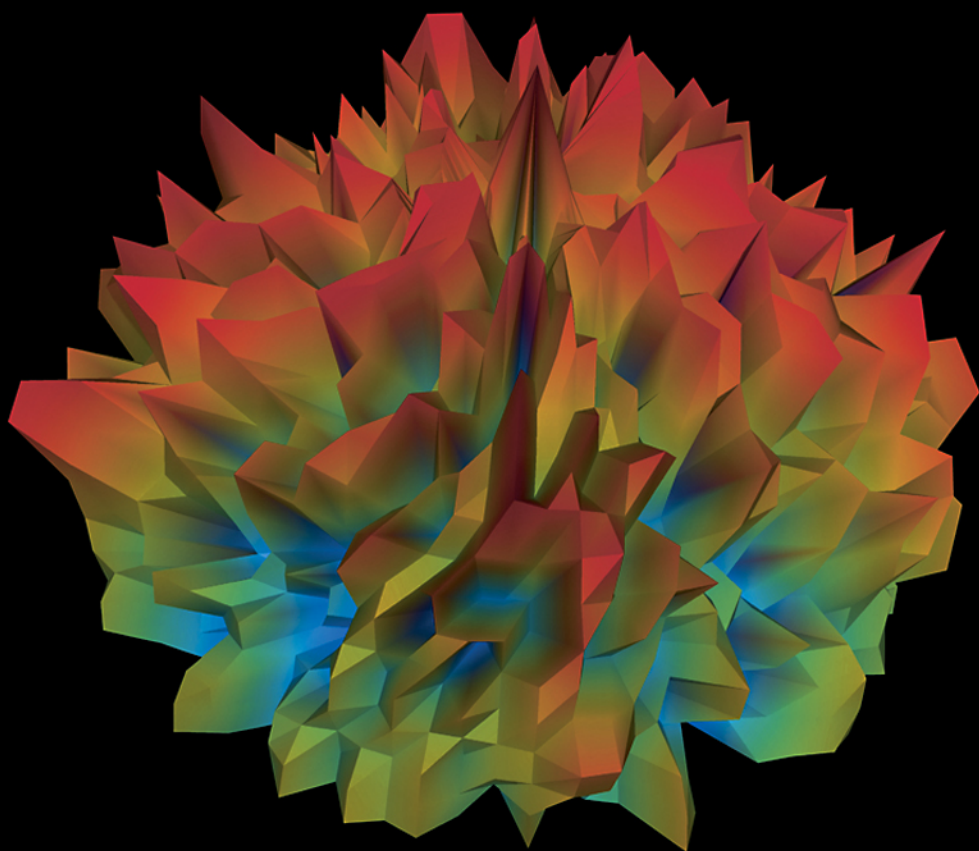# Acoustic Absorbers and Diffusers

Theory, design and application   Trevor J. Cox and Peter D'Antonio

Second edition

Taylor & Francis

Acoustic Absorbers and Diffusers

To our families

and

Manfred Schroeder

Acoustic Absorbers and Diffusers

Theory, design and application

Second edition

Trevor J. Cox
University of Salford, UK

and

Peter D'Antonio
RPG Diffusor Systems, Inc., USA

This publication presents material of a broad scope and applicability. Despite
stringent efforts by all concerned in the publishing process, some typographical
or editorial errors may occur, and readers are encouraged to bring these to our
attention where they represent errors of substance. The publisher and author
disclaim any liability, in whole or in part, arising from information contained
in this publication. The reader is urged to consult with an appropriate licensed
professional prior to taking any action or making any interpretation that is within
the realm of a licensed professional practice.

Contents

Preface to the first edition

Every book tells a story and there is a story behind every book. This story begins in 1980, in the conference room of the Laboratory for the Structure of Matter at the Naval Research Laboratory (NRL) in Washington, DC, where Peter D'Antonio was employed as a diffraction physicist. Knowing Peter's interest in music, a colleague handed him the latest issue of *Physics Today* with a cover photo of Manfred Schroeder seated in an anechoic chamber. The article suggested using number theoretic diffusers in concert halls. While Peter's interest at the time was not in concert halls, he became fascinated with the thought of using these diffusers in a renovation of Underground Sound, a private studio he originally built in 1972 with Jerry Ressler. The acoustic renovation utilized a new concept called live end dead end® proposed by Don and Carolyn Davis of Synergetic Audio Concepts (Syn-Aud-Con) and implemented successfully by Chips Davis.

At that time, Peter was examining the three-dimensional (3D) structure of matter in various phases using electron and X-ray diffraction techniques. Peter shared the article with John Konnert, a colleague at NRL, and it became apparent that the 'reflection phase gratings' suggested by Schroeder were in effect two-dimensional (2D) sonic crystals, which scatter sound in the same way that 3D crystal lattices scatter electromagnetic waves. Since the diffraction theory employed in X-ray crystallographic studies was applicable to reflection phase gratings, it was straightforward to model and design the diffusers. At this time, Peter's only link to the field of acoustics was a love of composing, recording and performing music. Having scientific backgrounds, John and Peter approached acoustics as they did the field of diffraction physics, and began researching and publishing findings in the scientific literature. The Audio Engineering Society (AES) and Syn-Aud-Con offered a unique forum and community for discussing the research. In October 1983, at the 74th AES Convention in New York, Peter met Bob Todrank following a presentation of Peter and John's first paper on Schroeder diffusers. Bob was designing a new studio for the Oak Ridge Boys in Hendersonville, TN and was interested in utilizing these new acoustical surfaces. The studio was a resounding success and turned out to be a harbinger of many exciting things to come.

In 1983, Peter and John measured quadratic residue and primitive root diffusers with a TEF 10 analyzer at a Syn-Aud-Con seminar in Dallas, TX, with the assistance of Don Eger of Techron. Here Peter met Russ Berger who was a pioneer in the use of new products in his firm's recording studios. In 1984, an intensive measurement programme was carried out using Richard Heyser's time delay spectrometry implementation. Farrell Becker was very helpful in the initial evaluation of these exciting new surfaces.

Not having access to an anechoic chamber, a boundary measurement technique was developed. These measurements were initially carried out at full scale in large spaces like open fields and parking lots, eventually moving indoors to a sports arena, a motion picture sound stage, and a local high school gymnasium. The measurements enabled the theories to be validated.

The Oak Ridge Boys' Acorn Sound Recorders project was celebrated with a Syn-Aud-Con control room design workshop in 1984. This project led to many others and collaborations with a growing community of new studio designers were undertaken. Neil Grant was an early staunch proponent of the research and products. Some of his milestone designs include Peter Gabriel's Real World Studios, Box, UK; Reba McEntire's Starstruck Studios, Nashville, TN; Sony Music, New York, NY and Cinerama Theater, Seattle, WA. In 1989, John Storyk integrated diffusive technology in many of his designs, including Whitney Houston Studio, Mendham, NJ; Electronic Arts, Vancouver, BC and Jazz at Lincoln Center, NY highlighting the list. Today much of the recorded music you hear is created in music facilities utilizing RPG Diffusor Systems Inc. technology. These fledgling years established relationships that continue to this day and produced many acoustical landmarks.

Interest in recording facilities naturally spread to broadcast facilities, where diffuser technology is now commonplace. Facilities include BBC, NPR, NBC, CBC and most of the broadcast networks due to Russ Berger's innovative designs. Being musicians and audiophiles led to significant involvement in residential high end audio listening rooms, as well as production studios.

In 1989, Peter was introduced to Jack Renner, President of Telarc Records, the company that started the classical high end recording industry on a digital journey. Jack was recording the Baltimore Symphony Orchestra at the Meyerhoff Symphony Hall and asked if RPG could assist him. Following initial experimentation, Telarc graciously credited RPG® as Telarc's exclusive acoustical system for control room and stage use for the Berlioz Symphonie Fantastique in 1990. The somewhat accidental stage use and overwhelming acceptance by musicians and conductor prompted an objective and subjective investigation of stage acoustics and acoustical shells both with small ensembles and with the Baltimore Symphony Orchestra. These chamber group studies were conducted with Tom Knab at the Cleveland Institute of Music, where Peter has been adjunct professor of acoustics since 1990, at the invitation of Jack Renner. In 1989, RPG was privileged to provide a custom number theoretic surface for the rear wall of Carnegie Hall, New York. This installation, along with the new diffusive acoustical shell development, launched RPG's involvement into performing arts applications, which eventually included the Fritz Philips Muziekcentrum, Eindhoven and the Corning Glass Center, Corning, NY.

Many of the acoustical consultants involved in the design of worship spaces began to include the use of diffusers for rear wall applications and acoustical shells. While RPG has collaborated with many acousticians, the relationship with Mike Garrison is noteworthy for the sheer number and size of the successful worship spaces produced using diffusers. The crown jewel of this collaboration is the 9,000 seat South East Christian Church in Louisville, KY.

In 1990, RPG funded the DISC Project in an attempt to devise a standard methodology for evaluating diffuser quality. In 1991, Peter proposed a directional diffusion coefficient and the AES invited him to chair standards committee SC-04-02 to formally develop an information document describing these procedures.

In 1993, David Quirt, Associate Editor of the *Journal of the Acoustical Society of America* (*JASA*), asked Peter to referee a paper by Trevor Cox entitled 'Optimization of profiled diffusers'. (Trevor's research journey had started a few years earlier in 1989 when, under the direction of Raf Orlowski and Yiu Wai Lam, he completed a PhD on Schroeder diffusers at Salford University, UK.) Trevor's paper outlined a process that combined boundary element modelling and multi-dimensional optimization techniques to make better diffusers. In Peter's view, this paper represented a creative milestone in diffuser development on par with Schroeder's seminal contribution. Peter and John's review of the paper consumed many months. It required the writing of boundary element codes and developing the first automated goniometer to measure these optimized surfaces. During the summer of 1994, Paul Kovitz helped to complete the measurement software. Trevor's revised paper, accompanied by a refereed paper of Peter and John's review, were published in 1995. Since this was nearly three years after Trevor submitted the paper to *JASA*, this must have seemed to be the peer review from hell, especially as the referees' comments were 36 pages long.

Peter finally met Trevor in Amsterdam at an AES SC-04-02 standards committee meeting in 1994 and again in Arup Acoustics' office in London. Our strong mutual interests led to an informal collaboration. In 1995, Trevor became a research consultant to RPG Diffusor Systems, Inc. This relationship started with developing an automated program to optimize loudspeaker and listening positions in a critical listening room and blossomed to generate much of the contents of this book.

Realizing that good acoustical design results from an appropriate combination of absorptive, reflective and diffusive surfaces, as mentioned in the Introduction, Peter (and later with Trevor) began developing absorption technologies as well, including hybrid abffusive (absorptive/diffusive) and diffsorptive (diffusing/absorbing) systems, concrete masonry units, low frequency absorbing arena seating risers, nestable open-cell foam systems and dedicated absorptive low frequency membrane systems.

In 1995, Peter and Trevor became aware of the diffusion research of James Angus on amplitude gratings and modulated phase gratings. James has made significant contributions to the field of diffuser design and we both have great respect for his insight and enjoy our collaborations with him. Also in 1995, we met Eckard Mommertz and Michael Vorlander at the 15th International Congress on Acoustics (ICA) in Trondheim, Norway. It was at this meeting that we learned of their work developing a procedure to measure the random incidence scattering coefficient. We have maintained close collaboration to this day, especially as members of the ISO WG 25, chaired by Jens Holger Rindel.

To further the development of the diffusion coefficient, RPG co-funded a three year grant with the Engineering and Physical Sciences Research Council of the United Kingdom, beginning in 1996. Trevor, Yiu Wai Lam and Peter were the investigators and Tristan Hargreaves was the doctoral student. This research was very fruitful in that it produced the first 3D measurement goniometer and yielded a robust diffusion coefficient, which has since been published as AES-4id-2001.

This diffusion coefficient has since been used as a metric to develop a range of new diffusing surfaces, including optimized welled diffusers, profile diffusers, 1D and 2D curved diffusers, baffled diffusers, genetic binary hybrid surfaces, flat and curved binary amplitude gratings, fractal and aperiodically modulated surfaces – in effect, many of the topics included in this book. These new optimized custom curved surfaces have found application in performance spaces like Kresge Auditorium, Boston, MA; Hummingbird

Center, Toronto, Canada; Edwina Palmer Hall, Hitchin, UK and also recording facilities like Sony Music's premier mastering room M1, in New York.

Things began falling into place and all of the relevant diffusion research was collected into a special edition of *Applied Acoustics*, entitled 'Surface Diffusion in Room Acoustics', guest edited by Yiu Wai Lam and published in June of 2000. Lam also organized a symposium in Liverpool that year. In September of 2001, a special structured session on scattering in room acoustics was organized by Michael Vorlander at the 17th ICA in Rome. Having played a pioneering role in making Schroeder's theoretical suggestions a practical reality, it was personally very gratifying for Peter to be part of a session dedicated to a topic which started as an intellectual curiosity, and has now turned into a diffuser industry and a field of research actively being studied by the leading acousticians of our time.

There have been many significant accomplishments over the past 20 years. We now know how to design, predict, optimize, measure, characterize and standardize the performance of scattering surfaces. While there is still much to do, there is a general consensus in the architectural acoustics community that a solid theoretical and experimental foundation has been laid, that diffuser performance can now be quantified and standardized and that diffusers can now be integrated into contemporary architecture, taking their rightful place along with absorbers and reflectors in the acoustical palette. The future holds many exciting possibilities.

It is a good time in the history of diffuser development to tell this story. This book has allowed us to chronicle developments with sufficient scientific detail, and to collect in one volume much of what is known about both diffusers and absorbers. In an effort to make this book 'timeless', we are providing a website www.rpginc.com/research, at which we will provide updates, polar responses of 1D and 2D diffusers, and additional diffusion and correlation scattering coefficients for 2D diffusing surfaces. You can contact us and tell us about technology and techniques we may have inadvertently missed in the book. So stay tuned and 'Listen to the Music, Not the Room'.

Peter D'Antonio
Trevor Cox
Authors

Preface to the second edition

As society evolves, new problems arise and these challenges must be met with new technology. For instance, sustainability is influencing the materials used in absorbers and diffusers. Intractable problems, such as environmental noise, continue to drive innovative new solutions. Furthermore, the general expectation of better quality design in the built environment has meant that designers have to concern themselves about the visual aesthetics of treatments alongside acoustic performance.

This second edition brings the technology of absorbers and diffusers up to date. For instance, the ubiquitous fabric wrapped panel and acoustical ceiling tile no longer address all of the concerns of our day. Therefore, we have expanded the description of other absorber technologies, such as microperforated designs. The sound diffuser continues to evolve to improve performance and to meet new demands for artistic shapes. Each stage in the evolution of these technologies overcame a particular shortcoming and increased performance.

But it isn't just the absorbers and diffusers that are changing; there have been new developments in measurement methods, standards and prediction models. For instance, recent advances in 3D solid prototyping printers greatly simplify the fabrication of diffuser test samples. To take another example, new time domain methods are being developed to predict how absorbers and diffusers interact with sound.

It is often said that new technology takes many years to be assimilated into the culture. Well 2008 was the 25th anniversary of the founding of RPG Diffusor Systems, Inc. and it is fair to say that diffusion technology is fully integrated into every aspect of architectural acoustics. Acousticians are routinely including absorption and diffusion coefficients into design specifications and architects are embracing the innovative diffusive shapes into their projects.

Peter D'Antonio
Trevor Cox
Authors

Acknowledgements

Glossary of frequently used symbols

Vectors are denoted in bold

a	Half diffuser or reflector width (m)
a	Fibre or hole radius (m)
A	Total absorption of a room (m²)
A	Scaling constant
A_n	Coefficients for grating lobes (Pa)
b	Half diffuser length (m)
c	Speed of sound (ms⁻¹), in air unless otherwise stated. Subscript 0 denotes value in air where ambiguity might arise otherwise ($\approx$343 ms⁻¹)
c_p	Specific heat capacity of air at constant pressure ($\approx$1.01 JKg⁻¹K⁻¹)
d	Cavity depth Helmholtz absorbers (m)
d	Diffusion coefficient
d	Thickness of materials (m)
$d\psi$	Diffusion coefficient for incident angle ψ
d_n	Depth of the nth well in a Schroeder diffuser (m)
D	Cell width for Helmholtz absorbers (m)
E	Ratio of the specimen perimeter to the specimen area absorption samples
f	Frequency (Hz)
f_0	Design frequency (Hz)
g	Acceleration due to gravity (ms⁻²)
G	Green's function
$H_0^{(1)}$	Hankel function of the first kind of order zero
H	Transfer function
FT()	Fourier transform
j	√-1
k	Wavenumber (m⁻¹). Subscript 0 denotes value in air where ambiguity might otherwise arise
k_x	Wavenumber component in x direction, similar expressions for y and z (m⁻¹)
k_s	Tortuosity
K_e	Effective bulk modulus (kgm⁻¹s⁻²)
l	Depth of materials (m)
m	Mass per area (kgm⁻²)
m	Order of diffraction or grating lobes
m	Energy attenuation coefficient for absorption in air
m	Constant relating finite to infinite sample absorption coefficients

MLS	Maximum Length Sequence
n	Normal to surface, for BEM modelling this is pointing out of the surface
N	Number of wells per period
N	Prime number generator and/or length of pseudorandom sequence
N_p	Prandtl number (≈ 0.77)
p	Pressure (Pa or Nm^{-2}). Subscript 0 denotes value in air where ambiguity might otherwise arise
p_1	Pressure from a single diffuser/reflector (Pa)
p_a	Pressure from an array (Pa)
p_i	Pressure incident direct from a source (Pa)
p_m	Pressure of the mth order diffraction lobe (Pa)
P_0	Atmospheric pressure ($\approx 101,320$ Pa)
p_s	Pressure scattered from a surface (Pa)
PRD	Primitive Root Diffuser
QRD®	Quadratic Residue Diffuser
r	Distance (m)
r	Primitive root of N
r′	Distance from image source (m)
r	Receiver position
r$_0$	Source position
r$_s$	Point on surface
R	Pressure reflection coefficient
s, s_n	Number sequence
s	Diffuser surface
s	Standing wave ratio
s	Scattering coefficient
S	Surface area of a room (m²)
S	Area of holes in Helmholtz resonator (m²)
sinc(x)	$= \sin(x)/x$
S_{xxm}	Maximum energy in autocorrelation side lobes
S_{xym}	Maximum energy in cross-correlation
t	time (s)
t	Sheet thickness for Helmholtz and membrane absorbers (m)
t'	Sheet thickness for perforated sheet including end corrections (m)
t_a	Resistive layer thickness for Helmholtz and membrane absorbers (m)
T_{60}	Reverberation time (s)
u	Particle velocity (ms^{-1})
V	Volume (m³)
w	Well or slot width (m)
W	Repeat distance or periodicity width (m)
x	Cartesian coordinate (m)
y	Cartesian coordinate (m)
z	Specific acoustic impedance (Pa s m^{-1} or MKS rayl)
z	Cartesian coordinate (m)
z_c	Characteristic impedance of a medium (MKS rayl)
z_f	Flow impedance (MKS rayl)
z_n	Normalized specific acoustic impedance ($=z/\rho c$)
α	Absorption coefficient

α_s	Random incidence absorption coefficient
α_∞	Random incidence absorption coefficient for an infinite sized sample
β	Admittance (rayl^{-1})
β'	Admittance with outward pointing normal (rayl^{-1})
β_n	Normalized admittance ($=\beta\rho c$)
ε	Porosity or fractional open area
δ	End correction factor (i.e. ≈ 0.85 if baffled)
δ	Delta function
δ_c	Correlation scattering coefficient
δ_v	Size of viscous boundary layer (m)
δ_h	Size of thermal boundary layer (m)
γ	Ratio of specific heat capacities (≈ 1.4 in air)
η	Viscosity of air (1.84×10^{-5} poiseuille)
κ	Thermal conductivity of air ($\approx 2.41\times 10^{-2}$ WmK^{-1})
λ	Wavelength (m)
λ_0	Design wavelength (m)
ν	Kinemetric viscosity of air (15×10^{-6}m^{2}s^{-1})
θ	Angle of reflection
ρ	Density; ρ_0 denotes value in air where ambiguity might otherwise arise (kgm^{-3})
ρ_e	Effective density of porous absorber (kgm^{-3})
ρ_f	Density of porous absorber's fibres or grains (kgm^{-3})
ρ_m	Bulk density of porous absorber (kgm^{-3})
σ	Flow resistivity (MKS rayl m^{-1})
σ_s	Flow resistance (MKS rayl)
τ	Relaxation times (s)
ω	Angular frequency (s^{-1})
ψ	Angle of incidence
Λ	Viscous characteristic dimension for porous absorber modelling (m)
Λ'	Thermal characteristic dimension for porous absorber modelling (m)

Introduction

The sound that is heard in most environments is a combination of the direct sound straight from the source or sources and the indirect reflections from surfaces and other objects. For instance, in room acoustics, both the direct sound and the reflections from the walls, ceiling and floor are key in determining the quality of the acoustic. To take another example, outdoors, the reflection from the ground can significantly reduce noise at certain low frequencies. Hence, one of the central topics in acoustics is how to manipulate these reflections that affect the way the sound propagates, and is ultimately perceived.

Sound striking a surface is transmitted, absorbed or reflected; the amount of energy going into transmission, absorption or reflection depends on the surface's acoustic properties. The reflected sound can either be redirected by large flat surfaces (specularly reflected) or scattered by a diffusing surface. When a significant portion of the reflected sound is spatially and temporally dispersed, this is a diffuse reflection, and the surface involved is often termed a diffuser. Figure 0.1 illustrates temporal and spatial characteristics of absorbing, specularly reflecting and diffusing surfaces, which form the acoustical palette. In addition to the surface types shown in the figure, there are also hybrid surfaces, which can both absorb and diffuse to varying degrees.

For over 100 years, since the founding of architectural acoustics by Sabine, there has been considerable effort devoted to studying surface absorption. Over this time, a considerable library of absorption coefficients has been tabulated based on accepted standards of measurement and a reasonable understanding of how absorbers should be designed and applied has been achieved. This development continues, and in recent decades many innovative absorber designs have been developed, and new ways to predict and measure absorptive materials have been found. For noise control, the focus of attention is naturally on absorbers to remove energy, however, in architectural acoustics, both absorbers and diffusers have a role in creating a good acoustic. However, significant scientific knowledge about the role of scattering (diffusely reflecting) surfaces has only been developed much more recently. Over the past 30 or so years, significant research on methods to design, optimize, predict, measure and quantify diffusing surfaces has resulted in a growing body of scientific knowledge and understanding. All these issues, and many more, are covered in this book.

Good architectural acoustic design requires the right room volume, the right room shape and surface treatments, utilizing an appropriate combination and placement of absorbers, diffusers and flat surfaces. Architectural acoustic spaces can be loosely divided into sound production, sound reproduction and noise control environments.

An example of a sound production room is the performing arts facility, such as

Acoustical Treatment   Temporal Response   Spatial Response

Absorption

Direct Sound

Attenuated
Reflection

-30°   0°   30°
-60°   60°
-90°   90°
                    10dB

Reflection

Specular
Reflection

6dB

Diffusion

Diffuse
Reflections

10 ms   Time (ms)
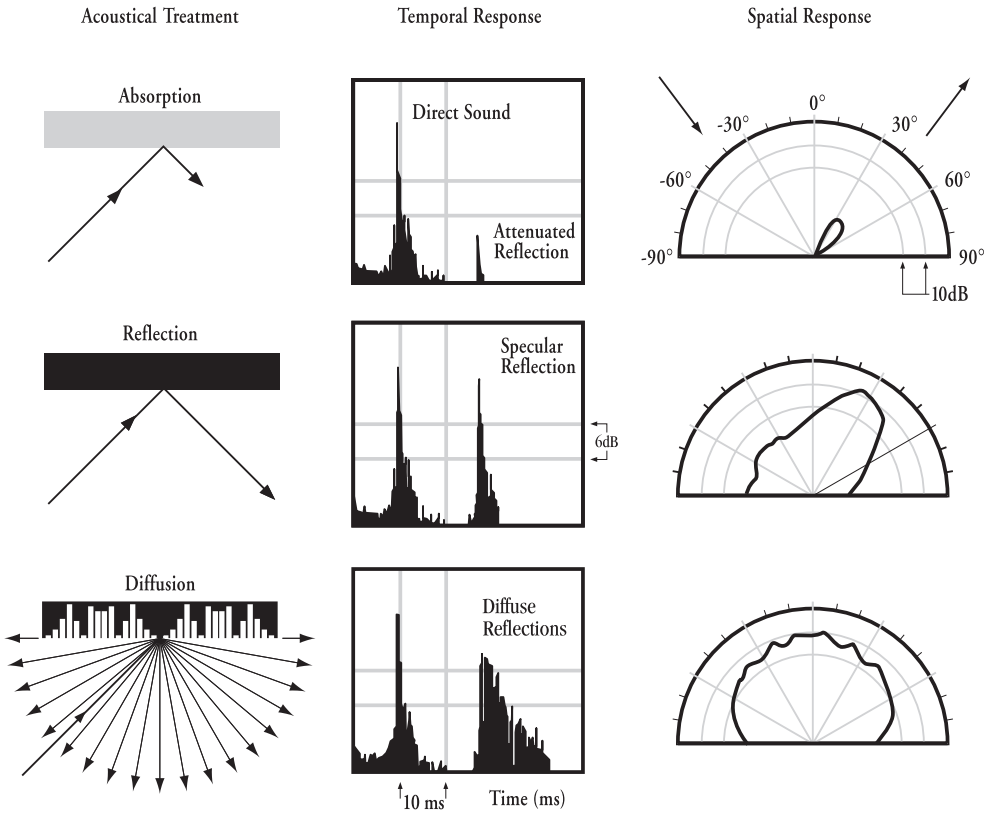
Figure 0.1   The temporal and spatial characteristics of absorbing, specularly reflecting and diffusing surfaces.

concert halls for classical music or a theatre for speech. The room acoustic contributes greatly to the perceived sound of the music or speech. The arrival time, direction and temporal density, and level of the early reflections, coupled with the balance of the early to late energy, decay time, temporal and spatial density of the late reflections, define the quality of sound that is heard and the degree of envelopment a listener experiences. In large sound production rooms, reflection and diffuse reflection are the primary acoustic tools. This is schematically illustrated in Figure 0.2. Absorption may be used to control reverberance, but the unavoidable absorption due to paying customers must also be considered.

In contrast, the acoustics of sound reproduction rooms, like recording studios and home theatres, should be neutral. All of the spectral, timbre and spatial information is pre-recorded on the playback media, and the reproduction room is only there to allow a listener to hear what has been recorded, as it was recorded. In a sound reproduction room, absorption and diffuse reflection play a key role, and specular reflection is a minor contributor. This is illustrated in Figure 0.3. Absorption and diffusion are used to control the coloration that would otherwise occur in the space from early arriving reflections and low frequency modes.
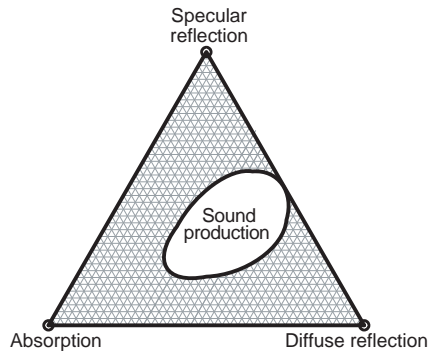
Figure 0.2 The relative importance of three acoustic treatments for sound production rooms such as concert halls, recital halls, auditoria, theatres, conference halls, courtrooms and worship spaces.

In noise control situations, like gymnasiums, swimming pools and factories, the objective is simply to reduce the reverberance and sound level. This might be done to reduce sound levels to prevent hearing damage or to improve the intelligibility of speech. Uniform distribution of absorption is the primary acoustic tool, and specular reflection and diffuse reflection have more minor roles. This is illustrated in Figure 0.4. (It has been suggested that diffusers can play a useful role in disproportionate spaces, but then the figures are all generalizations of the true situation.)

Surface acoustic treatment also plays an important role outdoors. For instance, the absorption of the ground can have a significant impact on sound levels from ambient noise sources, such as roads and industrial premises. The treatment of noise levels might involve the use of noise barriers, and these might be treated with absorption, or less commonly, diffusers to reduce the noise levels.

This introductory description has sketched out a few of the issues concerning where and why absorbers and diffusers are applied. More detailed descriptions can be found in Chapter 1 for absorbers and Chapter 2 for diffusers. The following section, however, tries to give an overview of the relative merits of absorption and diffuse reflections.
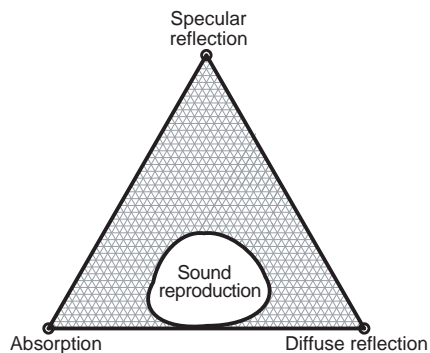
Figure 0.3 The relative importance of three acoustic treatments for sound reproduction rooms such as recording and broadcast studios, video conferencing rooms and home theatres.
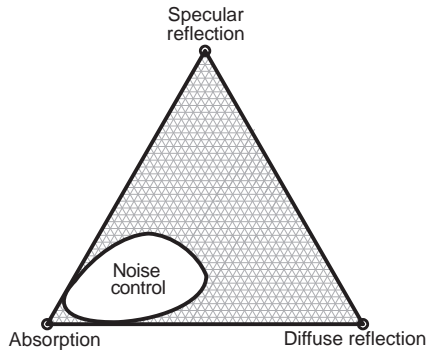
Figure 0.4 The relative importance of three acoustic treatments for noise control such as for factories, gymnasiums, swimming pools, libraries, atria and road side barriers.

Absorption versus diffuse reflections

Both absorbers and diffusers can be used to prevent acoustic distortion. For example, both can be effective in controlling echoes, coloration and image shift, which would otherwise be caused by strong reflections. This raises the question as to which is the best treatment in which situation.

   Whether absorbers or diffusers are better depends to a considerable degree on other acoustic factors, primarily on whether a decrease in reverberation and/or sound level is desirable. If a wall is causing an echo or coloration problem, and the designer wishes to conserve the reverberation time and sound energy in the space, then a diffuser is the best solution. The diffuser is placed on the wall to disperse the reflection and to reduce the distortion without removing sound energy from the space. For this reason, in concert halls, where acoustic energy is at a premium, diffusers are to be preferred. In smaller rooms, say a lecture theatre, where intelligibility is important, a balance must be reached in which absorption is used to adjust the reverberation time and level, and diffusers are used to ensure that early reflections, which can constructively support speech, do not produce distortion. When reflections cannot be constructively used for intelligibility, then these reflections can either be absorbed, if it doesn't make the room too dead, or diffused, thereby improving ambiance and coverage.

   In critical listening rooms, a mixture of absorbers and diffusers is used to control the acoustics of a space. Treatment is placed to control first order reflections. When absorbers are used, the sonic images forming the soundstage are points in space. When diffusers are used, these images take on a more natural width and depth. Which material is correct, absorber or diffuser, is to a certain extent a matter of personal taste. If all the treatment is absorption, then the room turns out to be rather dead. While some people favour this for mixing audio, others do not, and for a listening room a very absorbent environment is not best. Consequently, if some liveliness is to be left in the room, a combination of absorbers and diffusers must be used. Current psychoacoustical research in multi-channel surround listening rooms indicates the importance of generating lateral reflections to enhance envelopment, using single plane diffusers on side/rear walls and ceiling. Broad bandwidth absorption is most effective on the front wall and in corner locations. To provide low frequency modal control both

absorbers and diffusers require considerable depth to work, and the depths of acoustic treatments are often limited, because of space constraints and cost. Because of this, resonant absorbers requiring limited depth are often used to deal with the problems in a space efficient manner. In listening rooms, resonant absorbers provide effective low frequency control when placed in high pressure corner locations. For example, a membrane absorber might be used. The speed of sound in a porous absorber is lower than in air, and consequently a given thickness of absorber can work to a lower frequency than the same thickness of diffuser. For this reason, a partially absorbing diffuser, such as a hybrid structure, or a resonant absorber is usually favoured to treat low frequencies when space is a premium.

Diffusers have the advantage of generally being more robust than absorbers. Most absorber technologies involve fibrous materials, which do not stand up well to the effects of wind, rain and toxic environments. For example, in railway stations or on streets a large amount of particulate pollution may be generated, which over time can clog the pores of fibrous absorbents. There is a great risk with outdoor installations that fibrous absorbents will wash away over time. Recently, recycled, sintered glass absorbers have shown promise in both indoor and outdoor applications. Consequently, if it is possible to meet the acoustic requirement using a hard diffuser, it is possible to generate a much more robust treatment than with many absorbents. Alternatively, fibreless absorbers, such as microperforated absorbers, might offer a solution.

Both absorbers and diffusers have a role to play in good acoustic design. They have a complementary function, which means when they are used appropriately, better acoustics can be achieved.

1 Applications and basic principles of absorbers

This chapter is intended to introduce the fundamental principles of absorption, along with a basic explanation of the physics behind the absorption processes and some fundamental formulations which will be used in later chapters. Since the book is aimed at practitioners and researchers, most chapters begin with an application-driven, qualitative description, followed by a quantitative description of the technology and design. Following this type of philosophy, this introductory chapter on absorption is written from an application or case study perspective. The style is intended to make the more theoretical sections more palatable. Rather than start with a section labelled 'A little light mathematics' – which in most books is anything but light – the mathematical explanations will be formed around application examples. The chapter will also introduce some of the issues concerning the design, prediction and measurement of absorbers that will be treated in more detail in future chapters.

This chapter naturally introduces principles of airborne acoustics related to absorbers, such as some key issues in room acoustics. Readers familiar with these principles can skip these sections. Readers very unfamiliar with the subject should refer to the appropriate references. The first application example concerns the control of reverberance.

1.1 Reverberation control

Readers should be familiar with excessively reverberant spaces; this might be a restaurant or railway station, where the sound echoes around the space making it noisy and difficult to communicate. In these types of spaces, people tend to slow down their speech, talk louder and try to pronounce words more precisely in an effort to make the received speech intelligible. For some reason, many restaurateurs seem to think that to create the right atmosphere, it is necessary to make speech communication virtually impossible. The issue here is reverberation.

Reverberation is the decay of sound after a sound source has stopped and it is a key feature in room acoustics.[1] Reverberation is most audible in large spaces with hard surfaces, such as cathedrals, where the sound echoes around long after the sound was emitted from the source. In small spaces, with plenty of soft, acoustically absorbent materials, such as living rooms, the absorbent materials quickly absorb the sound energy, and the sound dies away rapidly. When people talk about rooms being 'live' or 'dead', this is usually about the perception of reverberance.

The amount of reverberation in a space depends on the size of the room and the amount of sound absorption. The solution to the reverberant restaurant is to add

acoustic absorbers. This will reduce the reflected sound energy in the room and so reduce the reverberance and sound level. Problems arise in dining rooms, because any surfaces close to eating or preparation areas need to be robust and washable, and many acoustic absorbers are soft and so are inherently unsuitable. Consequently, the best place for absorption is the ceiling or high up on the walls out of the way.

Figure 1.1 shows a large feature wall covered in an absorbing wood finish in an atrium. This treatment has the advantage of being architectural, yet absorptive, so it does not visually impose on the space as being an add-on treatment. Chapters 5 and 6 discuss innovative and more mundane absorber technologies. A less expensive solution would be standard absorbent ceiling tiles made out of compressed mineral wool, mounted in a T-bar grid; but this is not as elegant. The visual quality of acoustic treatment is extremely important to architects and absorbers need to fit within a design scheme rather than look like obvious add-ons. Consequently, one of the drivers for developing new acoustic materials is visual aesthetics, which is one reason why there is great interest in microperforated absorbers (see Section 6.2.4). Microperforations or microslits are barely visible at normal viewing distances and can be applied to wood and light transmitting plastics. The plastics provide absorption while maintaining visibility in projects with large amounts of glass, like atria. Microperforated wood veneers allow architects to use absorbing wood panelling in conjunction with traditional reflective wood panelling. Alternatively, acoustic plasters provide absorbing walls and ceilings that resemble traditional plaster or painted dry-wall.

In recent years, the issue of sustainability has become increasingly important. For this reason there is great interest in porous absorbents made from recycled materials, as discussed in Section 5.2.3. The need for thermally efficient buildings also poses a

Figure 1.1 Perforated, absorptive wood panelling covering the entire feature wall opposite an exterior glass wall (out of shot) in Morgan State University in Baltimore, MD. (Acousticians: Shen, Milsom and Wilke, Ballston, VA. Photo courtesy of RPG Diffusor Systems, Inc.)

challenge to acoustic consultants. More hard surfaces are being left exposed to exploit the thermal mass of ceilings and floors. These surfaces were traditionally covered with absorption to control reverberance. Therefore, new methods for controlling reverberance and sound reflections grazing across ceilings are now required.

Getting the correct amount of reverberation in a space is vital to the design of most rooms, whether the aim is to make music sound beautiful, to make speech intelligible, to reduce noise levels or simply to make a space a pleasant place to be in.

An extreme example of the use of absorption is the anechoic chamber, which is an acoustically dead space, an example of which is shown in Figure 1.2. This is a room where, above a certain cut-off frequency, there are no reflections from the walls, floor or ceiling. This means it is ideal for testing the response of diffusers, because the room does not affect the measurements. Anechoic chambers are also immensely quiet. To remove reflections from the boundaries, every surface is covered in absorbing wedges made of open-cell foam or fibreglass. Forming the absorbent into wedges reduces reflections from impedance discontinuities at the boundaries. Some have also made chambers from multiple layers of flat absorbents, where a gradual change in impedance is used to prevent strong reflections from the flat absorbent (see Section 5.5.4).

Another extreme example is the non-environment, which are acoustically (almost) dead spaces designed for control rooms.[2] The room has highly absorbing, broadband absorption on the side walls, rear wall and ceiling. The front wall is hard, diffusing, and the loudspeakers are flush mounted into the front wall. The floor is also hard and reflective. The idea is to replicate (near) free field conditions, to enable the monitoring of the direct sound and nothing else. Advocates of non-environments prefer certainty and detail over the reverberance and the more natural sound that is found in more conventional control rooms, examples of which can be found in Chapter 2.

Returning to more general reverberation, the primary technique for control is absorption. In discussing the design, application and measurement of absorbers, it is necessary to understand a statistical model of sound within an enclosure.[1,3] This is discussed in the next section.

Figure 1.2   The anechoic chamber at the University of Salford, UK.

1.1.1 A statistical model of reverberation

A simple model of sound propagation in a room is of particles of energy bouncing around the room in an analogous way to a snooker ball bouncing around a billiard table. The room can be characterized by the impulse response, an example of which is shown in Figure 1.3. The impulse response is a pressure versus time graph showing the response at a receiver position when somewhere else in the room a short impulse is created. For example, a balloon burst or a starting pistol might generate the short impulse, and the response might be measured with a microphone. First of all the direct sound from the source to receiver is received. Soon after, a series of reflections arrive, the level of these reflections generally decaying with time, due to absorption at the room surfaces. The effects of the boundaries dominate the behaviour of sound in rooms, and it is at the boundaries where absorption is normally found. (Only in large rooms does absorption by the air become important.) There is an increase in reflection density with time, and when the reflections become very dense this is termed the reverberant field. The energy of the reverberant reflections around the room is roughly constant and can be readily predicted, provided the sound field is diffuse.[4]

The reverberation time T_{60} measures the time taken for the sound pressure level to decay by 60 dB when a sound stops. From the impulse response, the Schroeder curve must be calculated first by backwards integration, before evaluating the reverberation time.[5] Sabine showed that the reverberation time could be calculated from the room volume and absorption by:[6]
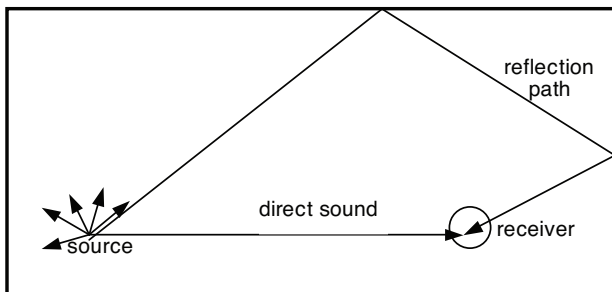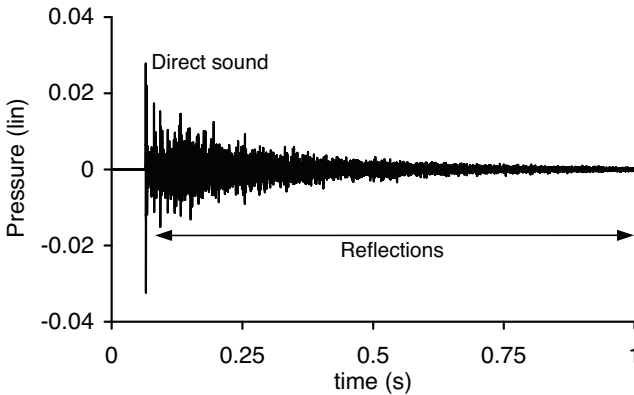
Figure 1.3   The generation of an impulse response in a room, and a typical example impulse response from a concert hall.

$$T_{60} = \frac{55.3V}{cA} \tag{1.1}$$

where V is the room volume; c the speed of sound, and A the total absorption of all room surfaces.

The total absorption of the room can be calculated from the individual absorption coefficients of the room surfaces, using the following expression:

$$A = \sum_{i=1}^{N} S_i \alpha_i \tag{1.2}$$

$$= S\overline{\alpha}$$

where S_i is the surface area of the ith surface element in the room; S is the total surface area of the room; α_i the absorption coefficient of the ith surface element in the room, and $\overline{\alpha}$ the average absorption coefficient of the room.

The absorption coefficient of a surface is the ratio of the energy absorbed by the surface to the energy incident. It typically lies between 0 and 1, which represent non-absorbing and totally absorbing surfaces, respectively. Values greater than 1 are often found in random incidence measurements, although theoretically impossible. This usually occurs due to diffraction/edge effects – see Chapter 3 for further details of the measurement methods. The absorption coefficient can be defined for a specific angle of incidence or random incidence as required.

Equations 1.1 and 1.2 form the basis for the standard method for measuring a random incidence absorption coefficient. The reverberation time in a reverberation chamber is measured with and without the test sample. The test sample adds absorption to the room and so reduces the reverberation time. From the change in reverberation time, the absorption coefficient can be obtained. This technique is described in detail in Chapter 3. Chapter 12 examines how to use this measurement data in room predictions and geometric models.

For large rooms, the absorption of air should also be accounted for. The total air absorption A_{air} in a room of volume V is given by:

$$A_{air} = 4Vm \tag{1.3}$$

where m is given in Table 3.1 or formulations can be found in ISO 9613-2.[7]

To allow for air absorption in the reverberation time predictions, the additional absorption calculated from Equation 1.3 should be added to the denominator of Equation 1.1 to give:

$$T_{60} = \frac{55.3V}{cA + 4mV} \tag{1.4}$$

Sabine's formulation does not correctly predict the reverberation time for rooms with a large amount of absorption. Over the years many new formulations have been

developed, the most popular of these being the Eyring equation,[8] also known as the Eyring–Norris equation:

$$T_{60} = \frac{55.3V}{-cS\ln(1-\overline{\alpha})} \tag{1.5}$$

where ln() signifies the natural logarithm. A little-used formulation, but one needed in Chapter 12, when the translation between coefficients measured in the reverberation chamber and those used in geometric models is considered, is the Millington equation:[9]

$$T_{60} = \frac{55.3V}{-c\sum S_i \ln(1-\alpha_i)} \tag{1.6}$$

Alternate reverberation time equations are the topic of considerable interest. Many formulations attempt to be catch-all equations for reverberation time estimation, but it is often difficult to know a priori, whether a formulation will work in a particular room. It is conceivable that better equations can be developed by analyzing rooms in more detail (such as surface size and orientation statistics, and absorber and diffuser distribution), but any such attempt would require a computer model of the room to be made for the analysis. As geometric models exist (ray tracing and variants thereof), where the impulse response of a room can be predicted, there is little need nowadays to search for ever more complex reverberation time formulations.

The relative advantages of the reverberation time formulations given in Equations 1.1, 1.5 and 1.6 will become important when discussing absorption measurement in Chapter 3. In recent years, researchers have also been revisiting alternative reverberation time formulations in an effort to improve the accuracy of predictions in geometric room acoustics models; this is discussed in Chapter 12. Using geometric models for reverberation time estimation also requires diffuse reflections to be taken into account, which is still the subject of standardization and investigation, as discussed in Chapters 4 and 12.

Despite many studies, the application of absorption coefficients in computer models is fraught with difficulty, mainly because it is difficult to know what the absorption coefficients are for surfaces, and this is a key input to the model. The accuracy of absorption coefficients is particularly important when a significant portion of the surface area of a room is very reflective, for instance if much of the room is made from concrete, glass or wood. Furthermore, when the absorption is restricted to one plane, as is typically the case in concert halls, swimming pools, sports halls and classrooms, this means that the late decay is very dependent on the exact value of the absorption coefficient selected for the reflective surfaces. Even in a room entirely made of one material, such as a room made only of concrete, accurate absorption coefficients are critical. Changing the absorption coefficient of the concrete from 0.02 to 0.01 in such a room will double the reverberation time (except at higher frequencies where air absorption will dominate in a large room). In other words, when a hard material is dominating, a very accurate estimate of the absorption coefficient is necessary for purely numerical reasons. Consequently, while there are tables of absorption

coefficients in the literature, and in Appendix A of this book, these cannot be blindly applied. The measured absorption coefficients can vary greatly from laboratory to laboratory, even for the same sample, as Figure 3.6 shows. Furthermore, for some products the absorption can vary greatly from manufacturer to manufacturer – an example being carpets as discussed in Chapter 5. Consequently, *in situ* methods for measuring absorption both within rooms and for outdoor applications are of interest, and these methods are discussed in Chapter 3.

The reverberation time formulations are statistical models of room acoustic behaviour, and are only applicable where there are a large number of reflections and the sound field is diffuse. For instance, at low frequencies, the modal behaviour of the room makes the sound field non-diffuse. Consequently, there is a lower frequency bound on the applicability of statistical absorption formulations. The lower bound is usually taken to be the Schroeder frequency[10] given by:

$$f \geq 2000\sqrt{T_{60}/V} \qquad (1.7)$$

Although this formal limit has been known for many years, it does not prevent many practitioners, standards and researchers still defining and using absorption coefficients below the Schroeder frequency, as it is convenient, even if not strictly physically correct. Geometric models are also used below this limit, although they have difficulties predicting at frequencies where there is a low modal density, where correct modelling of phase is needed.

1.2 Noise control in factories and large rooms with diffuse fields

The noise levels within working environments must be controlled to allow safe working, as excessive levels can cause hearing loss. Consequently, there are regulations to limit the exposure of workers. There are several methods for controlling noise exposure. The most efficient of which is usually to control the noise at the source, but this may not always be possible. Another technique is to reduce the reverberant sound level within a space. This is only effective if the reverberant field makes a significant contribution to the noise level. For instance, the approach is ineffective if the worker is close to a noisy machine, because the direct sound will dominate. The reverberant field level is reduced by the addition of absorption and hence the noise exposure is decreased by typically up to 3–4 dB(A). Typically, porous (or bulk) absorbers, such as mineral wool, are used as it is inexpensive, light and effective.

The porous absorber often has to be protected from dust, and so is frequently wrapped in plastic, but this decreases high frequency absorption. There are situations where the absorbent needs to be washable, and there are a few types of porous absorber that achieve this. There are also situations where the absorbent needs to be fibreless to prevent contamination. Chapter 5 discusses the design and modelling of porous absorbents, including some innovative materials. Chapter 6 includes sections on microperforation, which is one way of making fibreless absorbers. Porous absorbers are only effective at mid- to high frequencies, but this is where the ear is most sensitive and consequently where noise control is most needed in the working environment.

Factories tend to be very disproportionately dimensioned; they have very low ceilings compared to their widths and lengths. This means that the simple diffuse field

equations, such as Equation 1.1, are unlikely to work. For statistical room acoustics to hold, the space needs to be diffuse. A diffuse field is one where there is uniform reflected energy density across the whole room, and all directions of propagation are equally probable. There are many reasons why real rooms do not have even energy density and equally probable propagation directions:

1   At low frequencies there are standing wave modes similar to those found in ducts (see Section 1.3).
2   If the room's dimensions are very dissimilar, there is a tendency to get different reverberation times in different directions as happens with many factories. Sound will decay faster if it is propagating perpendicular rather than parallel to the floor, as the perpendicular propagating sound will reflect more often, and it is at the reflections that most absorption occurs.
3   The absorption in a room should ideally be evenly distributed across all surfaces. For many cases this is not true: the factory absorption might all be on the ceiling; a swimming pool may also have all the absorption in the ceiling; a reverberation chamber with a test sample has all of the absorption on the floor; and a classroom usually has absorption on the ceiling and floor, but not the walls.
4   If the room has a distinctive shape, e.g. cylindrical, the curved surfaces can focus sound to a point, like a curved mirror does with light. The result will be an uneven sound field (see Section 2.9 for solutions involving diffusers).

The relevance of the diffuseness of the space to absorption technologies is as follows. The absorption coefficient of a building element will be measured in a reverberation chamber, using Sabine's reverberation time formulation (see Section 3.4). When the absorption is applied, however, the acoustic conditions might be dramatically different, for instance non-diffuse, which means that the anticipated changes in noise levels and reverberance might not occur. The absorption might be more or less effective than predicted; this is discussed in Chapter 12. A special example of the problem is considered in Sections 3.4.1 and 7.1 when auditorium seating is considered. Chapter 12 discusses the application of absorption coefficients to room acoustic models, where the issue of non-diffuseness is again important.

1.3 Modal control in critical listening spaces

Small rooms, like recording/broadcast studios, home theatres and conference rooms, usually suffer from problems due to low frequency modes. At low frequencies, the standing wave modes of the room are separated in frequency. Figure 1.4 shows the frequency response for a small room. The frequency response is uneven, meaning that some frequencies are emphasized, where mode(s) are strong, and some suppressed, where mode(s) are weak, leading to coloration of the received sound. This is most critical for music applications, particularly with the increasingly widespread use of sub-woofer technology and reproduction of modern music with high bass content. Common solutions include choosing the room dimensions, loudspeaker and listening positions correctly to flatten the frequency response of the room as much as possible and avoid degenerate modes.[11] Even when the room dimensions have been carefully chosen, however, the frequency response of the room will still be uneven and acoustic treatment is needed.
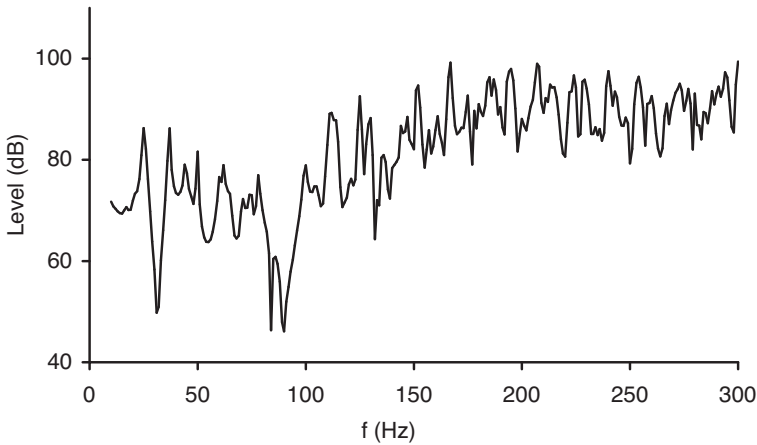
Figure 1.4 Low frequency response of a small room.

Particularly prominent modes are usually treated with bass absorption, often referred to as bass traps or bins. (It is not usually possible to treat this problem with diffusion because the sizes of the diffusers become prohibitively large, although Section 2.2.3 discusses a case where this has been done.) Porous absorbers are not usually used, as they would have to be extremely thick to provide significant bass absorption. Porous absorption is most effective when it is placed at a quarter wavelength from a room boundary, where the particle velocity is maximum. For a 100 Hz tone, this would be roughly 1 m from the boundary. Placing porous absorbers directly on a room boundary, while the most practical, is not efficient, because the particle velocity at a boundary is zero. Too often, many people place porous absorption in corners of rooms thinking this will absorb sound, since all the modes have a 'contribution' in the corners. However, while the modes have a maximum pressure in the corners, the particle velocity is very low and so the absorption is ineffective. For these reasons, resonant absorbers are preferred for treating low frequencies.

Resonant absorbers are mass spring systems with damping to provide absorption at the resonant frequency of the system. The mass might come in the form of a membrane made of plywood or mass-loaded vinyl. Alternatively, the vibrating air in the neck of a hole might form the mass, as is the case for a Helmholtz resonant absorber. The spring usually comes from an air cavity. Damping is most often provided by sound being forced through a porous resistive material: mineral wool, fibreglass or acoustic foam.

The problem with resonant absorbers is that they usually only provide a narrow bandwidth of absorption. To cover a wide bandwidth, a series of absorbers are required, each tuned to a different frequency range. Alternatively, double-layered absorbers can be used, but are expensive to construct. In recent years, a new resonant absorber has been constructed where the vibrating mass is a metal plate and the spring is formed from foam or polyester, and this provides absorption over a broader bandwidth.

Resonant absorbers are discussed in Chapter 6, including microperforated absorbers, which are currently attracting considerable interest. An alternative, but expensive solution to bass absorption is to use active surfaces. Active absorbers have much in common with active noise control systems, and are discussed in Chapter 13.

One problem with low frequency modal control is knowing how much resonant absorption to use. Although the theories set out in Chapter 6 allow the performance of Helmholtz absorbers to be estimated, the meaning and interpretation of absorption coefficients at low frequencies is not straightforward. (Even more tricky is the lack of good prediction models for membrane absorbers, but that is another story.) At low frequency, the sound field is not diffuse, and consequently the effect that an absorber has is not calculable through simple statistical laws. Often, practitioners pragmatically apply diffuse field theory anyway; a more complex, but exact approach, would use a wave based modelling method such as finite or boundary element.

1.4 Echo control in auditoria and lecture theatres – basic sound propagation models

A late arriving reflection appears as an echo, if its level is significantly above the general reverberation level. In a large auditorium, the reflection from the rear wall is a common source of echo problems for audience members near the front of the stalls (main level seating) or performers on the stage. Echoes are very likely if the rear wall forms a concave arc, which focuses the reflections at the front of the hall. The physical and subjective processes are the same as for echoes heard in mountain ranges or in cities with large building facades. One technique for removing the echo is to apply absorption to the rear wall. The absorption attenuates the reflection making it inaudible as a separate acoustic source. Figure 1.5 shows the Royal Festival Hall where such a solution was used when it was first built. The problem with using absorption in auditoria is that it removes acoustic energy, which is at a premium in large spaces for orchestral performance, and so diffusion is currently the preferred solution (see Section 2.1).

For smaller spaces, where absorption is being used anyway for reverberation control, absorption is a possible treatment for echo problems. The absorption needs to act

Figure 1.5   The Royal Festival Hall, London. (Photo courtesy of Bridget Shield.)

at mid- to high frequencies, as echoes are most notable for directional instruments. Consequently, a layer of porous absorber can be used. Alternatively, hybrid surfaces controlling reverberation at low to mid-frequencies, but providing diffuse reflections at higher frequencies might be used; these are discussed in Chapter 11.

Flutter echoes can occur in spaces with two large parallel walls. The regular pattern of reflections caused by sound bouncing back and forth between the parallel walls causes coloration. By coloration, it is meant that the frequency response of the sound is detrimentally altered. If you go into many stairwells with parallel walls and clap your hands, a high frequency ringing will be heard; this is the flutter echo. Flutter echoes are common in lecture theatres. One remedial measure is to apply absorbent to at least one of the two parallel walls to absorb the reflections. Again, a relatively thin layer of porous absorber can achieve this, as it is mid- to high frequency treatment that is needed. Alternatively, diffusers are sometimes preferable, because they control the flutter echo, while also uniformly dispersing the sound for better coverage and intelligibility.

Porous absorbers are any material where sound propagation occurs in a network of interconnected pores in such a way that viscous effects cause acoustic energy to be dissipated as heat. Common examples are mineral wools, fibreglass, open cell foams, acoustic tiles, carpets and curtains. Current concerns about sustainability have also led to porous absorbers being constructed from recycled materials. To gain a proper theoretical understanding of porous absorbers, it is necessary to understand the theories of sound propagating in a medium. Some basic models of sound propagation, which are the basis for much of the absorber and diffuser modelling in the book, are presented in the next section.

1.4.1 Sound propagation – a wave approach

To understand and design absorbers, it is necessary to have a basic understanding of the terminology used and the fundamental mathematical constructs used for sound propagation. This section introduces some basic constructs, concepts and terms.

A complex number representation of waves will be adopted throughout the book. The pressure of a plane wave propagating in a direction **r** is:

$$p(t, \mathbf{r}) = Ae^{j(\omega t - \mathbf{k} \cdot \mathbf{r})} = Ae^{j(\omega t - k_x x - k_y y - k_z z)} \tag{1.8}$$

where $\mathbf{k} = \{k_x, k_y, k_z\}$ is the wavenumber ($\propto$ propagation constant) with k_x being the component in the x direction, $k^2 = |\mathbf{k}|^2 = k_x^2 + k_y^2 + k_z^2$; A is a constant related to the magnitude of the wave; $\mathbf{r} = \{x, y, z\}$ is the location of the observation point; t is time, and $\omega = 2\pi f = kc$ is the angular frequency, where f is the frequency and c the speed of sound.

The same conventions as used in Reference 3 are being adopted, so this is useful background reading for those who find this introduction too brief. The time dependence is $e^{+j\omega t}$. Unfortunately, there is no standard convention for the sign of this time dependence, so some of the literature uses a negative power in the exponential, leading to equations and results which are complex conjugates of those given in this book. Some texts and papers used a propagation constant, $\gamma = jk$, in their equations instead of the wavenumber, but this will be not often be used in this book.

Consider a plane wave propagating through an acoustic medium; this could be air or a porous absorber. The plane wave will be taken to propagate in the x-direction for convenience. The pressure and particle velocity are given by:

$$p = Ae^{j(\omega t - kx)} \tag{1.9}$$

$$\mathbf{u} = \frac{A}{\rho c} e^{j(\omega t - kx)} \tag{1.10}$$

where ρ is the density and c the speed of sound of the acoustic medium. The ratio of pressure to velocity gives the characteristic specific acoustic impedance of the medium, z_c:

$$z_c = \rho c \tag{1.11}$$

The characteristic acoustic impedance is a very useful property of the material when calculating the transmission of acoustic waves within and between different acoustic media.

   The characteristic impedance of plane waves in air is purely real with a value of about 415 MKS rayls. In an acoustic medium it will be complex, with a characteristic resistance and reactance, which are the real and imaginary parts of the impedance respectively. The characteristic impedance is analogous to the characteristic impedance of an electronic transmission line.

   Once the characteristic impedance and wavenumber within an acoustic medium are known, it is possible to predict the sound propagation. While it is possible to characterize a medium with the characteristic impedance and the wavenumber, it is also possible to use two other variables, the effective density ρ_e and bulk modulus K_e. The term effective is used to signify that this is the density experienced by the acoustic waves rather than the more normal definition of mass divided by volume. The bulk modulus is the ratio of the pressure applied to a material to the resultant fractional change in volume it undergoes. It is the reciprocal of the compressibility. For a porous absorber, the effective density and bulk modulus can be related to the characteristic impedance and wavenumber by the following formulations. The characteristic impedance is given by:

$$z_c = \sqrt{K_e \rho_e} \tag{1.12}$$

and the propagation wavenumber by:

$$k = \omega \sqrt{\frac{\rho_e}{K_e}} \tag{1.13}$$

Where possible, this book will work with the impedance and wavenumber, as multiple inter-related parameters are a potential source of confusion. Some porous absorbent prediction formulas, however, explicitly give values for the bulk modulus and the effective density, so these terms will sometimes be met in the literature.

1.4.2 Impedance, admittance, reflection coefficient and absorption coefficient

The effect that a surface has on an acoustic wave can be characterized by four inter-related acoustic quantities: the impedance, the admittance, the pressure reflection

coefficient and the absorption coefficient. The first three (impedance, admittance and pressure reflection coefficient) give information about both the magnitude and phase change on reflection. The absorption coefficient does not contain phase data, but only gives information about the energy change on reflection.

Understanding these four acoustic quantities is fundamental to understanding absorbing materials. These will now be defined mathematically by considering a wave propagating between two media. Consider a plane wave incident at an angle to a boundary between two acoustic media at $x = 0$, as illustrated in Figure 1.6. A simple model for a porous absorber assumes that it behaves as an acoustic medium like air, only with a different speed of sound c_1 and density ρ_1. The incident p_i, reflected p_r and transmitted p_t pressures are given by:

$$p_i = A_i e^{j[\omega t - kx \cos(\psi) - ky \sin(\psi)]} \tag{1.14}$$

$$p_r = A_r e^{j[\omega t + kx \cos(\theta) - ky \sin(\theta)]} \tag{1.15}$$

$$p_t = A_t e^{j[\omega t - k_1 x \cos(\phi) - k_1 y \sin(\phi)]} \tag{1.16}$$

where A_i, A_r and A_t are the magnitudes of the plane waves incident, reflected and transmitted, and the angles are defined in the figure.

Applying continuity of pressure gives the following relationship:

$$A_r e^{j[\omega t + kx \cos(\theta) - ky \sin(\theta)]} + A_i e^{j[\omega t - kx \cos(\psi) - ky \sin(\psi)]} = A_t e^{j[\omega t - k_1 x \cos(\phi) - k_1 y \sin(\phi)]} \tag{1.17}$$

This must be true for all times and for all values of y as this was a plane wave. Consequently, a relationship relating the angles of propagation is obtained, more commonly known as Snell's law:

$$\sin(\psi) = \sin(\theta) \tag{1.18}$$

$$\frac{\sin(\psi)}{c} = \frac{\sin(\phi)}{c_1} \tag{1.19}$$

or

$$k \sin(\psi) = k_1 \sin(\phi)$$

The behaviour of the sound wave therefore depends on the relative values of the speeds of sound in the two media. For most absorbents, the speed of sound is much less than that in air. Consequently, the angle of propagation in the medium is smaller than in the air. In fact for many absorbents, the angle of propagation can be assumed to be normal to the surface, i.e. $\phi \rightarrow 0$.
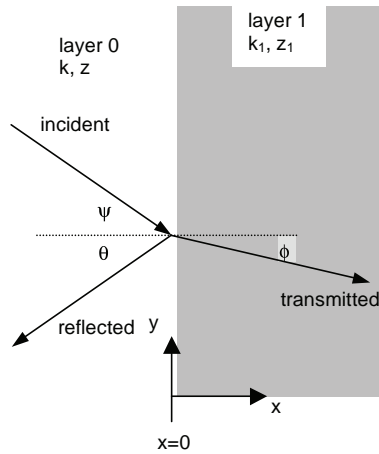
Figure 1.6 Sound hitting a surface.

The pressure reflection coefficient, R, (sometimes referred to as a reflection *factor*) gives the ratio of the reflected and incident pressure, i.e.:

$$R = \frac{p_r}{p_i} \tag{1.20}$$

Therefore, the pressure reflection coefficient includes both magnitude and phase information about the reflection of sound. There is also an intensity reflection coefficient, but this is not used in this book.

The need for continuity of particle velocity normal to the surface enables the derivation of an expression for the specific acoustic impedance of the surface. The relationships between pressure reflection coefficient and impedance will be used repeatedly in the book. For oblique incidence, these are:

$$R = \frac{\frac{z_1}{\rho c}\cos(\psi) - 1}{\frac{z_1}{\rho c}\cos(\psi) + 1} \tag{1.21}$$

$$\frac{z_1}{\rho c}\cos(\psi) = \frac{1 + R}{1 - R} \tag{1.22}$$

The admittance is the reciprocal of the impedance:

$$\beta = 1/z_1 \tag{1.23}$$

Often the surface admittance and impedance are normalized to the characteristic impedance of air, and these are denoted with a subscript of *n*.

The surface impedance is often split into the real term (resistance) and imaginary term (reactance). In general, the real term of surface impedance is associated with energy losses, and the imaginary term with phase changes. So a simple inspection of the surface acoustic impedance gives more insight into the absorbing properties of a material than the absorption coefficient.

Remembering from Section 1.1.1 that the absorption coefficient, α, is a ratio of the absorbed and incident energy enables the following expression to be derived:

$$\alpha = 1 - |R|^2 \tag{1.24}$$

where $|R|$ is the magnitude of the pressure reflection coefficient.

The above formulations have assumed a plane wave case, however in certain cases, for example for a source close to a reflecting surface, then a spherical wave formulation is most appropriate. The F-term solution of Nobile and Hayek[12] gives the velocity potential at a distance d above an impedance plane as:

$$\phi(d) = \frac{e^{-jkr_1}}{r_1} + Q\frac{e^{-jkr_2}}{r_2} \tag{1.25}$$

where r_1 and r_2 are defined in Figure 1.7. Q is the spherical wave reflection coefficient given by:

$$Q = R + (1 - R)F \tag{1.26}$$

where R is the plane wave reflection coefficient as previously used. So this asymptotic solution uses the plane wave solution plus a correction term. F is the boundary loss function given by:

$$F(w) = 1 - j\pi^{1/2}we^{-w^2}erfc(jw) \tag{1.27}$$

where $erfc()$ is the complementary error function and w is the numerical distance given by:

$$w = \sqrt{-\tfrac{1}{2}jkr_2}\left\{\cos(\psi + \beta_n)\right\} \tag{1.28}$$
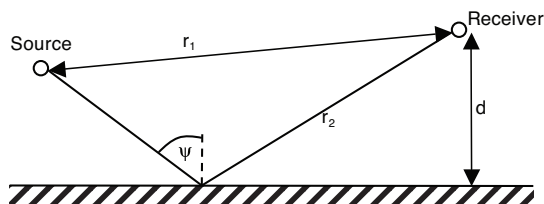
Figure 1.7   Geometry for spherical wave reflection coefficient.

While many reflections strictly speaking should be modelled using spherical wave reflection coefficients, in reality, in many cases the extra complication of the above equations is unnecessary. For instance, in the reverberant field in rooms where the number of reflections is large, a plane wave coefficient is sufficient. In contrast, when considering grazing reflections from sources close to the ground outdoors, the spherical wave reflection coefficient should be used.

This section has described a number of key terms for sound propagation fundamental to absorber and diffuser modelling. These will be used throughout the theoretical sections of this book where prediction models are developed for both absorbers and diffusers. These terms are also used in Chapters 3 and 4 when measurements are considered. But for now, it is time for some light relief by returning to some applications.

1.5 Absorption in sound insulation – transfer matrix modelling

Porous absorbent material is widely used in sound insulation. Lightweight constructions are often based on double leaf partitions with an air gap in-between, as shown in Figure 1.8. It is normal for the air gap to contain a porous absorber. The porous absorber is used to prevent a resonance of the air cavity. If cavity resonances are not removed by damping, at the resonant frequency sound will pass easier through the partitions, and so the sound insulation will be poorer. It is important that the absorbing material is lightly packed, otherwise it can form a vibration path bridging between the two partitions; this could greatly reduce the performance of the system. Many different porous absorbers will be effective in the partition; this is not the most critical application for the design of absorbents.

As the issue of transmission is being discussed, it seems appropriate to discuss the transfer matrix approach to modelling transmission through, and absorption from, porous and resonant absorbers. The transfer matrix approach is the basis for many of the prediction techniques given in Chapters 5 and 6. A similar process is used in transducer modelling, where the method is called a two port network.

1.5.1 Transfer matrix modelling

The transfer matrix approach to modelling sound propagation is a very powerful technique most often applied to porous absorption with and without membrane or perforated facings. It enables the surface impedance of single and multiple layers of
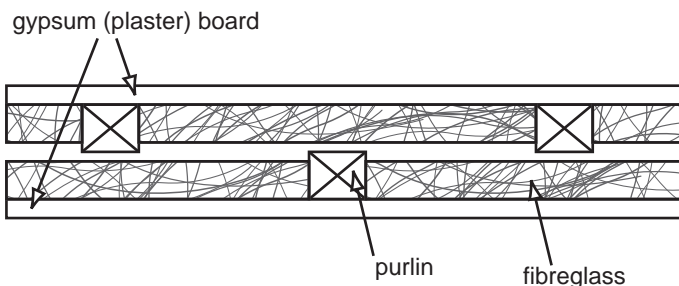
Figure 1.8 Mineral wool in a partition.
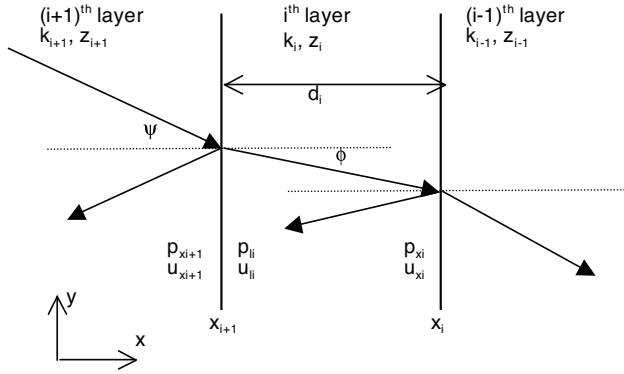
Figure 1.9 Geometry for transfer matrix modelling of a multi-layer absorbent.

absorbent to be calculated. For instance, it enables the case of a rigidly backed porous absorbent to be considered. This is the most important acoustic case, because it represents an absorbent placed on a wall, floor or ceiling.

Consider the situation shown in Figure 1.9. It is assumed that only plane waves exist within the layers. It is further assumed that the propagation is entirely contained in the *x-y* plane. By considering the continuity of pressure and velocity at the boundaries, it is possible to relate the surface pressure of one layer to the next.

$$\begin{Bmatrix} p_{li} \\ u_{li} \end{Bmatrix} = \begin{Bmatrix} p_{xi+1} \\ u_{xi+1} \end{Bmatrix} = \begin{Bmatrix} \cos(k_{xi}d_i) & j\dfrac{\omega\rho_i}{k_{xi}}\sin(k_{xi}d_i) \\ j\dfrac{k_{xi}}{\omega\rho_i}\sin(k_{xi}d_i) & \cos(k_{xi}d_i) \end{Bmatrix} \begin{Bmatrix} p_{xi} \\ u_{xi} \end{Bmatrix} \tag{1.29}$$

where p_{xi} and u_{xi} are the pressure and particle velocity at the bottom of the ith layer, for velocity this is defined to be in the *x*-direction; p_{xi+1} and u_{xi+1} are the pressure and particle velocity at the bottom of the $(i+1)^{th}$ layer; p_{li} and u_{li} are the pressure and particle velocity at the top of the ith layer; d_i is the thickness of the layer i^{th} layer; ρ_i is the density of ith layer, and k_{xi} is the *x*-direction component of the complex wavenumber for the ith layer.

The component of the wavenumber in the *x* direction is calculated by considering Snell's law (Equation 1.18):

$$k_{xi} = k_i\sqrt{1 - \sin(\phi)} = \sqrt{k_i^2 - k_{i+1}^2 \sin(\psi)} \tag{1.30}$$

Many porous absorbents have a small speed of sound in comparison to air, and so often $k_{xi} \approx k_i$ as $\phi \approx 0$.

Equation 1.29 is a recursive equation from which the pressure and velocity of any layer can be determined from boundary and incident sound wave conditions. Although this process can be used to determine absolute values for the pressure and velocity, the technique is most powerful in determining surface impedance values. The surface

impedance is calculated for the top of the ith layer, this is then used to calculate the impedance at the top of the $(i + 1)^{th}$ layer. The process is then repeated until all layers have been evaluated. The relationship that enables this process, relates the surface impedance at $x = x_{i+1}$ to the impedance at $x = x_i$:[13]

$$z_{si+1} = \frac{-jz_{si}z_i \dfrac{k_i}{k_{xi}} \cot(k_{xi}d_i) + \left(z_i \dfrac{k_i}{k_{xi}}\right)^2}{z_{si} - jz_i \dfrac{k_i}{k_{xi}} \cot(k_{xi}d_i)} \tag{1.31}$$

where z_{si} is the impedance at $x = x_i$; z_{si+1} is the impedance at $x = x_{i+1}$; k_i is the wavenumber in the ith layer, and x_i and x_{i+1} are defined in Figure 1.9.

To illustrate the application of Equation 1.31, consider the most common case, which is a rigidly backed single layer. In this case, $z_{si} \rightarrow \infty$, and the equation reduces to give a formulation for the surface impedance of the rigid back absorbent as:

$$z_{si+1} = -jz_i \frac{k_i}{k_{xi}} \cot(k_{xi}d_i) \tag{1.32}$$

1.6 Pipes, ducts and silencers – porous absorber characteristics

Air conditioning ducts and other pipelines are a common source of noise.[14] The noise generated by fans, blowers and internal combustion engines can propagate along the duct with little attenuation and radiate from outlets and exhausts. In addition, breakout noise can radiate from the sides of the pipelines and ducts. The most effective treatment is to reduce the noise at the source, but where this is not possible, the application of absorbent material can be effective.

For pipelines internal treatment is not often possible, and in this case external lagging can be used to reduce breakout noise. The external lagging is often a combination of mineral wool and a heavy limp mass jacket made of metal, although the evidence is that foam is more effective. Below 300 Hz, the lagging of pipelines is not effective, and indeed treatment around 300 Hz can often result in increased noise breakout. References 14 and 15 give design charts and equations to enable the effectiveness of pipeline and duct lagging to be calculated, although the prediction can be inaccurate unless proper manufacturer's data is known.

For ventilation ducts, internal lining of the duct is most effective and 2.5–5 cm thick linings are typically used. Internal duct liners are generally made of porous absorbent although the type of porous material is not that important from an acoustic perspective. It is often necessary to use a protective coating, which might be materials such as a spray-on polyurethane coating, impervious lightweight plastic sheet, neoprene or perforated metal. The protective coating can have a significant effect on the absorption obtained.

Porous absorbers are also used as part of silencers and mufflers used to attenuate sound within pipe work. It is important to know the environmental conditions that the absorbent will be subject to, both to be able to evaluate whether the material will be sufficiently robust overtime and not, for instance, become clogged, but also

because temperature and flow affect the acoustic properties of the material. In harsh environments, perforated or sintered metal is a good choice. In situations where sound pressure levels are very high, the non-linear behaviour of sound within the absorbent will need to be considered. Introducing a silencer will introduce a pressure drop, as it will somewhat inhibit the flow through the system, and this needs to be considered alongside the acoustic performance, size and cost.

Silencers come in three main forms: reactive, absorptive and a combination of reactive and absorptive. Reactive silencers change the cross-section of pipes to achieve attenuation at selective frequencies,[15] and are commonly used on outlet exhausts in harsh environments, but because they do not feature acoustic absorption, they will not be discussed further. Absorptive or reactive/absorptive silencers, as the names imply, are of more interest because they remove sound energy using porous absorbents. The porous material will be most effective at mid- to high frequencies. Absorptive silencers are most useful where a minimum pressure drop is required, and so are commonly used in applications such as ventilation ducts, intake and exhaust ducts of gas turbines and access openings of acoustic enclosures. Figures 1.10 shows one of the most common types of parallel-baffle silencers, where the shaded regions are made of porous absorbent. The attenuation is proportional to the perimeter area ratio, P/A, where P is the lined perimeter and A the cross-section of the silencer. The porous material should have a low enough flow resistivity so the sound enters the absorbent, but not too low otherwise no dissipation occurs (flow resistivity is defined in the next section). The spacing between baffles should be less than a wavelength; above the frequency where the wavelength equals the baffle spacing the attenuation falls off quite rapidly. The low frequency performance is determined by the thickness of the baffles, with $d \approx \lambda/8$ being optimal. Thickness rarely exceeds 200 mm, with thinner baffles usually producing more attenuation. Detailed design equations are given in Reference 15.

1.6.1 Characterizing porous absorbers

To theoretically model the sound propagation through a porous material, it is necessary first to have measurements characterizing the acoustic properties of the absorber as an
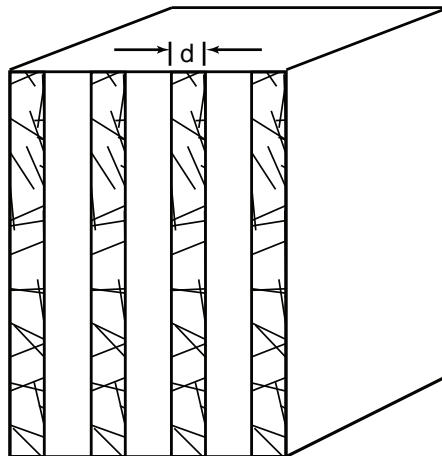

Figure 1.10   A typical parallel-baffle absorptive silencer used in a ventilation system.

acoustic medium. So far in this chapter, the wavenumber and characteristic impedance have been discussed, but these cannot be directly measured. There are other parameters which are needed by absorber designers. Given a piece of porous absorbent material to characterize, often a researcher would start by measuring the flow resistivity σ and porosity ε. The flow resistivity gives a measure of the resistance to flow that the porous absorber offers and porosity the amount of open volume in the absorber available to sound waves. Chapter 3 outlines measurement methods for obtaining these values, although for many porous absorbents it is possible to assume a porosity of 1. These are probably the two most important determining parameters for porous absorbents. Once the flow resistivity and porosity are known, it is then possible to get the characteristic impedance and wavenumber via empirical laws, such as those outlined in Chapter 5, and predict the absorption properties of the sample.

It is possible to go further and use a more refined model of porous absorbers, which need further measurements of properties (methods are given in Chapter 3). There are a variety of models in the literature, but the one outlined in Chapter 5 uses three additional parameters; two characteristic lengths and tortuosity. Measuring the characteristic lengths is somewhat problematic, but there are a variety of methods for getting the tortuosity accurately.

It is possible to directly measure the surface impedance, pressure reflection coefficient or absorption coefficient of a sample. This is often done in the development of prediction models for absorbents. As mentioned previously, the absorption coefficient can be measured through a reverberation chamber method, but the absorption coefficient is often influenced by edge effects. Furthermore, it is not possible to get phase information from the reverberation chamber, and this is very useful in understanding how an absorber works or why a theory succeeds or fails. To get phase information, a measurement for a particular incident angle needs to be made. The easiest system is to measure the impedance in a tube, where only normal incidence plane waves exist. To get oblique incidence coefficients, it is necessary to use large samples in an anechoic chamber; the most common technique is a two microphone method, which is limited to homogeneous, isotropic, planar samples. All these techniques are discussed in Chapter 3.

1.7 Enclosures, barriers and roads

Enclosures might be used around a single machine to reduce noise, or they might be a personnel enclosure, a sealed room which workers go into to get away from noise. Issues such as access and ventilation must be considered, and the need for these can compromise performance. Enclosures should be lined with porous absorbents to reduce the build up of reverberant energy, which otherwise would compromise the sound attenuation.

Traffic is a major cause of noise problems, and although modern cars are quieter than their older ancestors, the increase in traffic levels has meant that average noise levels have not changed very much in recent decades. One possibility is to use porous asphalt, the properties of which are discussed in Chapter 5, to reduce noise. Another possibility is to use traffic noise barriers to reduce noise propagation from roads to neighbouring houses. However, double reflections from high sided vehicles enable some of the noise to bypass barriers, as shown in Figure 1.11a. Even more important, reflections from barriers on one side of the road can pass over barriers on the other side, as shown in Figure 1.11b. These additional reflections typically change sound levels by between
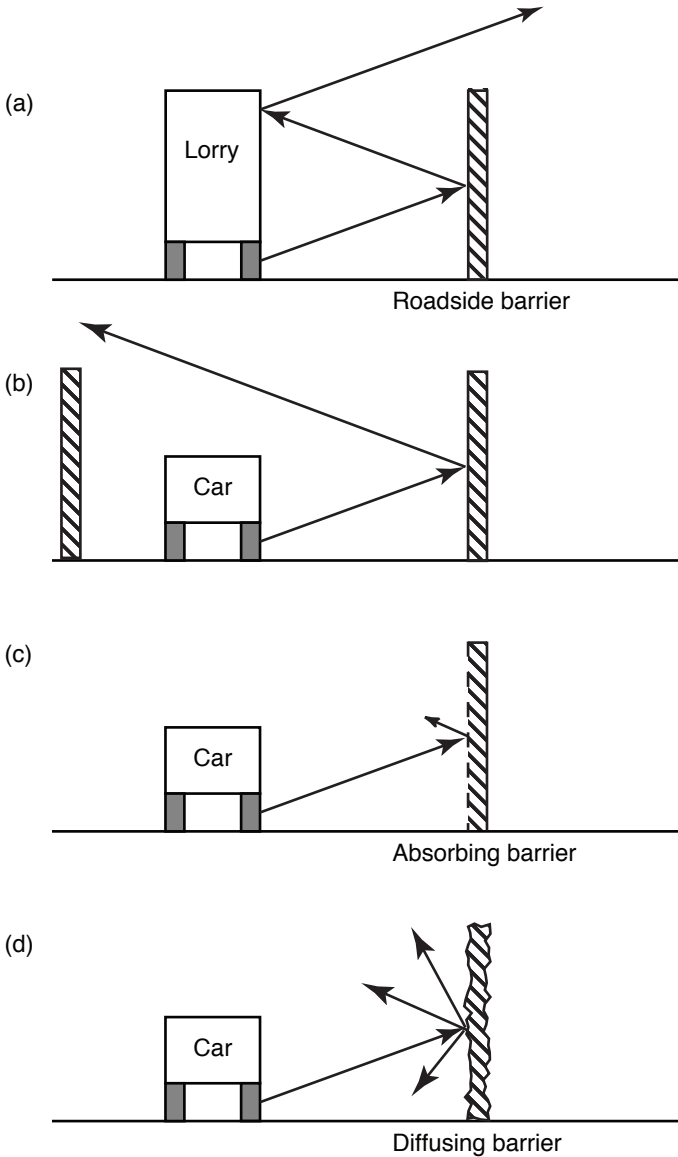
Figure 1.11 Schematic illustrating absorbers and diffusers to reduce reflection problems with noise barriers.

2 and 6 dB(A).[16] One solution is to apply absorption as shown in Figure 1.11c. The problem with absorption is that it tends to wear badly under the harsh conditions of high winds, salt and water, which are common next to busy roads. Consequently, absorber performance is likely to decrease over time unless specialized and expensive durable absorbers are used.

Barriers also have a role indoors, for example office screens are used to give acoustic isolation from noisy equipment, between workplaces and to slightly reduce the reverberant

noise levels in open plan areas. However, barriers are often ineffective in a highly reverberant environment. The performance of indoor barriers can be improved by hanging absorptive baffles from the ceiling or by placing sound absorbing material directly on the ceiling.

1.8 Natural noise control

It is common to find grass or tree covered areas around major noise sources and optimizing the natural features to maximize attenuation offers a sustainable solution to noise. Recent research findings have challenged the conventional wisdom that natural elements, such as trees, either on their own or with purpose built barriers, vegetation and ground, have no practical part to play in the controlled reduction of noise in the propagation path between source and receiver. Where space allows, the use of natural means (trees, shrubs and ground) rather than artificial barriers, has the advantage of contributing to other issues in sustainability such as: reducing air pollution; generating corridors to encourage walking and cycling; generating access to local green areas, and reversing the long term decline in wildlife habitats and populations. Chapter 5 discusses how ground conditions affect noise levels outdoors, and how the absorptive behaviour of the ground is modelled. Chapter 7 examines the use of trees and shrubs to attenuate sound.

1.9 Hearing protection devices

Ear defenders are used to reduce noise exposure, although where possible it is better to control the noise at the source or along the path between the source and listener. They have cups which are designed to resist sound transmission, resting on cushions which should provide a comfortable and leak-free seal between the cup and the side of the head. Within the cup a cavity is formed, and unless absorption is provided within the cavity, there will be a build up of reverberant energy. Acoustic foam is most commonly used because it does not deteriorate in the warm and moist atmosphere next to the head.

1.10 Loudspeaker cabinets

Most conventional loudspeakers are mounted within cabinets to prevent sound generated by the rear of the driver interfering with that radiating from the front. The enclosure changes the behaviour of the driver, because the air cavity forms a compliance which alters the mechanical behaviour of the driver, and this must be allowed for in the loudspeaker design. An empty enclosure has a series of resonances, which means the effect of the cavity on the driver varies greatly with frequency. By placing absorption within the cavity, the resonant modes are damped and the sound quality improved because the effect of the enclosure is more even with respect to frequency. Usually it is sufficient to use a porous absorbent wadding which has relatively low resistivity, because it can fill the cavity. Some have used activated carbon within the cabinet, because as well as providing absorption, the sorption of air molecules on and off the surface of the carbon changes the compliance of the cavity. Section 5.2.9 discusses activated carbon further.

1.11 Summary

This chapter has outlined some absorber applications, and touched on some of the issues that will be important in future chapters. It has also introduced some necessary mathematical principles. The remaining chapters concerning absorption are as follows:

- *Chapter 3* discusses measuring absorber properties from the microscopic to the macroscopic.
- *Chapter 5* discusses the application, design and theoretical modelling of porous absorbers.
- *Chapter 6* discusses the application, design and theoretical modelling of resonant absorption, especially Helmholtz and membrane devices.
- *Chapter 7* sets out some miscellaneous absorbers, which did not obviously fit into Chapters 5 and 6. Seating in auditoria, turning Schroeder diffusers into absorbers, sonic crystals, trees and vegetation are considered.
- *Chapter 11* discusses hybrid diffusers, and as these cause absorption, they are also an interesting absorber technology.
- *Chapter 12* discusses how to use predictions and laboratory measurements of single absorbent properties (mainly absorption coefficients), in room predictions, including the role of absorption coefficients in geometric room acoustic models.
- *Chapter 13* rounds off the work on absorbers by looking at active impedance technologies.

The next chapter introduces diffusers.

1.12 References

1 H. Kuttruff, *Room Acoustics*, 4th edn, Spon Press (2000).
2 P. Newell, *Recording Studio Design*, Focal Press (2003).
3 L. E. Kinsler, A. R. Frey, A. B. Coppens and J. V. Sanders, *Fundamentals of Acoustics*, 4th edn, John Wiley & Sons (2000).
4 M. Barron and L.-J. Lee, "Energy relations in concert auditoriums, I", *J. Acoust. Soc. Am.*, **84**(2), 618–28 (1988).
5 M. R. Schroeder, "New method of measuring reverberation time", *J. Acoust. Soc. Am.*, **37**, 409–12 (1965).
6 W. C. Sabine, *Collected Papers on Acoustics*, Harvard University Press (1922); republished, Acoustical Society of America (1993).
7 ISO 9613-2:1996, "Acoustics – Attenuation of sound during propagation outdoors. Part 2: General method of calculation".
8 C. F. Eyring, "Reverberation time in 'dead' rooms", *J. Acoust. Soc. Am.*, **1**, 217–26 (1930).
9 G. Millington, "A modified formula for reverberation", *J. Acoust. Soc. Am.*, **4**, 69–81 (1932).
10 M. R. Schroeder and H. Kuttruff, "On frequency response curves in rooms. Comparison of experimental, theoretical, and Monte Carlo results for the average frequency spacing between maxima", *J. Acoust. Soc. Am.*, **34**(1), 76–80 (1962).
11 T. J. Cox and P. D'Antonio, "Determining optimum room dimensions for critical listening environments: a new methodology", *Proc. 110th Convention Audio Eng. Soc.*, preprint 5353 (2000).
12 M. A. Nobile and S. I. Hayek, "Acoustic propagation over an impedance plane", *J. Acoust. Soc. Am.*, **78**(4), 1325–36 (1985).

13 J. F. Allard, *Propagation of Sound in Porous Media: Modelling Sound Absorbing Materials*, Elsevier Applied Science (1993).

14 D. A. Bies and C. H. Hansen, *Engineering Noise Control: Theory and Practice*, E&FN Spon, 2nd edn (1996).

15 L. L. Beranek and I. L. Vér (eds), *Noise and Vibration Control Engineering*, John Wiley & Sons (1992).

16 C. S. Y. Lee and G. G. Fleming, "Measurement of highway-related noise", Report no. FHWA-PD-96-046 and DOT-VNTSC-FHWA-96-5, US Department of Transportation (1996).

2 Applications and basic principles of diffusers

In this chapter the basic principles of diffusers will be developed. Following the same style of Chapter 1, the chapter will be driven by application. In many respects, the right and wrong places to use diffusers are still being worked out.[1,2] There are locations, such as rear walls of large auditoria, where there is a general consensus that diffusers are a good treatment to prevent echoes and better than traditional absorbers. The case for using diffusers in some other places is less clear cut, and until further research is undertaken, some applications of diffusers are going to be based more on precedence and intuition, rather than scientific fact. Having said this, much has been learned in recent decades which can help to ensure that diffusers are used where they are needed.

This chapter will outline how diffusers can be applied and the effects their application will have on the physical acoustics and the listener response. It will also be used as an opportunity to introduce some basic physics, which will be needed to understand the more detailed chapters on diffuser prediction, design, measurement and characterization later in the book.

2.1 Echo control in auditoria

In Section 1.4 the problems of echoes and flutter echoes in rooms were discussed. To recap, echoes are caused by late arriving reflections with a level significantly above the general reverberance. For instance, they are often heard at the front of badly designed auditoria, with the echo being caused by a reflection from the rear wall. The echo might also come from a balcony front or many other multiple reflection paths. Flutter echoes are caused by repeated reflections from parallel walls and are often heard in lecture theatres, corridors and meeting rooms.

In Chapter 1, absorbers were suggested as a treatment for echoes, but diffusers should be used when sound energy needs to be conserved. This would be the case in a large auditorium with an orchestra, because every part of the sound energy generated by the musicians should be preserved and not lost by avoidable absorption. In other cases, the choice between diffusers and absorbers will rest on whether the energy lost to absorption will detract or improve other aspects of the acoustics, such as the reverberance, envelopment and intelligibility.

2.1.1 Example applications

There is a growing trend away from the traditional use of absorbers on the rear wall of auditoria towards the use of diffusers. Figure 2.1 shows Quadratic Residue Diffusers

Figure 2.1 Schroeder diffusers (QRD®s) applied to the rear wall of Carnegie Hall to prevent echoes (after D'Antonio and Cox[2]).

(QRD®s) applied to the rear wall of Carnegie Hall in New York. QRDs are a type of Schroeder diffuser described in Chapter 9. This form of reflection phase grating was the starting catalyst for modern diffuser research about three decades ago. The diffusers were installed in Carnegie Hall because a long delayed reflection from the rear wall caused an echo to be heard on the stage, making it difficult for musicians to play in time with each other. Adding diffusers dispersed the reflection, reducing the reflection level arriving on the stage and consequently making the echo inaudible. The diffusers also improved spaciousness on the main floor by uniformly diffusing rear wall reflections and masking echoes from the boxes.[3]

Figure 2.2 shows the application of optimized curved diffusers to the side walls of the Hummingbird Centre in Toronto. A refurbishment of the hall was going to involve adding a reverberation enhancement system. This system added additional reflections from loudspeakers mounted in the side walls. Unfortunately, this was a shallow splay, fan shaped hall, and as is common with halls of this shape, if sources are on the side walls, echoes across the width of the audience area are heard. This was not a problem while the sound was being generated from the stage, but would have been a problem when the artificial reflections were generated from the side walls. It made no sense to treat the echoes with absorption, since this would just remove sound energy, which would rather defeat the point of having the artificial enhancement system installed in the first place. The solution was therefore to use diffusers, which break up lateral propagating reflections in the audience area.

The original concept was to use Schroeder diffusers, which were to be covered in cloth to hide their visual appearance. This is a common story in diffuser design. The acoustical treatment needs to complement the visual appearance of the room to be acceptable to architects. If the visual aesthetic is not agreeable, the treatment will have to be hidden behind fabric; but as discussed in Chapters 7 and 9, this would have turned the side wall diffusers into absorbers. (Another solution architects often apply to acoustical treatment that does not fit with the visual requirement of a space, is to remove the treatment completely. This not only solves the visual aesthetic

Figure 2.2 Application of optimized curved diffusers (OptiCurve™) in the Hummingbird Centre, Toronto. (Consultant: John O'Keefe, Aercoustics Engineering Ltd.; after D'Antonio and Cox[1].)

problem, but it also saves money!). In the Hummingbird Centre, designers tried a new method for designing optimized curved surfaces, which is outlined in Chapter 10. The finished design then complemented the appearance of the space, and met the visual requirements of the architect. The concept was a basket weave that would thread in and out of the cherry wood side walls. O'Keefe comments:*"The renovated room and, in particular, the enhancement system have been well received by the owners and their tenants, including the National Ballet and the Canadian Opera Company."*[4]

2.1.2 Aesthetics

For acoustics to be considered part of a project, it is important to be involved in the initial stages, so that appropriate budgets can be established. If acoustic treatments are introduced later in the process, the chances of them being included are greatly reduced. Therefore, acoustic consultants and treatment manufacturers must present the idea to

the architect that including the proper acoustical design does not have to infringe on the intended aesthetic design. On many projects, architects prefer custom products, so that the design has their signature on it and not that of an acoustical manufacturer's catalogue products. There are exceptions for functional projects, where absorbing ceiling tiles and fabric wrapped absorbers are chosen to reduce costs. How can acoustic treatments integrate with the architecture? This is very important, because every project has a function, in addition to its appearance, whether that is achieving intelligible speech or clear and enveloping music.

In classical architecture, scattering surfaces were an integral part of the form, with elements such as columns, relief ornamentation, statuary and coffered ceilings. These surfaces provided structural, aesthetic and acoustic functions. As architecture evolved into less ornate and simpler rectangular forms, very few of these architectural motifs were retained, which has altered the acoustic. Today, the architecture seems to be evolving into curvilinear lines and the challenge is to find options to complement contemporary architecture. One approach for designing diffusers is optimization – the results of which are shown in many figures in this chapter and the methodology of which is discussed in Chapter 10 – which offers the opportunity to collaborate with the architect in shaping treatment to satisfy acoustic and visual requirements. For these diffusing surfaces, any reflective material can be used. It is possible to shape concrete, wood, glass or other materials the architect has in mind. These custom designed materials then function in a similar way to the relief ornamentation, columns and statuary of classical architecture in that they complement the contemporary design. Of course, there remains the possibility to cover treatments with acoustically transparent fabrics and perforated metals, although this approach is falling out of favour.

2.1.3 Wavefronts and diffuse reflections

This section is an introduction to how diffusers disperse reflections. Figure 2.3 shows a cylindrical wave reflected from a planar hard surface, calculated using a finite difference time domain (FDTD) model. (The case shown is where the wavelength is much smaller than the surface width.) An impulse was generated, and so a single cylindrical wavefront is seen in frame 0, which is travelling from right to left towards the surface. The wave simply changes direction on reflection, travelling back in the specular reflection direction, where the angle of incidence equals the angle of reflection (in this special case back towards the source). The reflected wavefront is spatially unaltered from the incident sound. Consequently, the sound from the source reflects straight back, and is unchanged and not dispersed. This could lead to the reflection being perceived as an echo, especially if the source is a directional instrument, such as a trumpet. Therefore, the role of a diffuser is to break up or diffuse the reflection, so that the sound energy is dispersed, and sound from directional instruments does not remain in narrow beams.

Figure 2.4 shows the effect of changing a surface to help disperse reflections. In this case, part of an ellipse is used. It can be seen that the reflected wavefront is more bowed. The change is not great, because the curve of the ellipse was quite gentle; even so, in the far field the sound will be more spatially dispersed. The wavefront generated is still very ordered, however, so although single semicylinders or ellipses are good at spatial dispersion, they are not the best diffusers, because temporal dispersion is not achieved; this will be discussed further in Chapter 10.

Figure 2.5 shows the effect of using a Schroeder diffuser; the reflected wavefront is
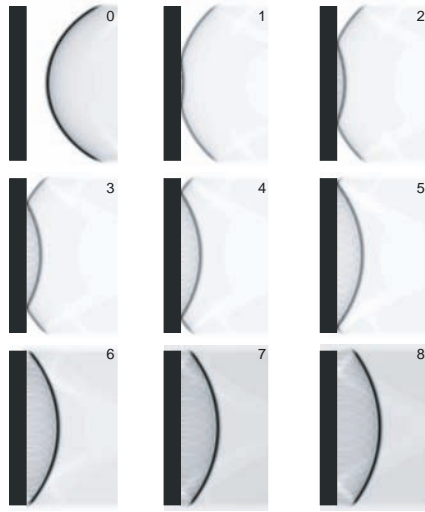
Figure 2.3 Cylindrical wave reflected from a flat surface calculated using an FDTD (Finite Difference Time Domain) model. The numbers indicate the frame order of the snapshots (FDTD courtesy of Brian Horner).

much more complex than the previous examples. Inspection of the different frames shows why this complexity arises. Sound can be seen taking time to propagate in and out of the wells, causing parts of the reflected wavefronts to be delayed. The different depths of the wells cause different delay times, and the resulting interference between the reflected waves forms a complex pattern. Chapter 9 gives details of what depths are chosen to gain dispersion and why. An observer listening to the reflection from the
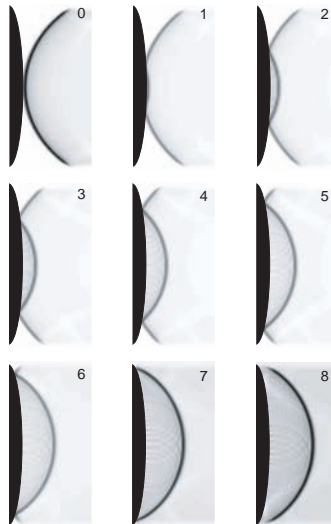
Figure 2.4 Cylindrical wave reflected from a curved surface calculated using an FDTD model.

Figure 2.5 Cylindrical wave reflected from a Schroeder diffuser calculated using an FDTD model.
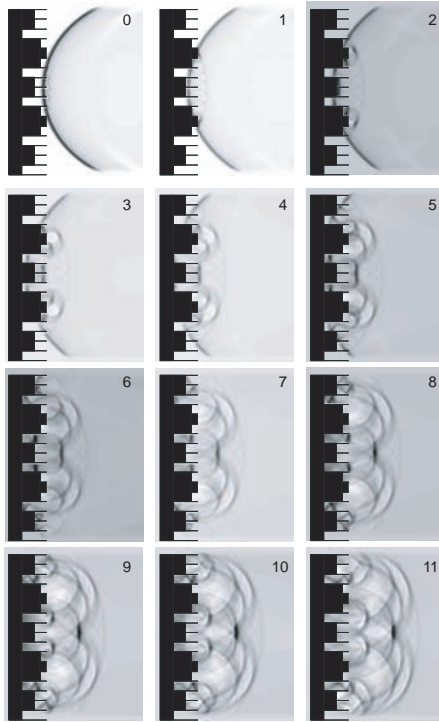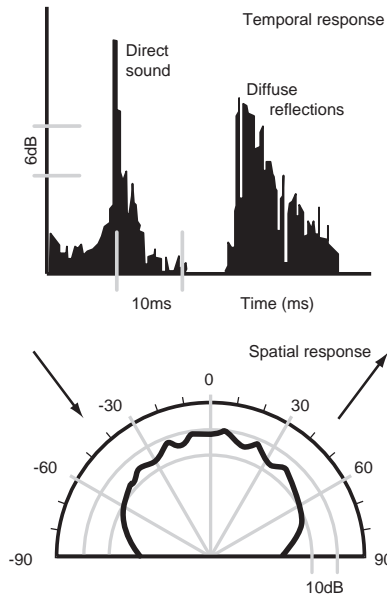

Figure 2.6 Measured spatial and temporal dispersion generated by a Schroeder diffuser.
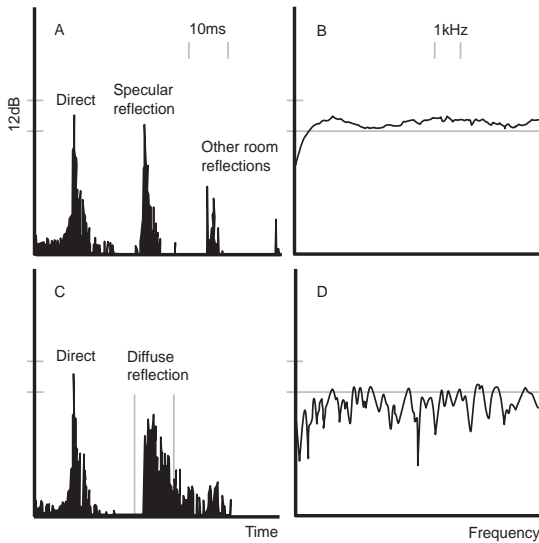
Figure 2.7 Measured temporal and frequency responses for a flat surface (top) and a diffuser (bottom). The frequency responses are for the reflected sound only (after D'Antonio and Cox[1]).

surface will receive sound arriving over an extended time as these different reflected waves move past. So as well as generating spatial dispersion, Schroeder diffusers also generate temporal dispersion. This can be seen in Figure 2.6 where the impulse response for a Schroeder diffuser is shown.

The consequences of temporal dispersion can be seen in the frequency domain. In Figure 2.7 the temporal and frequency response of a single specular reflection from a flat surface and a diffuse reflection from a diffuser are shown. In Figure 2.7a, the direct sound, a specular reflection and the room interference are shown. In Figure 2.7b, the frequency response of the specular reflection alone is given. (The time window is illustrated by the two vertical lines in Figure 2.7c.) The frequency response of the specular reflection is characterized by a high pass filter response, determined by the size and shape of the reflecting surface (see Chapter 10 for discussions of flat reflectors). In Figure 2.7c, where the reflection from a diffuser is given, the specular reflection is now temporally dispersed and shown as a diffuse reflection. The frequency response of the diffuse reflection in Figure 2.7d is characterized by a random distribution of irregularly spaced nulls and peaks. Many heuristic diffuser designs assume that any temporal distribution will provide a satisfactory frequency spectrum, when in fact coloration is often inadvertently introduced.

In Figure 2.8 the temporal and frequency responses of the total fields, consisting of the direct sound and the reflection(s), are shown. When the direct sound and a specular reflection combine, they form a comb filter. The time delay between the direct sound and the reflection determine the frequency spacing of the minima and maxima, and the relative amplitudes of the sound, the levels of the minima and maxima. Comb filtering is an effect that should be avoided in critical listening rooms and performance spaces. It can happen if large flat reflectors and nearby walls are not treated with absorbers or diffusers. When the direct sound combines with a diffuse reflection, the regularity of
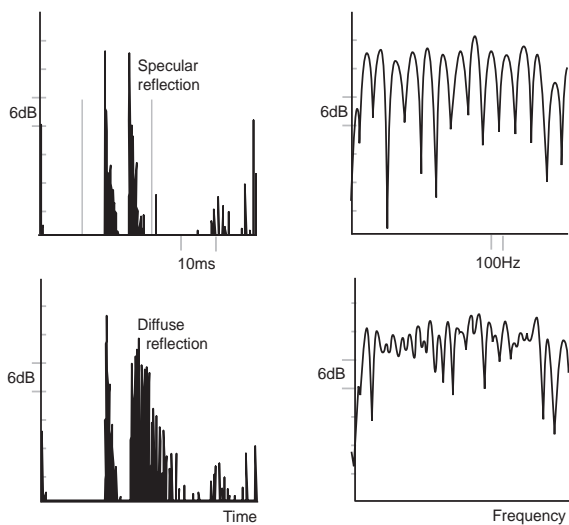
Figure 2.8 Measured temporal and frequency response of the total field, consisting of the direct and reflected sound. The top case is for specular reflection, the bottom case is for diffuse reflection (after D'Antonio and Cox[1]).
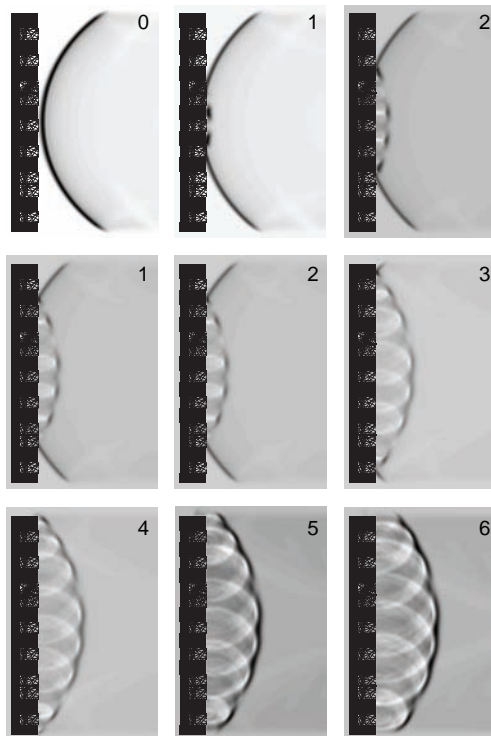

Figure 2.9 Cylindrical wave reflected from a hybrid surface using an FDTD model; the shaded wells are filled with absorbent.

the comb filtering is removed and the variation in levels reduced. The spectral content of the direct sound can be more fully perceived. In addition to providing uniform spatial dispersion, reducing comb filtering is a principal reason for using diffusers in many applications.

Another way of forming a diffuser is to combine reflection and absorption. By putting patches of absorbent on a wall, reflections from parts of the surface will be absent, and dispersion is generated. Figure 2.9 shows a FDTD prediction of this case; the absorbent is placed inside wells for convenience of prediction. The temporal dispersion is not as great as generated by Schroeder diffusers, however. To gain more dispersion, the surface can be curved or a ternary sequence used (see Chapter 11). Traditionally, acousticians have utilized patches of absorption on walls to obtain dispersion. But this only leads to modest dispersion below frequencies where the dimension of the patches is roughly half a wavelength. To obtain high frequency diffuse reflections, the dimension of the patches must be much smaller and the distribution of the patches is important. This approach forms a hybrid surface, which partially absorbs and diffuses reflected sound, i.e. providing diffsorption. This type of surface is discussed in more detail in Chapter 11. These types of hybrid surfaces cause partial absorption, therefore they need to be used where reverberation control and dispersion are simultaneously needed.

2.1.4 Coherence and terminology

Many might describe the reflection from a flat surface as being coherent, and the reflections from diffusers as being incoherent, however this is a misleading use of terminology. From a purely physical standpoint, coherence occurs when there is a fixed, time invariant phase relationship between separate parts of a wavefront. For both flat surfaces and complex diffusers there is a fixed phase relationship. In this linear system, there is usually time variance. The wavefront from a diffuser is just complicated, not incoherent. To achieve physical incoherence, the surface would have to move or change shape over time.

Another terminology commonly used is to say the reflection is diffuse. There is no formal definition of this, but it refers to the case where the reflection is dispersed both spatially *and* temporally. The sound should be distributed more widely, and the impulse response at a receiver should have more reflections spread over a longer time. Many diffusers are designed by examining the spatial dispersion, and assuming that this will be accompanied by temporal dispersion. In addition, many diffusers are designed simply assuming that any temporal variation will produce uniform spatial dispersion and an acceptable frequency response, however this is not necessarily the case.

It is also important that surface diffusion and volume diffusion are not confused. For surfaces, the diffusion being discussed is that generated by surface reflections in terms of the spatial and temporal dispersion. Whether these diffuse reflections then contribute to make a sound field more diffuse, is not what is being referred to. Indeed, diffusers might be applied simply to treat first order reflection problems, such as echoes, and the effect these have on the reverberant sound field in the space might be of little concern. Both surface and volume diffusion refers to cases where the sound field, or surface reflections, become more complex. Section 2.10 further discusses some of the effects that diffusers have on the volume diffusion in the space.

The effect of surface roughness and impedance changes is to generate diffraction, i.e. the breaking up of sound wavefronts due to edges and other effects. Acousticians do not

seem to favour the term diffraction, however, but prefer diffusion, diffuse reflection or scattering. To complicate matters further, the use of these terms is inconsistent between different disciplines in acoustics. The only place where some clear differentiation has been set is with surface scattering and diffusion coefficients. A scattering coefficient refers to the ability of a surface to remove energy from the specular reflection direction; the diffusion coefficient is a measure of quality referring to the spatial uniformity of the reflections from a surface. Measuring and characterizing surface reflections is discussed in Chapter 4. This is also relevant to Chapter 12, where the application of scattering coefficients to geometric models is discussed.

Finally, it seems appropriate to discuss the spelling of diffusers. Schroeder and D'Antonio chose to use the spelling 'diffusor' to distinguish between acoustic and other diffusers, such as those used for lighting and air dispersion. However, common usage has drifted towards diffuser, and this will be employed throughout this book.

2.2 Reducing coloration in small sound reproduction rooms

Of interest in this section are small rooms where sound is being reproduced through a loudspeaker system; examples include recreational listening rooms, recording or broadcast critical listening control rooms, teleconferencing or distance learning rooms.

It is often useful to consider extreme boundary conditions when attempting to solve a room acoustic problem. In the case of a critical listening room, one extreme is an anechoic chamber, and the other a reverberation chamber. Anyone who has spent any time in these rooms realizes that neither is an exciting place for music listening. An ideal critical listening room will usually lie somewhere between the two extremes. It is also important to realize that since this is a sound reproduction room, the room can only corrupt what is being reproduced by the playback system. The unwanted artefacts added by the room are acoustic distortion.

In general, these rooms are not used for recreational listening, but rather as acoustical sonoscopes to accurately perceive spectral balance and spatial imaging. Modern diffuser design has played a significant role in developing these state-of-the-art sound reproduction facilities.

For late reflections, there has been general agreement in most designs, over many decades, that the decay time should be small, say with a reverberation time of about 0.3–0.4s. But opinions about what should be done about the otherwise inevitable strong early reflections have varied over many decades. It is interesting to map out how opinions have evolved, from the early 2-channel designs to today's multi-channel surround.

Early 2-channel designs of Tom Hidley emphasized early ceiling reflections, using a 'compression' ceiling, and promoted a reflective front surrounding the monitors with the rear of the room being anechoic. The introduction of time delay spectrometry by Dick Heyser fostered an era that aimed at eliminating early frontal reflections, due to the measurable comb filtering that otherwise resulted. This led to the live end dead end (LEDE®)[5] studio control room developed by Don and Carolyn Davis, suggesting the front of the room should be absorptive, or dead, and the rear live. Designers became aware of the research of Schroeder[6] describing the importance of early lateral reflections in providing envelopment in concert halls. This led Peter D'Antonio[7] to the use Schroeder diffusers on the rear wall of LEDE control rooms to provide passive surround sound; he also proposed broadband control of early frontal reflections, by creating a temporal and spatial reflection free zone (RFZ™)[8] surrounding the mix position. Some

of the concepts have been adapted and adopted for listening room standards.[9] Tom Hidley and Philip Newell promoted the idea of non-environment approaches, with significant broadband sound absorption, thus removing early reflections. D'Antonio, James Angus and George Massenburg then experimented with diffusing early frontal reflections, rather than absorbing them in control rooms, leading to reflection rich zones and significant diffusion – a control room with massive amounts of diffusion will be described later in Section 2.2.3.

As the industry moved from 2-channel to multi-channel, early reflections began to be viewed constructively, rather than being seen as destructive to the critical listening process. This concept was further promoted by a review of psychoacoustics research by Floyd Toole.[10] There are still studio engineers and producers that prefer to control early reflections with absorption; an analogy to music performance may be informative. When a musician practices, she generally prefers a somewhat dead space, so that she can hear every nuance of her instrument. However, in performance she prefers a more reverberant space to support the instrument. These practice rooms may be analogously compared to critical listening rooms, where spatial and spectral nuances must be monitored and tailored. The performance space may be compared to a recreational listening room in which enveloping reflections enhance the listening experience.

2.2.1 Example: reflection free zone (RFZ)

The debate about the best small critical listening design continues, and probably will never be resolved because tastes change! However, for now, consider one of the most successful approaches, the RFZ. This design strives to minimize the influence of the room acoustic on the sound reproduced and so provide a neutral critical listening room. The design creates a spatial and temporal reflection free zone surrounding the primary mixing or listening position(s). The zone is spatial, because it only exists within a certain area in the room; and it is temporal, because the interfering reflections are only controlled over a certain time window, between the arrival of the direct sound, and prior to reflections arriving from the rest of the room.

It is well established that early reflections affect the perceived sound[11,12] and acoustical treatment can be used to create a space in which spatial and spectral textures can be accurately perceived. Furthermore, the room aberrations can mask important artefacts on recordings. Even though the auditory system adapts rather well to interfering acoustic distortion, if undesirable artefacts are masked by room aberrations, they will not be perceived even after the listener has habituated to the room acoustic. Absorption can be used to control first order reflections between the source and the listener and so remove early arriving, strong reflections, which might produce coloration and image shift (image shift meaning that the sound source appears to be coming from the wrong place). Applying large numbers of absorbers leads to a dead room, and so diffusers are used to delay and temporally diffuse reflections while preserving sound energy. This is done to minimized distortion caused by interference with the direct sound. Diffusers on the rear wall essentially produce passive surround sound that provides ambience in the room and envelopment.

Figure 2.10 shows the energy time curves measured before and after treatment in a small critical listening room. At the top of the figure, the direct sound and interfering side wall, floor, ceiling and sparse reflections from the room are identified. Isolated and intense early specular reflections cause coloration, image shifting and broadening of
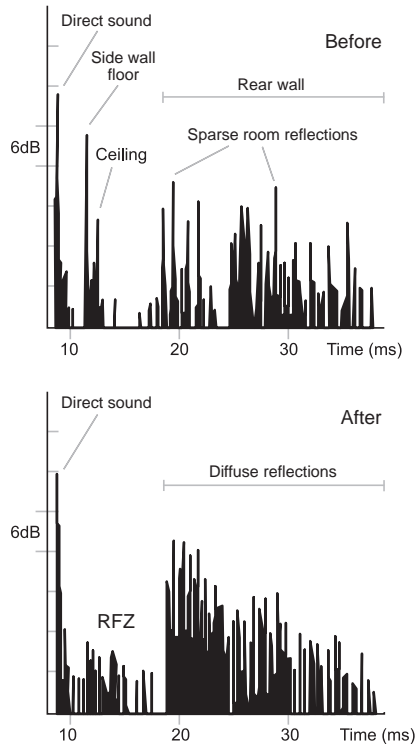
Figure 2.10   The impulse responses in a small critical listening room before treatment (top), and after (bottom) (after D'Antonio and Cox[1]).

the image width and depth. The sparse specular reflections from the rear of the room also interfere with the direct sound, further colouring the reproduction. These problems can be addressed by controlling the competing early reflections from the walls, floor and ceiling by application of absorbers and diffusers. This creates an initial time delay gap before the reflections from the rear wall arrive, forming the reflection free zone described above; this extends to roughly 18 ms as shown in the lower graph in the figure. If absorption is used to remove early reflections, psychoacoustic experiments indicate that the sonic images in the soundstage will be extremely small, as if sound comes from a point in space. If diffusers are used, the sonic images take on greater size and appear more realistic. Following the application of diffusers on the rear wall, the effects of which are shown in the lower part of the figure, the sparse room reflections more resemble a reverberant field of a larger room, with increased spatial and temporal reflection density. Using this technique, it is possible to create a reverberant sound field with a linear slope within a small room.

D'Antonio *et al.*[13] carried out a study on a recording control room; a drawing of the room can be seen in Figure 2.11. In this example, a reflection free zone is achieved by flush mounting the loudspeakers (L) with the woofers close to the front trihedral corners of the room. The massive front walls are splayed outward and treated with porous absorption to provide broadband control of first order reflections. The rear wall surfaces are treated with broadband diffusers (QRDs) to disperse first order rear

wall reflections away from the listeners, while providing ambience and envelopment. The shaded area represents the spatial reflection free zone, 24 dB below the direct sound, with an initial time delay gap of approximately 17 ms, where the predominant energy is from the monitor loudspeakers. Two types of reflections are indicated in Figure 2.11; an undesirable specular reflection from the glass doors forming the machine room (S) and diffuse reflections which arise from 7 m² of diffusers located on the rear wall (D).

The rear wall diffusers reduce the level of the reflections reaching the listener early and so coloration effects are reduced. Figure 2.8 (top row) shows the time and frequency response for a listener close to a large plane surface with no other surfaces present. The similarity between the incident and reflected time responses can be seen. (Some minor differences are seen, because the measured surface was finite in extent.) The incident and reflected sounds interfere to cause a comb filter response, shown to the right. This gives emphasis to some frequency components, while others are absent. This will change the relative magnitude of the harmonics in music and so lead to a coloured sound where the timbre is not true. Figure 2.8 (bottom row) shows the case for a listener close to a diffuser. The diffuser introduces temporal dispersion of the reflected sound, which leads to a more complicated frequency response. The regularity of the comb filtering is minimized, and consequently its audibility is diminished.

Unfortunately, although the coloration can be measured, there is no formal method for evaluating the audibility of comb filtering. Chapter 4 discusses some possible approaches but cannot draw any definite conclusions about a suitable method. Furthermore, a more complete model is required which allows for the masking effects which occur due to other room reflections. Comb filtering becomes less of a problem when there are either many additional reflections to mask it, or when you have multi-channel
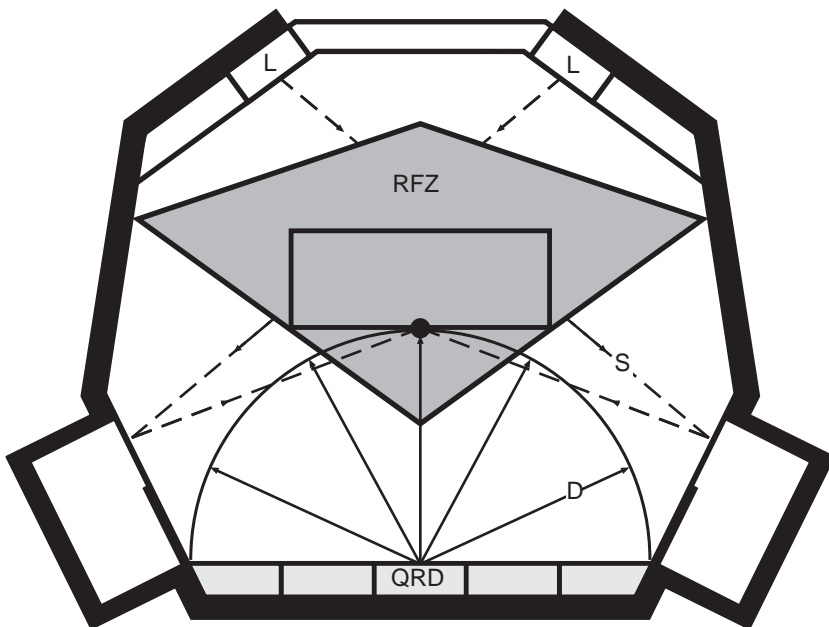

Figure 2.11   A sound reproduction room, with a designed reflection free zone (RFZ) shown shaded (after D'Antonio and Cox[1]).

loudspeakers which dominate the natural acoustics of the listening room.

The most efficient placement for a diffuser (or an absorber for that matter), is at the points where the first order specular reflections are produced – the geometric reflection points. Consider a room in which all of the surfaces are mirrors. The geometric reflection points are the locations on the boundary surfaces at which a listener can see the sources.

The number of diffusers that should be used depends on personal preference. If interfering reflections are absorbed, then one experiences the highest resolution sonic images, which are essentially points in space. If diffusers are used to control these reflections, the apparent size of the image is broadened. If done properly, some have described this as a more natural size image, similar to what might be experienced in the presence of an actual sound source. So a balance has to be reached in which the desired apparent source width and depth is achieved, while creating an appropriate ambiance. While some people favour very dead spaces for mixing audio, others do not. Some studio designers like to create a non-environment where only the direct sound is received by the sound engineer. Whether this is a desirable acoustic or not seems to be a matter of personal preference. High levels of absorption remove most of the room effects such as coloration, but lead to a very dead room that some find oppressive. It leaves the sound engineer the tricky job of interpolating between the dead mixing room and more-normal listening environments such as living rooms, but does ensure that the engineer receives a very pure sound where details can be easily detected.

If some liveliness is to be left in the room, a combination of absorbers and diffusers is better than absorption and flat walls, which generate specular reflections. Consequently, many of the industry's leading mastering facilities use this combination of treatments. To take a few examples, one of the industry's most successful mastering rooms is Gateway Mastering + DVD, Portland, ME, shown in Figure 2.12 and one of the most successful recording studios is the Hit Factory, New York, shown in Figure 2.13. Live performance studios also usually employ a mixture of absorbers and diffusers. Figure 2.14 shows the live performance studio at XM Satellite Radio. The glass wall is a Schroeder

Figure 2.12 Gateway Mastering, Portland, ME, showing a fractal diffusing rear wall (Diffractal®). (Photo courtesy of Gateway Mastering + DVD.)

Figure 2.13   The Hit Factory, New York. (Photo courtesy of The Hit Factory, New York and Harris, Grant Associates.)

diffuser and on the opposite wall there are optimized curved diffusers. Both are used to diffuse sound in the performance space – Chapters 9 and 10 discuss these designs. Other treatments not visible in the photo include hybrid absorber-diffusers, which are discussed in Chapter 11.

In a small critical listening room, the walls, floor and ceiling are usually rather close

Figure 2.14   A live performance studio seen through a glass Schroeder diffuser. The opposite wall features Waveform® Spline, an optimized curved diffuser. XM Satellite Radio, Washington, DC. (Acoustician: Francis Daniel Consulting Alliance. Photo courtesy of Michael Moran Photography.)

to the listener. How far away should a listener be from the diffusers? The distance between listener and diffusers can be determined by considering the scattered and total field. First consider the scattered field, in other words just the reflections from the diffuser. A diffuser requires a certain time or distance to form a wavefront. There is an analogy to loudspeakers that can be made here. A listener would not consider sitting 30 cm from a multi-way loudspeaker, because the listener would be in the near field of the device. At some distance from the loudspeaker, all individual high-, mid- and low frequency waves from the individual drivers will combine to form a coherent wavefront. The same holds true for scattering surfaces. They also can be thought of in terms of near and far field, although the situation is a bit more complex than for loudspeakers.

It is common to describe the scattered field by its spatial response. This is similar to the far field polar response of a loudspeaker, however the polar response of a diffuser is much more difficult to measure and this has been the subject of extensive research as reported in Chapter 4. In the far field, the polar response of an ideal diffuser is invariant to the angle of incidence, the angle of observation and the frequency, within its operational bandwidth. Unfortunately, in most critical listening rooms, it is usual for sources and receivers to be in the near rather than the far field. Consequently, listeners should be positioned as far from scattering surfaces as possible. Precedence has shown that it is best if the listener is at least three wavelengths away from diffusers. Since diffusers used in listening room applications have a lower frequency limit of roughly 300–500 Hz, this means a minimum distance of 3 m is recommended. In some situations this distance may have to be compromised.

A listener positioned near a multi-way loudspeaker with their ear close to the mid-range driver hears sonic anomalies, and the same is true when the listener gets too close to a diffuser. Many of the phasing anomalies reported by room designers are due to the fact that they are listening too close to the diffuser and they are hearing near field comb filtering effects. Some listeners have even put their heads in the wells of large low frequency diffusers, and then claim something is wrong, because it sounds odd! Furthermore, getting too close to a diffuser means that the temporal response is overly dominated by the surface close to the ear, which means the temporal and spatial dispersion generated by the diffuser is not heard. The direct and reflected sounds are then rather similar and comb filtering gets worse. This naturally leads to a consideration of the total field.

When listening to music in a room, the total field is heard, which is a combination of the direct sound and reflections. If the scattered sound predominates, aberrations are heard. Just as room reflections affect the size and directionality of sonic images, they also can introduce coloration by changing the frequency response, distorting the spectral content or timbre of the direct sound. Studying the total field offers some insight into why scattering surfaces may introduce coloration.

Consider a listener approximately 1 m from a scattering surface. If the reflection comes from a flat surface, the reflected and direct sound are comparable in level and the result is a comb filter (Figure 2.8, top). This is not very representative of the content of the direct sound. While this looks rather bad, the comb filtering may or may not be perceived depending on the relationship between the frequency of the nulls/peaks and auditory critical bands. In addition, masking by other reflections may reduce audibility of the coloration. If the reflection comes from a diffuser, the scattered energy is dispersed in time, and the frequency response consists of an irregular spacing of nulls and peaks (Figure 2.8, bottom). The frequency response of the total field more

closely resembles the direct sound, since the diffuse reflections have minimized the interference. Importantly, the listener no longer picks up the regularity of the peaks and troughs that occur for a flat surface, and so the spectral changes introduced may be less noticeable. Figure 2.8 shows the case for a diffuser which scatters in one plane. Diffusers which scatter hemispherically will direct more energy away from the listener and so will further reduce the comb filtering.

More recent research has led to hybrid surfaces, which consist of reflective and absorptive areas. These surfaces provide absorption at low to mid-frequencies and diffuse reflection at mid- to high frequencies; these may allow the listener to get even closer to the scattering surface. The design of hybrid surfaces is described in detail in Chapter 11.

The level of the scattered sound and the resulting interference in the total field decreases in the following order: flat surface, curved surface, 1D phase grating, 2D phase grating, 1D amplitude grating, 2D amplitude grating and absorber. In light of these remarks, it is important to consider the temporal, spatial and spectral response of a sound diffusing surface. Casual or arbitrary shaping of surfaces is unwise and designers should solicit theoretical or experimental proof of the performance characteristics for diffusers. Chapter 4 discusses how this might be done.

2.2.2 Surround sound

How should listening spaces be adapted for surround sound? The design of these spaces is heavily dependent on how one controls reflections from the front and surround loudspeakers, as well as how the subwoofers couple with the room. The goal is to have the room complement the additional speakers. Today, with surround sound reproduction formats becoming increasing popular, the 2-channel concepts given above are still valid but need to be employed differently. The rooms are not polarized between live and dead zones, and tend to be more uniform, with diffusers being used to enhance the envelopment and immersion provided by the surround speakers and to provide the desired degree of ambience. One approach to designing a surround listening room suggested by D'Antonio utilizes broadband absorption down to the modal frequencies in all the corners of the room and across the front wall behind the left, centre and right loudspeakers (see Chapter 6 for possible designs). The side wall space between the front loudspeakers and the listeners can be controlled with broadband absorbers or 1D diffusers. Broadband, 1D modulated, optimized diffusers are used on the side and rear walls to disperse sound from the surround loudspeakers, which are preferably wall mounted or free standing (it is important to keep in mind that loudspeakers have better performance when they are surface mounted or far from boundary surfaces). These wall mounted diffusers work in conjunction with the surround loudspeakers and enhance envelopment. Diffusing clouds – with or without broadband absorption down to the modal frequencies – are placed above the listeners. These ceiling diffusers provide enveloping lateral reflections, additional modal control and a convenient surface for lighting and HVAC.

The room height can be divided roughly into thirds with diffusers in the central section, to the extent that the ear is covered in both seated and standing positions. The lower and upper areas can remain untreated. There is the possibility of using distributed absorbers or diffusers on the upper third to control flutter echoes, if it is a problem. Wall-ceiling soffits and wall-wall intersections should be used to provide low frequency absorption. Many dedicated listening rooms utilize massive

construction for sound isolation, thus low frequency control is required. The use of optimal dimensional ratios and multiple in-phase subwoofers properly placed can offer significant advantages.[14]

2.2.3 Ambechoic

A final extreme example of a critical listening environment is the so-called ambechoic space, a concept devised by George Massenburg. Figure 2.15 shows a picture of the front of the room. The room uses very large amounts of very deep and complex diffusers to alter the sound field within the space. Figure 2.16 shows the impulse response measured, showing many interesting features, including the extremely high reflection density at very early times for a small room. There is no time delay before the reverberance begins. This space can be described as an ambient anechoic or ambechoic space, because although the reverberant level is low and somewhat similar to an anechoic chamber, the decay time is about 0.3 s and there is nonetheless a definite sense of reverberance. One can comfortably hold a conversation while listening to music in the room – the room is not like an anechoic chamber. However, the low level of the reverberance means that acoustic images are very precise.

Unusually, the diffusers operate down to 50–100 Hz, and so are important in controlling the low frequency modal response of the room as well. (Additional resonant absorbers are also used as seen in the corners of the photo.) Forming rooms from very much more complex shapes by, for example, covering them in very deep diffusers, can increase the number of standing wave modes at low frequencies.[15–18] This can reduce the unevenness of the frequency response somewhat. However, it is unusual for this

Figure 2.15 Blackbird Studios, www.blackbirdstudio.com. (Photo courtesy of George Massenburg and Blackbird Studios.)
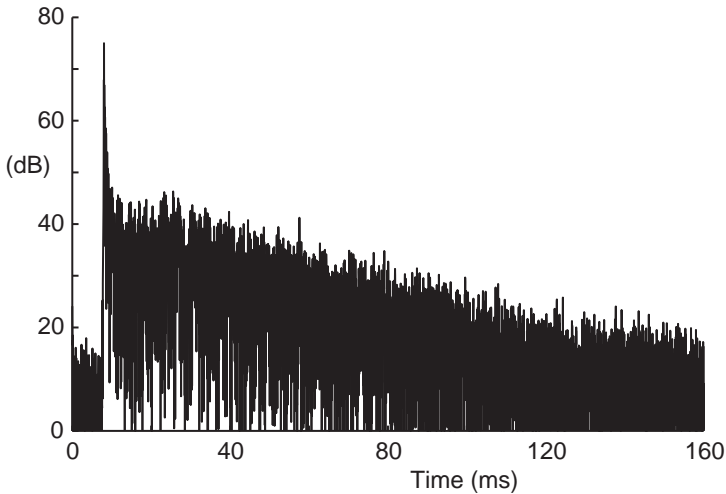
Figure 2.16 The impulse response in an ambechoic listening room.

to be done in a room, because of the space required and normally resonant absorbers would be used on their own to treat low frequencies. Another solution might be to use active diffusers, as discussed in Chapter 13.

2.3 Music practice rooms

Individual practice rooms play an essential role in music education. For all the extensive hours students spend in them, they are usually very uninviting and uninspiring cubicles. They usually are small rectangular rooms, 8–25 m³, fabricated from concrete block, with traditional compressed acoustic ceiling tiles, some curtains to allow the acoustics to be varied, a concrete floor and a full length mirror, which students use to monitor their posture and fingering. In other words, a low cost, functional and student proof space. Since the surfaces are usually concrete and the volume is small, the rooms typically have audible distortions caused by modes. Some designs feature non-parallel walls to minimize flutter echoes. In addition to awareness of the unwanted buzzes and squeaks, students studying articulation, tone production and intonation are hampered by poor room acoustics. Another approach to making a music practice room is to use a prefabricated isolation cubicle. These rooms are typically small with absorbent on the room surfaces making the space relatively dead. As with other small rooms, these spaces can benefit from diffusers to give the musician some reverberance while minimizing coloration.

Consider a candidate room, which was 4.5 m long, 2.1 m wide on one end, 2.4 m wide on the other and 2.7 m high. The room had a conventional compressed acoustical ceiling glued to dry-wall, concrete floor, cinder block walls and a thin curtain to allow the acoustics to be varied somewhat. Before and after acoustical changes were carried out, objective measurements and subjective musician impressions were evaluated. The study introduced three acoustical elements: (i) an acoustical concrete masonry block; (ii) a hemispherically scattering ceiling diffuser; and, (iii) a wall mounted hemispherically

Figure 2.17   A music practice room treated with diffusers (Skyline® on the ceiling[20] and DiffusorBlox® on rear wall[19]) and absorbers (after D'Antonio and Cox[1]).

scattering hybrid diffuser-absorber. The first two of these elements are shown in Figure 2.17. The acoustical concrete masonry block[19] provided low frequency modal control via resonant absorption, structural walls and diffuse reflections in a single plane to promote ambience, intonation, tone production and support. In this connection the
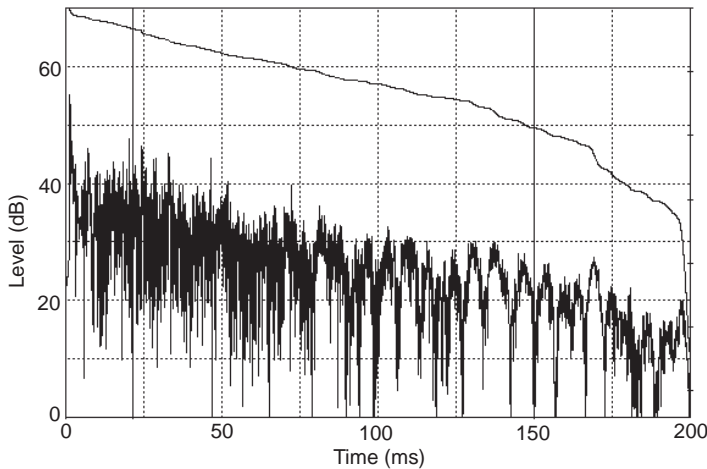

Figure 2.18   Impulse response and decay curve of music practice room shown in Figure 2.17 at early stages of treatment (after D'Antonio and Cox[1]).
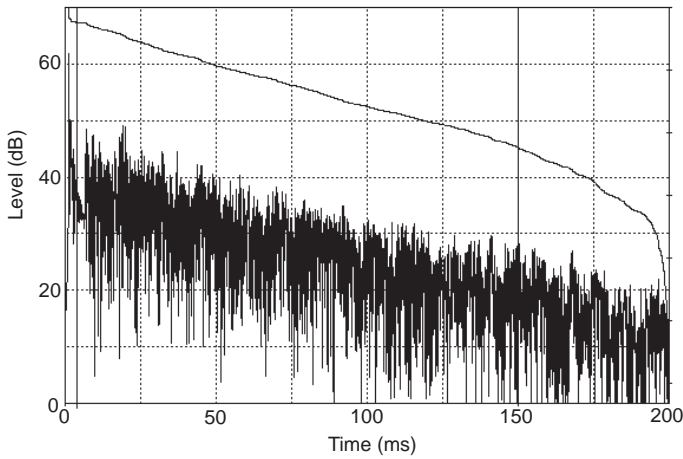
Figure 2.19   Impulse response of music practice room shown in Figure 2.17 at end of treatment (after D'Antonio and Cox [1]).

word ambience is used to denote a high spatial impression and envelopment. The hemispherically scattering ceiling diffuser[20] provided ambience, enhanced ability to hear intonation issues and a more diffuse sound field. The hemispherically scattering hybrid absorber-diffuser provided partial absorption, with any reflected energy being diffused. This provided the desired amount of articulation control for critical listening. Thus, the practice room provided detailed resolution, space or ambience, improved feedback for intonation and tone production, support, reduced modal coloration and lessened playing fatigue.

The impulse response of the room was measured during various stages of treatment as shown in Figures 2.18 and 2.19. The time response shows the sound decay becoming
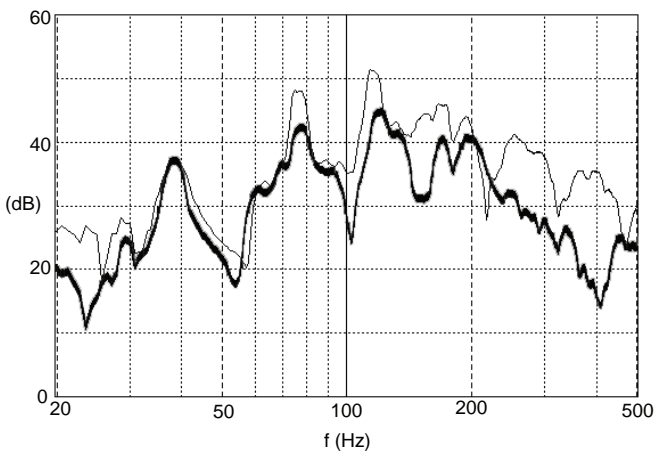

Figure 2.20   Frequency response of the music practice room:
————— before; and
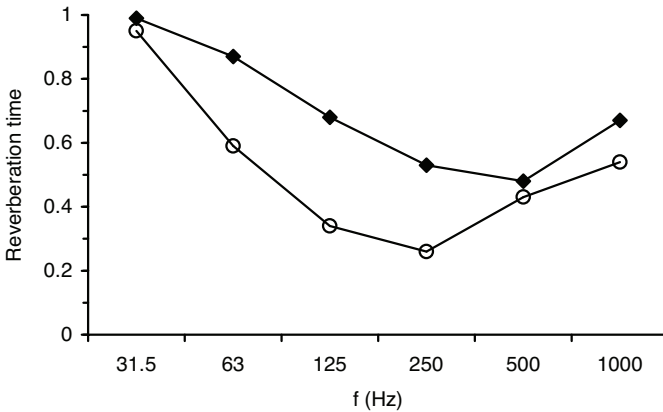**—————** after bass treatment (after D'Antonio and Cox[1]).

Figure 2.21   Change in reverberation time caused by adding absorbing/diffusing masonry
units in the music practice room:
◆ without; and
○ with masonry units (after D'Antonio and Cox[1]).

more even after treatment is added. Low frequency modal measurements were made
before and after the addition of acoustical masonry units. The masonry units made
a significant improvement in reducing the unevenness in the frequency response
produced by the modes as seen in Figure 2.20. Figure 2.21 shows the decrease in
the reverberation time in the frequency range where the masonry units are tuned for
maximum absorption. The experiments verified that with treatment, a very functional
and enjoyable practice room could be attained.

2.4 Promoting diffuse fields in reverberation chambers

Reverberation chambers are designed to produce a diffuse sound field, one where the
reflected energy density is the same throughout the room and all directions of propa-
gation are equally probable. Reverberation chambers need to achieve this condition
because they are a reference test environment providing repeatable results, which can be
interpreted and matched by other laboratories. Unfortunately, a completely diffuse field
is not achievable, and this is one of the reasons that round robin tests on reverberation
chamber methods usually show significant anomalies (see Chapter 3) and why the ab-
sorption coefficients measured in reverberation chambers need to be used with care in
prediction models (see Chapter 12).

   One of the methods used to achieve a more diffuse field is applying surface or
volume diffusers. Standing wave modes in the reverberation chamber cause the energy
density to be uneven. Placing diffusers in the paths of modal propagation creates
additional modes, which make the sound field more uniform spatially and with respect
to frequency. Surface diffusers need to be of the order of half a wavelength or deeper
to have a significant effect on the sound field. The diffusers must also be applied to at
least three of the boundaries, so that opposite surface pairs have at least one surface
treated (e.g. treat the floor or ceiling). Consequently, surface diffusers need to be large
and can be prohibitively expensive. A more economic solution is to hang diffusers in the

Figure 2.22 The small reverberation chamber at RPG Diffusor Systems, Inc. (Photo courtesy of RPG Diffusor Systems Inc.)

volume of the room. Surface diffusers can only influence sound over a hemisphere, as they only receive waves from 2π space. Volume diffusers, on the other hand, can influence a full sphere, and so it is possible to get greater diffusion from this type. Figure 2.22 shows a typical application in a reverberation chamber. A final option is to use rotating elements, but these will presumably become less common as test signals which require time invariance, such as maximum length sequences and swept sine waves, become more popular.

It may be that using volumetric diffusers away from wall surfaces might offer a useful acoustic treatment in other rooms. Absorbers hung in the volume of large performance spaces are used to control reverberation, so there are places in some rooms which volumetric diffusers could be placed without interfering with sight lines. Diffusers could be hung in the propagation path of echoes. They could also influence the reverberance and distribution of sound in the room. Sonic crystals are examples of such devices – Chapter 7 discusses their use for absorbing sound – where periodic arrangements of spheres and cylinders are used. However, to achieve good scattering and broadband performance, periodicity must be avoided. A fractal would be a good choice, because it has objects on various length scales to scatter sound of different wavelength and so can cover a useful bandwidth.

## 2.5 Improving speech intelligibility in underground or subway stations

Many underground (subway) stations are non-diffuse spaces. The long and narrow shape results in the mean free paths along the length of the station being much longer than those for transverse propagation (where the mean free path is the average time between reflections). Consequently, the sound decays much faster for transverse propagating sound than for sound travelling up and down the length of the station. This results in a double decay and two reverberation times in the space. The long reverberation time causes problems with speech intelligibility, as the reverberance causes

words to run into each other and become difficult to distinguish. Kang[21] showed that by applying diffusers to the side walls of the station, more transverse propagation can be promoted to decrease the reverberance of the space and improve speech intelligibility.

2.6 Promoting spaciousness in auditoria

One of the pioneering applications of Schroeder diffusers was by Marshall and Hyde in the Michael Fowler Centre, New Zealand.[22,23] Figure 2.23 illustrates the application. Marshall and Hyde used large overhead reflectors to provide early reflections to the audience in the balconies. This was a method whereby a hall could have good clarity, and yet maintain a large volume for reverberance. The large volume partly comes from the space behind the diffusers.

Not many years before the design of the hall, it was established that lateral reflections were important in concert halls as these promote a sense of envelopment or spatial impression in rooms.[24] Music outdoors may be popular when accompanied with fireworks, but the quality of the sound is usually poor. Move indoors and the sound
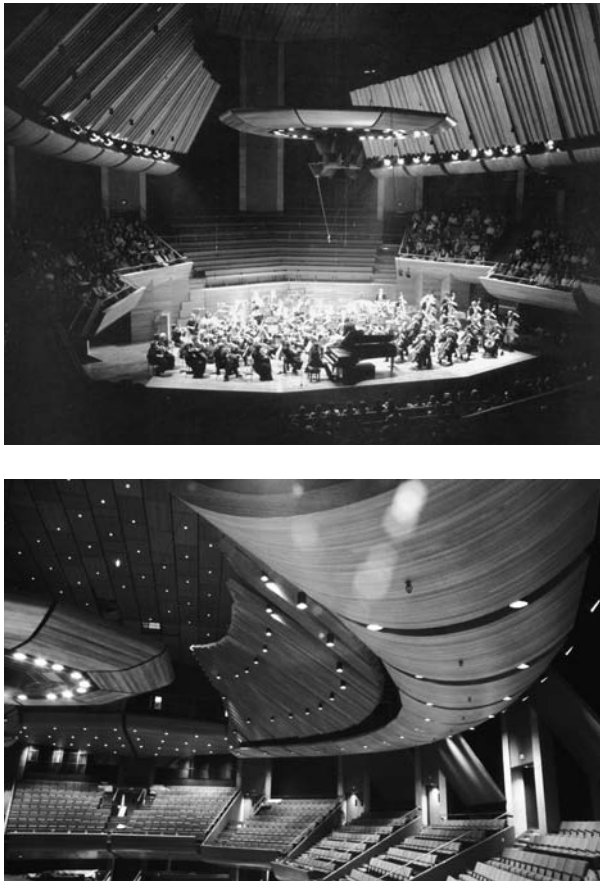
Figure 2.23   Schroeder diffusers in the Michael Fowler Centre, New Zealand. (Photos courtesy of Dr Harold Marshall of Marshall Day Acoustics.)

comes alive, enveloping and involving the listener in the music making process. Outdoors, listeners receive sound straight from the orchestra, there are no reflections from walls, and the sound appears distant. When music is played in a room, reflections from the walls, ceiling and floor embellish the sound, especially if there are plenty of reflections arriving from the side. When sound reaches the listener straight from the stage, the same signal is received at both ears, because the head is symmetrical and the sound to both ears travels an identical path. When reflections come from the side, the signal at each ear is different, as sound to the furthest ear has to bend around the head. This means the sound arrives later and is significantly altered. The brain senses it is in a room, because of the differences between the ear signals, and a feeling of being enveloped by the music occurs.

   This need for lateral reflections influenced Marshall and Hyde to apply diffusers to the large overhead surfaces shown in the figure. The diffusers promote early arriving lateral reflections for spatial impression and clarity.

2.7 Reducing effects of early arriving reflections in large spaces

In Section 2.2 it was discussed how early arriving reflections can cause problems in small spaces due to coloration. Problems also arise in large rooms, for example in rooms with low ceilings. The ceiling reflection can arrive soon after the direct sound for audience members at the rear of the room, and this can lead to coloration, as comb filtering may result. Figure 2.24 shows an application of diffusers in the Cinerama Theatre, Seattle, WA. Mainstream cinemas tend to be very dead spaces with the room effects added artificially through the surround sound reproduction system. The design brief for Cinerama, by Grant of Harris–Grant Associates, was to generate an acoustic with high envelopment and some reverberance, a first in modern commercial cinema design, by using diffusers on the ceiling and walls. While there is an extensive use of surface diffusion, experimental measurements showed that the cinema satisfied THX design criteria. The curved diffusers were used to disperse reflections from the relatively low ceiling to minimize comb filtering. The diffuser used on the ceiling is

Figure 2.24 Cinerama Theatre, Seattle, WA, with a diffusing ceiling (OptiCurve™). (Photo courtesy of University of Salford.)

an optimized curved diffuser – the design process for this surface is discussed in more detail in Chapter 10.

A secondary effect of using ceiling diffusers can be to reduce the level of early arriving non-lateral reflections from the ceiling. This can increase the spatial impression, but whether this happens depends on the geometry of the room and the diffusers used.

2.8 Stage enclosures

During musical performances there is a need for surfaces or enclosures, conventionally called acoustical shells, that surround the musicians. These shells reinforce and blend the sound that is projected toward the audience. It also heightens the ability of the musicians to hear themselves and others. Acoustical shells typically incorporate a rear wall, flared side walls and an overhead canopy.

2.8.1 Overhead canopies

Overhead reflections from stage canopies can cause coloration if the canopy effectively covers the whole stage area. Overhead canopies might be used to hide the presence of a fly tower, or may simply be an integral part of the stage canopy design. Figure 2.25 shows a typical case at Kresge Auditorium, Boston, MA (Acoustician: Rein Pirn, Acentech, Boston) and Figure 2.26 another at First Baptist Church, Eugene, OR (designed by Steve Diamond, AGI, Inc.). The canopy provides reflections back to the stage, which are necessary for the musicians to hear themselves and others. Without early reflections from the stage shell, musicians will find it difficult to create a good balance among themselves and keep in time. Canopies with little open area provide plenty of overhead reflections back to the musicians, but if the canopy elements are flat, there is a risk that the overhead reflections will be too strong and so cause coloration. The solution to this is to shape the canopy, so that some breaking up of the reflected wavefronts occurs. The diffusers spatially and temporally disperse the reflections, and so reduce coloration. The design of overhead stage canopies is discussed in more detail in Chapter 10.

Figure 2.25 Overhead stage canopy (Waveform™) at Kresge Auditorium, Boston, MA. (Photo courtesy of RPG Diffusor Systems Inc.)

Figure 2.26   Rear towers and overhead stage canopy (Overture®) at First Baptist Church, Eugene, OR. (Photo courtesy of Steve Diamond, AGI, Inc.)

Overhead stage canopies can have a much greater open area than that discussed above. Figure 2.27 shows an example, where the canopy serves both the performers and the audience at Rivercenter for the Performing Arts, Columbus, GA (Acoustician: JaffeHolden Acoustics). Again the canopy is designed to promote better communication between musicians across the orchestral stage, leading to better ensemble among musicians and consequently better quality concerts. This is achieved by ensuring an

Figure 2.27   Rivercenter for the Performing Arts, Columbus, GA. (Photo courtesy of Jaffe-Holden Acoustics.)
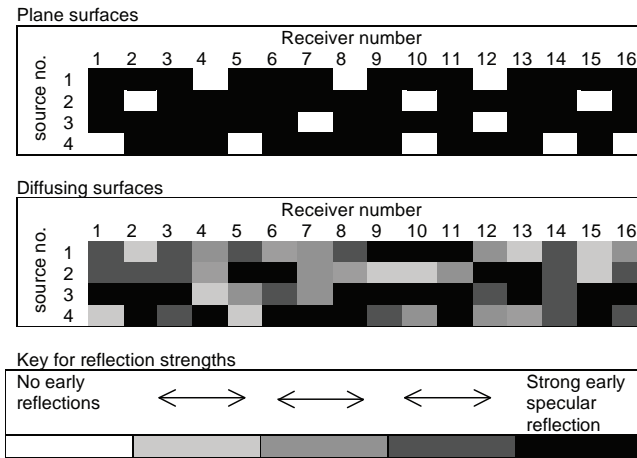
Plane surfaces

Diffusing surfaces

Key for reflection strengths

Figure 2.28   Schematic of pressure distribution from fairly open canopies with different surface treatments (adapted from Dälenback et al.[26]).

even distribution of reflected energy from each of the instruments on the stage to all musicians, with the reflected energy being delayed by about 20–30 ms.[25] A canopy may also be used to reflect sound towards audience areas lacking sound energy. There is risk, however, that providing extra overhead reflections from the stage canopy could lead to coloration. Canopies with large open areas are usually designed so much of the sound will go through the stage canopy to the void above, to be returned to the audience or stage from the true ceiling of the auditorium, and so provide additional reverberance.

If the canopy elements are sparse and flat, then the pressure distribution will be uneven. For some receiver positions there will be specular reflections from a canopy element, and so at mid-high frequency a strong reflection level results. For other receiver positions, the geometric reflection point misses the canopy elements, and a low reflection level results. Figure 2.28 shows a comparative sound pressure level distribution from a canopy with open areas and plane surfaces, and a canopy with open areas and diffusing surfaces after Dalenbäck et al.[26] Consequently, canopies with spaces between the reflectors benefit from using diffusing elements, as they enable a more uniform coverage over the stage area by scattering sound to receivers, which would otherwise lack reflections due to the gaps between the canopy. Chapter 10 discusses stage canopy design in more detail.

2.8.2 Rear and side of stage enclosures

In addition to the orientation of the shell surfaces with respect to the performers, the nature of the surfaces is critical to good performance. A shell can contain reflecting and diffusing surfaces[27] and less often absorption.

Marshall et al.[28] suggested that early reflections among musicians greatly improve their sensation of playing as a group if the reflections:

(a) occur within a temporal window that is dependent on the nature of the musical programme material, typically between 17 and 35 ms after the direct sound;

(b) include high frequency content roughly between 500 Hz and 2,000 Hz, containing the attack transients that are cues for rhythm and expression;
(c) contain a balance of all the parts in the ensemble at all performance positions.

Condition (a) is easily met by spacing the shell an appropriate distance from the performers, while (b) and (c) depend more on the surface topology. Acoustical shells have used a wide variety of surfaces ranging from flat reflecting panels to various forms of surface irregularity, such as curved surfaces, poly-cylinders, fluted columns, and reflection phase gratings. The current state-of-the-art is to utilize multi-dimensional optimization to obtain the optimal shape and orientation; a technique discussed in Chapter 10. In Figure 2.29, the reflections from a flat and diffuse shell are compared. The diffuse reflections are spread over time and are of reduced level, lowering the chances of coloration and harshness due to comb filtering. The diffusion also satisfied the requirements (b) and (c).

D'Antonio[29] carried out a series of experiments using objective measures as well as musician's perceptual evaluations, to determine the appropriate combination and orientation of reflecting, diffusing and absorbing surfaces to optimize performance. The study began by looking at small chamber groups. An example of the test arrangement with a string ensemble is shown in Figure 2.30. Five different microphone systems were used for each playing environment to obtain five simultaneously recorded signals:

1. A mannequin, with microphones at the entrance to the ear canal, was placed within the group to determine ensemble blend without self-masking.
2. Probe microphones, Figure 2.31, were inserted into the ear canal to determine ensemble blend with self-masking of the musician's instrument.
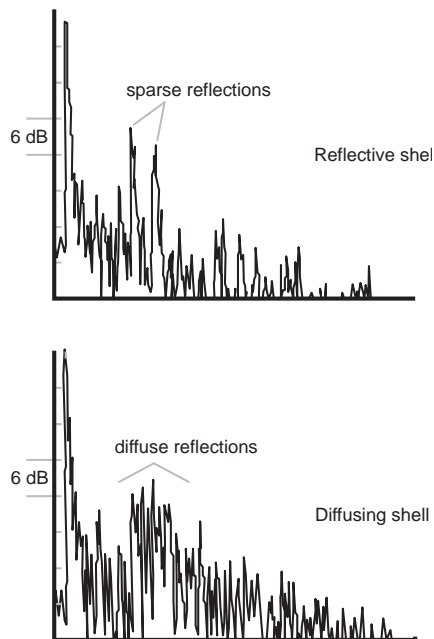

Figure 2.29   The reflections from a flat and diffusely reflecting shell.

Figure 2.30 Cavani string quartet performing in front of VAMPS® shell[23] at the Cleveland Institute of Music (after D'Antonio and Cox[2]).

3. Headband microphones, located at the entrance to the ear canal, were also used to monitor ensemble blend with self-masking.
4. An omnidirectional microphone was placed within the group as a monophonic control.
5. Spaced omnidirectional microphones were placed at the front of the house.

The string ensemble preferred a mixed orientation shell with lower vertical wells and upper horizontal wells, producing lateral and vertical diffusion respectively. Some

Figure 2.31 Probe microphone inserted into the ear canal of the first violinist. Microphone is inserted to a point just in front of the ear drum (after D'Antonio[29]).

musicians preferred flat surfaces on the lower surfaces for better bass coupling. Mutual and self-hearing were unanimously improved. The general reaction was that the diffusive shell provides warmth and intimacy and minimizes harshness. The preferred shell distance for warmth and intimacy was approximately 0.9–1.8 m. The preferred shell distance for projected sound quality was 2.7–3.7 m. There was unanimous agreement that a height of 4.9 m was better than 2.4 m.

A brass quintet experienced harshness from a completely reflective shell and preferred lower diffusers with vertical wells and upper diffusers with horizontal wells. The preferred distance for mutual and self-hearing as well as projected sound quality was 2.7 m. A horn duo preferred a mixture of flat surfaces and diffusers at approximately 1.8 m.

Following the chamber group research, the requirements of a symphony orchestra were investigated. There is an inherent imbalance in an orchestra, because the percussion and brass are naturally louder than the strings and woodwinds. Many traditional shells employ an average acoustic solution to satisfy a majority of the players, using fixed acoustical elements designed for existing musical formats and orchestral arrangements. Since each musician and musical section has a different preference for its own local acoustical environment, and since musical format, orchestral arrangements, and conductor's preferences change, the benefit of a variable acoustical design was explored. The result was an open architecture modular framework, which would allow local acoustical environments in the rear of the orchestra, where the loudest and most problematic instruments are located. A study was done with the Baltimore Symphony Orchestra at the Meyerhoff Symphony Hall, Baltimore, MD, using questionnaires and experimental measurements.

The various sections of the orchestra were asked to mark the quality of the acoustic on a 4 point scale before and after treatment. For instance, the oboe section was asked how the addition of the diffusive shell affected synchronicity, intonation, tone production, distant hearing, mutual hearing and self hearing, compared to the flat existing enclosure. All aspects were improved, with the average score increasing from 1.5 to 3.5. Over the whole orchestra, the average score increased from 1.9 to 3.3.

Figure 2.32 Diffusers around the stage of the Corning Glass Center, NY. (Photo © Paul Warchol Photography, www.warcholphotography.com)

The shell was placed around the entire perimeter of the stage, similar to the shell shown in Figure 2.32. There was no change to the overhead circular disc canopy. The shell consisted of a lower open support that allowed sound to reflect from the hard existing wall behind the shell. The next 0.6 m high tier consisted of horizontally diffusing single plane Schroeder diffusers with the centre of this level at seated ear height. The next 0.6 m in height contained all vertical diffusion, resulting from the wells being oriented horizontally. A 0.6 m cantilever canopy was oriented on top of the vertically diffusing diffusers, at an angle of 45° with respect to the face of the diffusers. The purpose of the experiment was to blend the outer strings into the woodwinds, decrease the harshness of the brass, intensify the fullness and warmth of the strings and control strong specular reflections to enhance the sense of ensemble and rhythmic performance of the musicians. Musicians reported improved ensemble playing through the questionnaires.

2.8.3 Orchestra pits

Semi-enclosed stages are often an acoustically challenged space for music performance. The ceiling is typically low as is the volume. Sound levels can become excessive and

Figure 2.33   Two views of the pit at Nicholas Music Center, Rutgers University. (Architects: Bhavnani & King Architects, NY; photos courtesy of RPG Diffusor Systems Inc.)

ensemble hearing is often lacking. The situation is even worse within an orchestral pit in an opera or ballet house. These situations can be improved with the use of absorption and diffusion with low-mid frequency absorption to control sound levels and diffusion to improve ensemble. Figure 2.33 (bottom) shows the ceiling and walls of an orchestra pit treated with hemispherically scattering diffusers and single plane diffusers, respectively. The pit rail, shown on the left in the top of the figure, is also an important surface for communication between the stage and orchestra on the left. It is shown with upper diffusers having horizontal dividers to scatter sound in a vertical hemi-disc and lower diffusers to provide horizontal scattering for the benefit of the conductor and orchestra. Diffusive concrete masonry units, such as those shown in Figure 6.10, are also becoming popular for use in orchestra pits.

2.9 Blurring the focussing from concave surfaces

Concave surfaces can cause focussing in a similar manner to concave mirrors. This can lead to uneven sound levels around a room, which is usually undesirable. Furthermore, as the concave surface concentrates energy in particular locations, there is a risk that this reflection will be significantly above the general reverberation of the space and so cause echo problems or coloration. A famous example of this is the Royal Albert Hall, where the large dome caused problems with long delayed and focussed reflections. The solution was to place volume scatterers, the 'mushrooms', to disperse sound and also to provide earlier reflections to the audience. Assuming the concave surface cannot be removed, the only treatments available are absorbers or diffusers. Both treatments will work; the choice depends on other acoustic considerations, such as reverberance.

Figure 2.34 shows the polar response near a concave wall, which was to be part of a music rehearsal room at the Edwina Palmer Hall, Hitchin, England. The concentration of sound at the focus is clear. To overcome this problem, a diffuser was specified by Raf Orlowski of Arup Acoustics, UK. An optimized diffuser was developed and applied as shown in Figure 2.35, and Figure 2.34 shows that the dispersion of the focused energy is quite dramatic. It would have been possible to remove the echo with absorbers, but then the musicians would not have received reflections from this wall. This would potentially have a detrimental effect on ensemble. In this case, the wall
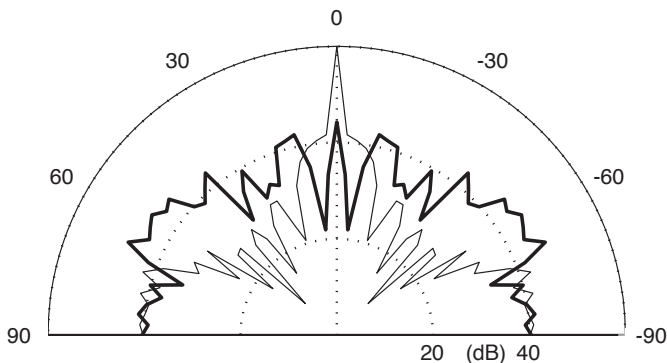

Figure 2.34 Scattering from a concave arc compared to an optimized curved diffuser at 3 kHz:
——— concave arc, and
━━━ optimized curved diffuser.

Figure 2.35   Optimized curved surface (OptiCurve™) in the Edwina Palmer Hall. (Photo courtesy of Arup Acoustics.)

reflection had to be preserved, but the focussing removed, and hence diffusers were preferred over absorbers. Orlowski commented that:

> For architectural reasons, a concave form was developed for the hall, which obviously gave rise to concerns about focussing. Curve shape optimization was used to minimize focussing by the concave wall using a geometrical motif based on an amplitude modulated wave. Subjective listening tests to piano and clarinet music in the hall indicated a very uniform sound field with no evidence of focussing. Furthermore, both instruments produced an expansive sound with a very good balance between clarity and reverberance. Musicians found the hall easy to play in. The success of this project has led Arup Acoustics to consider curve optimization for providing diffusion for other projects, including a rehearsal hall with curvature in two dimensions.

See Chapter 10 for detailed discussions of geometric diffusers and optimized diffuser design.

2.10 In audience areas – diffuse fields

Canopies of reflectors are commonly seen above audiences in concert halls. An example is shown in Figure 2.36. Similar to overhead stage canopies discussed previously, making these canopy elements diffusing can reduce coloration and make the distribution of sound more uniform across the audience.

But do diffusers have a broader application in auditoria, for example on the side

Figure 2.36 Optimized curved audience canopy (Waveform® Bicubic) in Patterson Mill Middle and High School, MD (CSD Architects, Baltimore, MD; photo courtesy of RPG Diffusor Systems Inc.)

walls? And how does surface diffusion, dispersion created by diffusers, relate to volume diffusion or the diffuseness of a space? If a space is non-diffuse, for instance if the absorption is not very evenly distributed or the dimensions of the space are not very similar, then applying diffusers to the space will have a number of effects. In the case of very disproportioned rooms, such as underground stations, the reverberation time will decrease when diffusers are added, because the mean free path is reduced, giving more absorption from the increased number of reflections per second (see Section 2.5).

Consider another case, a room with just absorption on the floor and flat hard surfaces for the walls and ceiling. This non-diffuse space is likely to have a reverberation time different to that predicted by Eyring formulation (Equation 1.5), which would be correct for a diffuse space.[30] When the room is tall relative to its width and length, then some sound will be able to propagate in the horizontal plane without being absorbed by the highly absorbent floor, and consequently a longer reverberation time can result. Adding surface diffusers to the walls which scatter sound vertically will cause sound paths to more evenly involve all the surfaces in a room, and consequently, the floor absorption will become more important and the reverberation time will decrease.

Unfortunately, there is no simple formulation to relate the reverberation time in the space to the number of diffusers applied. Gerretsen[31] outlines a set of formulations for reverberation time, which includes both absorption and scattering coefficients. There are a large number of equations involved, however, and it is probably just as easy to gauge the change in reverberation using a geometric room acoustic model.

As the reverberation time is altered, so is the level of the reverberant sound field. However, it would be incorrect to assume that as diffusers are added, the sound levels will become identical across the room because the space is more diffuse. This is because even in ideal reverberant conditions there is scatter in measured levels.[32] Furthermore, as discussed below, the early reflected sound can be changed by introducing diffusers,

which can have a significant effect on the sound level. On the other hand, as diffusers are added, the reverberation time variation across a space does decrease and decays become more linear[33–35] (see also the discussion of sound reproduction rooms in Section 2.2). Indeed monitoring the difference between the T_{15} and T_{30} predicted within a computer model and the calculated statistical T_{60}, as acoustic treatment is altered, is one indication of how mixing an environment is.

A few people have examined the effect of large scale diffusion on the acoustics of concert halls and looked beyond reverberation. Fujii *et al.*[36] examined two similar halls, one with side wall columns, which promote scattering, and one without. Chiles[37] and Jeon *et al.*[38] examined the effect of large scale scattering in physical scale models; Chiles also examined computer models. In some of the measurements in some of these studies, it appears that the diffusers may also have been partly absorbing the sound, and this makes interpreting some of the results more difficult.

For shoebox shaped auditoria, hemispherically-scattering side wall and ceiling diffusers promote more early sound being reflected back towards the stage than would be the case for flat walls. This gives an increase in clarity and sound level for the front seating and a decrease for the audience at the rear of the hall – generally these would not be desirable effects. However, it would also be possible to overcome these effects by using single plane diffusers or designing diffusers with specific polar responses, for instance by using diffusers which just scatter laterally on the ceiling. Putting diffusers on the rear wall of a concert hall can help to promote a diffuse space with less effect on the early reflected sound distribution. However, this raises the interesting question as to whether a diffuse sound field is desirable within a concert hall. While a diffuse field makes the prediction of sound behaviour more straightforward, what is currently unknown is whether this is desirable for the audience. Do people prefer strong specular or diffuse reflections?

Furthermore, the situation is different for other auditoria layouts. For instance, in fan shaped halls, the promotion of additional lateral reflections by introducing single plane side wall diffusers would be desirable for promoting spaciousness. Incidentally, for rectangular halls, one study[38] showed that 1-IACC (Internal Aural Cross Correlation[25]) is increased for front and side seats, as might be expected, whereas another study showed that IACC is not strongly affected.[36]

2.11 Barriers and streets

Barriers can be used to reduce noise propagation from roads and railway lines to neighbouring houses. One problem that roadside barriers suffer from is double reflections from high sided vehicles, which enables some of the noise to bypass the barrier – this is shown in Figure 1.11a. Another problem is reflections from barriers on one side of the road, which then pass over barriers on the other side, as shown in Figure 1.11b. Chapter 1 discusses absorption as a solution, but common absorbents wear badly under the harsh conditions of high winds, salt and water which are common next to busy roads. Diffusers may offer a solution to this problem, as shown in Figure 1.11d. By dispersing the sound, the reflection problems are decreased. The difficulty with this solution is that sound energy has not been removed by the diffusers, just scattered into other directions. There is a risk that wind and other meteorological conditions could cause the noise to be scattered or refracted to noise sensitive areas. Consequently, there is a need to make this solution robust under a wide range of weather conditions. Recent

studies have indicated that trees can be used to reduce turbulence around roadside barriers, and so natural wind breaks might enable the performance of diffusing (and other) barriers to be more robust to changing meteorology.[39]

Various studies have been carried out into the how diffusers on top of barriers can alter the sound diffraction and hence improve performance,[40] however this is probably not a cost effective way of improving barrier performance.

Street canyons are roads with high sided buildings on both sides, which form a semi-enclosed space where sound levels can build up and noise levels can become unacceptable. The surface structures of the buildings forming the street canyon influence the sound levels. For example, balcony fronts can have the unfortunate effect of reflecting sound back down to street level thereby exacerbating noise problems. On the other hand, other types of surface roughness may have a role in breaking up the reflected sound on the building fronts, causing it to disperse and therefore be minimized at street level. Kang[41] and Onaga and Rindel[42] used geometric computer models to examine the influence of the building façades on noise levels in streets. Scattering increases the noise level by very small amounts close to the source, but further away, they reduce the sound level from traffic by 2–4 dB, because surface roughness promotes more cross-street propagation which attenuates rapidly, especially if directed upwards!

2.12 Conclusions

In recent decades, an understanding of where and why diffusers should be used has been created. While this knowledge is still incomplete, in many common applications it is now well established how diffusers should be used. This chapter has detailed some of these applications, as well as presenting some of the key principles to be further developed later in the book. The remaining chapters concerning diffusers are as follows:

- *Chapter 4* discusses the measurement of reflections from surfaces, and the characterization in terms of scattering and diffusion coefficients.
- *Chapter 8* discusses methods for predicting diffuser scattering, presenting both complex and simple methods in the frequency and time domains.
- *Chapters 9*, *10* and *11* deal with the design of key diffuser types: Schroeder, geometric and hybrid diffusers.
- *Chapter 12* discusses the role of scattering coefficients in geometric room acoustic models.
- *Chapter 13* rounds off the diffuser chapters by looking at active diffuser technologies.

2.13 References

1 P. D'Antonio and T. J. Cox, "Diffusor application in rooms", *Appl. Acoust.*, **60**(2), 113–42 (2000).
2 P. D'Antonio and T. J. Cox, "Two decades of sound diffusor design and development part 1: applications and design", *J. Audio Eng. Soc.*, **46**(11), 955–76 (1998).
3 L. L. Beranek, *Concert and Opera Halls: How They Sound*, AIP Press, 69–74 (1996).
4 J. P. O'Keefe, T. J. Cox, N. Muncy and S. Barbar, "Modern measurements, optimized

diffusion, and electronic enhancement in a large fan-shaped auditorium", *J. Acoust. Soc. Am.*, **103**(5), 3032–3 also *Proc. 16th ICA* (1998).

5 D. David and C. Davis, "The LEDE concept for the control of acoustic and psychoacoustic parameters in recording control rooms", *J. Audio Eng. Soc.*, **28**, 585–95 (1980).

6 M. R. Schroeder, "Binaural dissimilarity and optimum ceilings for concert halls: more lateral sound diffusion", *J. Acoust. Soc. Am.*, **65**, 958–63 (1979).

7 P. D'Antonio and J. H. Konnert, "The Reflection Phase Grating Diffusor: Design Theory and Application", *J. Audio Eng. Soc.*, **32**(4), 228–38 (1984).

8 P. D'Antonio and J. H. Konnert, "The RFZ/RPG approach to control room monitoring", *Proc. Audio Eng. Soc.*, preprint 2157 (I-6) (October 1984).

9 ITU-R BS.1116-1, "Methods for the subjective assessment of small impairments in audio systems including multichannel sound systems" (1997).

10 F. E. Toole, *Sound Reproduction*, Focal Press (2008).

11 J. Blauert, *Spatial hearing*, MIT Press, Cambridge, MA (1983).

12 S. E. Olive and F. E. Toole, "The detection of reflections in typical rooms", *J. Audio Eng. Soc.*, **37**(7/8), 539–53 (1989).

13 P. D'Antonio, F. Becker and C. Bilello, "Sound intensity and interaural cross-correlation measurements using time delay spectrometry", *J. Audio Eng. Soc.*, **37**(9), 659–73 (1989).

14 T. Welti, and A. Devantier, "Low-frequency optimization using multiple subwoofers", *J. Audio Eng. Soc.*, **54**, 347–64 (2006).

15 P. D'Antonio, "New types of acoustical materials simplify room designs", *Proc. 81st Convention Audio Eng. Soc*, preprint 2365 (1986).

16 J. A. S. Angus, A. C. Marvin and J. Clegg, "The effect of acoustic diffusers on room mode density", *Proc. 96th Convention Audio Eng. Soc.*, preprint 3851 (1994).

17 X. T. Zhu, Z. M. Zhu and J. C. Cheng, "Using optimized surface modifications to improve low frequency response in a room", *Appl. Acoust.*, **65**(9), 841–60 (2004).

18 S. Felix, M. Asch, M. Filoche, B. Sapoval, "Localization and increased damping in irregular acoustic cavities", *J. Sound Vib.*, **299**(4–5), 965–76 (2007).

19 P. D'Antonio, *Acoustical Diffusing and Absorbing Cinder Blocks*, US patent 5, 193, 318 (1993).

20 P. D'Antonio, *Two-dimensional Primitive Root Diffusor*, US patent 5, 401, 921 (1995).

21 J. Kang, "Experimental approach to the effect of diffusers on the sound attenuation in long enclosures", *Bldg. Acoust.*, **2**, 391–402 (1995).

22 A. H. Marshall and J. R. Hyde, "Some practical considerations in the use of quadratic residue diffusing surfaces", *Proc. 10th ICA*, Sydney, paper E7.3 (1980).

23 A. H. Marshall, J. R. Hyde and M. F. E. Barron, "The acoustical design of Wellington Town Hall: design development, implementation and modelling results", *Proc. IoA (UK)*, Edinburgh (1982).

24 M. Barron, "The subjective effects of first reflections in concert halls – the need for lateral reflections", *J. Sound Vib.*, **15**, 475–94 (1971).

25 M. Barron, *Auditorium Acoustics and Architectural Design*, E&FN Spon (1993).

26 B.-I. Dalenbäck, M. Kleiner and P. Svensson, "A macroscopic view of diffuse reflection", *J. Audio Eng. Soc.*, **42**, 793–807 (1994).

27 P. D'Antonio, *Variable Acoustics Modular Performance Shell*, US Patent 5, 168, 129 (1992).

28 A. H. Marshall, D. Gottlob and H. Alrutz, "Acoustical conditions preferred for ensemble", *J. Acoust. Soc. Am.*, **64**(5), 1437–42 (1978).

29 P. D'Antonio, "Performance acoustics: the importance of diffusing surfaces and the variable acoustics modular performance shell", *Proc. 91st Convention Audio Eng. Soc.*, New York, preprint 3118 (B-2) (October 1991).

30 H. Kuttruff, *Room Acoustics*, 4th edn, Spon Press (2000).

31 E. Gerretsen, "Estimation methods for sound levels and reverberation time in a room with irregular shape or absorption distribution", *Acta Acustica uw Acustica*, **92**, 797–806 (2006).

32 D. Lubman, "Precision of reverberant sound power measurements", *J. Acoust. Soc. Am.*, **56**, 523–33 (1974).

33 J. L. Davy, I. P. Dunn, and P. Dubout, "The variance of decay rates in reverberation rooms", *Acustica*, **43**, 12–25 (1979).

34 J. L. Davy, "The variance of impulse decays", *Acustica*, **44**, 51–6 (1980).

35 S. Chiles and M. Barron, "Sound level distribution and scatter in proportionate spaces", *J. Acoustic. Am. Soc.*, **116**(3), 1585–95 (2004).

36 K. Fujii, T. Hotehama, K. Kato, R. Shimokura, Y. Okamoto, Y. Suzumura and Y. Ando, "Spatial distribution of acoustical parameters in concert halls: comparison of different scattered reflection", *J. Temporal Des. Arch. Environ.*, **4**, 59–68 (2004).

37 S. Chiles, "Sound Behaviour in Proportionate Spaces in Auditoria", PhD thesis, University of Bath, UK (2004).

38 J. Y. Jeon, J. K. Ryu, S. Sato and Y. H. Kim, "Subjective and objective evaluation of the scattered sound in a 1:10 scale model hall", *Proc. Forum Austicum*, Budapest, Hungary (2005).

39 T. Van Renterghem, D. Botteldooren, W. M. Cornelis and D. Gabriels, "Reducing screen-induced refraction of noise barriers in wind by vegetative screens", *Acta Acustica uw Acustica* **88**(2), 231–8 (2002).

40 M. R. Monazzam and Y. W. Lam, "Performance of profiled single noise barriers covered with quadratic residue diffusers", *Appl. Acoust.*, **66**(6), 709–30 (2005).

41 J. Kang, "Sound propagation in street canyons: Comparison between diffusely and geometrically reflecting boundaries", *J. Acoustic. Am. Soc.*, **107**(3), 1394–1404 (2000).

42 H. Onaga and J. H. Rindel, "Acoustic characteristics of urban streets in relation to scattering caused by building facades", *Appl. Acoust.*, **68**, 310–25 (2007).

3   Measurement of absorber properties

This chapter covers a variety of methods used to measure and characterize acoustic absorbers. For many practitioners, the only important measurement is that which gives the random incidence absorption coefficient in a reverberation chamber. While this may be the absorption coefficient that is needed for performance specifications in room design, other measurements are needed to understand and model absorptive materials. For instance, the prediction of the random incidence absorption coefficient is problematic, and consequently it is necessary to measure materials in a more controlled environment to allow direct comparison between theory and experiment.

The more controlled environment that is often used is the impedance tube, which allows normal incidence impedance and absorption to be determined. Less often, but nevertheless valuable, are the free field measurements on large area samples done in hemi-anechoic spaces. The most common free field method uses a two-microphone approach, but this is often only applicable to isotropic, homogeneous samples. Consequently, attention has recently turned to using more than two microphones; however, the measurements appear to be problematic and very noise sensitive. These techniques can be adapted for *in situ* measurements, the next subject in the chapter.

Chapter 12 discusses how to convert between the absorption coefficients resulting from the different measurement methods. It also examines how absorption coefficients can be applied to real room predictions as well as their use in geometric room acoustic models.

There is also a need to be able to characterize the propagation within the absorbent material, to enable theoretical modelling. For instance, the well-known Delaney and Bazley empirical model outlined in Chapter 5 requires the flow resistivity and porosity of the porous material to be known. For this reason, methods to measure all the key parameters that characterize the propagation within the absorbent are outlined.

The intention of this chapter is to provide information on the different measurement techniques. It is not intended that each description is a comprehensive standard with a foolproof description of how to carry out the measurements. What is intended is that the reader should be able to make an informed decision about the different techniques described, understand the advantages and disadvantages, and supplement the descriptions given here with those available in the referenced literature.

3.1 Impedance or standing wave tube measurement

The standing wave tube enables both the normal incidence absorption coefficient and surface impedance to be measured. This is a very useful test method as it enables the

absorption coefficient and impedance to be measured under well defined and controlled conditions. Consequently, it is frequently used in validating prediction models for porous materials. This method has the advantage of only needing small samples (a few centimetres in diameter) and this makes it ideal for developers of materials, as the alternative is to construct large samples for reverberation chamber tests, which is more difficult and expensive. The final key advantage is that the impedance tube method can be carried out with relatively simple apparatus in a normal room and does not need specialist test chambers. Problems with the method arise when the absorption from the small sample is not representative of the behaviour of a large sample, as would happen with some resonant absorbers. For this reason, the method is most used with local reacting porous absorbers.

Figure 3.1 shows some typical set-ups, and the concept is as follows. A loudspeaker generates plane wave propagation in the impedance tube and the plane wave propagates down the tube before reflecting from the sample. A standing wave is set up within the tube. The impedance of the sample alters how sound is reflected and, by measuring the resulting standing wave, it is possible to calculate the normal incidence absorption coefficient and surface impedance of the sample. This is such a common technique in acoustics that it has been enshrined in international standards.[1,2]

The necessity for plane wave propagation imposes many limitations on the system which are discussed as follows.

1. The losses into and through the tube should be minimized so that the plane waves propagate without significant attenuation. Consequently, thick metal is a common construction material for the mid- to high frequency ranges of most concern in building design and noise control. For impedance tubes that are to work at bass frequencies, more extreme construction is needed to prevent significant losses from
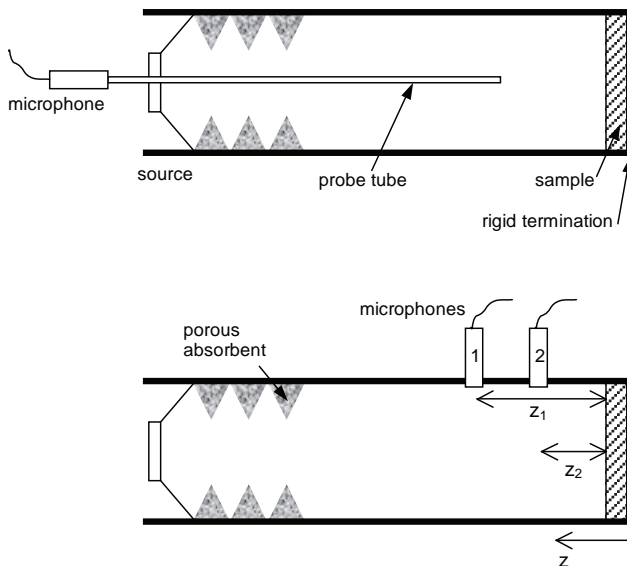
Figure 3.1 Set-ups for impedance tube measurement. Top: probe tube for standing wave method; bottom: two-microphone technique.

the tube. For example, thicker walls are required or steel-lined concrete tubes can be used; these can work down to the limit of human hearing (20 Hz). Whatever the size, to minimize losses the tube should be smooth on the inside and clean.

2. The tube should have constant cross-section over the measurement region where the sample and microphone positions are located. The actual shape is not that important; square and circular tubes are most popular. Although circular tubes seem to be less prone to cross-mode problems within porous absorbents, square tubes are useful, as in some cases square samples are easier to construct.

3. The loudspeaker should be a few tube diameters (or widths) from the first microphone position so that any cross modes generated by the loudspeaker have decayed away. It is sometimes necessary to place absorbent at the loudspeaker end of the tube to reduce the effect of resonances within the impedance tube.

4. The microphone positions should not be too close to the sample so that any evanescent waves generated on reflection have had time to die away. For a homogeneous, isotropic sample that means the first measurement microphone should be at least half a tube diameter (or width) away. For samples that are structured and anisotropic, no microphones closer than two diameters away from the sample surface should be used.

5. The highest frequency, f_u, that can be measured in a tube is then determined by:

$$f_u = \frac{c}{2d} \tag{3.1}$$

where d is the tube diameter or maximum width and c the speed of sound. This is a statement that there should not be any cross modes in the tube; the first mode appears when half a wavelength fits across the tube. The limitation imposed by Equation 3.1 means that to cover a wide frequency range, several different impedance tubes of different diameter or width are required.

It is possible to measure at higher frequencies if multiple microphones are used across the width of the tube. The sound field within the tube can be considered to be a sum of the plane wave and higher modes, in a similar way to how a room sound field is decomposed into its modes. In a circular tube and an isotropic sample, one additional microphone enables the impedance of the sample for the plane wave and first cross mode to be determined (circular symmetry can be exploited to reduce the number of additional microphones in this case). For a square tube, four microphones can be placed as shown in Figure 3.2, and the measured signals summed.[3] In this case the first and third cross modes in the tube in each direction cancel, while the microphones are at nodes of the second order mode, so leaving the fourth order mode to dominate. This quadruples the limit shown in Equation 3.1. However, the disadvantage of the multi-microphone method is that for frequencies where cross modes dominate, the sample is not receiving plane waves, so the absorption coefficient measured is harder to relate to prediction models.

The experimental detail that is most critical is the requirement for the sample to be cut and mounted correctly. It is vital that the sample fits snugly into the tube. Any gaps around the edge must be filled and sealed, otherwise the gaps will allow absorption by the edge of the sample and the measured absorption will be too high. Worse still, if the small gaps open up to an air cavity behind, a Helmholtz device could be formed, and the absorption overestimated by a large margin. The normal way of providing proper
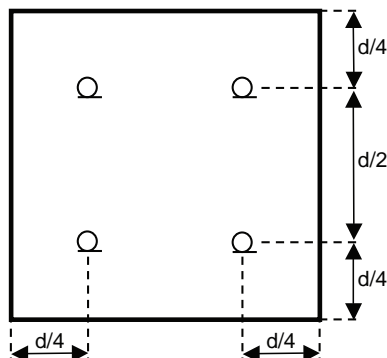
Figure 3.2 Set-up for impedance tube measurement at higher frequencies using four micro-
phones.

sealing is to use petroleum jelly (Vaseline®), Plasticene® or mastic to fill the edges of the sample. It is also important, however, not to wedge porous absorbers into the tube – this changes the mechanics of the absorber frame and can lead to incorrect measurements due to the constrained vibration of the absorber frame.[4] Rapid variations in the impedance data is seen around the resonant frequency of the frame. Consequently, the sample should be 0.5–1 mm smaller than the diameter (or width) of the tube;[5] then the impedance and absorption coefficient measured are effectively the same as a sample with infinite lateral dimensions.

It is also important that the rear of the absorber is properly terminated. Air gaps between the absorber and the backing plate will lead to excess absorption being measured, unless of course it is planned to mount the absorber with an air gap, in which case the measurement would be correct.

The impedance tube is not often useable for extended reaction absorbers, unless the impedance tube happens to coincidentally be the same size as the extended reaction device. For instance, the performance of a membrane absorber is usually dependent on the mounting of the membrane. It is not possible just to mount a smaller membrane absorber in an impedance tube, and expect the same performance as the larger device.

3.1.1 Standing wave method

The advantage of the standing wave method is that it is very dependable, and relatively idiot proof. Unfortunately, it only measures one frequency at a time and the procedure for locating minima in the standing wave, which is needed to get phase information, is rather slow and so measuring a large number of frequencies is tedious. It is, however, more robust and reliable than the transfer function method discussed in Section 3.1.2 and is a useful second check on results from that method.

If plane waves are assumed to propagate in the tube, then the theories outlined in Chapter 1 for the reflection of sound from a plane infinite absorbent can be used. The steady state pressure in the tube is given by:

$$p = A\left(e^{jkz} + \mathrm{Re}^{-jkz}\right) \tag{3.2}$$

where R is the reflection coefficient; k is the wavenumber; the sample is assumed to be at $z = 0$, and A is a complex constant. The first term represents the incident wave and the second the reflected wave.

There are two standard approaches for sampling the pressure within the tube, the first is the standing wave ratio method and the second is the transfer function technique. For the standing wave method, the minimum and maximum pressures are measured. The maximum pressure p_{max} occurs when the first and second terms in Equation 3.2 are in phase, and the minimum pressure p_{min} occurs when they are completely out of phase. In terms of formulations:

$$\begin{aligned} p_{max} &= 1 + |R| \\ p_{min} &= 1 - |R| \end{aligned} \tag{3.3}$$

The standing wave ratio s is defined as the ratio of p_{max} to p_{min} and is given by:

$$s = \frac{p_{max}}{p_{min}} = \frac{1 + |R|}{1 - |R|} \tag{3.4}$$

This formulation can be rearranged to allow the magnitude of the reflection coefficient to be obtained:

$$|R| = \frac{s - 1}{s + 1} \tag{3.5}$$

From the reflection coefficient it is possible to get the absorption coefficient as $\alpha = 1 - |R|^2$ – see Section 1.4.2.

To find the pressure maximum and minimum, it is necessary to have a probe microphone mounted on a moving trolley. The advantage of this formulation is that no pressure calibration is needed, provided the equipment remains time invariant, as any factors relating the acoustic pressure to the voltage monitored by the measurement equipment, such as the effects of the probe tube, cancel out.

By noting the distance of the first minimum from the sample, z_{min}, and considering the necessity for the incident and reflected phase to be different by exactly π at this position, it is possible to also calculate the impedance of the sample. The phase angle of the reflection coefficient is given by:

$$\angle R = 2kz_{min} - \pi \tag{3.6}$$

Using Equation 1.22, it is then possible to obtain the normal incidence surface impedance.

Moving back from the sample, the first minimum met should be measured, and then the next maximum. This minimizes the effect of tube losses. It is possible to add loss

factors into Equation 3.2 if the tube absorption is significant, and formulations are given in the standard[1] to do this. It is far better, however, to make sure the losses are negligible in the first place. For samples with low absorption, this measurement becomes rather inaccurate as the measured standing wave ratio has a large error associated with it, as the pressure minimum becomes too small to be accurately measured.

3.1.2 Transfer function method

Equation 3.2 has two unknowns: the magnitude and phase of the reflection coefficient. By measuring the pressure at two points in the tube, it is possible to set up and solve simultaneous equations for the reflection coefficient and from there get the impedance and absorption coefficient. This is the principle of the transfer function, often called the two-microphone method. (Although, as this is often used with one microphone which is moved, calling this a two-microphone method is nowadays rather misleading!)

The primary advantage of using this approach is that it obtains the absorption coefficient and impedance of the surface for all frequencies (within limits) with only a couple of quick measurements. It is therefore much more efficient than the standing wave method. It is also a method where if something is done wrong, for example the microphone positions are incorrect, then the formulations yield results which are clearly unphysical – it is easy to spot common measurement errors with this approach.

The transfer function between two microphone positions in the tube is measured as shown in Figure 3.1. Remembering that the transfer function is simply the ratio of pressures, $H_{12} = p(z_2)/p(z_1)$, and applying Equation 3.2, the transfer function between microphone positions 1 and 2 is given by:

$$H_{12} = \frac{e^{jkz_2} + Re^{-jkz_2}}{e^{jkz_1} + Re^{-jkz_1}} \qquad (3.7)$$

where z_1 and z_2 are the positions of the microphones shown in Figure 3.1. Rearrangement then directly leads to the complex pressure reflection coefficient:

$$R = \frac{H_{12}e^{jkz_1} - e^{jkz_2}}{e^{-jkz_2} - H_{12}e^{-jkz_1}} \qquad (3.8)$$

Using the equations set out in Section 1.4.2, the absorption coefficient and surface impedance are then obtained.

There are restrictions on the microphone spacing. If the microphones are too close together, the transfer function measured will be inaccurate because the change in pressure will be too small to be accurately measured. This leads to a lower frequency limit, f_l, for a given microphone spacing $|z_1 - z_2|$:

$$f_l > \frac{c}{20|z_1 - z_2|} \qquad (3.9)$$

Problems also arise, if the microphone spacing becomes too wide. As the spacing approaches a wavelength the simultaneous equations become impossible to resolve as the

pressure measured at both microphones is identical. This leads to an upper frequency limit f_u due to microphone spacing given by:

$$f_u < \frac{0.45c}{|z_1 - z_2|} \qquad (3.10)$$

Consequently, there are two upper frequency limits given by Equation 3.1 and 3.10, and the lowest figure should be taken.

The lower and upper frequency limits mean that to cover a reasonable number of octaves it is often necessary to use more than two microphone positions in a tube; three positions are typically used. Three positions give three possible microphone spacings. By appropriately setting the frequency ranges for each of the spacings, it is possible to cover a wider frequency range.

There is a choice of methods for measuring the transfer function in Equation 3.7. A dual channel FFT analyzer can be used with a matched pair of microphones, using a white noise source. In that case, it is necessary to compensate for differences in the microphone responses by measuring once, then interchanging the microphones and measuring again. A more efficient method is to use a deterministic signal such as a maximum length sequence[6] or swept sine wave.[7] This means that one microphone can be used to measure the transfer function to each microphone position and the ratios of these transfer functions are used to obtain Equation 3.7. This negates the need for matched microphones. Using a deterministic signal rather than white noise also removes the need for time consuming averaging.

It is important that any unused holes are blocked, and that microphones are mounted flush to the tube sides. Better results appear to be obtained for fixed microphones than for a probe microphone. The likely reason is that positioning the microphone accurately is crucial, and this is harder to obtain with a probe. This problem can be overcome by measuring many different microphone positions along the impedance tube with the probe and averaging the different results, but this is rather tedious and not recommended.

Horoshenkov *et al.*[8] carried out a round robin test on impedance tube measurements involving seven acoustics laboratories. They used three samples; reconstituted porous rubber, reticulated foam and fibreglass and Figure 3.3 shows some of the results. The mean absorption coefficient is shown for each material, along with dotted lines indicating the 95 per cent confidence limit in any one laboratory measurement.

The biggest errors are seen for the reconstituted porous rubber in the top graph, however, and this is most likely due to the fact that the sample varies considerably even when taken from the same block of material, so the large variations probably reflect true sample variation and not just experimental error. The fibreglass results shown in the bottom graph are similarly affected by sample variation. The foam samples were more consistent, but the effects of mounting were seen. Individual laboratory results showed patterns of minima and maxima indicative of structural resonances. This evidence is somewhat lost in producing the average plots in Figure 3.3, but the increase in errors around 2,500 Hz are due to this effect.
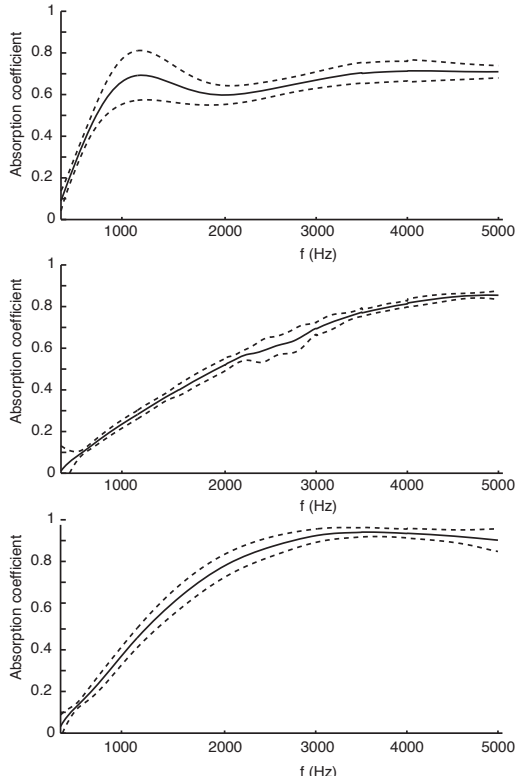
Figure 3.3   Comparison of impedance tube measurements of the absorption coeffcient for three materials at up to seven laboratories. Top graph: reconstituted porous rubber; middle: reticulated foam, and bottom: fibreglass. The mean absorption coefficient is shown, along with dotted lines indicating the 95 per cent confidence limit in any one laboratory measurement. <3,500 Hz data from seven laboratories is used; 3,500–4,000 Hz from six laboratories; and >4,000 Hz from four laboratories. (Adapted from Horoshenkov *et al.*[8], graphs kindly prepared by F-X. Bécot.)

3.1.3 Least mean square method

This is essentially an adaptation of the transfer function method. It is usual to use three microphone measurements to cover the frequency range an impedance tube offers. There will be a region of frequency overlap where two sets of measurement results are applicable, and each will yield a slightly different answer. By applying a least mean square approach it is possible to gain a formulation which produces one unambiguous result from the three (or more) microphones.[9] The complex reflection coefficient is given by:

$$R = -\frac{\displaystyle\sum_{n=1}^{M-1}\sum_{m=n+1}^{M}\left(e^{-jk(L-z_n)}H_{nm} - e^{-jk(L-z_m)}\right)\left(e^{-jk(L+z_n)}H_{nm} - e^{-jk(L+z_m)}\right)^{*}}{\displaystyle\sum_{n=1}^{M-1}\sum_{m=n+1}^{M}\left|e^{-jk(L+z_n)}H_{nm} - e^{-jk(L+z_m)}\right|^{2}} \qquad (3.11)$$

where H_{nm} is the transfer function measured between microphones n and m; z_n and z_m the distances of the nth and m^{th} microphones from the test specimen, and * indicates complex conjugate.

3.1.4 Transmission measurements

The impedance tube method can also be extended to allow the measurement of transmission through materials. Figure 3.4 shows a typical arrangement. The right hand side might be an anechoic termination, generated by a thick porous layer of gradually increasing flow resistivity. The quality of the anechoic termination is crucial for accurate measurement,[10,11] because any reflected sound will pass back through the test material and be measured by microphones 1 and 2 as reflections from the front of the test sample. (This leads to a transmission coefficient spectrum which inaccurately oscillates with respect to frequency due to interference.) Provided the sample being tested has low flow resistivity and high porosity, a very good anechoic termination will yield accurate results; indeed in theory a fourth microphone is not even needed.

However, a more robust technique is the two-load method, which can cover a wider range of samples. Two test conditions are measured, one where the right hand termination is rigid, and the other where it is open. The formulations for this method are derived below.[12]

The pressure amplitudes A–D of the various plane wave components in the tube are defined in Figure 3.4. To the left of the sample, the pressure and velocity are given by:

$$p = Ae^{jkz} + Be^{-jkz}, \quad u = \frac{1}{\rho c}\left(Ae^{jkz} - Be^{-jkz}\right) \tag{3.12}$$

and to the right of the sample:

$$p = Ce^{jkz} + De^{-jkz}, \quad u = \frac{1}{\rho c}\left(Ce^{jkz} - De^{-jkz}\right) \tag{3.13}$$

Using the pressures measured at the four microphones, $p(z_1) \ldots p(z_4)$, it is possible to derive expressions for the pressure amplitudes:

$$A = \frac{p(z_1)e^{-jkz_2} - p(z_2)e^{-jkz_1}}{2j\sin(k(z_1 - z_2))}, \qquad B = \frac{p(z_2)e^{-jkz_1} - p(z_1)e^{-jkz_2}}{2j\sin(k(z_1 - z_2))} \tag{3.14}$$

$$C = \frac{p(z_3)e^{-jkz_4} - p(z_4)e^{-jkz_3}}{2j\sin(k(z_3 - z_4))}, \qquad D = \frac{p(z_4)e^{-jkz_3} - p(z_3)e^{-jkz_4}}{2j\sin(k(z_3 - z_4))}$$

Once the amplitudes are calculated from the measured pressures it is then possible to evaluate the pressures and velocities on the front and rear of the test sample, at $z = 0$ and $z = -d$, using Equations 3.12 and 3.13. The propagation through the test sample can be described by a transfer matrix, as described in Section 1.5.1:
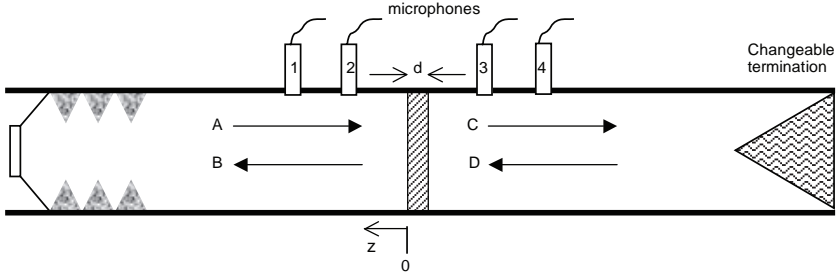
Figure 3.4 Set-up for transmission measurement in an impedance tube.

$$\begin{bmatrix} p \\ u \end{bmatrix}_{z=0} = \begin{bmatrix} T_{11} & T_{12} \\ T_{21} & T_{22} \end{bmatrix} \begin{bmatrix} p \\ u \end{bmatrix}_{z=-d} \tag{3.15}$$

where the pressures p and velocities u are known. To obtain the transmission coefficient, the four transfer matrix components, T_{11}, T_{12}, T_{21} and T_{22}, which determine how the sample reacts to sound, are needed. By making two sets of measurements, with different termination conditions at the right hand end of the tube, enough independent equations are generated to enable the matrix components to be solved:

$$\begin{bmatrix} p^r & p^o \\ u^r & u^o \end{bmatrix}_{z=0} = \begin{bmatrix} T_{11} & T_{12} \\ T_{21} & T_{22} \end{bmatrix} \begin{bmatrix} p^r & p^o \\ u^r & u^o \end{bmatrix}_{z=-d} \tag{3.16}$$

where a superscript r indicates the measurements with a rigid termination and o the measurements with the open end (roughly a pressure release case). It is vital that the termination impedances are very different across the frequency range of interest, or otherwise the additional equations derived will not be independent and the solution will become inaccurate. These sets of simultaneous equations can be solved to yield the transfer matrix elements.

These transfer matrix elements determine what happens to sound as it propagates through the test sample, but they involve velocities, and the transmission loss is defined purely in terms of a ratio of pressures. Consequently, some further work is needed to get the transmission loss from the matrix elements. The pressures at $z = 0$ and $z = -d$ from Equations 3.12 and 3.13 can be substituted into Equation 3.15. After some manipulation, it is possible to derive a new matrix which relates the pressure amplitudes in the system:

$$\tag{3.17}$$

$$\begin{bmatrix} A \\ B \end{bmatrix} = \begin{bmatrix} \frac{1}{2}\left(T_{11} + \frac{T_{12}}{\rho c} + \rho c T_{21} + T_{22}\right)e^{-jkd} & \frac{1}{2}\left(T_{11} - \frac{T_{12}}{\rho c} + \rho c T_{21} - T_{22}\right)e^{jkd} \\ \frac{1}{2}\left(T_{11} + \frac{T_{12}}{\rho c} - \rho c T_{21} - T_{22}\right)e^{-jkd} & \frac{1}{2}\left(T_{11} - \frac{T_{12}}{\rho c} - \rho c T_{21} + T_{22}\right)e^{jkd} \end{bmatrix} \begin{bmatrix} C \\ D \end{bmatrix}$$

This equation is true for any termination condition. From inspection of Figure 3.4, the transmission loss (*TL*) is given by $20 \log_{10}(|A/C|)$ which is easiest to work out when there is a perfect anechoic termination, in other words when $D = 0$. Consequently, the transmission loss is given by:

$$TL = 20 \log_{10} \left(\frac{1}{2} \left| T_{11} + \frac{T_{12}}{\rho c} + \rho c T_{21} + T_{22} \right| \right) \tag{3.18}$$

The above formulations are sufficient for carrying out the calculation, but with some algebraic manipulation, it is possible to derive a single equation for the transmission loss, which bypasses the need to explicitly calculate the transmission matrix elements. Equation 3.17 shows that it is possible to relate the pressure amplitudes by a simple matrix. Consider the amplitudes derived from the two different measurements in a matrix form:

$$\begin{bmatrix} A^r & A^o \\ B^r & B^o \end{bmatrix} = \begin{bmatrix} a_{11} & a_{12} \\ a_{21} & a_{22} \end{bmatrix} \begin{bmatrix} C^r & C^o \\ D^r & D^o \end{bmatrix} \tag{3.19}$$

where the superscripts denote the different measurement conditions. The element a_{11} gives the transmission loss (again, by considering the case $D = 0$). So by manipulating the simultaneous equations represented in Equation 3.19 it is possible to show that:

$$TL = 20 \log_{10}(a_{11}) = 20 \log_{10} \left(\frac{A^r D^o - A^o D^r}{C^r D^o - C^o D^r} \right) \tag{3.20}$$

So the transmission loss can be calculated directly from the pressure amplitudes under the different measurement conditions using this one formulation.

3.2 Two-microphone free field measurement

The disadvantage of the impedance tube is that it does not readily allow oblique incidence measurement. In contrast the two-microphone free field method allows this to be done. By its very nature, the test method needs a large sample, which can be difficult to produce. It also needs an anechoic or hemi-anechoic space for the measurement. This method, like the impedance tube, is of most use to porous absorber designers or modellers.

The method can be thought of as an extension of the transfer function, impedance tube method. Readers unfamiliar with the impedance tube method should read Section 3.1 before proceeding here. The technique is most straightforward for homogeneous, isotropic materials. Consider a large sample of absorbent being irradiated by a loud-speaker a long way from the surface as shown in Figure 3.5. The measurement can be done in an anechoic or hemi-anechoic chamber; it can even be done in a large room providing that time windowing is used to remove unwanted reflections from other boundaries. It is assumed that plane waves are incident on the surface. Furthermore, for
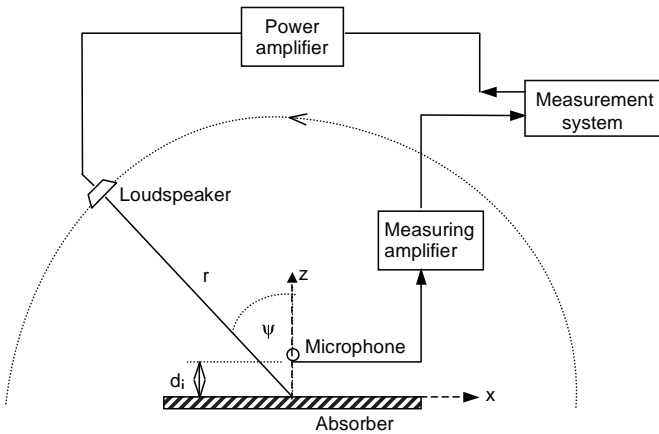
Figure 3.5 Experimental set-up for two- or multi-microphone free field measurement.

large isotropic, homogeneous samples, it can be assumed that the reflected sound is also a plane wave. In which case the equations set out in Section 3.1.2 for the transfer function measurement in the impedance tube can be applied directly to the free-field case.

Some practical details need careful consideration. Although in theory the sample should be infinite, in reality the sample will be finite in extent and so edge diffraction becomes important. The diffraction from the edges at low frequencies causes the reflected wave to no longer be planar, and so the simple theories no longer apply. A rough lower frequency limit is when half a wavelength fits across the smallest sample dimension. Consequently, samples are typically several square metres in area. When large samples are not available, one solution is to bring the source close to the surface, say 20 cm away, so the edge waves become less significant.[13] In which case, it is necessary to use spherical wave equations rather than the plane wave formulations given above. The drawback of using spherical wave formulations is that the interpretation of the measured impedance becomes less straightforward.

Returning to the plane wave case, the first microphone is typically 5 mm from the surface, and the second 15 mm from the surface; the lower and upper frequency limits discussed for the impedance tube related to microphone spacing are still relevant. The microphones must be small enough that they do not cause significant disturbance to the acoustic sound field. While it is possible to use two microphones, one microphone that is moved may be preferred as it disturbs the sound field less significantly than a microphone pair. It also removes the need for calibration. A deterministic test signal such as a maximum length sequence or swept sine must be used in this case.

The method can be extended to deal with oblique incidence, in which case the formulations should be re-derived. For an incident angle of ψ, the transfer function between the two microphones positions is given by:

$$H_{12} = \frac{e^{jkz_2\cos(\psi)} + \mathrm{R}e^{-jkz_2\cos(\psi)}}{e^{jkz_1\cos(\psi)} + \mathrm{R}e^{-jkz_1\cos(\psi)}} \qquad (3.21)$$

where it has been assumed that the two microphone positions have the same x and y displacement in the coordinate system defined in Figure 3.5. A rearrangement leads directly to the reflection coefficient:

$$R = \frac{H_{12}e^{jkz_1\cos(\psi)} - e^{jkz_2\cos(\psi)}}{e^{-jkz_2\cos(\psi)} - H_{12}e^{-jkz_1\cos(\psi)}} \tag{3.22}$$

The impedance can then be calculated using Equation 1.22 and from Equation 1.24 the absorption coefficient at that particular angle of incidence can be found.

Problems arise for large angles of incidence. As the angle of incidence increases, the effects of edge diffraction become more significant at higher frequencies. Consequently, very large angles of incidence are difficult to measure due to the effects of edge scattering unless very large sample sizes are available.

3.3 Multi-microphone techniques for non-isotropic, non-planar surfaces

For non-isotropic or non-planar surfaces, it is still possible to carry out a free field measurement using methods similar to those detailed in Section 3.2, although the system becomes more elaborate and rather sensitive to measurement error. The formulations for the two-microphone free field method have assumed that the dominant reflected wave is a plane wave, which is true for isotropic, homogeneous, infinitely large planar surfaces. As soon as the surface becomes rough, or there are impedance variations, then there is potential for non-plane wave propagation. For example, if a periodic impedance variation is considered, a set of grating or diffraction lobes in non-specular directions are generated. (See for example Figure 9.3, where the Schroeder diffuser generates 11 lobes.) To measure the absorption in the periodic case, it is necessary to measure the magnitude and phase of each of these reflected waves. This requires the measurement using more than two microphone positions, because there are additional unknowns – the magnitude and phase of each of the grating lobe waves – to be resolved. To measure the eleven propagating waves seen in Figure 9.3, 12 microphone positions would be needed. In reality, it is unlikely that this case could be measured, because multi-microphone systems become prone to measurement noise and errors,[14,15] as the number of microphones increases.

The next section details a multi-microphone method for surfaces with periodic impedance variation[14] to give an idea of how such a multi-microphone system might work. Although it is difficult to implement and get accurate measurements, it does enable incident angle dependent absorption to be measured.

3.3.1 Multi-microphone free field measurement for periodic surfaces

There will be multiple reflected waves, not just the plane waves considered in the two-microphone method. By using more than two microphone positions, it is possible to measure the amplitude and phase of these reflected waves. The set-up is shown in Figure 3.5. The pressure at the mth microphone, p_m measured at coordinates (x_m, z_m), is given by:

$$p_m(x_m, z_m) = P_i e^{j(-x_m k_x + z_m k_z)} + \sum_{n=-\infty}^{\infty} A_n e^{j(-x_m \beta_n - z_m \gamma_n)} \tag{3.23}$$

The first term on the right hand side is an incident plane wave p_i and the second term the scattered or reflected pressure. In this equation:

$$k_x = k \sin(\psi), k_z = k \cos(\psi); \beta_n = k_x + n\frac{2\pi}{W}, \gamma_n = -jk\sqrt{(\sin(\psi) + n\frac{\lambda}{W})^2 - 1}$$

A_n are complex coefficients describing each of the reflected waves; P_i is a constant; ψ is the incident angle; k is the wavenumber; λ is the wavelength; and W is the width of one period. The surface is periodic and (assumed) infinite so that a Fourier representation of the reflected sound field is used. Readers are referred to Chapter 7 for more details of the theory.

The scattered pressure is an infinite sum of waves, with complex coefficients A_n. Not all of these waves will propagate into the far field. The waves which are confined to the near field, the evanescent waves, need not be modelled, which means the sum over n is finite. The upper and lower limits for the sum in Equation 3.23 are determined by:

$$\left[\sin(\psi) + n\frac{\lambda}{W} \right]^2 \le 1 \tag{3.24}$$

Let the lower limit be denoted n_1 and the upper limit n_2; the number of coefficients to be determined must be small for this measurement to work.

The absorption coefficient is found by taking one minus the ratio of the reflected to incident energy, which gives:

$$\alpha(\psi) = 1 - \left| A_0 \Big/ P_i \right|^2 - \frac{1}{\cos(\psi)} \sum_{n=n_1, \neq 0}^{n_2} \left| A_n \Big/ P_i \right|^2 \sqrt{1 - (\sin(\psi) + n\lambda/W)^2} \tag{3.25}$$

When only the $n = 0$ term exists, then a two-microphone approach can be used as the only radiating wave is the plane wave term. When more than one term is present, $|n_1| \vee |n_2| > 0$ then more microphones are needed. In this case $N = (|n_1| + |n_2| + 2)$ points need to be measured since the transfer functions between two measured positions will be used.

In the data processing, it is convenient to use the transfer functions between adjacent measurement positions $H_{m,m+1} = p_m / p_{m+1}$:

$$H_{m,m+1} = \frac{p_m}{p_{m+1}} = \frac{P_i e^{j(-x_m k_x + z_m k_z)} + \sum_{n=n_1}^{n_2} A_n e^{j(-x_m \beta_n - z_m \gamma_n)}}{P_i e^{j(-x_{m+1} k_x + z_{m+1} k_z)} + \sum_{n=n_1}^{n_2} A_n e^{j(-x_{m+1} \beta_n - z_{m+1} \gamma_n)}} \tag{3.26}$$

This means a $N - 1$ set of simultaneous equations can be obtained in terms of A_n/P_i:

$$\sum_{n=n_1}^{n_2} (\frac{A_n}{P_i})(e^{j(-x_m\beta_n - z_m\gamma_n)} - H_{m,m+1}e^{j(-x_{m+1}\beta_n - z_{m+1}\gamma_n)}) \qquad (3.27)$$

$$= H_{m,m+1}e^{j(-x_{m+1}k_x + z_{m+1}k_z)} - e^{j(-x_m k_x + z_m k_z)}$$

Once the simultaneous equations have been formed, these can be solved to give A_n/P_i, which can be substituted into Equation 3.25, and gives the absorption coefficient after a little manipulation.

The choice of measurement positions is critical. If the microphone is only allowed to traverse the z direction, then critical frequencies occur where there are insufficient unique simultaneous equations to resolve the coefficients. These critical frequencies manifest themselves as frequencies for which nonsensical absorption coefficients are obtained. These critical frequencies can be avoided by changing the microphone position in z and x. The typical spacings used give microphones 5–10 cm apart.

The multi-microphone method is very sensitive to evanescent (non-propagating) waves. The microphone must be far enough away from the sample to prevent the measurement of evanescent waves, as these have been neglected in the above theories, but if the microphone is too far from the surface, diffraction from the sample edges will cause the measured pressures to be inaccurate. The multi-microphone method is much more noise sensitive than the two-microphone method. Very accurate microphone positioning is needed. Others looking at multiple microphone techniques have found similar noise sensitivity.[15]

Figure 7.11 shows an example measurement result. It is compared to two prediction models. Good accuracy is achieved with the multi-microphone measurement system in this case. At low frequencies only two microphone positions are used as there is only one plane wave reflection. At mid-high frequencies three microphone positions are needed as an additional reflected wave is present.

3.4 Reverberation chamber method

In most applications, the sound will be incident on an absorptive material from a multitude of incident angles at once. It is not efficient to laboriously measure the absorption coefficients for all angles of incidence in the free field and reconstruct these into a random incidence absorption coefficient (although this can be done, as is discussed in Chapter 12). Consequently, a quicker method is needed, and this is afforded by the reverberation chamber method.[16] The random incidence absorption coefficient is the parameter used most in the design of spaces to specify the absorption performance of materials. It is well known and defined; however, it is notoriously difficult to predict. So while the random incidence absorption coefficient is needed to enable room design, it is not very useful for those interested in validating prediction models.

The reverberation chamber test requires large sample sizes and a specialist test room, and so is expensive to undertake. It also only gives absorption coefficients; the impedance cannot be measured. Consequently, developers of absorptive materials will often use the impedance tube to build up an understanding of the material properties on small samples, before undertaking reverberation tests.

The reverberation time of a room is dependent on the total absorption in the room

– see Equation 1.1. Consequently, by measuring the reverberation time of a room before and after a sample of absorbent is introduced, it is possible to calculate the random incidence absorption coefficient. It is necessary to have defined acoustic conditions for the test, and the normal technique is to try and generate a diffuse field. A diffuse field can be roughly defined as requiring the reflected sound energy to be the same across the whole room and the energy to be propagating evenly in all directions. To achieve this, reverberation chambers often use diffusers in the volume of the room, and the chamber walls are often skewed (splayed). Furthermore, the room should be of a certain minimum size, and room dimensions should be irrationally related to reduce the influence of room modes. The minimum requirements are given in the appropriate standard.[16]

Despite these measures, a diffuse field is not completely achieved, and consequently the reverberation time is position dependent. For this reason, it is normal to use multiple source and receiver positions and to average the results to reduce the effect of non-diffuseness. The source is normally placed in the corner of a room, pointing into the corner, because it maximally excites the modes of the room and reduces the amount of direct radiation from the loudspeaker to the test sample. Receivers should be at least 1 m from the room boundaries, room diffusers and the sample, and should be chosen to obtain a diverse sampling of the room volume. Even with all these measures, the measured absorption coefficients are often more inaccurate at low than high frequencies due to modal effects.

The reverberation time before the sample is introduced is given by:

$$T_0 = \frac{55.3V}{c\alpha_0 S + 4Vm_1} \tag{3.28}$$

where V is the room volume, c the speed of sound, α_0 the average absorption coefficient of the empty room and S the surface area of the room. m_1 allows for air absorption in the room and typical values are shown in Table 3.1.

Table 3.1 Air absorption constant m_1 at 20°C and normal atmospheric pressure in 10^{-3} m^{-1}

Relative humidity (%)	Frequency (Hz)							
	63	125	250	500	1000	2000	4000	8000
20	0.06	0.16	0.32	0.6	1.5	4.96	17.2	50
30	0.044	0.14	0.33	0.58	1.15	3.25	11.26	38.76
40	0.035	0.12	0.32	0.6	1.07	2.58	8.39	29.94
50	0.028	0.1	0.3	0.63	1.07	2.28	6.83	24.24
60	0.024	0.088	0.28	0.64	1.11	2.14	5.9	20.48
70	0.021	0.077	0.26	0.64	1.15	2.08	5.32	17.88

Complete formulations for air attenuation can be found in ISO 9613-2.[17]

The reverberation time after the sample is introduced is given by:

$$T_1 = \frac{55.3V}{c(\alpha_0[S - S_s] + \alpha_s S_s) + 4Vm_1} \tag{3.29}$$

where S_s is the surface area and α_s the absorption coefficient of the sample. By rearranging Equations 3.28 and 3.29 it is possible to obtain the absorption coefficient of the sample. If ISO 354:1985 is followed, the factor $[S - S_s]$ is approximated to S, which simplifies the end formulation.

The current standards are based on Sabine's formulations as used above. It is well known that this equation becomes inaccurate for large absorption coefficients, in which cases other formulations like the ones derived by Eyring and Millington can be used (these were given in Equations 1.5 and 1.6). Indeed, Chapter 12 discusses how some geometric room acoustic modellers are advocating the use of alternative reverberation time formulations to give better room predictions. While it can be argued that using other reverberation time formulations produces more correct answers, the databases of absorption coefficients available to designers have been derived from Sabine's formulation. Consequently, while it is known that Sabine's equation produces systematic (or bias) errors, it continues to be industry practice to use this approach. Appendix A gives a table of typical measured absorption coefficients for common materials.

The reverberation times can be measured by interrupted noise, maximum length sequences or swept sine waves. Maximum length sequences allow rapid measurement, but problems in getting sufficiently long decays can arise due to non-linearities in loudspeakers.[18]

To get an accurate measurement, it is necessary to have a big difference between T_0 and T_1. This necessitates a large sample area of 10–12 m². Even with such a large sample, the accuracy is compromised due to edge effects. Sound is diffracted around the edges of the sample, which usually leads to excess absorption. It is normal practice to cover the edges of the sample and to use rectangular samples to reduce edge effects. Nevertheless, even with the edges covered, absorption coefficients greater than 1 can be measured. Chapter 12 discusses this further, including how these edge effects might be compensated for in real room predictions.

It is also possible to measure discrete objects, for example people. They are arranged randomly around the room, and a total absorption per object calculated from the reverberation times.

Given the standard deviations of the reverberation times T_0 and T_1, it is possible to calculate the random experimental error. The standard deviations are calculated from the set of reverberation times for all source and receiver combinations. If the standard deviation of the reverberation time measure T_0 is σ_0, then the 95 per cent confidence limit is given by:

$$\delta_0 = \frac{2\sigma_0}{\sqrt{n}} \tag{3.30}$$

where n is the number of source and receiver pairs. (It is assumed that n is sufficiently large that two standard errors is equivalent to the 95 per cent confidence limit.) A similar relationship exists for T_1. The accuracy (95 per cent confidence limit) of the empty room average absorption coefficient is given by:

$$\delta_{\alpha_0} = \left| \frac{55.3V}{cT_0^2 S_0} \right| \delta_0 \tag{3.31}$$

where the effect of inaccurate estimation of air absorption has been assumed to be smaller than the effect of reverberation time variation between measurement positions. The accuracy of sample absorption is given by:

$$\delta_{\alpha_s} = \sqrt{\left|\frac{55.3V}{cT_1^2 S_s}\right|^2 \delta_1^2 + \left(\frac{c[S_0 - S_s](\delta\alpha_0)^2}{S_s}\right)^2}$$

(3.32)

While good repeatability within a laboratory can be achieved, there are reproducibility problems between laboratories. The measured absorption coefficients can vary greatly from laboratory to laboratory. Figure 3.6 shows the average absorption coefficient for an identical fibreglass sample measured in 24 reverberation chambers. The error bars indicate the 95 per cent confidence limits in one of the laboratory measurements. To explain this figure further, when the sample was sent to one laboratory, 95 per cent of the time the absorption coefficient would be within ±0.2 of the mean value at 1 kHz. This indicates that the absorption coefficients could vary by as much as 0.4 between two different laboratories, a huge error in the absorption coefficient.

The reverberation chamber method can also be used to measure single items.[16] Sakagami *et al.*[19] detail a method for measuring absorbents hung in the reverberation chamber, as might happen in the case where a porous absorbent is hung in a factory to reduce reverberant noise levels.

Chapter 12 takes the discussion of random incidence absorption coefficients further, examining how the values measured in laboratories are used in predictions, including their use in geometric room models. The chapter also quantifies the effects of edge absorption and sample size. Seating is a common absorbent with very significant edge absorption, and the measurement of this particular surface is dealt with in the next section.
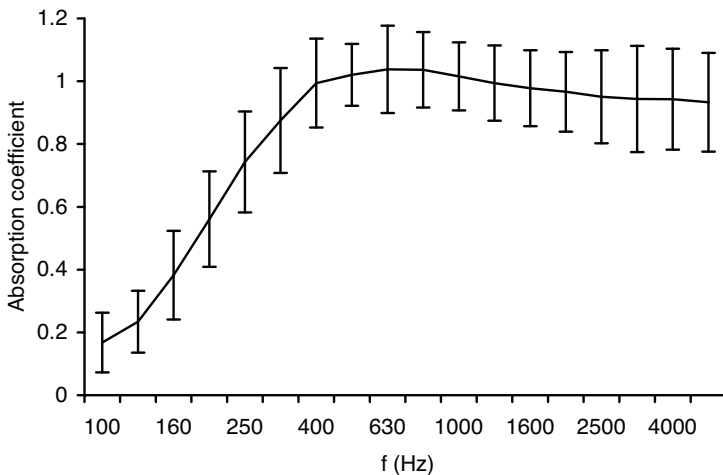
Figure 3.6 Comparison of measured absorption coefficients for a single sample in 24 laboratories. The mean absorption coefficient across all laboratories is shown, along with error bars indicating the 95 percent confidence limit in any one laboratory measurement.

3.4.1 Measurement of seating absorption

The reverberation time in a concert hall is dominated by the absorption of the seating and audience and it is essential that these can be measured or predicted accurately in the early stages of design. The wrong estimation of seating absorption has been blamed for acoustic problems in many halls, and consequently a measurement procedure is given here. Davies *et al.*[20] compared seating absorption coefficients in a reverberation chamber and in concert halls for 10 different cases, and showed that the Kath and Kuhl method[21] is best for estimating seating absorption in a real hall. Beranek[22] showed that it is best to calculate seating absorption coefficients based on absorption per unit floor area rather than by absorption per seat.

The aim of measuring the random incidence absorption coefficients of a small sample of seats in a reverberation chamber is to predict the total absorption that a larger area of the same seats will exhibit when installed in an auditorium. There are problems, however, because the small sample of chairs in the reverberation chamber (say 24), is unrepresentative of the larger block of seating in the auditorium, because edge effects are overemphasized in the reverberation chamber measurements.

The Kath and Kuhl method involves placing the seating in the corner of the reverberation chamber in rows with their intended row spacing. The exposed edges are obscured with barriers for some of the measurements. The barriers need to be massive and stiff to reduce low frequency absorption. The barriers should be at least as high as the seating, and higher if any audience is present for an occupied measurement. Excessive extra height (say, more than 100 mm above the top of the seating for the unoccupied case) should be avoided. The set up is schematically shown in Figure 3.7. Though it seems that the array is mirrored in the adjacent walls of the chamber, thus effectively increasing its size, it is not effectively infinite as Kath and Kuhl suggested. Diffraction effects will still be present and so the measured absorption coefficient may still vary with sample size.

The concept is to separately measure three absorption coefficients by carrying out measurements with and without barriers. The measurements are:

- for an infinite array with no edges, yields an absorption coefficient α_∞, with side and front barriers in place;
- for the front edges, α_f, by measuring with the side barrier only in place and combining the result for α_∞; and
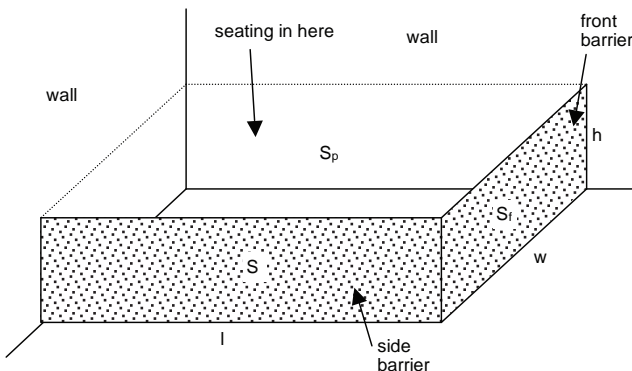
Figure 3.7 Set-up for the Kath and Kuhl method for measuring seating absorption.

- for the side edges, α_s, by measuring with the front barrier only in place, and combining with the result for α_∞.

Then in the hall, if the areas of the front edges S_f, side edges S_s and plan area S_p are known, the absorption coefficient of the audience block is given by:

$$\alpha = \alpha_\infty + \alpha_f \frac{S_f}{S_p} + \alpha_s \frac{S_s}{S_p} \qquad (3.33)$$

In the reverberation chamber the absorption coefficients α_∞, α_f, and α_s are determined by the following formulations. First with both the front and side barriers in place the infinite array absorption coefficient is obtained:

$$\alpha_\infty = \frac{A_1}{(l + \lambda/8)(w + \lambda/8)} \qquad (3.34)$$

where A_1 is the total absorption of the sample with both barriers in place, and the $\lambda/8$ terms correct for pressure doubling at the chamber walls, where λ is the wavelength of the centre frequency in the octave band.

With an additional measurement of the total absorption A_2 with the front barrier missing, the absorption of the front edge is determined.

$$\alpha_f = \frac{A_2 - A_1}{h(w + \lambda/8)} \qquad (3.35)$$

Finally, with an additional measurement of the total absorption with the side barrier missing A_3, the absorption of the side edge is determined.

$$\alpha_s = \frac{A_3 - A_1}{h(l + \lambda/8)} \qquad (3.36)$$

The corner placing of the seats is advantageous because it increases the effective size of the array. However, there is a disadvantage: the pressure in a reverberant field is increased at the boundaries,[23] so the absorption coefficients measured will be higher than those found when the sample is in the centre of the chamber. To compensate for this, Kath and Kuhl proposed[24] that the absorber areas used in the calculations should be increased by strips of width $\lambda/8$. This extra absorbing area accounts for the increase in measured total absorption due to the increase of up to 3 dB in sound pressure level close to the wall. In a corner, there is an increase of up to 6 dB, and a correction of $(\lambda/8)^2$ is needed. This is the reason for the extra terms in the denominators of the above formulations.

Figure 3.8 shows a comparison of the measured absorption coefficient in the auditorium and a prediction from the reverberation chamber results. Good prediction accuracy is achieved for this case. Discrepancies found by Davies *et al.*[20] for other halls
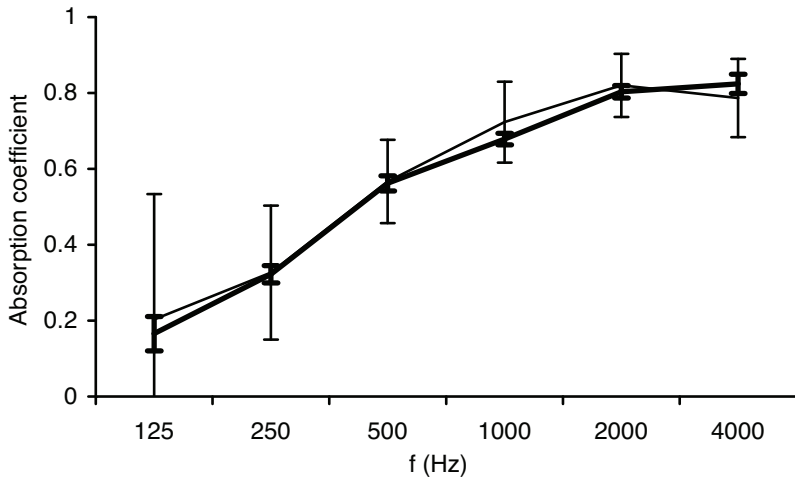
Figure 3.8 Random incidence absorption coefficient measured in an auditorium com-
        pared to a prediction based on a Kath and Kuhl reverberation chamber meas-
        urement.
        ——— prediction for full auditorium seating based on reverberation chamber
        measurement; and
        ——— full auditorium measurement (data from Davies *et al.*[20]).

were likely to be due to the non-diffuseness of the auditoria and indefinable changes
in the hall between the without and with seating measurements.

Bradley[25] also suggested a seating absorption measurement method which attempts to
take account of the variation of seating absorption with sample size. This involves making
measurements on five or six differently sized arrays of seats and then extrapolating to
the expected absorption for large seating blocks in auditoria. Although this is accurate,
it requires more tests than the above method.

3.5 *In situ* measurement of absorptive properties

There is great interest in being able to measure the absorption coefficient and surface
impedance of products *in situ*. To take one example, in geometric room acoustic models
the absorption coefficients of surfaces are required, but how can these be determined if
the room is already built? It is for this sort of problem that *in situ* techniques have been
developed. Indeed, *in situ* techniques for absorption measurement can be traced back
as far as 1934.[26] For those interested in the historical context of *in situ* measurement,
the paper by Nocke and Mellert[26] gives a comprehensive reference list of the important
literature.

One possible technique is to use the two-microphone free field method outlined in
Section 3.2. If the surface to be tested is large, homogeneous, isotropic and planar,
and the unwanted reflections from other surfaces can be removed by time gating
(windowing), then this process has been shown to work and give accurate results.[27]
This process will fail if the unwanted reflections cannot be removed, or non-plane wave
reflections are significant, which might arise if the surface is too small, or if the surface
to be tested is inhomogeneous.
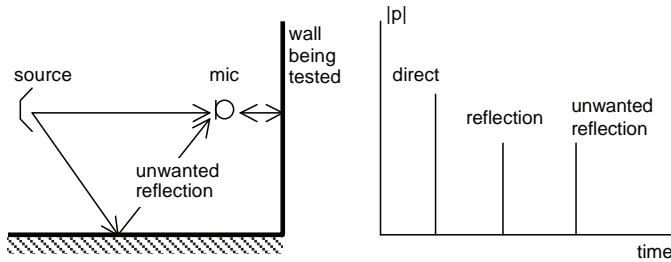
Figure 3.9 Measurement of *in situ* absorption properties using time gating.

Other techniques try to separate the incident and reflected sound from a surface by arrival times. This is schematically shown in Figure 3.9. An impulse response is measured and the reflected and incident sound isolated by applying rectangular windows. From this the reflection coefficient is calculated. To achieve this, however, requires considerable distance between the microphone and the surface, which means that problems often arise because of edge reflections from the test surface and unwanted reflections from other surfaces. Very large surfaces are needed otherwise there is poor accuracy at low frequencies. Consequently, while this technique is potentially accurate, its range of applicability is limited.

A more promising technique was developed by Mommertz,[28,29] as this exploits a subtraction technique which enables the microphone to be placed close to the test surface. The technique appears in standards concerning measuring noise barriers[30] and road surfaces.[31] This allows measurement from 250 Hz to 8 kHz for normal incidence on plane surfaces greater than 4 m². The low frequency accuracy is compromised for oblique incidence or smaller samples. The test arrangement is shown in Figure 3.9. The sound source is connected to the microphone by an anchored tube to ensure that the distance between the source and microphone remains constant. Precise positioning is vital if the measurement method is to be accurate. The impulse response between the source and microphone is measured with the microphone close to the test surface, and separately in the free field. These two impulses can be subtracted, which leaves the reflected sound and unwanted interfering reflections; these parasitic reflections can be removed by time windowing. To allow the subtraction, a deterministic test signal such as a maximum length sequence or swept sine must be used.

Placing the microphone very close to the surface ensures that the interfering reflections are maximally spaced from the wanted reflections, consequently allowing more accurate measurements. By de-convolving the loudspeaker's free field impulse response from the *in situ* measured impulse response, the length of the direct and reflected sound in the impulse responses can be shortened. This can help make the gating process more accurate. Mommertz advocates doing this de-convolution by pre-emphasizing the test signal – an approximate inverse of the loudspeaker impulse response is used to pre-filter the maximum length sequence before it is sent to the loudspeaker. Alternatively, this de-convolution could be done as part of the post-processing before the windows are applied. If overlap still exists between the wanted and parasitic reflections, then a window with a smooth transition should be used, like a half-Hanning.

If the microphone is very close to the surface, a simple ratio of the reflected and incident spectra can be taken to give the complex pressure reflection coefficient, and
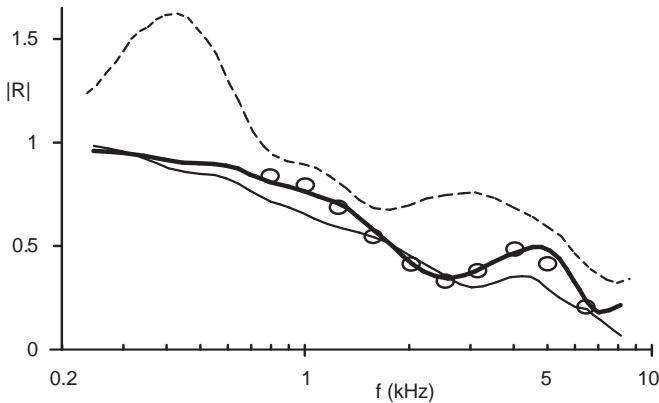
Figure 3.10 Measurements of reflection coefficient magnitude. *In situ* method:
———— $\psi=0°$;
——— $\psi=45°$;
– – – $\psi=81°$; and
○   Standing wave tube method (data from Mommertz[29]).

from there absorption coefficients and surface impedance. If the microphone is not close to the surface, a correction for spherical spreading and propagation phase must be made to the incident and reflected spectra before the ratio is taken.

Figure 3.10 shows a typical result. For normal incidence, the reflection coefficients of the sample obtained using the *in situ* method match those obtained using a standing wave method in an impedance tube. For oblique incidence and at low frequencies (<800 Hz), the method fails with the reflection coefficient exceeding 1. This occurs because there is an implicit assumption of plane waves in the methodology. At low frequencies, the edges of the test sample create other types of reflected waves, which then render the technique inaccurate. One solution to this is to consider spherical wave reflection.[32]

Problems arise with this *in situ* method if the acoustic medium changes between the free field and sample measurement. For instance, Mommertz gives an example of a temperature change of 1°C leading to an error of 0.03 in absorption coefficient.

The final *in situ* method detailed uses an alternative approach. No attempt is made to separate the incident and reflected sound; this removes some of the geometric restrictions on the measurement system. To make it work accurately, however, requires a good theoretical model of the sound field close to the test surface. The idea of the method is as follows: given measurements of the sound field in the vicinity of the test surface and a theoretical model for the sound propagation, it is possible to apply a numerical optimization or root finding scheme to derive the unknown properties of the test sample.

Figure 3.11 shows a typical set-up used by Nocke.[33] The transfer function between the source and receiver is measured, and from this the angle dependent impedance and absorption coefficient is derived by numeric inversion.

To simplify the description, consider a plane homogeneous sample. The pressure above the absorber is given by:

$$p(\mathbf{r}) = p_i(\mathbf{r}) - F(k, \mathbf{r}, \mathbf{r}_0, R(\mathbf{r}_s), p_i(\mathbf{r}_s)) \tag{3.37}$$
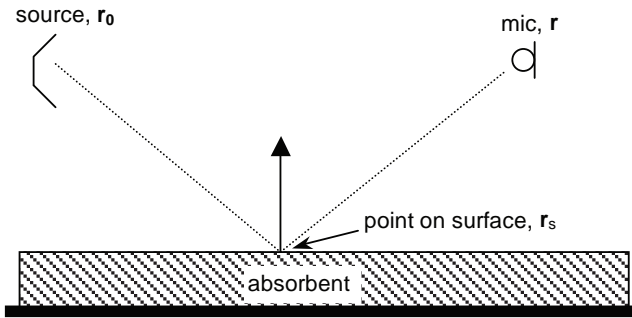
Figure 3.11 Typical set-up for *in situ* measurement (after Nocke[33]).

where $p_i(\mathbf{r})$ is the pressure direct from the source to the receiver; $\mathbf{r}$ is the receiver position; $\mathbf{r}_o$ is the source position; $\mathbf{r}_s$ is the position of a point on the surface; F() is a function which gives the pressure at the microphone due to reflections from the surface; k is the wavenumber, and R is the surface reflection coefficient.

There are various prediction theories that can be used to model the function F() which gives the reflected energy. For instance, it would be possible to use the theories outlined in Chapter 8. Nocke advocates using a spherical wave reflection theory – see Chapter 1. It would also be possible (and easier) to use simple plane wave formulations provided the surface is large so that edge diffraction is not significant and the source is not too close to the surface so the incident wave can be considered to be plane.

Given that the incident and reflected pressures have been measured and that the receiver and source positions given in Equation 3.37 are known, the only unknown in the equation is the complex reflection coefficient R, as a function of the vector on the surface $\mathbf{r}_s$. This reflection coefficient can therefore be found by using an iterative procedure. For simplicity, assume that R is the same for the whole surface. If the measured pressure is $p_m(\mathbf{r})$ and the predicted pressure $p(\mathbf{r})$, then a numerical optimizer can be tasked with the procedure of minimizing the mean square error between the measured and predicted pressures, $| p_m(\mathbf{r}) - p(\mathbf{r})|^2$ by finding the value of R which gives minimal error. There are a variety of numerical optimization methods that can be used for this process, such as genetic algorithms.

However, Taherzadeh and Attenborough[34] found numerical optimization formulated this way was rather slow when calculating the impedance of the ground from excess attenuation measurements, because spherical wave reflection coefficients must be used for the typical measurement geometries used. They advocated the use of a root-finding algorithm, which is more efficient because it exploits the Newton Raphson algorithm, using calculated derivates. This efficient formulation reduces computation time vastly.

Whichever numerical process is used, there is a risk of finding the wrong solution, because the measured pressures do not always map to a single unique reflection coefficient. A simple solution to this is to make measurements with a couple of different geometries to ensure the correct answer is found. In theory, this could work for samples where R varies across the surface. As a number of different surface reflection coefficients have to be derived, more microphone positions are needed. In this case,

the optimization problem becomes slower to solve and the risk of getting incorrect solutions from the optimizer increases. The experience with multiple microphone techniques is that the more receiver positions, the more problems with noise sensitivity and evanescent waves. Consequently, it might be anticipated that resolving a large number of different surface reflection coefficients might prove to be problematical.

Nocke[33] restricts himself to deriving an average absorption coefficient for inhomogeneous surfaces. Figure 3.12 shows a typical result showing the *in situ* method compared to impedance tube measurements. By using the spherical wave formulation, accurate results are achieved down to 80 Hz, but this requires a very large sample of 16 m² to prevent edge effects being significant. The upper frequency limit measured was 4 kHz, presumably limited by the accuracy of the microphone positioning. Kruse[35] examined the method for typical ground surfaces and found the results to be inaccurate below about 400 Hz and for hard ground. More measurements utilizing different geometries are needed to overcome these problems.
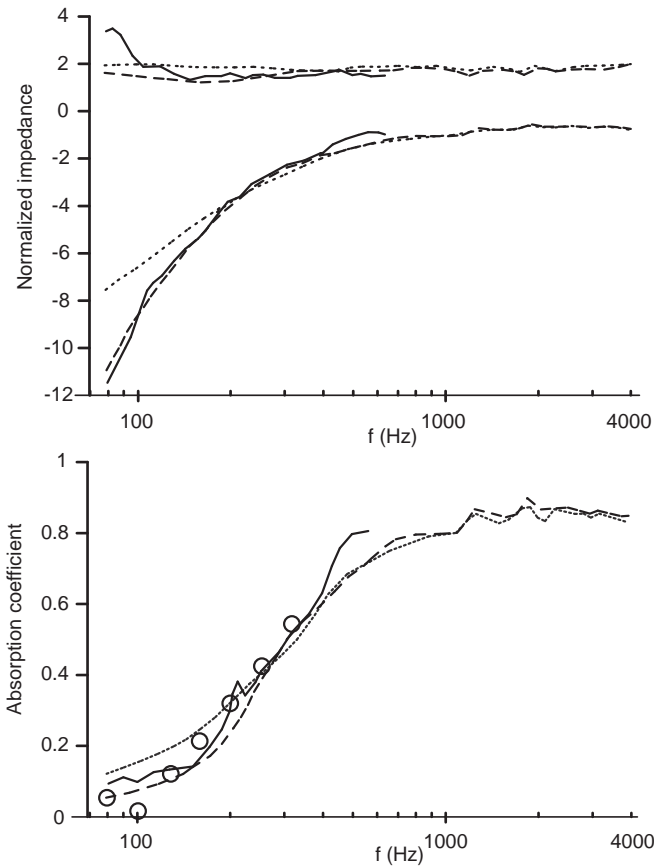
Figure 3.12   Comparison of *in situ* and impedance tube measurements for a fibrous absorber:
———— impedance tube A;
○   impedance tube B (on absorption coefficient graph only);
– – – *in situ* $\psi = 10°$; and
······ *in situ* $\psi = 12°$ (data from Nocke[33]).

3.6 Measurement of internal properties of porous absorbents

The remaining sections of the chapter are devoted to the measurement of properties within absorbents, characterizing the sound propagation within the porous materials either in terms of propagation constants and characteristic impedances or finding key parameters, such as flow resistivity, tortuosity, porosity and characteristic lengths. These are key measurements for those involved in the development or modelling of porous materials.

3.6.1 Flow resistivity

The flow resistivity of a porous absorber is one of the most important defining characteristics. Once the flow resistivity is known, simple empirical models can be used to find the characteristic impedance and wavenumber, and from there, the surface impedance and absorption coefficient can be obtained. The importance of this parameter is discussed in more detail in Chapter 5. For now, three techniques for measurement will be considered. These are the preferred techniques, because they are non-acoustic and so are the most robust approaches.

The measurement techniques presented here follow directly from the definition of flow resistivity. Consider a slice of the porous material of thickness d subject to a mean steady flow velocity U. The pressure drop across the sample ΔP is measured, and from these quantities the flow resistivity σ is given by:

$$\sigma = \frac{\Delta P}{Ud} \qquad (3.38)$$

The measurement of flow resistivity has been enshrined into International Standards,[36] where more details of the procedure can be found. In the direct flow method, a steady air supply pushes air through the porous material. Sensors are used to measure the air flow and pressure drop to atmospheric pressure, and hence the flow resistivity is obtained. This is shown in Figure 3.13.
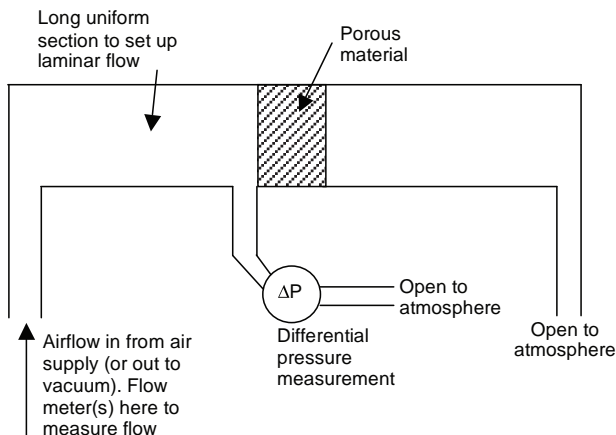
Figure 3.13 Set-up for direct airflow method for measuring flow resistivity.

It is important that flow rates are kept small because otherwise the relationship between the pressure drop and velocity become non-linear. Flow rates between 5×10^{-4} and 5×10^{-2} ms^{-1} are recommended by Bies and Hansen.[37] Ingard[38] produces results that show that the flow rate should not be greater than 0.1 ms^{-1} to get results consistent with the velocity amplitude of typical sound waves in absorbents (0.01 ms^{-1}). (However, note that at this flow rate, the flow resistivity varies with flow rate following either a linear[39] or quadratic relationship.[40]) The flow resistivity is calculated from:

$$\sigma = \frac{\rho_0 \Delta P A}{md} \tag{3.39}$$

where ρ_0 is the density of air, A is the cross-sectional area of the specimen and m the air mass flow rate (kgs^{-1}).

In the alternative airflow method, a piston is used to generate a low frequency, alternating airflow through the test specimen; the piston should move at a frequency of $f = 2$ Hz. The set up is shown in Figure 3.14. The rms (root mean square) airflow velocity is then:

$$u_{rms} = \frac{\pi f h A_p}{\sqrt{2} A} \tag{3.40}$$

where h is the peak-peak displacement of the piston, A_p the cross-sectional area of the piston, and A the cross-sectional area of the porous material. The standard recommends 0.5 mms^{-1} $<u_{rms}<4$ mms^{-1}. A condenser microphone is used to measure the rms pressure relative to atmospheric pressure.

The problem with these experimental techniques is that there is a great variation between results from different laboratories. Garai and Pompoli[41] found that repeatability within a laboratory is good, with an error of about 2.5 per cent with repeat measurements on one sample and about 5 per cent with five samples cut from the same material. Reproducibility between laboratories, on the other hand, is a problem with errors around 15 per cent.

There are alternative methods for obtaining the flow resistance. Ingard[38] devised a measurement system which does not require blowers and flow instrumentation and so greatly simplifies the apparatus required. The set up is shown in Figure 3.15. A piston
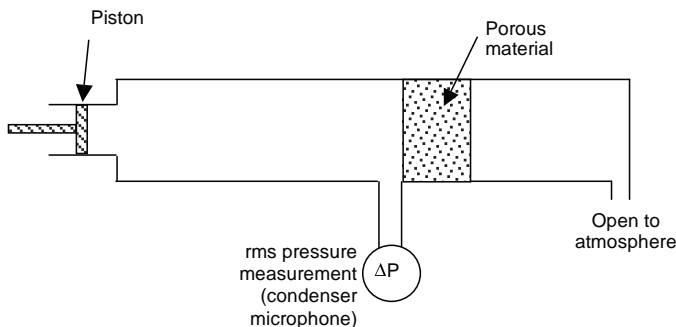
Figure 3.14   Set-up for alternating airflow method for measuring flow resistivity.
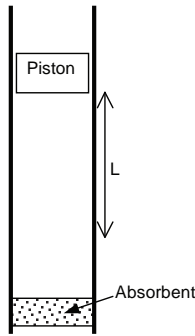
Figure 3.15 Set-up for Ingard's method for measuring flow resistivity.

within a tube falls under gravity and pushes air through the porous absorbent. When the piston has reached terminal velocity, the pressure drop ΔP across the sample is given by:

$$\Delta P = \frac{Mg}{A_p} \tag{3.41}$$

where M is the mass of the piston, g is the acceleration due to gravity and A_p the cross-sectional area of the piston or tube. The flow velocity U is given by:

$$U = \frac{A_p}{S_s} v \tag{3.42}$$

where S_s is the cross-sectional area of the sample, and v is the terminal velocity of the piston found by timing how long it takes the piston to travel a set length. Equations 3.41 and 3.42 can be combined with Equation 3.38 to give the flow resistivity. It is first necessary, however, to carry out two calibration measurements. There will be frictional forces between the piston and the tube walls, and there will be leakage between the piston and the tube wall. Consequently, it is necessary to calibrate for these; in total, three timed falls of the piston are made as summarized in Table 3.2.

Table 3.2 Measurements needed for flow resistivity measurement using falling piston method

Time measured	Condition
t	Sample in tube, both ends of tube open
t_0	No sample in tube, both ends of tube open
t_1	No sample in tube, one end of tube closed (either end)

The time taken for the piston to fall in the tube with no sample over a set length is measured in two cases. First with the tube open, t_0, and second with one end of the tube closed (it does not matter which), t_1. Then a calibration factor is found:

$$C = \frac{1 - t_0 / t}{1 - t / t_1} \tag{3.43}$$

where t is the time it takes the piston to drop over the same measurement distance L with the sample present. Then the flow resistance is then given by:

$$\sigma = \frac{CMg \cos(\psi) S_s t}{L A_p^2} \tag{3.44}$$

where ψ is the angle of the tube to the vertical.

Ingard[38] reports using a tube with an inner diameter of 0.08 m, a length of 1.2 m and $L = 0.6$ m. The piston was 264 g and 10 cm long. The gap between the cylinder and the tube wall was about 0.2 mm. The system does not work for materials with very small or large flow resistivities due to problems with accurate timing and calibration.

3.6.2 Flow impedance

Strictly speaking, porous materials are not just resistive but contain some reactance as well.[38] The reactance comes from additional mass due to viscous boundary layer effects and constrained flow. Consequently, while Section 3.6.1 has given methods for flow resistance, there could be interest in measuring the flow impedance to get the reactance. As the resistive term dominates, this type of measurement is not that commonly undertaken. While these methods give alternative methods for measuring the flow resistivity, they are not the most independent and robust, because they use sound waves.

This flow impedance is measured within an impedance tube.[42] Figure 3.16 shows an arrangement that can be used; the tube is about 5 cm in diameter. A pure tone plane wave is produced by the sound source. The frequency is adjusted so that the distance w is an odd integer multiple of a quarter of a wavelength:

$$w = n\lambda / 4 \tag{3.45}$$
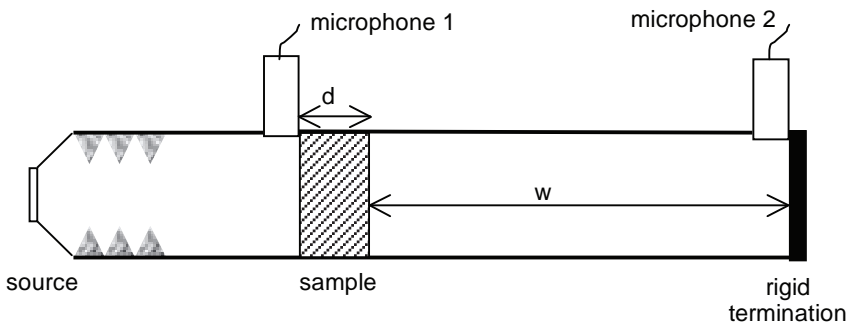
Figure 3.16   Apparatus for determining flow impedance using an impedance tube (after Ingard and Dear[42]).

where n is the number of quarter wavelengths in the length w and n must be odd. There are an infinite set of frequencies which satisfy this condition, but a low frequency (say less than 100 Hz) is needed to get accurate results, as the sample should be thin compared to wavelength. This forces the pressure and surface impedance at the rear of the sample to be zero. The flow impedance z_f is then a ratio of the pressures measured at microphones 1 and 2:

$$z_f = j\rho_0 c_0 (-1)^{(n-1)/2} \frac{p_1}{p_2}$$
(3.46)

where p_1 and p_2 are the complex pressures for microphones 1 and 2. This formulation can be derived as follows. As the impedance at the rear of the sample is zero, the flow impedance equals the difference in the pressures on either side of the sample divided by the particle velocity (which should be the same on both sides of the sample). This impedance can be derived, using the transfer matrix method outlined in Section 1.5.1. The calculation yields a complex impedance, of which the real part is the flow resistance and the imaginary part the flow reactance (the latter is generally small).

Others have also produced variants on this type of measurement.[43] Section 3.1.4 detailed a method for measuring the transmission through a sample using: an impedance tube; four microphones, and two different tube terminations (see Figure 3.4). Once the transmission matrix coefficients in Equation 3.15 are known, it is possible to calculate the pressure difference across the sample by considering the case $p(z=-d) = 0$ at low frequency. Provided the sample is thin compared to wavelength, the flow impedance is given by T_{12}.

It is also possible to derive the flow resistivity from the effective density, which can be found in impedance tube measurements[44] and reasonable accuracy[45] ($\approx$20 per cent) can be obtained. However, this method is not as independent as the techniques outlined in Section 3.6.1, so if possible, methods which do not use sound waves should be used.

3.6.3 Direct measurement of wavenumber

The wavenumber (or propagation constant) for a porous medium can be directly measured.[46] It is a crucial parameter describing how sound propagates in a medium and was defined in Section 1.4.1. The direct measurement process is rather slow, but accurate and robust. An impedance tube is filled with the material to be tested. A loudspeaker at one end of the tube generates sound waves, which propagate through the absorbent. If it is assumed that no reflection happens from the opposite end of the tube from the loudspeaker, the steady state pressure in the tube is given by:

$$p = Ae^{-jkz}$$
(3.47)

where z is the distance along the tube, and A is a constant. As the wavenumber k is complex, this can be rewritten as:

$$p = Ae^{\mathrm{Im}(k)z}e^{-j\mathrm{Re}(k)z}$$
(3.48)

By measuring the decay in the amplitude of the sound wave and plotting the log of the amplitude versus distance, the imaginary part of the wavenumber can be obtained.

Measuring the changing phase of the sound wave and plotting another log-linear graph yields the real part of the wavenumber.

It is necessary to ensure there are no reflections from the tube end remote from the loudspeaker. This necessitates a long length of absorbent to ensure full absorption – it is not sufficient just to leave the end of the tube open. Typically 0.5 m of the test absorbent might be used, followed by another 0.5 m of loosely packed porous absorber such as mineral wool to give an anechoic termination.

The sensing microphone must be placed in the bulk of the absorbent in the tube and this can be achieved by using a probe tube microphone similar to that shown in Figure 3.1. The probe tube moves within a hole pre-drilled through the centre of the absorbent material.

3.6.4 Inverse methods for wavenumber and characteristic impedance

Given a theoretical model for the propagation of sound in a porous absorbent and some measurements on a simple experimental set up, it is possible to derive the wavenumber and the characteristic impedance of porous absorbers.[47–49] For example, a numerical fit can be carried out between the experimental data and the theoretical model to find values for unknown parameters in the theoretical model. Such a technique is similar to that used for *in situ* measurements discussed at the end of Section 3.5 and is also used to gain other porous parameters, such as tortuosity as discussed in Section 3.6.8. There are various arrangements that can be used for this measurement. The most convenient methods are probably those that use the impedance tube, as this is more readily available in laboratories. The advantage of these methods over the direct measurement of wavenumber described in Section 3.6.3 is that it is faster and it yields the characteristic impedance, as well as the wavenumber.

Smith and Parrott[47] review two possible methods, of which the two thicknesses method is most convenient and so will be described here. The surface impedance is measured for two different thicknesses of the absorbent with a rigid backing. For a thickness of d_1, the surface impedance is z_1:

$$z_1 = -jz_c \cot(kd_1) \tag{3.49}$$

where z_c is the characteristic impedance of the sample. A similar relationship gives the surface impedance $z_2 = -jz_c\cot(kd_2)$ for a depth d_2. These relationships were derived in Section 1.5.1. For simplicity, assume that $d_2 = 2d_1$; typically d_1 would be a couple of centimetres. The equations for z_1 and z_2 can then be rearranged using trigonometric identities and solved to give the characteristic impedance z_c and wavenumber k:

$$z_c = \sqrt{z_1(2z_2 - z_1)} \tag{3.50}$$

$$k = \frac{-j}{2d_2} \ln\left(\frac{1 + \sqrt{\dfrac{2z_2 - z_1}{z_1}}}{1 - \sqrt{\dfrac{2z_2 - z_1}{z_1}}}\right) \tag{3.51}$$

It is necessary to choose depths so that $z_1 \neq z_2$ otherwise the results become unreliable. This happens when $kd_1 = kd_2 \pm n\pi$, where n is an integer. Unfortunately, there is no way to test for this before the measurements, as the wavenumber is unknown. Consequently, this must be checked for in analysing the results, and if necessary, another set of thicknesses measured.

Another approach is to exploit the transmission measurement approach shown in Figure 3.4 and described in Section 3.1.4. The transmission measurement enables the transfer matrix that describes how sound propagates through a sample to be determined. Combining Equation 3.15 with the general formulation for sound propagation through an impedance layer (Equation 1.29) yields:

$$\begin{bmatrix} T_{11} & T_{12} \\ T_{21} & T_{22} \end{bmatrix} = \left\{ \begin{array}{cc} \cos(kd) & jc\rho\sin(kd) \\ j\sin(kd)/c\rho & \cos(kd) \end{array} \right\} \tag{3.52}$$

where k is the wavenumber, $c\rho$ the impedance and d the depth of the material. The material properties can be derived from Equation 3.52:

$$k = \frac{1}{d}\cos^{-1} T_{11} \tag{3.53}$$

or

$$k = \frac{1}{d}\sin^{-1}\sqrt{-T_{12}T_{21}}$$

$$z = \sqrt{\frac{T_{12}}{T_{21}}} \tag{3.54}$$

Results from Song and Bolton[10] indicate a 5 cm thick sample is reasonable for common porous materials.

3.6.5 Measurement of porosity

The porosity of interest here is a ratio of the pore volume involved in sound propagation to the total volume; this is the open porosity. For specialist absorbers, such as mineral wool, the porosity is close to one, and so the value is often assumed rather than measured. Table 5.2 gives a table of typical porosities and the surrounding text discusses the significance of this parameter in more detail. While it is possible to measure the density of the sample and compare this to the density of the matrix material, this will not necessarily yield the correct porosity for sound waves, because it will include the porosity of closed pores which are relatively inaccessible to sound.

The best (more robust) measurement techniques do not use sound waves and there are three methods that satisfy this requirement: one involving liquid saturation; another which uses the isothermal compression of air, and a final approach which simply uses mass measurements in air and in a vacuum. However, it is best if the experiment uses air rather than liquid saturation of the sample, as it cannot be guaranteed that the

liquid will fill all the available pores. Liquid saturation is commonly used for geological samples,[50] but many other porous materials will be damaged by liquids and so this is inappropriate. This leaves two approaches which are detailed below.

Figure 3.17 shows a set-up used by Beranek,[51] which exploits the isothermal compression of the air volume within and external to a porous absorber. This summary is partly taken from Cremer and Müller.[52] In recent years, improvements of this technique have been developed and these are outlined later.

There is a chamber of known volume connected to a U-shaped manometer. The material to be tested is placed in the chamber. The valve at the top of the chamber can be open or closed. With the valve open, the liquid in both legs will have the same height, h. This height is measured. The valve is then closed and the pressure in the vessel increased by raising the right leg of the manometer. The surface of the liquids are now at h_1 and h_2 in the two legs and these heights are measured. The difference in the liquid levels in the two legs ($h_2 - h_1$) is the increase in pressure in the sample in metres of water ΔP. This needs to be converted to SI units:

$$\Delta P = \rho_w (h_2 - h_1) g \tag{3.55}$$

where ρ_w is the density of the liquid in the manometer and g is the acceleration due to gravity. The height difference multiplied by the cross-sectional area of the manometer tube S_s is the reduction in the volume, ΔV, in the chamber:

$$\Delta V = S_s (h - h_1) \tag{3.56}$$

Assuming this is an isothermal system, the product of the pressure and volume is constant ($PV = nRT$). This gas law is needed in a differential form for the derivation:

$$\Delta PV + \Delta VP = 0 \tag{3.57}$$

By considering the volumes of air being compressed in the chamber, both within and external to the test sample, and remembering that the porosity ε gives the ratio of the pore to total volume of the sample, Equation 3.57 can be expanded to:
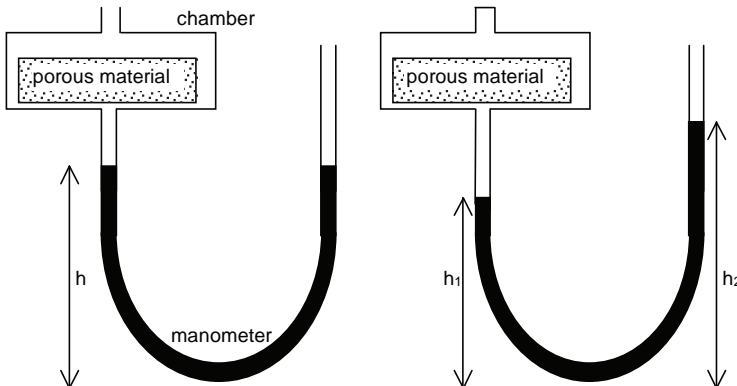
Figure 3.17   Apparatus for measuring porosity (after Beranek[51]).

$$\Delta P(V - V_a + \varepsilon V_a) + \Delta V P_0 = 0 \qquad (3.58)$$

where P_0 is atmospheric pressure; V_a the volume of the material being tested in the chamber and V the volume of the chamber. Rearranging then gives the porosity:

$$\varepsilon = \frac{P_0}{V_a}\frac{\Delta V}{\Delta P} + 1 - \frac{V}{V_a} \qquad (3.59)$$

Leclaire et al.[53] improved this method by using a reference chamber to reduce the influence of temperature and atmospheric pressure changes. Calibration needs only to be done once, and so this also reduces the number of operations in the measurement process. However, the method is still relatively slow, taking 20 minutes for calibration and 15 minutes per sample for the measurement. Porosities are accurate to about 5 per cent.

Champoux et al.[54] produced a more elaborate apparatus, which exploited the same physical principle, but without the liquid in the manometer. A micrometer drive produces precise small changes in volume, and the pressure differences are measured, using a differential pressure transducer. As the formulations assume isothermal conditions, care must be taken to insure that temperatures are stable. The paper discusses the various precautions needed to ensure the system is isothermal and isolated from atmospheric pressure fluctuations, such as the use of a heat sink, thermal insulation material and a large air reservoir. Porosities measured over a wide range of materials were accurate to better than 1 per cent.

If a measurement apparatus was being made from scratch and the desire was to utilize the above methods, the best approach might be to combine the approaches of Champoux et al. and Leclaire et al.

Panneton and Gros[55] produced a method, which employs a completely different approach and uses equipment which is readily available in many laboratories. Two masses are required: the mass when the sample is in air M_a, and the sample mass when in a vacuum M_v. The porosity is given by:

$$\varepsilon = 1 - \frac{M_v - M_a}{\rho_0 V} \qquad (3.60)$$

where ρ_0 is the density of air and V the sample volume. Precise measurement scales are needed, because the difference in the two masses on the numerator will be a few tenths of a gram typically, however this approach can yield porosities accurately provided the sample volume is chosen appropriately so the mass difference is measured accurately.

There are a variety of approaches for getting the porosity using sound waves and porous absorber models (particularly the phenomenological model outlined in Section 5.4.3). Some of these are given in the next section, which looks at tortuosity measurement, because the porosity is found as a bi-product of the process. On the whole, these are not the best approaches because they rely on prediction models. They are, however, very useful in laboratories which lack the equipment for the measurement approaches outlined above.

3.6.6 Measurement of tortuosity

For a non-conducting porous absorber, which does not get damaged by being soaked, the tortuosity can be measured by saturating the material with a conducting fluid and measuring the electrical resistivity.[56,57] The electrical resistance of the conducting fluid is measured alone, r_f, and then the electrical resistance of the porous material impregnated with the conducting fluid, r_a. Then the tortuosity can be found from:

$$k_s = \frac{\varepsilon \, r_a}{r_f} \tag{3.61}$$

This is the best approach for getting the tortuosity because it does not involve sound. Consequently, it is independent of any prediction models which might use the value and therefore more robust.

Using ultrasonic sound waves is another possibility and, as the test frequencies are beyond the audible range, this approach has a certain amount of independence from any prediction model using the measured values. Starting from the phenomenological model shown in Section 5.4.3, and considering sound propagation at high frequency, it is possible to show that the tortuosity, k_s is given by:[58]

$$k_s = \lim_{\omega \to \infty} \left(\frac{c_0}{c(\omega)} \right)^2 \tag{3.62}$$

where c_0 is the speed of sound in air, and c the wave speed in the porous material. By measuring the time-of-flight of short ultrasonic impulses, say at 50–100 kHz, the tortuosity can be derived. The increase in time of flight is measured when the porous material is introduced to estimate the ratio in the above formulation. The sample must be thin (typically a few millimetres thick), because there is an assumption of negligible absorption and dispersion, and the sample must have relatively small grains, pores or fibres (<1 mm). It can be difficult to make such thin samples that are representative of large amounts of the material. A powerful source is required, because sound waves are easily attenuated at these frequencies. Allard *et al.*[58] found errors of 1–8 per cent for the ultrasonic method in comparison to the electrical resistivity measurement in plastic foams.

The porosity can also be derived from these ultrasonic measurements, but the errors are rather large. More accurate estimations of the porosity can be achieved – while simultaneously obtaining the tortuosity – by measuring the reflection of ultrasonic waves from materials at two incident angles.[59]

For porous materials with larger grains, pores or fibres (>1 mm), then the wavelength of the ultrasonic waves becomes comparable to these structural elements, and consequently, the assumptions behind the above method breaks down. Umnova *et al.*[60] used lower frequencies (~3–20 kHz) produced using laser-generated sparks and larger samples which were several centimetres thick. Both reflected and transmitted waves were measured and used to derive the tortuosity and porosity. Tortuosity is estimated from Equation 3.62 and porosity from the high frequency limit of the reflection coefficient using:

$$\varepsilon = \sqrt{k_s} \frac{1-|R(\omega)|}{1+|R(\omega)|}\bigg|_{\omega\to\infty} \tag{3.63}$$

Tortuosity errors were small for three of the samples tested (<4 per cent), and for porosity the errors ranged from 1–20 per cent.

Tortuosity can also be deduced from the real part of the characteristic impedance for mixes where the grain size and pores are large.[61] Above some critical frequency, the real part of the characteristic impedance $Re(z_c)$ approaches asymptotically to a limit value:[62]

$$k_s = \mathrm{Re}\left(\frac{z_c}{\rho_0 c_0}\right)^2 \varepsilon^2 \bigg|_{\omega\to\infty} \tag{3.64}$$

The next section on characteristic length measurement includes a method using two gases that also yields tortuosity.

3.6.7 Measurement of characteristic lengths

There are a few methods available for gaining the viscous (Λ) and thermal (Λ') characteristic lengths. However, getting accurate results is problematic. Leclaire *et al.*[63] used ultrasound frequencies; two gases (air and helium); and a phenomenological model similar to that given in Section 5.4.3 to measure the characteristic lengths. Using the formulations in that section, it is possible to show that the complex wavenumber in the high frequency limit is given by:[64]

$$k = \omega\sqrt{k_s \frac{\rho_0}{\gamma P_0}} \left\{ 1 + (1-j)\frac{\delta_v}{2}\left(\frac{1}{\Lambda} + \frac{\gamma-1}{N_p \Lambda'}\right)\right\} \tag{3.65}$$

where ω is the ultrasonic angular frequency; k_s is the tortuosity; ρ_0 is the density of air; γ is the ratio of the specific heat capacities; P_0 is atmospheric pressure; N_p is the Prandtl number, and δ_v is the size of the viscous boundary layer.

To get the two characteristic lengths, it is necessary to generate two different equations for the wavenumber. This can be done by measuring the system with two gases, say air and helium or, for better accuracy, air and argon.[65] Argon gives a better signal-to-noise ratio than helium for two reasons. First, there is better coupling between the ultrasonic transducers and the gas as the characteristic impedance of argon is closer to that of air, and second the viscous boundary layer for argon is closer to that of air. Measuring with two gases also enables the tortuosity to be found. Time of flight and attenuation of ultrasonic pulses are measured and from this the characteristic lengths are determined. Defining the accuracy is difficult because no easy reference values are available to compare values to, but errors of the order of 10–20 per cent are typical.

Panneton and Olny[44] also started with the phenomenological model in Section 5.4.3 but worked within the audible frequency range. (They also examined the Wilson relaxation model of Section 5.4.4.) By rearranging the phenomenological formulation for

the real and imaginary parts of the effective density and assuming the porosity and flow resistivity are known from other measurements, it is possible to derive expressions for the tortuosity and the viscous characteristic length. The effective density is measured in the impedance tube. Because the technique works within the audible frequency range and relies on the phenomenological model, the method lacks independence from prediction models. However, the formulations are such that some checks on applicability of the model are possible which enables the reliability of the results to be tested. Simulations show that the tortuosity is accurate to within a few per cent, but the viscous characteristic length has a bias error of up to 20 per cent. Working with equations for the bulk modulus enables the thermal characteristic length to be determined in a similar manner.[66]

3.6.8 Inverse methods for multiple material parameters

A variety of methods for gaining different parameters have been suggested, but no single technique discussed previously yields all of them accurately. By measuring both sound reflected from and transmitted through porous material at ultrasonic frequencies it is possible to gain all the required parameters from a single measurement.[67] Although, to get both characteristic lengths, it is necessary to assume a given ratio between the two, say $\Lambda'/\Lambda = 2$.

A series of measurements of transmitted and reflected pressure are made, and then a numerical fit is carried out, using a model which predicts the sound propagation in the porous material. The prediction model could be the phenomenological model outlined in Section 5.4.3 in the high frequency limit or a relaxation model. The fit is carried out directly in the time domain. The values for the internal acoustic properties of the material – porosity, tortuosity and characteristic lengths – are changed until the least mean square error between the measured and predicted reflected and transmitted pressures is minimized across the measurement bandwidth. This fitting process is essentially a constrained numerical optimization, for which a number of different algorithms can be used.

The quality of the results is dependent on how well the prediction model can predict the material behaviour. For instance, if the pores are too big for the prediction model used in the measurement bandwidth, then the numerical optimization will yield incorrect answers.

A similar procedure can be carried out in the audible frequency range. Again a series of reflection and transmission measurements are undertaken, but this time in an impedance tube. Then a numerical fit is carried out by changing the values for the internal acoustic properties of the material until the mean squared error between the measured and predicted surface impedance (and maybe transmission coefficients) are minimized across the measurement bandwidth using a constrained numerical optimization. At the end of the fitting process, parameters such as flow resistivity will have been deduced.[68]

Again, this technique relies on the prediction model being able to represent the material behaviour correctly. For instance, if a frame resonance is prominent in the measurements, this is going to make the results incorrect. There is also a risk that the numerical optimization will not find the correct parameter values, either because a local minimum is found or because there is not a unique set of solutions for a particular measured impedance. This approach is most successful[45] in predicting porosity and

tortuosity where average errors of 1 per cent and 13 per cent respectively have been observed. It is less successful for flow resistivity and the characteristic lengths where average errors of 30–50 per cent occur.

3.7 Summary

This chapter has reviewed the methods used to measure and characterize absorbing materials. Chapter 5 gives details about how these measured parameters are exploited in porous absorber models. The next chapter details the measurement of diffusion.

3.8 References

1 ISO 10534-2:1998, "Acoustics – determination of sound absorption coefficient and impedance in impedance tubes. Part 1: Method using standing wave ratio".
2 ISO 10534-2:1998, "Acoustics – determination of sound absorption coefficient and impedance in impedance tubes. Part 2: Transfer-function method".
3 W. Schneider, M. Leistner, F. Zickmantel and R. Tippkemper, "Large scale impedance tubes", *Proc. Joint Congress CFA/DAGA*, **1**, 469–70 (2004).
4 B. H. Song and J. S. Bolton, "Investigation of the vibrational modes of edge-constrained fibrous samples placed in a standing wave tube", *J. Acoust. Soc. Am.*, **113**, 1833–49 (2003).
5 N. Kino and T. Ueno, "Investigation of sample size effects in impedance tube measurements", *Appl. Acoust.*, **68**, 1485–93 (2007).
6 D. D. Rife, and J. Vanderkooy, "Transfer function measurement with maximum-length sequences", *J. Audio Eng. Soc.*, **37**(6), 419–43 (1989).
7 A. Farina, "Simultaneous measurement of impulse response and distortion with a swept-sine technique", *Proc. 108th Convention Audio Eng. Soc.*, Paris 18–22 (2000).
8 K. V. Horoshenkov *et al.*, "Reproducibility experiments on measuring acoustical properties of rigid-frame porous media (round-robin tests)", *J. Acoust. Soc. Am.*, **122**(1), 345–53 (2007).
9 Y. Cho, "Least Squares Estimation of Acoustic Reflection Coefficient", PhD thesis, University of Southampton, UK (2005).
10 B. H. Song and J. S. Bolton, "A transfer-matrix approach for estimating the characteristic impedance and wave numbers of limp and rigid porous materials", *J. Acoust. Soc. Am.*, **107**(3), 1131–52 (2000).
11 G. Pispola, K. V. Horoshenkov and F. Asdrubali, "Transmission loss measurement of consolidated granular media", *J. Acoust. Soc. Am.*, **117**(5), 2716–19 (2005).
12 O. Olivieri, J. S. Bolton and T. Yoo, "Measurement of transmission loss of materials using a standing wave tube", *Proc. Inter-Noise* (2006).
13 J. F. Allard, *Propagation of Sound in Porous Media: Modelling Sound Absorbing Materials*, Elsevier Applied Science (1993).
14 T. Wu, Y. W. Lam and T. J. Cox, "Measurement of non-uniform impedance surface by the two microphone method", *Proc. 17th ICA*, Rome (2001).
15 W. Lauriksa, G. Jansensa, J. F. Allard, L. De Geeterea and G. Vermeira, "Evaluation of free field techniques for the measurement of the surface impedance of sound absorbing materials", *Proc. 17th ICA*, Rome (2001).
16 BS EN ISO 354:2003, "Acoustics – measurement of sound absorption in a reverberation room".
17 ISO 9613-2:1996, "Acoustics – attenuation of sound during propagation outdoors. Part 2: General method of calculation".
18 J. S. Bradley, "Optimizing the decay range in room acoustics measurements using maximum-length-sequence techniques", *J. Audio Eng. Soc.*, **44**(4), 266–73 (1996).
19 K. Sakagami, T. Uyama, M. Morimoto and M. Kiyama, "Prediction of the reverberation absorption coefficient of finite-size membrane absorbers", *Appl. Acoust.*, **66**, 653–68 (2005).

20 W. J. Davies, R. J. Orlowski and Y. W. Lam, "Measuring auditorium seat absorption", *J. Acoust. Soc. Am.*, **96**, 879–88 (1994).

21 U. Kath and W. Kuhl, "Messungen zur schallabsorption von personen auf ungepolsterten stuhlen", *Acustica*, **14**, 49–55 (1964).

22 L. L. Beranek, "Audience and chair absorption in large halls. II", *J. Acoust. Soc. Am.*, **45**, 13–19 (1969).

23 R. V. Waterhouse, "Interference patterns in reverberant sound fields", *J. Acoust. Soc. Am.*, **27**, 247–58 (1955).

24 U. Kath and W. Kuhl, "Einfluss von streuflache und hallraumdimensionen auf den gemessenen schallabsorptionsgrad", *Acustica*, **11**, 50–64 (1961).

25 J. S. Bradley, "Predicting theater chair absorption from reverberation chamber measurements", *J. Acoust. Soc. Am.*, **91**, 1514–24 (1992).

26 C. Nocke and V. Mellert, "Brief review on *in situ* measurement techniques of impedance or absorption", *Proc. Forum Acusticum, Sevilla* (2002).

27 G. Dutilleux, T. E. Vigran and U. R. Kristiansen, "An *in situ* transfer function technique for the assessment of the acoustic absorption of materials in buildings", *Appl. Acoust.*, **62**(5), 555–72 (2001).

28 E. Mommertz, "Untersuchung akustischer wandeigenschaften und modellierung der schallrückwürfe in der binauralen raumsimulation", Dissertation RWTH Aachen, Shaker Verlag (1996).

29 E. Mommertz, "Angle-dependent *in situ* measurements of reflection coefficients using a subtraction technique", *Appl. Acoust.* **46**(3), 251–64 (1995).

30 BS CEN/TS 1793-5:2003, "Road traffic noise reducing devices – test method for determining the acoustic performance. Part 5: Intrinsic characteristics – *in situ* values of sound reflection and airborne sound insulation".

31 BS ISO 13472-1:2002, "Acoustics – measurement of sound absorption properties of road surfaces *in situ*. Extended surface method".

32 C. Nocke, V. Mellert, T. Waters-Fuller, K. Attenborough, and K. M. Li, "Impedance deduction from broad-band point-source measurements at grazing incidence", *Acustica*, **83**(6), 1085–90 (1997).

33 C. Nocke, "*In situ* acoustic impedance measurement using a free-field transfer function method", *Appl. Acoust.*, **59**(3), 253–64 (2000).

34 S. Taherzadeh and K. Attenborough, "Deduction of ground impedance from measurements of excess attenuation spectra", *J. Acoust. Soc. Am.*, **105**(3), 2039–42 (1999).

35 R. Kruse, "Application of the two-microphone method for *in situ* ground impedance measurements", *Acta Acustica uw Acustica*, **93**, 837–42 (2007).

36 BS EN 29053:1993, ISO 9053:1991, "Acoustics – materials for acoustical applications. Determination of airflow resistance".

37 D. A. Bies and C. H. Hansen, *Engineering Noise Control: Theory and Practice*, E&FN Spon, 2nd edn (1996).

38 U. K. Ingard, *Notes on Sound Absorption Technology*, Noise Control Foundation (1994).

39 O. Umnova, K. Attenborough, E. Standley, and A. Cummings, "Behavior of rigid-porous layers at high levels of continuous acoustic excitation: Theory and experiment", *J. Acoust. Soc. Am.*, **114**(3), 1346–56 (2003).

40 Y. Auregan and M. Pachebat, "Measurement of the nonlinear behaviour of acoustical rigid porous materials", *Phys. Fluids*, **11**, 1342–5 (1999).

41 M. Garai and F. Pompoli, "A European inter-laboratory test of airflow resistivity measurements", *Acta Acustica uw Acustica*, **89**(3): 471–8 (2003).

42 U. K. Ingard and T. A. Dear, "Measurement of acoustic flow resistance", *J. Sound Vib.*, **103**, 567–72 (1985).

43 J. D. McIntosh, M. T. Zuroski and R. F. Lambert, "Standing wave apparatus for measuring fundamental properties of acoustic materials in air", *J. Acoust. Soc. Am.*, **88**, 1929–38 (1990).

44 R. Panneton and X. Olny, "Acoustical determination of the parameters governing viscous dissipation in porous media", *J. Acoust. Soc. Am.*, **119**(4), 2027–40 (2006).

45 P. Bonfiglio and F. Pompoli, "Comparison of different inversion techniques for determining physical parameters of porous media", *Proc. 17th ICA*, Madrid (2007).

46 R. A. Scott, "The absorption of sound in a homogenous medium", *Proc. Phys. Soc. London.* **58**, 165–83 (1946).

47 C. D. Smith and T. L. Parrott, "Comparison of three methods for measuring acoustic properties of bulk materials", *J. Acoust. Soc. Am.*, **74**, 1577–82 (1983).

48 C. K. Amédin, Y. Champoux and A. Berry, "Acoustical characterisation of absorbing porous materials through transmission measurements in the free field", *J. Acoust. Soc. Am.*, **102**(2), 1982–94 (1997).

49 J. Tran-vana, X. Olnyb, F.C. Sgard and Y. Gervais, "Global inverse methods for determining the acoustical parameters of porous materials", *Proc. 17th ICA*, Rome (2001).

50 ASTM C830-00, "Standard Test Methods for Apparent Porosity, Liquid Absorption, Apparent Specific Gravity, and Bulk Density of Refractory Shapes by Vacuum Pressure" (2006).

51 L. L. Beranek, "Acoustic impedance of porous materials", *J. Acoust. Soc. Am.*, **13**, 248–60 (1942).

52 L. Cremer and H. A. Müller, *Principles and Applications of Room Acoustics*, Applied Science Publishers (translated by T. J. Schultz) (1978).

53 P. Leclaire, O. Umnova, K. V. Horoshenkov and L. Maillet, "Porosity measurement by comparison of air volumes", *Rev. Sci. Instrum.*, **74**(3), 1366–70 (2003).

54 Y. Champoux, M. R. Stinson, G. A. Daigle, "Air-based system for the measurement of porosity", *J. Acoust. Soc. Am.*, **89**, 910–6 (1991).

55 R. Panneton and E. Gros, "A missing mass method to measure the open porosity of porous solids", *Acta Acustica uw Acustica*, **91**, 342–8 (2005).

56 R. J. S. Brown, "Connection between formation factor for electrical resistivity and fluid-solid coupling factor in Biot's equations for acoustic waves in fluid-filled porous media", *Geophysics*, **45**, 1269–75 (1980).

57 E. Sarradj, T. Lerch and J. Hűbelt, "Input parameters for the prediction of acoustical properties of open porous asphalt", *Acta Acustica uw Acustica*, **92**, 85–96 (2006).

58 J. F. Allard, B. Castagnede, M. Henry and W. Lauriks, "Evaluation of tortuosity in acoustic porous materials saturated by air", *Rev. Sci. Instrum.*, **65**, 754–5 (1994).

59 Z. E. A. Fellah, S. Berger, W. Lauriks, C. Depollier, C. Arisetgui and J. Y. Chapelon, "Measuring the porosity and the tortuosity of porous materials via reflected waves at oblique incidence", *J. Acoust. Soc. Am.*, **113**(5), 2424–33 (1983).

60 U. Umnova, K. Attenborough, H.-C. Shin and A. Cummings, "Deduction of tortuosity and porosity from acoustic reflection and transmission measurements on thick samples of rigid-porous materials", *Appl. Acoust.*, **66**, 607–24 (2005).

61 N. N. Voronina and K. V. Horoshenkov, "A new empirical model for the acoustic properties of loose granular media", *Appl. Acoust.*, **64**, 415–32 (2003).

62 K. Attenborough, "Acoustical characteristics of rigid fibrous absorbents and granular materials", *J. Acoust. Soc. Am.*, **73**(3), 785–99 (1983).

63 P. Leclaire, L. Kelders, W. Lauriks, M. Melon, N. Brown and B. Castagnède, "Determination of the viscous and thermal characteristic lengths of plastic foams by ultrasonic measurements in helium and air", *J. Appl. Phys.*, **80**(4), 2009–12 (1996).

64 D. Lafarge, J. F. Allard, B. Brouard, C. Verhaegen and W. Lauriks, "Characteristic dimensions and prediction at high-frequencies of the surface impedance of porous layers", *J. Acoust. Soc. Am.*, **93**(5), 2474–8 (1993).

65 N. Kino, "Ultrasonic measurements of the two characteristic lengths in fibrous materials", *Appl. Acoust.*, **68**, 1427–38 (2007).

66 X. Olny and R. Panneton, "Acoustical determination of the parameters governing thermal dissipation in porous media", *J. Acoust. Soc. Am.*, **123**(2), 814–24 (2008).

67 Z. E. A. Fellah, F.G. Mitri, M. Fellah, E. Ogam and C. Depollier, "Ultrasonic characterization of porous absorbing materials: Inverse problem", *J. Sound Vib.*, **302**, 746–59 (2007).

68 Z. E. A. Fellah, M. Fellah, W. Lauriks and C. Depolier, "Direct and inverse scattering of transient acoustic waves by a slab of rigid porous materials", *J. Acoust. Soc. Am.*, **113**, 61–72 (2003).

4 Measurement and characterization of diffuse reflections or scattering

While surface scattering elements have been used accidentally or by design in rooms for centuries, it is only in recent decades that a concerted effort has been made to develop methods for measuring and characterizing the scattering from these surfaces.[1] Without measurements of surface reflections, it is impossible to confidently design and apply diffusers. Consequently, this chapter starts by describing methods for measuring the scattering produced by a surface. This mainly concentrates on measurements in terms of polar responses, as this is the primary way that surface reflection has been measured for diffuser design and evaluation.

The polar response of a source, like a loudspeaker, can be determined by measuring the sound energy distribution on a semicircle or hemisphere surrounding the source. With care, this concept can be translated from loudspeaker measurements, and used for backscattering from architectural surfaces. While polar responses tell designers much about how a surface reflects sound, they contain a considerable amount of data and a different polar response is required for each frequency band and angle of incidence. This is one of the reasons why single figure parameters have been developed, which condense the polar response data and allow characterization in terms of diffusion coefficients.

The reflection from a surface can also be characterized using a scattering coefficient, which is different from a diffusion coefficient. The differences between the coefficients will be discussed in some depth later in this chapter, but for now, it is opportune to give the contrasting definitions of diffusion and scattering coefficients:

> *Diffusion coefficient*, *(d)*, is a measure of the uniformity of the reflected sound. The purpose of this coefficient is to enable the design of diffusers, and to also allow acousticians to compare the performance of surfaces for room design and performance specifications.

> *Scattering coefficient*, *(s)*, is a ratio of sound energy scattered in a non-specular manner to the total reflected sound energy. The purpose of this coefficient is to characterize surface scattering for use in geometrical room modelling programs.

Both the coefficients are simplified representations of the true reflection behaviour. It is necessary to come up with simple metrics, rather than trying to evaluate the reflection characteristics for all possible source and receiver positions, because the amount of data is otherwise too large. The coefficients attempt to represent the reflection by a single parameter, maximizing the information carried by that single number. The

difference between diffusion and scattering coefficients is the emphasis on which information is most important to be preserved in the data reduction. For diffuser designers and acoustical consultants, it is the uniformity of all reflected energy which is most important; for room acoustic modelling, it is the amount of energy scattered away from specular angles. The difference between the definitions may appear subtle, but it is significant.

In this chapter, diffusion and scattering coefficients are described after a discussion of the direct ways of measuring the energy reflected from surfaces. For example, what are the best ways of obtaining the scattered and total sound fields? The chapter concludes by describing some other techniques for characterizing surfaces which have yet to find great favour, but may in the future be useful techniques.

4.1 Measurement of scattered polar responses

In order to characterize a diffuser's performance, it is necessary to be able to both measure and/or predict how the surface reflects sound. Currently, this is most often done by looking at how the scattered energy is spatially distributed. This spatial distribution is conventionally described by polar responses in one-third octaves, for a given angle of incidence. An ideal diffuser produces a polar response that is invariant to the angle of incidence, the angle of observation and the frequency (within its operational bandwidth). Figure 4.1 shows a measured polar response for normal incidence, at 2 kHz, from an array of 2D number theoretic diffusers, one of which is also shown in the figure. There are various techniques for measuring such a scattered polar distribution, as discussed below. (Chapter 8 details some possible prediction methods.)
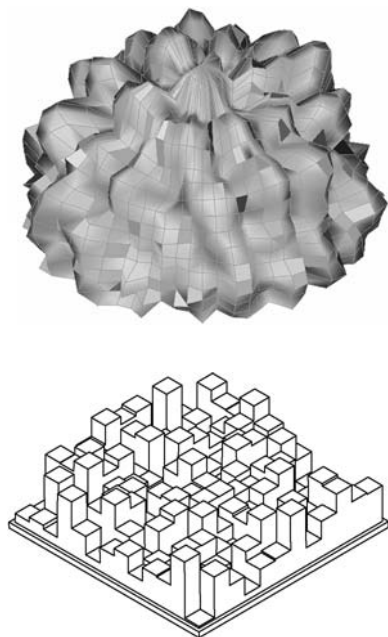
Figure 4.1 Three-dimensional polar balloon measured from a Skyline® diffuser, which is shown below the polar response.
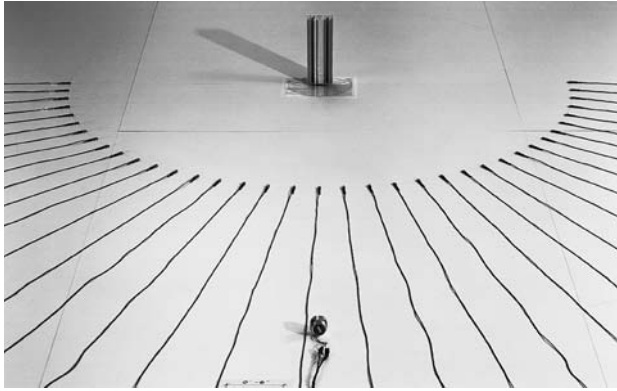
Figure 4.2   A system for measuring the scattering from a surface in a plane using a boundary plane measurement. The diffuser (a Schroeder diffuser) is shown top middle. There are 37 microphones arranged on an arc. The source loudspeaker is in the bottom middle of the picture (reproduced from the Audio Engineering Society Information Document AES-4id-2001, with permission[2]).

A source is used to irradiate the test surface, and measurement microphones at radial positions in front of the surface record the pressure impulse response. The microphone positions usually map out a semicircle or hemisphere, for a single plane or hemispherical measurement, respectively. Once the pressure impulse responses are measured, time gating is used to separate the reflections from the incident sound. Various methods can be used to measure the impulse responses. The most common uses a maximum length sequence (MLS) signal. Other signal possibilities include swept sine

Figure 4.3   A system for measuring the scattering from a surface over a hemisphere. The diffuser being tested is the small pyramid in the centre. The source arc is most obvious, the receiver arc is acoustically transparent and so is difficult to see (reproduced from AES-4id-2001, with permission[2]).
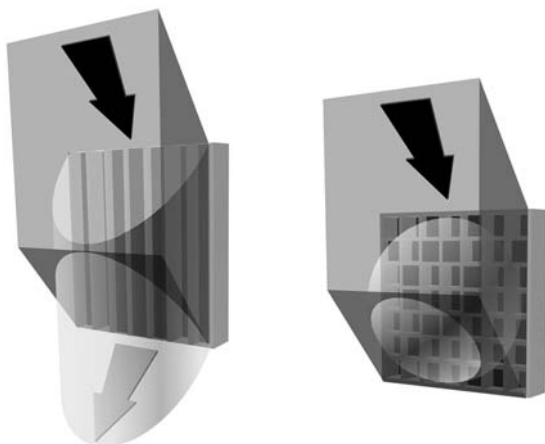
Figure 4.4 Scattering from a single plane (left) and hemispherical diffuser (right) (after D'Antonio and Cox[3]).

waves and impulses. Time delay spectroscopy might also be used. As time variance and non-linearity are not an issue, MLS signals are currently the most efficient to use.

Polar response measurements can be made in a single plane using a 2D goniometer on a semicircle,[4] as shown in Figure 4.2, or over a hemisphere, using a 3D goniometer, as shown in Figure 4.3. The choice of single plane or hemispherical measurement depends on the type of diffuser, and the fact that a hemispherical measurement system is difficult and expensive to construct. Figure 4.4 (left) illustrates that an extruded diffuser (known as a single plane or 1D diffuser) produces scattering in one plane, and consequently a single plane evaluation is appropriate.[3] If the surface produces scattering in multiple planes, as shown in Figure 4.4 (right), then a hemispherical evaluation is ideal. However, for practical reasons, carrying out a couple of single plane measurements in orthogonal directions might be done. Figures 4.2 and 4.3 show 1:5 scale measurement systems. Scale model measurements are needed, because otherwise the source and receiver radii become too large (see below).

In Figure 4.2, a fixed microphone array is used. In Figure 4.3, a single microphone is moved on a lightweight scaffolding, which then traces out a hemisphere. It is also possible to use a boom arm to rotate a microphone on a single arc, as shown in Figure 4.5.

The single plane measurement can be made in an anechoic chamber,[5] but it is also possible to use a boundary layer technique;[4] this latter technique is shown in Figure 4.2. This can be done in a large room, provided that the ceiling and walls are sufficiently far away from the test set up. The scattering sample is shown in the top middle, along with 37 pressure zone microphones arranged on a semicircle 1 m from the sample. The source loudspeaker, for normal incidence, is shown at the bottom middle located 2 m from the sample. Ideally, somewhat larger source and receiver distances should be used to allow wider samples to be measured. The measurement geometry is shown in plan view in Figure 4.6, and from this geometry it is possible to calculate the size of the non-anechoic room needed for the measurement. In this case, the loudspeaker (L), microphone (M) and diffuser (D) are placed on a flat, hard surface on the floor. The microphone radius is denoted by *R* and the loudspeaker radius is *2R*. Figure 4.6
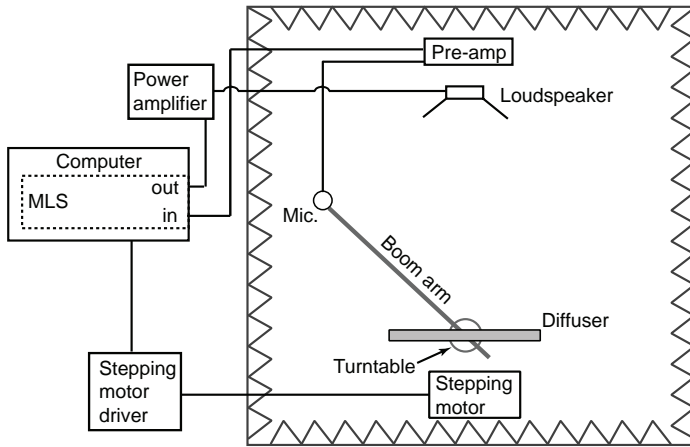
Figure 4.5 A schematic of a measurement system.

illustrates the ellipsoidal area (dashed) necessary to make a reflection free zone measurement. Consider the respective sound paths of the direct sound (LM = R), the scattered sound (LDM = $3R$) and the limiting reflection from the second order reflection from the speaker (LDLM = $5R$). Therefore, the reflection free zone, which measures only scattering from the sample, is $4R$. It is possible to determine the ellipsoidal area from the measurement geometry. If the limiting path is $5R$, then the total path travelled from the loudspeaker to the room boundary, B, and back to the microphone is also equal to $5R$ = LBM (LB + BM). The minor axis of the ellipsoid, H, equals $2.45R$ and the major axis, W, equals $2.5R$. If $R=5$ m, then this requires a room 12.2 m high, by 24.4 m wide, by 25 m long. Since this is an unreasonably large room, measurements have been done at 1:5 scale in which $R = 1$ m.
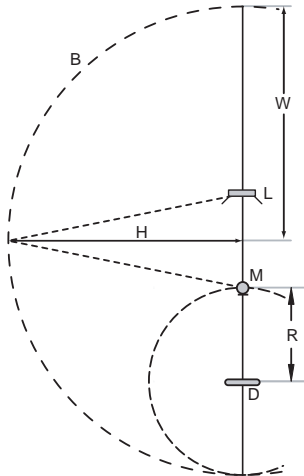
Figure 4.6 Plan view of reflection free zone geometry for boundary measurement technique. Loudspeaker (L), microphone (M), diffuser (D), microphone radius (R), room boundary (B), ellipse axes (H) and (W).
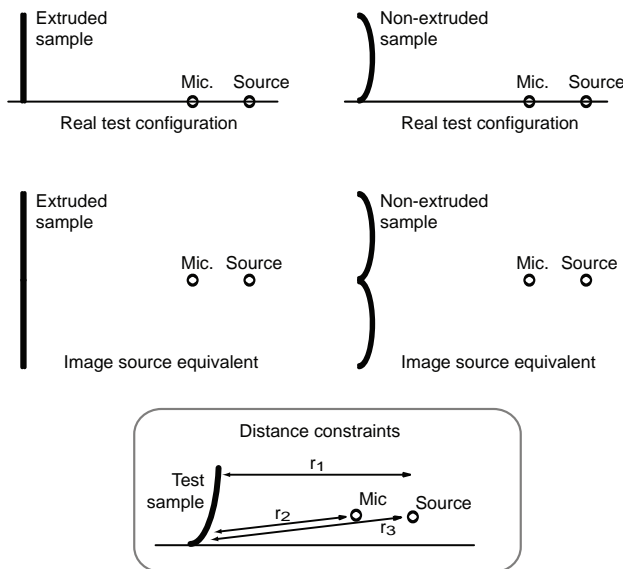
Figure 4.7 Top row: boundary plane measurement and below that the equivalent image source configuration. Left column: extruded sample; right column: non-extruded surface. The insert shows distances used for calculating the maximum frequency.

In the boundary layer measurement, the floor acts as a mirror image and what is measured is effectively the diffuser paired with a mirror image of the diffuser, as illustrated in Figure 4.7, where a section is shown. In Figure 4.7 (left) a diffuser is shown in a real test condition and its image source equivalent. The diffuser is extruded in the vertical direction, and so it can be seen that what is actually measured is a sample twice as high, with the source and receiver at the midpoint. In Figure 4.7 (right) a non-extruded shape (arc) is shown in the real test configuration and its image source equivalent. For this sample, the actual sample and its mirror image is being measured.

As the source and receivers are not located exactly on the boundary, there is an upper frequency limit for this measurement. The longest and shortest propagation paths must not differ by more than half a wavelength. In terms of the geometry shown in Figure 4.7, the path difference $|r_1 - r_2 - r_3| \ll \lambda/2$, where r_1, r_2 and r_3 are defined in the figure.

A potential problem with this measurement process is that the microphone(s) will get in the way of the sound propagating from the source to the panel. For this reason, the fixed microphone array or the boom arm used to move a single microphone must be small enough not to cause significant reflections or disturbance to the sound field. Where possible, supports should be located not in a direct line between source and diffuser, and be covered in absorbent material or be acoustically transparent. Fixed microphone arrays have been constructed using small pressure zone microphones. This potential interference by the microphones on the sound field makes diffuser measurements more awkward than measuring the polar responses from loudspeakers, because for loudspeakers it is possible just to rotate the loudspeaker.

The single plane measurement is quick and easy to carry out. In contrast, measurements with a hemispherical goniometer require considerably more complex engineering to achieve the acoustically transparent microphone positioning in an anechoic chamber. Hemispherical measurements are also more time-consuming, due to the great increase in the number of measurements required. A spatial resolution of 5° in azimuth and elevation requires 1,296 measurement positions for every angle of incidence. (5° was chosen because tests have shown that this is a sufficient resolution to gain the polar response accurately without overburdening measurements with excessive sampling points.) Consequently, for hemispherical evaluation, it is much easier to use validated prediction models. For this reason, a better approach is to follow the suggestion of Farina[6] to measure two semicircular arcs rather than measuring the whole hemisphere. Incidentally, if symmetry in the sample exists, and the source lies in the plane of symmetry, it is possible to reduce the number of measurements. For the hemispherical measurement, symmetry is worth exploiting.

Figure 4.8 illustrates the sequence of events in determining the scattered impulse
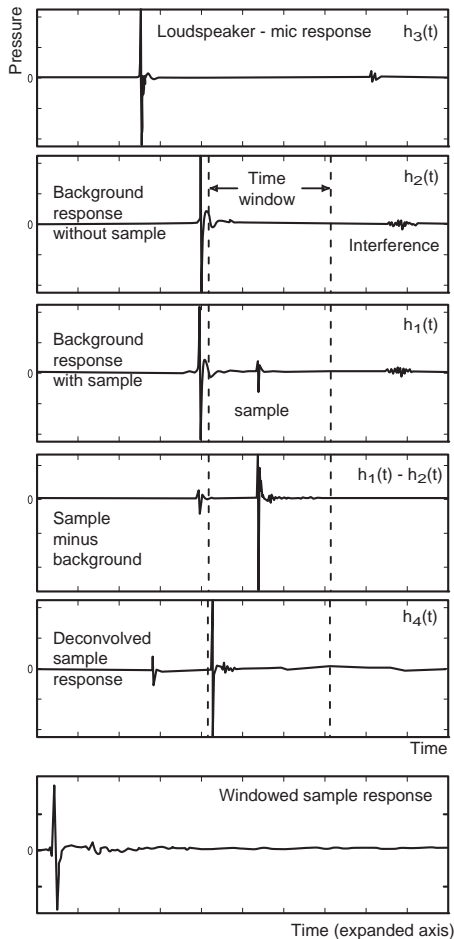
Figure 4.8 Data reduction process to extract the scattered impulse response from a test sample at a given observation angle.

response at a particular observation angle, for a given angle of incidence. As an illustration, consider the measurement in a single plane illustrated in Figure 4.2. To obtain the impulse response of a sample under test, it is necessary to de-convolve the loudspeaker/microphone response at each scattering angle, $h_3(t)$. It is also necessary to minimize any room interference and reflections from microphone supports and wires within the time window of interest. To obtain the 'Loudspeaker mic response' (top panel in the figure) at each scattering angle, the loudspeaker is placed at the sample position and rotated so its on-axis response is coincident with the on-axis response of each microphone for each angle.

The loudspeaker is then placed in its normal source position, without any sample present, and the 'Background response without sample', $h_2(t)$, at each angle is auto-matically measured via computer control by emitting 37 impulses and sequentially switching each microphone on. A vertical dotted line representing the time window of 10 ms used to isolate the reflections is also shown. The sample under test is then placed in position and the scattered sound is measured, obtaining the 'Background response with sample', h_1(t), in Figure 4.8.

Data are collected at 5° intervals. The measurement system selects a microphone, emits a selected maximum length sequence stimulus, records the data, selects the next microphone position, and so on. Since the microphones are stationary and the measurement process is rapid, the respective background response can be subtracted from each microphone position, prior to de-convolution. This is illustrated as 'Sample minus background' in Figure 4.8. The direct sound is significantly decreased and is not providing interference in the time window with the scattered sound. The room interference is also decreased. The loudspeaker/microphone response can now be de-convolved as illustrated in 'Deconvolved sample response', $h_4(t)$, which is calculated using:

$$h_4(t) = IFT\left\{\frac{FT[h_1(t) - h_2(t)]}{FT[h_3(t)]}\right\} \tag{4.1}$$

where FT and IFT are the forward and inverse Fourier transforms. The data within the time window is gated to isolate the 'Windowed sample response'.

This process assumes that the system remains time variant over the time it takes to determine all 2 x 37 impulse responses for the with and without sample measurements. For full-scale measurements, this can be problematic. One way of mitigating this difficulty is to measure the with and without sample responses for each microphone immediately after each other. Many modern measurement systems are capable of making multi-microphone measurements simultaneously. Therefore, 37 impulse responses can be measured with one stimulus with and without sample present, to significantly improve the accuracy of the background subtraction.

The data are further post processed to provide frequency responses, polar responses and finally diffusion coefficients, as shown in Figure 4.9.

At the top, Figure 4.9A shows the 2D boundary measurement geometry with the exciting loudspeaker at an angle of incidence of –60° with respect to the normal. Also shown are the 37 receiving microphones. A flat non-absorbing sample is being measured. Below that, Figure 4.9B shows the impulse response for the microphone at 0°, with the scattered data outlined in a box, corresponding to the time window in Figure 4.8. The
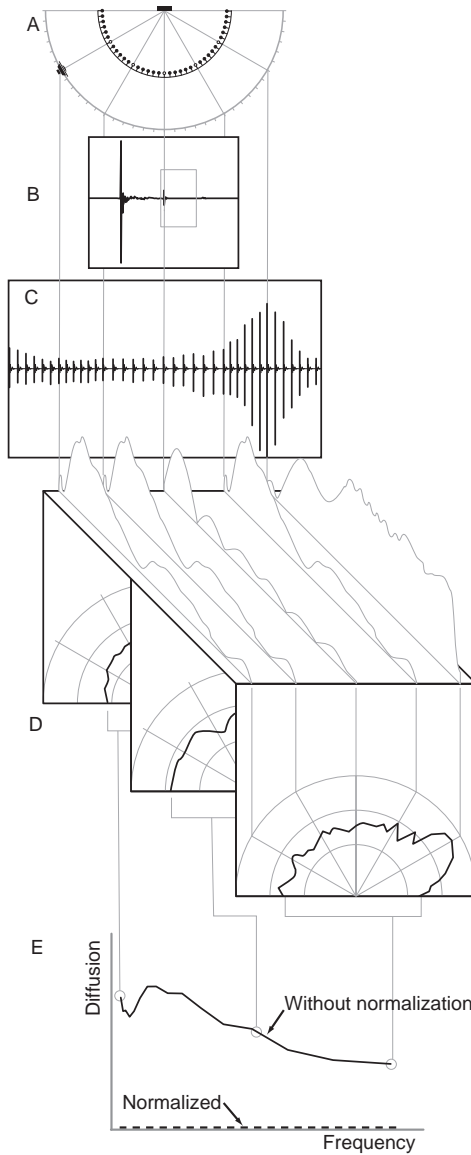
Figure 4.9 Summary of data processing technique from a flat reflector at −60° incidence.

scattered data are windowed for all of the angles of observation, of which five are highlighted at −60, −30, 0, 30 and 60° and concatenated in Figure 4.9C in the form of a temporal angular impulse response. A Fourier transform is then applied to each of the impulse responses to get the frequency responses, shown in Figure 4.9D. Five of the 37 frequency responses are only shown for clarity. The frequency response energy is summed over one-third octave bands and three of the polar responses are shown in Figure 4.9D. The visible polar response at high frequency is narrow and directed in the specular direction of +60°, as would be expected. The polar responses can then be
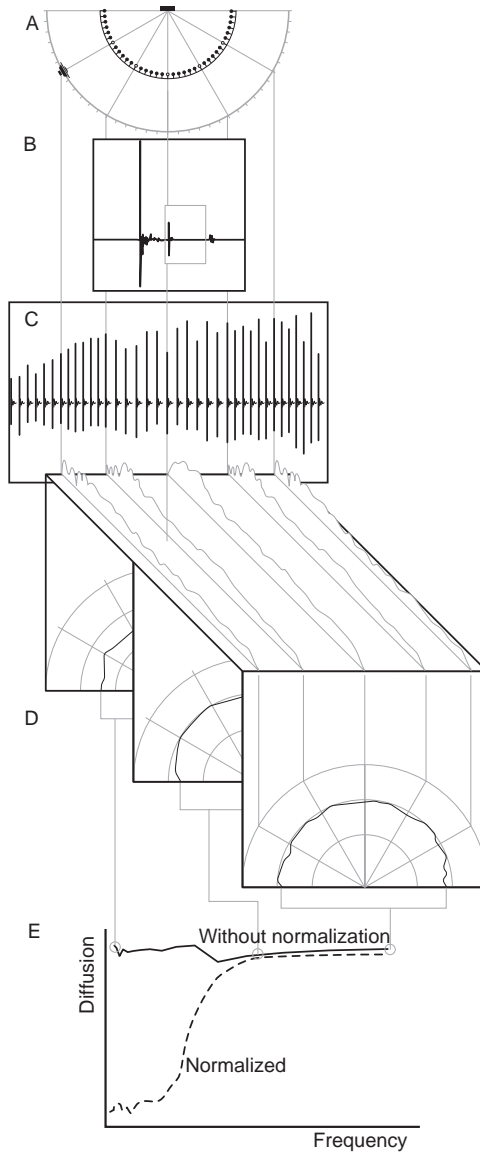
Figure 4.10   Summary of data processing technique from a diffuser at −60° incidence (reproduced from AES-4id-2001, with permission[2]).

further processed to give a diffusion coefficient, which is plotted versus frequency to obtain the diffusion response in Figure 4.9E. Without normalization, the diffusion coefficient decreases as the frequency increases. This happens because the width of the panel becomes increasingly large compared to the wavelength and the scattering becomes more specular. To remove these finite-panel effects, a normalized diffusion coefficient is used and because a flat reflector is being measured, this is zero for all frequencies in this case.

In Figure 4.10, the same procedure is shown for a diffusing sample for –60° incidence. The polar responses are more semicircular and the diffusion coefficient without normalization is closer to 0.6, the maximum value for complete diffuse reflection on real surfaces. By normalizing the diffusion coefficient with the flat reflector value, the frequency at which surface scattering becomes important is clearer and the results are easier to interpret. Normalization also removes edge diffraction scattering effects, so that the normalized diffusion coefficient represents the uniformity of scattering from the surface topology only.

In Figure 4.11, a presentation format for a sample of three semicylinders is shown. The top row shows a photo of the three semicylinders on the left, the diffusion coefficient of the test sample compared to a reference flat reflector in the middle and the normalized diffusion coefficient on the right. The remaining images are the one-third octave polar responses of the test sample compared with a reference flat reflector. Round robin testing on a reference sample has been shown to be effective in comparing the results from different laboratories. Three semicylinders, which can easily be fabricated from PVC pipe as a test sample, can be used to calibrate different goniometers.
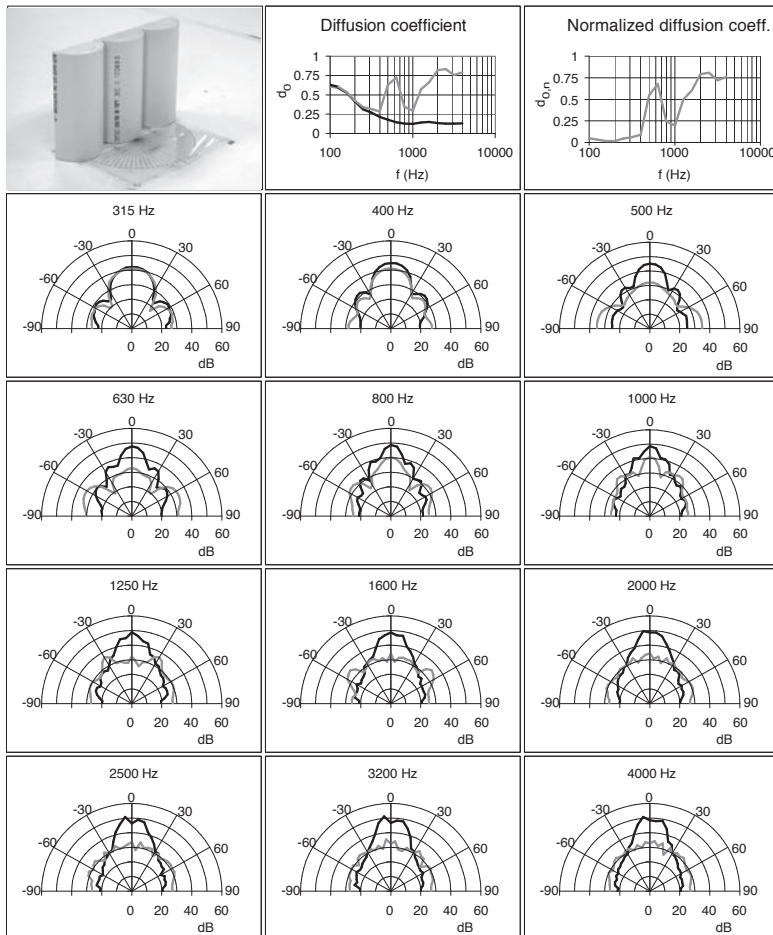
Figure 4.11   Presentation format for diffusing surfaces at normal incidence. Diffuser light line, reference reflector dark line.
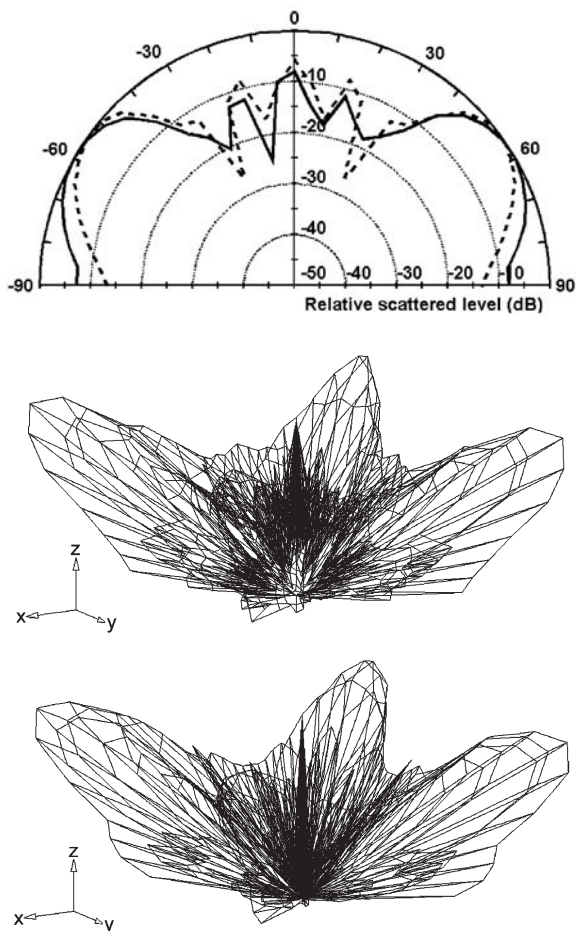
Figure 4.12 Comparison of measured and predicted polar responses for a square-based
pyramid and normal incidence.
Top: ——— measurement (2D) using boundary plane;
and – – – single plane BEM prediction (1 kHz).
Middle: 3D measurements at the University of Salford (2 kHz).
Bottom: 3D BEM prediction (2 kHz) (after Hargreaves *et al.*[7]).

Figure 4.12 compares the measured and predicted scattering from a surface meas-
ured both on a single plane and a hemisphere. The agreement between theory and
measurement is good; this is a measurement process that yields accurate results.

4.1.1 Near and far fields

All free field measurements suffer from the problem that the relative levels within the
polar response are dependent on distances from the source and receiver to the surface,
unless the source and receivers are in the far field. (The far field being where the
scattered pressure falls by 6 dB per distance doubling for 3D geometries, and 3 dB per
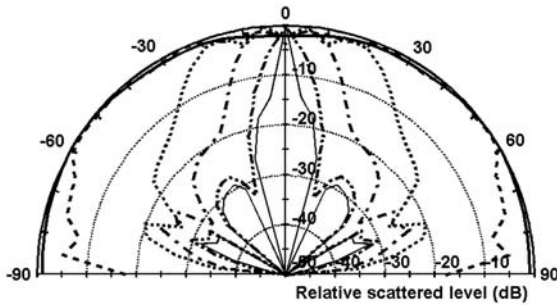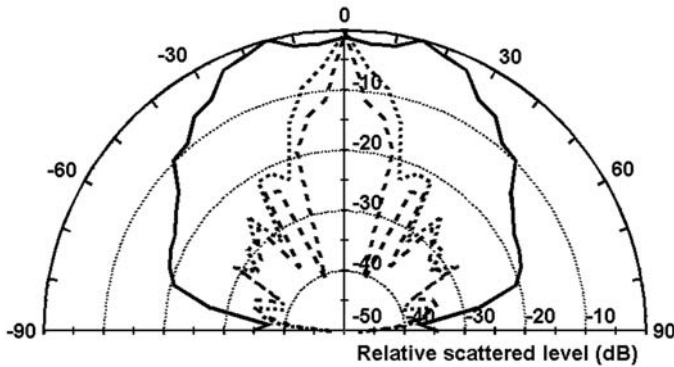
Figure 4.13 Effect of receiver arc radius on the polar response of a 1 m square plane
panel. Single plane BEM prediction, 5 kHz, normal incidence, source
distance = 100 m. Receiver distances ———— 0.1 m, – – – 0.5 m, ······· 1 m,
·—·—·· 2 m, ··—··—··· 5 m, ———— 100 m (after Hargreaves *et al.*[7]).

distance doubling in 2D geometries.) Unfortunately, in most room applications, it is
usual for sources and receivers to be in the near rather than the far field, unless the test
surface is small. Figure 4.13 shows the scattering from a plane surface for a variety
of receiver distances. As the receiver approaches the surface, the scattered pressure is
more evenly distributed over the polar response. A plane surface appears to be a very
good diffuser when measurements are made close to the surface. In fact, close enough
to the surface the reflection is provided by an approximate image source that radiates
the same energy to all receivers except for minor effects due to spherical spreading
and path length differences. This seemingly contradicts conventional wisdom in room
design that a plane surface is a poor diffuser.

To understand this contradiction, it is necessary to understand why plane surfaces
can cause problems in real applications. Problems can occur with plane surfaces with
directional sources such as trumpets. The reflected energy will be concentrated over a
narrow solid angle, leading to a risk of detrimental effects such as echoes, coloration or
image shift for receivers within this solid angle. The results shown in Figure 4.13 were
produced using an omnidirectional source. Furthermore, the plane surface does not
produce any temporal diffusion, and as discussed in Chapter 10, this is another important
reason why it is a poor diffuser. The polar responses do not consider the wavefront phase.

The solution usually adopted is for scattering measurements based on polar dis-
tributions to be taken in the far field, even when this is further than any real listeners
would ever be. Then some receivers will be outside the specular zone (which is defined
in Figure 4.14), and it is possible to measure the energy dispersed from receivers in the
specular zone to those outside the zone. In the spatial domain and in the far field, the
effect of a diffuser should be to move energy from the specular zone to other positions.
So, unless receivers are placed both outside and within the specular zone, measuring
energy levels alone will not detect the effects of diffuse reflections.

There are standard formulations for approximately calculating the required distance
for measurements to be in the far field.[8] These criteria apply to both sources and
receivers, but for now, only receivers are considered to simplify explanations – the
source will be assumed to be at infinity. There are two criteria to satisfy: the receiver
radius should be large compared to wavelength and the differences between path lengths
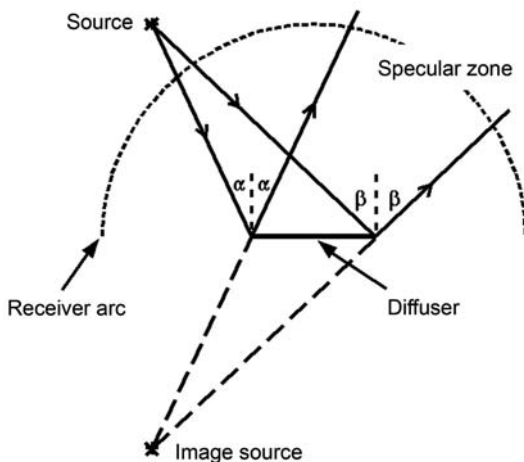
Figure 4.14   Definition of the specular zone – the region over which a geometric reflection occurs. (Although the specular zone is strictly a high frequency construction, practice has shown it to be a useful concept for the geometries and frequencies typically used in diffuser design) (after Hargreaves *et al.*[7]).

from points on the surface to the receiver should be small compared to wavelength. With the geometries and frequencies used for measuring diffuser scattering, it is the latter criterion that is most exacting.

Unfortunately, the common far field formulations are not applicable to the case of oblique receivers, where significant destructive interference occurs. Problems arise because the amount of destructive interference is very sensitive to the relative magnitudes of the waves coming from the secondary sources on the scattering surface (assuming the scattering is modelled following Huygen's principle). Consequently, the receiver distance required to achieve the true far field for oblique receivers is often so large that measurements cannot be accommodated in normal test facilities. Figure 4.15 shows the scattering from a surface as a function of distance; it takes a receiver distance of hundreds or even thousands of metres to reach a completely stable far field polar response!

Fortunately, a pragmatic approach may be taken, as knowing the minima in a polar response to very exact detail is not necessary. This is particularly true if a diffusion coefficient is going to be evaluated, as the calculation of the coefficient involves reducing the many scattered pressure values in a polar response to a single figure of merit. Consequently, errors from the slight misrepresentation of notches in the polar response will have negligible effect on the diffusion coefficient value. The situation is also less critical when one-third octave bandwidths are used, as is normal practice. So, the true far field does not have to be obtained. It is sufficient to ensure that the majority of receivers are outside the specular zone, so that the diffuser's ability to move energy out of the specular zone can be measured. Then a reasonable approximation to the far field polar response can be obtained.

The Audio Engineering Society standard information document, AES-4id-2001,[2] recommends that 80 per cent of receivers are outside the specular zone, ideally in revisions of the standard this figure should be referenced to Fresnel zones or panel
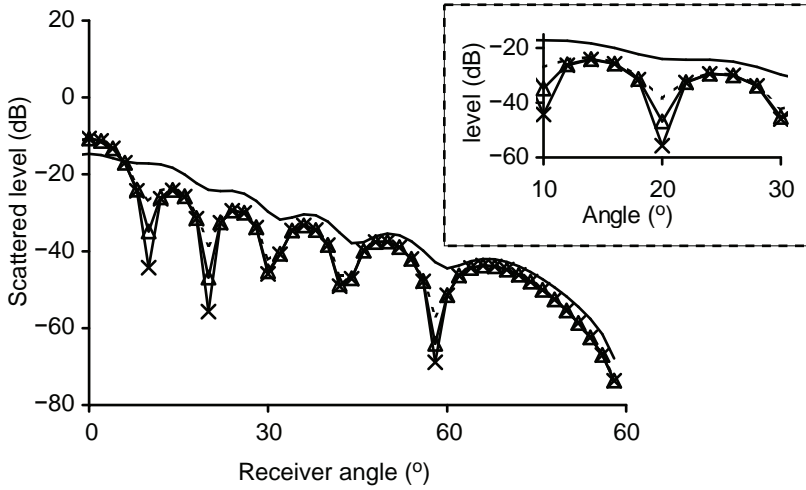
Figure 4.15   Variation of the scattered polar response with receiver distance to illustrate extent of near field. Receiver angle on a linear scale for clarity; insert graph is an enlargement of a section of the main graph. 1 m plane surface at 1 kHz using BEM predictions. A distance correction of $1/\sqrt{r}$ has been used to correct for cylindrical wave spreading. Receiver distances:
———— 2.94;
– – – 12;
—△— 32; and
—✕— 100 m;
(after Hargreaves *et al.*[7]).

critical frequencies.[9] In Figure 4.16 the diffusion coefficients (the single figure of merit derived from the polar responses) for two surfaces, as a function of receiver distance, are shown. The point where 80 per cent of the receivers are outside the specular zone is shown. The plane panel case shown is one of the worst case scenarios and the error introduced into the diffusion coefficient is only 0.1. Furthermore, this is a single frequency prediction. Once summing across one-third octave bands is used, this error
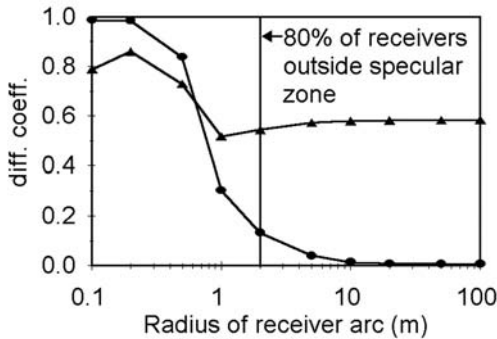
Figure 4.16   Effect of receiver arc radius on the diffusion coefficient. Single plane BEM predictions, normal incidence, source distance = 100 m.
—●— 1 m wide plane panel, 5 kHz;
—▲— 1 m wide random binary panel, 400 Hz (after Hargreaves *et al.*[7]).

Figure 4.17 Effect of receiver arc radius on the polar response of a concave arc. Single plane BEM predictions, 2 kHz, normal incidence, source distance = 10 m: ——— near field; – – – focal distance; ······ far field (after Hargreaves et al.[7]).

approximately halves. Consequently, a reasonable approximation to the true far field polar responses and diffusion coefficients can be obtained.

An alternative solution is to use near field acoustic holography[10] to enable near field measurements to be projected into the far field, but this method has disadvantages, such as the problems of mounting the surface in a manner similar to typical applications. Another solution is to use validated numerical models, as predicting in the far field is always possible.

For some surfaces, however, it is not sufficient just to measure in the far field. For concave surfaces and others that might have significant aberrations closer to the surface, it is necessary to monitor in the near, as well as the far field to ensure that effects such as focussing are found. This is illustrated in Figure 4.17 where the scattering from a concave surface is shown as a function of distance. It can be seen that receivers very close to the surface detect a good diffuser, but a little further out the reflected sound is highly focussed. In the far field, some diffusion is created. In summary, a pragmatic approach requires receivers to be both inside and outside the specular zone and measurements at application realistic distances are also needed to check for focussing with concave surfaces.

4.1.2 Sample considerations

It is important to test a sample which is representative of the entire structure to be applied in real applications. For instance, one period of a Schroeder diffuser should not be tested alone if the intention is to apply the surface periodically; this is because the scattering from the periodic and single diffuser will be very different. Where the whole sample cannot be tested, because of geometric constraints on source and receiver distances, the following techniques are suggested in AES-4id-2001:[2] for a periodic sample at least four complete repeat sequences should be included so the effects of lobing from repetition is measured. (Although the width of the diffraction lobes depends somewhat on the number of repeat units in the sample.[11]) Figure 4.18
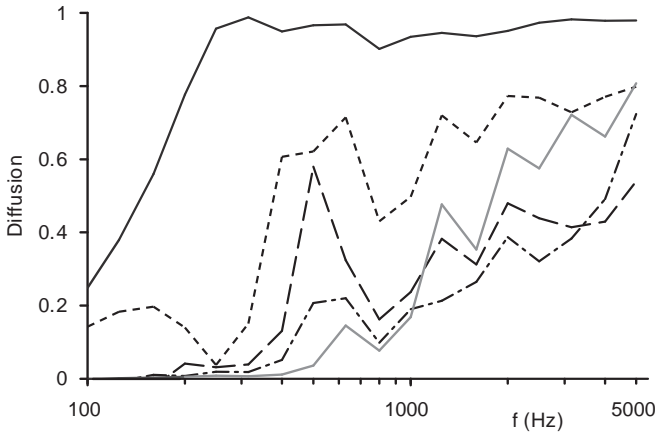
Figure 4.18 The normalized diffusion coefficient for various sets of semicylinders. The number of cylinders in each set is:
——— 1;
········ 2;
– – – 4;
·—·—· 6;
——— 12.

shows the normalized diffusion coefficient from five different sets of semicylinders. The plots show that one cylinder is not representative of the scattering from an array of semicylinders. For random surfaces, representative samples of the surface roughness should be tested, large enough so that surface, rather than edge, effects are more prominent in the scattering.

Some have said that the diffusion coefficient method will not work for large surfaces with small surface roughness and that it is intended to be used for single diffusers only. This is not true, and the evaluation method can theoretically be used on any sized surface. The problem is that, when the surface becomes large, the measurement becomes impractical because it is impossible to get far enough away from the surface. In this case, the evaluation can still be done, but only with the use of prediction or scale models.

When scale models are used, it is important that a representative test sample is constructed. For scale models, the absorption properties should be the same for both the full scale surface at full scale frequencies and the test surface at the equivalent model scale frequency. When considering absorption from samples, losses due to viscous boundary layer effects should be included. This consideration can limit the usable model scales, because viscous boundary layer effects do not scale in the same way as physical dimensions.

Tremendous advances have been made in 3D solid prototyping printers and scale samples can easily be fabricated with solid reflective backs for diffusive/reflective comparison tests in the goniometer. A photo of samples made using this rapid proto-typing system is shown in Figure 4.19. The software layers a 3D CAD file into thin layers. The printer lays down a thin layer of powder and a print head with resin rasterizes this layer and successive layers, depositing resin wherever there is a contribution from the sample in the layer. At the end, a 3D physical scale model is created.
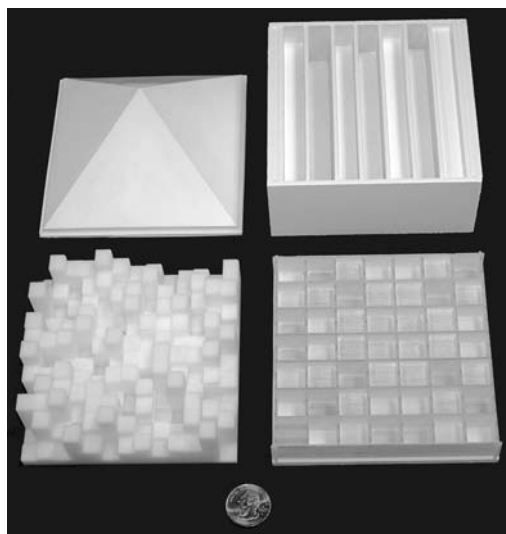
Figure 4.19 Samples generated using a 3D printer.

4.2 Diffusion and scattering coefficients – a general discussion

While polar responses can give much information about the sound reflecting from a surface, the problem is that they can yield too much detail. There is a need to reduce the large amount of data in a polar response to a single value, to allow a more ready comparison of diffuser quality. This then helps diffuser designers to evaluate the worth of a product and room designers to produce product specifications for surface designs. However, it is important that the polar responses are not disregarded; they should also be available for designers to consider alongside the diffusion coefficient. In addition, there is a need for a scattering coefficient to evaluate the amount of dispersion generated by a surface and so allow accurate predictions using geometric room acoustic models.

Unfortunately, there does not appear to be one ideal coefficient which meets the needs of all interest groups – the room modellers, diffuser manufacturers and room designers. There are no diffusion or scattering coefficients currently in the literature that do not have flaws in their use. While on first examination it appears possible to produce a watertight definition of a coefficient, detailed analysis reveals problems. For this reason, two different coefficient definitions are, or are about to be, enshrined in international standards. While this may appear unsatisfactory, it should be remembered that room acoustics has for a century used an absorption coefficient which has well defined limitations in application. For example, there are two primary techniques for measuring absorption – the impedance tube and reverberation chamber methods – and each measurement method has advantages and disadvantages and is used for different reasons. In an analogous manner, the methods for characterizing diffusion can be classified either as free or diffuse field.

Diffuse field methods have the advantage of quickly obtaining a random incidence coefficient, but are difficult to predict. A measurement method for obtaining a random

incidence scattering coefficient is now part of an ISO standard;[12] this is based on the Mommertz and Vorländer technique.[13,24] Free field methods are often more laborious measurements to carry out, but can be readily predicted. A free field method for a diffusion coefficient, based on the Cox and D'Antonio technique, has recently been published in AES-4id-2001[2] and is likely to become part 2 of the ISO standard.

The terms scattering and diffusion are used in different ways and are interchanged in different subject fields. It would be possible to have a long argument about whether diffusion or scattering is a better terminology for a given coefficient, but it would be impossible to get a unanimous agreement on nomenclature. Consequently, in this book the nomenclature that is being used in the standards will be adopted. This defines the diffusion and scattering coefficients as follows:

- A diffusion coefficient measures the quality of reflections produced by a surface, in the case of the AES coefficient, by measuring the similarity between the scattered polar response and a uniform distribution.
- A scattering coefficient is a measure of the amount of sound scattered away from a particular direction or distribution. This has the greatest similarity to the coefficients required as inputs to current geometric room acoustic models.

4.3 The need for coefficients

4.3.1 Diffuser manufacturer and application

When Schroeder introduced his revolutionary design of diffusers, which are described in Chapter 9, he also introduced a possible measure for complete diffuse scattering. This was different from Lambert's law. Schroeder defined optimum diffuse scattering as being when the level of the grating lobes produced by a periodic phase gratings have the same energy. Since the 1970s, many other types of diffusers have been produced, and to enable the merits of these designs to be evaluated, it is necessary to have a better measure of the quality of the diffuse reflections than lobe energy. The idea of measuring the similarity of the lobe energy is not a useful criterion, because surfaces do not have to be periodic and non-periodic surfaces do not necessarily have grating lobes. Consequently, new definitions to measure the diffuseness of reflections have been developed.

For a diffusion coefficient to be useful to designers, the primary characteristic of the coefficient is that it must rank diffusers correctly according to quality. This will not necessarily be achieved by the scattering coefficient, and this is why a separate coefficient has been developed for quality. An ideal diffusion coefficient would:[7]

- have a solid physical basis;
- be clear in definition and concept, and related to the current and future roles of diffuse reflections in airborne acoustics, especially in rooms;
- consistently evaluate and rank the performance of diffusers;
- apply to all the different surfaces and geometries found in rooms;
- be measurable by a simple process;
- be bounded;
- be easy to predict.

This turns out to be like searching for the Holy Grail, but it is possible to produce a diffusion coefficient that does satisfy most of the above criteria.

The current state-of-the-art in diffuser design is numerical optimization, as described in Chapters 9 and 10. Using diffusion coefficients in a numerical optimization has enabled designs to move away from the rigid geometric constructs imposed by phase grating diffusers. This has enabled designs in which both acoustic and visual requirements can be considered and their conflicting requirements resolved. It is now possible to make diffusers which blend in with architectural forms rather than appearing as add-ons and this is important for acoustic treatments to be acceptable to architects. Enabling shape optimization has been one of the main drivers behind the development of a diffusion coefficient.

When a designer requires absorbing surfaces in a space, a performance specification in terms of the absorption coefficient is currently used to ensure quality and compliance with design requirements. One of the aims of research into diffusion coefficients was to be able to state the amount of diffuse reflections required in performance specifications; this can now be done by specifying diffusion coefficients measured or predicted according to AES-4id-2001. Without standardization, the industry is vulnerable to published performance data which have no basis in fact and diffusers that do not perform as intended.

The evaluation criteria developed do not just have to be applied to especially designed surfaces; they can also be used to monitor the diffuse reflections by accidental diffusers. It appears that surface diffusion is often applied in a haphazard fashion, because there is not a good understanding of when and where to apply diffusers. For instance, discussions with consultants produce examples where it is claimed that too much or too little surface diffusion has resulted in acoustic aberrations. A priori to developing a better understanding of where diffusers are needed is an index to measure their quality. This measure is now provided by the uniformity diffusion coefficient.

4.3.2 Geometric room acoustic models

Originally, geometric room acoustic models did not include the effects of scattering due to edge effects and surface roughness. However, there is now plenty of evidence that incorporating scattering into the geometric models enhances prediction accuracy. For instance, it has been shown that without surface scattering, geometric room acoustic models tend to over predict reverberation time.[15–17] This is especially true in spaces where absorption is unevenly distributed, as happens in many concert halls, or where rooms are highly disproportionate, as happens in many factories. Moreover, for acoustic parameters that are highly dependent on early reflection prediction accuracy, such as early lateral energy fraction and clarity, there can be great sensitivity to the modelling technique used for diffuse reflections and to the value of scattering coefficients assumed.[18] In the first round robin study of room acoustic models,[17] three models were found to perform significantly better than others. These three models produced results approximately within one subjective difference limen, while the less successful models produced predictions inaccurate by many difference limen. What differentiated the three best models from the others was the inclusion of a method to model surface scattering. Scattering in geometric room acoustic models is discussed in detail in Chapter 12.

There are many different methods for incorporating diffuse reflections into a geometric

room acoustic model[19] (see Chapter 12). This process is inevitably approximate, because geometric models cannot explicitly model the true wave nature of sound. The geometric models use a scattering coefficient to determine the proportion of the energy that is reflected in a specular manner and the proportion that is scattered. (In the computer models, these coefficients are sometimes referred to as diffusion coefficients just to confuse matters!) Problems arise, because until recently, there has not been a procedure for determining the values of the scattering coefficients, except for trial and error and through precedence. Consequently, a key driving force behind the ISO process was to standardize a method to enable scattering coefficients to be determined in a rigorous manner.

The scattered energy in a geometric model is usually distributed according to Lambert's cosine law.[20] Lambert's law is used because it fits with the philosophy of the geometric models which are based on high frequency modelling techniques. The law is correct for high frequency, point incoherent scattering. As shall be discussed below, diffusion coefficients used by diffuser designers are based on uniform energy distribution. Uniform energy distribution is a possible design goal, because the reflected sound from surfaces display strong coherent interference effects at the most important acoustic frequencies. Indeed, this coherence is explicitly exploited in many diffuser designs – just try and explain how a Schroeder diffuser works without referring to interference! Consequently, Lambert's law is inapplicable for evaluating diffusers, and despite what some have claimed, diffuser designers are not violating the second law of thermodynamics. Conversely, using the diffusion coefficients measured according to AES-4id-2001 in geometric room acoustic models is likely to produce incorrect results, unless the model has been explicitly designed to use this coefficient.

4.4 The diffusion coefficient

4.4.1 Principle

The general method for evaluating diffuser quality is as follows. First, the scattering from a surface is measured or predicted in terms of a polar distribution, as discussed in Section 4.1. Then the diffusion coefficient is a frequency dependent, single figure of merit derived from the polar distribution. This is evaluated in one-third octave bandwidths, which has the advantage of smoothing out some of the local variations in the polar responses, so the diffusion coefficient is based more on the overall envelope. There have been various statistical operations suggested to calculate a diffusion coefficient from the polar distributions: standard deviation,[21–23] directivity,[24,25] specular zone levels[26,27] and spherical harmonics,[28] percentiles and autocorrelation.[7] In any such data reduction, there is a risk of losing essential detail. It has been shown that the autocorrelation coefficient seems to offer significant advantages over other published statistical techniques.

The autocorrelation function is commonly used to measure the similarity between a signal and a delayed version of itself; looking for self similarity in time. It is also possible to use the autocorrelation to measure the scattered energy's spatial similarity, with receiver angle. A surface which scatters sound uniformly to all receivers will produce high values in the spatial autocorrelation function; conversely, surfaces which concentrate reflected energy in one direction will give low values. To form a single figure diffusion coefficient, the circular autocorrelation function is first calculated and

then an average taken. This is a rather laborious process, but fortunately the whole calculation can be simplified to a single equation. For a fixed source position, the autocorrelation diffusion coefficient, d_ψ, can be calculated using:

$$d_\psi = \frac{(\sum_{i=1}^{n} 10^{L_i/10})^2 - \sum_{i=1}^{n} (10^{L_i/10})^2}{(n-1)\sum_{i=1}^{n} (10^{L_i/10})^2} \tag{4.2}$$

where L_i are a set of sound pressure levels in decibels in a polar response, n is the number of receivers and ψ is the angle of incidence. This equation is only valid when each receiver position samples the same measurement area. This is automatically achieved for single plane measurements on a semicircle with an even angular spacing between receivers. (The fact that receiver positions at ±90° actually sample half the area of the other receivers can be ignored, because applying a correction makes an insignificant difference to the diffusion coefficient.)

Figure 4.20a shows the diffusion coefficient for a few commercial products and a reference flat surface. At low frequency, edge scattering causes the diffusion coefficient
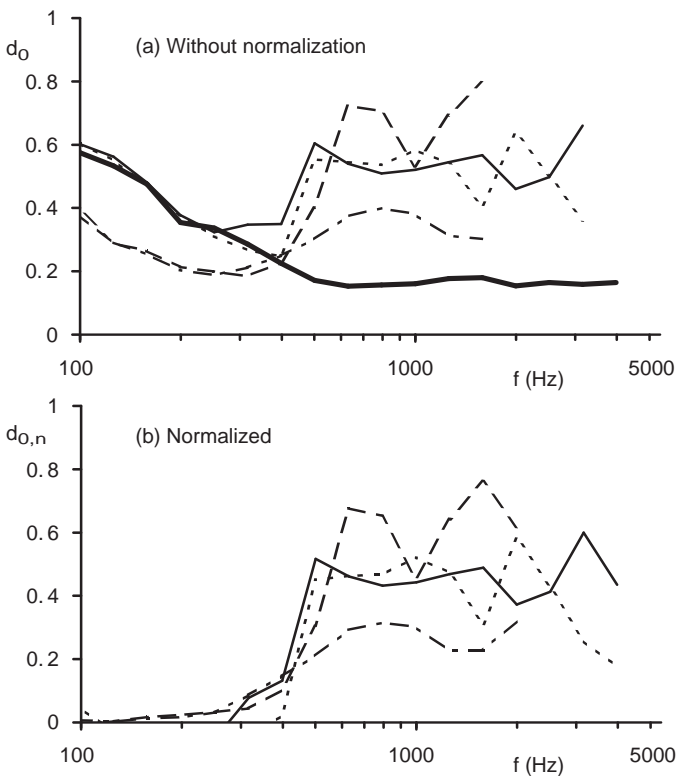
Figure 4.20 Diffusion coefficient for four commercial products. Top: not normalized; bottom: normalized. The thick line in the top picture is the diffusion coefficient for a flat reflector.

to increase with decreasing frequency because the sample acts as a point source scattering omnidirectionally. While there is a clear physical explanation for this effect, it does lead to confusion and so a normalized diffusion coefficient is introduced to remove this effect. The result of normalization is shown in Figure 4.20b. This gives the more intuitive response, with surfaces producing little diffusion at low frequency. It also more clearly illustrates the frequency where diffusion begins. The normalized diffusion coefficient, $d_{\psi,n}$, is calculated using the following formulation:

$$d_{\psi,n} = \frac{d_\psi - d_{\psi,r}}{1 - d_{\psi,r}} \tag{4.3}$$

where d_ψ and $d_{\psi,r}$ are the diffusion coefficients calculated using Equation 4.2 for the test sample and a reference flat surface of the same overall size as the test sample. At low frequency, sometimes the normalized diffusion coefficient dips below zero, due to experimental 'error'. In these cases, the negative values should be set to zero.

The concern with diffusion measurement is to determine the ability of diffusers to uniformly scatter in all directions, rather than with just the ability of a surface to move energy away from the specular angles. This restriction is placed because of experiences of diffuser designers. From the standpoint of a designer, it is important that a diffusion
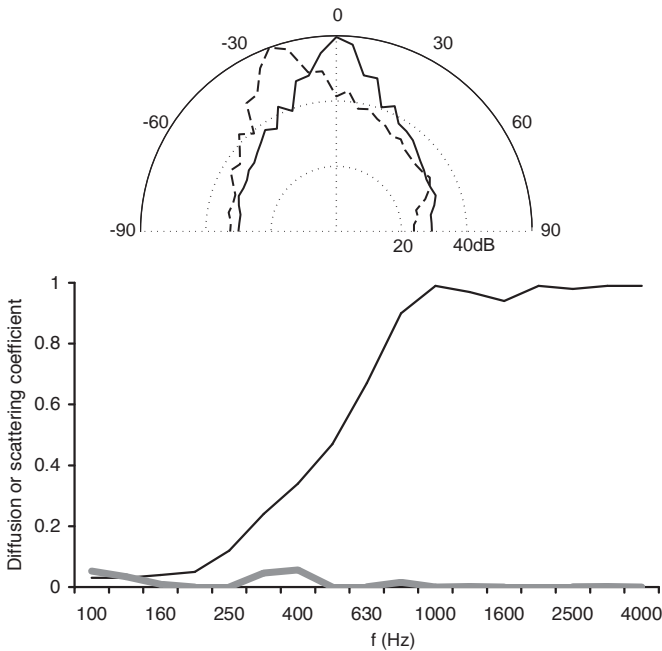
Figure 4.21   Top: the polar responses for ——— a plane surface and – – – a rotated plane surface.
Bottom: the diffusion and scattering coefficient frequency responses:
——— correlation scattering coefficient; and
——— normalized diffusion coefficient rotated plane surface (adapted from Cox and D'Antonio[29]).

coefficient differentiates between redirection and dispersion. Figure 4.21 shows the scattering from a flat surface, and the same flat surface which has been rotated by 20° to redirect the specular reflection in another direction. The normalized diffusion coefficient measures the rotated plane surface to have little dispersion capabilities, as would be anticipated. The scattering coefficient, however, sees the redirection of energy from the specular reflection angles as scattering, and therefore gives a high coefficient for the rotated plane surface, even though this is only achieving redirection, not dispersion. Diffusers are often applied to treat first order reflections, for example to prevent echoes from the rear wall of concert halls. If all the diffuser achieves is redirection, there is a risk that the echo problem will simply move to another place in the hall. On the other hand, if the diffuser achieves spatial dispersion, this has the potential to reduce the echo problem, without creating new difficulties elsewhere. This is the reason why the Mommertz and Vorländer[13,14] free field method has not found favour with diffuser designers.

4.4.2 Obtaining polar responses

Section 4.1 already discussed how measurements might be made to obtain the polar responses. Predictions can also be used. AES-4id-2001[2] recommends a receiver every 5°, with the source at 10 m and receiver arc radii 5 m (equivalent full scale). It recommends that to obtain a random incidence diffusion coefficient, source positions should be measured with a maximum angular separation of 10°, covering a semicircle or hemisphere measured about the reference normal. Random incidence is achievable for single plane measurements, but the number of measurements in the hemispherical case is unrealistically large (0.5 million source and receiver combinations). To overcome this, the pending ISO standard suggests measuring the directional diffusion coefficient at 0, ±30 and ±60°. The average incidence coefficient can be obtained from the average of the five normalized directional diffusion coefficients. In reality, the measurement over a hemisphere is difficult to perform, and therefore a better option is to measure in two planes and average the diffusion coefficient values obtained for each plane.

In many applications the source position is well known. In performance spaces, for example, this is the location of the stage. In that case, it makes most sense to evaluate the diffusion coefficient for this specific angle of incidence, as the first order effects of a diffuser are of primary importance, especially if the concern is to remove echoes or coloration.

AES-4id-2001 stipulates that different radii polar responses might be used to check for focussing effects. If measurements are made at different radial distances from the surface, it is necessary to apply a correction to allow for the normal drop in level due to spherical or cylindrical spreading. Otherwise the diffusion coefficient is overly biased by drops in levels that naturally occur due to effects that are not related to a surface's ability to diffuse.

4.4.3 Discussion

The autocorrelation diffusion coefficient ranks diffusers correctly and separates different surfaces along the diffusion axis. The coefficient has a clear physical basis in the autocorrelation function. However, it is not known exactly how the diffusion coefficient values relate to subjective response, which would be useful in evaluating the merits of diffusers.

The experimentally measured and theoretically predicted diffusion coefficient values tend to be small. This can be seen by glancing at the coefficient values given in Appendix C. Values for the autocorrelation coefficient can in theory spread over the entire range from 0 to 1. A value close to zero has been measured for a concave surface designed to focus sound on a single receiver. A value of 1 can be measured for a small single semicylinder, but a single semicylinder on its own is not much use, because it cannot cover a wide area. As soon as more complex surfaces are introduced, such as a set of semicylinders, the diffusion coefficient is reduced, because of the lobing introduced. This lobing is unavoidable in extended structures, and so the diffusion coefficient is rarely close to 1 for usable and realistic diffusers and diffuser arrays. A single semicylinder may produce complete diffusion, but to cover a wall a set of semicylinders are needed. This is why it is important to measure application realistic samples, as the scattering from a single object is not representative of the response from a periodic or modulated array.

4.4.4 Diffusion coefficient table

Appendix C gives calculated values for normalized diffusion coefficients, for various surfaces, following the procedure in AES-4id-2001. The predictions were carried out using a 2D Boundary Element Model as described in Chapter 8. All surfaces were modelled as thin panel extrusions and the rear of the surfaces were not enclosed. Therefore, these represent the diffusion coefficient for single plane devices such as semicircular arcs. The source and receiver were 100 m and 50 m respectively from the surface. Each one-third octave band polar response was found by averaging seven single frequency responses. The random incidence diffusion coefficient values were found by an arithmetic average of the diffusion coefficient values for ten different angles of incidence (Paris's formulation was not applied). The table reports three incident angles; normal, 57° and random incidence.

The first part of the table shows the effect of changing the number of diffusers in an array, illustrating that the diffusion coefficient for single and multiple devices are very different. The rest of the table keeps all the test sample widths the same, at about 3.6 m, to allow ready comparison. When comparing other diffusers in the table, it is important to compare like with like. For example, ensure that the diffusers being compared have the same maximum depth.

The second section shows the effect of diffuser depth on the diffusion coefficient. To do this, a set of semi-ellipses are used. As might be expected, as the semi-ellipses get deeper, they start diffusing at a lower frequency – although period width becomes a limiting factor for deeper devices, as discussed in Chapter 10. The third section shows the diffusion coefficients for different triangles – the scattering from triangles is discussed in detail in Chapter 10. The fourth section gives examples of what happens when ellipses are mounted on a flat baffle with spaces between – as might be expected, this reduces the dispersion generated at high frequencies.

The fifth part shows the performance that can be obtained from optimized curved surfaces, the design of which is discussed in detail in Chapter 10. The table values illustrate that the optimization design process is very effective. The sixth part gives results for flat and planar hybrid surfaces, where absorptive patches are used to generate dispersion; these diffusers are discussed in detail in Chapter 11. The seventh and last part gives data for a variety of reflection phase gratings: simple Schroeder

diffusers, fractal designs and optimized surfaces. These designs are discussed in Chapter 9. The Schroeder surfaces were modelled by meshing the entire surface so the predictions are valid above (and below) the limit where plane wave propagation becomes less dominant in the wells.

4.5 The scattering coefficient

4.5.1 Principle

The principle of a scattering coefficient is to separate the reflected sound into specular and scattered components. The specular component is the proportion of energy which is reflected in the same way as would happen for a large plane surface. The scattered components give the energy reflected in a non-specular manner. This is illustrated in Figure 4.22. The coefficient has a clear physical meaning and the definition is very useful for geometric room acoustic models, because these tend to have separate algorithms dealing with specular and scattered components. Therefore the separation of terms mimics the modelling methods. With this definition it is then possible to define a scattering coefficient, *s*, as the proportion of energy not reflected in a specular manner.

This definition takes no account of how the scattered energy is distributed, but assumes that in most room acoustic applications there is a large amount of mixing of different reflections. Therefore, any inaccuracies that arise from this simplification will average out. This is probably a reasonable assumption for the reverberant field, where there are many reflections. However, it could well be troublesome for the early sound field, where the impulse response is dominated by a few isolated reflections and the correct modelling of these is essential for gaining accurate predictions. Section 4.4.1 has already illustrated how scattering coefficients can give misleading results for the first order reflections from redirecting surfaces.

The scattering coefficient, like the diffusion coefficient, generally depends on frequency and angle of sound incidence. Similar to the random incidence absorption coefficient obtained in reverberation rooms, an angular average of the scattering coefficient – the random incidence scattering coefficient – can be defined. As a general assumption, the surface under test is assumed to be large and not too rough. The method will not work for isolated items and deep surfaces, as it is trying to measure the scattering from the surface roughness and not the edges. It also has problems when the surface absorption is high, as the coefficient estimation becomes inaccurate.
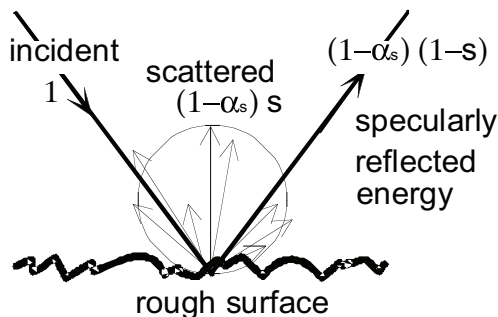
Figure 4.22 Definitions used for scattering coefficient (after Vorländer and Mommertz[14]).

4.5.2 Rationale and procedure

The energies of reflections (normalized with respect to a reflection from a non-absorbing flat surface) are expressed as follows:[13]

$$E_{spec} = (1-\alpha_s)(1-s) \equiv (1-\alpha_{spec}) \tag{4.4}$$
$$E_{total} = 1-\alpha_s$$

where E_{spec} is the specular reflected energy; E_{total} is the total reflected energy; s is the scattering coefficient, α_s is the absorption coefficient, and α_{spec} is the apparent specular absorption coefficient.

The apparent specular absorption coefficient warrants further description. It is the energy dispersed from specular reflection directions. This energy is not dissipated to heat; it is reflected into non-specular directions. Rearranging the above formulations gives the following equation for the scattering coefficient:

$$s = \frac{\alpha_{spec} - \alpha_s}{1-\alpha_s} = 1 - \frac{E_{spec}}{E_{total}} \tag{4.5}$$

The measurement of this quantity is easiest to explain in the free field, although it is in the diffuse field measurement where this process is useful and powerful. The set-up is shown in Figure 4.23. The specular absorption coefficient is found by rotating the test sample, while phase locked averaging the reflected pulses. Figure 4.24 shows three band pass filtered pulses for different orientations of a corrugated surface. The initial parts of the reflections are highly correlated; these are the specular components of the reflection, and remain unaltered as the sample is rotated. In contrast, the later parts of the three reflected pulses are not in phase and depend strongly on the specific orientation; this is the scattered component. By averaging the reflected pulse pressure, while rotating the sample, the scattered components are averaged to zero, and only the specular energy remains.

Transferring this procedure to the reverberation chamber, the measurement technique is as follows. A circular test sample is placed on a turntable and rotated. While the turntable is rotated, the room impulse response is repeatedly measured. The latter parts of the impulse response, which are due to the scattering from the surface, will cancel out, and the averaged impulse response only contains the specular reflection
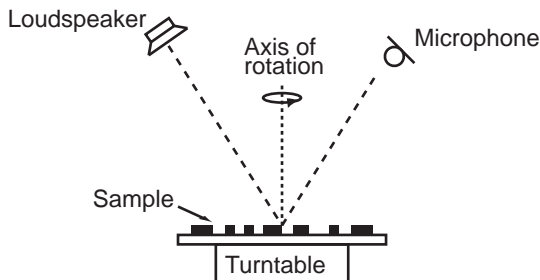
Figure 4.23   Set-up used for measuring the scattering coefficient (after Vorländer and Mommertz[14]).
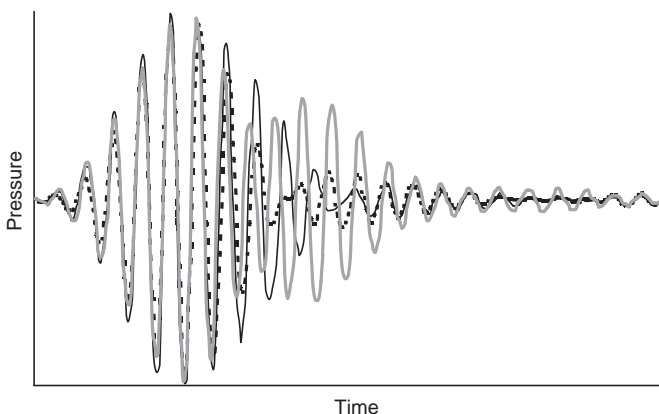
Figure 4.24 Band limited reflected pulses for different sample orientations (after Vorländer and Mommertz[14]).

component. This impulse response is then backward integrated to give the reverberation time, due to the specular reflection component. The reverberation time with the sample stationary (not rotating) can also be obtained and this decay is due to the total scattering – specular plus diffuse. By manipulating these reverberation times, it is possible to derive the specular and total reflected energy and, from Equation 4.5, the scattering coefficient.

In reality, four reverberation times are needed. It is difficult to get a perfectly flat and circular turntable; this is especially true for full scale measurements.[30–32] Consequently, the imperfections in the turntable must be compensated for by additional measurements. The four reverberation times that must be measured are shown in Table 4.1.

Table 4.1 The measurement conditions for the four different reverberation times

Reverberation time	Test sample	Turntable
T_1	not present	not rotating
T_2	present	not rotating
T_3	not present	rotating
T_4	present	rotating

Once these reverberation times are measured, the following formulations are used to get the scattering coefficient. The random incidence absorption coefficient α_s of the sample is calculated using:

$$\alpha_s \;=\; 55.3 \frac{V}{S}\left(\frac{1}{c_2 T_2} - \frac{1}{c_1 T_1} \right) \;-\; \frac{4V}{S}(m_2 - m_1) \tag{4.6}$$

where V is the volume of the reverberation room; S is the area of the test sample; c_1 is the speed of sound in air during the measurement of T_1; c_2 is the speed of sound

in air during the measurement of T_2; m_1 is the energy attenuation coefficient of air in m^{-1} during the measurement of T_1 (see Sections 1.1.1 and 3.4), and m_2 is the energy attenuation coefficient of air during the measurement of T_2.

The specular absorption coefficient α_{spec} is calculated using the following formulation:

$$\alpha_{spec} = 55.3 \frac{V}{S}\left(\frac{1}{c_4 T_4} - \frac{1}{c_3 T_3}\right) - \frac{4V}{S}(m_4 - m_3) \tag{4.7}$$

where c_3 is the speed of sound in air during the measurement of T_3; c_4 is the speed of sound in air during the measurement of T_4; m_3 is the energy attenuation coefficient of air during the measurement of T_3, and m_4 is the energy attenuation coefficient of air during the measurement of T_4.

Finally, the random-incidence scattering coefficient, s, is calculated using Equation 4.5. These reverberation times are measured using the standard procedures in ISO 354,[33] so multiple source receiver pairs are needed to average out spatial variation within the reverberation chamber. The measurement must use a deterministic source signal to allow the phase locked pressure averaging. In the original work, maximum length sequences were favoured, but these are rather sensitive to time variance, which means the measurement of the reverberation times with the turntable rotating must be done quickly. This is not a problem at model scale, but at full scale the turntable must move slowly. The signal periodicity must be longer than the reverberation time in the room, which means full scale measurements take a long time, as typically 72 measurements in a single rotation are needed. For this reason, some have favoured the use of swept sine waves, which are less sensitive to time variance errors.[30,32]

At full scale, the measurement is rather slow and laborious. There are some considerable logistical problems in fabricating a 3.6 m diameter flat turntable. For instance, the doors of the reverberation chamber are probably too small for the turntable to go through in one piece and so it needs to be dismantled, yet a completely flat and strong turntable when assembled must be made. Furthermore, a powerful, yet quiet motor is required.[30,32] For these reasons, model scale measurements are to be preferred for speed and efficiency.

4.5.3 Sample considerations

Since the measurement method is intended to measure surface roughness, the results are only reliable when the structural depth of the sample is small compared to the size of the specimen. An empirically derived limit is $h \leq d/16$, where d is the diameter of the turntable and h the structural depth. Figure 4.25 shows 1:10 samples of four commercial samples that were fabricated for scattering coefficient measurements. The measured scattering coefficients are very sensitive to edge conditions.[32,34] If there are large variations in the structure along the edges of the samples, then excess scattering from the edges are measured. Even with shallow surfaces, the edge effects cause measured scattering coefficients to be larger than 1 at high frequencies. For instance, if a square sample is placed on top of a round base plate, the scattering from the square edges results in excessive scattering and misleading results. The solution is to recess square samples within the circular base plate, as shown in Figure 4.26. Figure 4.27
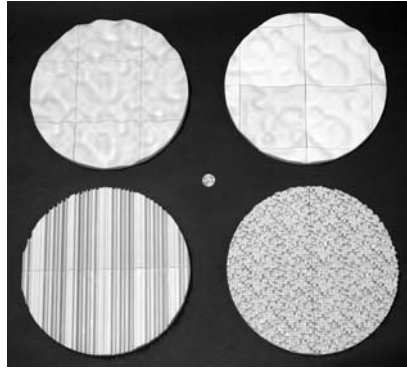
Figure 4.25   Four 1:10 scale models of commercial diffusers used to measure scattering coefficients. A small coin is placed in the centre of the photo to indicate scale.

shows measurements for the different mounting conditions, indicating that the recessed sample mounting gives the best results.

4.5.4 Anisotropic surfaces

The scattering coefficients give potentially misleading values when a surface is anisotropic. This is illustrated by Figure 4.28, where the scattering coefficients for a single plane and a hemispherical diffuser are compared. The single plane device produces a high value for the scattering coefficient, even though it is plane and extruded in one direction. To use a simplistic analysis, even if the scattering coefficient in the plane of maximum dispersion is 1, the scattering coefficient in the extruded direction must be close to 0. Therefore, it might be expected that the hemispherical coefficient would be somewhere around 0.5 – yet a value of 1 is obtained. This happens because the topology changes dramatically when the surface is rotated and, consequently, the surface is seen as being very good at scattering.
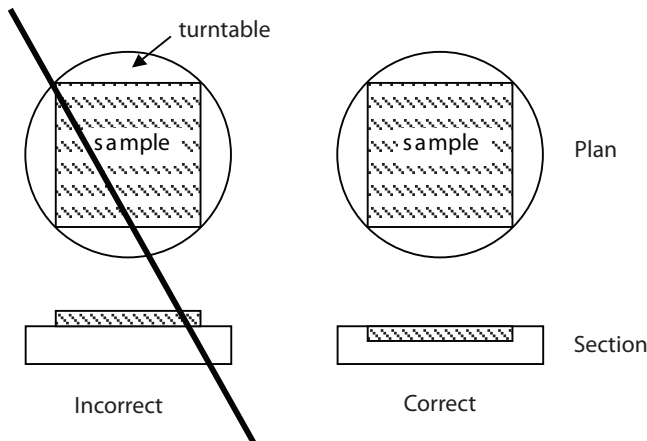
Figure 4.26   Mounting condition for non-circular samples.
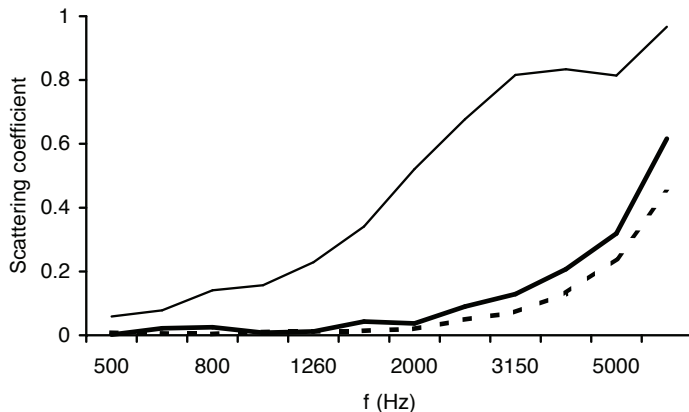
Figure 4.27 Scattering from a sinusoidal-shaped sample with different mounting conditions and sample shapes:
───── square sample, proud edges;
━━━━━ square sample, recessed edges; and
▬ ▬ ▬ circular sample (modified from Gomes *et al.*[34]).
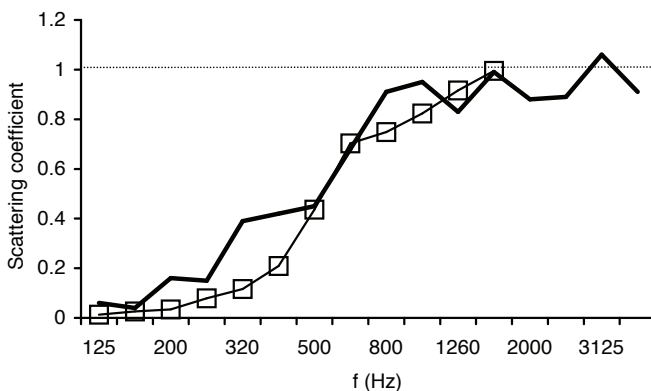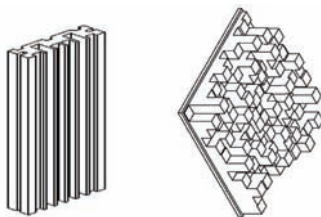
Figure 4.28 Scattering coefficients for two different diffusers and also the diffuser shapes. The left diffuser is a single plane device (FlutterFree®); the right diffuser is a hemispherical device (Skyline®). Multiple periods of each were used:
━━━━━ single plane; and
─▫─ hemispherical.

The ISO method often (if not always) produces high scattering coefficients for anisotropic surfaces. A more strict measure of diffusion ability would be two coefficients in two orthogonal directions, as is done for the AES diffusion coefficient. But then most current room acoustic models can only deal with single hemispherical based scattering coefficients, so this more strict evaluation is incompatible with current geometric models.

4.5.5 Predicting the scattering coefficient

It is awkward to predict the random incidence scattering coefficient. The necessity to carry out the predictions for a large number of sample orientations makes the prediction tedious with a boundary element model. Furthermore, it would be anticipated that the reverberation chamber would introduce inaccuracies due to non-diffuseness and other effects commonly seen in absorption measurement. Nevertheless, it is possible to carry out predictions for the free field scattering coefficient, as a function of incidence angle, and use Paris's formula (Equation 12.1) to get approximate random incidence values.

The free field scattering coefficient follows a similar principle to the random incidence coefficient. The measurement is done in an anechoic chamber and the receiver is placed in the specular reflection direction, as was shown in Figure 4.23. The surface is again rotated and the reflected pulses phase locked averaged. The energy remaining after the averaging is the specular energy. From this the scattering coefficient is obtained.

This measurement process can be mimicked in a boundary element model (BEM), although as noted above, it is rather tedious to do. Hargreaves[35] did this for a sample of rectangular battens and obtained accurate predictions, but this was only done for a few single frequencies.

If a simpler numerical model is used, the prediction time can be greatly decreased. Indeed, for Schroeder diffusers, it is possible to draw up a very simple formulation for the scattering coefficient. The far field scattering from a Schroeder diffuser can be predicted, using a simple Fourier model as described in Chapters 8 and 9. The Fourier model is not exact, but it does give reasonably accurate predictions of the scattering from the surfaces except at low frequencies and large angles of incidence or reflection. Under this approximate model, the pressure scattered from the surface, p_s, is given by:

$$p_s(\psi,\theta) \approx A \sum_{np=1}^{N_p} \sum_{n=1}^{N} e^{-2jkd_n} e^{jknw[\sin(\theta)+\sin(\psi)]} \tag{4.8}$$

where: ψ is the angle of incidence; θ the angle of reflection; N_p the number of periods; N the number of wells in a period; w the well width; k the wavenumber; d_n the depth of the nth well, and A is a constant.

This approximate theory enables a simple formulation for the scattering coefficient to be derived. In addition, the polar response can also be calculated from Equation 4.8 and so the diffusion coefficient can be found. Hence, a comparison of the diffusion and scattering coefficients can be made.[29] The scattering coefficient is not the ISO coefficient, however. Instead, it is a free field version of the Mommertz and Vorländer coefficient[13,14] derived following a similar philosophy.

The free field scattering coefficient is evaluated by finding the invariant energy, E_{spec}, in the specular direction ($\psi = -\theta$), when the surface is moved. Equation 4.8 is a single

plane formulation, so it is natural to translate the surface. The surface has been assumed infinitely large, so that edge effects are not significant. In this case, the averaging is done by translation over a complete period. In this ideal case, the scattering does not change with translation, because the receiver is in the specular reflection direction and all the terms, which vary when the surfaces moves, cancel out. The specular or invariant energy can be shown to be:

$$E_{spec} \approx \left| A' \sum_{np=1}^{N_p} \sum_{n=1}^{N} e^{-2\,jkd_n} \right|^2 \tag{4.9}$$

where A' is a constant.

The invariant energy is placed in a ratio with the energy from a flat plane surface for normalization purposes.[13] This then gives a specular reflection coefficient, R_{spec}:

$$R_{spec} = \frac{\left| A' \sum_{np=1}^{N_p} \sum_{n=1}^{N} e^{-2\,jkd_n} \right|^2}{\left| A' N_p N \right|^2} \tag{4.10}$$

This then represents the proportion of energy that is reflected in a specular manner by the surface, and so the scattering coefficient can be readily evaluated:

$$s = 1 - \left| \frac{1}{N} \sum_{n=1}^{N} e^{-2\,jkd_n} \right|^2 \tag{4.11}$$

The scattering coefficient is independent of angle of incidence and so averaging over multiple angles of incidence is not needed – in this special case the random incidence coefficient is numerically identical to the free field case. This is similar to the prediction model Embrechts *et al.*[36] produced for Gaussian rough surfaces.

Equation 4.11 shows that to get the greatest scattering, the sum of the reflection coefficients $\exp(-2kjd_n)$ must be evenly spaced around the unit circle. This is achieved for the modified versions of the primitive root diffuser[37,38] at integer multiples of a design frequency, as discussed in Chapter 9. This is illustrated in Figure 4.29 (the line labelled 'Correlation scattering coefficient' can be ignored for now). At multiples of the design frequency, the scattering coefficient, using Equation 4.11, is one. (Except at the flat plate or critical frequency of $(N-1)f_0 = 3$ kHz.) This complete scattering at the design frequency and multiples thereof, simply means no energy is in the specular direction. It does not necessarily say how good the dispersion produced is. This is why diffusion coefficients are numerically less than the free field scattering coefficient.

The free field scattering coefficient is given by the sum of the reflection coefficients squared – there is no dependence on the order of the wells in the diffuser. Although the distribution of polar response energy changes with the order of the wells, the energy actually moved from the specular reflection direction does not. Consequently, while the diffusion coefficient will vary if the order of the wells is changed, the scattering coefficient will not. This is another illustration of why the diffusion coefficient is a more strict test of diffuser quality.
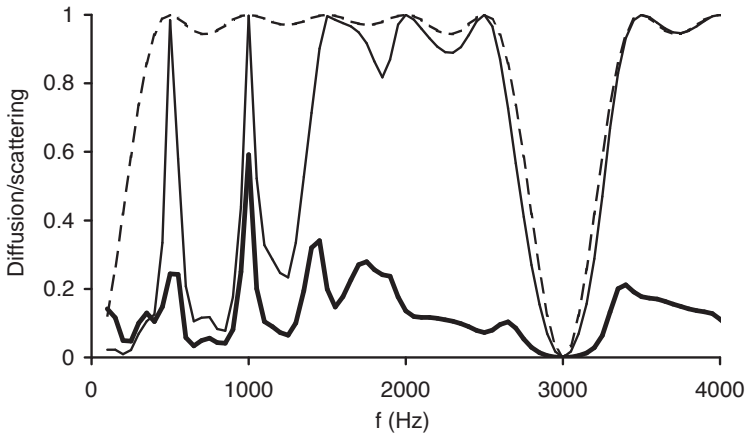
Figure 4.29 Various scattering and diffusion coefficients for a primitive root diffuser with a design frequency of 500 Hz:
– – – scattering coefficient using Equation 4.11;
────── normalized diffusion coefficient; and
────── correlation scattering coefficient (modified from Cox and D'Antonio[29]).

4.6 The correlation scattering coefficient – from polar responses to scattering coefficients

Mommertz presented a method for evaluating a scattering coefficient from polar responses. This correlates the scattered pressure polar responses from the test surface and a reference flat surface[39] to give a scattering coefficient. This will be called the correlation scattering coefficient δ_c. The coefficient is given by:

$$\delta_c = 1 - \frac{\left| \sum_{i=1}^{n} p_1(\theta_i) p_0^*(\theta_i) \right|^2}{\sum_{i=1}^{n} |p_1(\theta_i)|^2 \sum_{i=1}^{n} |p_0(\theta_i)|^2} \quad (4.12)$$

where p_1 is the pressure scattered from the test surface; p_0 is the pressure scattered from the flat surface; * denotes complex conjugate; θ_i the receiver angle of the ith measurement position, and n is the number of measurements in the polar response.

An alternative description of this coefficient was given by Embrechts *et al.*[36] who described it in terms of an LMS problem, which might be a more familiar description to anyone with a signal processing background.

This is not the same as the ISO coefficient or the free field scattering coefficient. This is illustrated in Figure 4.29, where the scattering coefficient from Equation 4.11 is compared to the correlation scattering coefficient for a primitive root diffuser. This difference arises because the coefficient definition is different. The free field Mommertz and Vorländer method measures the amount of energy moved from the specular direction when the surface is moved. The correlation scattering coefficient measures
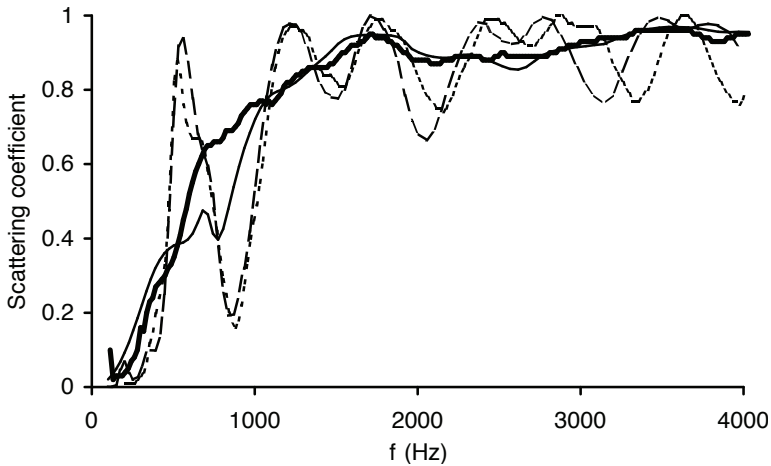
Figure 4.30 Comparison of predicted and measured correlation scattering coefficients:
———— prediction, 1 cylinder;
▬▬▬ measurement, 1 cylinder;
– – – prediction, 4 cylinders; and
------- measurement, 4 cylinders.

the dissimilarity between the test and flat surface scattering over a polar response. In the case of randomly rough surfaces, the two coefficients probably are similar, but for diffusers with distinct polar responses, this is not the case.

Although the correlation scattering coefficient is not identical to the ISO scattering coefficient, it does illustrate and help contrast the performance of diffusion and scattering coefficients.[29] One useful property of the correlation scattering coefficient is that it is readily predicted. Consequently, it is possible to compare prediction and measurement in a 2D polar response for a single cylinder and a set of cylinders. Predictions were carried out using a BEM (see Chapter 8) and measurements in a 2D goniometer (see Section 4.1). Figure 4.30 compares the predicted and measured correlation scattering coefficients and a good match is achieved. This provides evidence that the coefficient can be predicted and that the measurement system used is robust. It was feared that the measurement system might have difficulties, as accurate pressure magnitude and phase is needed, but this did not occur. Problems might occur, however, in measurements where exact microphone position replication is not achieved, for example, if a moving boom arm is used or where time variance cannot be maintained between the reference surface and diffuser measurements.

Kosaka and Sakuma[40] examined predicting the correlation scattering coefficient using a 3D BEM and explored some of the practical requirements for accurate results. The receiver and sources should be at least a diameter away from the test sample to ensure near field effects do not cause significant errors in the scattering coefficient. They found a 5° spatial resolution was required and that two single frequency evaluations per one-third octave band were useful for rough evaluation of scattering coefficients. At least 10 periods need to be tested for a periodic sample.

Embrechts *et al.*[41] examined a sine-shaped surface and found significant differences between prediction and measurements. At high frequencies, they mainly attribute the
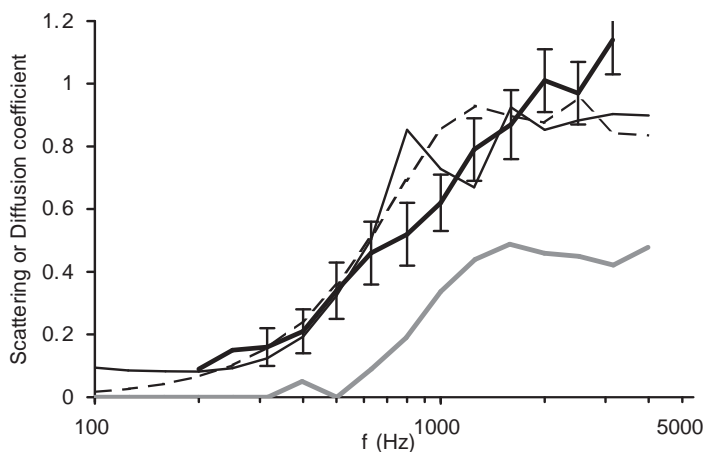
Figure 4.31 Various diffusion and scattering coefficients for a Schroeder diffuser. Diffuser
was shown top left in Figure 4.28.
———— correlation scattering coefficient;
——— random incidence ISO scattering coefficient (with error bars);
——— normalized diffusion coefficient;
– – – scattering coefficient predicted using Equation 4.11.

differences to a number of experimental issues leading to an over estimation of the
scattering. Low frequency measurement errors were thought to arise from the surface
producing low scattering. Therefore, the measurements became rather inaccurate and
uncertainties inherent in decay slope measurements mean a measured value of exactly
zero for the scattering coefficient can never be obtained.

A sample of a single plane QRD® has also been tested at 1:5 scale. One period of
the sample is shown as an insert in Figure 4.28. About 4 periods were used in the
final sample. The sample was measured in the 2D goniometer first with the QRD
wells perpendicular to the measurement arc and then with the wells parallel to the
measurement arc. For each sample orientation, three incidence angles (0, 30 and 60°)
were measured. These measurement results were then averaged to give an approximate
random incidence coefficient. A similar sample was measured using the ISO method
in a model reverberation chamber. The results are compared in Figure 4.31. There is
reasonable correspondence between the random incidence and correlation scattering
coefficients, although in two frequency bands the results are significantly different. For
example, for the 3.2 kHz octave band the random incidence measurement exceeds 1,
something that cannot happen with the correlation scattering coefficient. However,
considering one measurement is done in a diffuse field and the other in the free field,
the match is actually quite good, better than many have obtained when diffuse and free
field absorption coefficients are compared.

Also shown in Figure 4.31 is the scattering coefficient predicted using the simplest
Fourier model, Equation 4.11. The prediction accuracy is surprisingly good consid-
ering that the Fourier theory makes many assumptions which are not entirely correct
for this type of surface.

Figure 4.31 also shows the normalized diffusion coefficient for the diffuser. In this
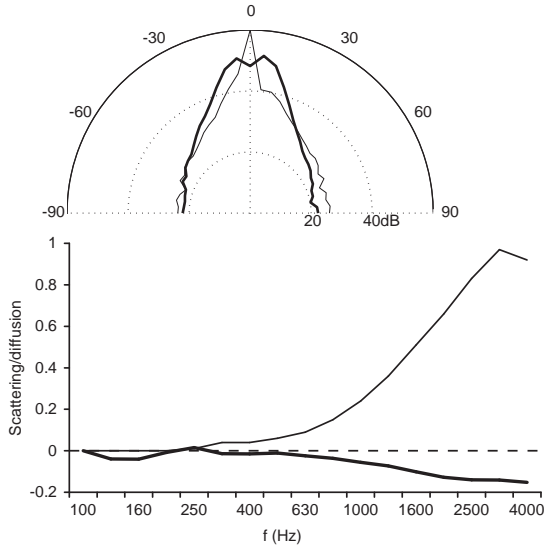
Figure 4.32 Top: polar responses for:
⎯⎯⎯ flat surface;
⎯⎯ concave sample.
Bottom: diffusion and scattering coefficients for concave sample:
⎯⎯ correlation scattering coefficient; and
⎯⎯⎯ normalized diffusion coefficient.

case, the scattering and diffusion coefficients agree as to the frequency at which significant scattering/diffusion begins ($\approx$500 Hz). Again, the diffusion coefficient is numerically less than the scattering coefficients, as discussed earlier.

   The polar response measurement system can also be used to illustrate some other key differences between scattering and diffusion coefficients. For example, in Section 4.4.1 the case of redirection was discussed. Another example is shown in Figure 4.32, which illustrates the effects of a focussing surface. The surface is designed to focus the sound on one microphone in the receiver arc. The diffusion coefficient interprets the focussing surface as being worse at diffusing sound than the plane surface. The normalized diffusion coefficient is less than zero for virtually every frequency. The correlation scattering coefficient, however, interprets the focussed polar response as being different from the plane surface and interprets this as being increased scattering. This illustrates that scattering coefficients should not be used to interpret single surface items, but should only be used for large surfaces with roughness. Furthermore, it shows that when evaluating diffusers, it is necessary not only to test the far field, but also to test at receiver positions where aberrations such as focussing may occur.

4.6.1 Scattering coefficient table

Appendix C gives a table of scattering coefficients for single plane diffusers. Some details of the geometry were given in Section 4.4.4, along with the rationale behind the choice of surfaces used in the prediction. The table includes all the surfaces included

in the diffusion coefficient table, except hybrid surfaces. The formulation for the correlation scattering coefficient needs to be revised for surfaces which partially absorb, because the current formulation interprets any absorption as being scattering.

The random incidence values tend to have raised values at low frequencies, especially for deep surfaces; values of up to 0.2 at 100 Hz are measured for many surfaces. At oblique incidence, edge scattering becomes important and the edges of the test samples are very different from the reference flat surface. Better results might be obtained if a reference surface with the same overall thickness as the test sample was used. Furthermore, because the rear of the test surfaces was not enclosed in a box, the scattering from the rear of the surface may also be having some effect at low frequency.

The scattering coefficient does not discriminate between different diffusers in a consistent manner – see the values for the optimized curved surfaces compared to the semi-ellipses, for example. The coefficient also interprets redirection as scattering. For instance, a 45° triangle returns a strong reflection back to a normal source, as discussed in Chapter 10, yet the scattering coefficient interprets this as dispersion. Nevertheless, with care, this published table of scattering coefficients can be used by geometric room acoustic modellers, as discussed in Chapter 12.

4.7 Contrasting diffusion and scattering coefficients – a summary

The scattering coefficient method gives a quick and rough estimate of the scattering process. It should not be used to evaluate the worth of surfaces when designing or specifying diffusers. The scattering coefficient is only concerned with how much energy is moved from the specular direction, it does not measure the quality of dispersion. For this reason, diffusing surfaces need to be evaluated using the diffusion coefficient when the quality of scattering is important. The diffusion coefficient should not, however, be blindly used in geometric room acoustic models as its definition is not compatible with the surface scattering models used in current geometric algorithms.

There are many issues surrounding these coefficients that remain to be resolved. One common question is whether there is a direct link between the coefficients and a physical property of the space. This arises because practitioners are used to a direct link between the absorption coefficient and the reverberation time. For diffusion and scattering there is no simple relationship, but maybe future research should include investigating what relationships, if any, exist between these coefficients and the room acoustic quality.

4.8 Other methods for characterizing diffuse reflections

There have been other methods developed to characterize the scattering from surfaces. They are noted here because they may yet develop into practical and used processes. The first method is a pragmatic approach, which has similarities to *in situ* absorption methods – maybe it will be developed into an *in situ* measurement method for diffusion coefficients. The second method tries to characterize the effect of diffuse reflections by investigating the change in diffuseness of a space. Finally, evaluating the comb filtering in the total sound field and temporal diffusion are discussed.

4.8.1 Measuring scattering coefficients by solving the inverse problem

This method was developed and published by Farina;[42] what is described below is a variation on the technique. In the description below, the general principle is discussed so that readers can get a sense of the process used.

The sound field in the vicinity of a diffuser is measured using a deterministic signal to gain the impulse response. It is necessary to make the measurements over many different spatial positions, these could be on an arc, as was done for the diffusion coefficient measurement, or if more convenient, these could be on a straight line parallel to the diffuser surface. The reflected impulse response is isolated by time windowing, as was done in Section 4.1, and then the frequency response found by using a Fourier transform. The frequency response is then normalized to a measurement of the incident sound field without the diffuser present to make the measurement independent of the source frequency response and sound power level.

The process is to predict the measured scattering from the surface using a geometric model and compare the predicted and measured polar response. The scattering and absorption coefficients within the geometric model are varied until the error between the predicted and measured polar responses are minimized. This is a trial and error process, which can be solved using an exhaustive search. The number of combinations to be tried is rather small if we assume the absorption and scattering coefficients only need to be varied in increments of say 0.01, and consequently, it is possible to simply do a complete check of every possible combination to find the correct coefficients.

This is a pragmatic approach to finding scattering coefficients. This process will probably give the coefficient most appropriate within the geometric model for randomly rough surfaces. Problems may arise, however, because the scattering coefficient will be dependent on the geometric model used, so this does not give a robust parameter for all models. The coefficient will only be as useful as the quality of the geometric model's diffuse reflection algorithm.

Problems also arise when the scattered polar response does not match any of the possible polar responses generated by the geometric model. Although Farina's paper shows good matches being achieved, many other diffusers have responses that do not match geometric models well. For instance, polar responses with a small number of distinct lobes (see Figure 10.11) are polar responses unlike anything that a geometric model will produce. In this case, the best matched scattering coefficient is likely to be nonsensical. This will happen with periodic devices at low- to mid-frequencies, as well as triangles and pyramids. This could be cured, however, by using more accurate dispersion patterns in the geometric model.

A further problem may occur from an ambiguity between the effects of scattering and absorption. There may be several good fits to the polar response, resulting from different combinations of absorption and scattering coefficients. Within experimental error, there will be a range of possible coefficients which could be used.

4.8.2 Room diffuseness

When surface diffusers are applied to a non-diffuse space, the volume diffuseness of the room will alter. Consequently, by measuring acoustic characteristics of a room before and after diffusers are introduced, it is possible to try and infer the scattering coefficient of the diffusers by the effect they have on the volume acoustic.[35]
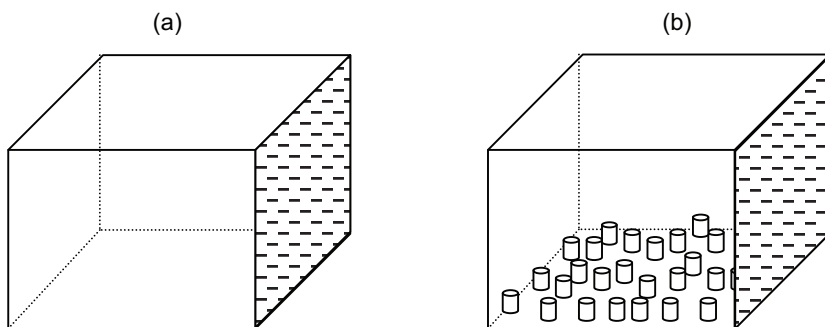
Figure 4.33   (a) A reverberation chamber with one wall made of absorbent (shown shaded).
(b) The chamber with a test sample on floor.

Consider the room shown in Figure 4.33a. It is a reverberation chamber with one wall covered in highly absorbent material. This is a highly non-diffuse space and the sound decay will be non-linear. If a diffuser is placed on another surface, Figure 4.33b, then the diffuser will scatter sound onto the absorbent, the reverberation times in the room will decrease, and the sound decays will become more linear. The issue here is the appropriate volume characteristic of the space to monitor the change in diffuseness.

A pragmatic approach, very similar in philosophy to Farina's method from the previous section, would be to use a geometric model to predict the sound field in the space. The geometric model is used to predict the acoustic in Figure 4.33a without diffusers, and this then enables the absorption of the walls of the reverberation chamber to be set by adjusting the values in the model until measurement and prediction match. Reverberation time would be an appropriate parameter to monitor. Then the diffusers are introduced. Again the model is tuned, this time changing the absorption and scattering coefficients on the floor with diffusers, until the best match between measurement and prediction is obtained. This process has the same disadvantages as that outlined for Farina's method in the previous section. The ambiguity between scattering and absorption is greater, as both affect the reverberation time. But most troublesome is the reliability and robustness of the geometric model used. These models are most inaccurate for non-diffuse spaces, which is exactly the test space deliberately created.

Consequently, it is best not to use a geometric model and to instead use the measured reverberation times in another way. The largest reverberation time obtained is for the test room before diffusers are applied (see Figure 4.33a). This is the case where the floor has a scattering coefficient of zero. If it were possible to obtain a lower limit for the reverberation time with diffusers present, the lowest achievable reverberation time when the maximally diffusing diffuser is applied, then this could be equated to a scattering coefficient of 1 for the floor. It would be straightforward to obtain a scattering coefficient from the actual measured reverberation time with a test sample by simple scaling. The problem, however, is obtaining this lower bounding limit. In theory, this limit would be the reverberation time predicted by Eyring's equation, but this can only be achieved if diffusers are applied to at least three surfaces, so that no surface and its opposite pair are untreated. For this reason, to carry out such a test method would involve large quantities of surface diffusion, far more than would be practical.

4.8.3 Temporal evaluation

The diffusion coefficient only monitors the sound energy scattered from the diffuser. Consequently, the phase and the temporal response have been neglected. With a single cylinder or hemisphere it is possible to produce good spatial dispersion, but without temporal dispersion. With most diffusers, on the other hand, good spatial dispersion also means that temporal dispersion is generated. Consequently, while current diffuser evaluation concentrates on energy dispersion, in the future it might also become necessary to look at the phase in the polar response or the reflected impulse response. Pertinent comments about this point can be found in Chapter 10, where the scattering from cylinders is discussed. The scattering coefficients implicitly deal with time dispersion, because of their definition.

One approach for evaluating the temporal dispersion is to look at decay characteristics. Redondo *et al.*[43] carried out a backwards integration[44] of the impulse responses of the sound scattered off various surfaces, to examine the decay time. Figures 10.3, 10.18, 10.26 and 10.28 show the impulse responses for a plane surface and various semi-cylinders (they can also be seen in Figure 4.36 later in this chapter). Figure 4.34 shows the decay curve for the four surfaces. Both the plane surface and the single semicylinder produce little temporal dispersion. This is reflected in the graph, as the sound energy decays rapidly. The four semicylinders have two strong reflection arrivals (because of symmetry there are two, rather than four, arrivals; see Figure 10.26 or Figure 4.36), and these arrivals appear as sudden drops in the decay curve. The surface that creates most temporal dispersion, the random array of semicylinders, has the longest decay time as might be expected. However, this analysis is only qualitative, and the perceptual significance of the different artefacts in the decay are currently not quantified.

In reality, the listener hears a fusion of the direct sound from the source and the reflection from the surface. This has led some to suggest that the total field (direct plus scattered) is an appropriate way of measuring the effectiveness of diffusers to reduce coloration. It certainly gets around all the problems of having to separate the direct and reflected sound by measuring impulse responses.
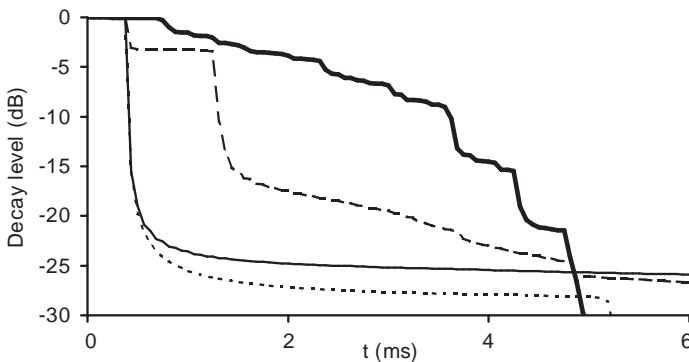
Figure 4.34   The decay of scattered sound from four surfaces:
- - - - - - flat surface;
———— 1 semicylinder;
– – – 4 semicylinders; and
▬▬▬ random array of semicylinders.
The corresponding impulse responses can be seen in Figures 10.3, 10.18, 10.26 and 10.28.
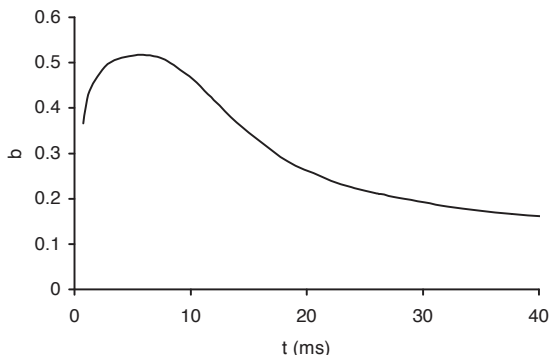
Figure 4.35 Weighting curve for examining coloration (after Bilsen[45]).

The autocorrelation function offers a way of checking for the randomness of signals, including impulse responses.[20,45,46] The weighted autocorrelation, s'_{xx}, is given by:

$$s'_{xx}(\tau) = b(\tau)s_{xx}(\tau)$$ (4.13)

where s_{xx} is the normal autocorrelation function, τ the delay variable and b a weighting function shown in Figure 4.35. This weighting function makes allowance for the time dependence of the reflections audibility. If a strong single reflection occurs at time τ_0, then it will cause audible coloration if:

$$s'_{xx}(\tau_0) > 0.063 s'_{xx}(0)$$ (4.14)

The results from examining the various impulse responses for a plane surface and semicylinders are shown in Figure 4.36. The maximum value in the sidebands of the autocorrelation function does decrease as more semicylinders are introduced and the sound becomes less specular. However, all of the plots shown exceed the threshold indicated by Equation 4.14. So coloration probably occurs in all cases. Furthermore, Equation 4.14 is based on the threshold of audibility, so it cannot be used to analyze whether there is an audible difference between the four cases, because they are all above threshold. Maybe the maximum value in the sidebands of the autocorrelation can be used as a measure of the amount of coloration, but that is untested.

However, both of the above approaches do not fully account for how the ear processes sound. Using an understanding of how the ear processes the total sound field, a more complete but complex method can be used.

For short delay times between the incident and reflected sound, say less than 25 ms[20,47] or a path length difference of 8.5 m, the dominating feature is the variation in the frequency response – the comb filtering – examples of which can be found in Chapter 10 and heard in most bathrooms.

For delays between 25 and 50 ms, equivalent to path length differences of 8.5 and 17 m, the dominant audible effect caused by the interference between direct sound and reflections is temporal fluctuations. To quantify this, one possible approach might be to use an adapted sound quality metric such as roughness,[48] which is used to quantify the
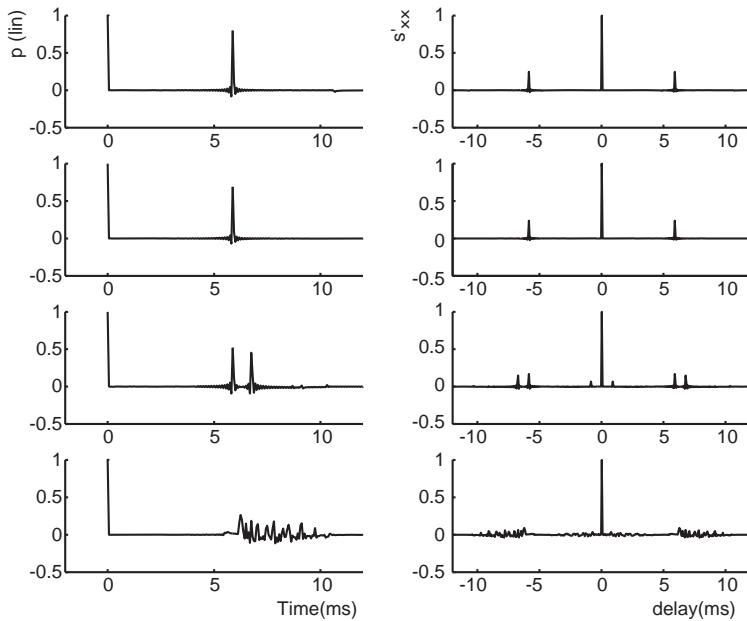
Figure 4.36 Left column: the impulse responses and right column: the weighted auto-correlation functions for the scattering from various surfaces. From top to bottom: plane surface, 1 semicylinder, 4 semicylinders, and random semi-cylinders.

subjective perception of rapid (15–300 Hz) amplitude modulation. However, even in sound quality testing, metrics such as roughness have a mixed history of success.

For delays beyond 50 ms, then strong reflections have the potential to be heard as separate sounds. Then criteria for the audibility of echoes could be considered[20] or, where there are large numbers of diffusers, some measure of the evenness of the reverberation.[49] Such criteria might be applied to monitor the effectiveness of diffusers *in situ* when used to control echoes, but the delay times are so long that they are not of interest for measuring diffusers within the laboratory.

As the above has shown, as the source and receiver positions change, the auditory effects alter because of the changing path lengths. The problem with total sound field evaluation is that it is so dependent on the geometry. The depth and frequencies of the minima and maxima in the comb filtering are strongly dependent on the delay time and relative level between the direct and reflected sound and hence on the source and receiver distances.

The total sound field might be analyzed in the critical bandwidths of the ears to examine whether the minima and maxima in the spectra are audible.[50] To be able to hear the effects of comb filtering, the analysis bandwidth of the ear, the width of the critical bands must be of a similar size to the frequency spacing of the minima and maxima. Provided delay times are <25 ms, so that frequency response variation dominates what is heard by the listener, then there are a number of options for quantifying the coloration. The most promising are those that attempt to mimic the processing of the ear.
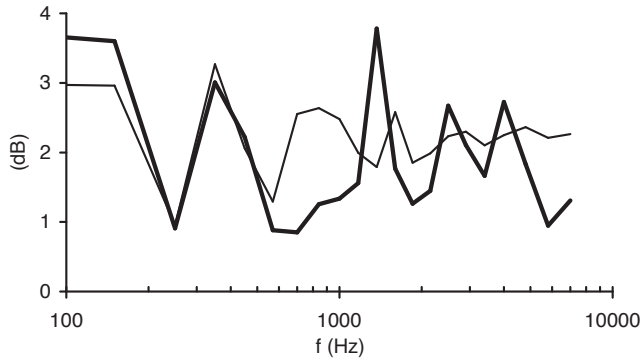
Figure 4.37   Level in the critical bands for total sound field:
────── plane surface; and
▬▬▬▬ random semicylinders.

The sound is initially passed through a bank of auditory filters that mimic the action of the cochlear which breaks sound into critical bands. This can be done according to the Bark scale[51] or similar. Figure 4.37 shows such an analysis for the plane surface and the random array of cylinders where equivalent rectangular bandwidths (ERBs) have been used.[52] Based on this representation, there are two evaluation methods: one based on the spectrum and the other on the autocorrelation.[53] Consider the former, which uses the ratio of the minimum and maximum energy in the spectrum. This ratio is examined to see if it exceeds some threshold value; this essentially quantifies the unevenness of the spectrum. Figure 4.37 shows an interesting result, however. Above 500 Hz, where the cylinders are diffusing, the spectrum for the plane surface has less variation than that for the diffuser, which contradicts expectation. When processing musical signals, the brain looks for regular harmonic structures to determine pitch and these periodic structures are also important for timbre. Consequently, further work is need to understand how the brain processes the regular periodic patterns that arise from comb filtering in comparison to the more random total field generated by a diffusing structure.

4.9 Summary

This chapter has mapped out some of the measurement techniques used for diffuse reflections. It might be anticipated that the use of scattering and diffusion coefficients might increase in the future, as practitioners want quantifiable evidence of how surfaces scatter and better predictions from geometric models. Having two coefficients gives potential for much confusion. Therefore, it is important that practitioners and researchers are educated about the difference, because using the wrong coefficient could lead to poor predictions or bad designs.

4.10 References

1 T. J. Cox, B-I. L. Dalenbäck, P. D'Antonio, J. J. Embrechts, J. Y. Jeon, E. Mommertz and M. Vorländer, "A tutorial on scattering and diffusion coefficients for room acoustic surfaces", *Acta Acustica uw Acustica*, **92**, 1–15 (2006).

2 AES-4id-2001, "AES Information document for room acoustics and sound reinforcement systems – characterisation and measurement of surface scattering uniformity", *J. Audio Eng. Soc.*, **49**(3), 149–65 (2001).

3 P. D'Antonio and T. J. Cox, "Diffusor application in rooms", *Appl. Acoust.*, **60**(2), 113–42 (2000).

4 P. D'Antonio, J. H. Konnert, and P. Kovitz, "The disc project: experimental measurement of the directional scattering properties of architectural acoustic surfaces", *Wallace Clement Sabine Centennial Symposium*, New York, 141–4 (1994).

5 T. J. Cox, "Objective and Subjective Evaluation of Reflection and Diffusing Surfaces in Auditoria", PhD thesis, University of Salford (1992).

6 A. Farina, personal communication.

7 T. J. Hargreaves, T. J. Cox, Y. W. Lam and P. D'Antonio, "Surface diffusion coefficients for room acoustics: free field measures", *J. Acoust. Soc. Am.*, **108**(4), 1710–20 (2000).

8 L. E. Kinsler, A. R. Frey, A. B. Coppens and J. V. Sanders, *Fundamentals of Acoustics*, John Wiley & Sons (1982).

9 J. H. Rindel, "Attenuation of Sound Reflections due to Diffraction", *Proc. Nordic Acoustical Meeting*, NAM86 (1986).

10 M. Kleiner, H. Gustafsson and J. Backman, "Measurement of directional scattering coefficients using near-field acoustic holography and spatial transformation of sound fields", *J. Audio Eng. Soc.*, **45**(5), 331–46 (1997).

11 P. D'Antonio and J. H. Konnert, "The reflection phase grating diffusor: design theory and application", *J. Audio Eng. Soc.*, **32**(4), 228–38 (1984).

12 ISO 17497-1:2004, "Acoustics – sound-scattering properties of surfaces. Part 1: Measurement of the random-incidence scattering coefficient in a reverberation room".

13 E. Mommertz and M. Vorländer, "Measurement of scattering coefficients of surfaces in the reverberation chamber and in the free field", *Proc. 15th ICA*, **II**, 577–80 (1995).

14 M. Vorländer and E. Mommertz, "Definition and measurement of random-incidence scattering coefficients", *Appl. Acoust.*, **60**(2), 187–200 (2000).

15 Y. W. Lam, "On the parameters controlling diffusion calculation in a hybrid computer model for room acoustic prediction", *Proc. IoA(UK)*, **16**, 537–44 (1994).

16 M. Hodgson, "Evidence of diffuse surface reflections in rooms", *J. Acoust. Soc. Am.*, **89**, 765–71 (1991).

17 M. Vorländer, "International round robin on room acoustical computer simulations", *Proc. 15th ICA*, **II**, 689–92 (1995).

18 Y. W. Lam, "Diffuse reflection modeling methods", *J. Acoustic. Soc. Am.*, **100**(4), 2181–92 (1996).

19 B. Dalenbäck, M. Kleiner and P. Svensson, "A macroscopic view of diffuse reflection", *J. Audio. Eng. Soc.*, **42**, 793–807 (1994).

20 H. Kuttruff, *Room Acoustics*, 4th edn, Spon Press (2000).

21 T. J. Cox, "Optimization of profiled diffusers", *J. Acoust. Soc. Am.*, **97**(5), 2928–41 (1995).

22 T. J. Cox, "Designing curved diffusers for performance spaces", *J. Audio. Eng. Soc.*, **44**, 354–64 (1996).

23 P. D'Antonio, "The disc project: directional scattering coefficient determination and auralization of virtual environments", *Proc. Noise-Con 93*, 259–64 (1993).

24 J. Angus, A. C. Marvin, J. Clegg and J. F. Dawson, "A practical metric for evaluating sound diffusers", *Proc. 98th Convention Audio Eng. Soc.*, preprint 3955 (D5) (1995).

25 D. Takahashi, "Development of optimum acoustic diffusers", *J. Acoust. Soc. Jpn (E)*, **16**(2), 51–8 (1995).

26 T. J. Cox, "Diffusion parameters for baffled diffusors", *99th Convention Audio Eng. Soc.*, paper 4115 (1995).

27 Y. W. Lam, "A boundary integral formulation for the prediction of acoustic scattering from periodic structures", *J. Acoust. Soc. Am.*, **105**(2), 762–9 (1999).

28 J. A. S. Angus, "Diffuser assessment using surface spherical harmonics", *J. Acoust. Soc. Am.*, **104**(3), 1857–8 (1998).

29 T. J. Cox and P. D'Antonio, "Contrasting surface diffusion and scattering coefficients", *Proc. 17th ICA*, 6B.09.01, Italy (2001).

30 J. J. Embrechts, "Practical aspects of the ISO procedure for measuring the scattering coefficient in a real-scale experiment", *Proc. Forum Acusticum Sevilla*, RBA-06-001-IP (2002).

31 L. De Geetere and G. Vermeir, "Investigations on real-scale experiments for the measurement of the ISO scattering coefficient in the reverberation room", *Proc. Forum Acusticum Sevilla*, RBA-06-004 (2002).

32 M. Vorländer, J. J. Embrechts, L. De Geetere, G. Vermeir and M. Gomes, "Case studies in measurement of random incidence scattering coefficients", *Acta Acustica uw Acustica* **90**, 858–67 (2004).

33 BS EN ISO 354:2003, "Acoustics – measurement of sound absorption in a reverberation room".

34 M. H. A. Gomes, M. Vorländer and S. N. Y. Gerges, "Aspects of the sample geometry in the measurement of the random-incidence scattering coefficient", *Proc. Forum Acusticum Sevilla*, RBA-06-002-IP (2002).

35 T. J. Hargreaves, "Acoustic Diffusion and Scattering Coefficients for Room Surfaces", PhD thesis, University of Salford (2000).

36 J. J. Embrechts, D. Archambeau and G. B. Stan, "Determination of the scattering coefficient of random rough diffusing surfaces for room acoustics applications", *Acta Acustica uw Acustica*, **87**, 482–94 (2001).

37 E. Feldman, "A reflection grating that nullifies the specular reflection: A cone of silence", *J. Acoust. Soc. Am.*, **98**(1), 623–34 (1995).

38 T. J. Cox and P. D'Antonio, "Acoustic phase gratings for reduced specular reflection", *Appl. Acoust.*, **60**(2), 167–86 (2000).

39 E. Mommertz, "Determination of scattering coefficients from reflection directivity of architectural surfaces", *Appl. Acoust.*, **60**(2), 201–4 (2000).

40 Y. Kosaka and T. Sakuma, "Numerical examination on scattering coefficients of architectural surfaces using the boundary element method", *Acoust. Sci. & Tech.*, **26**(2), 136–44 (2005).

41 J. J. Embrechts, L. De Geetere, G. Vermeir, M. Vorländer and T. Sakuma, "Calculation of the random-incidence scattering coefficients of a sine-shaped surface", *Acta Acustica uw Acustica*, **92**(4), 593–603 (2006).

42 A. Farina, "A new method for measuring the scattering coefficient and the diffusion coefficient of panels", *Acustica*, **86**(6), 928–42 (2000).

43 J. Redondo, R. Pico, B. Roig and M. R. Avis, "Time domain simulation of sound diffusers using finite-difference schemes", *Acta Acustica uw Acustica*, **93**(4), 611–22 (2007).

44 M. R. Schroeder, "New method of measuring reverberation time", *J. Acoust. Soc. Am.*, **37**(6), 409–12 (1965).

45 F. A. Bilsen, "Thresholds of perception of repetition pitch. Conclusions concerning coloration in room acoustics and correlation in the hearing organ", *Acustica*, **19**, 27–32 (1968).

46 S. Sato and J. Y. Jeon, "Evaluation of the scattered sound field by using the autocorrelation function of impulse responses", *Proc. IoA(UK)*, **28**(2), 210–7 (2006).

47 P. Rubak, "Coloration in room impulse responses", *Proc. Joint Baltic-Nordic Acoustics Meeting*, *Åland* (2004).

48 E. Zwicker and H. Fastl, *Psychoacoustics: Facts and Models*, Springer Series in Information Sciences (1999).

49 K. Srodecki, "Evaluation of the reverberation decay quality in rooms using the autocorrelation function and the cepstrum analysis", *Acustica*, **80**, 216–25 (1994).

50 F. A. Everest, *The Master Handbook of Acoustics*, 4th edn, TAB Electronics Technical Library (2000).

51 E. Zwicker, "Subdivision of the audible frequency range into critical bands", *J. Acoust. Soc. Am.*, **33**(2), 248 (1961).

52 B. C. J. Moore and B. R. Glasberg, "Suggested formulae for calculating auditory-filter bandwidths and excitation patterns", *J. Acoust. Soc. Am.*, **74**, 750–3 (1983).

53 A. N. Salomons, "Coloration and Binaural Decoloration of Sound Due to Reflections", PhD thesis, University of Delft (1995).

5   Porous absorption

Typical porous absorbers are carpets, acoustic tiles, acoustic (open cell) foams, curtains, cushions, cotton and mineral wools such as fibreglass. They are materials where sound propagation occurs in a network of interconnected pores in such a way that viscous and thermal effects cause acoustic energy to be dissipated. As discussed in Chapter 1, they are used widely to treat acoustic problems, in cavity walls and noisy environments to reduce noise and in rooms to reduce reverberance. This chapter will detail the physical processes producing the absorption and theoretical models for predicting absorption properties.

The first section gives a qualitative description of the use of porous absorbers; this will be followed by some example materials in Section 5.2. These materials range from standard well-known materials, such as mineral wool, to more recent developments, such as absorbent plaster systems. Section 5.3 and onwards then outlines the methods needed to predict the absorption. The theoretical sections start by outlining how the sound propagation within a porous absorbent might be modelled in terms of characteristic parameters of the material. There are empirical and semi-empirical approaches and both are detailed. The chapter then proceeds to show how these acoustic parameters are combined with mounting conditions, to enable the absorption coefficient and surface impedance to be predicted, which is ultimately what is required in design.

5.1 Absorption mechanisms and characteristics

When sound propagates in small spaces, such as the interconnected pores of a porous absorber, energy is lost. This is primarily due to viscous boundary layer effects. Air is a viscous fluid, and consequently sound energy is dissipated via friction with the pore walls. There is also a loss in momentum due to changes in flow as the sound moves through the irregular pores. The boundary layer in air at audible frequencies is sub-millimetre in size, and consequently viscous losses occur in a small air layer adjacent to the pore walls. As well as viscous effects, there will be losses due to thermal conduction from the air to the absorber material; this is more significant at low frequency. For the absorption to be effective there must be interconnected air paths through the material; so an open pore structure is needed. The difference in construction between an open and closed pore system is shown schematically in Figure 5.1.[1] Losses due to vibrations of the material are usually less important than the absorption as sound moves through the pores.

Figures 5.2 and 5.3 show the absorption coefficients for two porous absorbers illustrating the effect of material thickness. The porous absorber is mounted on a rigid
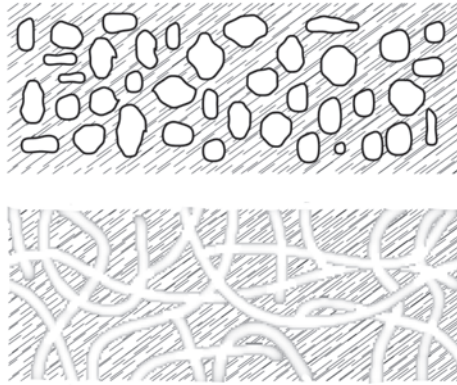
Figure 5.1 Illustration of the difference between closed (top) and open (bottom) pore structures (adapted from Cremer and Müller[1]).

backing. These curves follow the characteristic shape of porous absorption coefficients, a high pass filter response, although the curves can shift in frequency and move up and down in absorption depending on the characteristics of the particular material and how it is mounted.

   As the thickness of the porous material increases, the absorption at low frequency usually increases. For the porous absorber to create significant absorption, it needs to be placed somewhere where the particle velocity is high. The particle velocity close to a room boundary is usually zero, and so the parts of the absorbent close to the boundary generate insignificant absorption. It is the parts of the absorbent furthest from the backing surface which are often most effective, and this is why thick layers of absorbent are needed to absorb low frequencies. A rough figure sometimes quoted is that the material needs to be at least a tenth of a wavelength thick to cause significant absorption,[2] and a quarter of a wavelength to absorb all the incident sound. Consequently, substantial absorption cannot be achieved by simply applying a thin
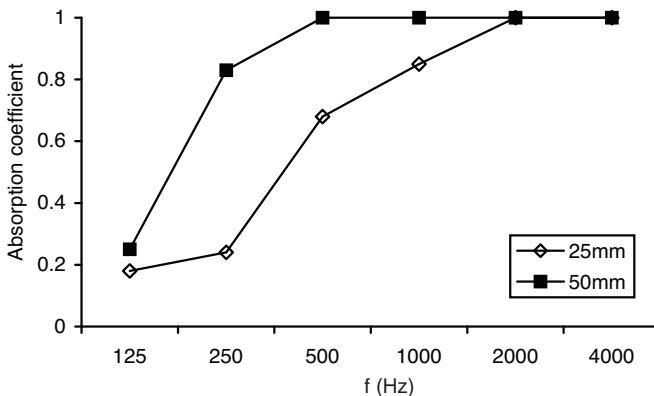
Figure 5.2 Random incidence absorption coefficient for rockwool of two different thicknesses on a rigid backing.
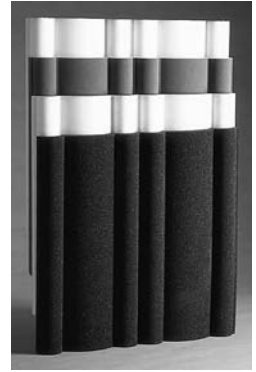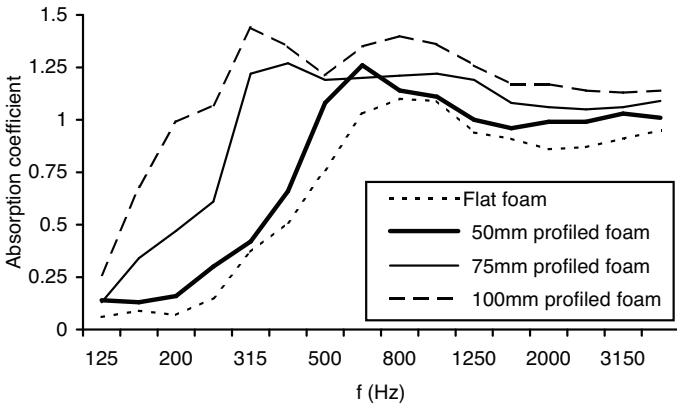
Figure 5.3 Random incidence absorption coefficients for a profiled acoustic foam on a rigid backing, sold as ProFoam™ ³.

layer of paint. As the material very close to the boundary is absorbing relatively little, it is possible to simply space porous absorbers away from a wall and get good performance. Figure 5.3 shows a simple way of achieving this by shaping acoustic foam into a rough sinusoidal shape.³ The acoustic absorption achieved is also given.

The amount of energy absorbed by a porous material varies with angle of incidence as illustrated in Figure 5.4. For a mineral wool with high absorption, as illustrated by
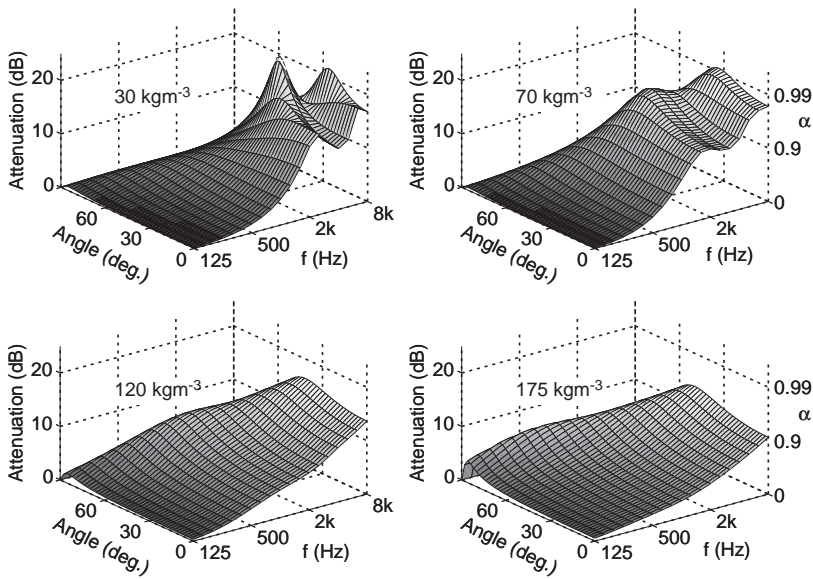
Figure 5.4 Attenuation of specular reflection from mineral wool as a function angle of incidence and frequency. Each plot represents a different mineral wool density as marked on the charts. On two of the charts, the equivalent absorption coefficient is also marked. 38 mm of mineral wool on a rigid backing, predicted using an empirical model.

the top right plot, then the absorption first increases as the angle of incidence moves away from the normal to the surface, before tailing off as the source moves around to grazing. The performance varies most with angle of incidence for the least dense mineral wools. Another feature of note is that it is important to get the right density of mineral wool (or to be more correct, the right flow resistivity). With too high a flow resistivity the impedance mismatch between the air and the absorbent causes the sound to reflect from the front face and the absorption reduces.

For low frequencies, where the wavelength is large, one has to go a considerable distance from the wall to reach a point where the particle velocity is significant. This makes porous absorbers inefficient and not particularly useful at low frequency. At bass frequencies, resonant structures will produce greater absorption from a given depth, as discussed in Chapter 6, or maybe this can be achieved through active absorbers, as discussed in Chapter 13. To get broadband passive absorption across the frequencies of most interest to design, usually requires a combination of resonant and porous absorption.

5.1.1 Covers

Often porous absorbers are covered in cloth or plastic. For instance, a thin impervious membrane might be used to wrap a fibrous absorbent when it is used as a duct lining material, to prevent fibres being lost within the ventilation system. Impervious membranes such as plastic will reduce the high frequency absorption, as the impedance tube measurements in Figure 5.5 show. At low frequencies, the membrane's acoustic mass is small and the sound passes through the membrane largely unaltered – although a small increase in absorption due to the added mass of the membrane may occur. At high frequencies, however, the membrane's acoustic mass is high and it will prevent some or all of the sound energy entering the porous absorber. This membrane effect is why porous absorbers should not be painted except with a non-bridging paint. Most paints will block the pores, prevent sound waves freely entering the structure and so reduce the absorption.

Within rooms, porous absorbers are often finished by cloth wrapping to protect the absorbent material and make it look better. The cloth wrapping potentially has
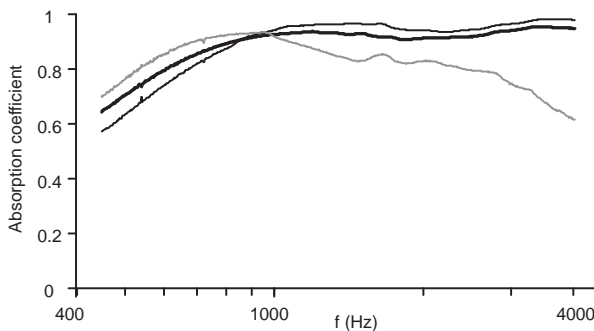
Figure 5.5 Measured normal incidence absorption coefficient for fibreglass with different finishes:
———— uncovered;
━━━━ cloth covering; and
———— perforated wood covering.

little effect on the absorption obtained, provided the cloth freely allows sound to enter the porous absorbent. If glue is used to fix the cloth to the front face of the absorber, however, care must be taken to ensure the high frequency absorption is not reduced, because the glue prevents sound entering the porous material.

Porous materials are often mounted behind perforated panels to protect the absorbent from damage. If the perforated sheet does not have a very open structure, with a large per cent open area, the mass effect of the holes will increase the absorption at low frequency but decrease absorption at high frequency, as shown in Figure 5.5. Although it is commonly quoted that a greater than 20 per cent open area means that the perforated sheet has no effect,[4] the results for hybrid diffuser-absorbers given in Chapter 11 illustrate that even a 50 per cent open area perforated sheet can have a significant effect on absorption. The transfer matrix techniques outlined in Chapter 6 can be used to predict the effects of perforated sheets on absorption. For membrane-wrapped porous material behind a perforated sheet, it is important that the membrane and perforated sheets are not in contact, otherwise the absorption is decreased.[4]

5.2 Some material types

5.2.1 *Mineral wool*

There is a bewildering array of materials available which exhibit porous absorption. Mineral wool is made from materials such as sand, basaltic rock and recycled glass. The raw materials are melted at high temperature and then spun or pulled into woolly filaments. The filaments are bonded together to give the product its physical shape, with roughly 1–5 per cent of the final product weight being binder.[5] Glass fibre is made up of the same raw ingredients as normal glass such as sand, limestone and soda ash, and the manufacturing process is similar to rock or basalt wool, although rock and basalt wool products tend to be heavier. The acoustic absorption achieved is determined by the fibre composition, fibre orientation, fibre dimensions, product density, and the quantity and nature of the binder used. The mineral wool can be in the form of semi-rigid boards or loose blanket. Compressed mineral fibre board is the basis of the ubiquitous absorbing ceiling tiles mounted in t-bar grids.

Man-made mineral wools are cheap to manufacture and can be partially recycled. However, the manufacturing process uses considerable energy which increases the environmental impact of the material. The acoustic performance of mineral wool can vary with density, and for low densities the high frequency absorption can be reduced. Density alone, however, is not sufficient to predict acoustic performance, because the fibre diameter is also a crucial factor, as the formulations later in this chapter show. Mineral wool is often laid down in layers and so is anisotropic. For this reason, the acoustic properties vary depending on whether sound is incident parallel or perpendicular to the fibres, although for simplicity this is often ignored in prediction models.

There have been some concerns about the long-term health effects of man-made vitreous fibres (MMVFs), which have helped develop a market for non-MMVF and fibreless absorbers. MMVFs are known to be irritants, causing skin, eye and upper respiratory tract irritation; the irritation is usually caused by mechanical action rather than an allergic reaction. Of particular concern are fibres with diameters of <3 μm, which can reach the pulmonary regions of the lung and form the greatest

cancer hazard. In the past, the lack of scientific data led authorities to give cautionary classifications to MMVF. However, more recent studies have failed to find evidence that MMVF are a significant risk to health. Indeed, in 2002, The International Agency for Research on Cancer, which is part of the World Health Organization, reclassified mineral wool as category 3: "not classifiable as to their carcinogenicity to humans", meaning there is no strong evidence that mineral wool is carcinogenic to humans.[6,7]

5.2.2 Foam

Foams can have open or closed cell structures. With open cell structures the pores are interconnected and significant absorption can result. Closed cell structures, on the other hand, do not permit the passage of sound and so the absorption is rather low. It is possible, however, to perforate closed foam structures at the end of manufacture and so provide moderate absorption by interconnecting the pores. Consequently, it is important to check that acoustic foam is used where sound absorption is needed. The fire rating of acoustic foams needs to be checked, especially when they are used in buildings.

5.2.3 Sustainable materials

To minimize environmental impact, acoustic treatments need to be made from recycled materials or resources that are natural, plentiful or renewable. The materials should be sourced locally or regionally. The product themselves should be recyclable, reusable and/or biodegradable. During manufacture, waste recycling, green power and resource-efficient manufacturing processes need to be considered. Recycled or recyclable product packaging needs to be used and the environmental impact of transportation considered. Ideally, a full life cycle of a product should be assessed, but in many cases this is not possible.

Sheep wool has been suggested as a possible replacement for mineral wool, and has the advantage of having a much lower impact on global warming than man-made mineral fibres.[8] However, in forms which are easy to manufacture, it is inherently a low density (10–100 kgm^{-3}), low flow resistivity material (500–15,000 MKS rayls m^{-1}), and so it needs to be relatively thick (5–10 cm) to achieve high absorption.[9] It is useful in sound insulation applications, filling cavity walls, where infill material does not have to have very high absorption coefficients to be effective.

There is great interest in trying to make acoustic absorbers from recycled materials, whether that be recycled cloth, metal, foams, wood, plastics or rubber. To take one example, researchers have been investigating recycling tyres as acoustic absorbers.[10] The hope is that the elastic properties of the material will also enable the rubber to cushion the effects of crashes if these are used in road side barriers. The other advantages that tyres offer are that they can be painted, and will survive the harsh environment around roads better than standard fibrous materials. The rubber is broken up into small granules, and these are then bonded together with a binder. The key is to use enough binder to hold the granules together without blocking the air pores, which are crucial to absorption, and to get the right grain size and shape. To take another example, Swift and Horoshenkov[11] showed that loose granulated mixes of waste foam with particle sizes <5 mm, can be pressed into consolidated, elastic, porous media with a high proportion of open and interconnected pores and good absorption properties.
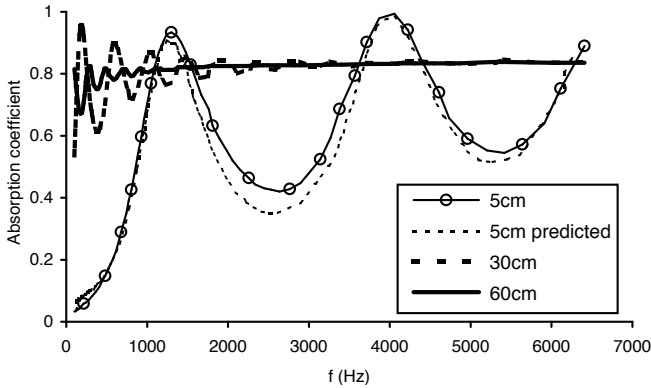
Figure 5.6   Absorption from granulated rubber 1 to 3 mm in size for different thicknesses. Measured in the impedance tube unless otherwise indicated in legend (modified from Pfretzschner[10]).

Pfretzschner[10] tested rubber granular diameters ranging from 1.4 to 7 mm. An example of the typical absorption coefficients are shown in Figure 5.6, mostly measured in an impedance tube. They found that, for a given sample thickness, the absorption coefficient increases when the diameter of the grains decrease.

The behaviour of granular materials is different from fibrous ones such as mineral wool, because grains pack together differently, usually resulting in a lower porosity for granular materials in comparison to fibrous ones. The absorption varies more with frequency for granular materials than for fibrous absorbents as shown in Figure 5.6 in comparison to Figures 5.2 and 5.3. There is a critical thickness for the granular material, beyond which additional depth does not increase absorption. The broadband absorption for thick samples of the granular material shown in Figure 5.6 is limited to around 0.8, whereas with fibrous absorbent, the value can rise to unity. Consequently, fibrous materials often give better acoustic absorption, but the recycled granular materials might be favoured for other reasons, such as sustainability. The performance of the recycled granular absorbent can be improved by forming wedges rather than flat boards. Also included in Figure 5.6 is a prediction of the absorption coefficient using a complicated porous absorber model showing that good results from such theories can be obtained; a similar theory is outlined later in this chapter.

In developing an environmentally friendly or sustainable absorbent, many issues have to be considered. It is preferable for the whole life cycle of the product to be considered. Products made from recyclable materials are welcomed, but issues such as energy consumption during manufacture and the environmental impact of binders need to be considered. Another issue is whether the product is recyclable at the end of its life. An example of product that achieves this is Reapor™,[12] which is a non-combustible inorganic foam. A combination of heat processes and sintering is applied to glass, much of it recycled waste, to form a granular absorbent where even the grains themselves contain small pores. Figure 5.7 shows the pore structure for the material measured using an electron microscope and also displays the absorption coefficients. The material is fibre-free, rugged, non-combustible, moisture resistant, and can be used indoors or outdoors.
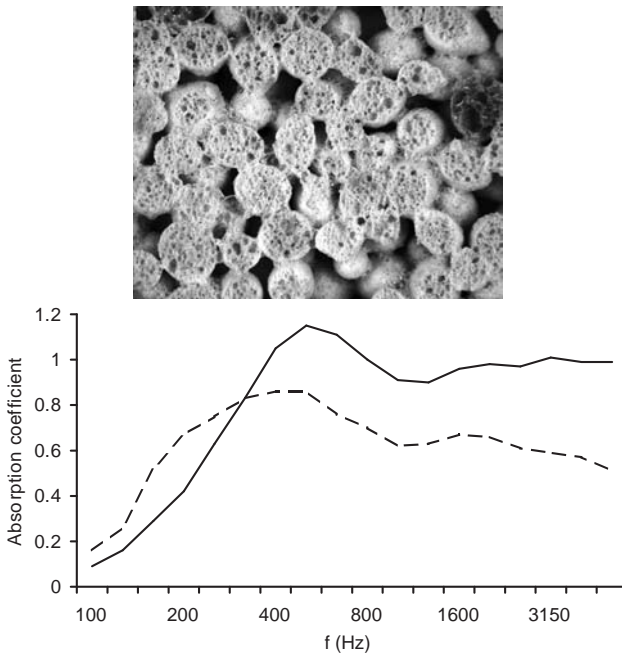
Figure 5.7 Top: pore structure for PhoneSTOP, an inorganic foam Reapor, showing double porosity. Bottom: random incidence absorption coefficient for:
———— Reapor; and
– – – – the material coated to form an acoustic plaster system (photo and data courtesy of Henkel KGaA).

Around the world various competing rating systems have been developed to encourage buildings which minimize environmental impact. An example of such a scheme in the US is the Leadership in Energy and Environmental Design (LEED®) rating system developed by the United States Green Building Council.[13] This lists detailed criteria against which building projects should be rated to gain accreditation. Relevant to acoustic materials, the system deals with issues such as recycled content, woods from certified sources and low-emitting paints and coatings. Four levels of LEED certification are available: Platinum (52–69 credits), Gold (39–51 credits), Silver (33–38 credits) and Certified (26–32 credits). To qualify under one of these four designations buildings must satisfy all of the LEED prerequisites, such as Elimination and Control of Asbestos, Smoking Ban, etc., then go on to earn a certain number of credits. The 69 credits are grouped into 6 areas: Sustainable Sites; Water Efficiency; Energy and Atmosphere; Materials and Resources; Indoor Environmental Quality, and Innovation and Design Processes.

5.2.4 Curtains (drapes)

Curtains or drapes are essentially porous absorbers. Most of the time, the deeper the folds, the greater the absorption,[14] as this means there is more resistive material and the absorbent is further from the rigid backing where the particle velocity is greater.
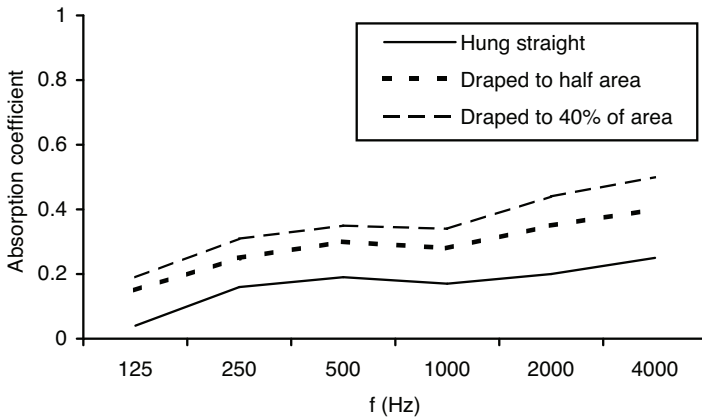
Figure 5.8   Curtain (drape) absorption with different fullness of draping (data from Harris[14]).

This is illustrated in Figure 5.8, where the same curtain is hung with different fullness. It is also possible to increase the absorption by hanging the curtain away from the rigid surface and so placing the resistive material where the particle velocity is higher, and hence producing more absorption. Increasing the density of the material generally increases the absorption produced,[15] as shown in Figure 5.9. Appendix A gives further data showing that the absorption coefficient varies greatly depending on the type of curtain and mounting.

5.2.5 Carpets

If present, carpet usually contributes a large proportion of the high frequency absorption present in a room. The amount of absorption created depends on the type of carpet and also the underlay used.[14,16] Essentially, the carpet is a porous absorber, and so it has little absorption at low frequencies, but causes significant attenuation at high frequencies. If the underlay is open celled, then its presence increases the thickness of
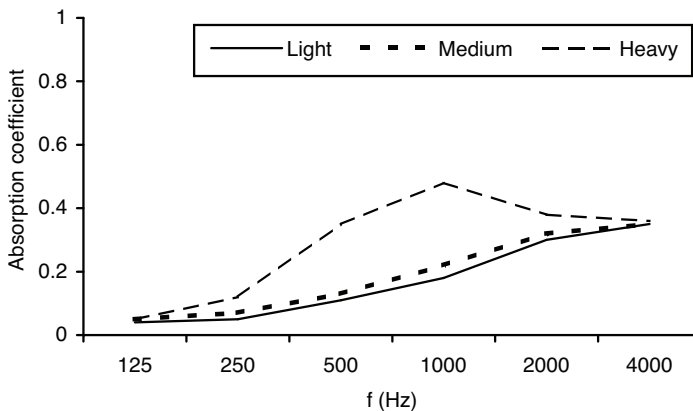
Figure 5.9   Curtain (drape) absorption for different material weights (data from Beranek[15]).
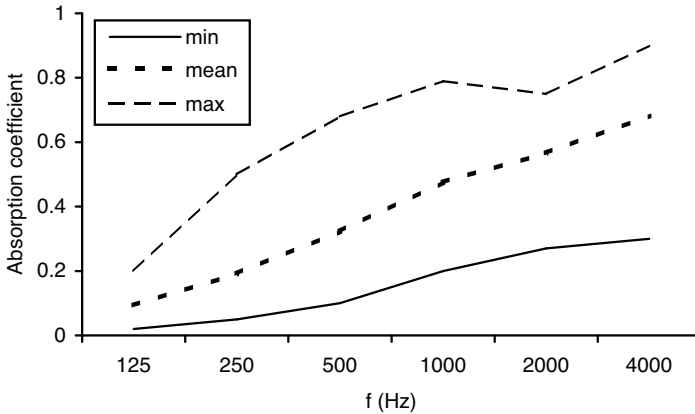
Figure 5.10 The minimum, mean and maximum values for carpet absorption from the literature.

the porous absorbent, and so increases the absorption. Some underlay types are open celled, such as old-fashioned felt hair and foam rubber. Sponge rubber, however, can be open or closed cell. The absorption generated is also very dependent on the type of carpet, for instance the way the pile is constructed. Appendix A gives a large number of absorption coefficients for different carpet types taken from literature. Everest notes[16] that the absorption coefficients reported for carpet vary quite considerably between different publications. This is illustrated in Figure 5.10, where minimum, mean and maximum absorption coefficients in the literature are shown. This emphasizes the need for measurement of the carpet to be used, rather than assuming that an average value from the literature will be accurate.

5.2.6 Acoustic plaster

Architects more often than not prefer their acoustic treatment to be hidden and certainly not defining the visual aesthetic. Consequently, an absorptive, smooth, seamless and durable plastered finish is useful in satisfying the aesthetic requirements of architects and interior designers. There are currently several approaches to achieving a seamless appearance which looks like plaster. However, current products are not really absorbent plasters in that they all involve an absorptive substrate, whether it be mineral wool or a non-combustible inorganic blown-glass granulate (2–4 mm grain size), and a surface layer which looks like plaster and is as acoustically transparent as possible. This surface layer is typically composed of some aggregate, such as marble particles, glass granulate and cotton, with a binder that allows the pores between the aggregate to remain open when the binder dries. The installation of seamless areas is possible up to a maximum of 200 m². The maximum length or width should not exceed about 15 m. Expansion joints are mandatory for larger areas and intersecting boundary surfaces to avoid cracking.

   All of these systems are applied on-site. To ensure that a seamless surface is achieved with a perfect optical finish, it is necessary to start with a ceiling that is perfectly level and clean by projecting a light across its surface. Once the absorptive substrate panels are
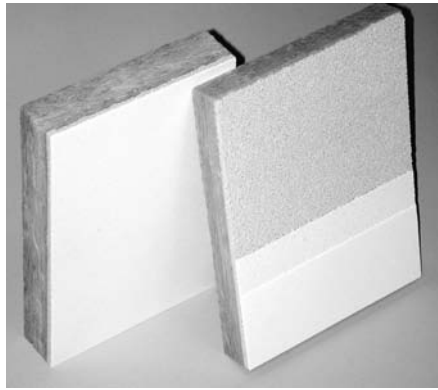
Figure 5.11   A proprietary system for achieving a flat porous plaster. The right sample shows the different layers of plaster which are used. (Photo courtesy of BASWA acoustic AG.)

glued or mechanically attached to the surface and levelled, the seams between the panels must be filled and sanded smooth. Next, depending on the desired smoothness of the finish, one or more surface layers of the plaster-like coating are applied. When the porous substrate is mineral wool and a smooth surface is desired, typically a base coat is hand applied or sprayed on, hand trowelled and sanded, followed by a finish coat which is applied and meticulously hand trowelled. If the final finish can be rougher, then a fine layer of the final coat may be sprayed on. When the absorptive substrate is blown glass granulate, the seam fill process is followed by several thin sprayed on coats of base, undercoat and finish coat with the desired degree of smoothness. Some sanding may be required to remove rough areas prior to the final coat. As is probably apparent from this description, the main disadvantage of this system is that they are slow to apply. The final acoustical performance is also dependent on the skill of the applicator to a certain extent.

A typical mineral wool substrate system, with a succession of acoustically transparent layers with the granule size decreasing with each layer, is shown in Figure 5.11. The top layer granules are so small that they provide the appearance of a smooth, seamless conventional gypsum-plastered surface. In fact, the top layer does seal the surface a little and acts as a thin membrane. As might be expected, this produces additional low frequency absorption, but at the cost of a little loss of absorption at high frequencies, in comparison to the mineral wool alone. The absorption coefficient for another acoustic plaster system is given in Figure 5.7, which shows how the top layer affects the absorption produced.

5.2.7 Coustone

Porous absorbers tend to be soft and prone to damage, for instance most do not survive repeated soakings. There is a need for a material which provides absorption and allows washing. Such an absorbent is Coustone. The ability to be washed means that Coustone can be used in places such as swimming centres, police interview rooms and firing ranges. The absorbent is a rigid, hard wearing material with a granulated
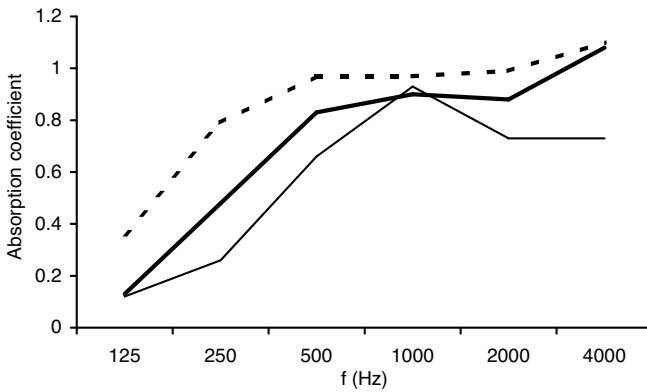
Figure 5.12   Random incidence absorption coefficient from a bonded flint absorber.
————— 14 mm absorber + 50 mm air gap;
————— 28 mm absorber + 50 mm air gap; and
– – – 28 mm absorber + 50 mm mineral wool (data courtesy of Sound Absorption UK Ltd).

surface. It is constructed from bonded flint in such a way as to keep the structure open and so allow absorption. It is heavy so it can also provide good sound insulation, but the weight also means that it can be expensive to use.

The material is formed by bonding flint aggregate together with a resin. Flint aggregate around a millimetre in size has a particular shape that means when bonded together with the right resin it forms an open pore structure. The cavities formed are of the order of millimetres in size. Furthermore, the pores are very irregularly shaped and joined; consequently the tortuosity is high. (Tortuosity, as the name suggests, is a measure of how tortuous the air paths are within the absorbent, and this influences the amount of absorption produced.) The high tortuosity is key to the high absorption; other aggregates form different pore shapes which absorb less efficiently. The resin must have the right properties. It must not fill the cavities, yet be strong enough to hold the absorber together. The resin is also elastic, and so the material can also offer a degree of vibration isolation.

Figure 5.12 shows typical absorption coefficients under different conditions. The material behaves like a porous absorber. Consequently, it can be spaced from walls to produce additional absorption by moving it away from where the particle velocity is low. It can also be backed by mineral wool to provide additional absorption at a lower cost and with less weight.

5.2.8 Aerogels

Aerogels are highly porous solids formed from a gel in which the liquid is replaced with a gas. They have very high porosities, being 95 per cent air, and so can be used as porous absorbents. Unfortunately, the lightest aerogels are rather fragile, and the denser ones are less suitable as acoustic absorbents because they do not have a suitable flow resistivity. However, it is possible to use them in a granular form,[17] and provided layers are built up to provide impedance matching to an incident wave, good absorption can be obtained.
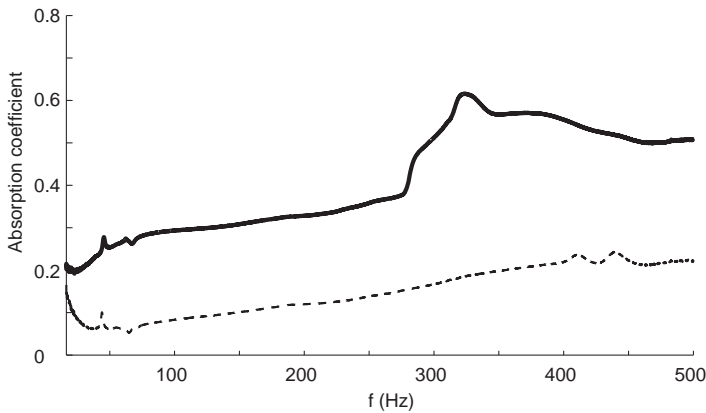
Figure 5.13   The low frequency absorption coefficient of:
━━━━ activated carbon, and
┄┄┄┄ sand. Normal incidence measured in impedance tube.

5.2.9 Activated carbon

Granular adsorbents (as opposed to absorbents), such as activated carbon, appear to have interesting acoustic properties. There are some experimental indications that adsorbent material can be used to enhance the compliance of acoustic enclosures.[18] Indeed, a loudspeaker manufacturer has exploited this property to enhance the low frequency performance of loudspeakers. Recent measurements show that, at low frequencies, a layer of activated carbon provides much stronger sound attenuation than other porous absorbers. For instance, Figure 5.13 shows the absorption coefficient for an activated carbon sample measured in an impedance tube compared to a sample of sand. The hypothesis is that adsorption and desorption are responsible for the excess sound attenuation of activated carbon.

Gas adsorption is a process whereby gas molecules adhere to a surface due to the Van der Waals potential. Adsorbed molecules form a film on the surface of the carbon with a thickness of one or several molecular layers. If the gas pressure increases, as happens in sound wave compressions, then the number of adsorbed molecules increases. Desorption is the opposite process, whereby the molecules leave the surface and return to the surrounding atmosphere, and this happens during sound wave rarefactions. This cycle of adsorption and desorption requires energy, which comes from the sound wave, and hence acoustic attenuation occurs. Because the density of the gas is being changed by the adsorption and desorption processes, if the activated carbon is placed in an enclosure, the compliance of the space changes.

To make this adsorption process effective, it is necessary to have a structure with two scales of porosity – large pores are needed to allow sound to enter the material, and much smaller pores are needed to facilitate the adsorption process. This is achieved by activated carbon. Because the adsorption process takes time to happen, the enhanced acoustic performance is only seen at low frequencies, as this gives sufficient time between the compression and rarefaction cycles.

5.2.10 Ground

When sound propagates outdoors from a source, a decrease in sound pressure level at low frequencies is often measured. This dip is due to the interference between the direct sound straight from source to receiver and the reflection from the ground. This is known as the 'ground effect'. What frequency this dip occurs at depends on the positions of the source and receivers relative to themselves and the ground, as well as the acoustic properties of the ground itself. The calculation of the frequency and depth of the ground effect is enshrined in many guides and standards for calculating environmental noise.[4] What is of interest here, however, is just the behaviour of the ground as an absorber.

The surface impedance of earth is significantly altered by the soil/earth composition, roughness, degree of compaction and moisture content. For instance, cultivated farmland offers significant decreases in A-weighted sound pressure levels for broadband sources in comparison to grassland, if subsoiling, discing and ploughing change the flow resistivity of the surface and the variation of the soil properties with depth. In addition, ploughing can result in periodic surface roughness which leads to a diffraction effect which can further attenuate sound. Attenborough *et al.*[19] showed that ploughed ground can produce up to 10 dB greater attenuation (A-weighted) for a broadband sound at 50 m range than would be expected from 'ISO-soft' ground. But whatever the surface texture and geometry, earth is normally modelled as a porous absorber, so Section 5.5.3 specifically details the application of empirical models to the ground.

5.3 Basic material properties

The rest of this chapter is devoted to the mathematical modelling of porous absorbents; given a particular material, how can the surface impedance and absorption coefficient be estimated? The mathematical models also give insight into how absorption is produced, and enable better designs to be produced. But first it is necessary to set down the two most important and fundamental quantities that determine the acoustic behaviour of sound within porous absorbents, namely flow resistivity and porosity.

5.3.1 Flow resistivity

Flow resistivity is a measure of how easily air can enter a porous absorber and the resistance that air flow meets through a structure. It therefore gives some sense of how much sound energy may be lost due to boundary layer effects within the material. A slice of the porous material of thickness d is subject to a mean steady flow velocity U. It is assumed that the flow velocity is small. The pressure drop ΔP is measured. From these quantities the flow resistivity σ is defined as:

$$\sigma = \frac{\Delta P}{Ud} \tag{5.1}$$

The flow resistance σ_s is defined as:

$$\sigma_s = \frac{\Delta P}{U} = \sigma d \tag{5.2}$$

The flow resistivity is effectively the resistance per unit material thickness. If the flow velocity is not small, then non-linear factors must be considered. For instance, the flow resistivity formulations quoted below will break down for high pressure sound waves, say when the sound pressure level exceeds 140 dB. Chapter 3 details how flow resistivity is measured. It is important to check the units used with flow resistance and resistivity as two systems have been in use. The unit of flow resistance in MKS units is Nm^{-3}s, often referred to as one rayl, and should nowadays be used. Older texts may use CGS rayls. To convert a CGS rayl to a MKS rayl, multiply by 10.

The flow resistivity is one of the most important parameters determining the absorption properties of a porous absorber – if not the most important. It is the parameter that varies most between common porous absorbent materials, and so is the most important to determine.

There are several empirical and semi-empirical formulations in the literature that can be used to estimate the flow resistivity. For fibreglass, the following empirical relationship derived by Bies and Hansen can be used:[4,20]

$$\sigma = 7.95 \times 10^{-10} \left(\frac{\rho_m^{1.53}}{a^2} \right) \tag{5.3}$$

where a is the fibre radius and ρ_m is the bulk density of the absorbent. For mineral and glass fibre, diameters are typically 1–10 μm. Bies and Hansen showed that fibrous materials have an approximately linear relationship between flow resistivity and density, but this is not necessarily true for foam. For fibrous materials, Bies and Hansen measured samples with resistivity values ranging from 2,000 to 200,000 rayls m^{-1}, and for one type of foam with flow resistivity between 2,000 and 40,000 rayls m^{-1}.

A number of other empirical relationships have been reported which deal with different materials, such as granular materials, and larger fibre sizes. These are summarized in Table 5.1. Flow resistivity values for the ground can be found later in the chapter in Table 5.4. Formulations to predict the effect of extreme heat on the properties of fibrous porous absorbers can be found in Reference 21; as the temperature increases, so does the flow resistivity. A simple formulation to allow for this is:

$$\sigma(T) = \sigma(20) \left(\frac{273 + T}{293} \right)^{1.65} \tag{5.4}$$

where T is the temperature in °C and $\sigma(20)$ the flow resistivity at 20°C. When using this with later formulations for impedance, it is necessary to also adjust the speed of sound and gas density for temperature:

$$c(T) = c(20) \sqrt{\frac{273 + T}{293}} \tag{5.5}$$

$$\rho(T) = \rho(20) \frac{293}{273 + T} \tag{5.6}$$

Table 5.1 *Various empirical relationships for flow resistivity. From References 5, 9, 22, 23, 67, 68, 69*

Material	Formulation
Parallel to the fibres, all fibres having the same radii	$\sigma = \dfrac{3.94\eta(1-\varepsilon)^{1.413}\left[1+27(1-\varepsilon)^3\right]}{a^2\varepsilon}$
Perpendicular to the fibres, all fibres having the same radii	$\sigma = \dfrac{10.56\eta(1-\varepsilon)^{1.531}}{a^2\varepsilon^3} \qquad 6\le a\le10\mu m$ $\dfrac{6.8\eta(1-\varepsilon)^{1.296}}{a^2\varepsilon^3} \qquad 20\le a\le30\mu m$
Random fibre orientation, all fibres having the same radii	$\sigma = \dfrac{4\eta}{a^2}\left[\dfrac{0.55(1-\varepsilon)^{4/3}}{\varepsilon}+\dfrac{\sqrt{2}(1-\varepsilon)^2}{\varepsilon^3}\right]$
Random fibre radius distribution with a mean radius of a, and random fibre orientation	$\sigma = \dfrac{3.2\eta(1-\varepsilon)^{1.42}}{a^2} \qquad \text{fibreglass}$ $\sigma = \dfrac{4.4\eta(1-\varepsilon)^{1.59}}{a^2} \qquad \text{mineral fibre}$
Polyester fibrous materials $18 \le 2a \le 48\ \mu m$ $12 \le \rho_m \le 60\ \text{kgm}^{-3}$ $900 \le \sigma \le 8{,}500\ \text{rayls m}^{-1}$	$\sigma = \dfrac{25.989\times10^{-9}\,\rho_m^{1.404}}{(2a)^2}$
Polyester fibre $6 \le 2a \le 39\ \mu m$ $28 \le \rho_m \le 101\ \text{kgm}^{-3}$ $4{,}000 \le \sigma \le 70{,}000\ \text{rayls m}^{-1}$	$\sigma = \dfrac{15\times10^{-9}\,\rho_m^{1.53}}{(2a)^2}$
Sheep wool $22 \le 2a \le 35\ \mu m$ $13 \le \rho_m \le 90\ \text{kgm}^{-3}.$	$\sigma = \dfrac{490\times10^{-6}\,\rho_m^{1.61}}{2a}$
Wood materials with short fibres $2a \approx 30\ \mu m$	$\sigma = 20.8\rho_m^{1.57}$
Loose granular material	$\sigma = \dfrac{400(1-H^2)(1+H^5)\mu}{HD}$ $H = 1 - \rho_m/\rho_f$
Consolidated granular material	$\log_{10}(\sigma) = -1.83\log_{10}(D) - 0.96$

Notes: η is the viscosity of air (1.84×10^{-5} poiseuille) and ε the porosity; $\varepsilon = \rho_m/\rho_f$ where ρ_f is the density of the fibres or the grain material and ρ_m the bulk density of the material. D is the characteristic particle dimension: $D^2 = V_g/0.5233$ where V_g is the number of the particles in a unit volume.

For thin materials which are used to cover porous absorbers it is better to define the properties in terms of the flow resistance. Wire, glass fibre and more normal cloths can be produced with a wide variety of resistance values.

5.3.2 Porosity

Porosity gives the fractional amount of air volume within the absorbent. It is a ratio of the total pore volume to the total volume of the absorbent. Good absorbers tend to have high porosity, for example most mineral wools have a porosity of about 0.98, but in designing an absorber, it is possible to trade off porosity against flow resistivity (and to a lesser degree the structural factors outlined later). When determining the porosity, closed pores should not be included in the total pore volume as these are relatively

Table 5.2 Typical porosity values for some materials from References 1, 5, 24, 45, 68, 70

Material	Typical porosities
Mineral wool	0.92–0.99
Reticulated vitreous carbon	0.91–0.97
Open cell acoustic foams	0.95–0.995
Felts	0.83–0.95
Wood fibre board	0.65–0.80
Vermiculite (granular)	≈0.65–68
Wood wool board	0.50–0.65
Perlite (granular)	0.60–0.78
Porous render	0.60–0.65
Pumice concrete	0.25–0.50
Rubber crumb	0.44, 0.54
Coustone	0.4
Glass beads (1.6 mm and 0.7 mm)	0.34, 0.38
Gravel and stone chip fill	0.25–0.45
Ceramic filters	0.33–0.42
Brick	0.25–0.30
Open porous asphalt	0.18–0.20
Sinter metal	0.10–0.25
Firebrick	0.15–0.35
Sandstone	0.02–0.06
Marble	≈0.005

inaccessible to sound waves (closed pores are most commonly found in foams, even ones designed to be open celled). The porosity is a key parameter, but for commonly used bulk absorbing materials, the value of porosity does not vary greatly and is close to unity. Table 5.2 gives some typical porosity values. Porosity values for the ground can be found later in the chapter in Table 5.4.

5.4 Modelling propagation within porous absorbents

Modelling the propagation of sound within a porous absorbent is difficult. Two approaches are found to be most useful. The first is a completely empirical approach as exemplified by Delany and Bazley. They measured a large number of samples of porous material and used curve fitting to arrive at relationships describing how the

characteristic impedance and propagation wavenumber vary with flow resistivity. When applied to an existing material type, this empirical technique is the simplest to apply and can be most effective. It is detailed in the next section.

A second approach to modelling porous absorbent is to formulate the problem using a semi-analytical approach. For instance, the propagation within the pores can be modelled semi-analytically by working on a microscopic scale. This approach results in complicated theoretical models, of which there are several variants in the literature. This approach is not for the faint hearted, and runs into difficulty because it is not possible to analytically derive all the necessary parameters within the models for most porous absorbents. In particular, factors related to the pore shapes are difficult to obtain except empirically. Consequently, the verification of the accuracy of the model is rather circular as measurements are needed to tune the model, and then the same measurements are sometimes used to show that the theory worked! This is not very satisfactory. Nevertheless, it is this type of modelling which holds the best chance of enabling the development of new porous absorbers to be undertaken without resorting to a completely experimental approach. Section 5.4.2 details some of the additional material properties that are needed in this approach, and Section 5.4.3 gives details of some of the models for rigid-framed materials.

Readers looking for a simple solution to porous absorber modelling are advised to read Section 5.4.1 and to use an empirical approach, before skipping to Section 5.5 to see how these empirical models can be applied to predict the absorption of absorbent layers.

5.4.1 Macroscopic empirical models such as Delany and Bazley

When predicting the absorption of porous absorbents it is necessary to know the characteristics of the material in terms of the characteristic impedance and (complex) wavenumber. These empirical models take a macroscopic view of the propagation, as the details of propagation through every pore are not considered, and the impedance and wavenumber are found empirically. For fibrous absorbent materials, Delany and Bazley[25] undertook a large number of impedance tube measurements and derived empirical relationships relating the impedance and wavenumber to the flow resistivity. These relationships are widely used as they give reasonable estimations across quite a wide frequency range.

The characteristic impedance, z_c, is given by:

$$z_c = \rho_0 c_0 \left(1 + 0.0571 X^{-0.754} - j0.087 X^{-0.732}\right) \tag{5.7}$$

and the wavenumber, k, by:

$$k = \frac{\omega}{c_0} \left(1 + 0.0978 X^{-0.700} - j0.189 X^{-0.595}\right) \tag{5.8}$$

where ρ_0 and c_0 are the density and speed of sound in air, and ω is angular frequency. X is given by:

$$X = \frac{\rho_0 f}{\sigma} \tag{5.9}$$

where f is the frequency and σ the flow resistivity of the fibrous material.

A good empirical match was achieved, but there are restrictions on the applicability of these formulations. These are only applicable where:

- The porosity, ε, is close to 1, which most purpose built fibrous absorbers achieve.
- $0.01 < X < 1.0$, which means the formulations only work over a defined frequency range.
- The limits of the flow resistivity in the measurements were

$$1000 \le \sigma \le 50{,}000 \; MKS \; rayl \; m^{-1}.$$

Figure 5.14 shows a large number of measurements undertaken by Mechel and Grundmann (reported in English in Reference 5) which give a visual indication of the accuracy of the empirical fit. These graphs show the normalized propagation constant k/k_0 and normalized characteristic impedance ($z_n = z_c/\rho_0 c_0$) for the measurements, alongside a thin dashed line giving the Delany and Bazley empirical values. The results shown are for glass fibre; similar accuracy is obtained for basalt and rock wool.

It is known that the Delany and Bazley model gives erroneous low frequency behaviour,[26] as this is outside its range of applicability. But often the absorption is low at these frequencies, and so the inaccurate predictions are not so important. However, several authors have attempted to produce improved relationships. For instance, Mechel and Grundmann produced a more complex set of empirical relationships.[5] They derive separate empirical relationships for mineral fibre and glass fibre, and this enables some improvement over the Delany and Bazley model. For many cases, however, the
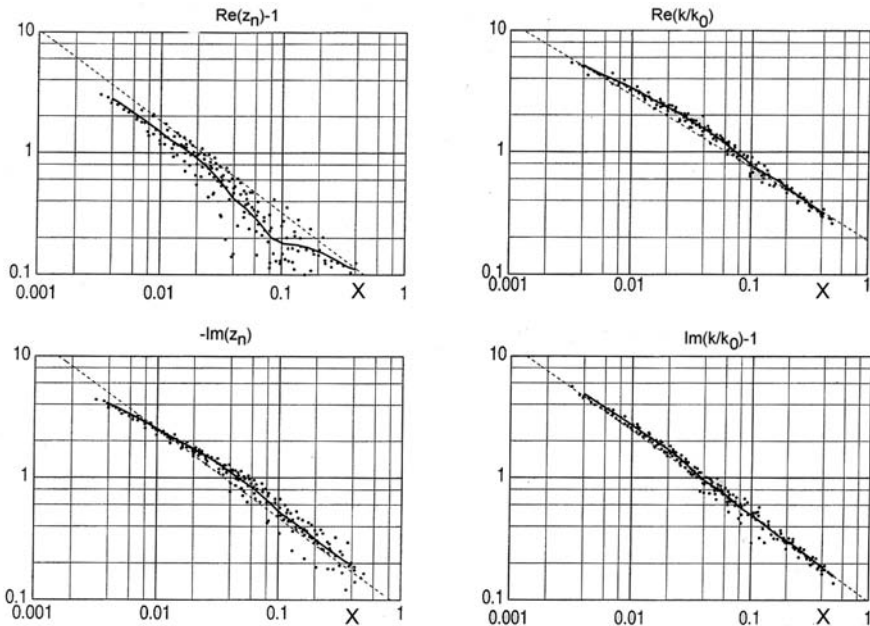
Figure 5.14   Normalized propagation constant and characteristic impedance ($z_n = z_c/\rho_0 c_0$) for fibreglass. Points show measured data; the dashed line the Delany and Bazley approximation; and the solid line a running mean (after Mechel[5]).

difference in the predicted quantities is relatively small. Figure 5.14 shows the floating average for the Mechel and Grundmann measurements, which is presumably close to their empirical predictions, compared to the measurements and the Delany and Bazley predictions.

The Mechel and Grundmann empirical can be most simply given as:

$$\left.\begin{array}{c} -jk/k_0 \\ z_n \end{array}\right\} = X^{-1}\beta_{-1} + X^{-\frac{1}{2}}\beta_{-\frac{1}{2}} + \beta_0 + X^{\frac{1}{2}}\beta_{\frac{1}{2}} + X_{1} + X^{\frac{3}{2}}\beta_{\frac{3}{2}} \qquad (5.10)$$

The coefficients are given in Table 5.3. The range of applicability is 0.003 <*X* <0.4. Other authors have also produced their own empirical models to update and improve on the Delany and Bazley model,[27] especially to expand the applicability to other materials such as polyurethane[28–30] and reticulated carbon[70] foams, other fibrous materials[22] and granular material.[68]

The ground is often modelled as a porous absorber. The Delany and Bazley empirical model has been used quite extensively to obtain the characteristic impedance and wavenumber, even though these formulations were developed for use with fibre glass rather than loose granular material. For this, flow resistivity values for typical ground surfaces are needed, and Table 5.4 gives appropriate values. While the Delany and Bazley model works reasonably well above about 250 Hz, at lower frequencies the characteristic impedance and wavenumber have significant errors resulting in inaccurate predictions of excess attenuations.[31]

Section 5.5 details how these empirical formulations can be used to get the surface impedance and absorption coefficient of a material.

The problem with these macroscopic empirical models is they do not readily give information about how the microscopic properties of the porous absorber, such as the pore size and orientation of the pores affect the absorption produced. This means

Table 5.3 Coefficients for Mechel and Grundmann empirical model of porous absorbers[5]

Coefficients	$-jk/k_0$	z_n
Mineral fibre (basalt or rock wool)		
β_{-1}	−0.003 557 57 − j 0.000 016 489 7	0.0026786 + j 0.003 857 61
$\beta_{-1/2}$	0.421 329 + j 0.342 011	0.135 298 − j 0.394 160
β_0	−0.507 733 + j 0.086 655	0.946 702 + j 1.476 53
$\beta_{1/2}$	−0.142 339 + j 1.259 86	−1.452 02 − j 4.562 33
β_1	1.290 48 − j 0.082 0811	4.031 71 + j 7.560 31
$\beta_{3/2}$	−0.771 857 − j 0.668 050	−2.869 93 − j 4.904 37
Glass fibre		
β_{-1}	−0.004 518 36 + j 0.000 541 333	−0.001 713 87 + j 0.001 194 89
$\beta_{-1/2}$	0.421 987+j 0.376 270	0.283 876 − j 0.292 168
β_0	−0.383809 − j 0.353 780	−0.463 860 + j 0.188 081
$\beta_{1/2}$	−0.610 867 + j 2.599 22	3.127 36 + j 0.941 600
β_1	1.133 41 − j 1.74819	−2.109 2 0 − j 1.323 98
$\beta_{3/2}$	0	0

Table 5.4 Effective flow resistivity values for ground surfaces and other parameters (data from References 35–38, 71, 72, 73)

Surface	Effective flow resistivity (MKS rayls m^{-1})	Water content (%)	Porosity	Porosity decay κ (m^{-1})
Dry snow, newly fallen 0.1 m over about 0.4 m older snow	$1 \times 10^4 - 3 \times 10^4$	–	–	–
Sugar snow	$2.5 \times 10^4 - 5 \times 10^4$	–	–	–
In forest, pine or hemlock	$2 \times 10^4 - 8 \times 10^4$	–	–	–
Grass, rough pasture, airport, public buildings etc.	$15 \times 10^4 - 30 \times 10^4$	–	–	–
Roadside dirt, ill-defined, small rocks up to 0.1 m mesh	$30 \times 10^4 - 80 \times 10^4$	–	–	–
Sandy silt, hard packed by vehicles	$80 \times 10^4 - 250 \times 10^4$	–	–	–
'Clean' limestone chops, thick layer (1–2.5 cm mesh)	$1 \times 10^6 - 4 \times 10^6$	–	–	–
Old dirt roadway, fine stones (5 cm mesh) interstices filled	$2 \times 10^6 - 4 \times 10^6$	–	–	–
Earth, exposed and rain-packed	$4 \times 10^6 - 8 \times 10^6$	–	–	–
Quarry dust fine, very hard-packed by vehicles	$5 \times 10^6 - 20 \times 10^6$	–	–	–
Asphalt, sealed by dust and light use	$\approx 3 \times 10^7$	–	–	–
Snow (new)	$1 \times 10^3 - 1 \times 10^4$	–	0.64–0.88	0–3
Snow (old crusted)	$8 \times 10^3 - 3 \times 10^4$	–	0.5	0–100
Forest floor	$7 \times 10^3 - 20 \times 10^4$	–	–	0–40
Tall crops	$4 \times 10^4 - 5 \times 10^4$	–	–	0
Loose sand or dry cultivated soil	$3 \times 10^4 - 3.1 \times 10^5$	–	0.36–0.52	0–10
Fine sand	3.1×10^5	–	0.44	
Grassland	$7 \times 10^4 - 8.5 \times 10^5$	–	–	0–250
Wet and compacted soil	4×10^7	–	–	−200 – 0
Coarse sand, pore size 98 µm	5×10^4	0	–	−14
	1×10^5	11	–	−82
	4.7×10^5	51	–	−141
	9×10^4	95	–	1290
Fine sand, pore size 65 µm	1.5×10^5	0	–	−28
	1.4×10^5	15	–	130
	1.5×10^5	48	–	620
	4.1×10^4	95	–	1130
Mineral layer beneath mixed deciduous forest	$(540 \pm 92) \times 10^3$	15	36.5	–
Loamy sand	$(420 \pm 17) \times 10^3$	11.2	37.5	–
Bare sandy plain	$(370 \pm 110) \times 10^3$	9.3	26.9	–
Humus on pine forest floor	$(230 \pm 220) \times 10^3$	16.1	58.1	–
Grass root layer in loamy sand	$(150 \pm 90) \times 10^3$	–	48 ± 4	–
Litter layer on mixed deciduous forest floor (2–5 cm thick)	$(30 \pm 30) \times 10^3$	–	–	–
Pine forest litter (6–7 cm thick)	$(9 \pm 5) \times 10^3$	28.6	38.9	–

that it is difficult to use this empirical approach to inform design, beyond finding the optimum flow resistivity required. To improve designs, more detailed models of the propagation are required. In the next section some of the key parameters needed for more physically based porous absorber models are discussed. Following on from this, some of these more complex models are presented.

5.4.2 *Further material properties*

The simplest theoretical models of porous absorbers assume that the material (or frame) of the absorbent is rigid. Then it is possible to apply some classical theories of sound propagation in small pores. It is only possible to gain analytical solutions for simple geometries such as bundles of cylindrical pores. Unfortunately, cylindrical pores are far removed from the complex geometry of the vast majority of porous absorbers. Consequently, a semi-empirical approach is often adopted, where a mixture of experiment and theory determines key properties of the material. The necessary parameters are detailed below; they are not independent.

5.4.2.1 *Pore shape factor and characteristic lengths*

While the porosity and the flow resistivity are usually the most important parameters in determining the sound absorption, other secondary parameters such as the shape factor and the tortuosity (see next section) can be important. The shape of the pores influences the sound propagation and hence the absorption. Different pore shapes have different surface areas and hence have different thermal and viscous effects. Analytically obtaining the shape factor for most porous absorbents is impossible as they do not usually conform to simple geometric shapes. Consequently, the pore shape factors are usually empirically found by best fitting the acoustic measurements of the effective density and bulk modulus of the material. The shape factors are therefore dependent on the model being used to predict the propagation within the absorbent. Later in this chapter, formulations for the effective density and bulk modulus are found, from which the characteristic impedance and wavenumber can be obtained; for now, the important shape factors (Λ and Λ') used in those formulations are defined. These factors are sometimes prefixed with the term 'dynamic' to emphasis that they apply to the dynamic, not static, case.

The characteristic length Λ is a weighted ratio of the volume to surface area of the pores. It is weighted according to the squared modulus of the microscopic velocity evaluated, including the effects of viscosity. It can be found for simple pore shapes using the following formulation:

$$\Lambda = \frac{1}{s}\sqrt{\frac{8\eta k_s}{\varepsilon\sigma}} \qquad (5.11)$$

where s is a constant. For most porous absorbers, s lies between 0.3 and 3. s is 1, 1.07, 1.14 for circular, square and triangular pores respectively, and 0.78 for slits. k_s is the tortuosity as defined in the following section, and η is the viscosity of air.

For materials with non-cylindrical pores and complicated internal structures, it is necessary to use another characteristic length.[32] The effective density of real porous

Table 5.5 Various characteristic length values from References 26 and 34–46

Material	Characteristic length (µm)	
	Viscous Λ	*Thermal Λ′*
Melamine foam	160	290
Plastic foam	25 & 230	70 & 690
Polyurethane	200	370
Metal foam	20	–
Porous aluminium	770	–
Fibreglass	60–180	125–400
Polyester fibres	50–270	100–540
Cellular rubber	9	15
Felt	30	60
Glass beads, 0.1 mm diameter	90	180
2.1 mm lead shot	280	490
4 mm lead shot	550	830
9 mm gravel	190	–

absorbers tends to be determined by parts of the pores with smaller cross-sections, whereas the bulk modulus is more determined by larger cross-sectional areas.[33] For this reason, a second characteristic length to supplement Λ is needed. The second characteristic length Λ' is given by:

$$\Lambda' = \frac{2V_p}{S_p} \tag{5.12}$$

where S_p and V_p are the surface area and volume of the pores respectively. This is the same ratio as used for Λ but without the weighting for microscopic velocity. Cylindrical pores are a special case where $\Lambda = \Lambda'$. In general $\Lambda' \geq \Lambda$, and to a first approximation $\Lambda' = 2\Lambda$ and $s = 1$ can be used in Equations 5.11 and 5.12 to derive simpler formulations for the sound propagation in rigid framed fibrous materials.[30]

The determination of these characteristic lengths poses a problem in the use of the theoretical models. For most absorbers, the pore shape is so complex that the characteristic lengths must be fitted from empirical measurements on samples, as detailed in Section 3.6, which in a sense defeats the point of theoretical modelling, because it is impossible to accurately predict the absorption from a material before it is built. Further complications arise when the material is anisotropic, which is common in many materials. For instance, mineral wool is often laid down in layers, in these cases the characteristic lengths depend on the incident angle of the sound wave. Chapter 3 gives some measurement techniques for the characteristic lengths and Table 5.5 some typical values.

5.4.2.2 Tortuosity

The orientation of the pores relative to the incident sound field has an effect on the sound propagation. This effect[35] is represented by the parameter tortuosity, denoted k_s.

Some authors use the term structural form factor for this property, and there are some differences in definition in the literature. Using tortuosity has the advantage that the term is almost self-explanatory. The more complex the propagation path through the material, the higher is the absorption, and the complexity of the path is partly represented by the tortuosity. Furthermore, the tortuosity affects how easily sound can penetrate the material. For simple cylindrical pores, all aligned in the same direction, the tortuosity is simply related to the angle between the pores and the incident sound ($k_s = 1/\cos^2(\psi)$). Formulations also exist for packed spheres. An empirical formulation is:[36]

$$k_s = \frac{1}{\sqrt{\varepsilon}} \qquad (5.13)$$

An alternative expression is:[37]

$$k_s = 1 + \frac{1-\varepsilon}{2\varepsilon} \qquad (5.14)$$

Real absorbents, however, are not normally that well ordered. Consequently, tortuosity needs to be measured. Techniques for doing this are discussed in Chapter 3. Some values are given in Table 5.6. Another approach is to calculate the tortuosity from the structure of the material at a microscopic scale. For instance, Koponen *et al.*[38] used a lattice-gas cellular automaton method to examine the tortuosity of a 2D lattice.

Table 5.6 Various tortuosity values from References 26, 35, 41–46, 39, 52 and 58

Material	Tortuosity
Fibrous materials e.g. rock wool	1–1.06
Polyester, hemp fibres	1.01–1.05
Plastic foam	1.06 & 1.7
Melamine foam	1.01
Polyurethane foam	1.08–1.41
Metal foam	1.27
Porous aluminium	1.05
Snow (new)	1.5–2.7
Snow (old crusted)	4
Loose sand or dry cultivated soil	1.27–3.32
Granular materials	1.1–1.8
Gravel	1.5–1.8
Glass beads, 0.1 mm diameter	1.87
2.1 mm diameter lead shot	1.56–1.72
4 mm diameter lead shot	1.46
Fused glass bead sample	1.75–3.84
Vermiculite	1.8–2.46
Perlite	1.17–2.22
Nitrile foam granulate	1.49
Open porous asphalt	3.2–15
Rubber crumb	1.38–1.56
Cellular rubber	2.64
Felt	1.01

5.4.3 Phenomenological theoretical models

Given the material properties (flow resistivity, porosity, tortuosity and characteristic lengths), it is possible to calculate the characteristic impedance and propagation wave-number by considering the microscopic propagation within the pores. Attenborough[40] produced a useful review of early methods, but these techniques have been much refined in recent years. Many people have been involved in the development of the models, the description below draws on the work by Johnson *et al.*[41] as summarized by Allard[42] and Allard and Champoux.[30] This is a simple phenomenological model. The absorber frame is assumed to be rigid.

The effective density of the porous material is given by:

$$\rho_e = k_s \rho_0 \left[1 + \frac{\sigma \varepsilon}{j \omega \rho_0 k_s} \sqrt{1 + \frac{4 j k_s^2 \eta \rho_0 \omega}{\sigma^2 \Lambda^2 \varepsilon^2}} \right] \tag{5.15}$$

The effective or dynamic bulk modulus of the air in the material is given by:

$$K_e = \frac{\gamma P_0}{\gamma - (\gamma - 1) / \left(1 + \frac{8\eta}{j \Lambda'^2 N_p \omega \rho} \sqrt{1 + \frac{j \rho \omega N_p \Lambda'^2}{16\eta}} \right)} \tag{5.16}$$

where γ is the ratio of the specific heat capacities (≈ 1.4), P_0 is atmospheric pressure $\approx 101{,}320 \ \mathrm{Nm^{-2}}$ and N_p is the Prandtl number given by:

$$N_p = \left(\frac{\delta_v}{\delta_h} \right)^2 \tag{5.17}$$

where δ_v and δ_h are the size of the viscous and thermal boundary layers. At 1 atmosphere and 20°C the Prandtl number is about 0.77; this can be found from the following formulations. The thickness of the viscous boundary layer is given by:

$$\delta_v = \sqrt{\frac{2\eta}{\rho \omega}} \tag{5.18}$$

Typically the viscous boundary layer is sub-millimetre in size, for example at 100 Hz it is ≈ 0.2 mm.

The thickness of the thermal boundary layer is given by:

$$\delta_h = \sqrt{\frac{2\kappa}{\rho c_p \omega}} \tag{5.19}$$

where $\kappa \approx 2.41 \times 10^{-2} \ \mathrm{WmK^{-1}}$ is the thermal conductivity of air and $c_p \approx 1.01 \ \mathrm{Jkg^{-1}K^{-1}}$ is the specific heat capacity of air at constant pressure.
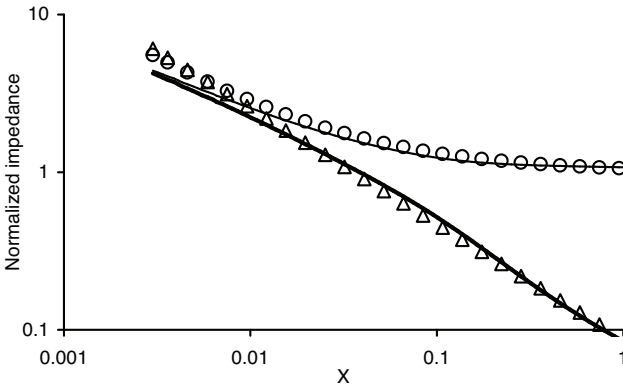
Figure 5.15   Two models for the normalized characteristic impedance ($z_c/\rho_0 c_0$) of a porous
absorber. The x-axis is $X = \rho_0 f/\sigma$.
    ○   Re (Delany and Bazley);
  ——— Re (Phenomenological);
    △   –Im (Delany and Bazley); and
  ━━━ –Im (Phenomenological).

Once the effective density and bulk modulus have been determined from Equations
5.15 and 5.16, it is then possible to calculate the characteristic impedance and propa-
gation wavenumber for the porous absorber, which are more often used in calculating
acoustic properties.

The characteristic impedance z_c is given by:

$$z_c = \sqrt{K_e \rho_e} \tag{5.20}$$
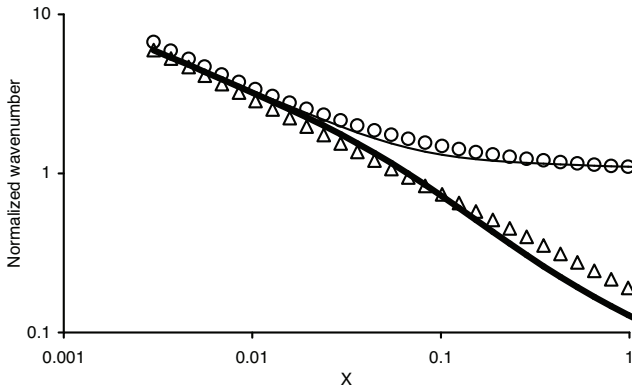
Figure 5.16   Two models for the normalized wavenumber (k/k_0, where k_0 is the wavenumber
in air) for sound propagation through a porous absorber compared. The
x-axis is $X = \rho_0 f/\sigma$.
    ○   Re (Delany and Bazley);
  ——— Re (Phenomenological);
    △   –Im (Delany and Bazley); and
  ━━━ –Im (Phenomenological).
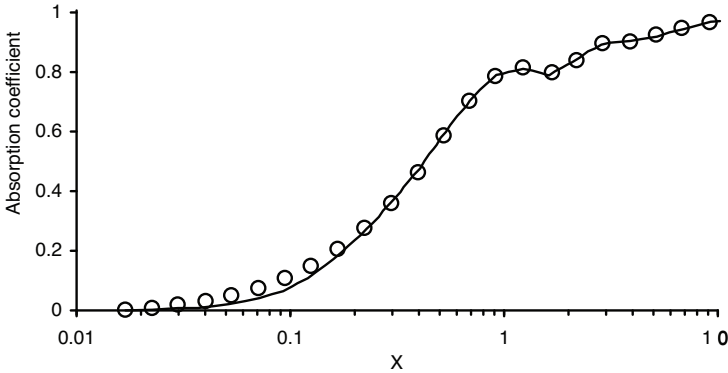
Figure 5.17   Two models for the absorption coefficient of a porous absorber compared. The x-axis is X = $\rho_0 f / \sigma$:
    O   Delany and Bazley; and
    ——— Phenomenological.

and the propagation wavenumber by:

$$k = \omega \sqrt{\frac{\rho_e}{K_e}}$$

(5.21)

The formulations in Equations 5.15 and 5.16 give the correct high and low frequency asymptotic behaviour, but is only approximately correct at mid-frequencies for complicated pore geometries.

Figures 5.15–5.17 show the normalized characteristic impedance, propagation constant and absorption coefficient for the model from Equations 5.15 and 5.16; these lines are labelled phenomenological. These values are compared to the Delany and Bazley formulations of Equations 5.7 and 5.8. The following assumptions were made to implement the phenomenological model: $k_s = 1$, $\Lambda' = \Lambda$, and $s = 1$. Both models give very similar results. As stated previously, the Delany and Bazley predictions are known to give inaccurate results at low frequency (the real part of the impedance of the surface of the porous absorber actually goes negative), but these are frequencies at which the absorption from the porous absorber is relatively small anyway.

The comparison in Figure 5.17 shows the absorption coefficient for a given absorber thickness on a rigid backing, rather than the characteristic impedance or wavenumber. How the absorption coefficient and surface impedance are calculated from the characteristic impedance and wavenumber is detailed in the next section.

5.4.4 Relaxation model

Wilson[43] took an alternative approach to modelling the propagation through porous absorbents, viewing the thermal and viscous diffusion as a relaxation processes. When

sound propagates through common porous materials, temperature perturbations result within the air inside the absorbent which relax over time towards the temperature of the frame material. The characteristic time for this thermal relaxation process is denoted τ_t. Similarly, the sound wave sets up pressure gradients that induce changes in the flow velocity which also relax towards the steady state by the absorbent's frame. The characteristic time for this viscous relaxation process is denoted, τ_v. Writing the inverse of the bulk modulus and effective density in a relaxational form allows the characteristic impedance and wavenumber of the acoustic absorber to be derived in terms of the relaxation times and other characteristics of the absorber:[56]

$$z_c = \frac{\rho_0 c_0 \sqrt{k_s}}{\varepsilon} \left[\left(1 + \frac{\gamma - 1}{\sqrt{1 + j\omega\tau_t}} \right) \left(1 + \frac{1}{\sqrt{1 + j\omega\tau_v}} \right) \right]^{-0.5} \tag{5.22}$$

$$k = \frac{\omega\sqrt{k_s}}{c} \sqrt{\left(1 + \frac{\gamma - 1}{\sqrt{1 + j\omega\tau_t}} \right) \Big/ \left(1 - \frac{1}{\sqrt{1 + j\omega\tau_v}} \right)} \tag{5.23}$$

With appropriate choice of relaxation times, these formulations give predictions which match the empirical and phenomenological models discussed earlier in this chapter. For instance, with $\tau_v = 2.54/\sigma$ and $\tau_v = 3.75/\sigma$, the above equations mimic the behaviour of the Delany and Bazley empirical formulation. The relaxation times are tuned to fit the behaviour of the porous material in the frequency range of interest either based on measurement or other prediction models. So for frequency domain modelling, this relaxation method does not offer any great advantages over other models. However, unlike other models, the formulations governing the relaxation process can be transformed into the time domain, and so this approach offers the possibility of enabling the modelling of porous absorbers through finite difference time domain (FDTD) techniques.[44]
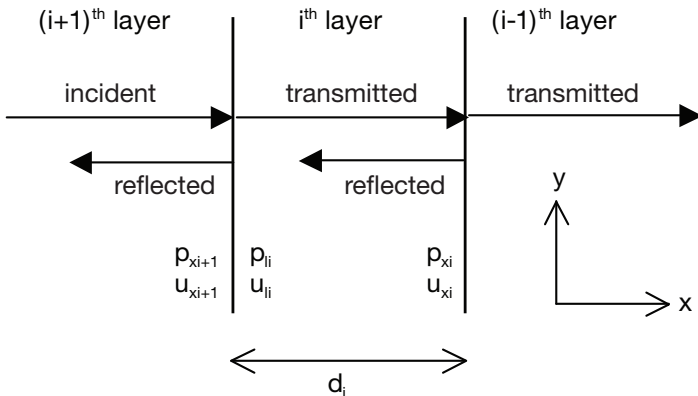
Figure 5.18 Geometry for propagation of sound through a layer of an acoustic medium.

5.5 Predicting the surface impedance and absorption coefficient of porous absorbers

Once the characteristic impedance and wavenumber for the material are known, it is necessary to convert these to the surface impedance and absorption coefficient for a particular thickness of the porous material with known boundary conditions. In this case, the most flexible way of predicting the surface properties of the porous material is to use the transfer matrix method. Consequently, this section starts by discussing the general case of propagation in one layer of porous absorber in a multi-layered system. Then the specific case of a single layer with a rigid backing will be presented. The prediction model can be extended to multiple layers of absorbent, but the most common situation is the single layer on a rigid backing.

Figure 5.18 shows the arrangement being considered. Only plane wave propagation in the absorbent will be considered, and for now normal incidence only is considered. Section 1.5.1 showed how sound behaves when propagating from one medium to another. At each interface between the layers, continuity of pressure and particle velocity is assumed. This allows a relationship between the pressure and particle velocity at the top and bottom of a layer to be produced which is compactly given in matrix format:

$$\begin{Bmatrix} p_{li} \\ u_{li} \end{Bmatrix} = \begin{Bmatrix} p_{xi+1} \\ u_{xi+1} \end{Bmatrix} = \begin{Bmatrix} \cos(k_{xi}d_i) & j\dfrac{\omega\rho_i}{k_{xi}}\sin(k_{xi}d_i) \\ j\dfrac{k_{xi}}{\omega\rho_i}\sin(k_{xi}d_i) & \cos(k_{xi}d_i) \end{Bmatrix} \begin{Bmatrix} p_{xi} \\ u_{xi} \end{Bmatrix} \tag{5.24}$$

where p_{xi} and u_{xi} are the pressure and particle velocity at the bottom of the ith layer; p_{xi+1} and u_{xi+1} are the pressure and particle velocity at the bottom of the $(i + 1)^{th}$ layer; p_{li} and u_{li} are the pressure and particle velocity at the top of the ith layer; d_i is the thickness of the layer; ρ_i the density of ith layer, and k_{xi} the wavenumber for the ith layer.

This formulation can be applied recursively to successive layers, and it is particularly powerful in allowing the calculation of the surface impedance of absorbers, rather than simply a way of gaining specific values for pressure and velocity at the layer boundaries. If the bottom of layer i has an impedance of z_{si}, and the layer i has a characteristic impedance z_i, then the impedance at the bottom of the $i + 1$ layer is:

$$z_{si+1} = \frac{-jz_{si}z_i \cot(k_{xi}d_i) + z_i^2}{z_{si} - jz_i \cot(k_{xi}d_i)} \tag{5.25}$$

This formulation can be applied repeatedly to calculate the surface impedance of a multi-layered absorbent. Next a simple case is considered.

5.5.1 Single layer porous absorber with rigid backing

Consider a single layer of absorbent with a rigid backing. The impedance at the surface of layer zero, z_{s0}, which is the backing, is taken to be infinite. Then Equation 5.25 simplifies and gives the impedance on the surface of the absorbent as:
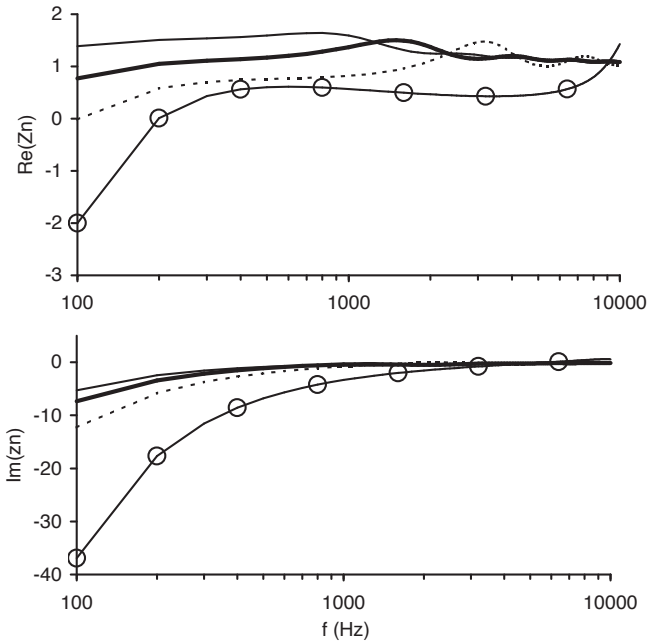
Figure 5.19 Effect of absorbent thickness:
—— 88.9;
—— 63.5;
- - - 38.1; and
—⊖— 12.7 mm on the normalized acoustic impedance. Using Delany and Bazley model combined with transfer matrix method.
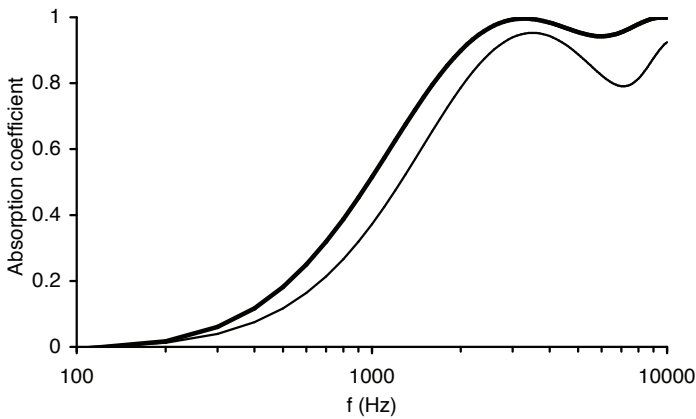
Figure 5.20 Comparison of absorption coefficient for two configurations of porous absorbent using transfer matrix methodology:
—— 12.5 mm absorbent with 12.5 mm air gap; and
—— 25 mm absorbent.

$$z_{si+1} = -jz_i \cot(k_{xi}d_i)$$ (5.26)

This can then be turned into absorption coefficients using Equations 1.21 and 1.24. Figure 5.19 shows the impedance changes as the thickness of the layer increases, using the Delany and Bazley empirical formulations for the porous material properties. As discussed previously, as the porous layer increases in thickness the absorption increases at low frequency as expected. Scripts 5.1–5.3 in Appendix B demonstrate the use of these equations.

It is also possible to demonstrate the usefulness of air gaps in increasing absorption. Consider two cases: 2.5 cm of porous absorber mounted on a rigid backing; and 1.25 cm of the same porous absorber mounted in front of a rigid backing with a 1.25 cm air gap. In the former case Equation 5.26 can be used as before. In the latter case, Equation 5.25 is applied first to the air layer, and second to the porous absorber layer. For the air layer (layer 1):

$$z_{s1} = -j\rho_0 c_0 \cot(kd_1)$$ (5.27)

and for the porous absorbent layer (layer 2):

$$z_{s2} = \frac{-jz_{s1}z_2 \cot(k_{x2}d_2) + z_2^2}{z_{s1} - jz_2 \cot(k_{x2}d_2)}$$ (5.28)

Figure 5.20 compares the absorption coefficients for the two configurations. It shows that the absorbent with the air gap has very similar performance to the thicker absorption alone. This confirms the usefulness of air gaps, as discussed in Section 5.1 and elsewhere.

5.5.2 Modelling covers

Often an absorbent is finished with a thin porous layer to make the absorber look better or more robust. If the porous surface layer is not free to vibrate then the resistance of the covering material should be added to the impedance predicted from the above formulations, such as Equation 5.26. If the covering material can vibrate then the effect of the moving mass can become significant. The following impedance should be added to the surface impedance to allow for this:

$$z = \frac{j\omega\rho_s r_s}{j\omega\rho_s + r_s}$$ (5.29)

where ρ_s is the mass per unit area and r_s the resistance of the covering material. When the covering is not porous, and the resistance large, this formulation simply adds the mass of the vibrating material.

5.5.3 Ground

A transfer matrix approach can be applied to the ground once the characteristic impedance and wavenumber have been determined. For surfaces such as grassland,

assumptions about the layering of the soil and the backing impedance conditions need to be made – what are especially important are the characteristics for the first few centimetres of depth. For many surfaces it is appropriate to assume a hard backing at some appropriate depth, but for others, such as forest floors, it is more appropriate to assume a non-hard backing.

More complex models, such as the phenomenological model outlined earlier can be used, but Attenborough[35] showed that in many cases it is possible to use a simplified two parameter model. The normalized surface impedance z_n of a single layer of ground of thickness d above an acoustically hard backing is approximately given by:

$$z_n \approx z_c - \frac{jc_0}{4\pi d\gamma f\varepsilon} \tag{5.30}$$

where z_c is the normalized characteristic impedance of the layer; c_0 is the speed of sound in air; ε is the porosity of the layer; γ is the ratio of specific heats for air; and f is the frequency in Hz. If it is assumed that the upper layer has a relatively high effective flow resistivity, and the frequency is not too high, then the normalized characteristic impedance of the layer is given by:

$$z_c \approx \sqrt{\frac{\sigma_e}{\pi\gamma\rho_0 f}}(1-j) \tag{5.31}$$

where ρ_0 is the density of air and σ_e is the effective flow resistivity given by:

$$\sigma_e \approx \frac{4s_p^2\sigma}{\varepsilon} \tag{5.32}$$
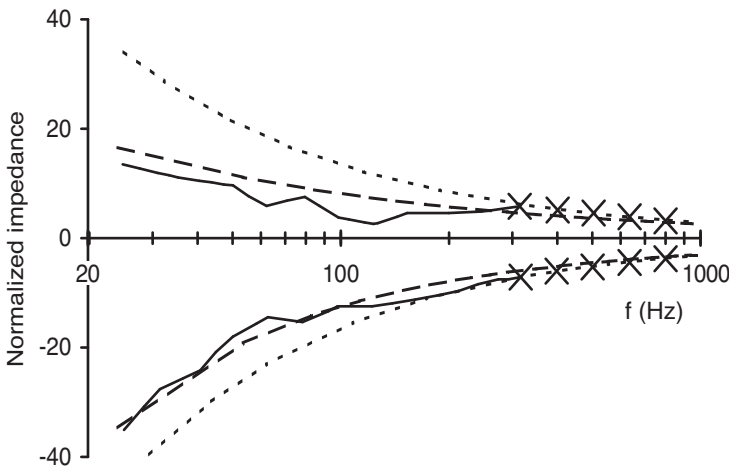
Figure 5.21   Comparison of two prediction models and measurements for grassland ground surface impedance:
——— and ✕ measurement;
······ one parameter model, and
– – – two parameter model with σ_e = 35,000 MKS rayls m^{-1} and κ = 45 m^{-1} (after Attenborough[35]).

where σ is the flow resistivity and s_p is a pore shape factor which can be taken to be 0.5 in many cases, meaning the effective flow resistivity is just the flow resistivity scaled by the porosity.

This model can also be used for the case where the deeper soil is more compacted; when the substrate has a lower porosity and higher flow resistivity. The change in soil properties is modelled as an exponential decrease in porosity with depth. The rate of change in porosity with depth is given by κ, and some values for this parameter are given in Table 5.4. The normalized surface impedance becomes:

$$z_n \approx z_c - \frac{jc\kappa}{8\gamma\pi f\varepsilon} \tag{5.33}$$

Figure 5.21 shows predicted and measured surface impedances for 'institutional' grass. The single parameter model is similar to one using the Delany and Bazley equations, and shows inaccuracy at low frequencies, below about 300 Hz. The two parameter model, based on the above equations is more accurate.

Horoshenkov and Mohamed[37] examined the effects of water saturation on sand in the laboratory. They found great changes in the surface impedance with the amount of moisture. They also found that the two parameter model of Attenborough was more suitable than one based on the Delany and Bazley formulations; the parameters for the model they deduced are shown in Table 5.4.

Porous road surfaces have been produced to reduce noise. Changing both the road texture and introducing open voids in asphalt is beneficial,[45] and reductions in A-weighted sound levels of 3 to 5 dB compared to a dense surface have been measured.[46] However, the pores will gradually become clogged as the surface is used, and then the noise reduction is lost. Asphalt consists of mineral grains bound together by a bituminous binder. Open porous asphalt uses an appropriate grain size distribution to form large voids which do not fill up with binder, although the porosity is rather small, typically around 20 per cent. This material can be modelled as a porous absorber. Using three parameters, namely porosity, tortuosity and flow resistivity in a relaxation or phenomenological model gives sufficient accuracy. Sarradj *et al.*[58] give empirical relationships for estimating these parameters from relevant technological parameters of the road material.

5.5.4 Multi-layer porous absorbers

By appropriately using layers of different absorbent materials it is possible to gain additional absorption from porous absorbers. Ideally, a porous absorbent should offer an impedance which matches that of air to remove reflections, while offering high internal acoustic attenuation. These two requirements are difficult to achieve in a thin layer of a single material, and can be more easily achieved in multi-layered linings. The front material has the necessary impedance matching that of air, and the inner layers attenuate the sound wave. This is achieved by having layers with the outside layer having a low flow resistivity, and the inner layers offering more resistance. Ideally, the impedance should only change gradually between internal layers to minimize reflections. This arrangement can be modelled by repeated application of the transfer matrix equations.[47] (An alternative approach to achieving impedance matching is to corrugate the front face of the porous absorber.)

An example of multi-layer impedance matching is in flat-walled linings for anechoic chambers. Traditionally anechoic chambers use wedges to achieve a gradual change in impedance from the air into the absorbent, and so prevent strong reflections from flat absorbent areas. The advantage of flat-walled linings is that they are simpler to make and install. Xu *et al.*[48] showed that it is possible to use a three-layered flat lining system with an overall thickness of about a sixth of a wavelength at the cut-off frequency. This is about 80 per cent of the depth normally used for anechoic linings made from wedges. A process of trial and error, or an optimization algorithm, can be used to find the appropriate materials to use.

5.6 Local and extended reaction

The propagation direction within many porous absorbers is normal to the surface, even for oblique incidence sound, because of refraction (see the next section). This means that the reaction of the material at any point is independent of the reaction at other points. In this case, the surface is termed locally reacting, as the surface impedance is independent of the nature of the incident wave. This is an extremely useful first order approximation. It means that in multi-layered absorbents the propagation can be assumed normal to the surface and are therefore much easier to evaluate. These assumptions will break down for large sound pressure levels when non-linear propagation is significant. Other common examples of locally reacting materials include resonant absorbers whose cavities are partitioned, and massive walls made of materials like concrete, where the stiffness effect is small enough to be ignored in comparison with the mass effect.

Unfortunately, man-made fibrous materials such as mineral wool often behave as an extended reacting surface because it is anisotropic with the material laid down in layers. The impedance produced is dependent on the incident wave type and angle of incidence. This is one reason why predictions of absorption from the Delany and Bazley model, which are based on normal incidence impedance tube measurements, are difficult to accurately translate into random incidence values measured in the reverberation chamber. A proper model of an extended reacting surface needs to deal with the entire wave field inside the medium. While there are formulations that allow for the anisotropic behaviour of mineral wool[55] (see the next section) these formulations produce similar results to the isotropic models because they do not account for the extended reaction.

5.7 Oblique incidence

Consider a sound wave in air incident at an angle ψ to a finite layer of porous material with a rigid backing. The geometry is shown in Figure 5.22. The wavenumber in air is k_0, and the wavenumber in the material is k. In vector form these are $k_0 = \{k_{0,x}, k_{0,y}, k_{0,z}\}$, $k = \{k_x, k_y, k_z\}$. For simplicity it is assumed that $k_{0,z} = k_z = 0$. Snell's law relates the angles of propagation to the speed of sound in the material, as discussed in Chapter 1. In terms of wavenumber this gives:

$$k_y = k_{0,y} = k_0 \sin(\psi) = k \sin(\beta) \tag{5.34}$$
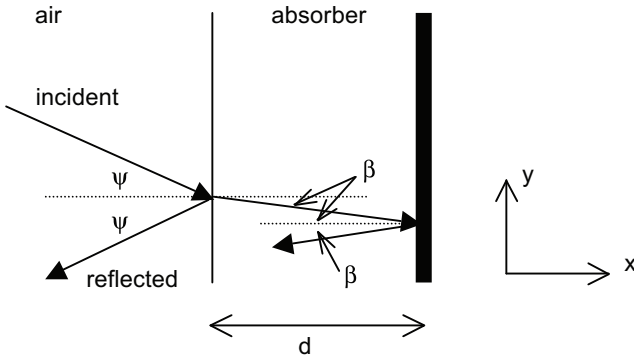
Figure 5.22 Geometry for propagation of sound through a finite layer of a rigid-backed porous absorber.

For many porous absorbents, the differences in wavenumber in air and the absorbent are so large that $\beta \rightarrow 0$ and the previous derived normal incident formulae are accurate. For cases where $\beta > 0$, a different formulation can be derived. As $k^2 = k_x^2 + k_y^2 + k_z^2$, this can be combined with Equation 5.34 to give:

$$k_x = \sqrt{k^2 - k_y^2}$$
(5.35)

The square root with the positive real part should be chosen. This can then be used to form an alternative form of the surface impedance for a rigidly backed absorbent for oblique incident sound.

$$z_{s1} = -jz_c \frac{k}{k_x} \cot(k_x d)$$
(5.36)

where z_c is the characteristic impedance of the porous absorbent. This is derived using Equation 5.24.

Figure 5.4 shows how the attenuation varies with angle of incidence using the Delany and Bazley formulations. The surface impedance does not vary much with angle of incidence but the reflection coefficient and absorption coefficient vary greatly as the pressure component perpendicular to absorbent drops off with a $1/\cos(\psi)$ relationship, where ψ is the angle of incidence. This was discussed in Chapter 1.

Fibrous porous absorbents can be anisotropic, in other words their acoustic properties vary depending on the angle of the wave to the fibre orientation. In this case, alternative forms for the surface impedance can be deduced. If the effective densities and bulk moduli are measured separately for propagation parallel and perpendicular to the fibres, Equation 5.21 can be applied to obtain the wavenumber parallel and perpendicular to the fibres. The wavenumber perpendicular to the fibres will be denoted k_N and parallel to the fibres k_p. The porous absorbent is placed so that the fibres are parallel to the rigid backing, as is most common; then the component of the wavenumber in the x-direction perpendicular to the backing and fibres is given by:[55]

$$k_x = k_N \sqrt{1 - \frac{k_y^2}{k_p^2}} \tag{5.37}$$

$$k_0 \sin(\psi) = k_y \tag{5.38}$$

$$z_{s1} = -jz_N \frac{k_N}{k_x} \cot(k_x d) \tag{5.39}$$

where z_N is the characteristic impedance for propagation perpendicular to the fibres.

A method for obtaining the parallel and perpendicular propagation wavenumber and characteristic impedance is to use different flow resistivities in the Delany and Bazley formulations. Typically the flow resistivity perpendicular σ_N and parallel σ_p to the fibres are related by a constant factor:[49,50]

$$\sigma_N \approx A\sigma_p \tag{5.40}$$

where A is a constant with a value of 0.6 or 0.5. When this formulation is used, it makes some difference to the absorption coefficient and surface impedance, but the change is not that large.

5.8 Biot theory for elastic framed material

In the above theories, the frame of the porous absorber was assumed to be rigid and waves only propagated in the air pores. In reality, porous absorbers have elastic frames which can support wave propagation. The consequence of this to the absorption properties of the material is not as great as might be supposed. For instance, if the porous absorber is anchored to a rigid surface, for example attached to the wall or resting on a floor, this will constrain the motion of the frame material. For this reason, the rigid frame models discussed above are mostly used, and models that allow for elastic motion of the frame are less commonly used.

Furthermore, as most of the previous models involve some form of empirical fitting, in many cases this fitting can partially compensate for some of the inaccuracies introduced by not properly modelling the additional wave types which propagate due to the frame being elastic, although strong frame and frame-air resonances cannot be well modelled. If the frame of the porous absorber is not constrained, for example if it is hanging in free air, then resonances of the frame material can be seen in the characteristic impedance of the surface. In this case, a more complete model may be required, and most authors favour using Biot theory.[51,52] Other models of note are presented by Ingard[2] and Zwikker and Kosten.[53]

Biot theory is summarized in more detail in References 5 and 55, where the necessary formulations are given. In this book, only the general principles and concepts will be discussed along with some indications of the relative accuracy of Biot theory and the rigid framed models discussed earlier in the chapter.

The equations of motion for the displacement and strain tensors of the air in the pores and the frame are defined. These equations of motion include a set of coefficients
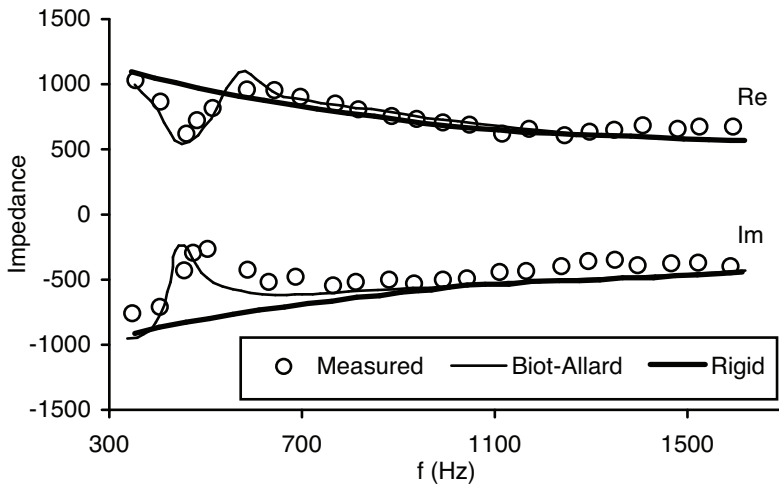
Figure 5.23 Comparison of two prediction models and measurements for a fibrous absorber with a distinct frame resonance (after Allard[55]).

which detail the coupling between the air and frame. These coefficients can be identified with physical properties such as the bulk modulus of the air in the pores and the elastic frame. The former, the bulk modulus of air is taken from the rigid framed theories detailed earlier. Once these coefficients are determined, the equations of motion can be solved to give the surface impedance of porous layers.

There are now three waves to consider in the structure. There are two compressional waves. In most air saturated porous materials, the coupling between the frame and air is negligible and these waves can be identified as the frame-borne and airborne waves. Where there is weak coupling, the airborne wave remains mostly within the pores, but the frame-borne wave actually propagates through both the frame and pores. The third wave, the shear wave is also frame-borne, and in most porous absorbents, is unaffected by the fluid air (for normal incidence this is not excited and can be ignored).

Figure 5.23 shows a comparison of theory and experiment from Allard.[55] For many frequencies the rigid framed model is accurate, but deviations occur around 500 Hz. These inaccuracies are due to the resonances of the frame material which by definition cannot be predicted by the rigid framed model. This is a dense fibreglass material, and so only the quarter wave resonance of the frame is seen. For these frequencies, Biot theory offers better predictions, although it should be noted that some fitting of prediction parameters had to be undertaken to gain this match. So even with Biot theory the rather circular nature of model verification is still a problem.

5.9 Summary

This chapter has described porous absorbers both qualitatively and quantitatively. There are a large number of possible porous absorbers, and they form an important part of the acoustic palette for acoustic designers both indoors and outdoors. Being able to predict the absorption caused by porous materials, and understanding what causes the absorption, is important to enable materials to be designed with maximum

absorption. In the next chapter, resonant absorbers will be discussed. Since many of these use porous absorbers within them, the understanding gained about porous absorber modelling from this chapter will be invaluable in the next.

5.10 References

1 L. Cremer and H. A. Müller, *Principles and Applications of Room Acoustics*, Applied Science Publishers (translated by T. J. Schultz) (1978).
2 U. Ingard, *Notes on Sound Absorption Technology*, Noise Control Foundation (1994).
3 P. D'Antonio, "Nestable sound absorbing foam with reduced area of attachment", US patent 5, 665, 943 (1997).
4 D. A. Bies and C. H. Hansen, *Engineering Noise Control: Theory and Practice*, E&FN Spon, 2nd edn, 42–3 (1996).
5 F. P. Mechel, *Formulas of Acoustics*, Springer, Section G (2002).
6 IARC Monographs on the Evaluation of Carcinogenic Risks to Humans, "Man-made Vitreous Fibres", **81** (2002).
7 R. A. Baan and Y. Grosse, "Man-made mineral (vitreous) fibres: evaluations of cancer hazards by the IARC Monographs programme", *Mutation Research*, **553**, 43–58 (2004).
8 V. Desarnaulds, E. Costanzo, A. Carvalho and B. Arlaud, "Sustainability of acoustic materials and acoustic characterization of sustainable materials", *Proc. 12th ICSV* (2005).
9 K. O. Ballagh, "Acoustical properties of wool", *Appl. Acoust.*, 48(2), 101–20 (1996).
10 J. Pfretzschner, "Rubber crumb as granular absorptive acoustic material", *Proc. Forum Acusticum*, *Sevilla*, MAT-01-005-IP (2002).
11 M. J. Swift and K. V. Horoshenkov, "Acoustic properties of recycled granular foams", *Proc. Euronoise* (2001).
12 H. V. Fuchs, "Alternative fibreless absorbers – new tools and materials for noise control and acoustic comfort", *Acustica*, **87**, 414–22 (2001).
13 US Green Building Council, http://www.usgbc.org/, accessed January 2008.
14 C. M. Harris (ed), *Handbook of Noise Control*, 2nd edn, McGraw-Hill (1991).
15 L. L. Beranek, *Acoustics*, McGraw-Hill (1954).
16 F. A. Everest, *Master Handbook of Acoustics*, 4th edn, McGraw-Hill (2001).
17 L. Forest, V. Gibiat, and A. Hooley, "Impedance matching and acoustic absorption in granular layers of silica aerogels", *Journal of Non-Crystalline Solids*, **285**(1–3), 230–5 (2001).
18 J. R. Wright, "The virtual loudspeaker cabinet", *J. Audio Eng. Soc.*, **51**, 244–7 (2003).
19 K. Attenborough, T. Waters-Fuller, K. M. Li and J. A. Lines, "Acoustical properties of Farmland", *J Agric. Engng. Res.*, **76**, 183–95 (2000).
20 D. A. Bies and C. H. Hansen, "Flow resistance information for acoustical design", *Appl. Acoust.*, **13**, 357–91 (1980).
21 L. L. Beranek and I. L. Vér (eds), *Noise and Vibration Control Engineering*, John Wiley & Sons (1992).
22 M. Garai and F. Pompoli, "A simple empirical model of polyester fibre materials for acoustical applications," *Appl. Acoust.* 66(12), 1383–98 (2005).
23 N. Kino and T. Ueno, "Experimental determination of the micro and macrostructural parameters influencing the acoustical performance of fibrous media", *Appl. Acoust.*, **68**, 1439–58 (2007).
24 K. V. Horoshenkov and M. J. Swift, "The acoustic properties of granular materials with pore size distribution close to log-normal", *J. Acoust. Soc. Am.*, **110**(5), 2371–8. (2001).
25 M. E. Delany and E. N. Bazley, "Acoustical properties of fibrous absorbent materials", *Appl. Acoust.*, **3**, 105–16 (1970).
26 J. F. Allard and Y. Champoux, "New empirical equations for sound propagation in rigid frame fibrous materials", *J. Acoust. Soc. Am.*, **91**(6), 3346–53 (1992).
27 Y. Miki, "Acoustical properties of porous materials – modification of Delany–Bazley laws", *J. Acoust. Soc. Jpn.*, **11**, 19–28 (1986).
28 J. P. Dunn and W. A. Davern, "Calculation of acoustic impedance of multi-layer absorbers", *Appl. Acoust.*, **19**, 321–34 (1986).

29 Q. L. Wu, "Empirical relations between acoustical properties and flow resistivity of porous plastic open-cell foam", *Appl. Acoust.* **25**(3), 141–8 (1988).

30 A. Cummings and S. P. Beadle, "Acoustic properties of reticulated plastic foams", *J. Sound Vib.* **1975**, 115–33 (1993).

31 K. Attenborough, "Ground parameter information for propagation modeling", *J. Acoust. Soc. Am.*, **92**(1), 418–27 (1992).

32 Y. Champoux and J. F. Allard, "Dynamic tortuosity and bulk modulus in air-saturated porous media", *J. Appl. Phys.*, **70**, 1975–9 (1991).

33 Y. Champoux and M. R. Stinson, "On acoustical models for sound propagation in rigid frame porous materials and the influence of shape factors", *J. Acoust. Soc. Am.*, **92**(2), 1120–31 (1992).

34 X. Olny and R. Panneton, "Acoustical determination of the parameters governing thermal dissipation in porous media", *J. Acoust. Soc. Am.*, **123**(2), 814–24 (2008).

35 K. Attenborough, "On the acoustic slow wave in air filled granular media", *J. Acoust. Soc. Am.*, **81**, 93–102 (1982).

36 K. Attenborough, "Models for the acoustical characteristics of air filled granular materials", *Acta Acust.*, **1**, 213–26 (1993).

37 J. G. Berryman, "Confirmation of Biot's theory", *Appl. Phys. Lett.*, **37**, 382–4 (1980).

38 A. Koponen, M. Kataja and J. Timonen, "Tortuous flow in porous media", *Phys. Review E*, **54**(1), 406–10 (1996).

39 U. Umnova, Keith Attenborough, H.-C. Shin and A. Cummings, "Deduction of tortuosity and porosity from acoustic reflection and transmission measurements on thick samples of rigid-porous materials", *Appl. Acoust.*, **66**, 607–24 (2005).

40 K. Attenborough, "Acoustical characteristics of porous materials", *Phys. Rep.*, **82**, 179–227 (1982).

41 D. L. Johnson, J. Koplik and R. Dashen, "Theory of dynamic permeability and tortuosity in fluid-saturated porous media", *J. Fluid Mechanics*, **176**, 379–402 (1987).

42 J. F. Allard, *Propagation of Sound in Porous Media: Modelling Sound Absorbing Materials*, Elsevier Applied Science (1993).

43 D. K. Wilson, "Simple, relaxational model for the acoustical properties of porous media", *Appl. Acoust.*, **50**(3), 171–88 (1997).

44 D. K. Wilson, V. E. Ostashev, S. L. Collier, N. P. Symons, D. F. Aldridge and D. H. Marlin, "Time-domain calculations of sound interactions with outdoor ground surfaces", *Appl. Acoust.* **68**, 173–200 (2007).

45 E. Sarradj, T. Lerch and J. Hubelt, "Input parameters for the prediction of acoustical properties of open porous asphalt", *Acta Acustica uw Acustuca.* 92, 86–96 (2006).

46 M. C. Berengier, M. R. Stinson, G. A. Daigle and J. F. Hamet, "Porous road pavements: Acoustical characterization and propagation effects", *J. Acoust. Soc. Am.*, **101**(1), 155–62. (1997).

47 I. P. Dunn and W. A. Davern, "Calculation of acoustic-impedance of multilayer absorbers", *Appl. Acoust.*, **19**(5), 321–4 (1986).

48 J. Xu, J. Nannariello and F. R. Fricke, "Optimising flat-walled multi-layered anechoic linings using evolutionary algorithms", *Appl. Acoust.*, **65**(11), 1009–26 (2004).

49 J. F. Allard, R. Bourdier and A. L'Esperance, "Anisotropy effect in glass wool for normal impedance in oblique incidence", *J. Sound. Vib.*, **114**, 233–8 (1987).

50 V. Tarnow, "Measured anisotropic air flow resistivity and sound attenuation of glass wool", *J. Acoust. Soc. Am.*, **111**(6), 2735–9 (2002).

51 M. A. Biot, "Theory of propagation of elastic waves in a fluid-saturated porous solid. I Low-frequency range", *J. Acoust. Soc. Am.*, **28**(2), 168–78 (1956).

52 M. A. Biot, "Theory of propagation of elastic waves in a fluid-saturated porous solid. II Higher frequency range", *J. Acoust. Soc. Am.*, **28**(2), 179–91 (1956).

53 C. Zwikker and C. Kosten, *Sound Absorbing Materials*, Elsevier (1949).

54 D. L. Johnson, J. Koplik and R. Dashen, "Theory of dynamic permeability and tortuosity in fluid-saturated porous media", *J. Fluid Mechanics,* **176**, 379–402, (1987).

55 J. F. Allard, *Propagation of Sound in Porous Media: Modelling Sound Absorbing Materials*, Elsevier Applied Science, (1993).

56 D. K. Wilson, "Simple, relaxational model for the acoustical properties of porous media", *Appl. Acoust.*, **50**(3), 171–88, (1997).

57 D. K. Wilson, V. E. Ostashev, S. L. Collier, N. P. Symons, D. F. Aldridge and D. H. Marlin, "Time-domain calculations of sound interactions with outdoor ground surfaces", *Appl. Acoust.* **68**, 173–200, (2007).

58 E. Sarradj, T. Lerch and J. Hubelt, "Input Parameters for the Prediction of Acoustical Properties of Open Porous Asphalt", *Acta Acustica uw Acustuca.* **92**, 86–96, (2006).

59 M. C. Berengier, M. R. Stinson, G. A. Daigle and J. F. Hamet "Porous road pavements: Acoustical characterization and propagation effects", *J.Acoust. Soc. Am.*, **101**(1), 155–62. (1997).

60 I. P. Dunn and W. A. Davern, "Calculation of acoustic-impedance of multilayer absorbers", *Appl. Acoust.,* **19**(5), 321–4, (1986).

61 J. Xu, J. Nannariello and F. R. Fricke, "Optimising flat-walled multi-layered anechoic linings using evolutionary algorithms", *Appl. Acoust.,* **65**(11), 1009–26, (2004).

62 J. F. Allard, R. Bourdier and A. L'Esperance, "Anisotropy effect in glass wool for normal impedance in oblique incidence", *J. Sound. Vib.,* **114**, 233–8, (1987).

63 V. Tarnow, "Measured anisotropic air flow resistivity and sound attenuation of glass wool", *J. Acoust. Soc. Am.*, **111**(6), 2735–9, (2002).

64 M. A. Biot, "Theory of propagation of elastic waves in a fluid-saturated porous solid. I Low-frequency range", *J.Acoust. Soc. Am.*, **28**(2), 168–78, (1956).

65 M. A. Biot, "Theory of propagation of elastic waves in a fluid-saturated porous solid. II Higher frequency range", *J. Acoust. Soc. Am.*, **28**(2), 179–91, (1956).

66 C. Zwikker and C. Kosten, *Sound absorbing materials*, Elsevier, (1949).

67 C Wassilieff, "Sound absorption of wood-based 00.materials", *Appl. Acoust.*, **48**(4), 339–56, (1996).

68 N. N. Voronina and K. V. Horoshenkov, "A new empirical model for the acoustic properties of loose granular media", *Appl. Accoust.* **64**(4), 415–32, (2003).

69 M. Vasina, D. C. Hughes, K. V. Horoshenkov and L. Lapcik, "The acoustical properties of consolidated expanded clay granules", *Appl. Acoust.* **67**(8), 787–96, (2006).

70 R. T. Muehleisen, C. W. Beamer and B. D. Tinianov, "Measurements and empirical model of the acoustic properties of reticulated vitreous carbon", *J. Acoust. Soc. Am.* **117**(2), 536–44, (2005).

71 T. F. W. Embleton, J. E. Piercy and G. A. Daigle, " Effective flow resistivity of ground surfaces determined by acoustical measurements", **74**(4), 1239–44, (1983).

72 K. V. Horoshenkov and M. H. A. Mohamed, "Experimental investigation of the effects of water saturation on the acoustic admittance of sandy soils", *J. Acoust. Soc. Am.* **120**(4), 1910–21, (2006)

73 M. J. M. Martens, L. A. M. van der Haijden, H. H. J. Walthaus, and W. J. J. van Rens, "Classification of soils based on acoustic impedance, air flow resistivity and other physical soil parameters", *J. Acoust. Soc. Am.*, **78**, 970–80, (1985).

6 Resonant absorbers

By exploiting resonance it is possible to get absorption at low to mid-frequencies. It is difficult to achieve this with porous absorbers, because of the required thickness of the material. Furthermore, treatments are often placed at room boundaries where porous absorbers are inefficient as the particle velocity is low. For many resonant absorbers, placing the device at the boundaries will improve their effectiveness. The absorption characteristics of these resonant devices are a peak of absorption, as shown in the thick line in Figure 6.1. Unlike porous materials, wide band absorption is difficult to achieve in one device, and so one of the frequent challenges in the design of resonant structures is to extend the bandwidth.

There are two common forms of the device: the first is the Helmholtz absorber, which is named after the German physician and physicist Hermann von Helmholtz (1821–94) and the second is a membrane or panel absorber. The ideas and concepts of resonant absorption have been known for many decades. In recent years, some more specialist devices have been produced, for instance clear absorbers, but these are still based on the same basic physics. While some devices, such as many basic Helmholtz absorbers, can be predicted with reasonable accuracy, others, such as membrane devices, are still designed by trial and error. These treatments are commonly employed to treat low frequency room modes and as parts of silencers within ventilation systems.
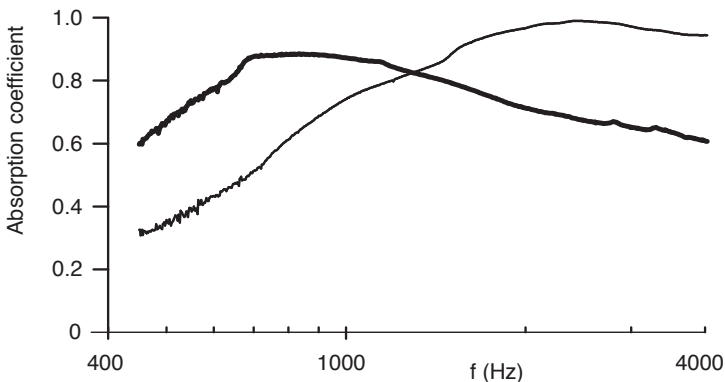
Figure 6.1 Normal incidence absorption coefficient measured in an impedance tube for:
———— mineral wool; and
———— the same material covered with the perforated sheet shown in Figure 6.9 to form a Helmholtz absorber.
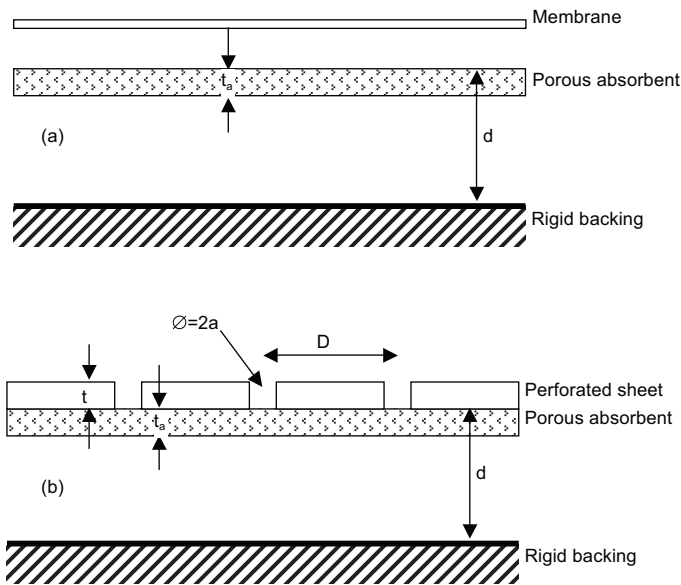
Figure 6.2 Typical constructions for (a) membrane, and (b) Helmholtz absorbers.

6.1 Mechanisms

Resonant absorbers involve a mass vibrating against a spring. The two common types of resonant absorber are illustrated in Figure 6.2. In the case of a Helmholtz absorber, the mass is a plug of air in the opening of the perforated sheet. The resonance is produced by the same mechanism which generates a note when you blow across a beer bottle. To make this into an absorber, losses are provided by damping to remove sound energy; this is often provided by a layer of mineral wool. For a membrane (or panel) absorber, the mass is a sheet of material such as rubber, mass loaded vinyl or plywood which vibrates. The spring in both cases is provided by air enclosed in the cavity. By changing the vibrating mass and the stiffness of the air spring, the resonant frequency of the device can be tuned, and it is at the resonant frequency that absorption is a maximum.

To achieve losses, damping is required. Often, this is best achieved by placing porous absorbent where the particle velocity is large – in the neck of the Helmholtz resonator or just behind the membrane in the panel absorber. In the latter case, the absorbent should not be so close as to inhibit movement of the membrane. Alternatively, for Helmholtz devices with small openings, viscous losses within the neck can be used to gain absorption; this is a technique which allows devices without porous absorbent, such as microperforated absorbers, to be produced. For panel absorbers there are also internal losses within the vibrating membrane, but these are usually too small to give high absorption. More significant are the losses that come from the mounting between the membrane and the enclosure. Problems arise in predicting performance of membrane absorbers, as the absorption from the boundaries is hard to characterize.

Before discussing the relevant design equations, some example constructions are given to provide a sense of what commercial devices are like. After the design equations, more complex and unusual constructions will be considered.

6.2 Example constructions

6.2.1 Bass trap membrane absorber

Small rooms often exhibit a poor low frequency response with significant emphasis due to standing wave modes and de-emphasis where modal excitation is small. There is also limited space within which to fit treatments. Porous absorbers are ineffective at these modal frequencies, because the particle velocity near walls and in corners is essentially zero for these long wavelengths; and also the treatment would have to be made so deep that significant space within the room would be lost. This problem can be solved by using a resonant absorber, such as a membrane design. A membrane absorber converts the high sound pressure fluctuations typically found at wall surfaces and in corners into selective absorption in the modal frequency range. As the use of sub-woofers has become more popular in small sound reproduction rooms in recent years, there is a growing need for modal frequency management. It has also been shown that the use of multiple in-phase subwoofers located at specific room locations can also be used to reduce excitation of room modes below their cut-off frequency.

Figure 6.2a shows a typical device. The membrane converts pressure fluctuations into air motion. As the membrane sympathetically vibrates over a selective low frequency
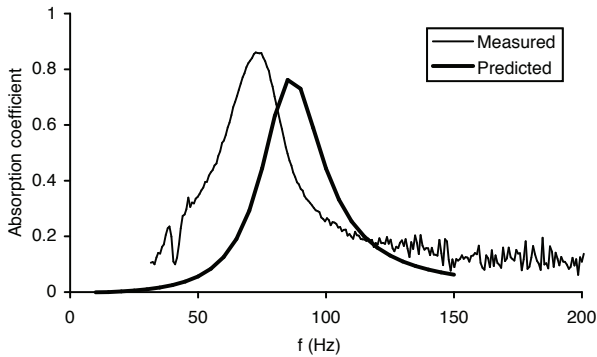
Figure 6.3 Top: Measured and predicted normal incidence absorption coefficient for a commercial membrane absorber (Modex™). Bottom: A typical installation in a small reproduction room, the absorber is in the corner of the room. (Photo courtesy of RPG Diffusor Systems, Inc.)

range, determined by its mass and the air spring stiffness, it pushes air through an internal porous layer producing low frequency absorption. Simple relationships exist between the design frequency of these resonant systems and the membrane mass, stiffness and cavity depth, and these will be outlined below. Figure 6.3 illustrates the absorption coefficient of this type of device and also shows an example application where the absorbent is placed in the corner where the pressure is a maximum for all room modes. There is also a prediction of the performance using a transfer matrix approach as discussed below. This prediction illustrates, however, that for membrane absorbers the design equations are often inexact in predicting the resonant frequency. There are many reasons for this. For instance the physical mass of the membrane is often different from the vibrating acoustic mass due to mounting conditions. Finite element analysis might be used to help overcome these problems.

If the absorber has a sharp resonant peak with a high Q factor, there is a risk of creating a notch at the wrong frequency, thus aggravating rather than ameliorating the modal problems. Consequently, experimental verification of the absorption is necessary, although at these low frequencies this is not easy. The results shown in Figure 6.3 were measured in an unusually large impedance tube.

Specific problem frequencies can be addressed with individually tuned absorbers, and while bass membrane absorbers can be designed for a specific frequency and offer a high absorption efficiency, their bandwidth over which they are effectively absorbing is rather limited. One can broaden the absorption by introducing additional damping in the air cavity, but this often lowers the maximum absorption efficiency. An alternative solution is to use a range of modules, each tuned to work in a different one-third octave band for more general broadband absorption. But a considerable amount of the room boundary must be covered with absorbent to get broadband low frequency absorption.

In multipurpose spaces, bass absorbers which can be turned on and off are useful to alter the acoustic for different uses. It has been suggested that this can be achieved using inflatable absorbers like air mattresses.[1]

6.2.2 *Conventional Helmholtz absorbers*

Currently, wood is more often than not the preferred surface treatment in general architectural spaces, as well as in critical listening and performance spaces. However, one of the problems is that flat wooden panels may generate problematic reflections compromising speech intelligibility and music quality. To treat offending reflections, upholstered fibreglass or stretch fabric systems are often used. But it is also possible to use flat attractive wooden panels and also provide absorption at specified frequencies. Figure 6.4 illustrates such a system and an example application. The grooves are mostly a visual trick to hide the holes as these are often not visually desirable. At the base of the grooves there is a single or double diameter hole, providing a sound path through the panel. By varying the groove (i.e. hole) spacing, the hole diameter, and the rear air cavity depth and content, it is possible to obtain absorption over a wide variety of frequencies. The design equations are given later in this chapter and are much more successful than when the formulations are applied to membrane absorbers.

These Helmholtz absorbers are constructed from class A medium density fibreboard (MDF) cores either painted or surfaced with wood veneers or simulated wood grain melamine. The rear of the panel is covered with a black non-woven glass matt to provide a resistive layer and also to conceal the contents behind the panel. In addition, a fibreglass
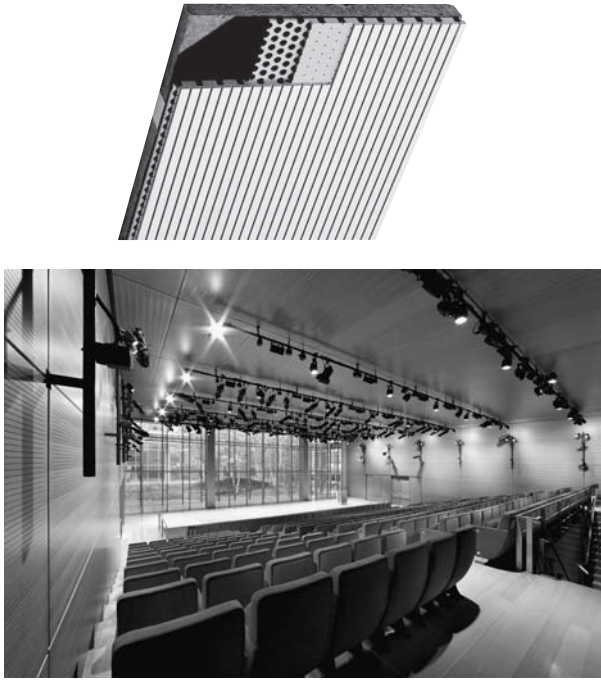
Figure 6.4 A commercial Helmholtz absorber and an application on the walls and ceiling in the auditorium of TheTimesCenter. (Architects: Renzo Piano Building Workshop. Acoustician: JaffeHolden Acoustics, Norwalk, CT. Photos courtesy of n'H Akustik + Design AG and RPG Diffusor Systems, Inc.)
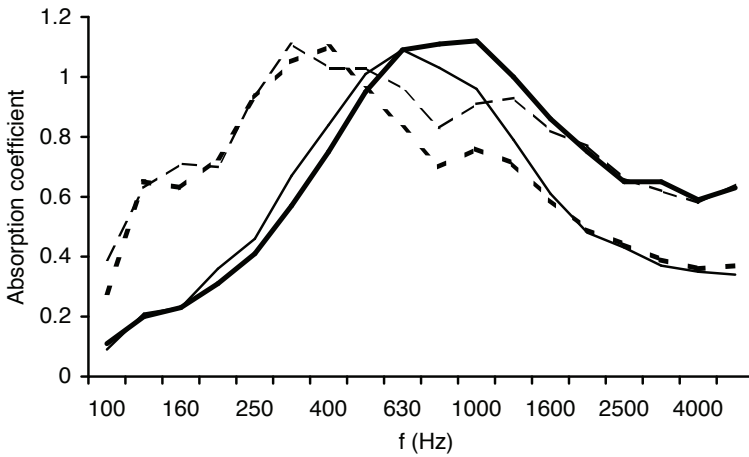
Figure 6.5 Random incidence absorption coefficient for different Helmholtz absorbers:
——— small hole, shallow cavity;
━━━ large hole, shallow cavity;
······· small hole, deep cavity; and
− − − large hole, deep cavity (data courtesy of n'H Akustik + Design AG).

panel is attached to the back of the glass matt to provide further resistance and losses.

Figure 6.5 shows typical absorption coefficients for different cavity depths and hole sizes. As the holes enlarge, the open area increases leading to greater absorption at higher frequencies; there is also a slight increase in resonant frequency. These trends can be predicted by the design equations given later, but they will not predict the absorption coefficient values greater than 1 shown in the graph. These arise because of issues with reverberation chamber measurements, such as edge diffraction, which is not included in the prediction models (see Chapter 12 for further discussion). Increasing the cavity depth causes the stiffness of the spring to decrease, and consequently the peak absorption decreases in frequency; again this is predictable.

The absorbers shown here are not particularly unusual in terms of the acoustics they exploit. The physics behind the mechanisms has been known for more than a century. The problem with this type of construction is getting the perforated sheet with the correct hole size and open area. Standard perforated board, such as peg board, has too small an open area; most perforated metals have too large an open area. Consequently, the perforated sheet often has to be specifically constructed for acoustic purposes, which makes it more expensive than if stock items could be used. However, CNC fabrication offers an unlimited choice of design parameters.
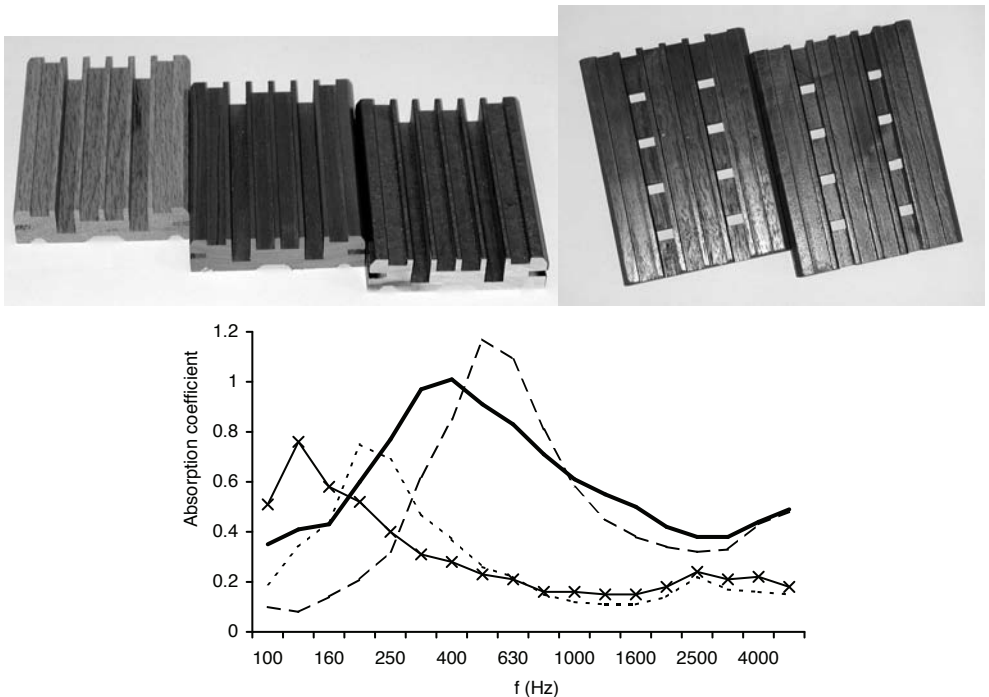
Figure 6.6 Top: a small scale Schroeder diffuser, FlutterFree® (top left) and a perforated version with square holes (top right) forming a Helmholtz absorber. Bottom: random incidence absorption coefficient for various systems:
------- no holes, Helmholtz mounts, shallow cavity;
– – – square holes, normal mount, shallow cavity;
—✕— no holes, Helmholtz mounts, deep cavity; and
—— square holes, normal mount, deep cavity.

6.2.3 Absorption and diffusion

Figure 6.6 shows a Schroeder style diffuser, which has square holes to provide mid-frequency absorption via resonance. These are relatively shallow diffusers and so are only efficient diffusers above 3 kHz, unless modulation is used to extend the bandwidth, as discussed in Chapter 9. Below 3 kHz, absorption is provided by a resonant mechanism via the square holes. The diffuser is mounted over porous absorbent with a cavity behind, similar to Figure 6.2b. Consequently, this is a hybrid device providing absorption and diffusion in different frequency ranges. As the frequency ranges are different, it is assumed that the absorption mechanism should not have too much effect on the diffusion performance and vice versa. The frequency of absorption can be varied by choosing the hole size, open area and cavity depth. Although in this case, the amount of variation in these design variables that is achievable is rather limited, because of restrictions imposed by the diffuser surface profile.

  This surface is also provided without holes. In Figure 6.6 the absorption coefficients for two mounting types are shown. The panel can be mounted with a 1.6 mm gap between the laths (planks) – this is labelled Helmholtz mounts. This gives a small slit opening to the back cavity and as this contains a porous absorbent it generates additional bass absorption via resonance. This additional bass absorption can be useful in treating spaces with excessive bass reverberation. Similar bass absorption can also be achieved by using tuned membrane absorbers, but a Helmholtz mechanism is generally easier to achieve in a device.

  The square holes shown in Figure 6.6 are responsible for the peaks in absorption around 500–600 Hz. The Helmholtz slits provide absorption at a few hundred Hertz or less. Again, the resonant frequency can be easily tuned by choosing an appropriate cavity depth and plank spacing.

6.2.4 Microperforation and clear absorbers

Acousticians have long sought a fully transparent absorbing finish to control reverberation in a room, while maintaining the view through glazing. Glazing is a popular building material, and there are considerable advantages in combining lighting and acoustic function into one device to save on materials and cost. This can be achieved by exploiting microperforation. Figure 6.7 shows a variety of clear microperforated materials. These are most often used as Helmholtz devices, but without the normal resistive material. For instance, the device might be rather like a double glazing unit, with the first pane being a 5 mm thick panel with sub-millimetre diameter holes spaced 5 mm apart, with the holes being drilled mechanically. Alternatively, narrow microslits cut into acrylic or PETG using lasers might be used, which is less expensive and gives the possibility of using decorative microslit patterns. These panels are typically suspended in front of glazing, rather than integrated into the window mullions.

  The device provides absorption through high viscous losses as air passes through the small holes, which are only a bit larger than the boundary layer. This inherent damping eliminates the need for fibreglass or other porous materials in the air cavity between the perforated sheet and the reflective surface behind it. Thus it is possible to provide fibreless, clear absorption. To augment the mid-to low frequency absorption, the device can be curved, tilted or shaped to provide redirection or diffusion at mid- and high frequencies. The surfaces are transparent when looked at from straight on, but at
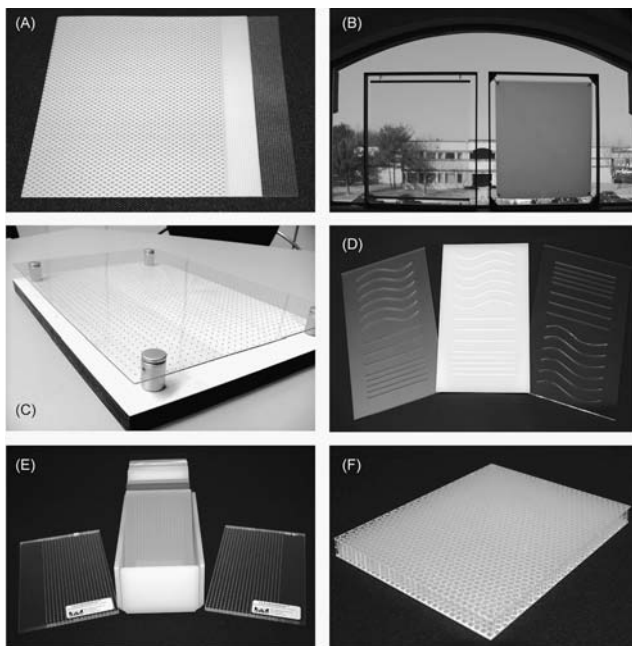
Figure 6.7 Some clear microperforated absorbers: (A) Kaefer 0.1 mm thick foil (printed, translucent and transparent); (B) transparent foil on left and translucent foil on right diagonally spring tensioned in mount; (C) Akustik & Innovation 1 mm thick sheet mounted with standoffs; (D) Deamp 4 mm thick frosted, translucent and transparent microslit panels; (E) Kaefer panels 3–15 mm thickness, and (F) Akustik & Innovation 17 mm thick honeycomb panel. (Photos courtesy of RPG Diffusor Systems Inc.)
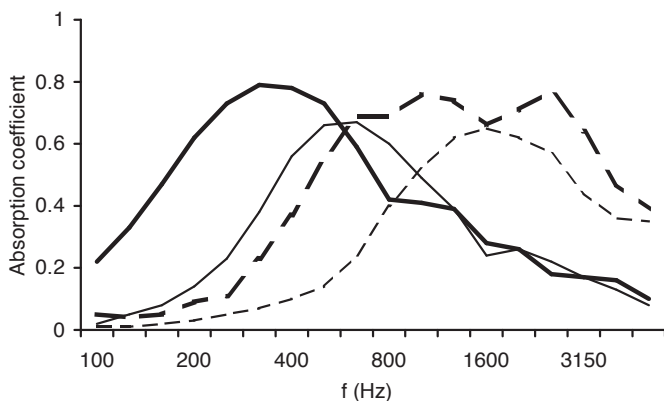
Figure 6.8 Measured random incidence absorption coefficient for four microperforated devices:
—— 1 mm sheet, 200 mm backing depth, 0.5 mm holes spaced at 5 mm;
—— 1 mm sheet, 50 mm backing depth, 0.5 mm holes spaced at 5 mm;
– – – two 0.1 mm foils, 50 mm backing depth, 0.2 mm holes spaced at 2 mm; and
– – – 0.1 mm foil, 50 mm backing depth, 0.2 mm holes spaced at 2 mm.

oblique angles the holes become more apparent, although the surface is still translucent.

Figure 6.8 shows typical absorption coefficients for these materials. For the thicker sheet material, the absorption is not as controllable as with Helmholtz devices with resistive material. The requirement for small holes restricts the frequency range over which the resonant absorption can be achieved within manufacturing constraints. So the thicker materials are useful devices for treating troublesome low to mid-frequency noise and reverberance in spaces such as atria.

Maa,[2] who developed the concepts of microperforation in the 1960s, showed that the sheet thickness and hole diameter should roughly be the same for high absorption. Consequently, to get absorption in the frequencies important for speech, it is necessary to use a thinner material, say 0.1–0.2 mm thick, and to make the holes smaller and closer together. Figure 6.8 shows typical absorption coefficients. The foil might be made from a material such as polycarbonate and stretched to provide a clear wrinkle-free finish or from substances such as polycarbonate or ETFE. Double layers can also be used to broaden the absorption bandwidth. An example result for two layers of microperforated foils is shown in the figure.

In addition, a 1 mm microperforated sheet can be bonded to both sides of a clear polycarbonate honeycomb (shown in Figure 6.7F), to form a structurally strong material that, for instance, might be used as part of a lighting system or as a suspended cloud, which can allow daylight into a space with a glass ceiling. Alternatively, the micro-perforated material might be fixed to another material with much larger holes to give a more structurally robust microperforated absorber.[3] Figure 6.9 shows such a device made from wood; the absorption coefficients are shown in Figure 6.1. Manufacturing the microperforations is easier in the thinner materials.

The advantage of clear microperforated absorbers is that being clear they can be hung some way from the backing surface without making the room appear smaller; the additional backing depth can help low frequency performance. To get absorption across a broader frequency range, a double layer construction is needed, or additional porous absorbent needs to be placed on the room surface.

Microperforated clear absorbers also have potential applications within double
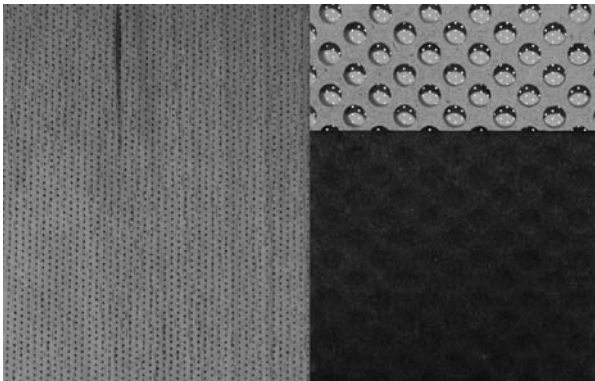
Figure 6.9 A microperforated wood absorber. Left: front view; right: rear of panel with and without non-woven glass matt. The light coming through the five microperforations in each larger hole can be seen. The panel can be used with only the non-woven substrate, but typically fibreglass is used behind the microperforated panel. (Photos courtesy of RPG Diffusor Systems Inc.).

glazing units; the absorbent could help prevent the built up of reverberant sound between the glazing panes and alter the mass-spring-mass resonance. The absorbent can also be used in glazing units which have natural ventilation openings.[4] It has even been suggested they can be used in transparent noise barriers.[5] The optical transmittance of a single microperforated sheet at normal incidence is about 80 per cent, so some loss of optical performance occurs.

Microperforation is also useful even when transparency is not needed. Made from the right material, these absorbers can be more robust than porous absorbers in harsh environments. Indeed the performance of these structures is largely independent of the material used (provided the material does not significantly vibrate). They also have a rather surprising ability not to get clogged up even in very dusty environments; probably due to the vibrating plug of air within the pores. Wood, metal and other materials can be microperforated to gain absorption. Such absorbents might be used where fibreless materials are required, for instance in situations where there are concerns about bacterial contamination, for instance in food and pharmaceutical industries. They might also be used where fibre contamination is a problem, such as in the microelectronic industries or ventilation system silencers.[6] They could also be used within double-leaf partitions where low weight is important, for instance in aircraft and cars.

Later in this chapter, the design equations for microperforated devices will be outlined and shown to be accurate. The use of double layers hung in free space as resistive absorbers will also be considered.

6.2.5 *Masonry devices*

In 1917 Straub patented the CinderBlox, the first concrete masonry unit (CMU). In 1965, slotted blocks were introduced to provide low frequency absorption. The slots produce a Helmholtz device to provide bass absorption. Figure 6.10 shows a modern equivalent. While the old blocks were useful for noise control, the flat or split face of these blocks can create reflection problems which degrade acoustics. Consequently, a phase grating diffuser is used to break up the reflected sound wavefronts. The design utilizes two slotted Helmholtz resonator chambers, as well as the phase grating pressure gradient absorption mechanism (see Chapter 7). Typical absorption coefficients are shown in Figure 6.11. Painting reduces the high frequency absorption as it seals the porous concrete surface, but does not affect low frequency absorption as would be expected. Good insulation against sound transmission is achieved because of the heavy construction.v

Figure 6.10   CMU (concrete masonry unit) which uses two slotted Helmholtz absorbers to provide bass absorption, DiffusorBlox® (one slot is difficult to see).
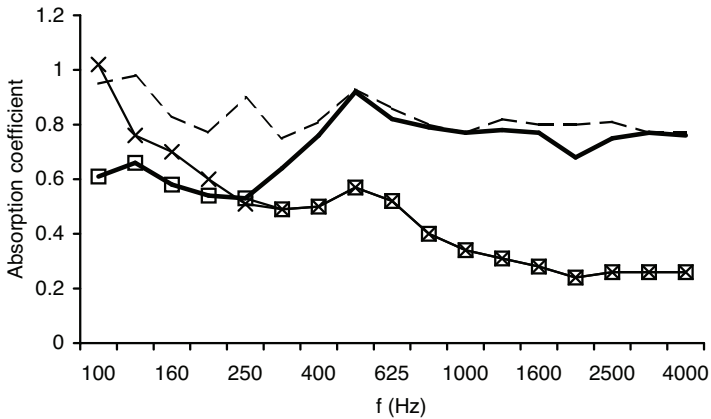
Figure 6.11 Random incidence absorption coefficient for a masonry unit. The slots provide absorption via a Helmholtz mechanism, producing low frequency absorption:
– – – slotted, unpainted;
⸻ not slotted, unpainted;
—×— slotted, painted; and
—☐— not slotted, painted.
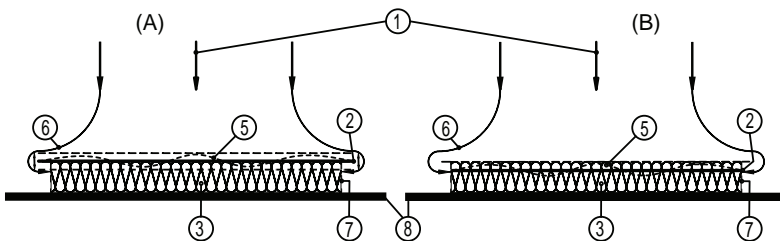
Figure 6.12 Above: illustrations show sound (1) striking two absorber systems. The steel plates (2) pistonically vibrate against the foam spring (3), mounted on a rigid backing (8). The porous absorption also damps plate bending modes (5) and absorbs higher frequencies which diffract around the plate (6) through a perforated (7) metal frame. The right hand device has some of the porous absorbent in front of the steel plate, protected by a perforated sheet, which generates additional mid-high frequency absorption. Top: pictures of the two systems.
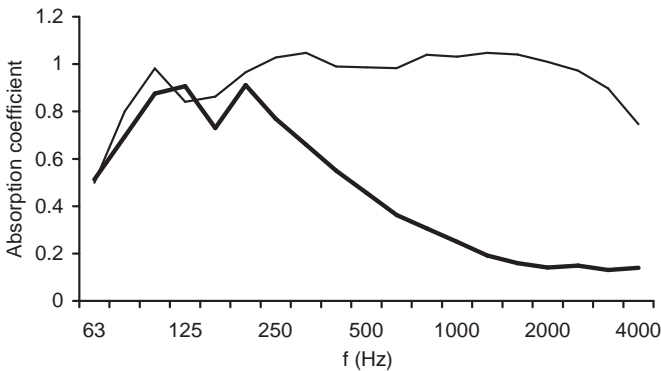
Figure 6.13   Random incidence absorption coefficients for two metal plate resonators: ———— with front perforations to exploit porous absorption at mid-high frequencies, and
▬▬▬ without perforations (data courtesy of Fraunhofer Institute for Building Physics, Stuttgart, Germany).

6.2.6 Metal plate resonators

Most devices described in this chapter use the air within a cavity to act as a spring. But it is also possible to make a resonant absorber where the spring of the porous material skeleton is exploited within a membrane absorber. As the spring is stiffer than would be the case for air, a more heavy mass is needed. A possible construction is a steel plate ≥1 mm in thickness, which vibrates against a foam or polyester spring.[7] Figure 6.12a illustrates the absorption mechanism. Sound strikes the steel plate which pistonically vibrates against the spring, mounted on a rigid backing. The porous absorption also damps plate bending modes and absorbs higher frequencies which diffract around the plate through a perforated metal frame. This arrangement provides low frequency absorption as seen in the heavy line in Figure 6.13. To provide broad bandwidth absorption, part of the rear porous material can be moved to the facing side of the plate resonator. In Figure 6.12b the foam also absorbs high frequencies striking the face. Photos of the devices are also shown in the figure.

By exploiting all three mechanisms it is possible to make an absorber which operates over about six octaves. Figure 6.13 shows the measured random incidence absorption coefficients for the two devices shown in Figure 6.12. Fuchs *et al.*[8] give formulations for calculating the key resonant frequencies of the absorber, but not the absorption coefficient.

6.2.7 Passive electroacoustic absorption

A sealed loudspeaker within an enclosure is like a membrane absorber: the diaphragm is a resonating mass; the compliance of the air in the enclosure is the restoring spring; and any porous material within the enclosure provides additional damping. So it is possible to use a loudspeaker as a resonant absorber. The loudspeaker is not being driven – this is not an active impedance system – it is just responding to the incident sound with passive electrical components across the input terminals. (A similar use of electromechanical systems has also been suggested for Helmholtz absorbers,[9] and for reducing cavity resonance in pipes.[10])
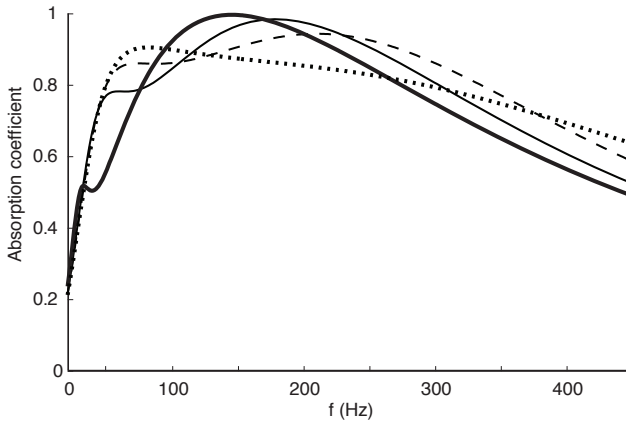
Figure 6.14 Predicted absorption coefficients for a loudspeaker with an inductor in series
with a 110 µF capacitor as a passive load:
-------- 1;
– – – 10;
——— 25; and
━━━ 100 H.

Using a loudspeaker as an absorber has several advantages: loudspeakers are cheap, readily available and already configured for rudimentary acoustic treatment. More importantly however, the electrical and magnetic properties of the loudspeaker will affect how the system responds to incident sound. Consequently, the bandwidth and quantity of absorption can be tuned, within certain limits, by altering the electrical coefficients of the loudspeaker.[11] By applying resistive loads across the terminal, the Q of the resonant absorption peak can be changed because the damping in the system is changed. Measurements show that the absorption bandwidth can be altered by up to 50 per cent. Applying capacitive loads across the terminals alters the resonant frequency by up to 30 per cent, but it also affects the damping in the system somewhat. Predictions indicate that by using inductors and capacitors together allows even greater changes in resonant frequency and broader absorption over two and a half octaves, as Figure 6.14 shows.

6.3 Design equations: resonant frequency

Having discussed some example designs, this section outlines the most simple design equations. Consider a simple absorber formed by a cavity with a covering sheet. The sheet could either be perforated to form a Helmholtz design, or solid but flexible to form a membrane absorber (Figure 6.2). It could even be a flexible perforated membrane, which is a combination of the two. In the first two cases, the impedance of the cavity given in Equation 5.26 will simply be altered by the addition of mass ($j\omega m$) and resistance (r_m) terms. These are the acoustic mass and resistance respectively, arising due to the perforated sheet or membrane. The surface impedance of the resonant system is:

$$z_1 = r_m + j[\omega m - \rho c \cot(kd)] \tag{6.1}$$

where $k = 2\pi/\lambda$ is the wavenumber in air; d the cavity depth; m the acoustic mass per unit area of the panel; ω the angular frequency; ρ the density of air; and c the speed of sound in air.

For now, the presence of porous absorbent within the cavity is ignored for simplicity. Systems resonate when the imaginary part of the impedance is zero, so to find the resonant frequencies the imaginary part of Equation 6.1 is set equal to zero. Consider a case where the cavity size is much smaller than the acoustic wavelength, i.e. $kd <<1$ and $\cot(kd) \rightarrow 1/kd$, then the resonant frequency f is given by:

$$f = \frac{c}{2\pi}\sqrt{\frac{\rho}{md}} \tag{6.2}$$

This is a general formulation. Now the specific instance of the Helmholtz resonator will be considered, followed by the case of the membrane absorber.

6.3.1 Helmholtz resonator

The perforated surface is divided into individual cells which are assumed to behave independently with a repeat distance D. D is defined in Figure 6.2, which shows a cross-section through the absorber. The absorber is assumed to be perforated in two directions, with the repeat length being the same in both directions. The individual cells will not be entirely independent at low frequency, and consequently physical subdividing of the volume may be required as the wavelength becomes large. This is especially true if absorption at oblique incidence is required, as would be needed for good random incidence absorption. In this case, lateral propagation within the cavity must be suppressed to maximize absorption. When a porous absorbent is placed in the cavity, sound propagation is generally normal to the surface, as discussed in Chapter 5, and so the need for subdividing is less critical, except at very low frequencies.

The hole spacing should be large compared to the hole diameter. The acoustic mass per unit area is then $m = \rho D^2 t'/\pi a^2$ where t' is the thickness of the perforated sheet with the end corrections (end corrections allow for the radiation impedance of the orifices and are discussed later) and other variables are as defined in Figure 6.2. The sheet thickness t and hole radius a are assumed to be much smaller than the wavelength of sound in air. Under these assumptions, the resonant frequency is:

$$f = \frac{c}{2\pi}\sqrt{\frac{S}{t'V}} \tag{6.3}$$

where $S = \pi a^2$ is the area of the holes, and V the volume = $D^2 d$ of each unit cell.

This is the same formulation as derived by other methods, such as lumped parameter equivalent electrical circuits.[12] The transfer function approach is used here because it can more easily generalize to non-lumped parameter cases, for example when the cavity size is no longer shallow compared to wavelength. It is also consistent with the theories used elsewhere in this book.

An alternative, but entirely equivalent formulation for the Helmholtz resonator uses the porosity, or fraction of open area, ε, of the perforated sheet. This is often more convenient to work with when using perforated sheets and can be derived by considering the geometry in Figure 6.2 to revise Equation 6.3:

$$f = \frac{c}{2\pi}\sqrt{\frac{\varepsilon}{t'd}}$$

(6.4)

$$\varepsilon = \frac{\pi a^2}{D^2}$$

(6.5)

The vibrating plug of air within the perforations provides the mass of the device. The length of the plug of air is not just the perforated plate thickness. The effect of radiation impedance must be considered, including the mutual interaction between neighbouring vibrating air plugs. Consequently, the vibrating plug of air has a length given by the thickness of the panel plus end corrections to allow for the radiation impedance of the orifice. A full expression for the mass in Equation 6.2 is:[13]

$$m = \frac{\rho}{\varepsilon}\left[t + 2\delta a + \sqrt{\frac{8v}{\omega}\left(1 + \frac{t}{2a}\right)}\right]$$

(6.6)

The last term in the equation is due to the boundary layer effect, and $v = 15 \times 10^{-6}$ m²s⁻¹ is the kinemetric viscosity of air. This last term is often not significant unless the hole size is small, say sub-millimetre in diameter. δ is the end correction factor which to a first approximation is usually taken as 0.85 and derived by considering the radiation impedance of a baffled piston. A value of 0.85 does not, however, allow for mutual interactions between neighbouring orifices because it is based on a calculation for a single piston. Consequently, other more accurate formulations exist. For a porosity of $\varepsilon < 0.16$, Ingard gives the correction factor as:[14]

$$\delta = 0.8(1 - 1.4\varepsilon^{1/2})$$

(6.7)

In the limit of only one hole in an infinite plane, this is roughly 0.85, as given earlier. An alternative formulation, which works for more open structures, was developed by Rschevkin and reported by Cremer and Müller.[15] This reportedly includes the limiting case of $\varepsilon = 1$:

$$\delta = 0.8(1 - 1.47\varepsilon^{1/2} + 0.47\varepsilon^{3/2})$$

(6.8)

For a square aperture, the formulation for $\varepsilon < 0.16$, Equation 6.7, changes slightly to:[14]

$$\delta = 0.85(1 - 1.25\varepsilon^{1/2})$$

(6.9)

For unusual shapes, the radiation impedance of the plug of air can be numerically evaluated using boundary or finite element models, but the changes this makes to the final resonant frequency are likely to be small.

An added complication with end corrections is that imperfections in constructions, such as burrs, may have an effect which will be ill-defined. For high amplitude sound, turbulence will reduce the acoustic mass and so the resonant frequency will increase. Grazing mean air flow is generally observed to also decrease reactance and increase resistance.

Figures 6.15 and 6.16 illustrate the effect of changing the open area on the resonant
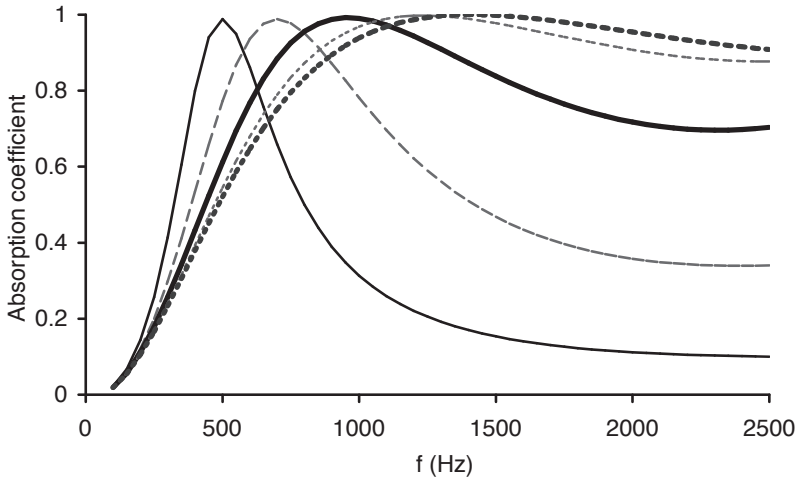
Figure 6.15 Absorption coefficient of a Helmholtz absorber showing effect of open area. Hole radius 2.5 mm; porous absorbent flow resistivity 20,000 rayls m⁻¹; thickness 2.5 cm; air layer thickness 2.5 cm; and perforated sheet thickness 6.3 mm. Open areas:

——— 6%;
– – – 12.5%;
——— 25%;
········· 50%; and
------ 100%.
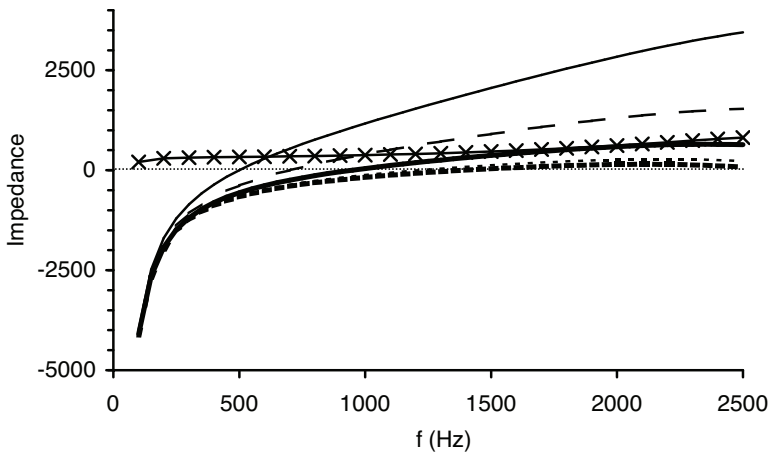
Figure 6.16 Impedance of some Helmholtz absorbers showing effect of open area. Geometry same as Figure 6.15. Only one real impedance is shown because the variation with open area is negligible. Open areas:

—✕— Re, 6%;
——— Im, 6%;
– – – Im, 12.5%;
——— Im, 25%;
········· Im, 50%; and
------ Im, 100%.
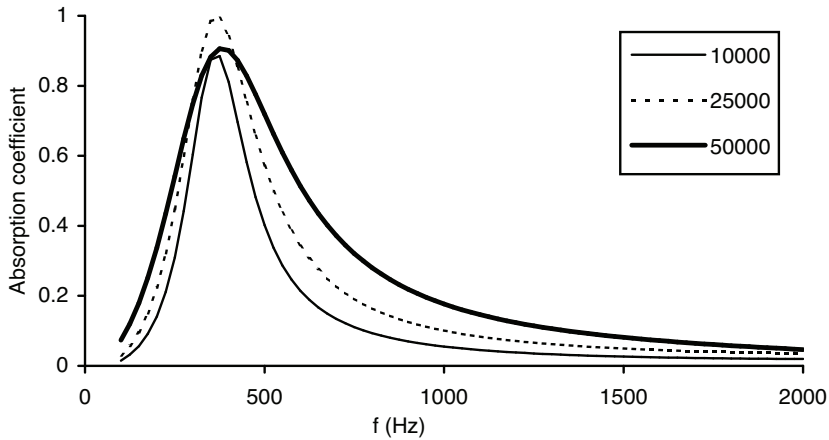
Figure 6.17   Effect of flow resistivity (shown in legend in rayls m⁻¹) on absorption of a Helmholtz resonator.

frequency. The first figure shows the absorption coefficient, with the frequency at which peak absorption occurs decreasing as the open area reduces. The second figure shows the change of resonant frequency in terms of impedance where the frequency of the zero crossing of the imaginary part decreases as the open area reduces. Script 6.1 in Appendix B gives the code to generate the results. As the open area decreases, additional low frequency absorption is generated mainly due to the increased stiffness of the spring in the unit cell as the volume reduces. The high frequency absorption decreases because the proportion of solid parts of the perforated sheet increases, and these parts reflect high frequency sound. Similar results are seen in measurements.[16]

The maximum absorption decreases somewhat as the resonant frequency decreases. If these absorbers were tuned to a lower frequency, this decrease would be more marked. The reason for this is that the impedance of the porous material moves further from the characteristic impedance of air at low frequencies, making the absorbent less efficient. The peak absorption can be altered by changing the porous material flow resistivity as illustrated in Figure 6.17. In the case shown, when the flow resistivity is 25,000 Nm⁻⁴s, the resistance is close to the characteristic impedance of air leading to high absorption. An additional effect of changing the flow resistivity is to change the bandwidth over which absorption is effective by altering the Q of the resonance. In this case, a higher flow resistivity would achieve a greater bandwidth, but will reduce the maximum absorption, as the resistance exceeds the characteristic value. A lower flow resistivity leads to an impedance less than characteristic, which results in a reduction in bandwidth and maximum absorption.

Figure 6.18 shows the trade-off between cavity depth and perforated sheet thickness. The perforated sheet thickness has been varied while keeping the total thickness of the device, cavity plus perforated sheet, constant. Making the covering sheet thicker can generate additional bass absorption. But this is at the expense of reduced bandwidth including decreased high frequency absorption.

Another common geometry is a Helmholtz device where slots are used instead of holes, see for example the CMU shown in Figure 6.10. This can have a considerable
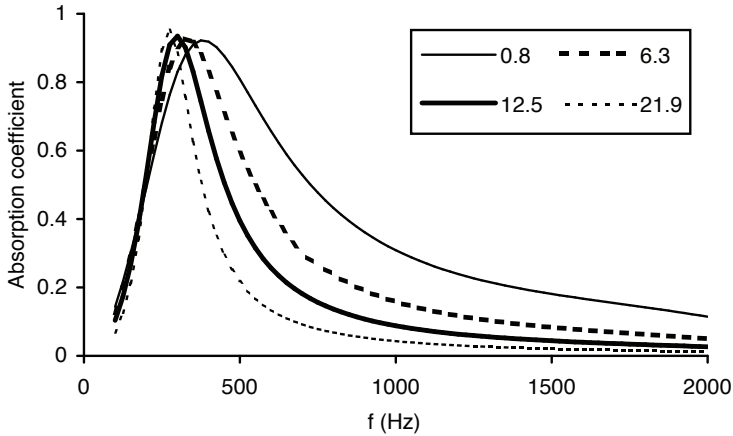
Figure 6.18   Effect of facing thickness (shown in legend in mm) on absorption of a Helmholtz resonator. The total thickness of the device (cavity plus facing) is kept constant.

advantage in some cases, as slots can be easier to make than holes. The orifices can be formed by sawing slots in board or by leaving spaces between parallel planks in wood claddings. For a lath or plank cladding, manufacturers can offer different mounting conditions, with and without spaces between the planks, which enables designers to choose the desired absorption characteristics (see Figure 6.6 for example). The difficulty with slotted Helmholtz devices is deriving the appropriate end correction. Kristiansen and Vigran[17] use a formulation originally derived by Smits and Kosten:[18]

$$\delta = -\frac{1}{\pi}\ln\left[\sin(\tfrac{1}{2}\pi\varepsilon)\right] \tag{6.10}$$

This then gives a mass term of:

$$m = \frac{\rho}{\varepsilon}(t + 2\delta w) \tag{6.11}$$

where w is the width of the slots. As shall be shown later, this gives accurate results.

6.3.1.1 Membrane absorber

For a membrane absorber, m in Equation 6.2 is simply the mass per unit area of the panel. A common simplification of the formulation is derived after straightforward algebraic manipulation. This gives the resonant frequency as:

$$f = \frac{60}{\sqrt{md}} \tag{6.12}$$

This is correct when the cavity is filled with air. If the cavity is filled with porous absorbent, then the system is no longer adiabatic, and an isothermal case must be

considered below about 500 Hz. In addition, the porosity of the porous absorber should be included although this is a minor effect for more commonly used materials as their porosity is close to unity. Under an adiabatic assumption, Equation 6.12 becomes:[19]

$$f = \frac{50}{\sqrt{md}} \tag{6.13}$$

This formulation holds for oblique incidence when a porous absorbent is in the cavity, because the porous absorbent enforces propagation normal to the front face. For an air cavity without partitions, a new formulation is required for oblique incidence:

$$f = \frac{60}{\cos(\psi)\sqrt{md}} \tag{6.14}$$

where ψ is the angle of incidence.

Unfortunately, these simple formulations for membrane absorbers are often inaccurate. The membrane system is not as simple to model as the perforated absorber. For example, these all assume that the membrane does not support higher order modes at the frequencies of interest. The mass of the membrane is being treated as a single mass, and therefore the membrane should move as one, like a piston. The effect of bending stiffness is to increase the resonant frequency, but usually Equation 6.2 is dominant. Problems can occur if the membrane is small, because the whole mass may not be able to vibrate freely if it is secured at the edges. In this case, the actual vibrating mass may be less than expected, and additional losses at the fixings may occur. One solution to this is to attach the edges of the membrane using resilient foam so that the whole membrane can vibrate including the edges. If such a fixing is used, it is important that the cavity remains air tight. Alternatively, a surround from a loudspeaker can be used to increase the effective moving mass; this can reduce the resonant frequency of a membrane absorber to 60–70 per cent of its original value.

As the angle of incidence increases, there is an increasing chance of bending waves being excited. Consequently, the simple formulations above can break down. Unfortunately, the modelling of such bending wave problems is complex, as it is very dependent on the construction used.

More complex modelling of panel absorbers does exist[20–21] but the prediction models presented are not that useful in designing practical surfaces. It is possible to model the plate vibration, and then use a mode matching approach to derive the power absorbed. This is complex, and many parameters concerning real surfaces, such as the mounting conditions of the panel, will not conform to simple conditions that the prediction models use. Consequently, predictions are unlikely to match measurements well. This has already been illustrated in Figure 6.3. For the prediction shown in the figure, a transfer function matrix method was used as detailed later. There is a 10 per cent error in the prediction of the peak frequency. In this case, the peak absorption frequency is somewhere between the values given by Equations 6.12 and 6.13. If a more accurate model is required, it is probably best to use a finite element analysis.[22]

6.3.2 Losses

So far, the above formulations have only allowed a calculation of the resonant frequency. A proper design method must also allow the absorption coefficient and surface impedance to be determined for all frequencies. To do this, the losses within the device must be modelled. These are determined by the resistance term r_m in Equation 6.1. For a Helmholtz device with no additional porous absorbent this can be calculated using:[13]

$$r_m = \frac{\rho}{\varepsilon}\sqrt{8v\omega}\left(1+\frac{t}{2a}\right) \tag{6.15}$$

This formulation assumes that the hole radius is not sub-millimetre in size, to ensure it is larger than the boundary layer thickness. An alternative formulation for this resistive term derived by Ingard is often used:[14]

$$r_m = \frac{\sqrt{2\rho\eta\omega}}{2\varepsilon} \tag{6.16}$$

where η is the viscosity of the air, with a value of 1.84×10^{-5} poiseuille. These theoretical equations do not allow for increased resistance that happens if burrs are present. Indeed, Ingard carried out empirical work to show that Equation 6.16 was approximately correct, but taking a value twice as large matches experimental results better. Equation 6.16 is more commonly quoted than Equation 6.15, but for most practical absorbers both are negligible, as is the difference between them! The exception is with devices such as microperforated absorbers where the size of the resistance is critical. For most designs, the losses contributed by Equation 6.15 are very small, and in order to get good absorption it is necessary to add porous material.

First, attention will be focussed on devices with additional porous material. The effect of the porous absorbent depends on where it is placed. Ideally, it should be placed where the particle velocity is a maximum. Porous absorption works primarily by viscous losses as sound penetrates the small pores. For this to be maximized, the air motion must be at its greatest, and this is achieved where the particle velocity is highest. For a Helmholtz resonator this means the absorbent being as close to the openings as possible, or even in the openings. A balance must be struck, however, as too much absorption in the neck might prevent resonance. The effect of placing an air gap between the perforated sheet and the porous absorbent is to reduce the resistance, and in most cases this will result in a decrease in absorption.[16]

For a membrane absorber, the porous absorbent should be just behind, but not touching, the membrane. Without the porous absorbent, the primary losses are most likely to come from within the membrane or from friction at the fixings between the membrane and the supporting structure. If the porous absorbent behind the membrane does not provide sufficient absorption, perforating the membrane to allow easier access to the porous absorber behind can be done. This then creates a hybrid Helmholtz-membrane design. Then the design equations should be altered somewhat. The impedance of the membrane alone, z_{mem}, will be a combination of resistance and mass:

$$z_{mem} = r_{mem} + j\omega m_{mem} \tag{6.17}$$

where r_{mem} and m_{mem} are the acoustic resistance and mass of the membrane. Similarly, the impedance of the perforated sheet forming the Helmholtz device, z_{helm}, will be formed from acoustic resistance and mass:

$$z_{helm} = r_{helm} + j\omega m_{helm} \qquad (6.18)$$

where r_{helm} and m_{helm} are the acoustic resistance and mass of the perforated sheet. It is necessary to make some assumptions about how these impedances interact. The simplest model is that the impedances act independently and in parallel; then a combined impedance can be derived. The impedance of the device with an air cavity is given by:

$$z = -j\rho c \cot(kd) + \frac{z_{mem} + z_{helm}}{z_{mem} z_{helm}} \qquad (6.19)$$

where d is the cavity depth. To find the resonant frequency of Equation 6.19, the easiest technique is to plot z versus frequency using a numerical tool such as a spreadsheet and inspect for the zero crossing of the imaginary part or use a numerical root-finding algorithm. Later on, this type of formulation will be discussed in more detail for a microperforated thin membrane. The problem with applying the above formulation is in properly defining the impedance of the membrane.

For a Helmholtz device the design equations for the case with porous absorbent depend on where the porous layer is located. First some relatively simple formulations are considered and then a more complex treatment using transfer matrixes will be considered. The accuracy of these formulations will be demonstrated later in the chapter.

6.3.2.1 Porous layer right behind perforations

When the porous layer is right in front or behind the perforated plate, then the resistance behaves as though it is actually in the openings. This comes from a consideration of the flow through the device. As sound is squeezed through the holes, the particle velocity is increased. On the other side of the perforated sheet, the flux lines return to a free field case somewhat gradually; this is shown schematically in Figure 6.19. If the porous
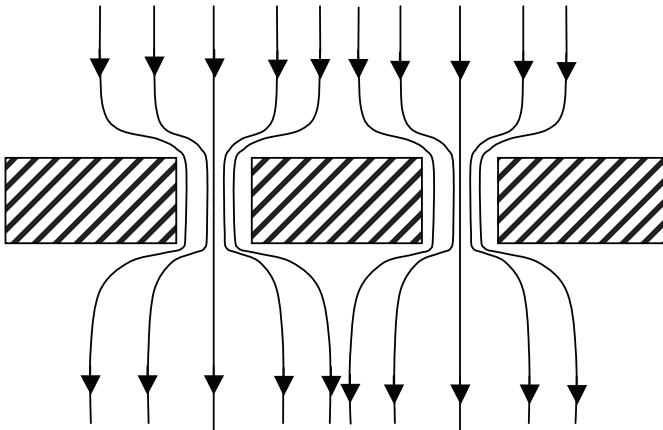
Figure 6.19   Flow through a perforated sheet.

layer is within a hole diameter of the perforated sheet, it is assumed that the flux has not yet had time to return to a free field state. Consequently, the resistance added by the porous material, r_m, is altered by the fractional open area of the perforated plate (porosity), ε. The resistance is:

$$r_m = \frac{\sigma t_a}{\varepsilon} \qquad (6.20)$$

where t_a is the thickness and σ the flow resistivity of the resistive layer. This form is assumed because the volume velocity is reduced by the open area (or porosity) ε, and has not yet had time to recover to a free space value. The key in absorber design is to make this resistance in Equation 6.20 as close to the characteristic impedance of air as possible, as this maximizes absorption. If characteristic impedance is achieved at resonance, absorption will be complete. Consequently, a balance between the open area, flow resistivity and absorbent thickness must be struck, while remembering that the resonant frequency of the device is also dependent on the open area of the per-forated sheet. In addition to changing the resistance, the presence of the porous material directly behind the perforations also increases the end correction. While the effect is smaller than the change in resistance, it can still vary by 30–100 per cent, depending on the open area of the perforated sheet,[23] with the biggest changes being for the most open sheets.

6.3.2.2 Porous layer in the middle of cavity with a perforated covering

It is assumed that the porous material is further than a hole diameter away from the perforated sheet; the materials are not too thick and are also away from the rigid backing. This is not a common situation as it is awkward to construct. As the bulk of the porous layer is away from the perforations, it is assumed that the velocity through the surface is the same as in free space. Consequently, the resistance term is given by:

$$r_m = \sigma t_a \qquad (6.21)$$

A more exact formulation would use a full transfer matrix approach as detailed in the following section.

6.3.2.3 More complete solution using transfer matrixes

A full multi-layer solution first calculates the impedance just below the perforated sheet or membrane, and then the effect of the sheet is considered by adding on this impedance. This is a very flexible solution method as it can allow for many different combinations in design. The solution discussed here is split into two forms: the first is when air is immediately behind the perforated sheet and the second when a porous absorber backs the perforated sheet.

The first case is shown in Figure 6.20. First, the impedance just behind the perforated sheet is calculated; this can be done to a first approximation using the equations set out in Section 5.5.1. Consider a simple case of a layer of absorbent of thickness d_1 and an air layer of thickness d_2. The impedance at the top of the absorbent is z_1:
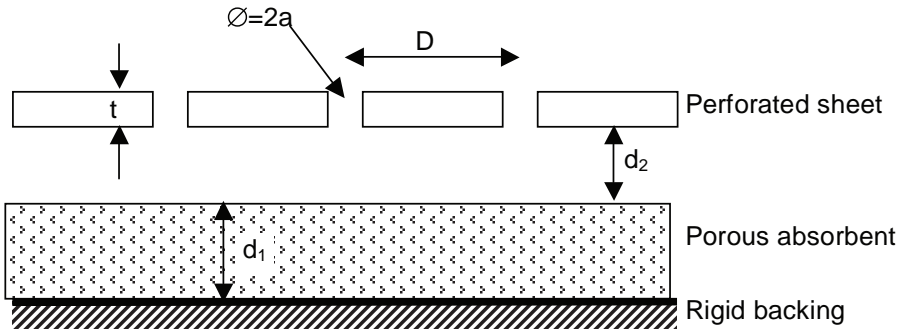
Figure 6.20   Construction for predictions around Equation 6.22.

$$z_1 = -jz_i \cot(k_i d_1) \tag{6.22}$$

where z_i is the characteristic impedance and k_i the wavenumber of the porous absorbent. The impedance at the top of the air layer and just below the perforation, z_2, can be found by using a transfer matrix as discussed in Chapter 5:

$$z_2 = \frac{-z_1 j\rho c \cot(kd_2) + \rho^2 c^2}{z_1 - j\rho c \cot(kd_2)} \tag{6.23}$$

The impedance of the Helmholtz absorber, z_3, is given by using Equation 6.6 and 6.15:[24]

$$z_3 = \frac{\rho}{\varepsilon}\left(\frac{t}{2a}+1\right)\sqrt{8v\omega} + (2\delta a + t)\frac{j\omega\rho}{\varepsilon} + z_2 \tag{6.24}$$

where the additional viscous term in Equation 6.6 is ignored as it is generally small.

   The second case, with the porous layer next to the perforated sheet is shown in Figure 6.2a. For simplicity, it is assumed that the entire cavity is filled with porous absorbent, and the cavity depth is d. This is a common construction because it is simple to make. Two solution methods can be attempted. The most simple is to consider that only plane waves propagating normal to the perforated sheet are present in the porous layer. Then the impedance immediately below the perforated sheet is given by:

$$z_1 = -jz_i \cot(k_i d) \tag{6.25}$$

where z_i is the characteristic impedance and k_i the wavenumber of the porous absorbent. Then the mass effect of the perforations can be added, and the effect of open area taken into account to give the surface impedance of the absorber, z_2, as:

$$z_2 = \frac{1}{\varepsilon}(2\delta a + t)j\omega\rho + z_1 \tag{6.26}$$

The mass and resistance terms due to viscous forces in and around the perforated plate are ignored because they will usually be negligible compared to the z_1 term.

A more complex solution to this problem allows for the multiple waves propagating in the porous media. The surface is considered in a series of elementary cells of size D by D, each containing one hole. The velocity at the cell boundaries parallel to the perforated sheet is assumed to be zero. Unless the cavity is actually partitioned, this is only an approximation. This enables the pressure within the cells to be decomposed into a sum of modes within the cell in an analogous way to solving the modes in a room. The impedance below the perforated sheet, z_1, is then given as a sum over modal terms:[24]

$$z_1 = \frac{z_{0,0}\varepsilon}{\phi} + \frac{4}{\pi} \sum_m \sum_{n,(n\neq 0 \& m \neq 0)} \frac{v_{m,n} z_{m,n} J_1^2 \left(\frac{2\pi a}{D} \sqrt{m^2 + n^2} \right)}{\phi \left(m^2 + n^2 \right)} \tag{6.27}$$

$$z_{m,n} = -jz_i \frac{k_i}{k_{m,n}} \cot(k_{m,n} d) \tag{6.28}$$

$$k_{m,n} = \sqrt{k_i^2 - \frac{4m^2\pi^2}{D^2} - \frac{4n^2\pi^2}{D^2}} \tag{6.29}$$

$$v_{m,n} = \begin{array}{ll} 0.5; & m = 0 \, or \, n = 0 \\ 1 & otherwise \end{array} \tag{6.30}$$

where k_i and z_i are the wavenumber and characteristic impedance of the porous absorber. ϕ is the porosity of the porous absorber, say 0.98 for mineral wool. J_1 is the Bessel function of the first kind and first order. The sum is carried out over all combinations of n and m when both are not equal to zero.

The sum converges as the contributions from higher modes reduce. In fact, in many cases only the plane wave term ($n = 0$ and $m = 1$) need be considered as the dominant propagation mode in a porous medium will be perpendicular to the perforations due to refraction. This is especially true when high flow resistivity materials are used. When only the first term is considered, Equations 6.27–6.30 give similar results to the more simple formulation given in Equation 6.25. Once the impedance, z_1, immediately below the perforated sheet is known Equation 6.26 can be applied to get the surface impedance of the whole system including the perforated sheet.

6.3.2.4 Oblique incidence

For oblique incidence it can be assumed to a first approximation that the impedance of the Helmholtz absorber will be very similar to the normal incidence value, provided there is a significant amount of porous absorbent in the cavity and/or the cavity is partitioned. With porous material in the cavity, the dominant propagation direction will be normal to the front face due to refraction. Lateral propagation could change the impedance of the device at oblique incidences, but this is not normally significant. Figure 6.21 shows the measured impedance for a sample at normal and 60° incidence[25]
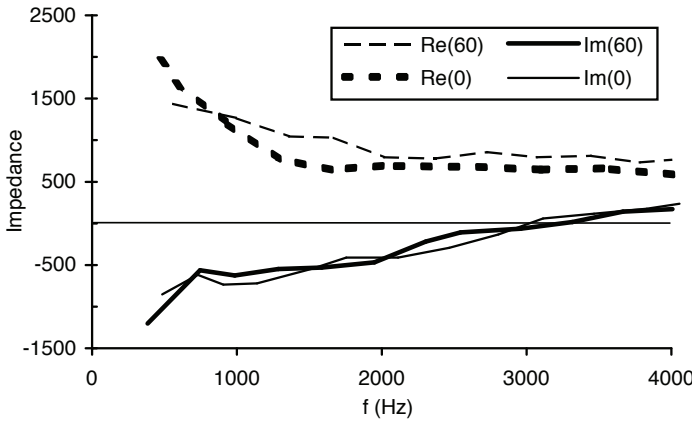
Figure 6.21 Measured impedance for two angles of incidence for a Helmholtz absorber. Angles indicated in legend in degrees (data from Guignouard *et al.*[25]).

confirming this assertion. At low frequencies, without partitions within the cavity, this may become less true as lateral propagation modes become more significant. Any lateral propagation would be expected to decrease the absorption achieved for most angles of incidence.

There is a more complex and complete prediction model for oblique incidence.[24] As the surface is periodic, it is possible to solve the problem with a Fourier decomposition. This method can only produce a solution when the wavelength in air projected onto the surface is an integer multiple of the spacing between the perforations, i.e:

$$ND = \lambda / \sin(\psi) \tag{6.31}$$

where N is a positive integer, and ψ is the angle of incidence. With this principle, it is possible to carry out a Fourier decomposition into a series of modes within the porous material. Consider the case of a Helmholtz device where there the cavity is filled with porous material. The impedance just below the perforated sheet is given by:[24,25]

$$z_1 = \frac{2}{\pi \phi} \sum_{m=0}^{\infty} \sum_{n=-1,-1\pm N,-1\pm 2N\dots} v_{m,n} z_{mn} \frac{J_1^2 \left\{ 2\pi a \sqrt{\dfrac{m^2}{D^2} + \dfrac{n^2}{N^2 D^2}} \right\}}{m^2 + \dfrac{n^2}{N^2}} \tag{6.32}$$

$$z_{mn} = -j\rho c \frac{k_i}{k_{mni}} \cot(k_{mni} d) \tag{6.33}$$

$$k_{mni} = \sqrt{k_i^2 - \chi} \tag{6.34}$$

$$\chi^2 = \left(\frac{2\pi m}{D} \right)^2 + \left(\frac{2\pi n}{ND} \right)^2 \tag{6.35}$$
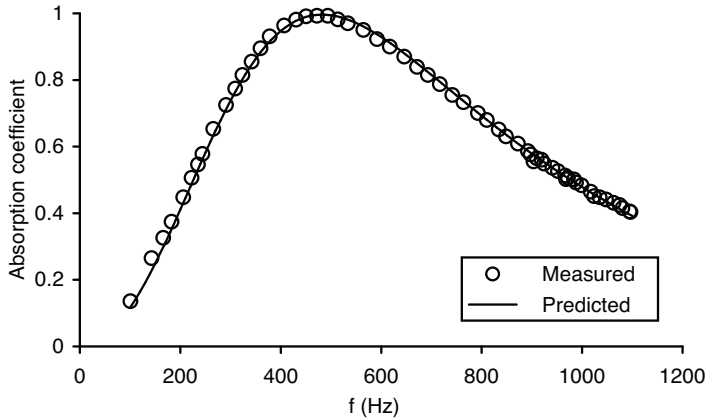
Figure 6.22 Predicted and measured normal incidence absorption coefficient for a slotted Helmholtz absorber (measured data from Kristiansen and Viglen[17]).

where the subscript i indicates that the wavenumber and impedance apply to the porous layer. The porous material has a depth d and porosity ϕ .$v_{m,n}$ is defined in Equation 6.30. Once z_1 has been evaluated, Equation 6.26 can be applied to get the impedance of the surface above the perforated sheet at the front face of the absorber.

6.4 Example calculations

6.4.1 Slotted Helmholtz absorber

Kristiansen and Vigran[17] carried out impedance tube measurements on a slotted absorber, which allows the accuracy of the above formulations to be partially tested. The absorber had an open area of about 24 per cent; the slots were 15 mm deep and 10 mm wide; the cavity depth was 150 mm and a material with an air flow resistance of 86 Pa s m⁻¹ was attached to the bottom of the slotted plate. Script 6.2 in Appendix B predicts the scattering from the slotted absorber, and it is compared with the experimental data in Figure 6.22. Using the transfer matrix method with Equations 6.10, 6.11, 6.20 and 6.1 gives accurate results as shown. Adding the resistance term, Equation 6.15 or 6.16 has a negligible effect and only changes the absorption coefficient by less than a hundredth.

A simple calculation of the peak of absorption using Equations 6.4 and 6.10 yields a predicted resonant frequency about 100 Hz greater than measured. This shows the power and usefulness of the transfer function matrix procedure for Helmholtz absorbers. Similarly accurate results were also found by Ingard when he examined circular perforations[14] with a thin resistive layer behind the perforated sheet.

6.4.2 Porous absorbent filling the cavity

Figure 6.23 compares the predicted and measured normal incidence impedance for a Helmholtz absorber. These use measurements by Guignouard *et al.*[25] using a two-microphone free field method to obtain both normal incidence and 60° incidence
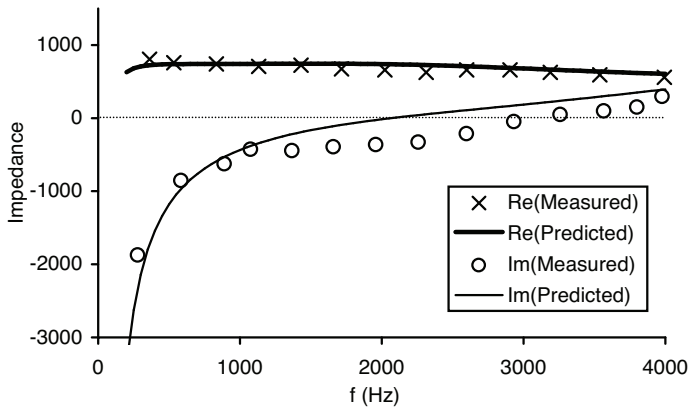
Figure 6.23   Impedance predicted and measured for a Helmholtz absorber (measured data from Guignouard *et al.*[25]).

results. The two-microphone technique is described in Chapter 3. Figure 6.24 shows the predicted absorption coefficients for three arrangements: a porous absorber, a porous absorbent faced with a porous sheet with and without an air gap between the porous absorber and the rigid backing. In addition, a measurement for one of the configurations is given. The predictions for normal incidence used the transfer function matrix technique given in Equations 6.22–6.24. The more complex modal decomposition model is unnecessary because the simple model gives satisfactory results. The porous absorber had a flow resistivity of 70,000 rayls m^{-1} and was 3 cm thick. For the perforated sheet, the holes had a radius of 2.5 mm, the open area was 17.5 per cent and the thickness was 0.75 mm. The prediction model gives reasonable accuracy.
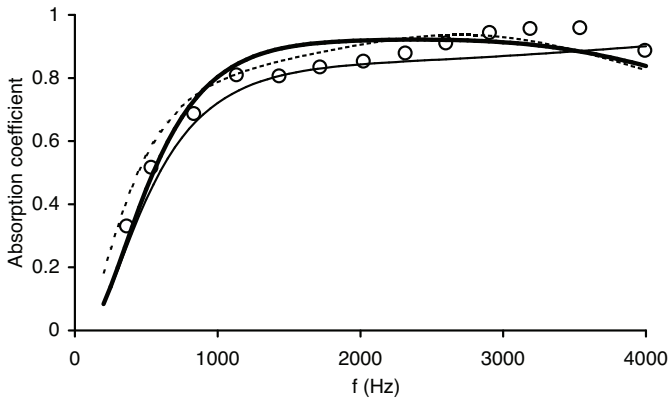
Figure 6.24   Absorption coefficient predicted for three absorbers, plus measurement for one case from Guignouard *et al.*[25] (some interpolation of the measured impedance data was used to obtain the measured absorption coefficient):
────── porous absorbent only, predicted;
━━━━━ porous absorbent with perforated facing, predicted;
------- porous absorbent with perforated facing and air gap, predicted; and
○   porous absorbent with perforated sheet, measured.

6.5 Other constructions

Having described the most common designs, more complex constructions and recent innovations will now be discussed. Much can be gained from application of the simple resonator design as discussed previously, but more complicated systems do exist. In trying to decide whether to use more complex constructions, the trade off lies mainly between acoustic performance and cost of manufacture and installation. After all, a piece of porous material covered with a perforated sheet is relatively inexpensive to produce. Once more complex designs are considered, like large scale microperforation or complex neck plates, the cost of the device will naturally increase. Consequently, the designs discussed in the following sections are most often used where space is a particular premium, or where special requirements, such as transparency, need to be achieved.

6.5.1 Shaped holes and slots

Vigran[26] examined the effects of making conical rather than cylindrical holes for Helmholtz absorbers where the front plate is at least 1 cm thick. The conical holes are such that the smallest opening faces the source. In comparison to cylindrical holes, conical holes broaden the bandwidth of absorption, however the frequency of peak absorption increases somewhat. The conical holes also have high order absorption modes which are broader, resulting in increased absorption at mid-high frequencies. While it may be complex to form conical holes, similar devices can be made from shaped slots very easily.

6.5.2 Double resonators

The problem with resonant absorbers is that they have a relatively limited bandwidth. It is common to have to cover a greater frequency range than can be achieved by a single resonator alone. One possibility is to use a device that has multiple absorption mechanisms, such as the metal plate resonators described in Section 6.2.6. Another possibility is to stack a high frequency Helmholtz device in front of a low frequency device. The disadvantage of this is that the surfaces become very deep, and depth is often restricted by non-acoustic constraints. This double system can be most easily modelled as a transfer function matrix. Such a double design was a standard construction used by the British Broadcasting Corporation for many decades in their studios.

6.5.3 Microperforation

If the holes of a Helmholtz resonator are made small enough, then losses will occur due to viscous boundary layer effects in the perforations. To achieve this, the perforations must be sub-millimetre in diameter so that they are comparable to the boundary layer thickness. Then it is possible to achieve absorption without using a porous material. This becomes a useful technique because the perforated sheet and the back of the cavity can be made from transparent acrylic or glass and so forming a clear absorber. Commercial realizations of this were discussed in Section 6.2.4. From an academic viewpoint, this is a neat device, because the physics of the system is very simple and so accurate predictions are readily achieved. A microperforated device was reported by Cremer and Müller,[27] where a multi-layer system originally devised by Rschevkin

is briefly outlined. It is Maa, however, who appears to have carried out the significant recent development of the concept.[2]

Formulations for the impedance of microperforated devices can be derived by considering the sound propagation within a cylindrical hole. This problem is well established and is the theoretical foundation of much work on microscopic propagation in porous absorbents. In fact, the earliest work was probably done by Lord Rayleigh. For a tube which is short compared to wavelength, it can be shown that the specific acoustic impedance of the tube is given by:[2]

$$z_1 = j\omega \rho t \left(1 - \frac{2J_1\left(k'\sqrt{-j}\right)}{k'\sqrt{-j}J_0\left(k\sqrt{-j}\right)}\right)^{-1}$$

(6.36)

$$k' = a\sqrt{\frac{\rho\omega}{\eta}}$$

(6.37)

where J_0 and J_1 are the Bessel functions of the first kind, of zero and first order respectively; t is the tube length, and a is the tube radius.

To get the specific acoustic impedance of the perforated sheet, Equation 6.36 must be divided by the plate open area ε. Maa details approximate solutions to the above equation, but with the advent of modern numerical tools on computers, it is as easy to implement Equation 6.36 directly as to use an asymptotic solution. To model the Helmholtz resonator, a transfer matrix must be used to get the surface impedance, z_h:

$$z_h = \frac{z_1}{\varepsilon} - j\rho c \cot(kd) + \frac{\sqrt{2\omega\rho\eta}}{2\varepsilon} + \frac{j1.7\omega\rho a}{\varepsilon}$$

(6.38)

The second term is the impedance of the cavity which is assumed to be d deep and to be filled with air. The final term is the end correction to allow for the radiation reactance of the tube. The penultimate term is the radiation resistance for an orifice. Maa uses the formulation from Ingard[14] given in Equation 6.16 above for the radiation impedance. Once the impedance is known, the normal incidence absorption coefficient can be readily obtained. These equations are most applicable for common sound intensities. For large intensities, the impedance will change due to non-linear effects; flow also affects the impedance, and formulations are given in Reference 28.

Figure 6.25 compares the prediction according to Equation 6.38 to measurements presented by Maa.[2] The hole separation is 2.5 mm, the hole radius 0.1 mm, the plate thickness 0.2 mm and the cavity depth 6 cm. Reasonable agreement between measurement and prediction is achieved, although not as good as given in the paper. Script 6.3 in Appendix B gives the code for the predictions. The prediction shows a sharp peak due to a second order resonance. Such resonances are relatively narrow in frequency, and so if the results are summed in one-third octave bands, the second order peak appears less significant.

The problem with these systems is getting broadband absorption. As it relies on resonance, the absorption will be limited to a certain bandwidth. To extend the bandwidth, Maa and others have shown that multiple layers can be used. Each layer is then tuned to a different frequency range. This can then be solved by a transfer matrix solution taking each layer in turn. The problem with double layer devices is
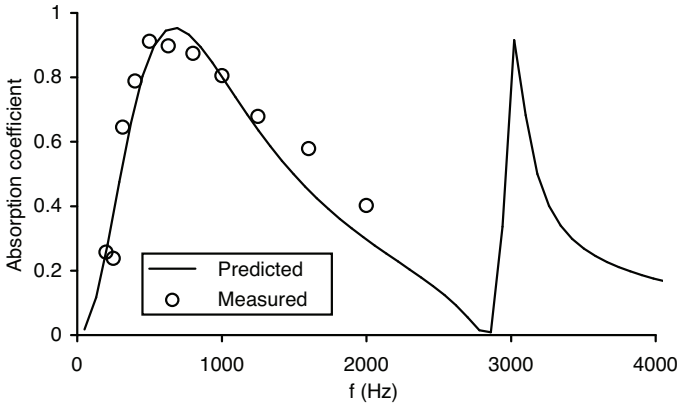
Figure 6.25 Predicted and measured absorption coefficient for a microperforated Helmholtz absorber (measurement data from Maa[2]).

they increase the depth and cost of the device, both of which are usually under strict restrictions by non-acousticians. Another solution to increasing the absorption at low frequency is to use a construction such as that shown in Figure 6.20, where porous absorbent is attached to the rigid backing.

For oblique incidence, the sound in the cavity travels at an angle to the normal, which is the angle of incidence. Consequently, Equation 6.38 should be altered to:

$$z_h = \left[\frac{z_1}{\varepsilon} - j\rho c \cot(kd) + \frac{\sqrt{2\omega\rho\eta}}{2\varepsilon} + \frac{j1.7\omega\rho a}{\varepsilon}\right]\cos(\psi) \qquad (6.39)$$

where ψ is the angle of incidence. The effect of this is to increase the resonant frequency, and so raise the frequency at which absorption is significant. For large angles of incidence, however, the lateral coupling between adjacent holes within the cavity will become significant. This might be expected to lower the absorption for most if not all frequencies. Consequently, in a diffuse field the absorption would be expected to be broader, but the maximum absorption would be lowered.

As discussed previously, it is possible to combine membrane and Helmholtz mechanisms in a single device. Kang and Fuchs[29] discussed the construction of such a device, which was a microperforated plastic membrane; the theory was also applied to glass fibre textiles. This treats the membrane and Helmholtz effects in parallel as discussed previously around Equation 6.19. Good agreement was found between impedance tube and reverberation chamber measurement, and the transfer matrix theory. An example result is shown in Figure 6.26, where random and normal incidence absorption coefficients are compared. The device had: a mass per unit area, $m = 0.14$ kgm^{-2}; thickness $t = 0.11$ mm; hole radius $a = 0.1$ mm; hole spacing $D = 2$ mm, and a cavity depth of $d = 10$ cm. As with the previous microperforated systems, the random incidence is less than the normal incidence absorption, and a shift in the frequency of maximum absorption is also seen.

If a microperforated material is used without a rigid backing, it can be used as a suspended absorber, attenuating sound incident from both sides. Figure 6.27
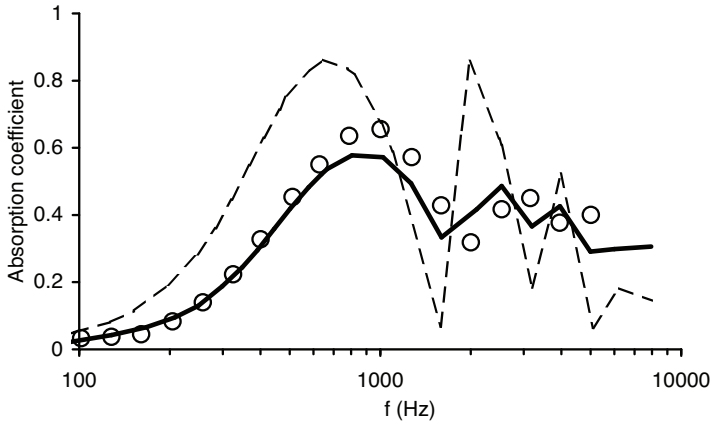
Figure 6.26   Measured and predicted absorption coefficient for a microperforated membrane for different incident sound conditions:
O   measured, random incidence;
───── predicted, random incidence; and
– – – predicted, normal incidence (after Kang and Fuchs[29]).

compares the attenuation generated by two microperforated materials with a rigid backing with that generated by a single and double layer device suspended in free space. (In the last two cases, the absorption is purely that which is dissipated in the device; the transmitted sound is not considered to be absorbed.) The single and double microperforated sheets suspended in free space provide low frequency absorption via the device's flow resistance only, and this is maximized when the flow resistance of the structure is $2\rho c$.[30] The additional low frequency absorption for the double layer
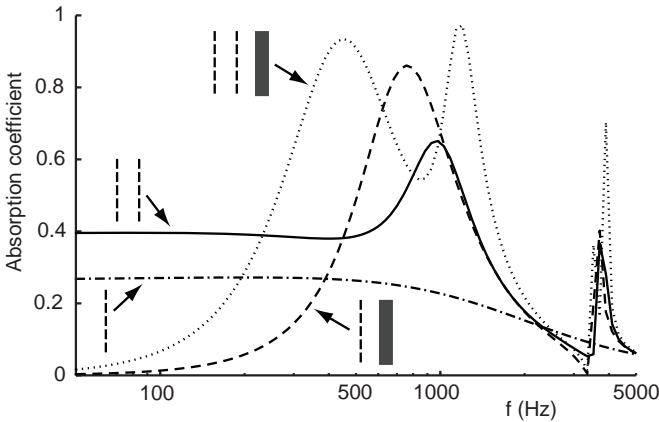
Figure 6.27   Predicted absorption coefficient for various microperforated devices:
·—·—·— single microperforated sheet in free space;
– – – single microperforated sheet in front of rigid backing;
··········· double microperforated sheet in front of rigid backing; and
───── double microperforated sheet in free space (figure concept from Sakagami *et al.*[30]).
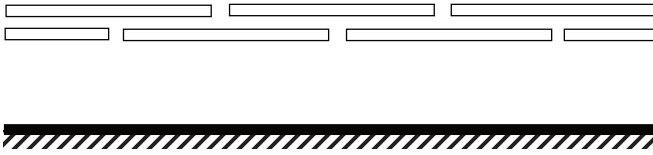
Figure 6.28 A Helmholtz absorber which uses lateral space between two perforated sheets as part of the neck of the device.

material suspended in free space is, however, at expense of some of the mid-frequency attenuation.

It is also possible to make microperforated devices using narrow slots instead of cylindrical holes.[31,32] This has advantages in making manufacture easier and allowing aesthetically pleasing etchings to be made. For an infinitely long slit of width w in a plate of thickness t the impedance can be written as:

$$z_h = \frac{j\rho_e \omega t}{\varepsilon} - j\rho c \cot(kd) - \frac{2j\rho\omega w}{\pi\varepsilon} \ln\left[\sin(\tfrac{1}{2}\pi\varepsilon)\right] \tag{6.40}$$

where ρ_e is the effective air density in the slit due to viscosity effects and is given by:

$$\rho_e = \frac{\rho}{1 - \dfrac{2}{k'w}\tan\left(\dfrac{k'w}{2}\right)} \tag{6.41}$$

where ρ is the density of air and $k' = \sqrt{-j\omega\rho/\eta}$

6.5.4 Lateral orifices

Another way to get clear absorption is to elongate the neck of the absorber laterally. Again the principle is to exploit viscous boundary layer losses in narrow openings and so remove the need for resistive material. Randeberg developed such a technique,[33] and Figure 6.28 shows the device. The front and rear plates are perforated with reasonably large perforations (1–3 mm in diameter); the viscous losses occur in the propagation parallel to and between the plates. Strict control of the plate spacing is required, which must be of the order of the boundary layer thickness, about 0.2 mm. This spacing must be achieved to a high precision, as the results by Randeberg demonstrate that a change in spacing of 0.05 mm makes significant difference to the absorption obtained. Predicting the absorption of the system is complicated and requires a finite difference solution of the Navier-Stokes Equation. A simple solution using a calculation of vibrating mass based on the volume of the openings and the elongated orifice does not work.

The device gives very similar performance to the microperforated systems discussed previously and as such offers a different construction rather than improved acoustic performance. The absorption is limited to low to mid-frequencies.

6.6 Summary

This chapter has outlined some design principles, typical applications and theoretical models for resonant absorbers. Resonant absorbers play a crucial role in improving acoustic conditions. They are exploited to control modes and reverberation within rooms and enclosures and for reducing sound levels in many noise control applications. The next chapter details some absorbers that did not fit neatly into other chapters, including seating and absorbers from Schroeder diffusers.

6.7 References

1 N. W. Larsen, E. R. Thomson and A. C. Gade, "Variable low-frequency absorber for multi-purpose concert halls", *Proc. Forum Acusticum*, 616 (2005).
2 D.-Y. Maa, "Microperforated-panel wideband absorbers", *Noise Control Engineering Journal*, **29**(3), 77–84 (1984).
3 J. Pfretzschner, P. Cobo, F. Simon, M. Cuesta and A. Fernandez, "Microperforated insertion units: An alternative strategy to design microperforated panels", *Appl. Acoust.*, **67**(1), 62–73 (2006).
4 J. Kang J and M. W. Brocklesby, "Feasibility of applying micro-perforated absorbers in acoustic window systems", *Appl. Acoust.*, **66**(6), 669–89 (2005).
5 F. Asdrubali and G. Pispola, "Properties of transparent sound-absorbing panels for use in noise barriers", *J. Acoust. Soc. Am.*, **121**(1), 214–21 (2007).
6 M. Q. Wu, "Micro-perforated panels for duct silencing", *Noise Control Engineering Journal*, **45**(2), 69–77 (1997).
7 H. V. Fuchs, "Alternative fibreless absorbers – new tools and materials for noise control and acoustic comfort", *Acustica*, **87**, 414–22 (2001).
8 H.V. Fuchs, X. Zha, X. Zhou and H. Drotleff, "Creating low-noise environments in communication rooms", *Appl. Acoust.*, **62**, 1375–96 (2001).
9 F. Liu, S. Horowitz, T. Nishida, L. Cattafesta and M. Sheplak, "A multiple degree of freedom electromechanical Helmholtz", *J. Acoust. Soc. Am.*, **122**(1), 291–301 (2007).
10 A. J. Fleming, D. Niederberger, S. O. R. Moheimani and M. Morari, "Control of resonant acoustic sound fields by electrical shunting of a loudspeaker", *IEEE Transactions on Control Systems Technology*, **15**(4), 689–703 (2007).
11 R. G. Oldfield and T. J. Cox, "Passive tuned loudspeakers as absorbers for room acoustics", *Proc. 19th ICA* RBA-16-008 (2007).
12 L. E. Kinsler, A. R. Frey, A. B. Coppens and J. V. Sanders, *Fundamentals of Acoustics*, 4th edn, John Wiley & Sons (2000).
13 A. W. Guess, "Result of impedance tube measurements on the acoustic resistance and reactance," *J. Sound Vib.*, **40**, 119–37 (1975).
14 U. Ingard, "On the theory and design of acoustic resonators", *J. Acoust. Soc. Am.*, **25**, 1037–61 (1953).
15 L. Cremer and H. A. Müller, *Principles and Applications of Room Acoustics*, Applied Science Publishers (translated by T. J. Schultz) (1978), p. 187.
16 W. A. Davern, "Perforated facings backed with porous materials as sound absorbers – an experimental study", *Appl. Acoust.*, **10**, 85–112 (1977).
17 U. R. Kristiansen and T. E. Vigran, "On the design of resonant absorbers using a slotted plate", *Appl. Acoust.*, **43**(1), 39–48 (1994).
18 J. M. H. Smits and C. W. Kosten, "Sound absorption by slit resonantors", *Acustica*, **1**, 114–122 (1951).
19 15, op. cit., 191.
20 R. D. Ford and M. A. McCormick, "Panel sound absorbers", *J. Sound Vib.*, **10**, 411–23 (1969).
21 F. P. Mechel, "Panel absorber", *J. Sound. Vib.*, **248**(10), 43–70 (2001).
22 W. H. Chen, F. C. Lee and D. M. Chiang, "On the acoustic absorption of porous materials with different surface shapes and perforated plates", *J. Sound Vib.*, **237**, 337–55 (2000).

23 I. Lee, A. Selamet, N. T. Huff, "Acoustic impedance of perforations in contact with fibrous material", *J. Acoust. Soc. Am.*, **119**(5), 2785–97 (2006).

24 J. F. Allard, *Propagation of Sound in Porous Media: Modelling Sound Absorbing Materials*, Elsevier Applied Science, Chapter 10 (1993).

25 P. Guignouard, M. Meisser, J. F. Allard, P. Rebillard and C. Depollier, "Prediction and measurement of the acoustical impedance and absorption coefficient at oblique incidence of porous layers with perforated facings", *Noise Control Engineering Journal*, **36**(3), 129–35 (1991).

26 T. E. Vigran, "Conical apertures in panels; sound transmission and enhanced absorption in resonator systems", *Acta Acustica uw Acustica*, **90**, 1170–7 (2004).

27 15, op. cit., 204–6.

28 L. L. Beranek and I. L. Vér (eds), *Noise and Vibration Control Engineering*, John Wiley & Sons (1992).

29 J. Kang and H. V. Fuchs, "Predicting the absorption of open weave textiles and micro-perforated membranes backed by an air space", *J. Sound Vib.*, **220**(5), 905–20 (1999).

30 K. Sakagami, M. Morimoto and W. Koike, "A numerical study of double-leaf microperforated panel absorbers", *Appl. Acoust.*, **67**, 609–19 (2006).

31 D. X. Mao and Z. M. Wang, "Theory and analogous design of microslitted-panel absorbers", *Journal of Tongji University* (in Chinese), **28**, 316–9 (2000).

32 T. E. Vigran, O. K. Ø. Pettersen, "The absorption of slotted panels revisited", *Proc. Forum Acusticum*, Budapest, Hungary, 2037–40 (2005).

33 R. T. Randeberg, "A Helmholtz resonator with a lateral elongated orifice", *Acustica*, **86**, 77–82 (2000).

7 Some other absorbers

This chapter deals with some absorbers that do not easily fit into categories, but are nevertheless important to airborne acoustics. The first subject is seating and audience absorption. In many auditoria, the seating and audience form the main absorption in the room, and consequently being able to correctly measure and predict the absorption coefficient of the audience area is very important. The second subject is how to make efficient absorbers from Schroeder diffusers. Researchers started by looking into why the absorption from Schroeder diffusers could be large, and ended up inventing a new style of absorber.

There has been considerable interest in sonic crystals that absorb sound. It could be argued that phase grating surfaces designed to absorb sound are sonic crystals, but the concern here is with volumetric devices analogous to photonic crystals which can produce high attenuations – but only over limited bandwidths.

Over the years, there has been some disagreement about the absorbing ability of trees and ground. The chapter ends by examining the mechanisms and ability of achieving noise control through natural materials.

7.1 Seating and audience

The reverberation time in performance spaces is often dominated by the absorption of the seating and audience; it is essential that these can be measured or predicted accurately for correct design. Section 3.4.1 discussed how the absorption of seating should be measured, and so this discussion concerns the actual values of absorption coefficients that are available in literature and what they mean.

Beranek[1] and Kosten[2] have both produced data for the average absorption coefficients of occupied and unoccupied seating. The data was averaged from measurements in many halls and is useful for estimating reverberation time in the early stages of design. The use of average data is not reliable for later design work, however, as there is too much variation in the construction for modern seating and consequently, seating absorption coefficients can vary greatly. Figure 7.1 shows the spread and mean of the absorption coefficients measured by Davies *et al.*[3] for nine seating types. Also shown are the average values from Beranek[1] which are in common use. Considering the range of the current data, the agreement between the means measured by Davies *et al.* and Beranek is quite good up to 1 kHz. At higher frequencies, as Bradley[4] explains, Beranek's absorption data is quite possibly affected by differences in air absorption between the many halls measured. Discrepancies may also arise because modern theatre seating has slightly more padding than the older ones forming the bulk of Beranek's data.
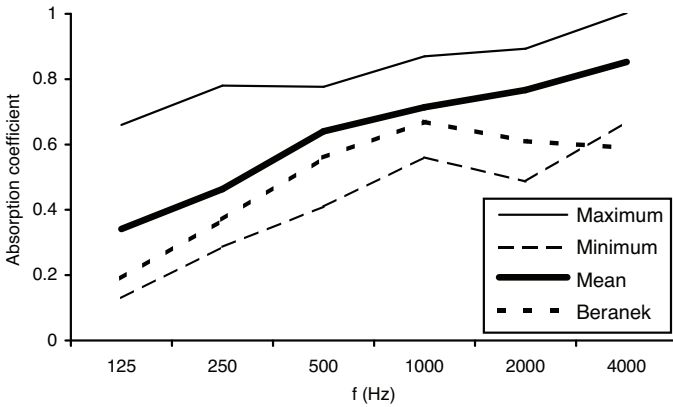
Figure 7.1   The minimum, maximum and mean absorption coefficients for audience seating from Davies *et al*.[3] Also shown are the mean values from Beranek.[1]

For occupied seating, measurements by different authors are much more similar.[5] It appears that the absorption of occupied upholstered seats is dominated by the absorption of the occupants and does not vary much over different seat types. Whether occupied or not, the absorption coefficients have the characteristic curve shape of a porous absorber.

Figure 7.2 shows the effect on the absorption coefficient of varying the row spacing over the small range commonly found in auditoria. Increasing the row spacing decreases the absorption coefficient. Figure 7.3 shows the effect of carpet on the absorption coefficient. The addition of carpet, even below the seating, significantly increases the absorption and so is generally avoided in large concert venues.

Figure 7.4 compares occupied and unoccupied absorption coefficients. Although it is normal practice to try and make the absorption of seating the same whether occupied or not, this is not entirely successful. On a related issue, Hidaka *et al*.[6] have suggested that draping the seats with felt can simulate occupied conditions. This appears to be
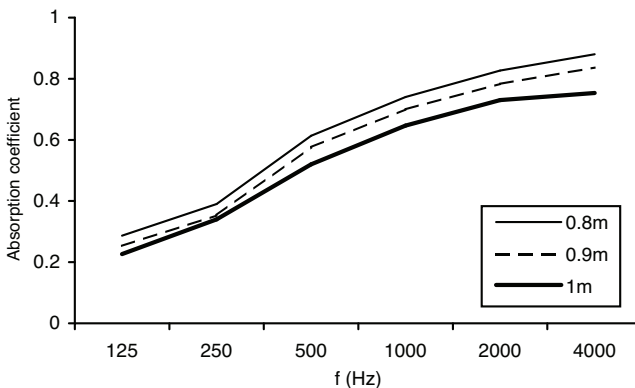
Figure 7.2   Effect of row spacing on the absorption coefficient for a large block of seating (after Davies[5]).
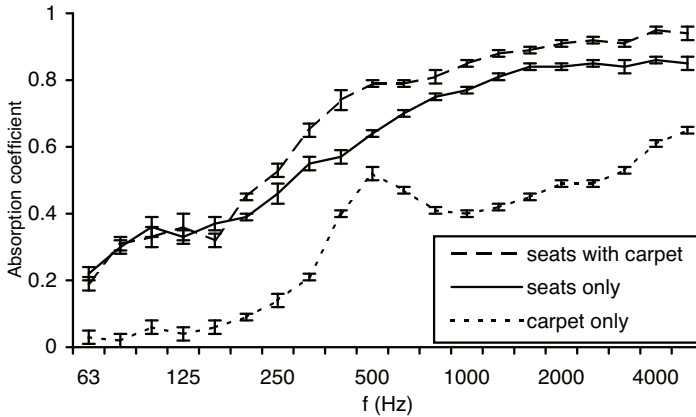
Figure 7.3   The absorption coefficient for seating with and without carpet (data from Davies[5]).

successful at mid-frequencies, but at low frequencies (100–200 Hz) it does not always work because the felt alters the seat dip effect.[7,8]

7.2 Absorbers from Schroeder diffusers

Numerous pictures and sketches of Schroeder diffusers can be found in Chapter 9, for example Figure 9.1. The Schroeder diffuser was designed to diffuse rather than absorb sound, although for sometime there has been anecdotal evidence of absorption. Now, some concerted scientific studies have been able to determine the source of the absorption, and even to show how to turn these diffusers into good absorbers. By changes in geometry and design, it is possible to change a Schroeder surface from a diffuser with low absorption to a highly absorbing surface. This is of great concern for diffuser installation, as it is very easy to accidentally make a highly absorbing surface through bad workmanship. Section 9.8 discusses some general principles to achieve
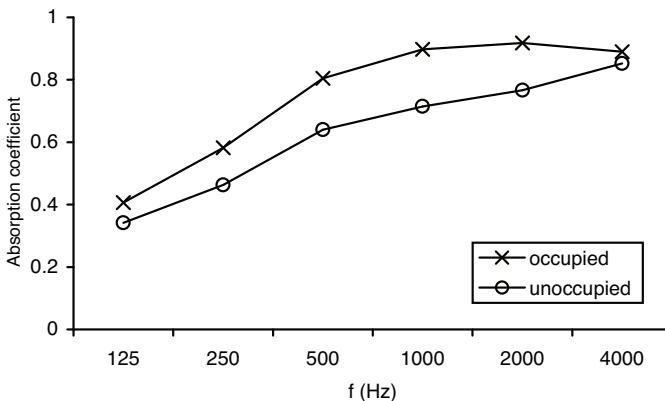
Figure 7.4   Absorption coefficients for occupied and average unoccupied seating (data adapted from Davies *et al.*[3]).

low absorption from Schroeder diffusers. What is discussed below is the mechanism of the absorption, and how this can be exploited to form a good absorber.

When Marshall and Hyde[9] implemented their revolutionary use of Schroeder diffusers in the Michael Fowler Centre (see Figure 2.23), they used rather shallow and wide wells. This was born out of a desire to achieve moderate diffusion, but also because of a concern that the diffusers could cause excess absorption. Dramatic levels of absorption from Schroeder diffusers were measured by Fujiwara and Miyajima[10] in 1992, with the absorption coefficient ranging from 0.3 to 1, and at the time this absorption could not be explained. Fujiwara and Miyajima[11] later reported that the quality of construction was to blame for some of the excess absorption; to achieve low absorption requires good workmanship. Commins *et al.*[12] experimentally investigated the absorption characteristics of a Schroeder diffuser and found values peaking at 0.5. They showed that by sloping the bottom of the diffuser wells, the absorption could be reduced. In 1983, D'Antonio made the first absorption measurements of a commercial QRD® with seven 86.4 mm wide wells, with a maximum depth of 196.9 mm. The average absorption coefficient was 0.24 between 125 and 4,000 Hz, with a maximum value of 0.35 at 500 Hz.

Although workmanship can explain the excess absorption in many cases, even diffusers constructed to a high standard can have absorption coefficients higher than expected. Resonant absorption occurs due to the one-quarter wave resonances in the wells, but the absorption measured is too high to be explained by one-quarter wave resonance alone. It was Kuttruff[13] who first postulated energy flow between the wells as a probable cause for the excess absorption, although his theoretical model could not predict the high absorption measured by others. Mechel[14] thoroughly discussed the theoretical basis for the absorption effect, and although his studies lacked direct experimental verification, the prediction model developed was shown by others to be accurate. Wu *et al.*[15] then brought together measurement and Mechel's prediction model to provide evidence that the energy flow or strong coupling between the wells was indeed responsible for the high absorption. This mechanism is described in the following section.

7.2.1 Energy flow mechanism

Consider a pure tone wave incident onto a Schroeder diffuser. For simplicity consider just two neighbouring wells. Furthermore, consider this to be a frequency where one well is in resonance, and the neighbouring well is not, as illustrated in Figure 7.5. The energy at the mouth of the resonating well will be much greater than that of the non-resonating well. This means that there will be energy flow from the resonating well to the well that is not resonating. Consequently, around the entrances to the wells there is high particle velocity. Indeed, Fujiwara *et al.*[16] showed that the particle
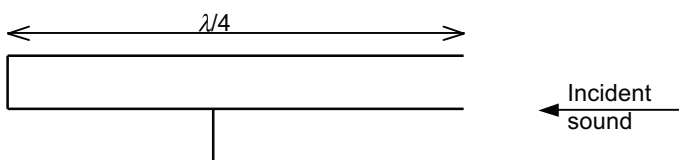
Figure 7.5 Two wells of a Schroeder diffuser.
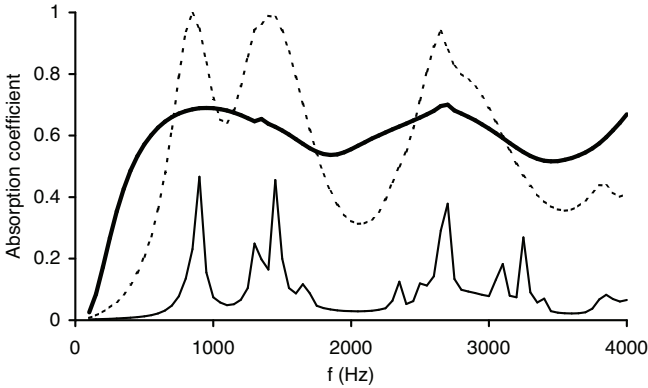
Figure 7.6 Normal incidence absorption coefficient for a quadratic residue diffuser with narrow wells, showing dependence on whether there is a covering at well entrance and what the flow resistance of the covering is:
—— no covering;
------ covering of 65 rayls; and
—— covering of 550 rayls.

velocity is up to 14 times greater at the mouth of the wells compared to the incident field. As sound moves around the front of the fins, from one well to the next, excess absorption occurs. This is the source of the additional absorption in Schroeder diffusers and occurs even in properly constructed structures.

Knowing that the front face of the diffuser is a region of high particle velocity, it makes sense to place resistive material at the well entrance if the desire is to make an absorber. Mechel[14] demonstrated that a resistive layer at the well entrances turns these
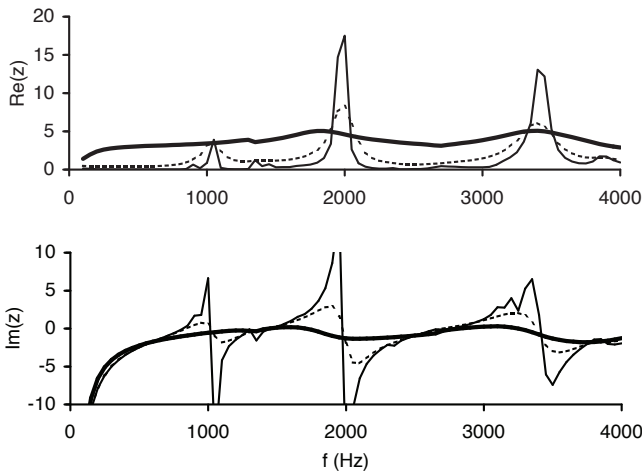
Figure 7.7 Normal incidence surface impedance for a quadratic residue diffuser with narrow wells showing dependence on whether there is a covering at well entrance and what the flow resistance of the covering is:
—— no covering;
------ covering of 65 rayls; and
—— covering of 550 rayls.

diffusers into potentially useful absorbers. Figures 7.6 and 7.7 show the absorption coefficient and surface impedance for a profiled structure with and without a resistive layer. Two different resistive layers of different flow resistance are illustrated. The effect of the resistive layer is to broaden the resonant peaks, thereby generating absorption over a greater bandwidth. It also increases the impedance closer to the characteristic impedance for air, and thereby gains more absorption. The resistive layer can be made from wire mesh, cloth or any material with an appropriate acoustic resistance. The advantage of using wire mesh is that the absorber is then washable and durable, which can be useful in some applications.

The resistance of the covering must be such that the total resistance of the wells are close to the characteristic impedance. Too large a resistance leads to an overly damped system and the peaks of absorption are significantly lowered. This is illustrated in Figures 7.6 and 7.7. Too little resistance (no covering) leads to an uneven performance; too much resistance (550 rayls) leads to over damping, whereas 65 rayls gives the highest peak absorption.

7.2.2 Boundary layer absorption

When the wells of a Schroeder surface become narrow, the losses at the well walls due to viscous boundary layer effects can become significant. This can be exploited to produce greater absorption, but the role of the resistive layer must be considered. The key to obtaining a high absorption is that the combination of the covering material and the losses at the well walls should approach the characteristic impedance of air. If the wells are wide, a higher resistance will be needed from the covering material to compensate for the lack of boundary layer absorption. Similarly, if the walls of the wells are rough, then there will be more boundary layer absorption than with a smooth material, and this must be allowed for in the design.

7.2.3 Absorption or diffusion

It is possible to construct Schroeder surfaces to maximize the absorption or maximize the diffusion. Although the surface used to produce high absorption has the same ancestry as those used to disperse sound, crucial design differences result in radically different absorption properties. The two different design remits are contrasted below in Table 7.1.

As indicated in Table 7.1, measurements show that 2D surfaces usually absorb more than 1D surfaces, as shown in Figure 9.37. The reason for this is probably twofold:

1. There are often a greater number of well depths in a 2D surface compared to a 1D surface. This means that there are more quarter wave resonances in the 2D surface, leading to more frequencies at which resonance is occurring. This in turn means that the absorption due to quarter wave resonance is significant for more frequencies, and the energy flow between the wells is also greater, leading to more losses.
2. There is a greater surface area of well boundaries in the 2D surface compared to the 1D surface. It is at these boundaries that viscous boundary layer losses occur. Consequently, it is expected that the greater the boundary area, the greater the absorption (unless a high flow resistivity covering is used).

Some of the other features summarized in Table 7.1 are discussed in the following sections.

Table 7.1 Construction differences between Schroeder diffusers and absorbers

	Absorber	*Diffuser with little absorption*
Well width	Usually narrow to exploit viscous boundary layer losses.	Usually>2.5 cm to minimize boundary layer losses.
Covering	Key to good absorption. Covering should be chosen so surface resistance is $\approx \rho_0 c$ when added to well resistance to maximize absorption.	Should not be covered. If covering unavoidable, use low flow resistivity material away from well entrances.
1D vs 2D	2D surface often gives more absorption.	2D surface gives hemispherical dispersion, 1D surface diffuses in a single plane.
Number of different depth wells, N	Determined by the need to have a sufficient number of quarter wave resonances in absorption bandwidth.	A larger N usually makes a better diffuser.
Depth sequence	Well depths should be chosen to evenly distribute well resonances across absorption bandwidth, best done using numerical optimization.	Chosen to maximize dispersion, best done using numerical optimization. Narrow period widths should be avoided.
Deepest well depth	Determines low frequency limit of absorption.	Determines low frequency limit of diffusion, except when period width is small.
Construction	Well sealed, no slits.	Well sealed, no slits.
Mass elements (addition of perforated sheets or membranes)	Can be used to lower bandwidth of absorption.	Can be used to lower bandwidth of diffusion.
Well sides	Can be rough.	Should be smooth.

7.2.4 Depth sequence

An optimum depth sequence for diffuse reflections does not necessarily produce the best absorption. It is possible to produce a set of depths that produces a better absorber than one based on the quadratic residue sequence (see Chapter 9 for definitions of different number sequences). This is done by using a set of well depths which produce more resonance frequencies, distributed more evenly in frequency, and optimally arranging to maximize energy flow between the wells. Mechel[14] was the first to suggest this; he discussed how using a primitive root sequence to determine the well depths of the structure could result in a better absorber than the more common quadratic residue sequence. This is because the primitive root sequence generates more different well depths than a quadratic residue sequence. The simple procedure outlined below to determine well depths works even better, however, as the primitive root sequence does not evenly space resonant modes in frequency. Another possibility is to use a numerical optimization to find the best well depth sequence. This can follow the principles outlined

in Chapters 9 and 10 for diffuse reflection optimization. The optimization can be tasked with maximizing the average absorption coefficient across the bandwidth of interest. As with diffuse reflection optimization, this is a slow and moderately complex procedure.

A simple procedure to determine the well depths is based on determining the resonant frequencies of the wells. To a first approximation, neglecting viscous boundary layer losses in the well, each well is a quarter wave resonator with resonant frequencies f given by:

$$f = \frac{(2m-1)c}{4d_n} \; ; \; m = 1,2,3.... \tag{7.1}$$

where d_n is the depth of the nth well, and c is the speed of sound.

To maximize the absorption it is necessary to evenly space these resonant frequencies over the design bandwidth avoiding degenerate modes – modes with similar resonant frequencies. This can be simply achieved by a trial and error process using a calculation tool such as a spreadsheet. Once the depths are determined, it is necessary to order them to maximize the losses due to energy flow between the wells. To achieve this, wells causing adjacent in-frequency resonances should not be physically next to each other. This can be done quickly by hand.

Figure 7.8 compares the performance of an absorber made following this simple design method to that of an absorber produced using a numerical optimization.[15] The performance of the absorber using the simpler design procedure is good. As might be expected, the optimization gives slightly better results, but that design involves considerably more computation and encoding effort. The resonant frequencies used during the simple design are also marked as vertical dashed lines. The drop at high frequencies >2.5 kHz occurs due to lack of resonances in the region above 3 kHz (beyond the frequency range shown in the figure). To illustrate that the ordering of
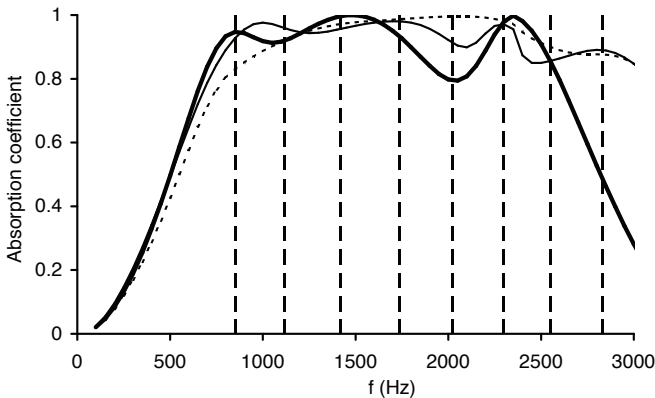
Figure 7.8 Absorption coefficient for profiled absorbers using different methods to determine the depth sequence:
  ------- simple design method;
  ——— designed using numerical optimization; and
  ——— simple design method, ascending well order.
Vertical lines indicate resonant frequencies for simple design method (data from Wu *et al.*[15]).

the wells is important, Figure 7.8 also shows the results when the absorber is designed using the simple design method, but has the wells stacked in ascending order. There is considerably less absorption at some frequencies.

7.2.5 Use of mass elements

High absorption at low frequencies is the most difficult to achieve. Consequently, an important challenge is to get more absorption at lower frequencies from a given profiled absorber depth. Interestingly, in a paper by Fujiwara and Miyajima,[11] it was reported that poorly constructed structures could provide high absorption below the lowest resonant frequency. It is speculated that this additional absorption came from cracks in the well bottoms forming Helmholtz resonators with air cavities behind. This inspired the idea that using perforated plates in some wells could significantly extend the absorption range towards the lower frequencies by adding mass to the system and so lowering the resonant frequency. Another possibility would be to use membranes to act as limp mass elements. A typical construction is shown in Figure 7.9.

Fujiwara *et al.*[16] were the first to publish measurement results on a structure with Helmholtz resonators in the wells, adding mass and so getting better absorption at low frequencies. Wu *et al.*[17] took this work further by producing a prediction model validated against measurement and some basic design methodologies. The simple concept of spacing resonant frequencies, as discussed in Section 7.2.4, can be used again, although predicting the resonant frequencies is more awkward with mass elements. In addition, multiple resonances from each of the wells need to be considered.

Wu *et al.*[17] found that wells with perforations and variable depth wells without perforations are needed to get a wide enough range of resonant frequencies. Both well types are shown in Figure 7.9. The added mass within the perforations makes it difficult to keep the reactance of the impedance small at high frequencies and so too many wells with perforations make it difficult to achieve high frequency absorption. The holes of the perforations must be carefully chosen. If they offer significant resistance, it may be necessary to lower the resistance of the resistive material to achieve good absorption.
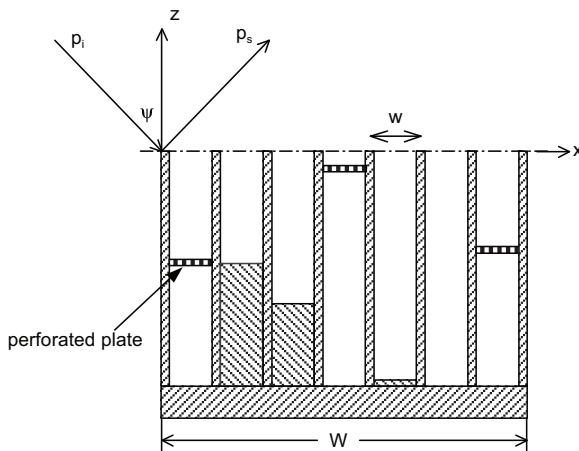
Figure 7.9 One period of a profiled sound absorber with perforated plates (adapted from Wu *et al.*[15]).
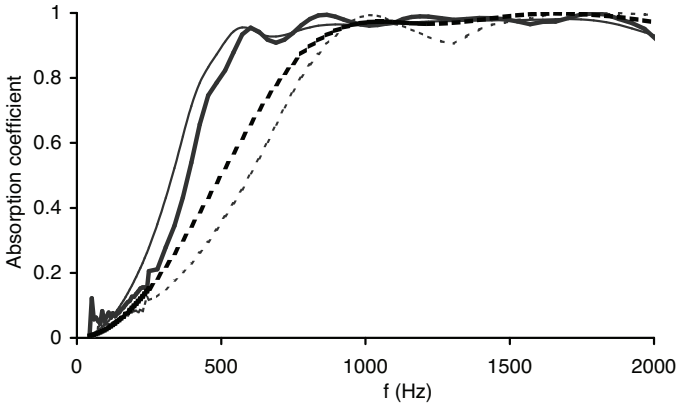
Figure 7.10 Measured and predicted absorption coefficient for two different profiled structures:
——— with perforated sheets, predicted;
⸺ with perforated sheets, measured;
······· no perforated sheets, predicted; and
– – – no perforated sheets, measured (after Wu *et al.*[17]).

These devices can produce greater absorption than a set of standard Helmholtz resonators stacked next to each other, because of the multiple resonances within some of the wells, but they are more expensive to construct.

Figure 7.10 shows a typical result for two optimized designs, one with perforated sheets, one without. Measurements from the impedance tube and predictions are shown. This demonstrates that adding mass elements can extend the low frequency performance of these devices.

7.2.6 *Number of wells*

For a narrow bandwidth only a few different well depths are needed. Reducing the number of wells would be useful as it simplifies the design and so reduces manufacturing costs. Wu *et al.*[17] designed a diffuser to work up to 3 kHz that only needed three different well depths. With this small number of wells, however, the density of resonances is insignificant above 3 kHz, and so the absorption decreases at higher frequencies. Incidentally, the choice of the correct value of the flow resistance for the resistive layer is even more important for absorbers with only a few wells.

7.2.7 *Theoretical model*

Having considered the mechanisms behind the absorption of the Schroeder diffusers qualitatively, a theoretical model for the absorber will now be presented. Boundary element methods could be used, but it is also possible to construct a theoretical model using a Fourier decomposition of the infinite periodic surface. This later model could also be used for profiled diffuser scattering. It is applicable to periodic structures and is almost as accurate as a boundary element model, but requires considerably less computation time. Both theoretical approaches divide into two parts: first the

admittance of the individual wells must be calculated and then the absorption should be calculated from these well admittances.

7.2.7.1 Admittance of wells

The approach follows similar lines to the transfer matrix approaches used for porous and resonant absorbers in Chapters 5 and 6 and also described in Chapter 1. Consequently, the following is given in brief, and readers are referred to other chapters for more details. The admittance (or impedance) is needed at the entrance of the wells. The well width of a profiled absorber is often narrow compared with diffusers to provide more absorption; therefore the energy losses caused by viscous and thermal conduction in the wells cannot always be neglected. Consider the case where the well width $w << \lambda/2$, where λ is the wavelength of the sound, so that only fundamental modes are considered to propagate in each well. The wavenumber in the wells, k_t, is:[18]

$$k_t \approx k + \frac{k}{2w}(1-j)[d_v + (\gamma-1)d_h] \tag{7.2}$$

where k is the wavenumber in air; γ the ratio of the specific heat $\approx 7/5$ for air; and d_v, d_h are the thickness of the viscous and thermal boundary layers respectively.

The thickness of the viscous and thermal boundary layers can be found from:

$$d_v = \sqrt{\frac{2\eta}{\rho\omega}} \approx \frac{0.0021}{\sqrt{f}} \tag{7.3}$$

where η is the coefficient of viscosity for air; ω the angular frequency; ρ the density of air; and f the frequency.

$$d_h = \sqrt{\frac{2K}{\rho\omega c_p}} \approx \frac{0.0025}{\sqrt{f}} \tag{7.4}$$

where K is the thermal conductivity and c_p is the heat capacity per unit mass of air at constant pressure.

For a slit with no perforated sheet present of depth l_n, the impedance at the top of the well is given by:

$$z_1 = r_m - \rho_e c \frac{k}{k_t} \cot(k_t l_n) \tag{7.5}$$

where r_m is the resistance of the covering material and ρ_e is the effective density of air in the slit.[19] The effective density can be calculated using:

$$\rho_e = \rho[1 + (1-j)d_v / w] \tag{7.6}$$

For a slit with a perforated sheet a distance d_n from the well bottom, the impedance at the top of the perforated plate is given by:

$$z_p = r_p + j(\omega m_p - \rho_e c \frac{k}{k_t} \cot(k_t d_n)) \tag{7.7}$$

where r_p and m_p are the added resistance and mass due to the perforated sheet. These can be calculated from Equations 6.6 and 6.15 or 6.16. The impedance at the top of the well is:

$$z_1 = \frac{-j\rho c z_p \cot(k_t l_n) + (\rho c)^2}{z_p - j\rho c \cot(k_t l_n)} + r_m \tag{7.8}$$

where l_n is the distance from the perforated plate to the top of the well.

7.2.7.2 *From well impedance to absorption: BEM*

Once the well impedances are known, a method for gaining the absorption coefficient is needed. One possibility is to apply one of the boundary element methods described in Chapter 8. The absorber is treated as a box with an impedance distribution on the front face. A source is placed in the far field and irradiates the absorber. An array of receivers on a sphere measures the far field scattered energy which is integrated to give the sound power reflected, P_a. A box with an infinite impedance on the front face of the same dimensions is placed in the same set up. The sound power reflected is calculated and in this case gives the incident power P_i. From these two powers, the absorption coefficient of the surface can be calculated:

$$\alpha = 1 - \frac{P_a}{P_i} \tag{7.9}$$
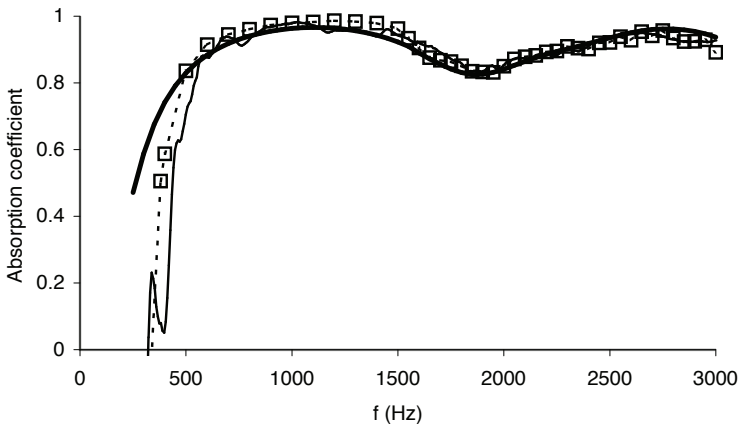
Figure 7.11   Measurement and prediction of absorption for a periodic profiled absorber:
──── multi-microphone measurement;
━━━━ infinite sample prediction; and
– ☐ – boundary element method (BEM) prediction (adapted from Wu *et al.*[20]).

Figure 7.11 compares a prediction of the absorption using a boundary element model compared to a multi-microphone free field measurement.[20] Reasonable agreement is achieved. The low frequency discrepancies are as likely to be due to measurement inaccuracies as the BEM model. The BEM is rather laborious, and consequently a different method can be used exploiting periodicity; this is detailed in the next section.

7.2.7.3 From well impedance to absorption: wave decomposition

As the surface is periodic it is possible to decompose the scattered wave according to the periodicity of the surface. This greatly reduces the computation burden compared to a BEM model. There is an assumption that the surface is infinitely wide, and consequently the prediction accuracy may be compromised at low frequencies for finite samples. The analysis below closely follows the method used by Mechel[14] and Wu *et al.*[15] The sound field in front of the absorber, shown in Figure 7.9, is decomposed into the incident plane wave $p_i(x,z)$ and scattered field $p_s(x,z)$, which is made up of propagating and non-propagating evanescent waves:

$$p(x,z) = p_i(x,z) + p_s(x,z) \tag{7.10}$$

$$p_i(x,z) = P_i e^{j(-xk_x + zk_z)}$$

$$p_s(x,z) = \sum A_n e^{j(-x\beta_n - z\gamma_n)}$$

where $W = Nw$ is the width of one period.

To use the above set of equations, the coefficients A_n need to be obtained for the non-evanescent (propagating) waves. These coefficients represent the magnitude of the grating lobes, and consequently one coefficient needs to be obtained for every grating lobe. The number of grating lobes is usually rather small and so this solution will be much faster than a BEM, where hundreds or thousands of simultaneous equations are common. The corresponding radiating harmonics indices n, which can propagate to the far field, must satisfy the following relationship:

$$(\sin(\psi) + n\frac{\lambda}{W})^2 \leq 1 \tag{7.11}$$

The outward particle velocity along the positive z direction and the pressure can be related to the surface impedance as discussed in Section 1.4.1 and 1.4.2. For this theory it is more convenient to work with admittance. The relationship between particle velocity u_z and pressure p is thus:

$$\rho c u_z(x,0) = -\beta(x)p(x,0) \tag{7.12}$$

where β is the surface admittance, which can be calculated from the well impedance using the transfer matrix approach outlined in Section 7.2.7.1. The relations in Equation 7.10 are differentiated to give the particle velocity and these are then related to the pressure relations in Equation 7.10 using the admittance relationship in Equation 7.12. This is imposing the boundary condition of the surface admittance onto the system of equations. This gives:

$$\cos(\psi)p_i - \sum_{n=-\infty}^{\infty} \frac{\gamma_n}{k} A_n e^{-j2\pi x n/W} = \beta(x) \left[p_i + \sum_{n=-\infty}^{\infty} A_n e^{-j2\pi x n/W} \right] \quad (7.13)$$

As the absorber is periodic, then the surface admittance is also periodic. This enables the surface admittance to be represented by a Fourier analysis. Since the period is W, this gives the admittance as:

$$\beta(x) = \sum_{n=-\infty}^{\infty} B_n e^{-j2\pi x n/W} \quad (7.14)$$

$$B_n = \frac{1}{W} \int_0^W \beta(x) e^{j2\pi nx/W} dx \quad (7.15)$$

Equations 7.13–7.15 are combined to impose the periodicity of the boundary conditions. After multiplication by $e^{j2\pi mx/W}$ and integration over W this gives:

$$\sum_{n=-\infty}^{\infty} A_n \left[B_{m-n} + \delta_{m,n} \left(\frac{\gamma_n}{k} \right) \right] = P_i \left(\delta_{m,0} \cos(\psi) - B_m \right) ; \quad m = -\infty,....,+\infty \quad (7.16)$$

$$\delta_{m,n} = \begin{cases} 1 & m = n \\ 0 & m \neq n \end{cases} \quad (7.17)$$

The infinite sum in m can be terminated by monitoring convergence as more terms are added into the sum. On the samples tested so far, the index limits may be taken as $|m| \leq 2N$, where N is the number of wells in one period.

Equation 7.16 gives a set of simultaneous equations relating the coefficients of the non-evanescent waves A_n to the surface admittance and other known factors of geometry, such as incident angle. These simultaneous equations can be solved using standard solution techniques to get the unknown coefficients.

By considering the energy in the scattered and incident waves shown in Equation 7.10 it is possible to derive an equation for the absorption coefficient. This is given by:

$$\alpha = 1 - \left| \frac{A_0}{P_i} \right|^2 - \frac{1}{\cos(\psi)} \sum \left| \frac{A_n}{P_i} \right|^2 \sqrt{1 - (\sin(\psi) + n\lambda/W)^2} \quad (7.18)$$

where the summation runs over radiating spatial harmonics only. The middle term is the specularly reflected energy, and the rightmost term the scattered energy. For a small period width W the specular reflection is the only non-evanescent reflection. In this case a normalized impedance on the surface of the structure, z_n, can be derived from:

$$z_n = \frac{1 + A_0/P_i}{1 - A_0/P_i} \quad (7.19)$$

Figure 7.11 compares predictions from this Fourier model with the BEM modelling described in the previous section. Free field measurements are also shown. Good agreement is obtained between the prediction models and measurements. Some discrepancies at low frequencies occur between the Fourier and BEM models; this is probably because the Fourier model assumes an infinite sample and the BEM model does not.

Figure 7.10 compared the Fourier theory and impedance tube measurements for two different samples. Again good accuracy is obtained. One of the keys to getting good comparisons between theory and measurement is to get good quality samples. Even apparently small imperfections in the samples can lead to large measurement errors.

This Fourier model can also be applied to periodic diffusers designed for scattering rather than absorption. Although this approach has not been verified, it is assumed that the predictions would be accurate. The advantage in using this method over a BEM model is the reduction in computation time and storage requirements.

7.3 Absorbing sonic crystals

When a wave passes through a periodic structure interesting effects happen. For instance when X-rays pass through a crystal, scattered energy is concentrated into particular directions to form grating lobes. The diffraction directions depend on the wavelength and the lattice spacings in the unit cell. In optics we have a similar phenomenon in what are called photonic crystals. In these periodic nanostructures of regularly repeating internal regions of high and low dielectric constant, photons propagate through the structure or not, depending on their wavelength. Wavelengths that pass through are known as modes and disallowed bands of wavelengths are called photonic band gaps. The acoustic equivalent is a phononic crystal, which is a material which exhibits stop bands for phonons, preventing phonons of selected ranges of frequencies from being transmitted through the material. A key factor for acoustic band-gap engineering is impedance mismatch between periodic elements comprising the crystal and the surrounding medium. If sound is incident on a set of periodically arranged cylinders, as shown in Figure 7.12, then there will be certain frequencies which will not pass

receiver

source

a
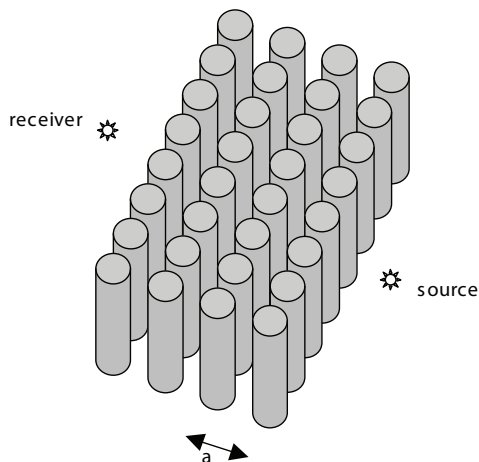
Figure 7.12   A 2D sonic crystal.
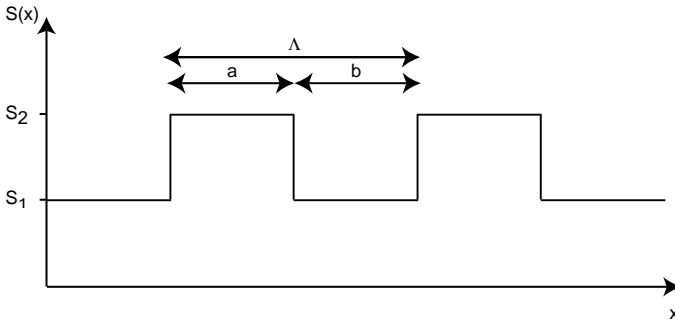
Figure 7.13 A 1D sonic crystal waveguide.

through the structure. Consequently, these sonic crystals offer the chance of reducing the transmission and/or absorbing particular frequencies. As described, such a structure is also known as a phononic crystal, because it is analogous to a photonic crystal.

To demonstrate why gaps appear, an analysis on a periodic waveguide will be used, which is a 1D sonic crystal. This is done because it simplifies the explanation, and the findings can be qualitatively generalized to 2D and 3D structures.

At low frequency, the crystal in Figure 7.12 has a periodic disturbance of the impedance, because sound cannot enter the cylinders. An analogous 1D structure would be a corrugated tube, as shown in Figure 7.13. This structure is best analyzed through a transfer matrix approach. A volume velocity rather than a particle velocity is used in the formulations to account for the change in cross-sectional area of the tube. The pressure p_n and volume velocity V_n in the nth unit cell can be related to the pressure p_{n+1} and volume velocity V_{n+1} in the $(n + 1)^{th}$ cell via an adapted form of Equation 1.29:

$$\begin{Bmatrix} p_n \\ V_n \end{Bmatrix} = \mathbf{P} \begin{Bmatrix} p_{n+1} \\ V_{n+1} \end{Bmatrix} = \begin{Bmatrix} P_{11} & P_{12} \\ P_{21} & P_{22} \end{Bmatrix} \begin{Bmatrix} p_{n+1} \\ V_{n+1} \end{Bmatrix} \tag{7.20}$$

where:

$$P_{11} = \cos(ka)\cos(kb) - \frac{S_1}{S_2}\sin(ka)\sin(kb) \tag{7.21}$$

$$P_{12} = j\rho_0 c \left(\frac{1}{S_1}\cos(ka)\sin(kb) + \frac{1}{S_2}\sin(ka)\cos(kb) \right)$$

$$P_{21} = \frac{j}{\rho_0 c}\left(S_2\sin(ka)\cos(kb) + S_1\cos(ka)\sin(kb) \right)$$

$$P_{22} = \cos(ka)\cos(kb) - \frac{S_2}{S_1}\sin(ka)\sin(kb)$$

where $b = \Lambda - a$ and the distances a and Λ and areas S_1 and S_2 were defined in Figure 7.13.

As the structure is periodic, then the pressure (and volume velocity) must be a periodic disturbance with the same periodicity of the structure:[21]

$$p(x) = e^{\pm jK\Lambda} f(x) \tag{7.22}$$

where $f(x)$ is the Bloch function, which has a periodicity arising from the lattice, i.e. $f(x + \Lambda) = f(x)$ and K is the Bloch wavevector. If the structure is considered to be infinitely long, both the right and left propagating waves must be Bloch waves. The pressure and volume velocities between two periods can be stated as:

$$\begin{Bmatrix} P_n \\ V_n \end{Bmatrix} = e^{\pm jK\Lambda} \begin{Bmatrix} P_{n+1} \\ V_{n+1} \end{Bmatrix} \tag{7.23}$$

Comparing Equations 7.20 and 7.23 shows that $e^{\pm \varphi K\Lambda}$ are the eigenvalues of **P**. The determinant of **P** is 1, and therefore the eigenvalue solutions of **P** are:

$$e^{\pm jK\Lambda} = \tfrac{1}{2}\left(P_{11} + P_{22}\right) \pm \sqrt{\tfrac{1}{2}\left(P_{11} + P_{22}\right) - 1} \tag{7.24}$$

Adding the two Bloch wave solutions and rearranging yields the Bloch wavevector:

$$K = \frac{1}{\Lambda}\cos^{-1}\left(\tfrac{1}{2}\left(P_{11} + P_{22}\right)\right) \tag{7.25}$$

Consequently, if $\tfrac{1}{2}(P_{11} + P_{22}) \leq 1$ then waves can propagate through the structure. But if $\tfrac{1}{2}(P_{11} + P_{22}) > 1$ then K is complex and the Bloch waves are evanescent, and band gaps arise. Figure 7.14 shows the measured and predicted transmitted intensity through a corrugated waveguide. In the case shown, $a = b$ and $2s_1 \approx s_2$. Using these
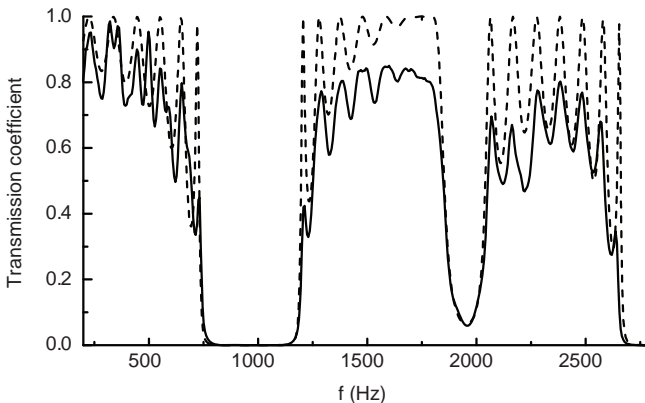
Figure 7.14   The transmission coefficient for 8 periods of a 1D sonic crystal with $a = b = 9.6$ cm formed in a waveguide with areas of $s_1 = 0.054^2$ m^2 and $s_2 = 0.038^2$ m^2:
———— measurement; and
– – – prediction (data from King and Cox[22]).
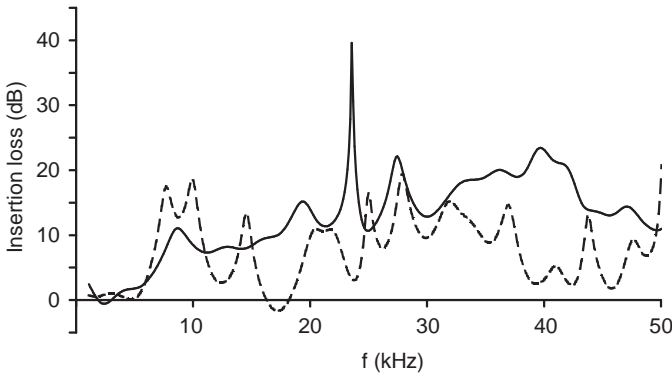
Figure 7.15 Insertion loss for two model-scale sonic crystals made from:
  – – – rigid cylinders; and
  ——— cylinders covered with felt (data from Umnova *et al.*[23]).

values in Equations 7.21 and 7.25 yields $\frac{1}{2}(P_{11} + P_{22}) = 1 - 9\sin^2(ka)/4$. So waves are not propagated when the frequency, f, is $775 \le f \le 1{,}200$ Hz and $2{,}750 \le f \le 3{,}180$ Hz.

Close inspection of the figure shows that the band gaps measured are slightly lower than these predicted limits and furthermore, there is an additional dip at around 2 kHz which is not expected by the above analysis. These effects are due to the radiation impedance as the size of the waveguide changes.[22] This is something that needs considering for accurate predictions, as was used for the predictions in Figure 7.14.

So a periodic crystal, whether 1D, 2D or 3D, has the potential to have band gaps – frequencies which are not transmitted. But whether band gaps arise depends on the geometry. Furthermore, to get full band gaps all the different periodicities need to be considered. For a square lattice structure shown in Figure 7.12, the smallest repeat distance is along the side of the lattice and is a, however, there is also periodicity diagonally across the crystal with a repeat distance of $\sqrt{2}a$. Consequently, the band gaps occur at different frequencies proportional to $1/a$ and $1/\sqrt{2}a$. If these band gaps can overlap then any wave is reflected completely from this periodic structure in the overlapping frequency range.

Umnova *et al.* measured sets of cylinders at model scale with and without an absorbent covering. The cylinders had a filling ratio of 33 per cent, meaning that the cylinders occupied a third of the volume of the array and were quite closely packed together. Figure 7.15 shows the insertion loss, which is the change in sound level between the measurement with the cylinders and a measurement without the cylinders. A large insertion loss means more sound is prevented from being transmitted. With hard cylinders, the reduction in sound level at the receiver is uneven with frequency, and shows evidence of band gaps. For most noise control applications, such an uneven response with frequency is not useful, and consequently the structure needs altering.

Adding defects to the crystals, removing some of the cylinders, or introducing local variations in the spacings can help generate additional pseudo-band gaps. However, the response is still uneven. The addition of absorbent material provides energy dissipation and so improves the attenuation and has potential to make the response more even with frequency. It is important to use the right amount of absorbent, however. Too much

absorbent and the structure will not resonate and so the band gaps will not appear. A careful balance needs to be achieved.

It is possible to make these absorbent cylinders from trees,[24] however consideration to how the trees will survive needs to be given. Trees packed close together will not thrive as they fight each other for light, nutrients and water. Published measurements on sonic crystals which give significant transmission loss use filling ratios in the range of 30 to 55 per cent. One possibility is to form the crystals from repeated rows of hedges – these are effectively 1D arrays. In this case, it is possible to achieve good attenuations at the band-gap frequencies, although the performance is rather uneven with frequency.

7.4 Trees and vegetation

It is generally believed that trees have no practical part to play in noise control, and certainly a single row of trees is not going to reduce noise significantly. However, there is substantial evidence that tall vegetation can cause significant sound reduction compared with open grassland,[25–28] provided a significantly wide tree belt is used, say greater than 30 m. Furthermore, whereas temperature inversion leads to higher sound levels over grassland, the levels in woodland are comparatively unaffected.[29] Consequently sound attenuation obtained with trees is fairly robust to changing weather.[30–31] When evaluating the attenuations achieved by the trees, it is important to compare the attenuation data to a reasonable alternative, such as grassland.

The way a mature forest affects sound propagation usually splits into different frequency ranges.[32] Figure 7.16 shows how the sound from a typical traffic noise spectrum is attenuated by the presence of either a 100 m tree belt of pine trees, or by open pasture. The results shown are for the excess attenuation, which is the measured level corrected for air absorption minus the free field level. The free field level is the level that would exist with no ground, obstacles and neutral metrology. The pine forest attenuated the overall A-weighted sound level by 10 dB more than the pasture.

At low frequency, the ground effect whereby sound reflected from the ground
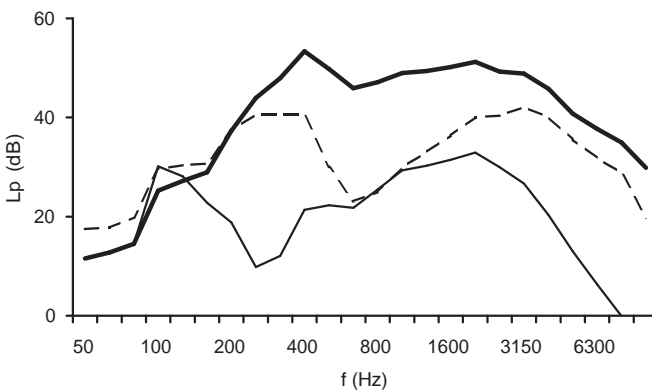
Figure 7.16   Sound pressure level from traffic after propagating 100 m:
──── in free field;
– – – over pasture; and
──── through a pine forest.
A-weighted corrections applied to spectrum (after Huisman and Attenborough[32]).

interferes with the direct sound between source and receiver is dominant. (The scattering from trunks and branches is small and the absorption from the leaves itself is negligible at these low frequencies.) The ground effect dip in the forest is usually around a few hundred Hertz, although this is geometry dependent. In a mature forest, a thick litter layer of partially decomposing vegetation usually lies on floor. In this case, the ground surface consists of a thick highly porous layer, with rather low flow resistivity resulting. The ground needs to be modelled as a complex layered structure; reported effective flow resistivity values range from 1×10^4 to 8×10^4 MKS rayls m^{-1}.[33] This means the ground effect occurs at a lower frequency for the forest in comparison to the pasture. Whether this shift to a lower frequency is useful or not depends on the frequency spectrum of the noise to be attenuated. For many environmental noise sources, this shift to a lower frequency is not desirable, because the overall sound pressure level (A-weighted) is attenuated less.

At mid-frequencies, say around 1 kHz, the trunks and large branches begin to scatter the sound out of the path between source and receiver. There is little difference in the attenuation between the pasture and forest, however. It has been suggested that, by arranging the trees in particular arrangements to form sonic crystals, it might be possible to gain additional attenuation at these crucial mid-frequencies – see the previous section.

At high frequency, typically above 1 kHz, scattering is still important, and in addition the foliage attenuates the sound by viscous friction. To achieve most absorption requires trees with large foliage surface areas to maximize viscous losses. In addition, the canopy should extend as low to the ground as possible to ensure there are no paths through the forest which bypass the foliage and are not scattered, and also to increase the amount of foliage surface area. Evergreen trees are also important if the sound attenuation is to be maintained at all times of the year.

Predictions of mid- to high frequencies might use multiple scattering theory for an idealized random infinite array of identical parallel impedance-covered cylinders, with the foliage represented by arrays of much smaller cylindrical scatterers than the trunks.[34] Huisman and Attenborough[32] used a stochastic particle-bounce method. In conjunction with a two-parameter impedance model and an assumption about the dependence of incoherent scattering on distance and frequency, good agreement was obtained with measurements in a monoculture of 29-year-old Austrian pines.

There is little data on propagation through shrubs, tall crops and hedging. Aylor[35] made a series of measurements that demonstrate significant attenuation of sound above 1 kHz through tall vegetation including corn, hemlock, brush and pine. There is a possibility of using these as natural noise control but more investigations are needed to prove the worth of this approach.

7.5 Summary

This chapter has discussed the absorption of seating; how to turn a Schroeder diffuser into an absorber; sonic crystals, and the absorption of trees. Accurate estimations of seating and audience absorption are vital to good room design, especially large concert halls for orchestral music. The absorption of Schroeder surfaces is a more esoteric subject. While the concept of a Schroeder absorber is interesting, and good absorption can be obtained, the cost of constructing such surfaces is rather high and this limits the commercial exploitation of these concepts. A similar comment could

be made about sonic crystals. The absorption of trees is interesting, because belts of vegetation are regularly planted, and the evidence is, with appropriate choice of trees and management, that these can provide useful amounts of absorption.

7.6 References

1 L. L. Beranek, "Audience and chair absorption in large halls. II", *J. Acoust. Soc. Am.*, **45**, 13–19 (1969).
2 C. W. Kosten, "New method for the calculation of the reverberation time of halls for public assembly", *Acustica*, **16**, 325–30 (1965).
3 W. J. Davies, R. J. Orlowski and Y. W. Lam, "Measuring auditorium seat absorption", *J. Acoust. Soc. Am.*, **96**, 879–88 (1994).
4 J. S. Bradley, "Predicting theater chair absorption from reverberation chamber measurements", *J. Acoust. Soc. Am.*, **91**, 1514–24 (1992).
5 W. J. Davies, "The Effects of Seating on the Acoustics of Auditoria", PhD thesis, University of Salford (1992).
6 T. Hidaka, N. Nishihara and L. L. Beranek, "Relation of acoustical parameters with and without audiences in concert halls and a simple method for simulating the occupied state", *J. Acoust. Soc. Am.*, **109**(3), 1028–42 (2001).
7 T. J. Schultz and B. G. Watters, "Propagation of sound across audience seating", *J. Acoust. Soc. Am.*, **36**, 855–96 (1964).
8 G. M. Sessler and J. E. West, "Sound transmission over theatre seats", *J. Acoust. Soc. Am.*, **36**, 1725–32 (1964).
9 A. H. Marshall, J. R. Hyde and M. F. E. Barron, "The acoustical design of Wellington Town Hall: design development, implementation and modelling results", *Proc. IoA(UK)*, Edinburgh (1982).
10 K. Fujiwara and T. Miyajima, "Absorption characteristics of a practically constructed Schroeder diffuser of quadratic-residue type", *Appl. Acoust.*, **35**, 149–52 (1992).
11 K. Fujiwara and T. Miyajima, "A study of the sound absorption of a quadratic-residue type diffuser", *Acustica*, **81**, 370–8 (1995).
12 D. E. Commins, N. Auletta and B. Suner, "Diffusion and absorption of quadratic residue diffusers", *Proc. IoA(UK)*, **10**(2), 223–32 (1988).
13 H. Kuttruff, "Sound absorption by pseudostochastic diffusers (Schroeder diffusers)", *Appl. Acoust.*, **42**, 215–31 (1994).
14 F. P. Mechel, "The wide-angle diffuser – a wide-angle absorber?", *Acustica*, **81**, 379–401 (1995).
15 T. Wu, T. J. Cox and Y. W. Lam, "From a profiled diffuser to an optimised absorber", *J. Acoust. Soc. Am.*, **108**(2), 643–50 (2000).
16 K. Fujiwara, K. Nakai and H. Torihara, "Visualisation of the sound field around a Schroeder diffuser", *Appl. Acoust.*, **60**(2), 225–36 (2000).
17 T. Wu, T. J. Cox, and Y. W. Lam, "A profiled structure with improved low frequency absorption", *J. Acoust. Soc. Am.*, **110**(6), 3064–70 (2001).
18 P. M. Morse and K. Ingard, *Theoretical Acoustics*, McGraw-Hill, New York, Chapter 6, 285–91 (1968).
19 J. F. Allard, *Propagation of Sound in Porous Media: Modelling Sound Absorbing Materials*, Elsevier Science, London, Chapter 4, 48–53, 59–62 (1993).
20 T. Wu, Y. W. Lam and T. J. Cox, "Measurement of non-uniform impedance surface by the two microphone method", *Proc. 17th ICA*, Rome (2001).
21 F. Bloch, "Uber die Quantenmechanik der Elektronen in Kristallgittern", *Z. Phys.*, **52**, 555–600 (1928).
22 P. D. C. King and T. J. Cox, "Acoustic band gaps in periodically and quasiperiodically modulated waveguides", *J. Appl. Phys.* **102**(1), 014902–014902-8 (2007).
23 O. Umnova, K. Attenborough, C. M. Linton, "Effect of porous covering on sound attenuation by periodic arrays of cylinders", *J. Acoust. Soc. Am.*, **119**, 278–84 (2006).
24 R. Martinez-Sala, C. Rubio, L. M. Garcia-Raffi, J. V. Sanchez-Perez, E. A. Sanchez-Perez and J. Llinares, "Control of noise by trees arranged like sonic crystals", *J. Sound Vib.*, **291**, 100–6 (2006).

25 G. A. Parry, J. R. Pyke and C. Robinson, "The excess attenuation of environmental noise sources through densely planted forest", *Proc. IoA(UK)*, **15**(3), 1057–65 (1993).
26 J. Kragh, *Road Traffic Noise Attenuation by Belts of Trees and Bushes*, Danish Acoustical Laboratory Report no. 31 (1982).
27 G. M. Heisler, O. H. McDaniel, K. K. Hodgdon, J. J. Portelli and S. B. Glesson, "Highway noise abatement in two forests", *Proc. Noise-Con*, 87 (1987).
28 L. R. Huddart, *The Use of Vegetation for Traffic Noise Screening*, TRRL Research Report 238 (1990).
29 W. H. T. Huisman WHT, "Sound Propagation Over Vegetation-covered Ground", PhD thesis, University of Nijmegen, The Netherlands (1990).
30 N. Barrière, "Theoretical and Experimental Study of Traffic Noise Propagation Through Forest", PhD thesis, Ecole Centrale de Lyon (1999).
31 J. DeFrance, N. Barriere and E. Premat, "Forest as a meteorological screen for traffic noise", *Proc. 9th ICSV* (2002).
32 W. H. T. Huisman and K. Attenborough, "Reverberation and attenuation in a pine forest", *J. Acoust. Soc. Am.*, **90**(5), 2664–7 (1991).
33 D. G. Albert, *Past Research on Sound Propagation Through Forests*, ERDC/CRREL TR-04-18 (2004).
34 M. A. Price, K. Attenborough and N. W. Heap, "Sound attenuation through trees: measurements and models", *J. Acoust. Soc. Am.*, **84**(5), 1836–44 (1988).
35 D. E. Aylor, "Noise reduction by vegetation and ground", *J. Acoust. Soc. Am.*, **51**(1), 197–205 (1972).

8   Prediction of scattering

Being able to predict the reflected pressure from a diffuser enables efficient evaluation, design and characterization of the performance. Currently, this is usually done by considering the surface in the free field in isolation of other objects and boundaries. The prediction techniques could in theory be used to predict the sound for whole rooms or in outdoor environments such as street canyons (if the effects of weather are ignored). At the moment, however, long computation times and storage limitations mean that algorithms dealing with large spaces are forced to use relatively crude representations of actual scattering processes. Consequently, when predicting the responses in rooms and semi-enclosed spaces, such as street canyons or pavilions, it is more common to use geometric models. The issue of modelling scattering in geometric models is discussed in Chapter 12.

Therefore, the issue for this chapter is predicting the reflection from isolated surfaces. There is a range of models, from the numerically exact but computationally slow to the more approximate but faster techniques. The prediction methods can also be differentiated as either time or frequency domain methods. In diffuser design, frequency domain methods have dominated. For this reason this chapter will concentrate on these methods. Table 8.1 summarizes the frequency domain prediction models which will be considered in this chapter, along with their key characteristics. The chapter also includes details of finite difference time domain (FDTD) models which could be the most efficient way of gaining reflected impulse responses.

The next section will start with the most accurate model, a boundary element method (BEM) based on the Helmholtz–Kirchhoff integral equation. It will then be demonstrated how the more approximate models can be derived from this integral equation, and the relative merits and limitations of the techniques will be discussed. To round off the chapter, an overview of less commonly used techniques will be given, including time domain modelling and FDTD.

8.1 Boundary element methods

When BEMs are applied to diffusers remarkable accuracy is achieved. The accuracy is much better than most acousticians are used to achieving from an acoustics theory. Acousticians are used to using empirical fixes to make measurements match predictions, but that is not often needed when BEMs are used to predict diffuser scattering. The disadvantages of BEMs are that the method is prone to human error in meshing the surface and, most importantly, it is slow for high frequencies and large surfaces. Some have attempted to apply the prediction methods to whole rooms for low frequencies but

Table 8.1 Key characteristics of various frequency-domain prediction models for scattering. The accuracy and computational efficiency columns are indicative; the rank ordering of the top four prediction models might vary depending on surface type being considered and the particular implementation of the algorithm.

Model	Accuracy	Computing time	Notes
Standard boundary element method (BEM)	Best	Slowest	Exact provided surfaces are locally reacting and viscous boundary layer losses are small. Slow, especially for large surfaces or high frequencies.
Thin panel BEM			An efficient method for thin surfaces, approximately halving the number of elements in a standard BEM model.
Kirchhoff	↑↓	↑↓	Uses the Kirchhoff boundary conditions to approximate surface pressures and so is much faster. Less accurate for oblique sources and receivers, low frequencies, rapidly changing surface impedance profiles and surfaces with steep gradients.
Fresnel			Replaces the numerical integration of Kirchhoff model by quicker to compute Fresnel integrals. Requires scattering across width and along length of surface to be orthogonal. Some useful simplifications available for flat and curved surfaces.
Fraunhofer or Fourier	Worst	Quickest	Simplifies numerical integral of Kirchhoff method, only useable in far field. Allows simpler Fourier principles to be applied. Good for understanding physical processes and designs, but least accurate.

this is very computationally intense, requiring super-computing facilities or a considerable amount of patience while waiting for results.

8.1.1 The Helmholtz–Kirchhoff integral equation

The Helmholtz–Kirchhoff integral equation forms the core of many of the prediction models used. It is defined below and the following section will then discuss how it is solved. For steady state, constant frequency motion, the acoustic wave equation reduces to the Helmholtz equation:

$$\nabla^2 p(\mathbf{r}) + k p(\mathbf{r}) = 0 \tag{8.1}$$

where p is the acoustic pressure, $\mathbf{r}$ is a point in space and k is the wavenumber. Green's first and second theorems are used to transform the differential equations based on Equation 8.1, which involve volume integrals, to an integral equation which is evaluated using integrals over the scattering surface. This Helmholtz–Kirchhoff integral equation formulates the pressure at a point, as a combination of the pressure direct from the

sources, and a surface integral of the pressure and its derivative over the reflecting surfaces. The single frequency form of the integral equation gives the pressure p as:[1]

$$
\left.\begin{array}{ll}
\mathbf{r} \in E & p(\mathbf{r}) \\
\mathbf{r} \in s & \frac{1}{2}p(\mathbf{r}) \\
\mathbf{r} \in D & 0
\end{array}\right\} = p_i(\mathbf{r},\mathbf{r}_0) + \int_s p(\mathbf{r}_s)\frac{\partial G(\mathbf{r},\mathbf{r}_s)}{\partial n(\mathbf{r}_s)} - G(\mathbf{r},\mathbf{r}_s)\frac{\partial p(\mathbf{r}_s)}{\partial n(\mathbf{r}_s)}ds
\tag{8.2}
$$

where $\mathbf{r} = \{x, y, z\}$ is the vector describing the receiver location; $\mathbf{r}_0 = \{x_0, y_0, z_0\}$ is the vector describing the source location; $\mathbf{r}_s = \{x_s, y_s, z_s\}$ is the vector for a point on the surface; $p_i(\mathbf{r}, \mathbf{r}_0)$ is the direct pressure radiated from the source at $\mathbf{r}_0$ to the receiver at $\mathbf{r}$; G is the Green's function; n is the normal to the surface pointing out of the surface; E is the external region; s is the surface, and D is the interior of the surface.

The geometry is illustrated in Figure 8.1. $p_i(\mathbf{r}, \mathbf{r}_0)$ is the pressure direct from the source at $\mathbf{r}_0$ to the receiver point at $\mathbf{r}$, and so the first term on the right hand side represents the direct pressure. The integral is carried out over the surface, with $\mathbf{r}_s$ being a point on the surface and n a normal to the surface pointing out of the surface, so the integral gives the contribution of the reflected energy to the pressure at $\mathbf{r}$. By single frequency it is meant that the system is in steady state conditions so that the time variation $\exp(j\omega t)$ can be neglected. G is the Green's function which gives how the pressure and its derivative propagate from one point in space to another point. Consequently, in 3D the Green's function is simply a point source radiation equation:

$$
G(\mathbf{r},\mathbf{r}_0) = \frac{e^{-jkr}}{4\pi r}
\tag{8.3}
$$

where $r = |\mathbf{r} - \mathbf{r}_0|$. Carrying out the solution in two dimensions is extremely useful for diffusers as it can greatly decrease the computational burden in terms of storage and calculation time. In that case, the Green's function is given by the Hankel function:

$$
G(r) = \frac{-j}{4}H_0^{(2)}(kr)
\tag{8.4}
$$
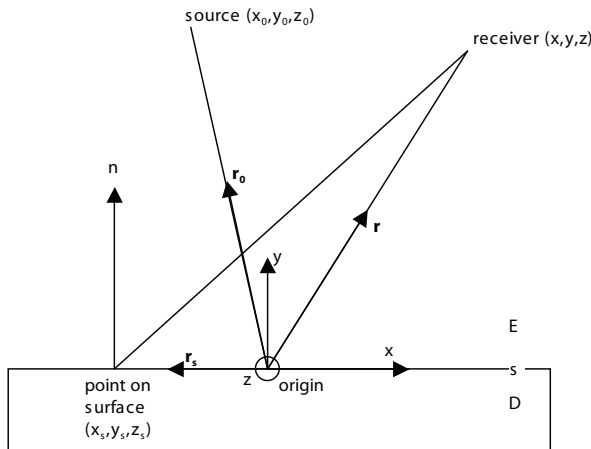
Figure 8.1 Geometry for prediction models.

where $H_0^{(2)}$ is the Hankel function of the second kind of order zero. The asymptotic version of the Hankel function when kr is large is:

$$G(r) \underset{kr \gg 1}{=} \frac{Ae^{-jkr}}{\sqrt{kr}} \tag{8.5}$$

where A is a constant. So this is a line source radiation equation as would be expected in a 2D world. The Hankel function is most efficiently evaluated by using polynomial expansions[2] when kr is small and by using the asymptotic form in Equation 8.5 when kr is large.

There are three possible equations shown in Equation 8.2. The top case is when the point $\mathbf{r}$ is external to the scattering surface ($\mathbf{r} \in E$), the middle case is when $\mathbf{r}$ is on a surface ($\mathbf{r} \in s$), and the bottom case when $\mathbf{r}$ is internal to the scattering surface ($\mathbf{r} \in D$).

The integral has two terms: one involving the surface pressure $p(\mathbf{r}_s)$ and one involving the surface pressure derivative $\partial p(\mathbf{r}_s)/\partial n(\mathbf{r}_s)$. If the surface is taken to be local reacting, the derivative of the surface pressure will be related to the surface pressure by the surface admittance:

$$jkp(\mathbf{r}_s)\beta'(\mathbf{r}_s) = \frac{\partial p(\mathbf{r}_s)}{\partial n(\mathbf{r}_s)} \tag{8.6}$$

where β' is the surface admittance. In BEM modelling, it is normal to define quantities in terms of an outward pointing normal. Surface admittances would normally be defined with an inward pointing normal. The prime is used to signify this difference, where $\beta' = -\beta$, where β is the more usual surface admittance. This definition of an outward pointing normal also affects the interrelations between admittance and surface reflection coefficient and is relevant when implementing the Kirchhoff solution. The assumption of local reaction means the surface admittance is independent of the incident and reflected pressure waves. For low absorption surfaces, where $\beta' \to 0$, the term involving the pressure derivative can be neglected.

8.1.2 General solution method

Having defined the terms and the nomenclature for the integral equation, the general solution technique for a BEM will be presented. The BEM involves the application of Equation 8.2 twice:

1   The surface pressures, $p(\mathbf{r}_s)$ on the scattering surface(s) are found.
2   A numerical integral is carried out over the surface to determine the pressures at the desired external points.

8.1.2.1 Determining surface pressures

The determination of the surface pressures is the rate-determining step of a BEM model. The surface pressures depend not only on the incident sound field but also on each other. This is a statement that there are mutual interactions across the surface, as

might be expected. To model the mutual interactions, the usual solution method is to discretize the surface into a number of surface (boundary) elements across which it is approximated that the pressure is constant. The elements must have sufficiently small dimensions to prevent errors in representing the continuous pressure variation by a set of discrete values. This is usually achieved by making elements smaller than a quarter of a wavelength in size for very simple surfaces. As surfaces become more complex it is safer to use element sizes of λ/8 or even smaller to ensure proper representation of the pressure variation, where λ is the wavelength of the highest frequency being modelled. Breaking the surface geometry into a series of elements – meshing the surface – can be a difficult process for complicated diffusers, but it can be greatly simplified by using specialist meshing programs. This is where human error is most likely to occur. Two-dimensional BEMs not only have computational speed advantages, they are also useful because it is far simpler to mesh a 2D shape.

Once the surface has been discretized, a set of simultaneous equations can be set up with one equation for each boundary element. The equations will be for the surface pressures with **r** being taken for positions on the surface in the middle of each of the elements. In matrix form, Equation 8.2 can be rewritten as:

$$\left(\tfrac{1}{2}\delta + \mathbf{A}\right)\mathbf{P} = \mathbf{P}_i \tag{8.7}$$

$$\delta_{nm} = 1; m = n \tag{8.8}$$
$$\delta_{nm} = 0; m \neq n$$

$$\mathbf{A}_{mn} = \int_{Sm} \frac{\partial G(\mathbf{r}_n, \mathbf{r}_s)}{\partial n_m(\mathbf{r}_s)} - G(\mathbf{r}_n, \mathbf{r}_s) jk\beta_m{}' ds_m \tag{8.9}$$

where **P** is a $(1 \times N)$ matrix of surface pressures; $\mathbf{P}_i$ is a $(1 \times N)$ matrix of incident pressures direct from the source(s) to the surface; N is the number of elements; the subscripts n and m refer to the $(n, m)^{th}$ element of the matrix or the contribution from the mth element to the nth element surface pressure, and s_m is the surface of the mth element.

The calculation of the matrix **A** is an important rate determining step in the boundary element method. It is roughly an N^2 process, where N is the number of elements. It is relatively slower for 2D processes when compared to 3D models. This is because the Hankel function is slower to evaluate unless it is in-built and optimized for speed by the computing language used to code the numerical model. But then there are great time savings to be had in a 2D model, as Equation 8.9 is only a line integral rather than a surface integration.

The integration of Equation 8.9 can use various algorithms and efficient numerical techniques[3] that can make significant time savings. It is also possible to use more approximate integration for elements that are far away from each other when the mutual interactions are less strong. This has to be done with care, however, because it risks compromising the accuracy of the solution. Evaluating Equation 8.9 when $m = n$, in other words evaluating the influence of an element on itself requires special consideration. The reason for this is the integral includes a singularity. The singularity

is relatively weak in this case, and so provided care is taken not to consider the case where $\mathbf{r}_n = \mathbf{r}_s$, then the numerical integration will converge to a correct value.

Once the simultaneous equations are constructed they can be solved using standard matrix solution techniques, which are now commonly available. The BEM method forms full matrixes so sparse matrix solvers used in techniques such as finite element analysis are not directly applicable.

If the simultaneous equations are solved, it is possible to get non-unique solutions at certain frequencies. These equate to eigensolutions of the interior of the surface being modelled. There are various methods for overcoming this problem. One solution is to form an over-determined set of equations; this is the CHIEF method.[4] By placing some receivers in the body of the diffuser, where the pressure must be zero, it is possible to add additional simultaneous equations which help to ensure the correct solution is found. In choosing the receivers inside the body of the surface, often referred to as internal points, it must be remembered that if these internal points are at a node of an incorrect eigensolution, then they do not help. Consequently, several internal points should be used, avoiding lines of symmetry and simple integer relationships between internal point locations. Another remedy to the non-unique solutions problem is to combine Equation 8.2 with its derivative; this is the Burton Miller approach.[1]

In reality, most diffuser geometries are such that non-unique solutions are not usually found. Non-unique solutions are most common when the wavelength is small compared to the geometry, but cases with such small wavelength to structural size are not often attempted in diffuser calculations because the computational burden becomes too large. Consequently, at the moment it appears that non-unique solutions are more of a worry for mathematicians than acousticians.

A significant reduction in computation burden can be achieved if there are planes of symmetry in the surface and the source lies on the planes of symmetry. In this case, a simple image source construction can be used to take the place of identical parts of the surface and so greatly reduce the computational burden. This is shown in Figure 8.2. The pressure on identical parts of the surface will be the same and consequently it is possible to construct a solution using about half the number of elements that would be required to mesh the whole surface. This does not reduce time in setting up the simultaneous equations but it greatly reduces the time required to solve the equations and decreases the memory requirements. The easiest method to exploit the image source construct is to modify the Green's function by an additional term:

$$G(r) = \frac{e^{-jkr}}{4\pi r} + \frac{e^{-jkr'}}{4\pi r'} \tag{8.10}$$

where r' is the distance from an image source which is reflected in the plane of symmetry. Multiple symmetry planes may exist, and so multiple image sources may need to be considered. A similar process can also be applied to the 2D Green's function.

It is also possible to assume non-uniform pressure variation across the elements. For instance, it is possible to define the matrices in terms of the pressures at the element boundaries and assume a linear relationship between these. This reduces the number of elements needed to correctly represent the pressure variation on the surface compared to constant pressure elements. This has potential to make a faster prediction model, but at the cost of a more complex implementation.
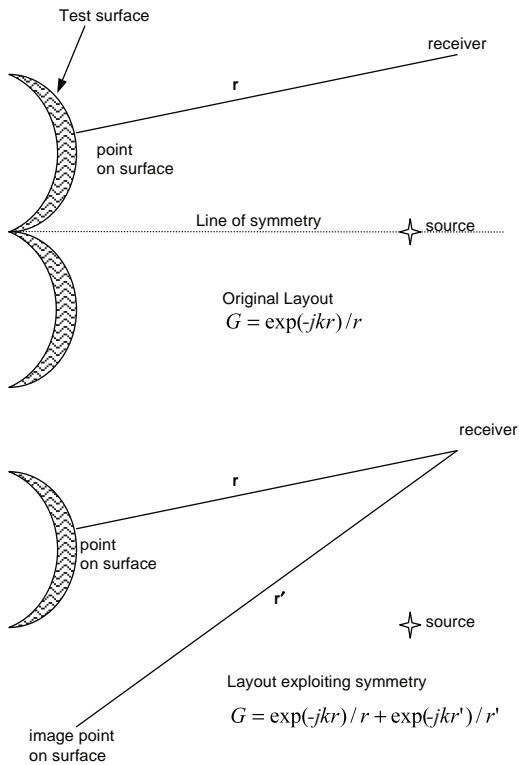
Figure 8.2 Illustration showing the use of an image source for a diffuser made of two arcs. The top illustration shows the original configuration where the source lies on a plane of symmetry. The bottom shows the exploitation of mirror symmetry to halve the number of elements required in the BEM model.

8.1.2.2 Determining external point pressures

Once the surface pressures are known, Equation 8.2 becomes a more straightforward numerical integration which must be solved. This process is relatively quick. The use of efficient numerical integration algorithms and asymptotic solutions for the 2D Green's function, when the receivers are far from the surface, can greatly speed up this process.

8.1.2.3 2D versus 3D

Cox[5] examined whether it is possible to predict the scattering from 3D diffusers using a 2D BEM model. The surfaces he tested were single plane surfaces which were extruded in one direction, like 1D Schroeder diffusers and cylinders. This meant that the scattering was roughly orthogonal across the width and along the extruded length. In these cases, 2D models provided accurate predictions except at low frequencies (for the surfaces tested, this meant below 500 Hz). Cox derived expressions to correct the 2D scattered polar response so that results matched the real (3D) diffuser scattering. These corrections affect the overall scattered sound power level and not the shape of the polar response.

8.1.3 Thin panel solution

When a surface becomes very thin the above solution method will not work. The front and back of the surface have elements which are too close to each other, and the solution method often becomes inaccurate. It is possible, however, to provide a formulation in terms of the pressure difference and sum across the panel. Not only does this regularize the equations to make them solvable, it also approximately halves the number of elements required and so speeds solution times and reduces storage requirements.

The solution method requires both Equation 8.2 and its derivative. Terai[6] showed that with correct regard for the jump relations, the integral equation and its derivative can be given by:

$$\tfrac{1}{2}\left\{p(\mathbf{r}_1) + p(\mathbf{r}_2)\right\} = p_i(\mathbf{r}_0, \mathbf{r}_1) + \tag{8.11}$$

$$\iint_s \left\{p(\mathbf{r}_{s,1}) - p(\mathbf{r}_{s,2})\right\}\frac{\partial G(\mathbf{r}, \mathbf{r}_{s,1})}{\partial n(\mathbf{r}_{s,1})} - \left\{\frac{\partial p(\mathbf{r}_{s,1})}{\partial n(\mathbf{r}_{s,1})} - \frac{\partial p(\mathbf{r}_{s,2})}{\partial n(\mathbf{r}_{s,1})}\right\}G(\mathbf{r}, \mathbf{r}_{s,1})\,ds$$

$$\tfrac{1}{2}\left\{\frac{\partial p(\mathbf{r}_1)}{\partial n(\mathbf{r}_1)} + \frac{\partial p(\mathbf{r}_2)}{\partial n(\mathbf{r}_1)}\right\} = \frac{\partial p_i(\mathbf{r}_0, \mathbf{r}_{s,1})}{\partial n(\mathbf{r}_{s,1})} + \tag{8.12}$$

$$\iint_s \left\{p(\mathbf{r}_{s,1}) - p(\mathbf{r}_{s,2})\right\}\frac{\partial^2 G(\mathbf{r}, \mathbf{r}_{s,1})}{\partial n(\mathbf{r}_1)\partial n(\mathbf{r}_{s,1})} - \left\{\frac{\partial p(\mathbf{r}_{s,1})}{\partial n(\mathbf{r}_{s,1})} - \frac{\partial p(\mathbf{r}_{s,2})}{\partial n(\mathbf{r}_{s,1})}\right\}\frac{\partial G(\mathbf{r}, \mathbf{r}_{s,1})}{\partial n(\mathbf{r}_1)}\,ds$$

where the 1 and 2 in the subscripts refer to the front and the back of an infinitesimally thick panel respectively. These are the equations for points on the surface ($\mathbf{r}_1$, $\mathbf{r}_2 \in s$) and should be used to set up the simultaneous equations which then yield the surface pressures. If the desire is to achieve a reduction in computational burden, further simplifications can be obtained if more assumptions are made. Two approaches will be considered: first, the case of a non-absorbing surface and second, the situation of a planar surface with non-zero surface admittance.

8.1.3.1 Non-absorbing surface

The surface is assumed to be non-absorbing and thin; then the differentials in the pressures on the front and rear surface are zero as the surface velocity is zero. Under this assumption, Equation 8.12 can be simplified to yield a single equation in terms of the pressure difference across the panel:

$$0 = \frac{\partial p_i(\mathbf{r}_0, \mathbf{r}_{s,1})}{\partial n(\mathbf{r}_{s,1})} + \iint_s \left\{p(\mathbf{r}_{s,1}) - p(\mathbf{r}_{s,2})\right\}\frac{\partial^2 G(\mathbf{r}, \mathbf{r}_{s,1})}{\partial n(\mathbf{r}_1)\partial n(\mathbf{r}_{s,1})}\,ds \tag{8.13}$$

Using this equation it is possible to discretize the front surface into a set of elements across which the pressure is assumed constant, and to set up simultaneous equations in the pressure difference between the front and rear of the panel $p(\mathbf{r}_{s,1}) - p(\mathbf{r}_{s,2})$. These simultaneous equations can then be solved to give the pressure difference for each element.

Once the pressure difference for each element is known, then the following equation is used to calculate the pressure at external points:

$$p(\mathbf{r}) = p_i(\mathbf{r}_0,\mathbf{r}_1) + \iint_s \{p(\mathbf{r}_{s,1}) - p(\mathbf{r}_{s,2})\}\frac{\partial G(\mathbf{r},\mathbf{r}_{s,1})}{\partial n(\mathbf{r}_{s,1})}\,ds \qquad (8.14)$$

Incidentally, for a planar surface, it is simple to get the pressures on the front and the rear of the panel if these are wanted (they are not explicitly needed to get the external point pressures). The sum of the pressures on either side of the surface is equal to twice the incident pressure $p(\mathbf{r}_{s,1}) + p(\mathbf{r}_{s,2}) = 2p_i(\mathbf{r}_{s,1})$. This fact can be used with the values for the pressure difference between the front and rear of the panel $p(\mathbf{r}_{s,1}) - p(\mathbf{r}_{s,2})$ to give the actual surface pressures on either side of the panel.

The matrix form of the integral Equation 8.13 is highly singular when the interaction of an element with itself is considered. To overcome this difficulty Terai suggested using an asymptotic solution for calculating the contribution of an element's radiation to its own surface pressure. For the 3D case this yields a line integral around the perimeter of the element:

$$\lim_{\mathbf{r}\to\mathbf{r}_s}\iint_s \frac{\partial^2 G(\mathbf{r},\mathbf{r}_s)}{\partial n^2}\,ds = \frac{-1}{4\pi}\left\{\oint \frac{e^{-jk\mathbf{r}(\theta)}}{\mathbf{r}(\theta)}\,d\theta + 2\pi jk\right\} \qquad (8.15)$$

where θ is defined in Figure 8.3.

For the 2D case the corresponding equation is:

$$\lim_{a\to 0}\int_0^a \frac{\partial^2 G(\mathbf{r},\mathbf{r}_s)}{\partial n^2}\,ds = \frac{1}{2\pi a} \qquad (8.16)$$

In many cases, it is possible to set the distance a as being the length of the element, and so the factor above can be used to directly calculate the contribution of the element to itself. For some problems with complex geometries, however, more accurate results are obtained if a smaller value of a is used and the rest of the element is integrated using normal numerical integration procedures.

Apart from this detail, the solution method proceeds in exactly the same way as for the standard BEM model. The thin panel formulation is very useful for many scattering
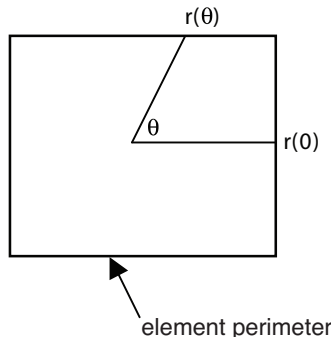
Figure 8.3 Definition of θ used for the asymptotic form of 3D thin panel BEM.

surfaces. An overhead canopy above a stage can be treated as a thin rigid surface, and this formulation allows a faster solution than the standard BEM. The accuracy is compromised close to grazing angles, as it does not model the scattering from the edges which exist with real surfaces. More details on the accuracy of this approach are given later.

The method can also be applied to Schroeder diffusers, which have thin fins as part of the construction. Schroeder diffusers are discussed in Chapter 9 and several pictures are shown in Figure 9.1. The thin panel solution method allows the Schroeder geometry to be exactly modelled and the scattering predicted for any frequency. This is not true of most prediction methods, which are generally frequency limited as they assume plane wave propagation in the wells. This method provides unique solutions, provided no enclosed volumes are created out of the elements. Consequently, there is no need to use an over-determined system in many cases. A slightly neater solution for the Schroeder diffuser is to use a BEM which uses a combination of both normal and thin elements.[7]

8.1.3.2 *Planar, thin surface with non-zero admittance*

By assuming the surface is planar, some of the terms in Equations 8.11 and 8.12 simplify. The aim is to reduce the number of elements involved in the calculation. One way of achieving a reduction in the number of elements is to assume that the admittances on the front and rear of the panel at any point are the same, i.e. $\beta(\mathbf{r}_{s,1}) = \beta(\mathbf{r}_{s,2})$. In room diffuser calculations this is not going to introduce large errors into the calculation because it is the scattering on the bright side which is of primary importance. For all but low frequencies the pressure is low on the rear of the panel, and consequently, what admittance is assumed on the rear is not terribly important. This admittance assumption might not be accurate in all cases. For example, if a diffusing roadside barrier is being considered, the scattering in the shadow zone at low frequencies is of interest.

Assuming that $\beta(\mathbf{r}_{s,1}) = \beta(\mathbf{r}_{s,2})$ is a reasonable approximation, and the surface is planar, then for receiver points $\mathbf{r}_1$ and $\mathbf{r}_2$ on the front and rear surface, Equations 8.11 and 8.12 can be re-written as:

$$\tfrac{1}{2}\{p(\mathbf{r}_1) + p(\mathbf{r}_2)\} = p_i(\mathbf{r}_0, \mathbf{r}_1) - jk \iint_s \beta'(\mathbf{r}_{s,1})\left[p(\mathbf{r}_{s,1}) + p(\mathbf{r}_{s,2})\right]G(\mathbf{r}, \mathbf{r}_{s,1})\,ds \tag{8.17}$$

$$\tfrac{1}{2}\beta'(\mathbf{r}_1)\{p(\mathbf{r}_1) - p(\mathbf{r}_2)\} = \frac{\partial p_i(\mathbf{r}_0, \mathbf{r}_{s,1})}{\partial n(\mathbf{r}_{s,1})} + \iint_s \{p(\mathbf{r}_{s,1}) - p(\mathbf{r}_{s,2})\}\frac{\partial^2 G(\mathbf{r}, \mathbf{r}_{s,1})}{\partial n(\mathbf{r}_1)\partial n(\mathbf{r}_{s,1})}\,ds \tag{8.18}$$

The surface is again discretized into elements that are small compared to the wavelength. Then two sets of simultaneous equations can be constructed from Equations 8.17 and 8.18. The first set of equations is in the sum of the pressures, using Equation 8.17, and the second is in the difference pressure across the panel, using Equation 8.18. These simultaneous equations are then separately solved. As two sets of simultaneous equations are being used, with half the number of elements when compared to a standard BEM, then the solution will be quicker by a factor of 4–8 times, depending on the implementation.

The propagation to external receivers is carried out using the following equation:

$$p(\mathbf{r}) = p_i(\mathbf{r}_0, \mathbf{r}_1) + \tag{8.19}$$

$$\iint_s \left\{ p(\mathbf{r}_{s,1}) - p(\mathbf{r}_{s,2}) \right\} \frac{\partial G(\mathbf{r}, \mathbf{r}_{s,1})}{\partial n(\mathbf{r}_{s,1})} - jk\beta'(\mathbf{r}_{s,1}) \left[p(\mathbf{r}_{s,1}) + p(\mathbf{r}_{s,2}) \right] G(\mathbf{r}, \mathbf{r}_{s,1}) ds$$

The accuracy of this technique will be presented later in this chapter.

8.1.4 Acceleration schemes

When large areas of diffusers are used BEM models can become too slow to be practical. Storage requirements for the full matrixes also cause problems. In recent times, fast multipole methods (FMMs) have been developed for BEM.[8] FMMs collect the boundary elements into clusters employing a classic BEM approach to elements in the near field and applying a more efficient FMM procedure for those in the far field. The computational effort for the conventional FMM increases for n elements by $n^{3/2}$ compared to the BEM, which increases by n^2. Storage requirements are also reduced. The implementation of this technique is complex.

Another approach to improving BEM predictions is to use information concerning the physical nature of the surface boundary conditions to reduce computational burden. In the case of periodic surfaces, considerable improvements in prediction times can be achieved by representing the periodicity in the Green's function. This technique is especially useful because diffusers are often applied in a periodic formulation.

Lam[9] developed formulations for periodic, 2D hard surfaces using Bloch's theorem.[10] For free waves in a periodic structure, all field quantities at two points exactly one period apart are related by the same factor. For surface scattering and a far field source, the incident pressure for identical parts of the structure will be related by a simple constant phase factor. The relationship between the total pressure at periodic points will be modified by the scattered wave. If the scattering is relatively weak, then it can be assumed that the constant phase factor relating the incident sound pressures between identical parts of the surface will also give the relationship for the total sound pressures. This may appear to be a large leap of faith as diffusers are designed to achieve strong scattering in the far field. Notwithstanding this design remit, it will be shown later in this chapter that the Kirchhoff boundary conditions form the basis of many reasonably good prediction methods, and there is an explicit assumption of weak scattering in applying the Kirchhoff boundary conditions. So this provides some hope that the weak scattering assumption may be reasonable.

Figure 8.4 illustrates a periodic structure and the geometry used. The pressure between identical points on adjacent periods is therefore:

$$\Lambda(\mathbf{r}_{s,i=0}, \mathbf{r}_{s,i=j}) = \frac{p_i(\mathbf{r}_{s,i=0})}{p_i(\mathbf{r}_{s,i=j})} \tag{8.20}$$

where $\mathbf{r}_{i=0}$ and $\mathbf{r}_{i=j}$ are vectors for identical points on the surface, where j is an integer and i is an index referring to the appropriate period number. This formulation can deal with non-plane wave incidence and so can be used for near field sources and receivers.
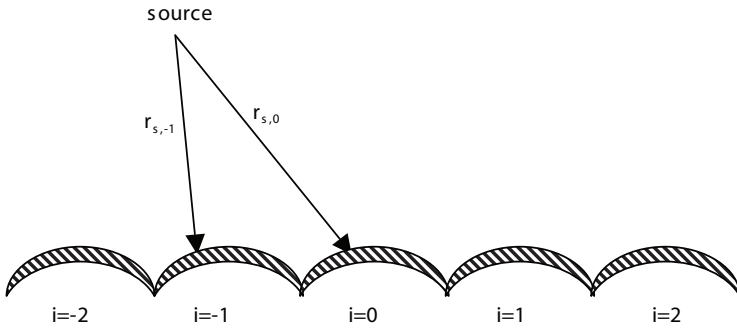
Figure 8.4 Geometry for periodic predictions illustrated for a set of arcs.

As Equation 8.20 gives the relationship between the pressures on identical parts of the diffuser, it is possible to produce a new version of Equation 8.2 for periodic surfaces:

$$
\left.\begin{array}{ll}
\mathbf{r} \in E & p(\mathbf{r}) \\
\mathbf{r} \in s & \frac{1}{2}p(\mathbf{r}) \\
\mathbf{r} \in D & 0
\end{array}\right\} = p_i(\mathbf{r},\mathbf{r}_0) + \int_{s_0} p(\mathbf{r}_{s,0}) \sum_{i=-\infty}^{\infty} \Lambda(\mathbf{r}_{s,i},\mathbf{r}_{s,i+j}) \left[\frac{\partial G(\mathbf{r},\mathbf{r}_{s,0})}{\partial n(\mathbf{r}_{s,0})} - jk\beta'(\mathbf{r}_{s,0})G(\mathbf{r},\mathbf{r}_{s,0}) \right] ds
$$

(8.21)

where $\mathbf{r}_{s,0}$ is the surface vector for the middle period only. The integration is only carried out over the middle period, surface s_0, since once the pressure is known on the middle period, it is known for the whole surface (Bloch[10]). Effectively, the Green's function has been modified in a way similar to the modelling of symmetry using image sources. The limits of the infinite sum can be taken as the physical number of periods present in the diffuser. Figure 8.5 shows the scattering from a periodic arrangement of six semicylinders. Measurements are compared to a standard BEM solution (modelling all six semicylinders explicitly), as well as the periodic formulation. Good agreement is obtained between the periodic and standard BEM, although some differences remain. One likely cause is that the number of periods used is relatively small and so edge
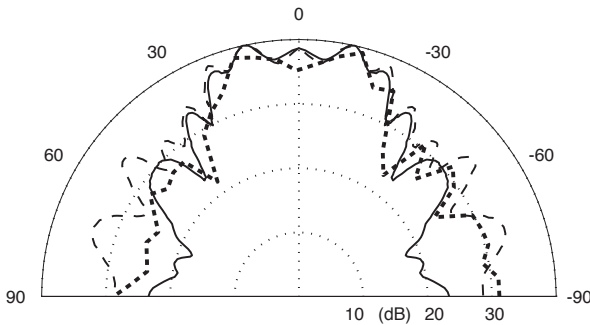
Figure 8.5 Scattering from six semicylinders. Two BEM models compared to measurement. 5 kHz, normal incidence, one-third octave band:
- – – measured;
——— standard BEM; and
– – – periodic BEM (data from Lam[9]).
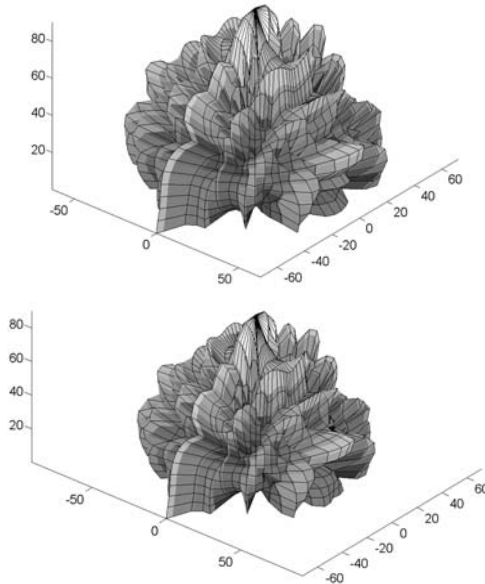
Figure 8.6 Comparison of predictions from standard BEM model (top) and a periodic formulation (bottom) for a planar hybrid surface.

diffraction effects may significantly alter the surface pressures of the outer periods. Alternatively, it may be evidence that the weak scattering assumption is not entirely true.

This technique can also be applied to other structures and in 3D. For example, Figure 8.6 shows the scattering from a planar hybrid surface. This is a flat surface with a complex array of hard and soft patches and is discussed in detail in Chapter 11, and a picture is shown in Figure 11.1. In Figure 8.6, a standard solution where all periods are meshed is compared to a periodic formulation. The case is an array of 4×1 periods at 2 kHz. The two prediction methods produce very similar results, validating the periodic formulation.

The reliance on the weak scattering theory for explaining the relationship between different periods of the device means that it is best to assume that this process works best where the Kirchhoff boundary conditions are accurate. Consequently, it might be expected that the periodic formulations would work less well at low frequencies, and for oblique sources and receivers, especially as these approach grazing angles. It would also be interesting to know how this formulation works for periodic arrangement of strongly scattering surfaces, such as pyramids or triangles.

8.1.5 *BEM accuracy: thin rigid reflectors*

The next two sections will examine the accuracy of BEMs. Consider first thin, rigid, planar and curved surfaces. These commonly occur in indoor and outdoor spaces and are relatively straightforward to mesh and predict using BEMs. It is also relatively easy to construct and measure the scattering from such surfaces, and so enable the accuracy of the prediction methods to be directly compared to scale model measurements (see Chapter 4 for the measurement techniques used).
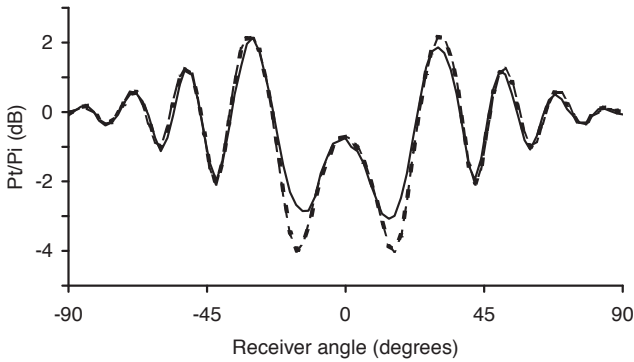
Figure 8.7 Comparison of total field (incident plus scattered) for a plane surface measured and predicted by two boundary element models. Normalized to incident sound at receiver:
———— measured;
− − − thin panel BEM; and
------- 3D BEM (data from Cox[12]).

The full BEM solution based on Equation 8.2 produces accurate predictions of the scattering over a wide range of frequencies[11,12] for plane and curved surfaces. Figures 8.7 and 8.8 compare predicted and measured results for the total and scattered pressure for a plane thin panel. Good prediction accuracy is achieved for both models. The thin panel model is based on Equations 8.13 and 8.14, and gives very similar results to the full BEM solution (for many angles the lines overlay each other) and is also quicker to predict. The thin panel and full BEM model only deviate for grazing angles and high frequencies. The deviations occur because the thin panel model does not properly represent the finite thickness of the panel, which becomes more critical at grazing angles when the wavelength is not large compared to the panel thickness. Inaccuracies arise because there are no edge elements in the thin panel case and so edge scattering is not properly modelled.
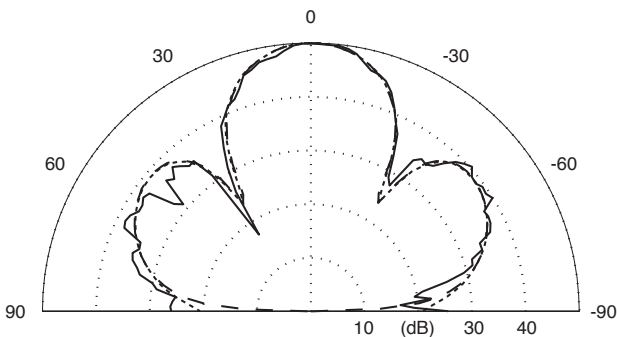
Figure 8.8 Comparison of scattered pressure from a plane surface:
———— measured;
− − − thin panel BEM; and
------- 3D BEM.
Normalized to incident sound at each receiver and offset by 57.5 dB (data from Cox[12]).
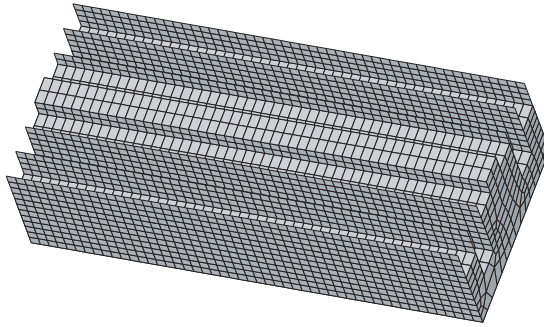
Figure 8.9   An example of a Schroeder diffuser meshed for prediction using a thin panel model.

8.1.6 *BEM accuracy: Schroeder diffusers*

Figure 9.1 shows pictures of Schroeder diffusers and Chapter 9 discusses the design of these surfaces in great detail. The diffuser consists of a series of wells of the same width but different depths. There are two approaches to modelling this surface. The first uses the thin panel solution and allows the diffuser shape to be exactly modelled; the second uses an approximate model of the surface as a box with a variable front face admittance (or impedance).

The thin panel solution allows explicit representation of the diffuser shape. The complete diffuser can be covered with thin panel elements. Figure 8.9 shows a typical example. The complete enclosure of the diffuser by thin panel elements forces the interior to have zero pressure provided no critical frequencies are found. Two other problems could arise from this representation: (1) a large number of thin panel elements with different sizes have to be sealed together, and the technique is therefore prone to meshing errors; and (2) the thin panel solution for a plane panel showed small inaccuracies for scattering at grazing angles, especially at high frequencies. This could be a problem for Schroeder diffusers with fins, as these are presented edge-on to sources normal to the surface. The main drawback of this method is that it uses a very large
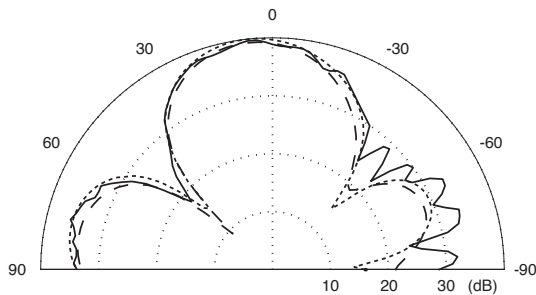
Figure 8.10   Comparison of scattered pressure from a Schroeder diffuser:
————— measured;
– – – thin panel BEM; and
------- BEM with box model.
Normalized to incident sound at each receiver and offset by 50 dB (data from Cox[12]).
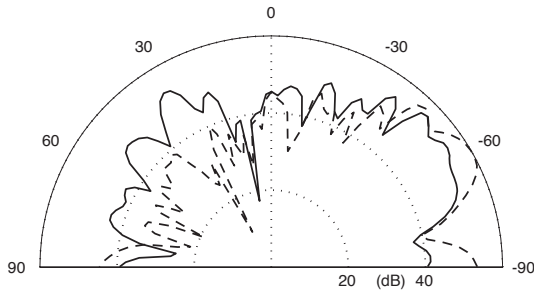
Figure 8.11 Comparison of two prediction models for the scattered pressure for oblique
sound incident on a Schroeder diffuser:
———— thin panel BEM; and
– – – BEM with box model.
Normalized to incident pressure at each receiver and offset by 66 dB (data
from Cox[12]).

number of elements and therefore predictions can exceed available computing power.

The approximate model, using a spatially-varying admittance on the front face of a
box, has been used by most authors investigating Schroeder diffusers. The admittance
on the front face at the entrance of each well is derived from the phase change of plane
waves propagating up and down the wells. This representation is expected to work
under certain conditions: (1) the frequency must be below the cut-off frequency of the
well so plane wave propagation in the wells dominates; and (2) the impedance at the
opening of the wells must be locally reacting, which means the radiation coupling
between the wells has to be small. Also, unless the radiation impedance of each well is
small, it should be represented in the admittance at the well entrances.

Comparisons with measurement show that the thin panel predictions of Schroeder
diffuser scattering are accurate. Figure 8.10 shows an example for the scattered pressure.
Similar accuracy is also achieved for the total field. The BEM model based on Equation
8.2, using the box representation with a spatially-varying front face admittance, is also
successful. This demonstrates that the simple phase change local reacting admittance
assumption is reasonable – this is discussed in more detail in Chapter 9.

For oblique incidence sources, there is greater interaction across the front face of the
diffuser and the box representation with a spatially-varying front face admittance will
be less accurate. Figure 8.11 shows an example for a source at 60°, where the thin panel
model, which is assumed to be correct, is compared to the BEM using the spatially-
varying admittance box model. The BEM using the box model is most accurate close
to the specular reflection angle and becomes more inaccurate for receivers further from
the specular reflection angle.

8.1.7 BEM *accuracy: hybrid surfaces*

Hybrid surfaces use a mixture of absorbent and hard surfaces to generate a combination
of absorption and dispersion. To test the accuracy of a BEM for such a surface, a single
plane surface shown in Figure 8.12 was constructed.[13] This was based on a fourth order
maximum length sequence, i.e. there were 15 patches of either absorption or reflection.
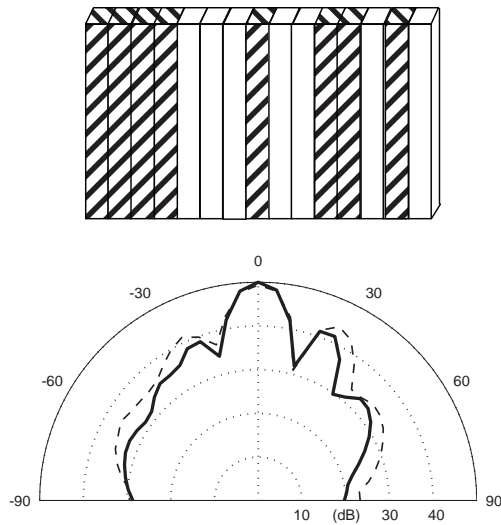
Figure 8.12   Scattered pressure for normal sound incident on the hybrid surface shown.
The shaded sections are constructed of MDF and the unshaded sections of
mineral wool.
━━━ BEM prediction and
− − − Measured (bottom figure after Xiao *et al.*[13]).

Each of the 15 patches was 127 mm wide. Absorption was provided by mineral wool
76 mm thick, and absorption by varnished wood 25 mm thick. The BEM was a con-
ventional solution using Equation 8.2 and a 2D Green's function for speed. For the
patches of absorbent, the impedance was modelled using the Delaney and Bazley empirical
formulation (see Section 5.4.1) with a flow resistivity of σ = 50,000 MKS Rayl m^{-1}
and a porosity of 0.98. Figure 8.12 shows a typical result from the measurements and
predictions at 1.25 kHz. The BEM model agrees well with the measurement.

8.2 Kirchhoff

The rate-determining steps in carrying out BEM predictions are setting up and solv-
ing the simultaneous equations to determine the surface pressures. Consequently,
faster methods for estimating the surface pressures have been derived and, for an
appropriate approximation, it is possible to turn to optics. Optics uses the Kirchhoff
approximation to determine the propagation of light through an aperture. The
Kirchhoff approximation gives the wave function and its derivative across the aperture
as unaltered from the incident wave. On the surround defining the aperture, both the
wave function and its derivative are assumed zero. Adapted for scattering in acoustics,
this approximation can be used to obtain the surface pressures and their derivatives,
and yield reasonably accurate results for far field scattering. There are cases, however,
when the method is not accurate, and so the approximation should be applied with care.

Consider a large planar surface, with uniform surface impedance across the whole
surface. By considering the definition of pressure reflection coefficient given in Chapter 1,
it would be anticipated that the pressure p on the surface at $\mathbf{r}_s$ would be given by:

$$p(\mathbf{r}_s) = \left[1 + R(\mathbf{r}_s)\right]p_i(\mathbf{r}_s, \mathbf{r}_0) \tag{8.22}$$

where R is the pressure reflection coefficient of the surface. Equation 8.22 is sometimes referred to as the Kirchhoff boundary condition. If the surface is completely non-absorbing, $R = 1$, then the surface pressure is simply double the incident pressure. When the surface is completely absorbing, $R = 0$, then the surface pressure is just the incident pressure. It is necessary to assume that the diffuser is thin, so that the pressure from the sides of the surface can be neglected. It is also assumed that the surface is large compared to wavelength so that the pressure on the rear of the panel can be assumed to be zero. Then substitution of Equation 8.22 into Equation 8.2 leaves a straightforward numerical integration over the front face which can be rapidly and readily evaluated.

Problems arise when applying the Kirchhoff boundary condition when the surface has significant thickness, is small compared to wavelength, or has a surface impedance which varies rapidly (spatially). Problems also arise for oblique sources and receivers. In the following paragraphs, these problems are highlighted and discussed.

When a surface becomes very deep, then it is possible for second order reflections to occur. These second order reflections are not modelled by the Kirchhoff approximation. This is illustrated in Figure 8.13 for a couple of triangles. A simple Kirchhoff model would predict significant grazing energy reflected from this surface from the middle of the surface, because it only models the first order reflections which result in grazing angle propagation. In reality, however, second order reflections mean that this scattered energy returns back towards the source. To prevent this problem, the Kirchhoff boundary conditions should only be applied to surfaces whose surface gradients are not too steep. It is generally assumed that when the surface is steeper than about 30–40°, then the prediction method is likely to become inaccurate.

When the surface becomes small compared to wavelength, the surface pressures on the rear of the panel become significant, and the assumption of zero pressure on the rear can be inaccurate. It is the problem of assuming zero pressure on the rear of the panel that can cause the predictions to become inaccurate if the angle of incidence or reflection becomes too large for finite sized surfaces. Furthermore, inaccuracies can occur because the scattering from the edges is not modelled, as the pressure on the edges is also assumed to be zero. Neglecting edge diffraction will also be more problematical for oblique sources and receivers.

A surface which has a non-uniform surface impedance, where the impedance variation is rapid, can also cause problems. Consider the hybrid diffuser shown as an insert in Figure 8.14. The dark patches are absorbent ($R = 0$), and the light patches
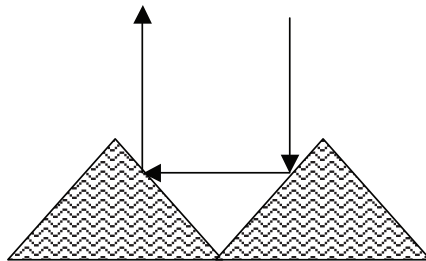
Figure 8.13 Example of a second-order reflection from a set of triangles. This reflection will not be properly modelled by the Kirchhoff boundary conditions.
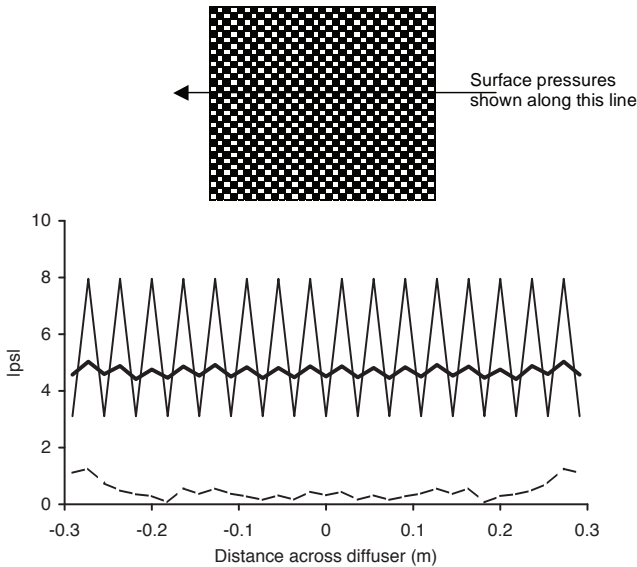
Figure 8.14 Surface pressures for a BEM compared to the Kirchhoff boundary conditions. Hybrid surface made up of a periodic arrangement of hard (white) and soft (black) patches as shown. The pressure distribution is shown for a line through the middle of the surface as indicated:
———— Kirchhoff boundary conditions;
━━━━ front pressure, thin panel BEM; and
– – – rear pressure, thin panel BEM.

reflective ($R = 1$). The figure also shows the surface pressures predicted by a BEM, and these are compared to the Kirchhoff boundary conditions. The Kirchhoff boundary conditions predict a rapidly fluctuating pressure distribution due to the arrangement of hard and soft patches. The more accurate BEM shows that mutual interactions across the surface significantly alter the pressure distribution, smoothing out the variation across the surface. This inaccuracy is not only a concern for the surface pressure calculation. If the far field polar response is considered, the Kirchhoff model in this case is most inaccurate.
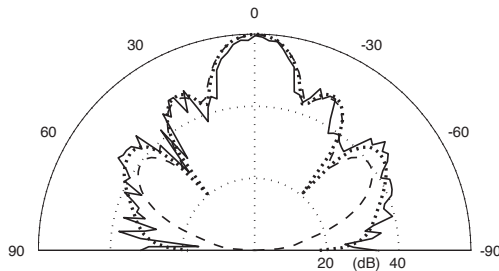
Figure 8.15 Pressure scattered from a plane surface. Comparing the accuracy of the – – – Kirchhoff solution to ······· BEM and ———— Experiment. Normalized to incident pressure at each receiver and offset by 65.5 dB for plotting (data from Cox[12]).
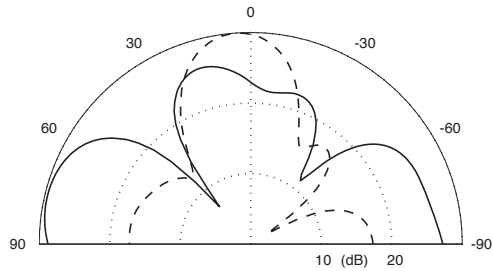
Figure 8.16   Pressure scattered from a Schroeder diffuser at a low frequency using two
different prediction models:
——— thin panel BEM and
– – – Kirchhoff.
Normalized to incident pressure at each receiver and offset by 49 dB for
plotting (data from Cox[12]).

The surface pressures are inaccurate, because there is an assumption in Equation
8.22 that the surface is large in extent. Consequently, it is necessary to have a surface
where the surface impedance spatial variation is large compared to wavelength; in other
words, the patches of different impedances should be larger than half a wavelength.
This is why the Kirchhoff boundary conditions fail for the case shown in Figure 8.14.
This would also appear to rule out the use of the Kirchhoff boundary conditions for
Schroeder diffusers, but fortunately the case of most Schroeder diffusers is less severe
than that shown in Figure 8.14 – in particular, the well width is wider for commercial
implementations, and good prediction accuracy can be achieved.

Given all the above reservations, the Kirchhoff solution is surprisingly good and
useful for many acoustic diffusers, the exception being hybrid surfaces. For a plane flat
surface, accurate results are achieved because the surface pressures are close to those
given by the Kirchhoff boundary conditions. Figure 8.15 shows a typical example.
Close to the specular reflection direction, the accuracy of the Kirchhoff solution
improves as the frequency increases. As the frequency increases, the pressure on the
rear of the panel decreases, as does the significance of edge diffraction and mutual
interactions across the surface. For single curved surfaces better accuracy is obtained,
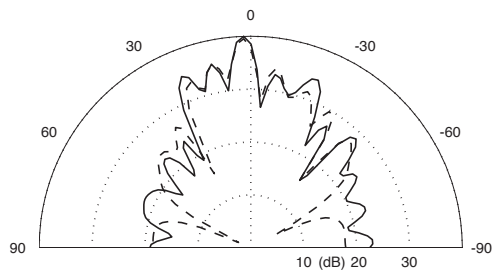
Figure 8.17   Pressure scattered from a Schroeder diffuser at a mid-high frequency using
two different prediction models:
——— thin panel BEM and – – – Kirchhoff. Normalized to incident pressure
at each receiver and offset by 48 dB for plotting (data from Cox[12]).

although there is a tendency for the Kirchhoff solution to incorrectly smooth out local minima in the polar distribution.

To use the Kirchhoff solution for Schroeder diffusers, the model of a box with a spatially-varying front face admittance must be used as described in Section 8.1.6. As the Kirchhoff boundary conditions do not allow for mutual interactions across the surface, it is not completely successful in predicting the sound field. This is most obvious at low frequencies. Figures 8.16 and 8.17 contrast the prediction accuracy achieved at low and mid-high frequencies. Again the accuracy is best near the specular reflection angle. The Schroeder diffuser tends to scatter more sound energy to the side than a plane surface, and this tends to mask the decreasing accuracy with angle that is normally found with the Kirchhoff model. For oblique receivers, the predictions become less accurate as the Kirchhoff boundary conditions break down.

8.3 Fresnel

Once the Kirchhoff boundary conditions have been assumed, the resulting numerical integration can be simplified further. This can be done either to facilitate faster computation or to enable the derivation and understanding of simple design principles. The Kirchhoff boundary conditions (Equation 8.22) are substituted into the Helmholtz–Kirchhoff integral equation (Equation 8.2). The usual relationship between surface admittance and pressure reflection coefficient, as given in Chapter 1, is also used. (Remembering that in this case the normal to the surface is pointing outwards, as is usually the case with BEM models, whereas surface admittance is normally defined with an inwardly pointing normal.) Combining these equations gives the following formulation:

$$p(\mathbf{r}) = p_i(\mathbf{r}, \mathbf{r}_0) + \int_s p_i(\mathbf{r}_s, \mathbf{r}_0)[1 + R(\mathbf{r}_s)]\left[\frac{\partial G(\mathbf{r}, \mathbf{r}_s)}{\partial n(\mathbf{r}_s)} - G(\mathbf{r}, \mathbf{r}_s)jk\cos(\psi)\frac{(R(\mathbf{r}_s)-1)}{(R(\mathbf{r}_s)+1)}\right]ds \quad (8.23)$$

where ψ is the angle of incidence. It is assumed that the receiver is sufficiently far from the surface so that the differential of the Green's function can be approximately given by:

$$\frac{\partial G(\mathbf{r}, \mathbf{r}_s)}{\partial n(\mathbf{r}_s)} \approx -jkG(\mathbf{r}, \mathbf{r}_s)\cos(\theta) \quad (8.24)$$

where θ is the angle of reflection. This relation is true for both the 2D and 3D Green's functions. Combining Equations 8.23 and 8.24 gives:

$$p(\mathbf{r}) = p_i(\mathbf{r}, \mathbf{r}_0) - jk\int_s p_i(\mathbf{r}_s, \mathbf{r}_0)[1 + R(\mathbf{r}_s)]G(\mathbf{r}, \mathbf{r}_s)\left[\cos(\theta) + \cos(\psi)\frac{(R(\mathbf{r}_s)-1)}{(R(\mathbf{r}_s)+1)}\right]ds \quad (8.25)$$

Fresnel diffraction is a method normally designed to work with non-absorbing panels, i.e. $R = 1$. In that case Equation 8.25 simplifies further:

$$p(\mathbf{r}) = p_i(\mathbf{r}, \mathbf{r}_0) - 2jk\int_s p_i(\mathbf{r}_s, \mathbf{r}_0)G(\mathbf{r}, \mathbf{r}_s)\cos(\theta)ds \quad (8.26)$$

For simplicity, just the 3D case will be considered, although the findings below are readily translated into a 2D representation. Consider a point source some way from a

planar diffuser, so the incident pressure p_i is given by the Green's function. It is necessary to come up with approximations for the distances $|\mathbf{r}_s - \mathbf{r}_0|$ and $|\mathbf{r} - \mathbf{r}_s|$. By considering the geometry shown in Figure 8.1 with the diffuser in the $y = 0$ plane, and a simple binomial expansion, it is possible to show that these distances are given by:

$$|\mathbf{r}_s - \mathbf{r}_0| \approx |\mathbf{r}_0| - \frac{x_0 x_s + z_0 z_s}{|\mathbf{r}_0|} + \frac{x_s^2 + z_s^2}{|\mathbf{r}_0|} \tag{8.27}$$

$$|\mathbf{r} - \mathbf{r}_s| \approx |\mathbf{r}| - \frac{x x_s + z z_s}{|\mathbf{r}|} + \frac{x_s^2 + z_s^2}{|\mathbf{r}|} \tag{8.28}$$

If Equations 8.27 and 8.28 are substituted into Equation 8.26, the following expression is obtained for the scattered pressure:

$$p_s(\mathbf{r}) \approx -\frac{jk}{8\pi^2} \frac{e^{-jk(r_0 + r)}}{r r_0} \cos(\theta) \iint e^{jk \frac{x x_s + z z_s + x_s^2 + z_s^2}{r}} e^{jk \frac{x_0 x_s + z_0 z_s + x_s^2 + z_s^2}{r_0}} dx_s dz_s \tag{8.29}$$

It has been assumed that the variation in $|\mathbf{r}_s - \mathbf{r}_0|$ and $|\mathbf{r} - \mathbf{r}_s|$ in the denominator of the integral is negligible compared to the variation in the phase of the complex exponential; an assumption often applied in optics. This enables the denominator of the Green's function to be moved outside the integral. Similar arguments allow the $\cos(\theta)$ factor to be moved outside the integration as well.

The phase terms of the complex exponentials are quadratic in x_s and z_s and so it is not possible to provide an analytical solution to this integration. In the past, this was overcome by using the Fresnel integrals, which were numerical solutions of the above functional form, which were readily available in tables. Nowadays, however, there is little point in using Fresnel integrals as computer power has increased to such an extent that the Kirchhoff approximation might as well be used. There are, however, some neat and simple short cuts to calculating the above integration suggested by Rindel,[14] which could be used if speed is at a premium. The Fresnel solution does, however, lead the discussion to far field prediction models, which are key to understanding diffuser design. Consequently, the discussion now continues with a far field solution.

8.4 Fraunhofer or Fourier solution

This solution is only valid in the far field, when both source and receiver are some distance from the surface. Then it is possible to neglect the quadratic terms in the integration in Equation 8.29 to obtain:

$$p_s(\mathbf{r}) \approx -\frac{jk}{8\pi^2} \frac{e^{-jk(r_0 + r)}}{r r_0} \cos(\theta) \iint e^{jk \frac{x x_s + z z_s}{r}} e^{jk \frac{x_0 x_s + z_0 z_s}{r_0}} dx_s dz_s \tag{8.30}$$

For a planar surface, this then gives an analytical equation that can be solved. Assuming the panel is $2a$ long in the x-direction, and $2b$ long in the z-direction, the scattering is given by two sinc functions:

$$p_s(\mathbf{r}) \approx -\frac{jkab}{2\pi^2} \frac{e^{-jk(r_0+r)}}{rr_0} \cos(\theta) \, sinc\left(k\left(\frac{x}{r}+\frac{x_0}{r_0}\right)a\right) sinc\left(k\left(\frac{z}{r}+\frac{z_0}{r_0}\right)b\right) \tag{8.31}$$

where $sinc(\theta) = \sin(\theta)/\theta$. (Note some definitions of sinc() contain an explicit factor of π, but that is not being used here.) This is a result familiar from optics and signal processing. The Fourier transform of a rectangular or top hat function gives a sinc() response. Equation 8.31 enables quick estimations of the far field scattering from a rigid flat surface and is very fast.

While the above case is interesting, the Fraunhofer solution is arguably going to be most useful in analyzing surfaces which do not have uniform reflection coefficient. The most obvious example is the Schroeder diffuser which can be modelled as having a spatially-varying admittance on the front surface of a box. To carry out this analysis, it is necessary to return to Equation 8.25 and to apply the distance approximations outlined above. For conciseness, consider just the scattered pressure:

$$p_s(\mathbf{r}) = -\frac{jk}{16\pi^2} e^{-jk(r+r_0)} \iint e^{jk\frac{x_0x_s+z_0z_s}{r_0}} \left[1+R(\mathbf{r}_s)\right] e^{jk\frac{xx_s+zz_s}{r}} \times \tag{8.32}$$

$$\left[\cos(\theta) + \cos(\psi)\frac{(R(\mathbf{r}_s)-1)}{(R(\mathbf{r}_s)+1)}\right] dx_s dz_s$$

To simplify the analysis, just normal incidence sound will be considered; furthermore, it will be assumed that the surface admittance variation is in the x-direction only. It is possible to keep all the terms included, but the equations become rather long and the key points of the analysis are lost in a forest of symbols. With these simplifications, it can be shown that the scattering is given by:

$$p_s(\mathbf{r}) = -\frac{jk}{8\pi^2} e^{-jk(r+r_0)} sinc\left(\frac{kb}{r}\right) \times \tag{8.33}$$

$$\left\{\int_{-a}^{a} R(\mathbf{r}_s) e^{jkx_s \sin(\theta)} \left[\cos(\theta)+1\right] dx_s\right\} + \left\{\int_{-a}^{a} e^{jkx_s \sin(\theta)} \left[\cos(\theta)-1\right] dx_s\right\}$$

The term with the $[\cos(\theta) - 1]$ term is usually less than the term with the term $[\cos(\theta) + 1]$, especially away from grazing angles. Consequently, it can be ignored. This leads to a scattered pressure of:

$$p_s(\mathbf{r}) = -\frac{jk}{8\pi^2} e^{-jk(r+r_0)} sinc\left(\frac{kb}{r}\right) \left[\cos(\theta)+1\right] \int_{-a}^{a} R(\mathbf{r}_s) e^{jkx_s \sin(\theta)} dx \tag{8.34}$$

This is essentially the equation used by Schroeder in the design of phase grating diffusers, although he derived his equations following a different philosophy. Furthermore, there are some additional factors outside the integral. Several authors neglect the $[\cos(\theta) + 1]$, and this simplified form is often called a Fourier theory because the integration is essentially a Fourier transform.
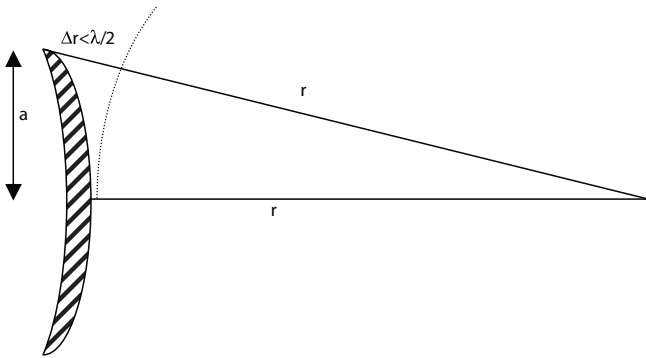
Figure 8.18 Standard construction for determining near field extent.

8.4.1 Near and far field

As the analysis is now considering a far field prediction model, it is expedient to define what the near and far field mean. Unfortunately, with diffusers the location of the near and far field is not as clear cut as for simple pistonic radiators, which is the case most often cited in text books. The far field is defined as the region where the difference between minimum and maximum path lengths from the panel to the receiver is small compared to the wavelength. In this region, all points on the panel are effectively at the same distance from the receiver.[15] This is illustrated in Figure 8.18. For diffusers there is an added complication that both the source and receiver need to be considered but to simplify discussions it will be assumed that the source is always at infinity. There is also a second requirement for the far field, which is that the receiver distance should be large compared to wavelength. This is, however, not usually the critical requirement for the geometries that occur with diffusers. Frequencies where the wavelength is large enough for this to be a consideration are usually below the lower frequency limit at which surface roughness effects are important. This can be important when receivers are close to diffusers, as might happen in poorly designed small rooms, as discussed in Chapter 2.

In the far field, the polar response is independent of the receiver distance from the surface – this makes it a useful place to test diffusers. By considering the geometry in Figure 8.18 for a planar surface, it is possible to derive the following formulation for an on-axis receiver to be in the far field:

$$r > \frac{a^2}{\lambda} \tag{8.35}$$

Unfortunately, this far field formulation is not applicable to the case of oblique sources and receivers. As Figure 4.15 demonstrated, the true far field is only achieved for many diffusers when the receiver radius is many hundreds of metres! For further discussion of this issue, see Section 4.1.1.
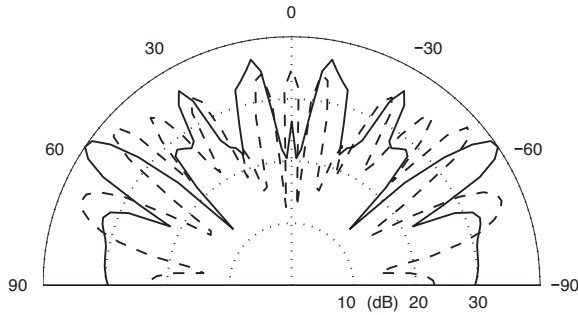
Figure 8.19   Scattered pressure from a surface. Comparison between ——— BEM and
– – – Fraunhofer solution in the near field. Normalized to incident pressure
at each receiver and offset by 49.6 dB for plotting (data from Cox[12]).

8.4.2 Fraunhofer theory accuracy

Provided sources and receivers are in the far field, for plane and Schroeder surfaces the accuracy of the Fraunhofer theory is similar to the Kirchhoff solution. So if the results in Figure 8.15 were predicted with the Fraunhofer solution, similar results to the Kirchhoff solution would be obtained. Consequently, in the far field the limiting factor for accuracy is the Kirchhoff boundary conditions. Where the Kirchhoff model fails, at low frequencies and for oblique sources and receivers, so does the Fraunhofer method.

Differences between Kirchhoff and Fraunhofer solutions occur when the receiver is in the near field, and this is true for nearly all diffusers. Consequently, high frequency predictions can become inaccurate as the near field extends further at higher frequency – a fact that can often surprise the unwary! Figure 8.19 shows the scattering from an N = 11 Schroeder diffuser in the near field. It is assumed the BEM model is accurate, and consequently this shows that the inaccuracies in the Fraunhofer model are significant at this distance. Figure 8.20 shows the same situation, but now the receiver is 50 m from the diffuser, which is safely in the far field. At these distances the Fraunhofer solution is as accurate as the Kirchhoff model. It is not often, however, that application realistic sources and receivers are this far from the panel. In diffuser design, however,
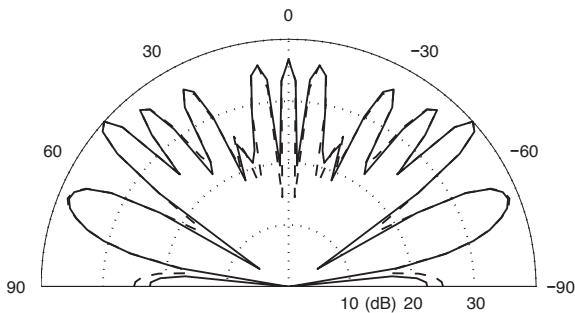
Figure 8.20   Scattered pressure from a surface. Comparison between ——— Kirchhoff and
– – – Fraunhofer solution in the far field. Normalized to incident pressure
at each receiver and offset by 77.6 dB for plotting (data from Cox[12]).

the usual assumption is that a good far field diffuser will also work in the near field, as discussed in Chapter 4.

8.5 Finite difference time domain (FDTD)[16]

Finite difference time domain (FDTD) is a widely used simulation technique in electro-magnetism and is becoming increasingly popular in acoustics. Both easy to understand and implement, it can cover a wide frequency range within a single prediction. It uses volumetric rather than surface meshes and can give accurate predictions of scattering.[17] (Chapter 2 used FDTD to generate pictures of wavefronts reflecting from various surfaces.) Figure 8.21 shows the scattering from a Schroeder diffuser predicted using three different models and illustrates that, especially near the specular reflection angle, the FDTD gives accurate results. By directly giving the impulse response, it is natural to evaluate the temporal dispersion diffusers generate using this method, however the interpretation of this data is not yet well established. Furthermore, one of the biggest strengths of FDTD, the simulation of systems that are time-variant, still remains unexplored.

   The main strength of FDTD is that it is an extremely intuitive technique so users can easily write and debug their own codes. Its main weakness is that the entire comput-ational domain must be meshed, and the spacing of the mesh must be small compared to the smallest wavelength and the physical features being modelled. Consequently, a very large system of equations must be considered which results in very long solution times. Near to far field transformations combined with absorbing boundary conditions can help to overcome this problem in some particular cases. The first technique (near to far field transformation) requires some post processing, and the second one (absorbing boundary conditions) can complicate the code, losing the simplicity of the prediction model.

   In the case of acoustics, the conservation of momentum and continuity equations are transformed to central-difference equations, obtaining update formulations for the
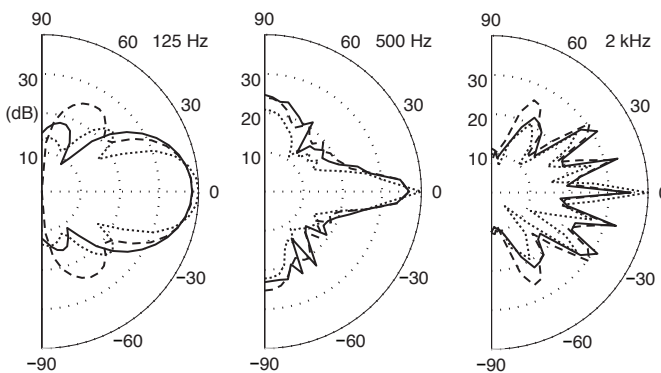
Figure 8.21   Scattered pressure level from a quadratic residue diffuser in the far field for three prediction models:
────── FDTD;
– – – BEM; and
------- FEA.
Three one-third octave bands as labelled on charts.

sound pressure and particle velocity. The equations are solved in a leapfrog manner; in other words, the sound pressure is solved at a given instant in time, then the particle velocity field is found at the next instant in time, and the process is repeated over and over again.

In 1966, Yee[18] described the first space-grid time-domain numerical technique in electromagnetism. Meloney and Cummings[19] adapted the method for acoustics based on the conservation of momentum and continuity equations:

$$\frac{\partial p}{\partial t} + \frac{(\vec{\nabla} \boldsymbol{u})}{K_e} = 0 \tag{8.36}$$

$$\vec{\nabla} p + \rho_0 \frac{\partial \boldsymbol{u}}{\partial t} = 0 \tag{8.37}$$

where p is the sound pressure, $\boldsymbol{u} = (u_x, u_y)$ is the particle velocity vector, ρ_0 is the density of the medium and K_e $(=1/\rho_0 c^2)$ is the bulk modulus of the medium.

For the sake of simplicity, only 2D schemes are considered here. Therefore, Equations 8.36 and 8.37 can be written as follows

$$\frac{\partial p}{\partial t} + \frac{1}{K_e}\left(\frac{\partial u_x}{\partial x} + \frac{\partial u_y}{\partial y}\right) = 0 \tag{8.38}$$

$$\frac{\partial p}{\partial x} + \rho_0 \frac{\partial u_x}{\partial t} = 0 \tag{8.39}$$

$$\frac{\partial p}{\partial y} + \rho_0 \frac{\partial u_y}{\partial t} = 0 \tag{8.40}$$

The sound pressure and particle velocity are considered at the points illustrated in Figure 8.22. Superscripts represent the time index, and the subscripts the spatial indices, namely:

$$p_{i,j}^{n+\frac{1}{2}} = p(i\,\Delta x, j\,\Delta y, (n+\tfrac{1}{2})\,\Delta t) \tag{8.41}$$

$$ux_{i+\frac{1}{2},j}^{n} = u_x((i+\tfrac{1}{2})\,\Delta x, j\,\Delta y, n\,\Delta t) \tag{8.42}$$

$$uy_{i,j+\frac{1}{2}}^{n} = u_y(i\,\Delta x, (j+\tfrac{1}{2})\,\Delta y, n\,\Delta t) \tag{8.43}$$

where Δx and Δy are the spatial interval in the x and y directions and Δt is the time interval between successive calculations.

The spatial grids are staggered in space to minimize the significance of higher order terms when discretizing spatial and time derivatives. For instance, the mesh for the x component of the particle velocity is shifted a distance of $\Delta x/2$ with respect to the pressure mesh. The same goes for the time mesh; the particle velocity meshes are shifted $\Delta t/2$ in
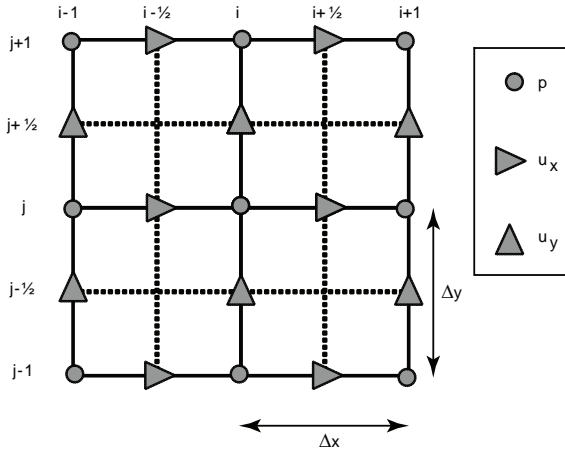
Figure 8.22 Position of pressure and particle velocity fields in an FDTD mesh (u_x is represented with a horizontal arrow while u_y is represented with a vertical arrow).

time with respect to the pressure mesh. This arrangement is termed a leapfrog scheme.

Then, the spatial and time derivatives of pressure and particle velocity can be approximated by central finite difference equations. For instance, the pressure derivative with respect to x is given by:

$$\frac{\partial p}{\partial x}\bigg|_{x=x_0} \approx \frac{p\left(x_0 + \frac{\Delta x}{2}\right) - p\left(x_0 - \frac{\Delta x}{2}\right)}{\Delta x} + O\left[(\Delta x)^2\right] \tag{8.44}$$

Using this approach, Equations 8.41–8.43 can be transformed into a set of update formulations which are used to obtain pressure and particle velocity:

$$p_{i,j}^{n+\frac{1}{2}} = p_{i,j}^{n-\frac{1}{2}} - \frac{1}{K_e}\Delta t\left(\frac{ux_{i+\frac{1}{2},j}^{n} - ux_{i-\frac{1}{2},j}^{n}}{\Delta x} + \frac{uy_{i,j+\frac{1}{2}}^{n} - uy_{i,j-\frac{1}{2}}^{n}}{\Delta y}\right) \tag{8.45}$$

$$ux_{i+\frac{1}{2},j}^{n+1} = ux_{i+\frac{1}{2},j}^{n} - \frac{\Delta t}{\rho_0}\left(\frac{p_{i+1,j}^{n+\frac{1}{2}} - p_{i,j}^{n+\frac{1}{2}}}{\Delta x}\right) \tag{8.46}$$

$$uy_{i,j+\frac{1}{2}}^{n+1} = uy_{i,j+\frac{1}{2}}^{n} - \frac{\Delta t}{\rho_0}\left(\frac{p_{i,j+1}^{n+\frac{1}{2}} - p_{i,j}^{n+\frac{1}{2}}}{\Delta y}\right) \tag{8.47}$$

All particle velocity computations are calculated and stored in memory for a particular time point using the previously stored values of the pressure. Then all the pressure computations are calculated and stored in memory using the previously calculated values of particle velocity. The cycle can be repeated as many times as needed to explore the changing sound field over time.

8.5.1 Stability: spatial and time steps

To ensure numerical convergence, the time step should be small enough to describe the wave propagation. The limit relationship between the spatial and time steps is given by the so-called Courant number, *s*, which in 2D can be defined as follows:

$$s = c\Delta t \sqrt{\left(\frac{1}{\Delta x}\right)^2 + \left(\frac{1}{\Delta y}\right)^2} \leq 1 \tag{8.48}$$

In addition, the maximum element size used in discretization is determined by the frequency, with at least 10 elements per wavelength being required for adequate accuracy. Thus, at high frequencies, a large numerical problem has to be solved. For instance, in room acoustics the upper limit of interest for predictions is often the 5 kHz one-third octave band. The highest frequency in the band is about 5,500 Hz, which leads to a spatial discretization step of 6 mm and a sampling frequency of 80 kHz to fulfil the Courant criteria.

8.5.2 Including objects in the integration area

Early papers in electromagnetism simulated objects by simply making the propagation media constants space dependent. The best approaches for modelling acoustic objects such as diffusers and absorbers are still being developed. Chapter 5 discussed time domain approaches to modelling sound propagation through porous absorbers, which might offer one approach. In the case of walls, there are several approaches depending on the different models used to simulate the propagation of vibrations in solids.[20] Drumm[21] coupled acoustic FDTD and finite element analysis (FEA) models to predict surface reflections; although the use of FEA significantly increases computation time.

   A perfectly rigid wall is the easiest case to deal with and can be modelled by setting some of the particle velocity points in the mesh to zero for the whole calculation run. Another possibility is to use an impedance boundary condition.[22] Assuming a locally reacting boundary, the particle velocity normal to the surface and the pressure can be related by the acoustic impedance. The simplest case is to assume the boundary is purely resistive. A more correct time-domain representation of a complex surface acoustic impedance is problematic because the impedance may not always be a causal function.[23] (Causal in this context means that knowledge of future sound field values are required before they are available.) One solution to this is to numerically fit an implementable filter which approximates the true impedance function. It is often the case that the true broadband impedance function is unknown anyway. For instance, it is possible that only the real part is known over a restricted frequency range from absorption coefficient values. In this case, the unknown parts can often be chosen to ensure the surface impedance function is causal. It is also important that the impedance function is also short in time to minimize the storage requirements for surface pressures and velocities. Using pressure reflection coefficients may offer an alternative approach with guaranteed causality,[24] however the reflection coefficient which should be used depends on the incident sound field and a physically correct scheme has yet to be formulated. Renterghem *et al.*[25] demonstrated that simple complex impedances can be modelled in a FDTD scheme using a mass-damper-spring

equation. Work continues to find a more accurate way of representing surfaces without a high computational cost.[26]

A final point of note is that when geometries are not aligned with the axis, for instance if there are curved surfaces, then conformal methods are required which are much more complicated.

8.5.3 Excitation

There are several ways to introduce sources into the mesh. In the first papers in electromagnetism, the excitation was introduced as an initial condition in the whole integration area. Researchers focussed on the scattering caused by perfect conductors, equivalent to rigid walls in acoustics, and so they took a plane wave as an initial condition and observed how it was transformed by the particular objects included in the simulation domain. Another possibility is to include one or more point sources within the mesh. This means that the evolution of at least one point of the mesh will not be given by the formulations given previously, but by an external driving function $g(t)$. For instance:

$$p_{i_{source}, j_{source}}^{n+\frac{1}{2}} = g(t) \tag{8.49}$$

Sources defined this way reflect the sound travelling in the mesh. To avoid these reflections, transparent sources must be used.[27]

There are many options for the source function $g(t)$. Gaussian pulses might be used because of their wide frequency range. Ricker wavelets (also known as Mexican-hat wavelets) are extremely useful because they do not introduce large-amplitude frequency components near D.C., which can be resonant with the mesh.

A Ricker wavelet is given by:

$$W(t) = -\sqrt{2}\,\pi\,f_{cent}\left[\left(\sqrt{2}\,\pi\,f_{cent}t\right)^2 - 1\right]\exp\left[-\frac{1}{2}\left(\sqrt{2}\,\pi\,f_{cent}t\right)^2\right] \tag{8.50}$$

where f_{cent} is the central frequency. In fact, the Ricker wavelet is nothing but the second derivative of a Gaussian function. Figure 8.23 shows the time and frequency response for these wavelets.

More complicated excitations have also been proposed to study scattering, mainly in the field of electromagnetism, in order to avoid the use of time windowing to separate incident and reflected waves. These techniques are known as the total scattered or pure scattered field formulations. Both methods produce the same results and are equivalent to a subtraction between a normal calculation (with all the scatterers included in the integration area) and one without scatterers.

Methods for simulating directional sources needs more development. Recently, Escolano[28] has presented a simple way to obtain arbitrary directivity patterns in the far field using a set of point sources.
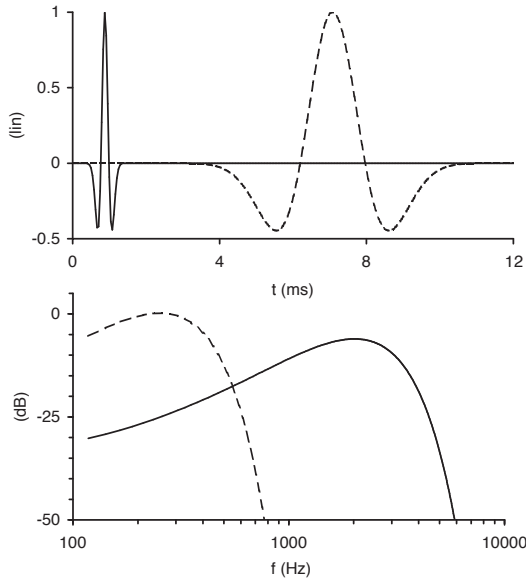
Figure 8.23   Time shifted Ricker wavelets and their spectra for a central frequency of 250 Hz and 2,000 Hz (after Redondo *et al.*[17]).

8.5.4 Anechoic boundary conditions

One of the main applications of FDTD is the analysis of scatterers. Usually an anechoic environment is desired. In order to do that, one can define the end of the integration area with an impedance equivalent to the characteristic impedance of air. In doing so, and due to inevitable small errors due to discretization, the absorption of the terminations will not be complete. To reduce the reflected waves further requires the used of perfectly matched layers (PMLs).[29] This technique defines a lossy medium in locations proximate to the boundaries, which in turn implies the modification of Equations 8.38–8.40 to include attenuation factors for each dimension considered (γ_x and γ_y), i.e.:

$$\frac{\partial p_x}{\partial t} + \gamma_x p_x + \frac{1}{K_e}\left(\frac{\partial u_x}{\partial x}\right) = 0 \tag{8.51}$$

$$\frac{\partial p_y}{\partial t} + \gamma_y p_y + \frac{1}{K_e}\left(\frac{\partial u_y}{\partial y}\right) = 0 \tag{8.52}$$

$$\frac{\partial p}{\partial x} + \rho\left(\frac{\partial u_x}{\partial t} + \gamma_x u_x\right) = 0 \tag{8.53}$$

$$\frac{\partial p}{\partial y} + \rho\left(\frac{\partial u_y}{\partial t} + \gamma_y u_y\right) = 0 \tag{8.54}$$
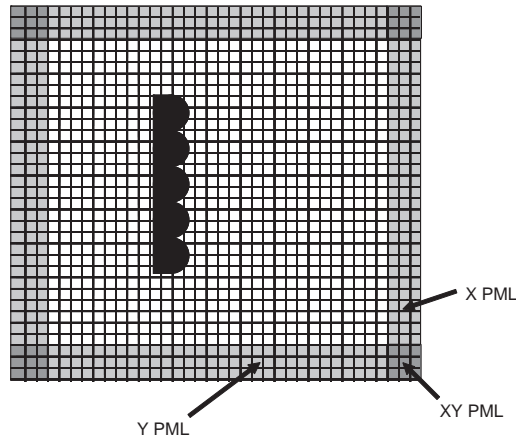
Figure 8.24 Structure of a two-dimensional PML with a test specimen in the middle.

where the sound pressure has been split into two additive components p_x and p_y that have no physical sense. The attenuation factors are zero inside the integration area, and are gradually increased in areas near the boundaries using the following expression:

$$\gamma_x = \gamma_{x\,max} \left| \frac{x - x_0}{x_{max} - x_0} \right|^n \tag{8.55}$$

where x_0 is the initial point in the PML, x_{max} is the last point of the PML, n is a number between 2 and 3, and $\gamma_{x\,max}$ is the maximum value of the attenuation factor. All these parameters should be optimized with some previous calculations.

Figure 8.24 illustrates the disposition of the different PMLs used in 2D simulations. At both the left and right sides of the grid there are x-direction PMLs ($\gamma_x \neq 0$, $\gamma_y = 0$) At both the upper and lower sides of the grid there are y-direction PMLs ($\gamma_x = 0$, $\gamma_y \neq 0$). At the four corners of the grid there is an overlap of two perpendicular PMLs. This scheme ensures the reflected sound is attenuated by at least 60 dB relative to the incident sound, provided the PML parameters are chosen correctly.

8.5.5 Near to far field transformation

One of the main weaknesses of FDTD is that the entire computational domain must be meshed. If the aim of a simulation is to obtain the sound pressure reflected by a scatterer in the far field, very large domains must be considered increasing the computational cost. To overcome this problem near field to far field transformations (NFFFT) should be used. The standard transformation is based on the contour equivalence theorem. In this approach, the scattered pressure field along a closed virtual contour surrounding the structure of interest is computed via FDTD and integrated over the entire contour to provide the far field response. Since the virtual surface is independent of the geometry of the scatterer which it encloses, it is usually chosen as a rectangular shape to conform to the standard Cartesian FDTD grid. As there are no sources outside the transformation

contour, the pressure at a far point can be computed via the Helmholtz–Kirchhoff integral, Equation 8.2; for further details see Taflove.[30]

8.6 Other methods

8.6.1 Time domain BEM

It is possible to formulate a transient boundary element model which operates in the time domain. The Kirchhoff integral equation and its normal derivative are used, instead of the time invariant frequency domain version, to derive surface and external point pressures. To solve the time dependent form the surface is again discretized. It can be shown from the time dependent integral equation[31–33] that the velocity potential and its derivative on the surface can then be represented by the incident velocity potential from the source plus contributions from the other elements at the current and previous times. Consequently, if initial silence is assumed, it is possible to formulate a system of equations for the velocity potential and its derivative that is marched on in time to obtain the full time history of the pressure on each element. Once the surface pressures are known, these can be propagated to find the pressure versus time response at external receiver points.

As with the constant frequency BEM, the underlying integral equation is known to possess non-unique solutions at certain frequencies. These happen for fully enclosed surfaces and are physically interpreted as cavity resonances. Despite the fact that these should be precluded by the initial conditions, they can be excited by numerical error and corrupt the external solution. This can be overcome by using the combined field integral equation.[32]

The marching on in time is an iterative process and therefore has potential for divergence. Although the actual physical system being modelled is stable, numerical inaccuracies in the discretized equations can, and often do, result in instability. The interaction matrixes have to be integrated to a high accuracy, particularly for complex real-life surfaces. The instabilities and high computational cost have prohibited widespread use of the time domain BEM.

The method has potential advantages over the constant frequency methods in that the impulse response may be generated. There is no need to separately calculate the response at many different frequencies and then combine these together to get the full frequency response, and from there the impulse response. However, the model needs further development, particularly for non-rigid bodies, as the formulation of surface admittance in the time domain is ill-defined.

8.6.2 Finite element analysis

Finite element analysis (FEA)[34] uses volumetric rather than surface meshes and can give accurate predictions of scattering.[17] Figure 8.21 shows the scattering from a Schroeder diffuser predicted using FEA and illustrates that, especially near the specular reflection angle, the model gives accurate results. As a mesh is formed in a space rather than just on the surface, as was done for BEM, the method yields a much larger system of equations. However, by applying a NFFFT, it is possible to get away with meshing only the volume close to the surface.

FEA is much slower than a BEM when dealing with exterior domain acoustic

problems such as the scattering from diffusers. Unlike FDTD, FEA does not produce a simple set of equations which compensate for the computational burden of using a volumetric mesh. Where FEA does have advantages is where there is fluid and structural motion. For example, it can model the behaviour of a non-rigid diffuser which exhibits structural vibration. As this sort of diffuser is currently rare, and structural motion is usually deliberately avoided in diffuser design, the use of FEA for scattering is not the most efficient method.

8.6.3 Edge diffraction models

Edge diffraction models can be used to produce the scattering from wedges and simple shapes. For a plane rigid surface, the total field can be seen as a sum of the direct sound, specular reflections and edge diffraction components.[35,36] Consequently, it is possible to solve the scattering problem by integrating over the edges present in a diffuser. This type of method becomes rather slow if high orders of edge diffraction need be considered, as would be the case for complex surfaces. It does, however, directly lead to a sampled impulse response, and consequently is particularly useful where broadband time domain scattering needs to be calculated, or if the results are to be integrated into geometric room acoustic models.[37]

8.6.4 Wave decomposition and mode matching approaches

It is possible to carry out a decomposition of the acoustic wave knowing the spatial distribution of the diffuser. Strube[38–40] used this approach to solve the scattering from Schroeder diffusers. In Chapter 7 an example of this type of theory was used to explain the absorption from Schroeder diffusers. For that reason, this type of theory is only briefly described here. In this theory it is assumed that the diffuser structure is periodic and then it is possible to decompose the scattered wave into the different diffraction lobes using a Fourier decomposition. Then, it is possible to set up and solve simultaneous equations into the diffraction lobe scattered amplitudes. These methods offer an alternative approach to BEMs, but BEMs are considerably more useful as they can be applied to arbitrary surfaces. The modal decomposition models are particularly powerful for large arrays of periodic structures, as the size of the problem to be solved is considerably smaller under this formulation than with a BEM model.

8.6.5 Random roughness

In the theories used so far, a deterministic approach has been taken, with the surface geometry and impedance properties being modelled exactly. For large-scale surfaces with small roughness this can turn out to be a very inefficient approach for carrying out predictions. In that case, it may be advantageous to use a statistical approach, whereby the surface is only determined by some shape statistics, such as the mean square surface height and the slope probability function.[41] In diffuser design, these theories are not often useful because the size of the surface roughness is large and the sample of roughness that might be used is small in width, and so a few shape statistics are not sufficient to accurately predict the scattering from the surface. This is illustrated in Figure 8.25. The top shape is meant to generically represent deliberately designed diffusers, where the scale of the roughness is deep and relatively slow varying. In this
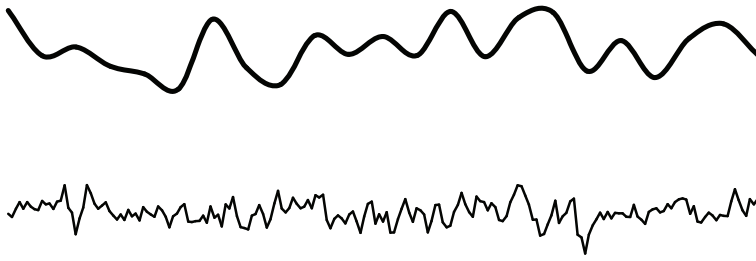
Figure 8.25   Two different randomly generated surfaces.

case, the small number of bumps on the surface will dominate the scattering in such a way that a statistical approach is not applicable. The bottom line in the figure, however, represents a more randomly rough surface, for which the theories based on a few shape statistics may be more applicable. To put it another way, there needs to be a sufficiently wide sample of the surface roughness for the shape statistics to be properly representative of the surface.

For accidental surface roughness, this statistical approach is more useful, especially as it may be impossible to get the exact geometry of all shapes in existing structures. Random rough theories are probably most commonly used in underwater acoustics, although both Cox and D'Antonio[42] and Embrechts *et al.*[43] have applied statistical approaches to diffuser scattering. In the case of Cox and D'Antonio, this was investigated with respect to the design of fractal diffusers. For Embrechts *et al.* a statistical approach was taken to investigate scattering coefficients from surfaces. These approaches usually assume the Kirchhoff boundary conditions, and so an additional limitation is that the surface gradients must not be too steep, otherwise second and high order reflections become important, and the statistical approach breaks down.

8.6.6 Boss models

Boss models are hybrid approaches.[41] They use a deterministic solution for the scattering from a single element – examples include cylinders and hemispheres – and then model the distribution of the elements in a statistical manner. Twersky developed the best known approach.[44] This theory allows high order scattering, across all frequencies, both in 2D and 3D, to be considered. Up to date versions of the theory also enable scattering from different sized bosses. One of the problems with applying this model is to represent complex surfaces by a series of regular sized bosses. In some cases this might be easy, but in the case shown at the bottom of Figure 8.25 this would be rather tricky. Torres *et al.*[45] have applied a boss model to predict scattering by hemispherical surface elements in auditoria.

8.7 Summary

In this chapter, some commonly used prediction models for scattering have been outlined and the necessary equations developed. These theories will be drawn upon in the design of diffusers, which is the subject of next three chapters.

8.8 References

1 A. J. Burton, *The Solution of Helmholtz Equation in Exterior Domains Using Integral Equations*, National Physical Laboratory Report NAC30 (1973).
2 M. Ambramowitz and I. A. Stegun (eds), *Handbook of Mathematical Functions*, Dover Publications Inc., NY (1965).
3 W. H. Press *et al.*, *Numerical Recipes*, Cambridge University Press, Cambridge (1989).
4 H. A. Schenck, "Improved integral formulation for acoustic radiation problems", *J. Acoust. Soc. Am.*, **55**, 41–58 (1968).
5 T. J. Cox, "Predicting the scattering from reflectors and diffusers using 2D boundary element methods", *J. Acoust. Soc. Am.*, **96**(2), 874–8 (1994).
6 T. Terai, "On the calculation of fields around three-dimensional objects by integral equation method", *J. Sound Vib.*, **68**, 71–100 (1980).
7 T. W. Wu, "A direct boundary element method for acoustic radiation and scattering from mixed regular and thin bodies", *J. Acoust. Soc. Am.*, **97**, 84–91 (1995).
8 N. Nishimura. "Fast multipole accelerated boundary integral equation methods", *Applied Mechanics Reviews*, **55**(4) 299–324 (2002).
9 Y. W. Lam, "A boundary integral formulation for the prediction of acoustic scattering from periodic structures", *J. Acoust. Soc. Am.*, **105**(2), 762–9 (1999).
10 F. Bloch,"Uber die Quantenmechanik der Elektronen in Kristallgittern", *Z. Phys.*, **52**, 555–600 (1928).
11 T. J. Cox and Y. W. Lam. "Evaluation of methods for predicting the scattering from simple rigid panels", *Applied Acoustics*, **40**, 123–40 (1993).
12 T. J. Cox, "Objective and Subjective Evaluation of Reflection and Diffusing Surfaces in Auditoria", PhD thesis, University of Salford (1992).
13 L. J. Xiao, T. J. Cox and M. R. Avis, "Active diffusers: Some prototypes and 2d measurements", *J. Sound Vibr.*, **285**(1–2), 321–39 (2005).
14 J. H. Rindel, "Attenuation of sound reflections due to diffraction", *Proc. Nordic Acoustical Meeting*, 257–60 (1986).
15 L. E. Kinsler, A. R. Frey, A. B. Coppens and J. V. Sanders, *Fundamentals of Acoustics*, 4th edn, John Wiley & Sons (2000).
16 The authors would like to acknowledge J. Redondo, who helped write this section.
17 J. Redondo, R. Pico, B. Roig and M. R. Avis, "Time domain simulation of sound diffusers using finite-difference schemes", *Acta Acustica uw Acustica*, **93**(4), 611–22 (2007).
18 K. S. Yee, "Numerical solution of initial boundary value problems involving Maxwell's equations in isotropic media", *IEEE Transactions on Antennas Propag.*, **14**, 302–7 (1966).
19 J. G. Meloney and K. E. Cummings, "Adaptation of FDTD techniques to acoustic modelling", *11th Annu. Rev. Prog. Applied Computational Electromagnetics*, **2**, 724 (1995).
20 P. Fellinger, R. Marklein, K. J. Langenberg, and S. Klaholz, "Numerical modelling of elastic wave propagation and scattering with EFIT – Elastodynamic finite integration technique", *Wave Motion*, **21**, 47–66 (1995).
21 I. A. Drumm, "Hybrid finite Element / finite difference time domain technique for modelling the acoustics of surfaces within a medium", *Acta Acustica uw Acustica*, **93**, 804–9 (2007).
22 D. Botteldooren, "Finite-difference time-domain simulation of low-frequency room acoustic problems", *J. Acoust. Soc. Am.*, **98**, 3302–8 (1995).
23 C. K. W. Tam and L. Auriault, "Time-Domain impedance boundary conditions for computational aeroacoustics", *AIAA Journal*, **34**(5), 917–23 (1996).
24 H. Jeong, B. Horner, and Y.W. Lam, "The modelling of frequency dependent boundary conditions in FDTD simulation of concert hall acoustics", *Proc. 19th ICA Madrid* (2007).
25 T. Van Renterghem and D. Botteldooren, "Numerical simulation of the effect of trees on downwind noise barrier performance", *Acta Acustica uw Acustica*, **89**, 764–78 (2003).
26 J. Escolano, F. Jacobsen and J.J. López, "An efficient realization of frequency dependent boundary conditions in a finite-difference time-domain model", *J. Sound Vib.*, 316(1-5). 234-47 (2008).
27 J. B. Schneider, C. L. Wagner and S. L. Broschat, "Implementation of transparent sources embedded in acoustic finite-difference time domain grids", *J. Acoust. Soc. Am.*, **133**(1), 136–42 (1998).

28 J. Escolano, J.J. López and B. Pueo, "Directive sources in acoustic discrete-time domain simulations based on directivity diagrams", *J. Acoust. Soc. Am.*, **121**(6), EL256-62 (2007).

29 X. Yuan, D. Borup, J. W. Wiskin, M,. Berggren, R. Eidens and S. Johnson, "Formulation and validation of Berenger's PML absorbing boundary for the FDTD simulation of acoustic scattering", *IEEE Transactions on Ultrasonics, Ferroelectrics, and Frequency Control*, **44**(4), 816–22 (1997).

30 A. Taflove, *Computational Electrodyamics, The Finite-Difference Time-Domain Method*, Artech House (2005).

31 Y. Kawai and T. Terai, "A numerical method for the calculation of transient acoustic scattering from thin rigid plates", *J. Sound. Vib.*, **141**, 83–96 (1990).

32 A. A. Ergin, B. Shanker and E. Michielssen, "Analysis of transient wave scattering from rigid bodies using a Burton–Miller approach", *J. Acoust. Soc. Am.*, **106**(5), 2396–404 (1999).

33 J. A. Hargreaves and T. J. Cox, "A stable time domain BEM for diffuser scattering", *Proc. 19th ICA*, Madrid, RBA-05-019 (2007).

34 D. G. Crighton, A. P. Dowling, J. E. Ffowcs Williams, M. Heckl and F. G. Leppington, *Modern Methods in Analytical Acoustics, Lecture Notes*, Springer-Verlag (1992).

35 U. P. Svensson, R. I. Fred and J. Vanderkooy, "An analytical time domain model of edge diffraction", *J. Acoust. Soc. Am.*, **106**(5), 2331–44 (1999).

36 U. P. Svensson UP and P. T. Calamia, "Edge-diffraction impulse responses near specular-zone and shadow-zone boundaries", *Acta Acustica uw Acustica*, **92**(4), 501–12 (2006).

37 P. T. Calamia and U. P. Svensson, "Fast time-domain edge-diffraction calculations for interactive acoustic simulations", *EURASIP Journal on Advances in Signal Processing*, 63560 (2007).

38 H. W. Strube, "Scattering of a plane wave by a Schroeder diffuser: a mode matching approach", *J. Acoust. Soc. Am.*, **67**(2), 453–9 (1980).

39 H. W. Strube, "Diffraction by a planar, local reacting, scattering surface", *J. Acoust. Soc. Am.*, **67**(2), 460–9 (1980).

40 H. W. Strube, "More on the diffraction theory of Schroeder diffusers", *J. Acoust. Soc. Am.*, **70**(2), 633–5 (1981).

41 D. Chu and T. K. Stanton, "Application of Twersky's boss scattering theory to laboratory measurements of sound scattered by a rough surface", *J. Acoust. Soc. Am.*, **87**(4), 1557–68 (1990).

42 T. J. Cox and P. D'Antonio, "Fractal sound diffusers", *Proc. 103th Convention of the Audio Eng. Soc.*, preprint 4578, Paper K-7 (1997).

43 J. J. Embrechts, D. Archambeau and G. B. Stan, "Determination of the scattering coefficient of random rough diffusing surfaces for room acoustics applications", *Acta Acustica uw Acustica*, **87**, 482–94 (2001).

44 V. Twersky, "On scattering and reflection of sound by rough surfaces", *J. Acoust. Soc. Am.*, **29**, 209–25 (1957).

45 R. R. Torres, G. Natsiopoulos and M. Kleiner, "Room acoustics auralization with boss-model scattering, compared with a Lambert diffusion model", *Symposium on Surface Diffusion in Room Acoustics*, Liverpool (2000).

9   Schroeder diffusers

One of the most significant occurrences in diffuser design, if not the most important event, was the invention of the phase grating diffuser by Schroeder.[1,2] Apart from very simple constructions, previous diffusers had not dispersed sound in a predictable manner. The Schroeder diffuser offered the possibility of producing 'optimum' diffusion, and also required only a small number of simple design equations. D'Antonio and Konnert[3] presented one of the most readable reviews examining the far field diffraction theory underpinning Schroeder's number theoretic surfaces; they experimentally measured performance and described applications in critical listening environments. Most crucially, they commercialized Schroeder diffusers and so made them widely available. Since the publication of Reference 3, there have been many new developments which have not been brought together and documented in one place. Therefore, the intention of this chapter is to tell the whole story of Schroeder diffusers. Much of this chapter was featured as a review article in the journal *Building Acoustics*.[4]

The chapter will start by outlining a largely qualitative view of the diffuser, how it works and the basic design principles. Following this, a more detailed quantitative and theoretical analysis of the diffuser will be given. In these descriptions, the ingenuity of the original design concept should become apparent. In addition, more recent developments will be presented, illustrating weaknesses in the original design which can be overcome by modifying the design procedure, sometimes using number theory – one of Schroeder's favourite subjects. Finally, it will be shown that better phase gratings can be made using an optimization procedure.

9.1 Basic principles

The top row of Figure 9.1 shows single plane or 1D Schroeder diffusers. They consist of a series of wells of the same width and different depths. The wells are separated by thin fins. The depths of the wells are determined by a mathematical number sequence, such as the quadratic residue sequence. Single plane diffusers cause scattering in one plane, in the other direction, the extruded nature of the surface makes it behave like a plane surface. Because of this, it is normal to just consider a cross section through the diffuser (Figure 9.2) which contains the plane of maximum dispersion. Multi-plane diffusers are possible, as shown in Figure 9.1 and are discussed later in Section 9.7.

Consider a mid-frequency plane wave incident onto the diffuser. Plane wave propagation within the wells in the y-direction occurs. The plane waves are reflected from the bottom of the wells and eventually re-radiate into the space. For now, it will be assumed that there is no loss of energy. The pressure at a point external to the diffuser is
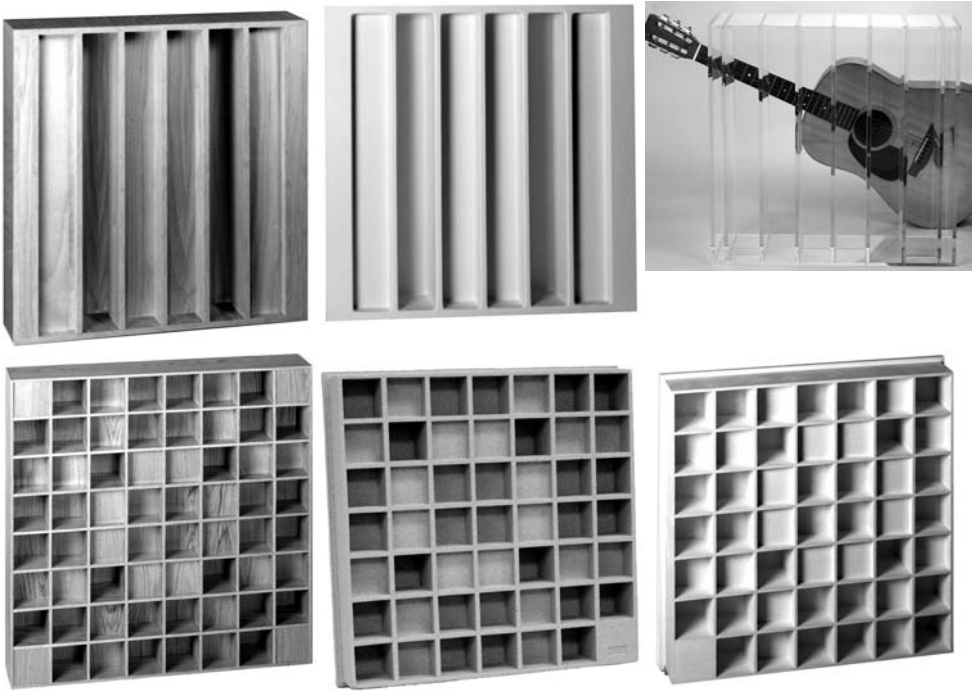
Figure 9.1 Various Schroeder diffusers. Top row: single plane or 1D diffusers made from wood, moulded plastic and plexiglass (from left to right). Bottom row: 2D diffusers made from wood, expanded polystyrene, and Glass Reinforced Gypsum (GRG) (from left to right).

therefore determined by the interference between the radiating waves from each well. All these waves have the same magnitude but a different phase because of the phase change due to the time it takes the sound to go down and up each well. Consequently, the polar distribution of the reflected pressure from the whole surface is determined by the choice of well depths. Schroeder showed that by choosing a quadratic residue sequence, the energy reflected into each diffraction lobe direction is the same. In Figure 9.3 an example of the reflection from the surface is given, as calculated by the
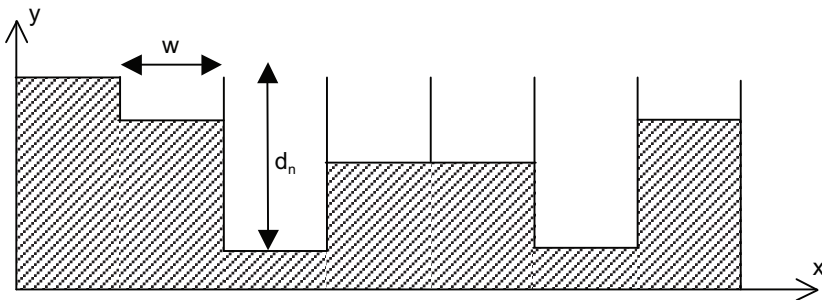
Figure 9.2 A cross-section through an $N = 7$ Quadratic Residue Diffuser (QRD®).
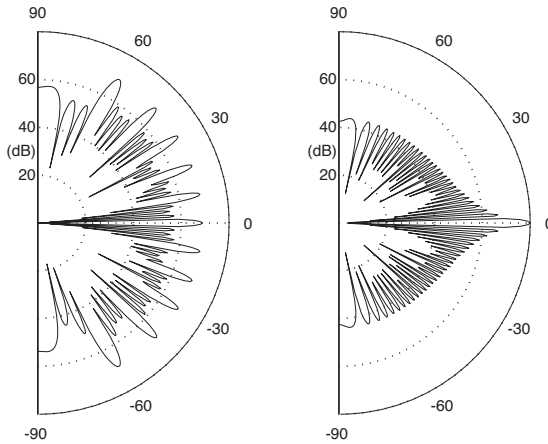
Figure 9.3 Scattered level from a Schroeder diffuser (left) and a plane surface (right) of the same size.

simplest and most approximate theory at a frequency where optimum diffusion is achieved. Eleven lobes of the same energy are found in this case. These lobes are generated because the surface is periodic.

9.2 Design equations

For the design theory to be correct, plane wave propagation within the wells must dominate. Consequently, an upper frequency for the diffusion to follow the simple design principles can be found from:

$$w = \lambda_{min} / 2 \tag{9.1}$$

where λ_{min} is the minimum wavelength before cross-modes in the wells appear, and w is the well width. Above this limit dispersion will continue to occur because these are complicated structures. Consequently, this is just a limit of applicability of a theory, and not necessarily an upper limit for the diffusion quality.

This need for plane wave propagation explains the need for fins to separate the different wells. The fins should be as narrow as possible, but not so narrow that they vibrate and cause significant losses.

A quadratic residue sequence is the most popular mathematical sequence used to form the well depths. The sequence number for the nth well, s_n, is given by:

$$s_n = n^2 \ modulo \ N \tag{9.2}$$

where modulo indicates the least non-negative remainder and is often written as *mod* for short. N is the number generator which in this case is also a prime and the number of wells per period. For example, one period of an $N = 7$ QRD has $s_n = \{0, 1, 4, 2, 2, 4, 1\}$.

Schroeder diffusers work at integer multiples of a design frequency, f_0. The design frequency is normally set as the lower frequency limit. However, it is more convenient to present formulations in terms of the corresponding design wavelength, λ_0. The depth d_n of the nth well is determined from the sequence via the following equation:

$$d_n = \frac{s_n \lambda_0}{2N} \tag{9.3}$$

The well depths consequently vary between 0 and approximately $\lambda_0/2$. The design frequency is not the lowest frequency at which the surface produces more dispersion than a plane surface, it is just the first frequency at which even energy diffraction lobes can be achieved. It has been shown that Schroeder diffusers reflect differently from a plane hard surface an octave or two below the design frequency.[5,6]

9.3 Some limitations and other considerations

Given the above equations, it is possible to design a diffuser to a desired bandwidth. There are some subtle details in the design that must be heeded to achieve the best possible diffusion.

If the period width (Nw) is too narrow, then at the first design frequency there is only one major lobe, and so this concept of even energy lobes is rather irrelevant. The period or repeat width is often significant in determining performance, especially when the repeat width is small. This is illustrated in Figure 9.4 where the scattering from diffusers of different period widths are shown. These are both $N = 7$ QRDs with a design frequency of 500 Hz. The well widths are 3 and 9 cm, which means that the period widths are 21 and 70 cm respectively. The number of periods for each diffuser is set so that the overall widths of the devices are the same for a fair comparison. For the narrow wells and period width, shown right, the low frequency limit of diffusion is
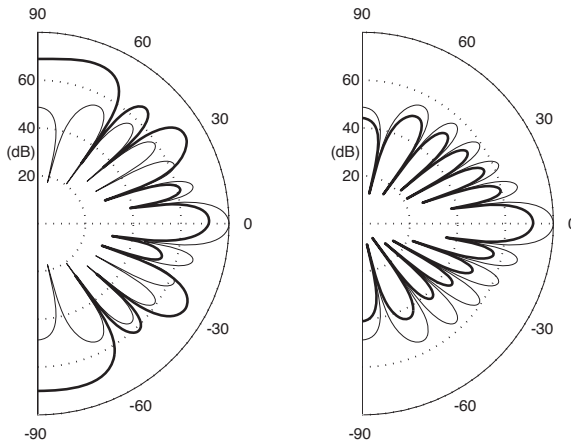
Figure 9.4 The pressure scattered from two QRDs at 1,000 Hz.
Left figure   Right figure
———— QRD well width 9 cm;   ———— QRD well width 3 cm;
———— plane surface.   ———— plane surface.
Overall width kept the same by changing number of periods.
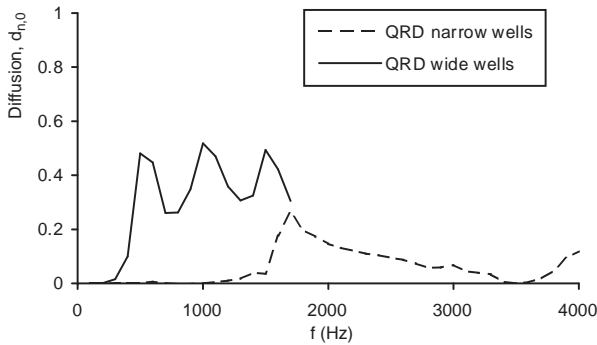
Figure 9.5 Normalized diffusion spectra for two QRDs showing that the lowest frequency
at which significant diffusion occurs can be determined by period width rather
than surface depth. The design frequency was 500 Hz.

determined by the period width and not by the maximum depth. This is illustrated in
Figure 9.5, where the normalized diffusion coefficient versus frequency is shown. The
narrow well width diffuser only starts causing significant diffusion over and above the
plane surface at 1.5 kHz, which is three times the design frequency. This is roughly
the frequency at which the first grating lobe appears and so is the lowest frequency
where significant scattering in oblique directions is achieved. For the wide well width,
the first grating lobe appears below the design frequency and so significant diffusion
is created at 500 Hz and above.

For the diffuser to behave 'optimally', the device must be periodic. The lobes are
generated by the periodicity of the surface. Without periodicity, all that the design
equations portray is the fact that in certain directions the scattering will have a similar
level. This is illustrated in Figure 9.6 where the scattering from one and multiple
periods of a diffuser is compared. The directions of similar level are marked. For the
periodic cases, the directions of similar level align with the lobes. For the single period
case, they are just points of identical level in the polar response; the points do not
align with the lobes. In this case, saying the levels are identical in some directions is
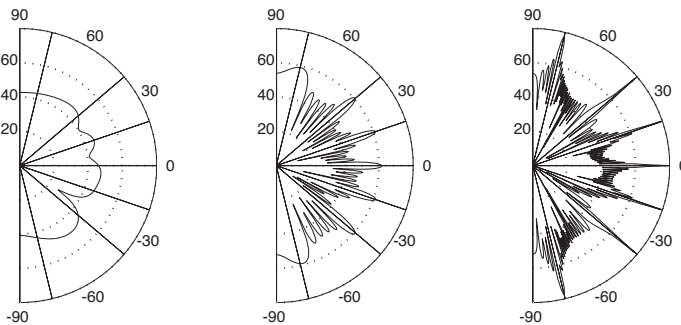
Figure 9.6 The scattering from N = 7 QRDs at 3,000 Hz for a different number of periods.
Left 1 period; middle 6 periods; right 50 periods. Locations of lobes and
directions of similar level marked by radial lines at ±76, ±40, ±19 and 0°.

almost a meaningless statement, because in most polar responses there will be angles where the scattering is identical to other angles. Consequently, using one period of the device spoils the point of using the quadratic residue sequence. Using one period therefore causes problems with the mathematical make-up and definition of Schroeder diffuser. However, the scattering from a single period diffuser is often more uniform than a periodic device, as Figure 9.6 shows. This issue will be returned to later when modulation is discussed.

If too many periods are included then the grating lobes become rather narrow; this leads to uneven scattering because there are large nulls present (see Figure 9.6). It must be remembered, however, that manufacturing and installation constraints are likely to mean that a narrow base shape with a large number of repeats is going to be the cheapest to build. Periodicity might also be preferred visually.

The points made in the last three paragraphs mean that the best design is one with a small number of periods, say five, to ensure periodicity, but with the diffraction lobes not too narrow. The period width must be kept large to ensure a large number of grating lobes, which then implies a reasonably large number of wells per period. Making the well width wide does not work as it can cause problems with specular-like reflections at high frequencies. Alternatively, modulation schemes can be used as discussed later in the chapter.

From the maximum frequency calculated from Equation 9.1, it might appear as though a Schroeder diffuser should have the narrowest wells possible to get the widest frequency range, but difficulty/cost of manufacture and absorption need to be considered. As the diffuser wells become more narrow the viscous boundary layer becomes significant compared to the well width and the absorption increases (see Section 9.8). Consequently, practical well widths are at least 2.5 cm, and usually around 5 cm.

The choice of prime number is limited by manufacturing cost, low frequency performance and critical frequencies. For a given maximum depth d_{max}, the design frequency achieved is:

$$f_0 = \frac{s_{max}}{N}\frac{c}{2d_{max}} \tag{9.4}$$

where s_{max} is the largest number in the quadratic residue sequence. The ratio of the largest sequence number to the prime number determines the low frequency efficiency of the device.[7] To take two examples: $N = 7$, $s_{max}/N = 4/7$; $N = 13$, $s_{max}/N = 12/13$. Consequently, an $N = 7$ diffuser will have a design frequency nearly an octave below that of an $N = 13$ diffuser. It is possible, however, to manipulate some sequences and increase the bass response. A constant phase shift can be introduced to yield a better bass response:

$$s_n = \left(n^2 + m\right)\text{modulo } N \tag{9.5}$$

where m is an integer constant. Consider two $N = 13$ diffusers:

   $m=0$, $s_n = \{0, 1, 4, 9, 3, 12, 10, 10, 12, 3, 9, 4, 1\}$, $s_{max}/N = 12/13$.

   $m=4$, $s_n = \{4, 5, 8, 0, 7, 3, 1, 1, 3, 7, 0, 8, 5\}$, $s_{max}/N = 8/13$.
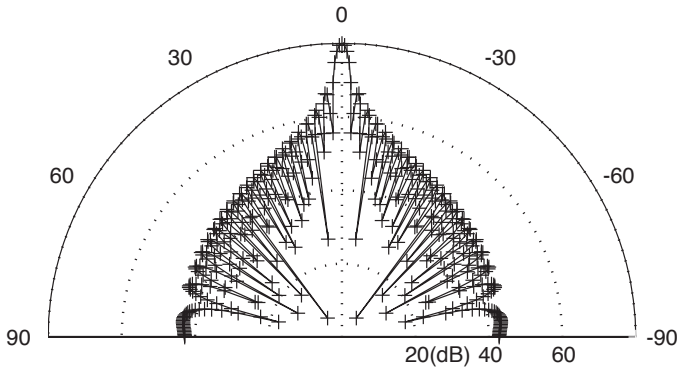
Figure 9.7   The scattering from a QRD at a critical frequency compared to a plane surface:
———— plane surface;
  +   QRD.
The two lines overlay each other.

Consequently, the design frequency has been lowered by two-thirds by this simple manipulation. It must be remembered, however, that this increased performance may not be realized if the repeat width is too narrow.

For a quadratic residue diffuser, critical frequencies occur at mNf_0 where $m = 1, 2, 3 ....$ These are frequencies where the diffuser behaves like a plane surface because all the wells re-radiate in phase. This occurs when all the depths are integer multiples of half a wavelength. Figure 9.5 illustrates such a critical frequency happening at 3.5 kHz in the diffusion spectrum for the narrow diffuser. Figure 9.7 shows the scattering at this frequency. To avoid these critical frequencies, it is necessary to place the first critical frequency above the maximum frequency of the device defined by Equation 9.1, i.e.:

$$N > \frac{c}{2wf_0} \tag{9.6}$$

9.4 Sequences

9.4.1 Maximum length sequence diffuser

Schroeder began his work by investigating maximum length sequences (MLSs).[1] Figure 9.8 shows one period of such a surface based on the sequence {0, 0, 1, 0, 1, 1, 1}. Schroeder chose an MLS because it has a flat power spectrum at all frequencies (except DC). There is a close relationship between the power spectrum and the surface scattering, indeed it is well established in optics that the far field scattering can be found by applying a Fourier transform to the 'surface'. Equation 8.34 gave the scattering in terms of the pressure magnitude $|p|$ from a surface when the Fraunhofer far field approximations are made:

$$\left|p(\theta,\psi)\right| = \left|A[\cos(\theta)+1]\int_s R(x)e^{jkx[\sin(\theta)+\sin(\psi)]}dx\right| \tag{9.7}$$
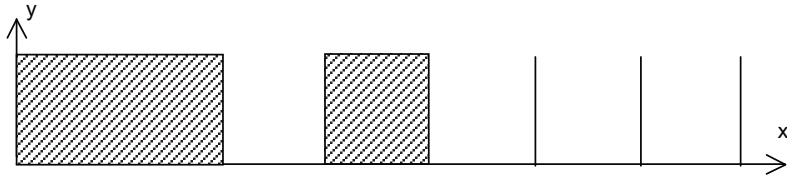
Figure 9.8 A cross section through one period of an N = 7 maximum length sequence diffuser.

where $R(x)$ is the pressure reflection coefficient; θ the angle of reflection; A is a constant; ψ the angle of incidence, and k the wavenumber.

This theory is based around representing the complex diffuser shape by a simple box with a variable admittance on the front face – the admittance being determined by considering the plane wave propagation in the wells. This is essentially the same theory used originally by Schroeder, except for the term in $[\cos(\theta) + 1]$. This extra term is an extension that makes the optical Fraunhofer theory more applicable for oblique incidence and reflection. For convenience and compatibility with previous work, this term will be ignored:

$$\left| p(\theta, \psi) \right| \approx \left| A \int_s R(x) e^{jkx[\sin(\theta) + \sin(\psi)]} dx \right| \qquad (9.8)$$

Equation 9.8 can be interpreted as a Fourier transform, but the transform is in the variable kx and transforms into $[\sin(\theta) + \sin(\psi)]$ space (rather than the more familiar time to frequency transformation). If the reflection coefficients $R(x)$ are chosen to have a flat power spectrum with respect to kx, then the amplitude is constant with respect to the transform variable $[\sin(\theta) + \sin(\psi)]$. This does not relate to a constant scattering in all directions, as the transform variable is not a simple function of θ and ψ; instead even energy lobes are achieved.

If the surface is assumed to be periodic, then there will be scattering directions where spatial aliasing produces grating (diffraction) lobes. These are directions where the path length difference from the source to receiver via parts of the panel exactly one period apart, is an exact multiple of a wavelength. This is illustrated in Figure 9.9 where
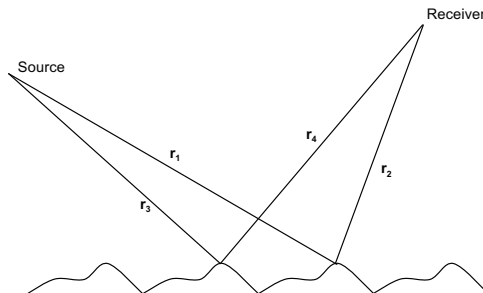
Figure 9.9 Geometry for generation of periodicity lobes.

periodicity lobes are generated when |**r**$_1$ + **r**$_2$ − **r**$_3$ − **r**$_4$| = *mλ*, where *m* is an integer. By considering the geometry of Figure 9.9 further it is possible to show that these grating lobes appear in the far field at the following angles:

$$\sin(\theta) = \frac{m\lambda}{Nw} - \sin(\psi) \ ; \ m = 0, \pm 1, \pm 2, ... \tag{9.9}$$

where *m* is the order of the lobes. If Equation 9.9 is substituted into Equation 9.8, the following results at the design frequency:

$$\left|p_m\right| \approx \left|A\int_s R(x)e^{j2\pi xm/Nw}dx\right| = \left|A\sum_{n=1}^{N}R_n e^{j2\pi nm/N}\right| \tag{9.10}$$

where it is assumed that each well radiates as a point source. Strictly speaking, a sinc function should be introduced to allow for the pistonic radiation, but for now the wells will be considered to be relatively narrow compared to wavelength, $w \le \lambda/4$. Consider a 7-well design. A length-7 MLS is {1, 1, 0, 1, 0, 0, 0}, so R_n are {1, 1, −1, 1, −1, −1, −1}. In this case, it can be shown that:

$$\begin{aligned}\left|p_m\right| &= A & m = 0, \pm N, \pm 2N \\ &= A\sqrt{N+1} & otherwise\end{aligned} \tag{9.11}$$

In other words, the grating lobes radiating into the far field ($\left|m\right| > 0$ & $|m| < N$) have the same level, whereas the main zeroth order lobe ($m = 0$) is lower by $10\log_{10}(N+1)$. Figure 9.10 shows the scattering from the MLS diffuser where the depth is a quarter of the wavelength, compared to a hard plane surface of the same size. At this frequency there are five lobes, with the central lobe being suppressed by $10\log_{10}(8)$ as expected from Equation 9.11. At an octave higher, however, when the depth is half a wavelength, the surface behaves like a plane surface because all waves re-radiate with the same phase – this is a critical frequency – the scattering will be rather like that shown in Figure 9.7. Consequently, the MLS diffuser is only useful over an octave. This problem can be overcome, however, by using different number sequences.
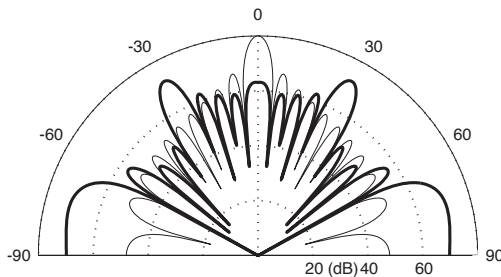
Figure 9.10 The scattering from 5 periods of an N = 7 MLS diffuser at its design frequency:
━━━ MLS diffuser;
──── Plane surface.

9.4.2 Quadratic residue sequence

When a quadratic residue sequence is used, the lobe pressure amplitudes are given by:

$$|p_m| \propto \sqrt{N} \ ; \ m = 0, \pm 1, \pm 2, ... \tag{9.12}$$

Consequently, all lobes will have the same energy, as has been shown in previous polar responses.

9.4.3 Primitive root sequence

A primitive root sequence is generated using the function:

$$s_n = r^n \bmod N \ ; \ n = 1, 2, ... N - 1 \tag{9.13}$$

where N is an odd prime, r is the primitive root of N and the diffuser will have $N - 1$ wells per period. A primitive root is one where s_n for $n = 1, 2, ... N - 1$ are all unique.[8] For example $N = 7$ has a primitive root of 3, so $s_n = \{3, 2, 6, 4, 5, 1\}$, which generates every integer from 1 to $N - 1$. Primitive roots can be found by a process of trial and error, alternatively, tables can be found in texts, such as Reference 8. Equation 9.13 can be re-written as a recursive relationship:

$$s_n = (r \cdot s_{n-1}) \bmod N \tag{9.14}$$

This form is useful because Equation 9.13 can cause overflow problems when being computed for large N.

The primitive root diffuser (PRD) is meant to reduce the energy reflected in the specular reflection direction and so produce a notch diffuser. In addition, it should have even energy in the other diffraction lobes. As with the QRD, the PRD achieves these performance criteria at integer multiples of the design frequency. At these frequencies,
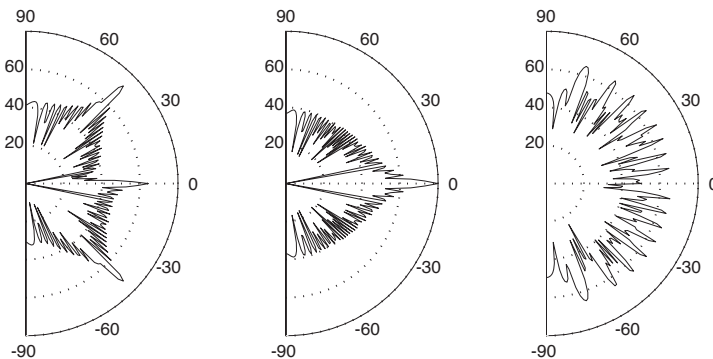
Figure 9.11 Scattering from two primitive root diffusers and a plane surface for normal incidence, showing that a large N number is required to get a significant notch in the specular reflection direction (0°). From left to right, N = 7 PRD; plane surface; N = 37 PRD.

the specular direction amplitudes from the PRD are attenuated by 20 $\log_{10}(N)$ in comparison with a plane surface. It is noted, however, that virtually any welled surface will achieve a reduced specular energy provided well depths are significant compared to wavelength. Equation 9.10 is a maximum when all radiating waves are in phase, as is the case for a flat surface. As soon as a depth sequence is introduced, partial destructive interference occurs between the waves, leading to a suppressed specular reflection.

The performance of the PRD in suppressing the specular reflection improves as the prime number, N, increases. This is shown in Figures 9.11, where the pressures scattered from two PRDs are compared to a plane surface. A large number of wells, say greater than 20–30, are needed before a pressure minimum appears at the specular reflection angle.

The pressure amplitude of the lobes can mathematically be expressed as:

$$\left|p_m\right| \quad = A \qquad m = 0, \pm N, \pm 2N \tag{9.15}$$
$$= A\sqrt{N} \qquad otherwise$$

Although there is an implication of a series of suppressed lobes for $m = \pm N, \pm 2N, \ldots$ these are not seen in the far field. The frequencies at which the high order suppressed modes occur will always be greater than the cut-off frequency for plane wave propagation in the wells and so can be ignored.

The specular reflection is attenuated, but it is not a pressure null at integer multiples of the design frequency. Feldman[9] developed a modified primitive root sequence to overcome the problem. The Feldman-modified PRD (FMPRD) contains an extra zero depth well so the sequence contains all integers from 0 to $N - 1$ (instead of from 1 to $N - 1$). This spaces the reflection coefficients evenly around the unit circle, on an argand diagram, for multiples of the design frequency, leading to an exact null in the specular reflection direction. This modification will, however, alter the evenness of the non-zero order lobes.
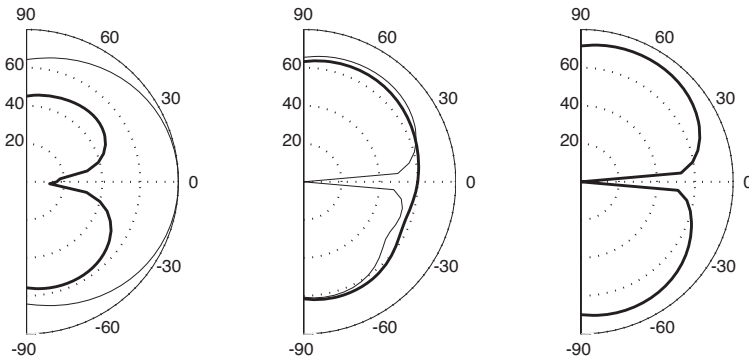
Figure 9.12 Scattering from a primitive root diffuser (PRD); Feldman modified primitive root diffuser (FMPRD); Cox–D'Antonio-modified primitive root diffuser (CDMPRD); plane surface; and optimized surface. N = 11. One period, w = 5 cm, normal incidence source, at the design frequency of 500 Hz (data from Cox and D'Antonio[10]).

Left figure	Middle figure	Right figure
▬▬ Optimized;	▬▬ PRD;	▬▬ CDMPRD.
——— Plane.	——— FMPRD.	
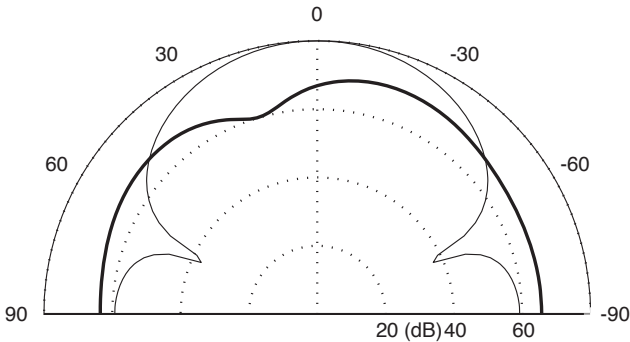
Figure 9.13   Scattering from a modified primitive root diffuser (PRD) and a plane surface. Design parameters given in Figure 9.12. At 750 Hz; not an integer multiple of the design frequency.
────── modified PRD;
────── plane surface.

A PRD does achieve nulls, but not at integer multiples of the design frequency. The nulls appear at frequencies given by $mNf_0/(N-1)$ where $m = 1, 2, 3, \ldots$; but it is at the integer multiples that the non-zero order lobes have the same energy. This realization led to Cox and D'Antonio[10] devising a revised formulation for notch diffusers. The technique is to introduce an effective frequency shift to align the reflection coefficients appropriately around the unit circle at multiples of the design frequency to achieve nulls. This is done by rewriting Equation 9.3 as:

$$d_n = \frac{s_n \lambda_0}{2(N-1)} \tag{9.16}$$

This will be referred to as the Cox and D'Antonio-modified PRD (CDMPRD). Figure 9.12 illustrates the two modified PRDs compared to a PRD and a plane surface. This demonstrates the introduced nulls that the modified schemes achieve. Also shown is a notch filter designed through optimization, a subject that will be returned to later in this chapter.

It is important to reiterate that these notches are only produced at discrete frequencies. Figure 9.13 shows the scattering from a modified PRD, but not at an integer multiple of the design frequency. No notch is found. While not achieving optimum scattering from a QRD at all frequencies is disappointing, it can be expected that between the frequencies of optimum diffusion the dispersion from a QRD will still be reasonable. The fact that PRDs only work at discrete frequencies, however, means the PRDs are impractical notch diffusers. This problem can be overcome to a certain extent by optimization,[10] to form a broader notch over a wider frequency range. Alternatively, triangles or pyramids may be used to get a more broadband notch, as discussed in Chapter 10, but then there are restrictions on the angle of incidence.

9.4.4 Index sequences

Schroeder[11] formed a complex Legendre sequence based on the index function. This has the following reflection coefficients:

$$R_n = \begin{cases} 0 \text{ for } n \equiv 0 \bmod N \\ e^{2\pi j s_n /(N-1)} \end{cases}$$

(9.17)

where s_n is the number theoretic logarithm or index function defined by:

$$r^{s_n} \bmod N = n, \quad n = 1,2,...,N-1$$

(9.18)

where r is a primitive root of N. For example, the $N = 7$, $r = 3$ sequence is {6, 2, 1, 4, 5, 3} as $3^6 = 1 \bmod 7$, $3^2 = 2 \bmod 7$, etc. To find a sequence for a given value of N requires a certain amount of trial and error. As the reflection coefficient for the $n = 0$ well is zero, this well should be filled with absorbent. Consequently, the diffuser absorbs a nominal 20 $\log_{10}(N-1)$ amount of power. The other wells are like those seen in other Schroeder diffusers. Apart from the absorption, the performance of the sequences should be very similar to the primitive root diffuser.

9.4.5 Other sequences

According to the Wiener–Khinchine theorem, the Fourier transform of an autocorrelation function gives the auto power spectrum. This can be related to diffusers and enable the use of other sequences to be understood. The Fourier transform of the surface reflection coefficients approximates to the scattered pressure distribution, although strictly speaking this is in [sin(θ) + sin(ψ)] space. Applying the Wiener–Khinchine theorem to this, if a Fourier transform is applied to the autocorrelation of the surface reflection coefficients, the scattered energy distribution should result. Consequently, a good diffuser is one which has a delta function autocorrelation function for the reflection coefficients, as this will lead to an even scattered energy distribution. (Although constant with sin(θ) + sin(ψ), which is not the same as being constant with θ and ψ.)

To demonstrate this, a familiar diffuser sequence can be considered. In Figure 9.14, the autocorrelation function for an $N = 13$ quadratic residue sequence is compared to that for a plane surface. It can be seen that the quadratic residue sequence has good autocorrelation properties with small side lobe energy, in other words the autocorrelation for index $\neq 0$ is small. This is one reason that a quadratic residue sequence makes a good diffuser.

Another way of viewing this is as follows. Peaks in an autocorrelation function away from zero indicate a sequence which has some similarity at some displacement. In terms of scattering, there will be angles at which this similarity will lead to lobes due to constructive interference. If all similarities can be removed, then in all directions no complete constructive interference can take place, and so the scattering in all directions will be the same.

Given the above, one approach to finding an appropriate sequence is to look for sequences with good autocorrelation properties. This is not difficult as sequences with
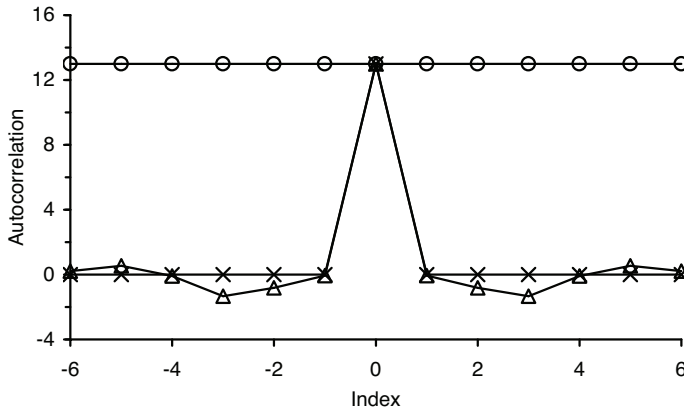
Figure 9.14 The autocorrelation for three different sequences:
—△— quadratic residue;
—✕— Chu (perfect); and
—⊖— constant (plane surface).

optimal autocorrelation properties are a keystone of digital communication systems, whether that is error checking systems for digital audio, code division multiple access (CDMA) systems used in mobile telecommunications or modulating waveforms for radar and sonar.

Datiotis *et al*.[12] examined Lüke and power residue sequences which both have good autocorrelation properties. In addition, these number sequences offer the opportunity to move the lowest frequency at which the wells all radiate in phase to outside the audible frequency range. The flat plate effect arises because there is a simple integer relationship between the different well depths. A way of mitigating this problem is to introduce an integer-based sequence which, although having a small number of wells per period, is generated using a larger integer. For instance, short power residue sequences can be formed by under-sampling longer primitive root sequences provided certain rules are followed. Consider a primitive root sequence based on prime 73; this will be of length 72. By taking every ninth sample from this sequence, a shorter-length 8 sequence is formed. Although this power residue sequence displays slightly worse autocorrelation properties than quadratic residue and primitive root sequences, the flat plate frequency will be at nine times the frequency that a more normal number theoretic diffuser would achieve.

Another approach is to use an optimization algorithm to find sequences with good autocorrelation properties.[8] The principle of optimization will be discussed in more detail later, but the basic principle is to get the computer to search for a sequence with minimum side lobe energy. This works well for a small number of wells, but when the number of wells becomes large the number of degrees of freedom in the optimization becomes too large for this to be an efficient or effective process.

A different sequence not considered before will be used to test the principle of choosing sequences with good autocorrelation properties. The Chu sequence is a perfect polyphase sequence; in other words the periodic autocorrelation function is a perfect delta function. Figure 9.14 shows the autocorrelation function for an $N = 13$
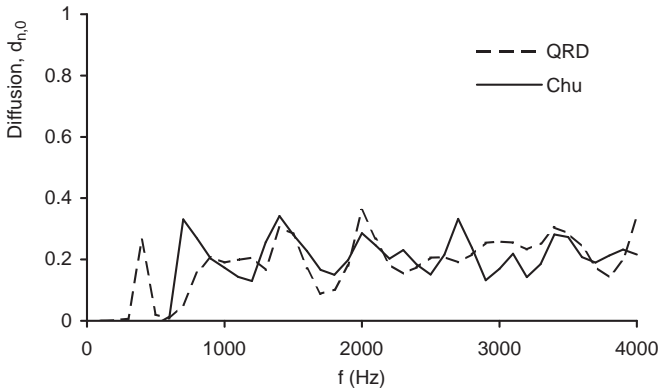
Figure 9.15 Normalized diffusion spectra for two diffusers.

case showing that there is no side lobe energy. The elements of a Chu sequence can be generated by:[13]

$$s_n = e^{j\varphi_n} \tag{9.19}$$

$$\varphi_n = \begin{cases} \dfrac{2\pi}{N}\left[\tfrac{1}{2}(n+1)n \ \bmod \ N\right] & N \ odd \\[2ex] \dfrac{2\pi}{N}\left[\tfrac{1}{2}n^2 \ \bmod \ N\right] & N \ even \end{cases}$$

$$0 \le n < N$$

The phase terms φ_n are converted to depths by equating the deepest depth to the design wavelength and maximum phase term, φ_{max}, i.e:

$$d = \frac{\lambda_0 \varphi_n}{2\varphi_{max}} \tag{9.20}$$

Figure 9.15 compares the normalized diffusion from an $N = 13$ Chu sequence, with a QRD and a plane surface. The performance from the QRD and the Chu sequence is overall very similar. Consequently, this presents an alternative design method, but not a better one.

9.5 The curse of periodicity and modulation

The scattered polar responses seen in Figure 9.6 are dominated by grating lobes generated by the fact that the diffusers are periodic. The lobe energy may be constant, but there are large minima between the lobes except at high frequencies when the number of lobes becomes very large. The scattered energy is not even in all directions. For this reason, significantly better performance can be obtained if the periodicity
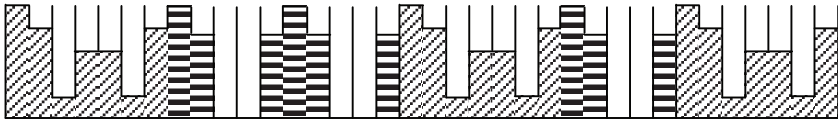
Figure 9.16 A cross section through a modulation scheme using N = 5 and N = 7 quadratic residue diffusers and the modulation sequence {1, 0, 0, 1, 0, 1}.

lobes can be removed by making the diffuser aperiodic or increasing the repeat distance. The small number of studies on the subjective effects of periodicity have all found that periodicity can cause audible coloration.[14] A phase grating diffuser which exploits number theory, such as a QRD, is in many ways cursed by periodicity. A QRD needs periodicity to form its even energy lobes, yet the periodicity lobes cause uneven scattering.

One possibility is to use a number sequence with good aperiodic autocorrelation properties. This means that a single period of the number sequence can be generated and used without repetition. There are two problems with this solution: first there are not many large aperiodic, polyphase sequences known, and second it will usually be cheaper to manufacture a small number of base shapes and use each of these many times.

Angus[15–20] presented a series of papers outlining methods for using two phase grating base shapes in a modulation scheme to deal with the problems of periodicity. Figure 9.16 shows such an arrangement for two QRDs, one based on N = 7, the other on N = 5. The idea is to use two or more base shapes and arrange them according to a pseudorandom sequence so there is no repetition.

As discussed previously, the far field scattering distribution is roughly given by the Fourier transform of the surface reflection coefficients. For a periodic device, the distribution of reflection coefficients can be expressed as the reflection coefficients over one period, convolved with a series of delta functions:

$$R(x) = R_1(x) * \sum_{n=-\infty}^{n=\infty} \delta(x - nW) \tag{9.21}$$

where $R_1(x)$ is the distribution of reflection coefficients over one period; n is an integer; * denotes convolution; $W = Nw$ is the width of one period of the device, and δ the delta function.

Equation 9.21 and the following process are illustrated in Figure 9.17. When a Fourier transform is applied to Equation 9.21 to obtain the scattering in $[\sin(\theta) + \sin(\psi)]$ space, then the convolution becomes multiplication:

$$FT\{R(x)\} = FT\{R_1(x)\} \cdot FT\left\{ \sum_{n=-\infty}^{n=\infty} \delta(x - nW) \right\} \tag{9.22}$$

where FT denotes Fourier transform. The Fourier transform of a delta function series, is another delta function series and it is the spikes in this for $[\sin(\theta) + \sin(\psi)] > 0$ that
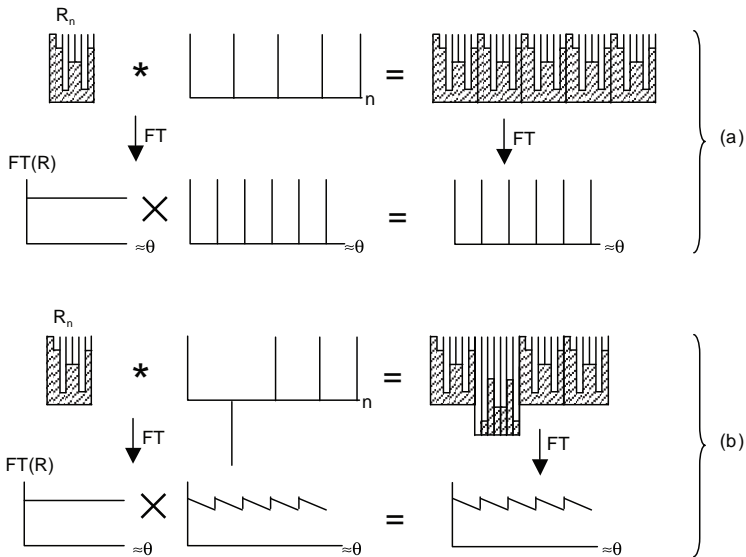
Figure 9.17 A modulation scheme illustrated. In the top case (a), a periodic arrangement is used and spatial aliasing causes grating lobes even though one period of the diffuser has a flat power spectrum. In the bottom case (b), the inverse of the diffuser is used in a modulation scheme to reduce periodicity effects.

cause the grating lobes. Consequently, rather than use a delta function series to form a periodic device, another function should be used which has better Fourier transform properties. Again, what is needed is a sequence with good autocorrelation properties. A good choice is a Barker sequence. This is a binary sequence whose aperiodic Fourier
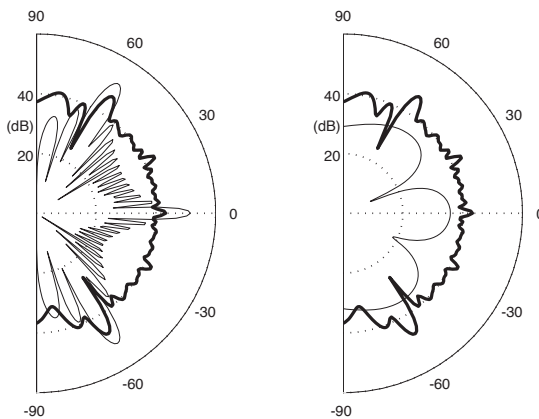
Figure 9.18 Scattered polar distribution from a single QRD, a periodic arrangement, and a Barker modulation using the QRD and its inverse. 2,000 Hz = $4f_0$.

Left figure	Right figure
━━━ modulated;	━━━ modulated (same as left figure);
─── periodic.	─── one period.
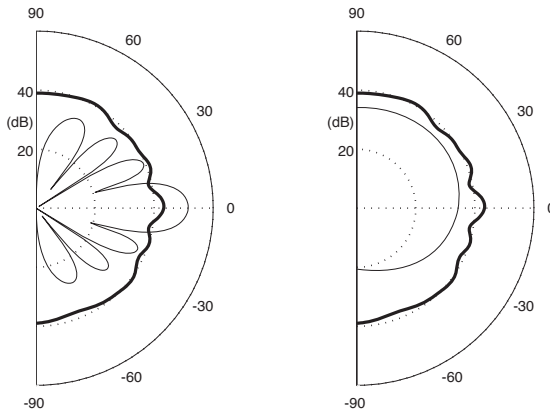
Figure 9.19   Same diffusers as Figure 9.18 but at 500 Hz, the design frequency.

Left figure	Right figure
▬▬ modulated;	▬▬ modulated (same as left figure);
── periodic.	── one period.

transform is flattest possible for a binary sequence. Consequently, the response of the whole array of diffusers is closer to the single diffuser alone than if a periodic arrangement is used. If a perfect binary sequence could be found then the single diffuser response would be recovered, but there are no such 1D sequences.

Consider forming a QRD with five periods. The Barker sequence for $N = 5$ is {1, −1, 1, 1, 1}. Consequently, where a 1 appears in the Barker sequence, the normal $N = 7$ QRD should appear. Where a −1 appears, an $N = 7$ QRD is needed, which produces the same scattering, except it is 180° out of phase. This can be done by using the rear of the normal $N = 7$ diffuser (provided the fins are extended far enough). This is illustrated in Figure 9.17. Consequently, one QRD has a number sequence of {0, 1, 4, 2, 2, 4, 1} and the other QRD has a number sequence of {7, 6, 3, 5, 5, 3, 6}. This second sequence is found by subtracting the first sequence from N. This is equivalent to changing the phase change due to the well depths from φ to $2\pi - \varphi$, i.e. obtaining an 180° out of phase surface.

Figures 9.18 and 9.19 show the scattering from the periodic arrangement of $N = 7$ QRDs compared to an arrangement according to the Barker sequence and a single diffuser for two frequencies. One of the frequencies where the diffusion improvement is most dramatic is 2 kHz; at other frequencies the improvement is less marked. Figure 9.20 shows the normalized diffusion coefficient versus frequency. A clear improvement is seen in the diffusion, and periodicity lobes are much reduced. As Figure 9.20 shows, the diffusion from the periodic array only becomes significant compared to a plane surface at 1–1.5 kHz, an octave or so above the design frequency (500 Hz). This is a case of the diffuser width, rather than the diffuser depth, limiting the low frequency response. At the design frequency, only one lobe appears in the scattered polar distribution, as shown in Figure 9.19. The Barker sequence means that there is reduced periodicity in the arrangement, and so the low frequency limit of the Barker modulated array is determined by the depth and not the periodicity. This is an important result, as it means the low frequency performance of some diffusers can be improved by modulation.
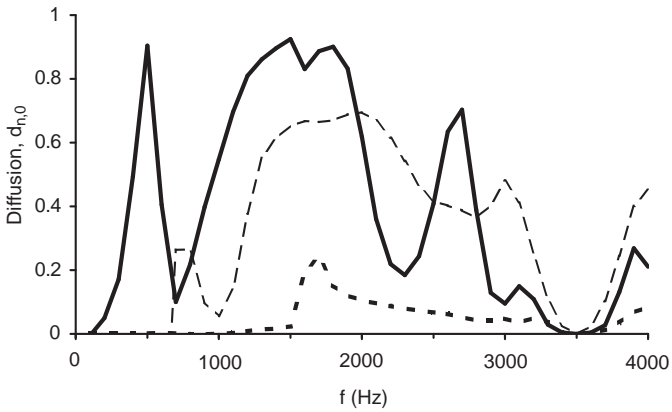
Figure 9.20 Normalized diffusion spectra for three diffuser arrangements:
– – – one narrow period of a QRD;
▬ ▬ ▬ QRD periodic (a wide array); and
▬▬▬ QRD Barker modulation (a wide array).
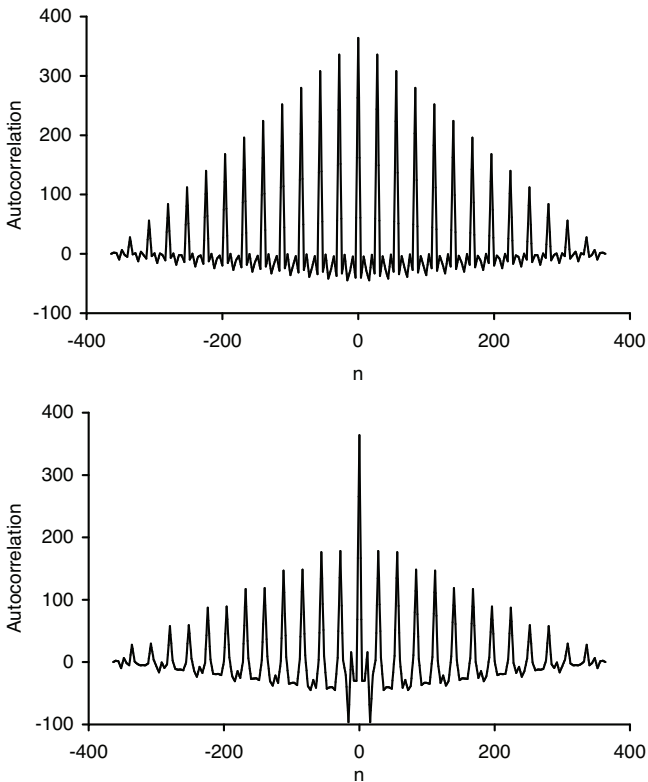
Figure 9.21 Autocorrelation function for two arrangements of QRDs. Top graph: periodic array; bottom graph: Barker modulated array.

The polar responses show that the scattering from the Barker modulated array is more similar to the single diffuser response, which is as expected from the theory outlined above. A single diffuser response is not recovered because the Barker sequence has good but not perfect autocorrelation properties. Figure 9.21 shows the autocorrelation properties for the diffuser arrangements at the design frequency. The spikes in the side lobes arise because of the repeat distance of 7 for the $N = 7$ diffusers. The Barker modulation has lower side lobe energy which means the periodicity is reduced. Although the Barker sequence has reduced the side lobe spikes they are not completely eliminated. This is why the single diffuser response is not completely recovered.

There are a variety of number sequences that can be used for modulation. The Barker sequence is a good choice as it has good aperiodic autocorrelation properties. As the modulation sequence does not repeat, a sequence with good periodic autocorrelation coefficient would not be optimal. Barker sequences only analytically exist for certain lengths: 2, 3, 4, 5, 7, 11 and 13, but computer-based search algorithms have been used to generate number sequences up to length 48.[8] For larger diffuser arrays, it may be necessary to use other number sequences, such as MLSs, which strictly speaking are only good with periodic use.

The modulation works best at multiples of the design frequency. Only at these frequencies do the diffuser and its inverse create exactly opposite pressures. At other frequencies, the modulation is likely to help with the scattering as it breaks up periodicity lobes, but in a more uncontrolled manner.
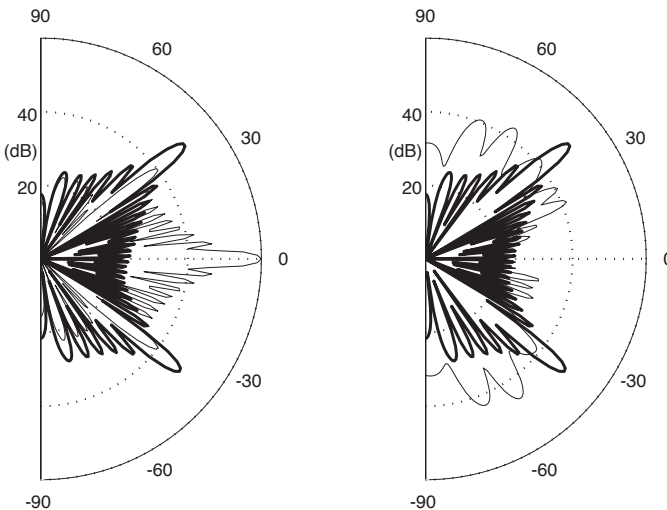
Figure 9.22   Comparison of a periodic arrangement of a modified primitive root diffuser (CDMPRD); a modulated sequence of the CDMPRD; and a plane surface. The periodic surface had 10 periods of $N = 11$ diffusers. $w = 0.05$ m, frequency is 1 kHz, design frequency 500 Hz. The modulated surface was formed from 12 periods of $N = 11$ and $N = 7$ placed in a random order (data from Cox and D'Antonio[10]).

Left figure	Right figure
▬▬ periodic;	▬▬ periodic (same as left figure);
—— plane.	—— modulated.

At high frequencies, say greater than 5 kHz for the typical geometries used in practical diffusers, the dispersion by a modulated array summed over a one-third octave band is often worse than for a periodic arrangement. This happens because the number of grating lobes in the periodic case saturates, so when the polar responses are summed over a one-third octave band the grating lobes average out. Having said this, the improvements generated by modulation in the more important low-mid frequency ranges far outweigh any slight decrease in performance at higher frequencies.

One other feature of note is that the critical frequency at Nf_0, where the diffusers behave as a flat plate, still remains even with the modulation. The flat plate frequency of 3,500 Hz can be seen in the diffusion spectra of Figure 9.20. Both the QRD and its inverse used in the modulation suffer the same critical frequency, and consequently this problem persists. While it is possible to reduce this problem by choosing a larger value for N, it is also possible to use modulation to reduce the effects. To do this, the two diffusers to be modulated must have different critical frequencies. There are further advantages to using two different diffusers. The QRD works at discrete frequencies based on integer multiples of the design frequency. By using diffusers with two different design frequencies, it is possible to achieve more frequencies with better diffusion.[17]

Cox and D'Antonio[10] used a combination of $N = 11$ and $N = 7$ PRDs. Figure 9.22 shows the scattering from this arrangement. Not only does the modulated array still achieve a notch at the specular reflection direction, but the two dominant first order lobes are broadened. The notch remains because each period of both diffuser types produce a null in the specular direction, and summing over all periods still leads to nothing scattered in the specular direction.

Angus[20] used a combination of $N = 5$ and $N = 7$ quadratic residue diffusers in an orthogonal modulation. Figure 9.23 shows the autocorrelation of the reflection coefficients at the design frequency for a modulation of $N = 5$ and $N = 7$ QRD. It shows that the original periodicity lobes are reduced, but other smaller peaks are produced elsewhere. The locations of the $N = 5$ and $N = 7$ diffusers can be determined by flipping a coin, or better still by using a pseudorandom sequence with good aperiodic
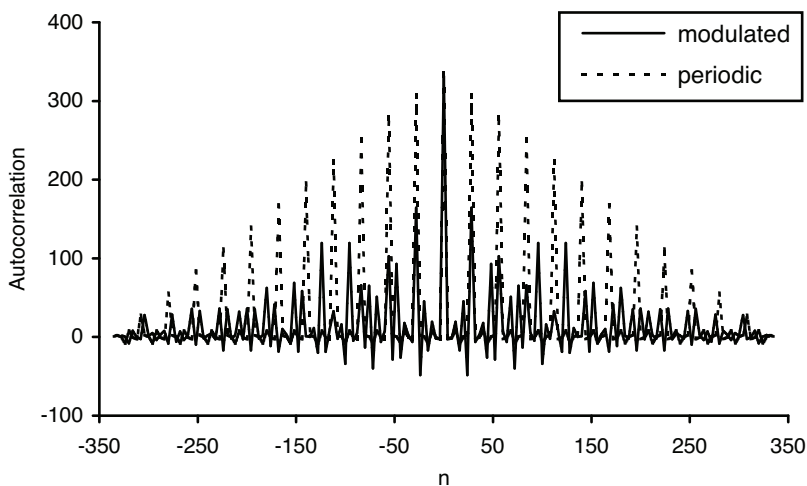
Figure 9.23 Autocorrelation function for a periodic arrangement of N = 7 QRDs and an orthogonal modulation using N = 5 and N = 7 QRDs and a Barker sequence.
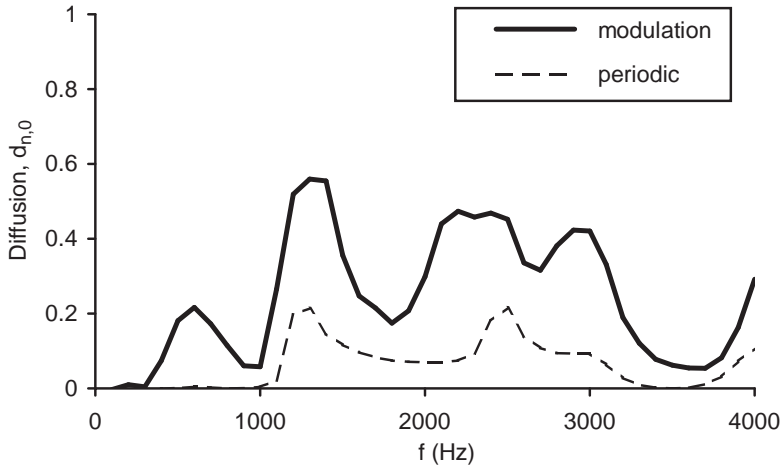
Figure 9.24   Normalized diffusion spectra for a periodic arrangement of N = 7 QRDs and an orthogonal modulation using N = 5 and N = 7 QRDs.

autocorrelation properties, such as a Barker sequence. Figure 9.24 shows the normalized diffusion spectra. The flat plate frequency at 3.5 kHz is removed by the orthogonal modulation, although there is still a decrease in performance around that frequency because at that frequency only the $N = 5$ diffusers are creating any dispersion and so a strong specular component still remains. Overall, the performance is not as good as the original Barker modulation using the QRD and its inverse described previously. Consequently, the best choice for modulation is to use a diffuser and its inverse, but choosing a diffuser where the critical frequency is above the high frequency limit where cross-modes in the wells appear.

The modulation techniques developed by Angus require two or more base shapes. It is possible to achieve cheaper modulation using a single asymmetrical base shape. Instead of inverting the diffuser to use the rear, an asymmetrical diffuser can be
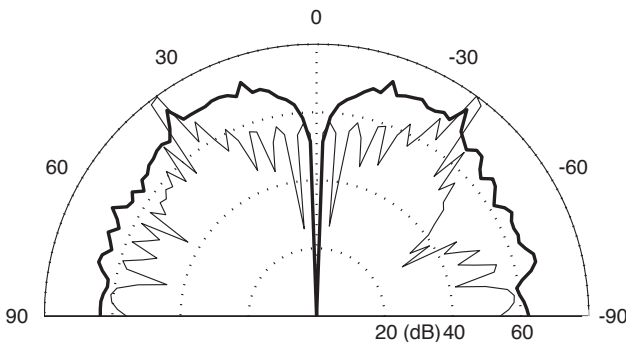
Figure 9.25   Scattering from a periodic and a modulated arrangement of primitive root diffusers, 2.5 kHz. Modulation using one base shape:
——— periodic; and
▬▬▬ modulated.
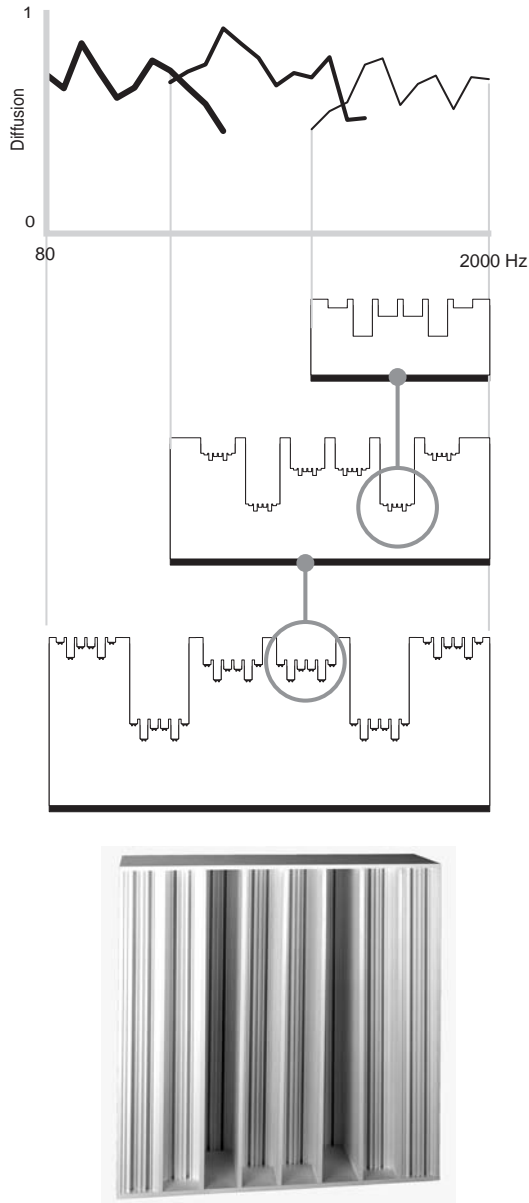
Figure 9.26   A Diffractal®, which imbeds high frequency diffusers within a low frequency diffuser to deal with periodicity, absorption and bandwidth problems (top figure after D'Antonio and Konnert[7]).

flipped about its mid-point. For example, an $N = 7$ PRD is {1, 3, 2, 6, 4, 5} and this can be rotated to form a new sequence {5, 4, 6, 2, 3, 1}. This modulation will not be successful with quadratic residue sequences or Chu sequences, however, because these are symmetrical. Instead, asymmetrical sequences are needed such as primitive root

or power residue sequences. Figure 9.25 shows the scattering from such a modulation using $N = 7$ primitive root sequences. The modulation reduces the non-zero order grating lobes, while still preserving the null in the specular reflection direction.

There is another approach to modulation to reduce periodicity effects and also to improve the bass frequency response. The bandwidth of a Schroeder diffuser is limited at high frequencies by the well width and at low frequencies by the maximum depth. To provide full spectrum sound diffusion in a single integrated diffuser, the self-similarity property of fractals can be combined with the uniform scattering property of Schroeder diffusers to produce a fractal diffuser. The surface consists of nested self-similar scaled diffusers, each of which covers a specific frequency range and offers wide area coverage (see Figure 9.26). Each diffuser provides uniform scattering over a specific range of frequencies so that the effective bandwidth is extended.

There are numerous natural phenomena exhibiting a macroscopic shape, which is repeated microscopically at progressively smaller and smaller scales. At each level of magnification we find a scaled replica of the original. These scaled replications are self-similar, that is they differ only in scale; they are invariant to scaling. The term fractal was first coined by Mandelbrot[21] to describe these structures, and hence these diffusing fractals have been termed Diffractals. It is possible to carry out the scaling many times; typical commercial implementations use two magnifications of self-similarity. Another analogy to this is a two-way coaxial loudspeaker system. The construction avoids using narrow deep wells to cover a wide bandwidth, and so decreases the absorption of the device. At low frequency, the small diffusers at the bottom of the wells will have negligible depth compared to wavelength, and so only the bass diffuser needs to be considered at low frequencies. At high frequencies, the small diffusers will act as a modulated array with phase modulation due to the depth of the deep diffuser. The phases introduced by the large diffuser on the small diffuser are conveniently also quadratic residues, and hence when they sum with the small diffuser phases, the result is still a quadratic residue sequence. This is a very useful outcome, because it is possible therefore to nest diffusers with overlapping frequency bandwidths. The two layers of magnification appear to operate orthogonally. In reality, however, in the overlap region at mid-frequencies the situation is likely to become much more complex. The cross-modes of the large wells will affect the scattering from the smaller diffusers. These difficulties make this surface impossible to model with a simple Fraunhofer approach; to properly model this surface requires a full BEM solution or similar.

A third-generation Diffractal is illustrated at the top of Figure 9.26 along with the overlapping frequency bandwidths of each generation. In the bottom of the figure, a photo of a commercial second generation Diffractal is shown. Figure 2.12 showed an application of this device at the rear of a studio.

9.6 Improving the bass response

The depth of a diffuser usable in design is often limited by non-acoustic factors. Ultimately, the designer or architect will limit the depth available for acoustic treatment. Furthermore, with the wavelength of sound extending to 17 m, it is impossible to construct a practical diffuser which will cover the full audible bandwidth and is also usable in most rooms. Consequently, there is always a need for extending the bandwidth of diffusing devices to a lower frequency.

By using well folding it is possible to gain a greater bandwidth from a given overall
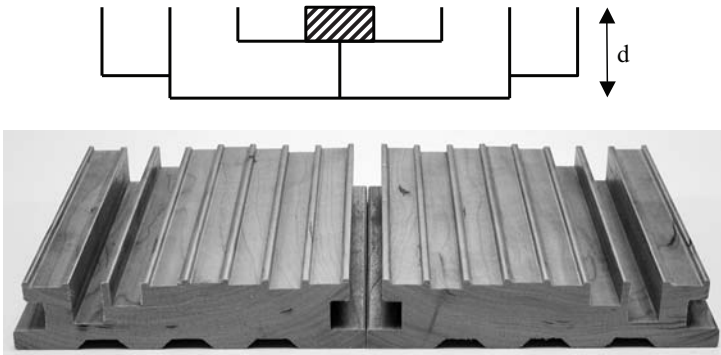
Figure 9.27 Top: an N = 7 QRD with 'folded' wells to reduce the depth to 63 per cent of its original size. Bottom: an optimized diffuser where side-cuts are used to form a folded well.

depth. Jrvinen *et al.*,[22] Mechel[23] and Hargreaves *et al.*[24] and others have investigated such a modification which improves the packing density. The standard Schroeder diffuser, Figure 9.2, has much wasted space at the rear which can be better utilized. Figure 9.27 shows the use of well folding to reduce the depth of an *N* = 7 quadratic residue diffuser. For low frequencies, the depth of the folded well should be calculated from the mid-line through the well. So in the case shown, the number sequence determining the depth is a quadratic residue sequence of {2, 4, 1, 0, 1, 4, 2}. At high frequency, the sound does not pass around the bend of the folded wells, and therefore the apparent depth is shallower, and the number sequence effectively becomes {2, 2½, 1, 0, 1, 2½, 2}. By bending the well such that the distance *d* shown in Figure 9.27 does not relate to the integers of the original quadratic residue sequence, it is possible to reduce the effect of critical frequencies where the surface looks like a plane surface.

Under these assumptions a simple Fraunhofer theory can be used. To properly model performance, especially at mid-frequencies, a full BEM solution is needed. As the depth sequence varies between different frequency ranges, the application of number sequences is less straightforward. The problem with folded wells is that they are awkward to manufacture. A neat solution is to form the folded well by cutting into the sides of a diffuser,[25] as shown in the bottom of Figure 9.27. When the diffusers are stacked side by side, folded wells are formed.

An alternative regime is to use perforated sheets to add mass to the impedance of the
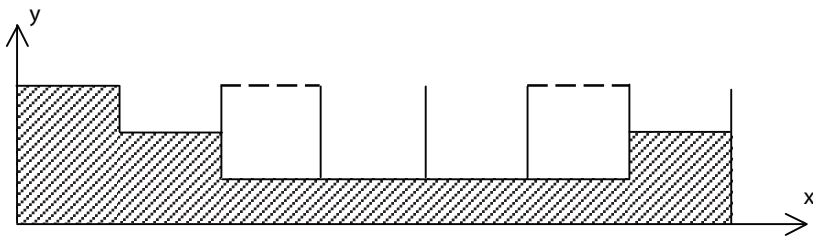
Figure 9.28 A cross section through a Schroeder diffuser using perforated sheets to add mass to the surface impedance of the longest wells and therefore enabling the longest wells to be shortened.
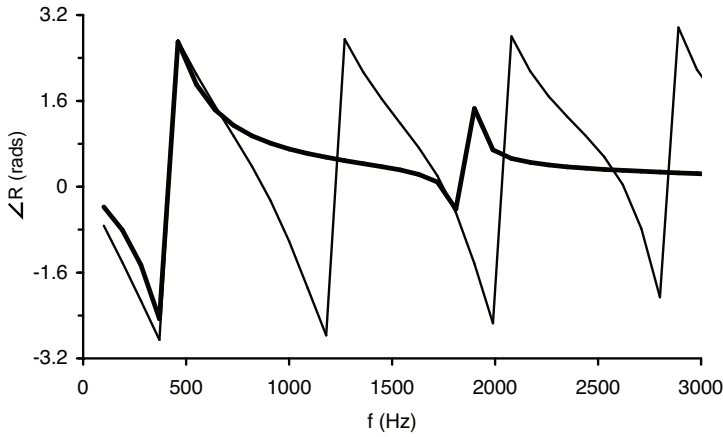
Figure 9.29   Reflection coefficient phase angle for two wells:
————— normal well; and
━━━━━ shorter well with perforated sheet to add mass.

wells, and so lower the resonant frequencies of the wells. This can then lower the design frequency. An example of such a device is shown in Figure 9.28, where the use of perforated sheets has enabled the longest wells to be shortened. Such an approach was tried for diffusion by Hunecke,[26] using microperforation, and for absorption by Fujiwara *et al.*[27] and Wu *et al.*[28] using larger diameter perforations. For a diffuser it is important that the perforation size is not too small, otherwise significant losses may result. The principle of the design is that for the first mode, the well reflection coefficient of a Helmholtz resonator and of a 1/4 wavelength tube can be made to be similar. Consequently, the 1/4 wave resonator tubes of the Schroeder diffuser can be replaced by Helmholtz devices. This is illustrated in Figure 9.29 where two well reflection coefficients are compared, one for a 1/4 wave resonator and the other for a well of half the depth but with a perforated sheet to create the correct resonant frequency. These reflection coefficients can be calculated using the transfer function matrix method
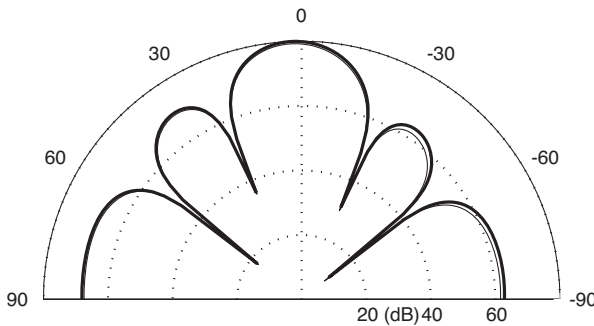
Figure 9.30   Scattering from an *N* = 7 QRD at the design frequency, and a similar QRD where the longest wells have been shortened and a perforated sheet used to add mass.
————— QRD; and
━━━━━ QRD using perforated wells.
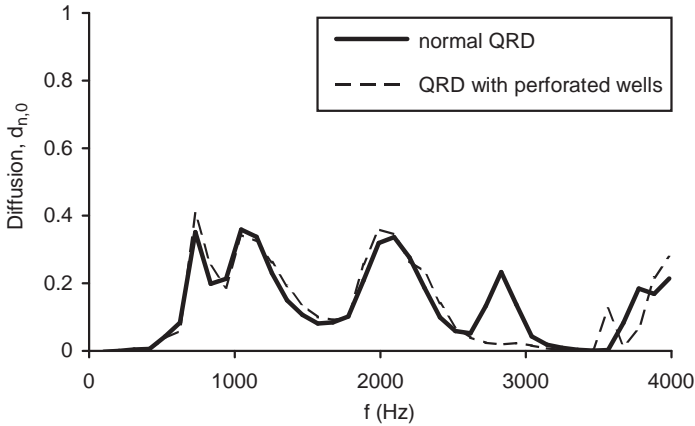
Figure 9.31   Normalized diffusion for a standard QRD and a QRD with perforated sheets to reduce the largest well depths.

outlined in Chapter 6. Unfortunately, for higher order modes, the reflection coefficients for the Helmholtz resonator and 1/4 wavelength tube diverge. Consequently, this design methodology can only work around the design frequency.

Figure 9.30 shows the scattering at the design frequency, illustrating that the two diffusers behave similarly. The Schroeder diffuser with perforations is about half the depth of the original diffuser, so considerable space savings have been made. A point to note when carrying out this calculation is that it is necessary to include the radiation impedance of the 1/4 wave tube. This has been ignored for other Schroeder diffusers because it is a constant term for nearly all wells and therefore does not affect the diffusion. With a mixture of Helmholtz and 1/4 wave devices, however, the correct radiation impedance must be included. Figure 9.31 shows the normalized diffusion coefficient, showing that for many frequencies similar performance is obtained from the perforated device and the normal Schroeder diffuser. At higher frequencies than shown, the scattering from the perforated sheet will become rather specular and so care in design and application is needed. As the principle is to add mass using perforations, mass can also be applied using limp membranes, probably to similar effect, but it may be difficult to reproduce mounting conditions consistently in manufacture.

To get a true broadband diffuser using this approach another design approach must be tried. Later in Section 9.10 an optimization approach will be discussed. This could equally be applied to a diffuser formed from a series of Helmholtz resonators.

9.7 Multi-dimensional devices

The diffusers discussed thus far have been single plane devices. They cause scattering into a hemi-disc, acting as a planar surface in the other directions. While this is the preferred diffuser design for some applications, there is a need for a diffuser that scatters into a hemisphere. For a Schroeder diffuser this can be achieved by forming a two-plane device, one that scatters optimally in the *x*- and *z*-direction, and therefore gives even lobes on a hemisphere. Examples of such surfaces were shown in the bottom row of Figure 9.1.

As 2D diffusers scatter in multiple planes, therefore, a receiver in the bright zone will experience a scattered energy that is reduced more than a 1D diffuser, provided multiple grating lobes are present. The number of grating lobes is squared if a 1D of width Nw and 2D diffuser of size $Nw \times Nw$ are compared. Therefore the energy in each lobe will reduce by $10 \log_{10}(m)$, where m is the number of grating lobes present for the 1D diffuser.

There are two common processes for forming 2D diffusers. The first involves forming two sequences, one for the x-direction, one for the z-direction and amplitude modulating the x sequence with the z sequence. For a quadratic residue sequence, this can be expressed as:[2]

$$s_{n,m} = \left(n^2 + m^2\right) \text{modulo } N \tag{9.23}$$

where n and m are integers and index the sequence for the nth and m^{th} wells in the x- and z-directions respectively. A similar procedure can be used for primitive root diffusers:

$$s_{n,m} = \left(r^n + r^m\right) \text{modulo } N \tag{9.24}$$

It is even possible to have a quadratic residue sequence in one direction and a primitive root sequence in the other, provided they are based on the same prime number, although it is hard to see why you would chose to do this.

A 2D QRD based on N = 7 is shown in Figure 9.32. In this case the indexes n and m were started from 4 to place the zero depth well in the middle of the diffuser. As the surface is periodic, it is possible to start the indexes n and m from any integer. Two-dimensional number theoretic diffusers will often have less bass diffusion efficiency than a 1D, as the ratio s_{max}/N tends to be close to 1 for 2D devices.

Figure 9.32 also illustrates other sequences that can be used. On the diagonal of the diffuser the following sequence appears {4, 1, 2, 0, 2, 1, 4}. This is the original sequence

4	6	3	2	3	6	4	4	6	3	2	3	6	4
6	1	5	4	5	1	6	6	1	5	4	5	1	6
3	5	2	1	2	5	3	3	5	2	1	2	5	3
2	4	1	0	1	4	2	2	4	1	0	1	4	2
3	5	2	1	2	5	3	3	5	2	1	2	5	3
6	1	5	4	5	1	6	6	6	1	5	4	5	1
4	6	3	2	3	6	4	4	4	6	3	2	3	6
4	6	3	2	3	6	4	4	6	3	2	3	6	4
6	1	5	4	5	1	6	6	1	5	4	5	1	6
3	5	2	1	2	5	3	3	5	2	1	2	5	3
2	4	1	0	1	4	2	2	4	1	0	1	4	2
3	5	2	1	2	5	3	3	5	2	1	2	5	3
6	1	5	4	5	1	6	6	6	1	5	4	5	1
4	6	3	2	3	6	4	4	4	6	3	2	3	6

Figure 9.32 A sequence array for a 7 × 7 quadratic residue diffuser; one period is highlighted.

{0, 1, 4, 2, 2, 4, 1} but with every fourth element used. This new sequence has the same Fourier properties as the original sequence due to the shift properties of quadratic residue sequences. This indicates that as well as producing good diffusion in the orthogonal directions x and z, good scattering in the directions along the diagonals should also be obtained.

The second method for making multi-dimensional diffusers is to use the Chinese remainder theorem.[29] This folds a 1D sequence into a 2D array while preserving the Fourier properties of the 1D sequence. The process is described in detail in Chapter 11, where it is applied to hybrid surfaces, but it can equally be applied to polyphase sequences.

The requirement for co-prime factors means that this folding technique cannot be applied to single periods of QRDs, because there is a prime number of wells. This can be overcome by using an odd-number generator N for the quadratic residue sequence which is not prime. For example, a quadratic residue sequence based on $N = 15$ will work perfectly well at the design frequency and can be wrapped into a 3×5 array. The problem is that the surface will have flat plate frequencies at 3 and 5 times the design frequency (as well as 6, 10, 9, 15 … times). Consequently, to use a non-prime N it is necessary to make sure the factors of N are sufficiently large that the flat plate frequency is above the frequency of interest. For example, $N = 143$ has factors of 11 and 13 and so would be a good choice as the flat plate frequencies will be beyond the upper limit of most diffusers. It is also possible to apply the Chinese remainder theorem to some primitive root sequences, or some other mathematical sequences, such as the Chu sequence outlined previously.

It has also been suggested by Pollack and Dodds[30] that the wrapping can be carried out in a hexagonal configuration:

$$s_{n,m} = \left(n^2 + m^2 + nm\right) \text{modulo } N \qquad (9.25)$$

Figure 9.33 illustrates a hexagonal QRD based on $N = 7$ generated using Equation 9.25.

Figure 9.34 illustrates the scattering from a 2D $N = 7 \times 7$ QRD and a plane surface as a 3D polar balloon, sometimes nicknamed a polar banana.[7] There are a regular set of
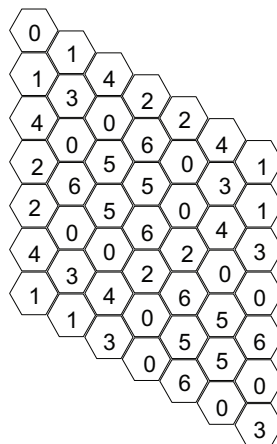
Figure 9.33 One period of a hexagonal quadratic residue diffuser based on N = 7.
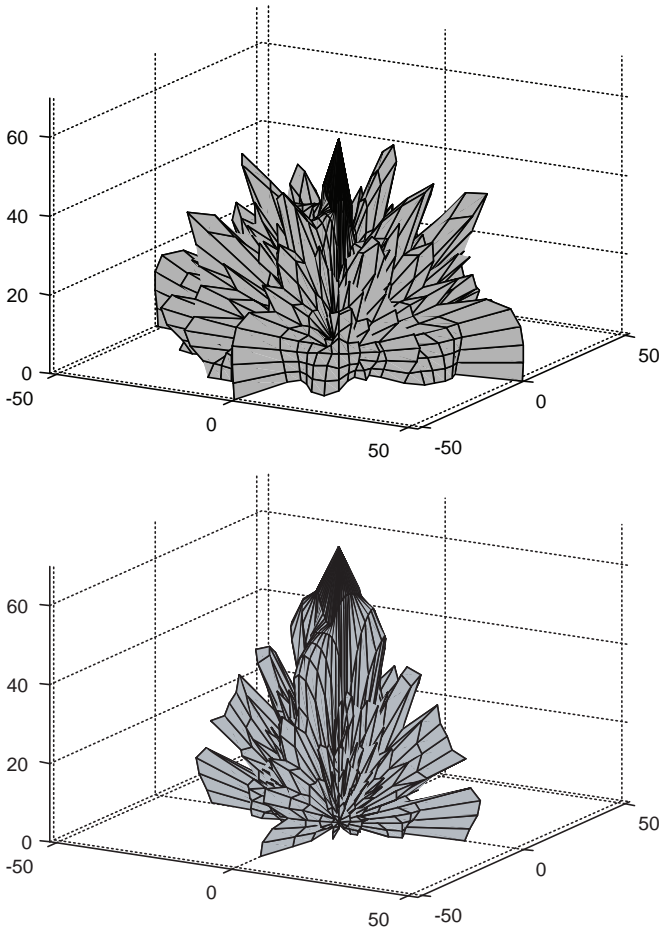
Figure 9.34   Scattering from an $N = 7$ QRD at four times the design frequency (top), and a plane surface (bottom).

grating lobes, but these are difficult to see unless the polar response can be animated and rotated. Figure 9.35 shows the data as a contour plot, where the grating lobes become more obvious. These grating lobes form a regular grid, the middle 9 in a 3 × 3 grid are most obvious in the case shown. These contour plots are effectively the contour on the surface of the hemisphere, looking down onto the hemisphere. Consequently, the *x*- and *z*- axes shown are non-linear.

Figure 9.36 illustrates the scattering from a diffuser formed using the Chinese remainder theorem. A Cox–D'Antonio-modified primitive root sequence based on the prime number $N = 43$ was generated, and so the sequence is 42 elements long. It was folded into a 6 × 7 array using the Chinese remainder theorem. Figure 9.36 shows the response at four times the design frequency, and the specular lobe, which would normally be pointing straight up the page, is missing. This demonstrates that the folding technique succeeds in preserving the primitive root properties. When amplitude modulation is used to form primitive root sequence arrays (Equation 9.24)
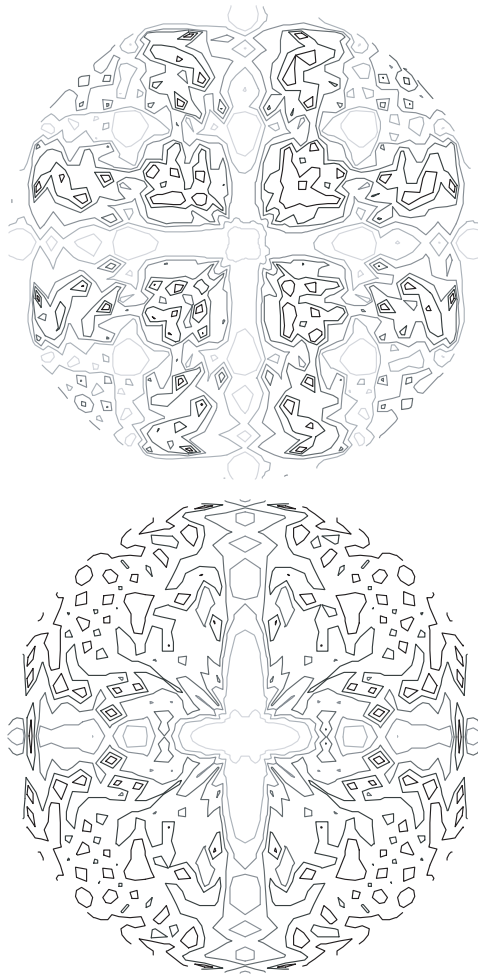
Figure 9.35 Contour plot of polar response shown in Figure 9.34 seen from above. The QRD (top) shows 13 grating lobes, where the 3 × 3 grid of lobes shown in the centre is clearest. The plane surface (bottom) just has a lobe in the specular reflection direction.

then planes of reduced scattering are produced. All the scattering in the directions given by $\phi = 0°$, $90°$, $180°$ and $270°$ will be suppressed.

Little measurement or prediction work on multi-dimensional devices has been carried out. It appears, however, that the understanding developed from a 1D analysis can be extended to multiple dimensions. Issues such as lobes, periodicity and frequency limits are all similar.

9.8 Absorption

Section 7.2 discussed in some detail how and why Schroeder diffusers absorb sound and how to make a phase grating into an efficient absorber. Briefly, Schroeder diffusers
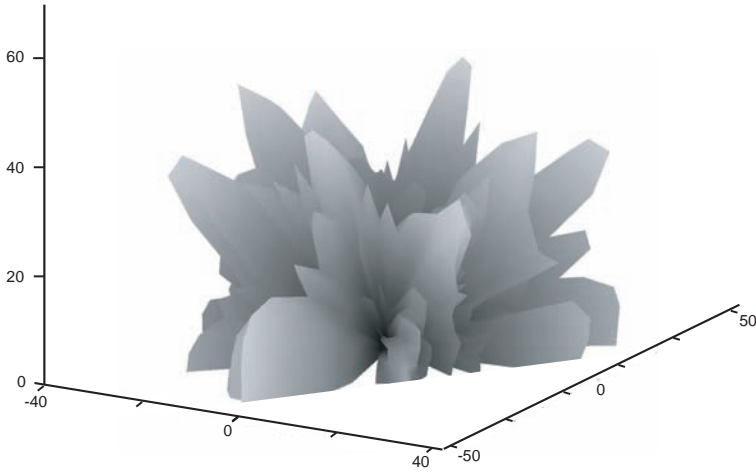
Figure 9.36   Scattering from a modified primitive root diffuser based on the prime 43, and wrapped into a 6 × 7 array using the Chinese remainder theorem.

primarily absorb because of: (1) high energy flows from wells in resonance to wells out of resonance, and (2) 1/4 wave resonant absorption in the wells, especially if the wells are rather narrow. Figure 9.37 shows the random incidence absorption coefficient for 1D and 2D commercial Schroeder diffusers which were similar to the wooden diffusers shown in Figure 9.1.

Figure 9.37 shows how important it is not to cover Schroeder diffusers with cloth, as this greatly increases the absorption. There is energy flow between wells of the absorber promoted by pressure gradients caused by wells being in resonance and having high energy adjacent to wells not being in resonance and having low energy. Consequently, there is high particle velocity around the front face of a Schroeder diffuser and any cloth covering will cause excess absorption, as might be expected if resistive material is
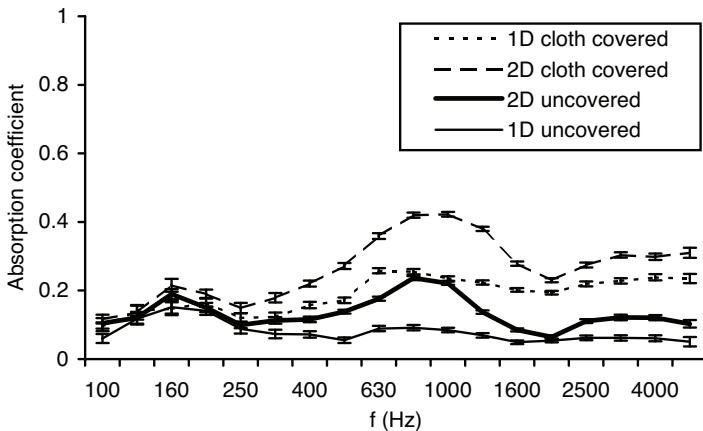
Figure 9.37   Random incidence absorption coefficients measured for 1D and 1D Schroeder diffusers based on $N = 7$ with and without cloth covering.

placed in a region of high particle energy flow. Any cloth covering should be placed at least a well width away from the front face. The cloth should have the lowest possible flow resistivity; indeed it is better if the cloth is not present at all.

There is a wide choice of construction materials for reflection phase gratings. Any smooth, reflective, non-diaphragmatic material is suitable. Over the years, diffusers have been manufactured from a wide variety of materials, such as wood in various species and finishes, light transmitting plastics to provide visibility, thermoformed plastics, Glass Reinforced Gypsum (GRG) and expanded polystyrene. Examples of these diffusers were shown in Figure 9.1.

Figure 9.37 also shows that 2D Schroeder diffusers absorb more sound than 1D devices. It is assumed that this is due to the greater number of different well depths in the 2D device, leading to more energy flow between the wells in addition to a greater density of 1/4 wave resonances. Furthermore, because there are more well walls present than in a 1D device, more losses due to viscous boundary layer effects can occur.

It is important that the Schroeder diffuser is constructed to a high precision. A little data has been published for Schroeder diffusers showing very high absorption coefficients, but this is generally due to poor construction. Small cracks in the bottom of the wells – between the well sides and bottoms – are difficult to avoid unless care is taken. If any cracks open up to cavities behind, these can cause excess absorption as a Helmholtz absorber/resonator has been formed. Proper sealing with varnish or paint is vital. Construction materials are generally not that important unless rough surfaces are used. Figure 9.38 shows the absorption of a concrete masonry Schroeder diffuser before and after it is sealed with paint. Before being fully sealed the rough and porous surfaces cause excess losses at the boundary layers and due to the energy flow between wells around the rough edges of the fins. Absorption is greatly reduced by sealing properly.

Commins *et al.*[31] experimentally investigated the absorption characteristics of a Schroeder diffuser. They showed that by sloping the bottom of the diffuser wells the absorption could be reduced. The effect of the slope is to broaden the resonances of the wells. This will decrease the energy flow within and between wells at resonance. Some early concert hall designs used very wide wells (30 cm), presumably to avoid
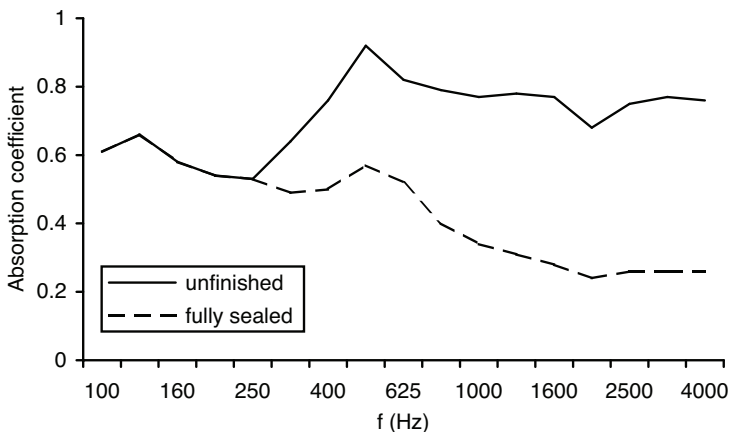
Figure 9.38 Random incidence absorption coefficients measured for a concrete masonry Schroeder diffuser before and after rough surfaces are sealed.

the problems of absorption. The problem with such wide well widths is that at high frequencies specular reflections from the bottom of the wells can cause problems.[32] Furthermore, the bandwidth of the device will be greatly reduced. Consequently, if the fear of absorption cannot be overcome, it might be better to use a fractal construction or a surface topology which does not generate strong resonances, such as a curved surface.

9.9 But …

All the above analysis has relied on a simplified model of acoustic scattering – the Fraunhofer theory. The performance of this theory can be divided into three frequency ranges, as discussed in Chapter 8. At low frequencies the theory is inaccurate as the mutual interactions across the surface are not correctly modelled by the Kirchhoff boundary conditions. At mid-frequencies, the theory is most accurate. At high frequencies, the theory becomes inaccurate again because application realistic sources and receivers are not in the far field. Berkhout *et al.*[33] pointed out that the theory used by Schroeder was approximate and concluded that the development of the diffuser should be based on a more complex model. While it is possible to use a more complex theory, it is only with the simplified Fraunhofer theory that the problem can be reduced to the point that the design can be carried out via simple design equations and using basic Fourier concepts. A more complex prediction model can be used in an optimization process, as will be discussed later, but numerical optimization is a brute force technique which often means the designer learns little about the basic principles of good diffuser design.

Schroeder *et al.*[34] replied to Berkhout *et al.* by pointing out that measurements and accurate theory were not too different from the approximate theory. It should also be argued that by understanding the Fourier properties one is in a better position to understand and exploit brute force techniques such as optimization, or the inverse problem alluded to by Berkhout *et al*. One probable advantage of working with dispersing surfaces is that the laws of physics and the tendency to disorder are going to aid diffusion. The difference between approximate and accurate theories is probably more crucial when exacting results such as notches formed from PRDs are required, or when there is a small number of wells. Even if the optimum diffusion as defined by Schroeder is not achieved, these are pretty complex surfaces which will create some dispersion.

There are other limitations that apply to the Schroeder design, some of which have been touched on before:

1.   The design methodology is based on an approximate model.
2.   Losses are ignored.
3.   The design is carried out for the far field, whereas most listeners are in the near field.
4.   The wells are assumed to be local reacting.

Assumption 3 may not be that limiting. There is some evidence that a diffuser that creates good energy dispersion in the far field also works well in the near field. In the near field, the path length differences from different points on the surface dominate and cause the scattering to have a large number of minima and maxima. Indeed, the polar plots for different diffusers have similar statistical features in the near field.

Some studies have compared periodic and aperiodic arrangements of diffusers either subjectively or objectively[35] using application realistic near field listener positions. In these cases, the aperiodic arrangements, which will create more dispersion in the far field than the periodic cases, are found to be more efficient diffusers in the near field. Consequently, it is assumed that Schroeder diffusers, which create good far field dispersion, will also be effective in the near field. A near field polar response normally neglects to show phase, and it is assumed that the phase of the wavefront must contain the information which enables listeners to distinguish between the periodic and aperiodic arrangements.

Schroeder gave an alternative solution to the near and far field problem. He suggested that by bending the diffuser the far field scattering pattern could be focussed at near field receivers. This means bending the diffuser to follow a parabolic concave mirror. This is not a very useful design because it is rather expensive to execute. A similar effect can be achieved by modulating the well depth phases by the locus of a parabolic mirror. In this case, the varying phases cause the far field beam to be focussed into the near field. It is rather like the use of phase changes in beam steering of transducer arrays. This process has been tested with a boundary element model and shown to work.[5]

Assumption 4 concerns whether the well admittances change due to the presence of the neighbouring wells. This assumption has undergone some limited tests. Cox and Lam[5] compared the admittance predicted by a BEM which models the surface shape precisely against the simple phase change admittance values derived from a reflection coefficient of $\exp(-2jkd_n)$. Figure 9.39 shows that reasonable agreement is found, indicating that the surface admittances are indeed local reacting to a reasonable accuracy. Some real parts are seen indicating losses or maybe mathematical inaccuracies in the BEM model. If these are true losses, they are due to evanescent waves as the BEM model did not include any absorption, and indicates the small inherent absorption present in these devices. Cox and Lam also looked at the admittance variation along the elongated dimension of a 1D Schroeder diffuser. They again showed that the admittance from a BEM model approximately matched the simple phase change admittance, except
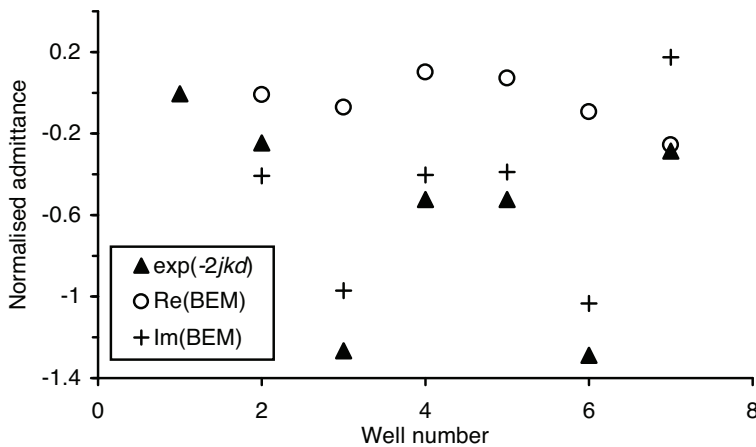
Figure 9.39 Admittance for an $N = 7$ QRD at a single mid-frequency. A BEM prediction was used to generate accurate admittances for comparison with the simple phase change calculation ($\exp(-2jkd)$). The first well is zero depth, and so no comparison is possible (after Cox and Lam[5]).

for positions close to the ends of the wells.

The most significant limitations of the above number theoretic designs are, however:

1. They only work at discrete frequencies.
2. Optimum diffusion means the same energy in the diffraction lobes; this is not the same as even energy in all directions.

As the number theoretic Schroeder diffusers are not truly broadband and do not completely disperse to all directions, it is possible to improve on the design. To do this, optimization algorithms can be used.

9.10 Optimization

9.10.1 Process

De Jong and van den Berg[36] developed the idea of using an iterative solution method to produce Schroeder style diffusers. It wasn't until Cox[37] rediscovered this idea in the early 1990s, however, and D'Antonio[38] provided experimental evidence for the improved performance over traditional number theoretic Schroeder diffusers, that this concept was exploited. de Jong and van den Berg used an approximate prediction model and narrow deep wells which were rather unrealistic for practical diffusers. Cox was able to use greater computing power to use more accurate BEMs, and also used more realistic geometries.

The concept of optimization is illustrated in Figure 9.40. The idea is to get a computer to go through a trial-and-error process searching for the best well depth sequence. First, a starting well depth sequence is randomly chosen. Then the computer predicts the scattering from the surface and evaluates the quality of the scattering in a single figure of merit or error parameter. The computer then adjusts the well depth sequence in an effort to improve the error parameter. When a minimum in the error
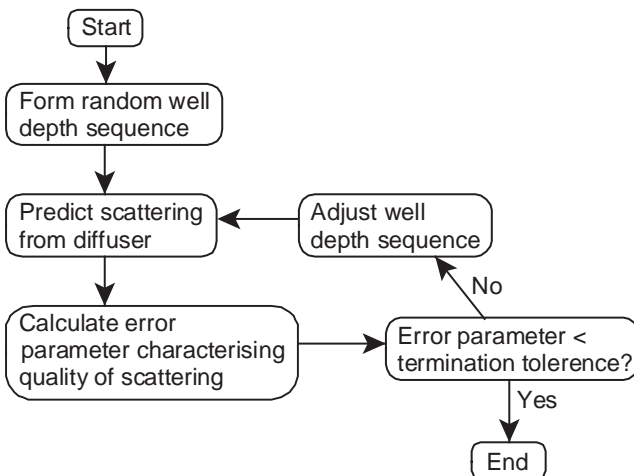
Figure 9.40   Flow diagram for optimizing the well depth sequence of a Schroeder diffuser.

parameter is achieved the iteration process ends, and a good diffuser has been found. Optimization processes are common techniques and have been exploited in a wide range of engineering applications.

To achieve an optimization of diffusers, several key ingredients need to be in place:

1. A validated prediction model.
2. A figure of merit or error parameter.
3. An optimization algorithm to change the well depth sequences.

A validated prediction model is needed and for this a BEM can be used. The disadvantage with a BEM is that it can be very slow to compute, but as computing power is constantly increasing, this is becoming less of a limitation. For computing power reasons, the diffusers that Cox originally optimized were rather narrow; now it is possible to carry this out with wider diffusers in large arrays over a wider bandwidth. It is also possible to use the simpler Fraunhofer models which means the optimization is very fast, but then the accuracy may be compromised. One possibility is to use simple models to carry out a course optimization, and then use the more accurate models to focus on solutions.

The diffusion coefficient can be used to evaluate the quality of the scattering produced by the surface in a single figure of merit. The diffusion coefficient is evaluated at each frequency band of interest, say each one-third octave band. The diffusion coefficients are then averaged across frequency to obtain a single figure of merit. The risk with this simplex averaging process is that the diffusion may be very uneven versus frequency. Frequencies with very good diffusion may compensate for frequencies with very poor diffusion, where a better solution might be moderate diffusion consistent across the whole frequency range. This problem is most easily solved by subtracting a standard deviation of the diffusion coefficients from the mean value across frequencies. This then penalizes cases with very uneven diffusion coefficient spectra.

An optimization algorithm is used to adjust the well depth sequence during the search. It is needed so that the different well depth sequences can be tried and tested in a logical manner rather than by a completely random trial-and-error basis. A usual analogy for a 2D optimization is finding the lowest point in a hilly landscape (while blindfolded). If a human was to carry out such a search, they would start by going downhill on the presumption that this will lead them to a lower point. The optimization algorithm must make similar decisions. It is vital that the solution is found in the fewest steps as otherwise the optimization process becomes rather tedious. The landscape is an optimization problem with two degrees of freedom; the analogous diffuser would only have two well depths. Practical optimization problems involve many more degrees of freedom which makes finding the minima more difficult.

There are a variety of algorithms available for optimization.[39] The key decision is whether the optimization is to take place with only the figure of merit, or with the figure of merit and its derivative. Knowledge of the derivative vastly speeds up the optimization processes and the derivative should always be used if available. To continue with the landscape analogy, it is much quicker if the person is told the downhill direction, otherwise they have to stagger around for a while trying to decide which way is downhill. The problem with diffuser optimization is that the derivative is not often known. With the Fraunhofer theory and a simple figure of merit, such as minimizing the specular zone energy, it is possible to derive the derivative of the figure of merit,[10] but that is an unusual case.

For most work on diffuser optimization, only function values are known. A downhill simple algorithm has been often used, which is rather slow. It is, however, extremely robust to non-linear constraints, something which will become important for the non-welled constructions discussed in Chapter 10. There are other techniques like genetic algorithms or quasi-Newton gradient descent methods. The disadvantage of a genetic algorithm is that it requires tuning by appropriately choosing variables such as population size and mutation rate. Methods which calculate gradients with finite differences such as quasi-Newton methods can cause problems with solution techniques such as BEMs, which often have small numerical inaccuracies which can greatly affect the estimated gradient. A downhill simplex method may not be trendy, but it just needs plugging in and it works.

When carrying out the optimization for a Schroeder diffuser, it is most efficient to use a BEM where the diffuser is modelled as a box with a variable admittance on the surface. Then all that changes during the optimization is the front face admittance and not the surface profile. This means that the time consuming processes of carrying out the Green's function integrations can be done once at the start of the optimization.

This greatly reduces optimization time. In fact, it should be possible to get the derivatives of the figure of merit in this case.[40] Time spent speeding up the prediction algorithm is time well spent; in a typical optimization process the scattering is typically evaluated a thousand times, so unless each individual case takes a matter of seconds, the optimization process will become very slow.

In any optimization problem there will be a large number of local minima, but somewhere there will be the numerically lowest point called the global minimum. To return to the landscape analogy, the blindfolded person might find a valley bottom and think the best point has been found, not realizing that over the next mountain ridge there is a lower valley. The key to a good optimization algorithm is not to be trapped in poor local minima, but to continue to find deep local minima. Provided a good optimization algorithm is chosen, this should not be a problem, especially if the optimization is tried many times from different starting points, as is customary good practice.

When there are a large number of degrees of freedom in an optimization problem, i.e. a large number of well depths to be optimized, the surface describing the variation of the figure of merit with the well depths becomes very complex. There will be a very large number of minima. It is virtually impossible to find the global minimum unless a large amount of time is used with the optimization algorithm being started over and over again from a wide variety of places on the error surface. Fortunately, as the number of degrees of freedom increases, the need to find the global minimum becomes less important. Experience has shown that there are a large number of good local minima solutions available and, although the scattering will be different in each case, there is often negligible difference in performance between the good local minima. There is usually no magical global minimum where the quality of scattering produced is significantly better than good local minima.

9.10.2 *Results*

When testing the results of an optimization, it is important to look at frequencies, source and receiver positions that are different to those used during the optimization. This checks to see whether the design process has found a robust solution. There is always a risk that the optimizer will over-fit a poor solution; this is where the solution is
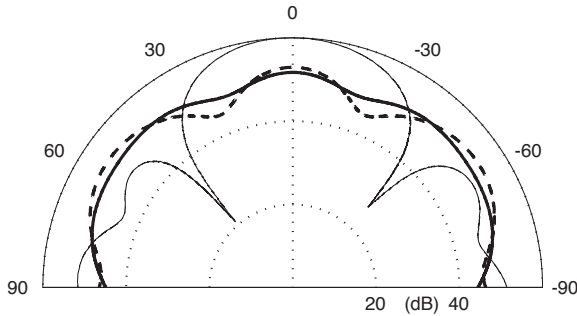
Figure 9.41 The scattering from an ———— N = 7 Schroeder diffuser; – – – an optimized Schroeder diffuser, ■■■■ an optimized stepped diffuser at 1,050 Hz (data from Cox[37]).

good only for the specific geometries and frequencies used during the optimization.

Figure 9.41 shows the scattering from two optimized diffusers compared to an $N = 7$ QRD. One of the optimized diffusers had fins; the other had a stepped profile – essentially a Schroeder diffuser with the fins removed. Both the optimized diffusers produce more even scattering than the QRD at this and other frequencies.

Cox[37] found that the optimized $N = 7$ diffuser with fins outperforms the QRD over a wide variety of frequencies. When the number of wells was increased to about 36 and compared to two periods of an $N = 17$ QRD, however, the gains were less marked. The scattering from the QRD was already fairly uniform at the low frequencies and so the room for improvement was relatively small. This was not, however, particularly due to the use of a quadratic residue sequence – even a diffuser with randomly determined well depths gave reasonable diffusion.

Removing the constraints on geometry imposed by a Schroeder style diffuser and forming a stepped surface produced better diffusion. The magic in the Schroeder diffuser geometry is not that it produces diffusion, but that it enables simple design methods to be brought to bear on the problem. Removing the fins enables a simpler geometry, which is cheaper to make. It has also removed the resonant wells and so will have lower absorption. The improved performance was seen for both the $N = 7$ and $N = 36$ cases. Interestingly, the $N = 7$ optimized stepped diffuser looked rather like a faceted semicylinder.

D'Antonio[38] carried out a thorough experimental evaluation of the work of Cox. The measurements confirmed that optimization produced better diffusers than number theory sequences. D'Antonio also looked at the performance of the diffusers outside the domain of optimization; at higher frequencies, at oblique angles of incidence, for different receiver radii and for a periodic arrangement. Outside the domain of optimization, the optimized diffusers were found to give roughly the same diffusion as the Schroeder diffusers – sometimes worse, sometimes better. The solution to this problem is to carry out the optimization including all frequencies, angles of incidence and source and receiver radii of interest. With modern computing power this is not a problem.

The original optimization work was limited to narrow single diffusers because of computing power. Now this optimization process can be applied to diffusers spread over larger areas. Figure 9.42 compares the normalized diffusion from an $N = 7$ QRD to an
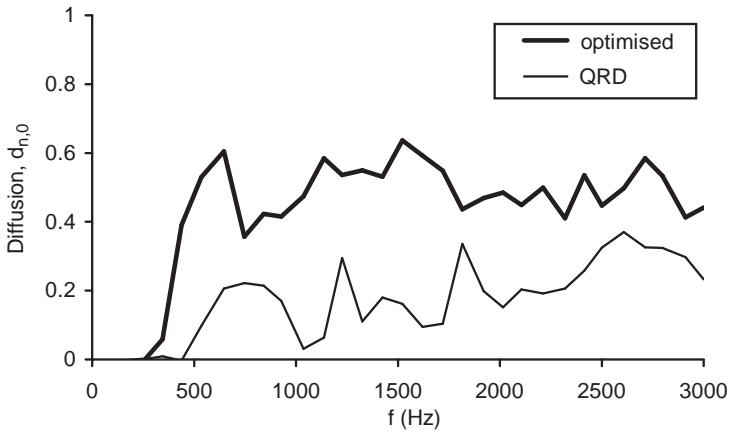
Figure 9.42   Normalized diffusion spectra for multiple periods of a Schroeder diffuser and an optimized phase grating diffuser.

optimized modulated arrangement of phase grating diffusers. The improvement in diffusion is quite marked.

It is also possible to optimize for a non-even scattering distribution. For example, Cox and D'Antonio[10] tried to minimize the energy in a particular direction; to produce a notch in the specular reflection direction to create an improved PRD. In Figure 9.43 the results from trying to optimize a diffuser to work from 500 to 3,000 Hz for an angular range of ±5° about the specular reflection direction are shown. The diffuser is labelled optimized and is compared to a plane surface and a modified PRD. Across the optimization range the specular reflection is reduced by about 25 dB compared to a plane surface, and by 10 dB when compared to the PRD. This was for a single period of the diffuser. When multiple periods were attempted, the results were far less
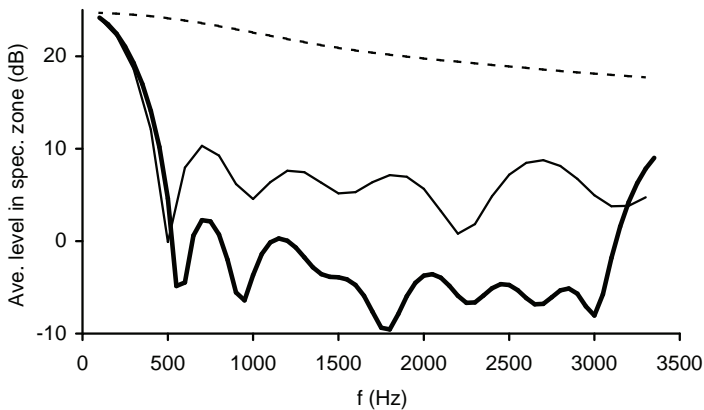
Figure 9.43   The average energy in the specular zone for three surfaces:
– – – plane;
——— optimized;
——— modified PRD (after Cox and D'Antonio[10]).

dramatic. Over the bandwidth 500–3,000 Hz the best optimized diffusers could achieve was an extra 4 dB attenuation of the specular and near-specular energy when compared to the modified primitive root. Although the reduction would probably be audible in certain applications, the improvement is not dramatic. Experience has shown that using optimization to shape polar responses or create notches is fraught with difficulty. Optimization is most successful when trying to create uniform dispersion.

9.11 Summary

Schroeder diffusers have been hugely successful thanks to their simple concept, straightforward design equations and their commercial exploitation. There has always been a certain reticence among designers to use this type of diffuser, however. The rumours of absorption have continued since their inception, with high absorption coefficients being published for poorly constructed surfaces. Now that there is a proper understanding of the absorption mechanisms, this should no longer be a problem. A few people have claimed to hear strange artefacts from Schroeder diffusers, but the designs they have been listening to have not followed some of the important design principles discussed in this chapter. Following proper design principles and applying all the current knowledge results in high quality sound from Schroeder diffusers. One of the main stumbling blocks to their use is, however, their visual appearance which is either loved or loathed. Consequently, other diffusers are needed which have defined acoustical properties but with different visual aesthetics. This will be addressed in the next chapter.

9.12 References

 1 M. R. Schroeder, "Diffuse sound reflection by maximum-length sequences", *J. Acoust. Soc. Am.*, **57**(1), 149–50 (1975).
 2 M. R. Schroeder, "Binaural dissimilarity and optimum ceilings for concert halls: more lateral sound diffusion", *J. Acoust. Soc. Am.*, **65**, 958–63 (1979).
 3 P. D'Antonio and J. Konnert, "The reflection phase grating diffusor: Design theory and application", *J. Audio Eng. Soc.*, **32**(4) (1984).
 4 T. J. Cox and P. D'Antonio, "Schroeder diffusers: A review", *Building Acoustics*, **10**(1), 1–32 (2003).
 5 T. J. Cox and Y. W. Lam, "Prediction and evaluation of the scattering from quadratic residue diffusors", *J. Acoust. Soc. Am.*, **95**(1), 297–305 (1994).
 6 W. R. T. Tenkate, "On the bandwidth of diffusors based upon the quadratic residue sequence", *J. Acoust. Soc. Am.*, **98**(5), 2575–9 (1995).
 7 P. D'Antonio and J. Konnert, "The QRD diffractal: a new one- or two-dimensional fractal sound diffusor", *J. Audio Eng. Soc.*, **40**(3), 113–29 (1992).
 8 P. Fan and M. Darnell, *Sequence Design for Communications Applications*, John Wiley & Sons, 49 (1996).
 9 E. Feldman, "A reflection grating that nullifies the specular reflection: A cone of silence", *J. Acoust. Soc. Am.*, **98**(1), 623–34 (1995).
10 T. J. Cox and P. D'Antonio, "Acoustic phase gratings for reduced specular reflection", *Applied Acoustics*, **60**(2), 167–86 (2000).
11 M. R. Schroeder, "Phase gratings with suppressed specular reflections", *Acustica*, **81**, 364–9 (1995).
12 K. Datiotis, T. J. Cox and J. A. S. Angus, "Lüke and power residue sequence diffusers", *Proc. 19th ICA*, Madrid, RBA-11-005 (2007).
13 8, op. cit., 187–8.
14 D. Takahashi and R. Takahashi, "Sound fields and subjective effects of scattering by periodic-type diffusers", *J. Sound Vib.* **258**(3), 487–97 (2002).

15 J. A. S. Angus, "Large area diffusors using modulated phase reflection gratings", *Proc. 98th Convention Audio Eng. Soc.*, preprint 3954 (D4) (1995).

16 J. A. S. Angus, "Using modulated phase reflection gratings to achieve specific diffusion characteristics", *Proc. 99th Convention Audio Eng. Soc*, preprint 4117 (1995).

17 J. A. S. Angus and C. I. McManmon, "Orthogonal sequence modulated phase reflection gratings for wideband diffusion", *Proc. 100th Convention Audio Eng. Soc.*, preprint 4249 (1996).

18 J. A. S. Angus and A. Simpson, "Wideband two dimensional diffusers using orthogonal modulated sequences", *Proc. 103rd Convention Audio Eng. Soc.*, preprint 4640 (1997).

19 J. A. S. Angus and C. I. McManmon, "Orthogonal sequence modulated phase reflection gratings for wide-band diffusion", *J. Audio Eng. Soc.*, **46**(12), 1109–18 (1998).

20 J. A. S. Angus, "Using grating modulation to achieve wideband large area diffusers", *Appl. Acoust.*, **60**(2), 143–65 (2000).

21 B. B. Mandelbrot, *The Fractal Geometry of Nature*, Freeman, San Francisco (1983).

22 A. Jrvinen, L. Savioja and K. Melkas, "Numerical simulations of the modified Schroeder diffuser structure", *J. Acoust. Soc. Am.*, **103**(5), 3065 (1998).

23 F. P. Mechel, "The wide-angle diffuser – a wide-angle absorber?" *Acustica*, **81**, 379–401 (1995).

24 J. A. Hargreaves and T. J. Cox, "Improving the bass response of Schroeder diffusers", *Proc. IoA(UK)*, **25**(7), 199–208 (2003).

25 P. D'Antonio and T. J. Cox, *Extended Bandwidth Folded Well Diffusor*, US Patent 7, 322, 441 (2006).

26 J. Hunecke, "Schallstreuung und Schallabsorption von Oberflächen aus Mikroperforierten Streifen", PhD thesis, University of Stuttgart (1997).

27 K. Fujiwara, K. Nakai and H. Torihara, "Visualisation of the sound field around a Schroeder diffuser", *Appl. Acoust.*, **60**(2), 225–36 (2000).

28 T. Wu, T. J. Cox, and Y. W. Lam, "A profiled structure with improved low frequency absorption", *J. Acoust. Soc. Am.*, **110**, 3064–70 (2001).

29 M. R. Schroeder, *Chaos, Power Laws: Minutes from an Infinite Paradise*, W. H. Freeman & Co (1991).

30 J.-D. Pollack and G. Dodd, personal communication.

31 D. E. Commins, N. Auletta, B. Suner, "Diffusion and absorption of quadratic residue diffusers", *Proc. IoA(UK)*, **10**(2), 223–32 (1988).

32 T. J. Cox and Y. W. Lam, "The performance of realisable quadratic residue diffusers (QRDs)", *Appl. Acoust.*, **41**(3), 237–46 (1994).

33 A. J. Berkhout, D. W. van Wulfften Palthe, and D. de Vries, "Theory of optimal plane diffusers", *J. Acoust. Soc. Am.*, **65**(5), 1334–6 (1979).

34 M. R. Schroeder, R. E. Gerlach, A. Steingrube and H. W. Strube, "Response to 'theory of optimal planar diffusers'", *J. Acoust. Soc. Am.* **65**(5), 1336–7 (1979).

35 T. J. Hargreaves, "Acoustic Diffusion and Scattering Coefficients for Room Surfaces", PhD thesis, University of Salford (2000).

36 B. A. de Jong and P. M. van den Berg, "Theoretical design of optimum planar sound diffusers", *J. Acoust. Soc. Am.*, **68**(4), 1154–9 (1980).

37 T. J. Cox, "Optimization of profiled diffusers", *J. Acoust. Soc. Am.*, **97**(5), 2928–41 (1995).

38 P. D'Antonio, "Performance evaluation of optimized diffusors", *J. Acoust. Soc. Am.*, **97**(5), 2937–41 (1995).

39 W. H. Press *et al.*, *Numerical Recipes*, *The Art of Scientific Computing*, Cambridge University Press, 289–92 (1989).

40 R. D. Ciskowski and C. A. Brebbia (eds), *Boundary Element Methods in Acoustics*, Kluwer Academic Publishers (1991).

10 Geometric reflectors and diffusers

Cylinders, pyramids and plane surfaces are common items in rooms. In this chapter the performance and design of these geometric surfaces will be considered as well as fractal and optimized curved surfaces. While most diffuser design is about breaking up wavefronts by surface roughness or impedance changes, it should be remembered that even a plane surface can cause significant diffraction from its edges, provided the surface has a similar size to the acoustic wavelength.

Triangles or pyramids can produce dispersion, redirection and specular reflection depending on the geometry used. Applied correctly, triangles and pyramids can form notch diffusers, where the energy in certain directions is much reduced. Curved surfaces are more obviously diffusers and more universally used; indeed a simple sphere or cylinder is very effective at spatially spreading reflections, but this is not the only ingredient needed for a good diffuser. Furthermore, a solitary sphere or cylinder is not very useful and so many spheres or cylinders next to each other are needed. Then the scattering is as much about how the objects are arranged, periodically or randomly, as about the scattering characteristic of the individual sphere or cylinder. A well-designed curved surface has the advantage of blending with modern architectural designs.

This chapter will first consider the role of plane surfaces, as an understanding of scattering from finite-sized surfaces is fundamental to diffraction and diffuse reflection.

10.1 Plane surfaces

Whether by accident or design, plane surfaces are probably the most common architectural surface. Consequently, understanding the reflection effects of finite-sized plane surfaces is important. Without surface roughness, any dispersion is generated by edge scattering. The effects of edge scattering for more complex surfaces can also be partly or fully explained using the concepts given below.

10.1.1 Single panel response

Consider the geometry shown in Figure 10.1, where a source and receiver are near a finite-sized plane surface. The surface is assumed rigid, hard and non-absorbing. If the source and receiver are chosen so that the geometric reflection point, the point at which the angle of incidence equals the angle of reflection, lies on the panel, then the scattered pressure as a function of frequency, as shown in the top line in Figure 10.2, resembles
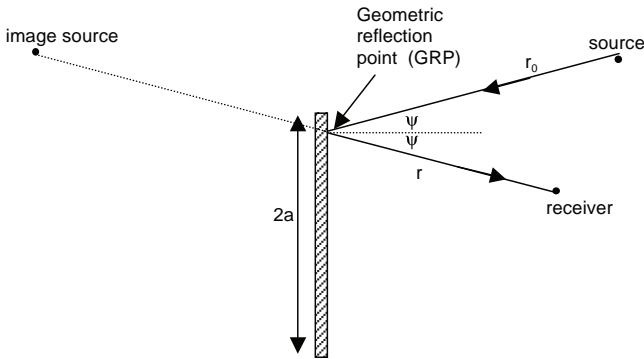
Figure 10.1   Geometry for sound reflecting from a plane surface.

an approximate high pass filter. At very low frequencies, when the wavelength is very large compared to panel size, little or no sound is scattered from the surface. At very high frequencies, when the wavelength is small compared to the surface size, strong specular reflection results.

It is useful to define the cut-off frequency for the plane reflector and the transition frequency between specular reflection and significant diffraction. To continue with the filter analogy, the transition frequency can be taken as the –3 dB point of the high pass filter.[1-4] This gives an approximate frequency below which the panel most effectively scatters sound in all directions and above which the panel produces more specular-like reflections. Rindel has derived a simple and useful formulation for the cut-off frequency. Rindel[4] used a simplified Fresnel solution method for the scattering from a plane surface, with the Fresnel integrals approximated by simple mathematical functions. Using this solution method, Rindel found a transition frequency above which the Fresnel integrals remain roughly constant. He defined this point as the cut-off frequency. For a plane panel it is given as:

$$f_{-3dB} = \frac{cr^*}{8a^2 \cos^2(\psi)}$$

(10.1)
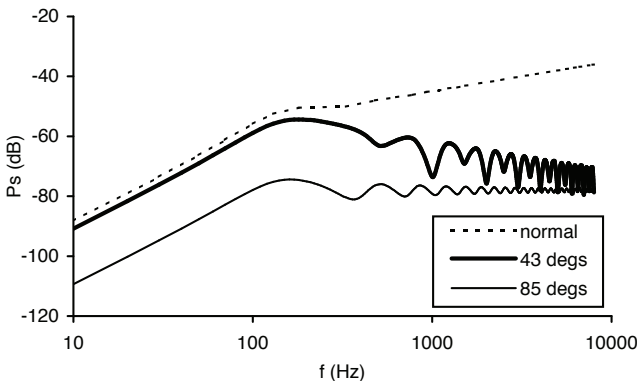
Figure 10.2   Scattered pressure level from a plane surface for three different receiver angles as shown in the legend. Normal incidence sound.

where r^* is given by:

$$r^* = \frac{2rr_0}{r + r_0}$$

(10.2)

where r_0 is the distance from the source to the panel centre; r is the distance from the receiver to the panel centre; $2a$ is the panel width; c is the speed of sound, and ψ the angle of incidence.

The use of a cut-off frequency is most valid for receivers close to the specular reflection direction. Figure 10.2 also shows predictions for the scattering at two oblique reflection angles. This shows that representing the scattered pressure by a simple high pass filter does not work for every direction. In this case, there is often a complicated pattern of minima and maxima. When the geometric point of reflection lies on the surface of the panel, it is reasonable to assume that the scattered pressure at high frequencies is going to be dominated by specular reflection. When the geometric reflection point does not lie on the surface, however, the scattered pressure is entirely due to diffraction. In this case, the diffracted energy reaching the receiver will decrease as the frequency increases. Consequently, the frequency response for these receivers is more likely to follow something closer to a band pass filter response. This is illustrated by the 43° receiver in Figure 10.2. This is not always true, however, as shown for the grazing reflection case. A rough guide to the region over which the cut-off frequency representation works is therefore the region over which the geometric reflection point lies on the panel. Incidentally, to simplify the calculation of these angles, an image source construction is a good idea as it greatly reduces the complexity of the trigonometry – this is shown in Figure 10.1.

For a plane panel, the case of scattering close to the specular reflection direction is usually of most interest, as this will have the largest amount of the scattered energy at high frequencies. Nevertheless, with significant energy scattered into other angles at low frequencies, the use of a cut-off frequency should be carried out with caution. Equation 10.1 has either assumed a square panel, where the azimuth and elevation incident angles are the same or a 2D world. For rectangular panels, and arbitrary
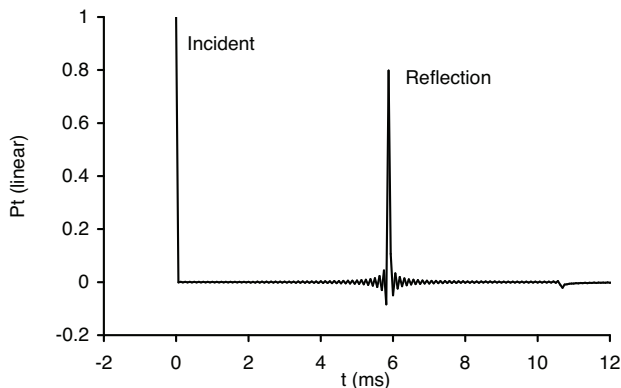
Figure 10.3 Time response for incident and scattered sound from a plane surface (NB, not the same case as Figure 10.2).
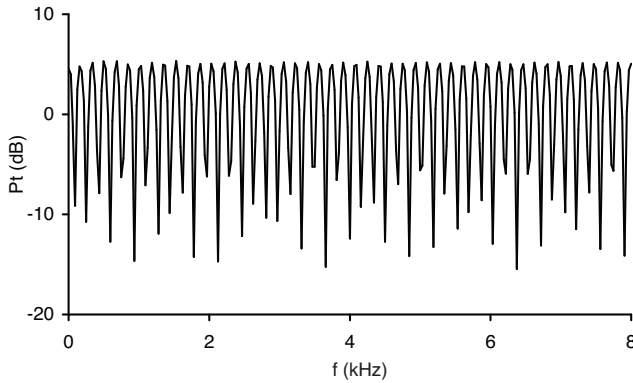
Figure 10.4   Total field frequency response for plane surface scattering.

incidence angles with square panels, there will be two different cut-off frequencies to consider. For circular or odd-shaped panels, the transition will be more complicated, but similar general principles to that shown in Figure 10.2 apply.

Figure 10.3 shows the total sound field impulse response – incident plus reflection sound – for plane wave scattering. The direct and reflected sounds are clearly distinguishable, as is the edge scattering wave which has a negative magnitude. Figure 10.4 shows the frequency response for the total sound field shown in Figure 10.3. The reflected sound from a plane panel is very similar to the incident sound unless the panel is small and so the frequency response shows distinct comb filtering. Comb filtering is characterized by minima and maxima at a regular spacing in frequency. The ear is particularly sensitive to this emphasis and de-emphasis of frequency components, and when audible, listeners will complain of harshness or glare from these reflections.

In diffuser design the ability of a surface to disperse the sound spatially is often monitored. Figure 10.5 shows the scattering from a plane thin rigid surface for several frequencies in the far field. For the largest wavelengths (lowest frequencies), the scattered response is exactly the same as that produced by a dipole, following a $|\cos(\psi)|$
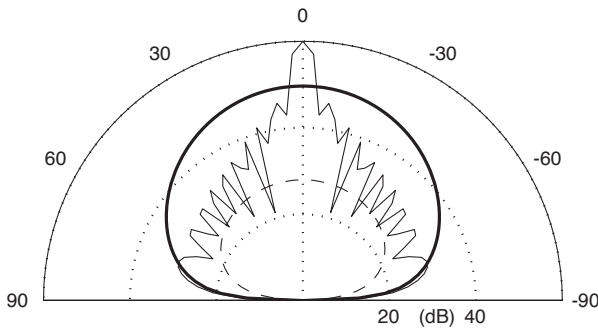
Figure 10.5   Scattered pressure level from a plane panel for three different frequencies:
– – – $\lambda = 20a$;
——— $\lambda = 2a$;
——— $\lambda = 0.2a$. Thin panel boundary element method (BEM) prediction.
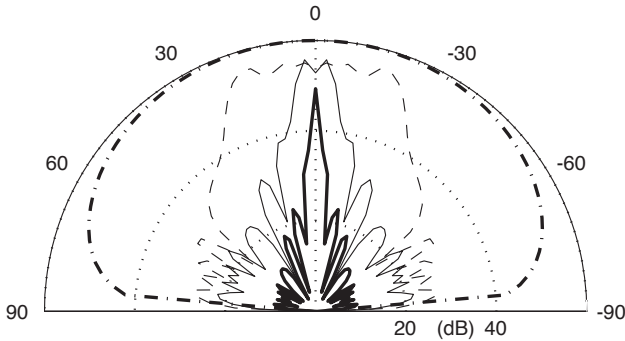
Figure 10.6 High frequency scattering from a plane surface 1 m wide (=30λ) for four
different receiver radii:
·—·—·· 0.8 m;
– – – 1.2 m;
——— 5.0 m; and
▬▬▬ 1000 m.

function typical of a low frequency dipole approximation. At grazing angles there is
zero pressure. This only happens for the infinitesimally thin surface, since surfaces with
finite thickness produce finite pressure. In fact, the pressure for all angles is relatively
low for large wavelengths as destructive interference is the dominant phenomenon, as
is true of dipoles. To put this in less technical language, when the wavelength is much
larger than the panel size, the wave does not 'see' the panel and propagates largely
undisturbed.

As the frequency increases and the wavelength becomes comparable and then smaller
than the panel size, eventually a specular reflection becomes apparent. Energy is
concentrated in the specular reflection direction obeying Snell's law, where the angle
of incidence equals the angle of reflection. This is a special case of Fermant's principle,
where the specular reflection direction is the shortest possible path length and so is
preferred.

Figure 10.5 presents the far field response. In real spaces, however, listeners and
sources can be quite close to surfaces. Figure 10.6 shows how the scattered pressure
distribution varies for a high frequency, as the receiver distance varies. At 0.8 m from
the panel, the receiver arc diameter is actually smaller than the panel width. For all
receivers on the 0.8 m arc the scattered pressure is high because for every receiver
there is a geometric reflection point on the panel giving a strong specular reflection.
As the receiver arc moves further from the panel fewer receivers get a strong reflection;
eventually the far field response is achieved.

Figure 10.6 implies that, close to the panel, the flat surface is good at dispersing
sound. In particular, good coverage is achieved because all receivers get similar energy
in the reflection. This does not mean, however, that the plane surface is a good diffuser.
In reality, the plots in Figure 10.6 are only telling part of the story. The polar plots
of scattered energy do not show how the direct and reflected sounds interfere, or the
effect this has on the sound heard by the listener. In fact, a comb filter response would
result, and this is likely to colour the sound, as discussed in Chapter 2.
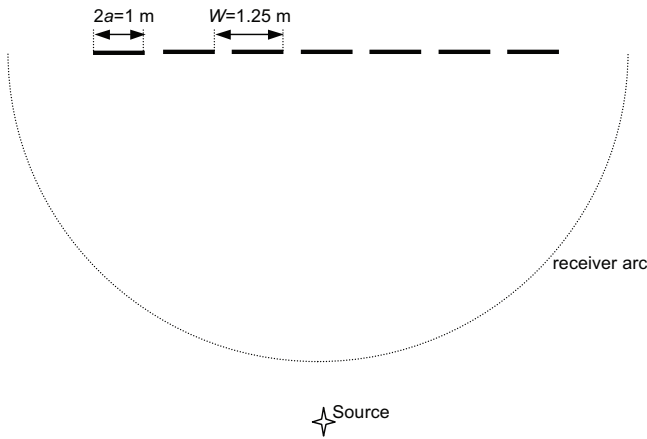
Figure 10.7   Sketch of an array of plane panels tested (source and receiver positions not to scale).

10.1.2 Panel array response: far field arc

When multiple plane panels in an array are used the response is a combination of both the response of a single panel and the periodic arrangement of the array. Figure 10.7 shows a sketch of an array which will be used to demonstrate the response. For simplicity, scattering in one plane predicted using a 2D model will be used. The findings can be generalized to a 3D array, as the principles are the same. Using the simple Fourier theory detailed in Chapter 8, it is possible to represent the array response, p_a, as a multiplication of the single panel response and a set of delta functions:

$$p_a(\beta) = p_1(\beta) \sum_{m=-\infty}^{\infty} \delta\left(\beta - \frac{m\lambda}{W}\right) \tag{10.3}$$

$$\beta = \sin(\psi) + \sin(\theta) \tag{10.4}$$

where β is the transform variable, as discussed in Chapter 9; ψ and θ are the incidence and reflection angles respectively; p_a is the pressure from the array; p_1 is the pressure from a single panel; m is an integer; λ the wavelength; $2a$ the single panel width; W the repeat distance; and δ the delta function.

This formulation is for the far field. It is an approximate representation, and so the graphs which are being shown are actually generated by an accurate BEM model, described in Chapter 8. Equation 10.3 is being used purely to aid understanding of the physical processes. This formulation is using similar arguments to those used for modulated forms of Schroeder diffusers in Chapter 9, where the concept is given in a little more detail.

Figure 10.8 shows the scattering for three contrasting frequencies. The last term in Equation 10.3 means that it would be expected that whenever:
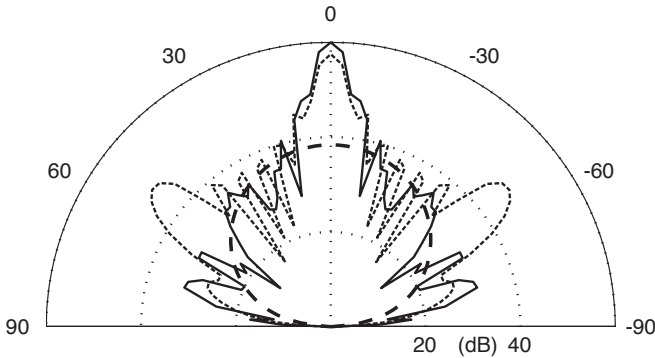
Figure 10.8   Scattering from an array of plane panels for three different frequencies:.
  – – – 34 Hz ($\lambda = 10{\cdot}2a$);
  ······· 340 Hz ($\lambda = 2a$); and
  ⎯⎯ 10 kHz ($30\lambda = 2a$).
  The $1/\sqrt{f}$ variation which naturally occurs with line sources has been removed to make comparison easier.

$$\beta = \sin(\psi) + \sin(\theta) = \frac{m\lambda}{W} \qquad\qquad (10.5)$$

there should be a reflection similar to the single panel alone. For the middle frequency in Figure 10.8, Equation 10.5 predicts lobes at 0, ±53° and this is borne out by the prediction of three grating lobes. Consequently, at mid-frequencies, periodicity effects will often dominate, and Equation 10.5 will predict their location.

At low frequencies the scattering from a single panel is rather small (20 dB less in the specular reflection direction) and follows a dipole response as the wavelength is large compared to panel size. In this case the single panel response $p_1(\beta)$ dominates the scattered level. The array produces a polar response which is very similar to a single panel, albeit with an increased power due to the greater surface area of the array of panels compared to a single panel. There are no periodicity lobes because the wavelength is so large that only the zeroth order mode ($m = 0$) can exist in the far field.

At the highest frequency, the scattering is dominated by a strong specular reflection. Equation 10.5 predicts a large number of side lobes (70), but these are not seen. The reason for this is that the response of the single panel p_1 is highly directional as was shown in Figure 10.5. Consequently, most of the side lobes have very low levels. In fact, the scattering from the array of panels is not too dissimilar to that of a single panel, except for a change in radiated power due to the greater surface area of the array.

10.1.3 Panel array response: near field

Simple reflector arrays are often used above stages and audiences in auditoria. In this case it is not just the response on a far field arc that should be considered, but also the response at application-realistic source and receiver positions. In many cases, this will be along a straight line 5–12 m below the reflector array. This produces a scattered
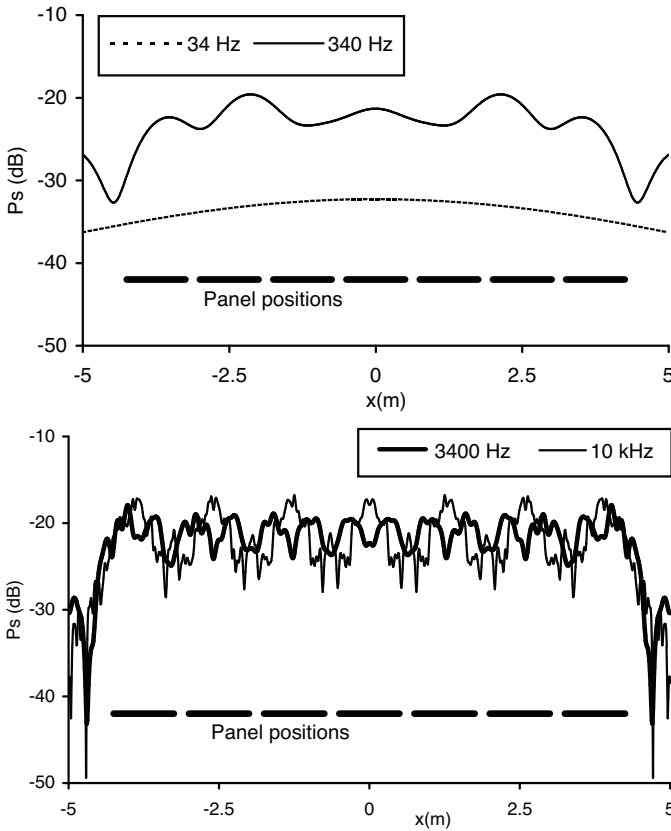
Figure 10.9   Near field scattered level from an array of plane panels along a straight line for various frequencies. The panel positions in the x-direction are shown at the bottom of both pictures.

response that is quite different in character to the far field arc. Figure 10.9 shows the scattering from the same array as shown in Figure 10.7 with a far field source and a line of receivers 8 m below the array running parallel to the array. (A far field source is used to simplify matters, but in reality the source would also be in the near field.) Figure 10.9 also indicates the panel locations.

At high frequency, the specular reflection from each panel is apparent. The scattered pressure is uneven, with a minimum where the geometric reflection point for a receiver is between panels, and a maximum where the geometric reflection point lies on a panel. For most designs of overhead canopies this uneven response is undesirable. Due to these absences between reflectors at high frequency, and the strong specular reflections between, shaped elements are usually used, such as arcs, to disperse energy more evenly to all receivers. This will be discussed in more detail later in this chapter.

For the middle two frequencies (340 and 3.4 kHz) the response is a complex pattern of minima and maxima. These are near field effects (the 10 kHz case was also in the near field, but the high directivity of the individual panel response weakened the near field effects). The rapidly changing path length differences from the array to the receiver,

as the receiver location is moved along the x-axis, cause a multitude of minima and maxima. The lowest frequency is in the far field, so something like the dipole response seen previously for the far field arc is obtained.

Rindel[5] used Fresnel theory to investigate arrays of ceiling reflectors. He used square reflectors and investigated the effect of reflector density on the frequency response. He found that if the geometric reflection point lay on a panel, a high pass characteristic with some similarity to the single panel response was obtained. Due to the fact that the reflections come from multiple panels, the actual frequency response had many more local minima and maxima than was the case for the single panel alone.

If the geometric reflection point was between panels, however, the scattering had a low pass filter response. In the latter case the energy is greatest when the scattering is greatest, and this occurs at the low frequencies. At high frequencies the energy is concentrated in specular directions and so the scattered energy for these receivers is small. Rindel showed that using smaller panels was advantageous, as it reduced the roll-off at high frequencies for receivers away from the geometric reflection points.

Either the size of the reflectors or the panel density determines the low frequency performance of an array. It is possible to imagine cases where it is a combination of these effects which is important. The mid- and high frequency performance is dominated by strong local variations due to the size of the reflectors and the repeat distance between them. The solution to this is to use non-plane surfaces, as shall be discussed later. Alternatively, a pseudorandom arrangement of different panel sizes and spacings could possibly be used. However, if the pseudorandom arrangement is based on a regular lattice, the reduction of periodicity effects maybe less dramatic than expected.

10.2 Triangles and pyramids

Triangles and pyramids can display a wide variety of scattering behaviour from a good diffuser to a surface that generates specular reflections, depending on the geometry. It will be shown that the scattering from an array of triangles or pyramids is very much determined by the steepness of the side slopes. For simplicity, the analysis below only considers a 2D case with triangles, but the arguments can easily extend to 3D surfaces, such as pyramids.

A simple ray tracing yields much information about how a triangle reflects sound.
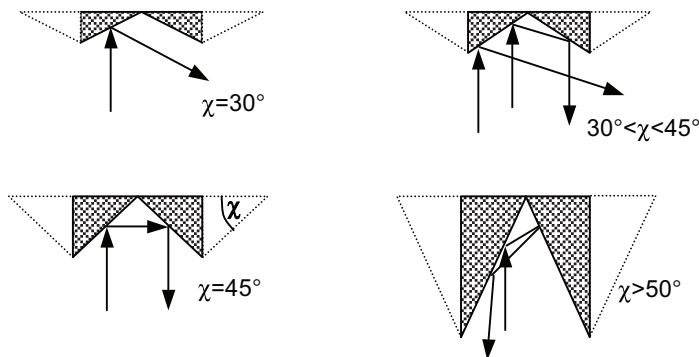
Figure 10.10 Ray tracing of sound reflecting from the centre of pairs of triangles.
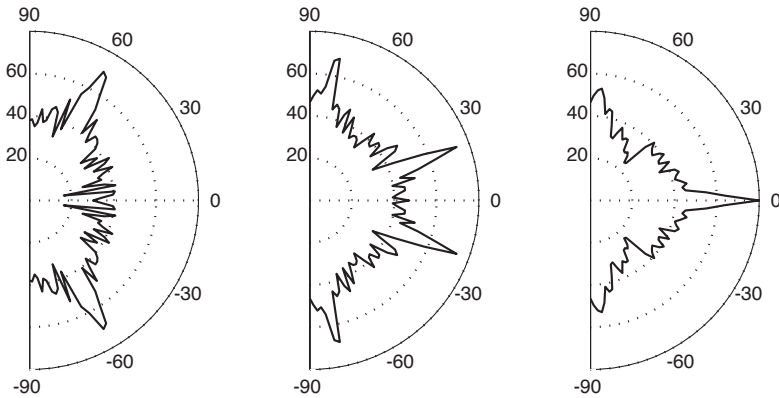
Figure 10.11 Scattered level from the centre of two triangles for three side angles, from left to right: χ = 30, 40, 45°.

Figure 10.10 shows some simple ray tracing examples. As the angle (χ) of the triangle varies, the reflection characteristic shifts between a notch response, diffuse reflection and a specular response. To understand a triangular arrangement very simple prediction theories based on the Kirchhoff method will not always work, because they do not model second and higher order reflections (see Chapter 8). Consequently, it is safer to use a BEM model or similar. Initially, only high frequencies will be considered at normal incidence. This makes the pattern of scattering clear. A further simplification is that the response for only the centre portion of two triangles will be considered, as this is more representative of what happens when an array of triangles is used.

For shallow angles ($\chi \leq 30°$) the ray tracing shows only a single reflection from each side as shown in Figure 10.10. This results in two distinct lobes being generated at angles of $\pm 2\chi$. An example of the far field scattering is shown in Figure 10.11. This then forms a notch response, with the energy returned to the specular direction being minimized. This is effectively a redirecting surface which generates two strong reflections in different distinct directions. Unlike primitive root diffusers discussed in Chapter 9, this surface forms a notch over a relatively wide frequency range, although the performance will be compromised at low to mid-frequencies, when finite-sized panel effects become important. Equation 10.1 could be used as a guide as to when each side will produce specular-like reflections and so produce a notch response, and when the scattering will be more dominated by edge diffraction. This finite panel effect is true for all the discussion below, but these comments will not be repeated again. With a $\chi \leq 30°$ triangle there is only a notch for certain incident angles, whereas a primitive root diffuser worked for any angle of incidence, but only at a few distinct frequencies.

For $30° < \chi < 45°$ a mixture of single and double reflections are seen in Figure 10.10. The single reflections will again form lobes in the directions of $\pm 2\chi$; the double reflection directions will be in the directions of $\pm(180 - 4\chi)$. Figure 10.11 shows four distinct lobes in the scattered polar response. By choosing an appropriate triangle slope angle, it is possible to have a notch in the specular reflection direction, but now the scattered energy is spread over four lobes, which is probably more desirable. However, the range of incidence angles over which this notch is achieved will be reduced.
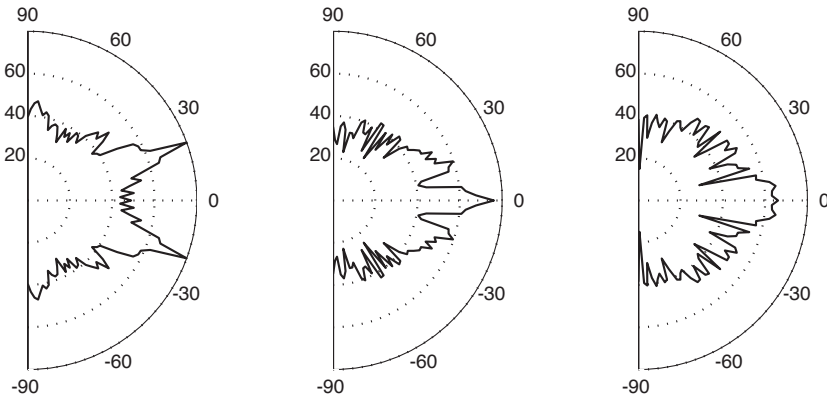
Figure 10.12   Scattered level from the centre of two triangles for three side angles, from left to right: χ = 50, 80, 85°.

χ = 45° is a special case because the energy is returned back towards the source, as shown in Figures 10.10 and 10.11. This is sometimes termed a corner reflector. The ability of a corner reflector to return energy back to sources is relatively well known and has been exploited in some auditoria as a way of returning energy back onto a stage to give reflections which help musicians and actors hear themselves and others.

For 45° <χ <54° double reflections always occur, but these only generate two lobes. An example is shown in Figure 10.12, for χ = 50°. As χ increases beyond 54° the number of reflections a ray undertakes before escaping the surface rises. A varying number of clear distinct lobes are still generated and simple ray tracing techniques can still be used to locate the directions of the most significant lobes. The relative level of the lobes varies, however, depending on the reflection paths. When the angle becomes very large (χ> 85°) then a single fairly broad lobe appears. The surface is in many ways acting like a horn loudspeaker in that a highly directional response is obtained. This occurs because the escape angles for the rays is limited to ±(90 – χ). This then returns the energy back to the source, but in a more diffuse manner than occurs with a χ = 45° surface. The simplistic analysis used here needs to be read with a little caution. Once these devices become very narrow and a great number of reflections occur then a resonant structure has been formed. Consequently, there is a risk of resonant absorption as is seen for Schroeder diffusers.

10.2.1 Arrays of triangles

The single triangle response is not that useful because usually large areas are needed to be covered and then the surface will become too deep, unless this is incorporated into the overall room shape in some way. Consequently, arrays of triangles need to be considered. Figure 10.13 shows the scattering from an array of χ = 15° triangles compared to a single triangle of the same size. Also shown is the response of two plane panels. An impressively large notch of almost 30 dB is generated for the array case compared to the plane surface. Additional lobes are also seen arising because of periodicity. The location of these can be predicted from Equation 10.5, however
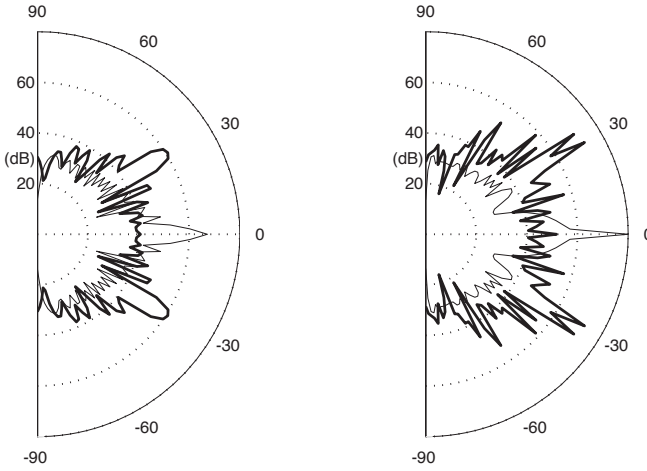
Figure 10.13 Scattered level from triangles and plane surfaces.

Left figure	Right figure
—— plane surface same size as one triangle;	—— plane surface same size as five triangles;
▬▬ one triangle.	▬▬ five triangles.

not all the lobes appear. The $m = 0$ and $m = 3$ lobes are attenuated because the single triangle response is weak in those directions. These periodicity lobes can be reduced by using modulation similar to that used for Schroeder diffusers discussed in Chapter 9. For example, two different triangle sizes could be chosen and arranged according to a pseudorandom number sequence.

Figure 10.13 actually represents a frequency where the notch diffuser is working well. Figure 10.14 plots the drop in the specular direction level as a function of frequency for the single triangle and the array. This shows that at other frequencies the attenuation is not as good; for example at 1.5 kHz the attenuation is only 13 dB. While this is a drop in level which is likely to be audible, it would be better if the performance could be improved. For example, the reflection free zone concept for small room design[6] would
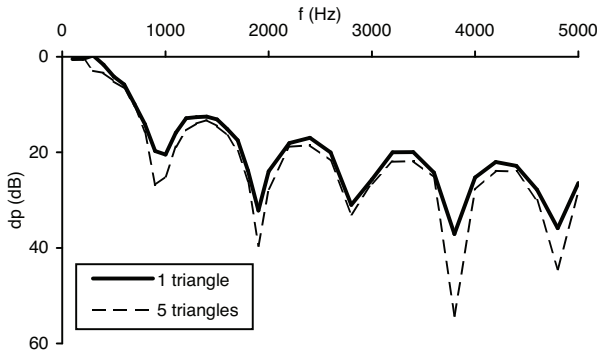
Figure 10.14 Decrease in specular zone pressure level when a triangle diffuser replaces a plane surface for different number of triangles. (Note: *y*-axis plotted in reverse order.)

typically be trying to achieve a 20 dB drop in the first order specular reflection level.

A brief parametric study looking at different triangle sizes shows that the peaks and dips in Figure 10.14 relate to the triangle depth. The maximum attenuation occurs when the depth is a multiple of $\lambda/2$. Unfortunately, if χ is increased further, say to 30°, this neat story relating the depth of the triangle to the wavelength of the minima and maxima is no longer true. Nevertheless, these results again lead to the thought that orthogonal modulation could solve the problem, following the ideas developed by Angus for Schroeder diffusers outlined in Chapter 9. By using two or more different depth triangles so that their frequency bands of higher specular reflection energy are different, it should be possible to improve the notch generated. By using two different depth triangles it might be expected that the improvement would be of the order of 3 dB, so a large number of different triangles would need to be used. Another solution to the problem is just to make the triangles much deeper, although overly deep surfaces are often not possible for non-acoustic reasons such as cost, weight and visual appearance.

10.3 Concave arcs

Concave surfaces such as domes are often an acoustician's nightmare. Used wrongly they lead to focussing effects that generate strong reflected energy in certain places. This can lead to uneven energy distribution across the room as well as echoes and coloration of timbre.

Whether an arc causes problems depends on the positions of the sources and receivers, and the radius of the arc. Figure 10.15 shows the scattering from a concave arc at a mid-high frequency for different receiver radii. Figure 10.16 schematically shows a ray tracing of the surface scattering. Figures 10.15 and 10.16 show that the
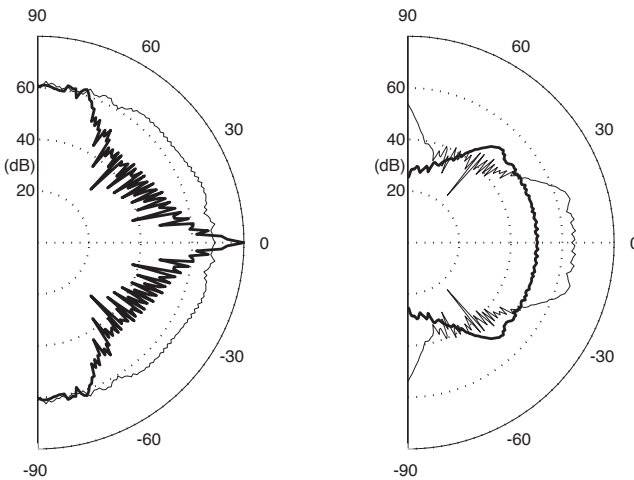
Figure 10.15   Scattered level from a concave arc for various receiver radii, r. r_f is the focal length of the concave surface.
Left figure   Right figure
────── $r < r_f$ ────── $r > r_f$
────── $r = r_f$ ────── $r \gg r_f$.
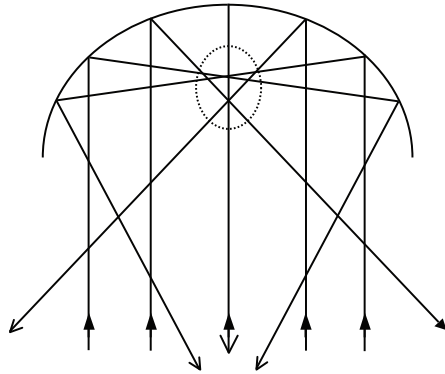
Figure 10.16 Ray tracing for scattering from a concave arc. The region marked with a dashed line will receive higher reflection levels than elsewhere.

focussing effect of the curved surface is only a problem for some receiver distances, close to the focal length of the arc. Consequently, it is possible to use a curved surface provided the focus of the surface is away from the listeners. For example, a concave ceiling in an auditorium is not a problem provided the curved surface focusses the sound well above or below the audience. If the focus is well above the audience, then the concave surface can paradoxically cause dispersion, but not as well as many other surface shapes. On the other hand, if the focus is below the audience, although the focussing may not be heard, the concentration of non-lateral sound from above may not be desirable for other acoustic reasons.

   If a concave arc with a focus on listeners is inevitable, there are two possible solutions: either treat the surface with an absorber or a diffuser. Absorbers can be placed in front of the surface to remove the reflection, although this must be considered alongside the reverberation time requirements of the room. There might also be a desire to produce some reflected energy from the concave surface, perhaps to provide ensemble reflections to musicians or early reflections to the audience to improve spaciousness or clarity. Diffusers can be used to break up the reflected wavefront and so disperse the focus while still maintaining the acoustic energy and avoiding absorption. Figure 2.34 showed a scattered polar distribution for a concave arc before and after treatment with an optimized curved diffuser. Figure 2.35 showed the curved surface used. The reduction in focussing is dramatic.

10.4 Convex arcs

A single cylinder is an efficient disperser of sound in one plane and a single sphere is efficient at dispersing hemispherically. They generate responses that mimic the behaviour of radiating line and point sources, respectively. Figure 10.17 shows the scattering from a semicylinder for three frequencies. The radial axis range of this graph is only 20 dB so at all frequencies the response from the semicylinder is fairly omnidirectional. The 400 Hz response is where the wavelength is roughly the width of the semicylinder and so some edge diffraction effects are seen. The lowest frequency, 40 Hz, is not omnidirectional because the rear of the semicylinder becomes important – it would be
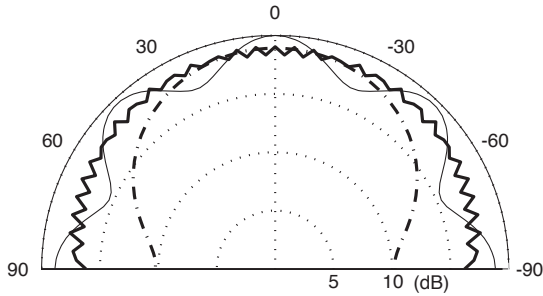
Figure 10.17 Scattered pressure from a 1 m diameter semicylinder for various frequencies (the $1/\sqrt{f}$ variation with frequency due to Green's function has been removed by normalization):
·–·–·· 40 Hz ($\lambda = 8.5d$, d = cylinder diameter);
——— 400 Hz ($\lambda = 0.85d$); and
▬▬▬ 4,000 Hz ($\lambda = 0.085d$).

more omnidirectional if a cylinder had been modelled. At the two highest frequencies the scattered level only varies by 2–3 dB over the receiver arc.

It might appear that the cylinder is the ideal diffuser – the Holy Grail of diffuser designs – but this unfortunately is not the case. A single cylinder on its own is rarely of much use. The example given in Figure 10.17 was 0.5 m deep – already deeper than many architects allow – and it was only 1 m wide, which is not wide enough for most applications. One solution is to use multiple cylinders in an array. Then the response of the cylinder array is dominated by how the cylinders are arranged, and the perfect response from a single cylinder becomes a secondary and less important issue. Another solution is to flatten the cylinder, but then the perfect angular dispersion will be lost for oblique sources.

There are also issues with cylinders and the total sound field response. Figure 10.18 shows the impulse response for a direct sound and a reflection from a large semicylinder.
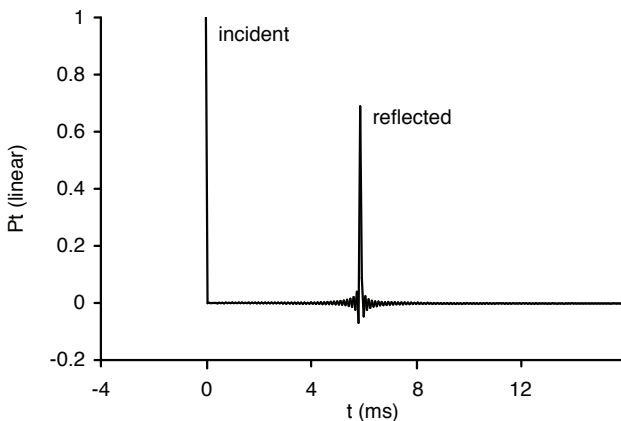
Figure 10.18 Incident and reflected time response for a semicylinder the same width as the plane surface used in Figure 10.3.
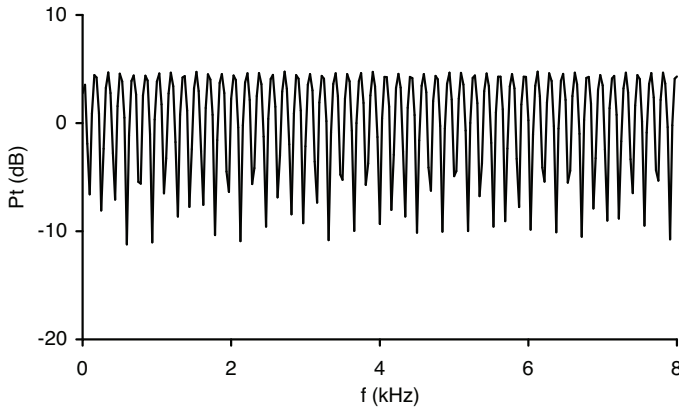
Figure 10.19 Total field frequency response for large semicylinder scattering.

The semicylinder has the same width as the plane panel used for Figure 10.3 to allow direct comparison between the surface types. The reflected sound is attenuated because of spatial dispersion, but the time signature is still very similar to the reflection from the plane surface. Consequently, large cylinders and semicylinders produce comb filtering similar to that generated by plane surfaces, as shown in Figure 10.19, however the minima and maxima variation is over a slightly smaller magnitude range for the semicylinder. The comb filtering is thought to give rise to the harsh sound that some large semicylinders generate, although a more detailed set of subjective tests would be interesting and could clarify the situation. Certainly, semicylinders are an enigma; they appear to be a near perfect diffuser from dispersion graphs, but they do not sound like a perfect diffuser.

10.4.1 *Geometric scattering theory and cut-off frequencies*

One method that has been proposed to predict the scattering from a curved surface is geometric theory.[3,7] The scattering is split into two processes. First the diffraction from the finite-sized panel is considered and then the effect of curvature added. The finite-sized surface effect is predicted using Fraunhofer or Fresnel theory. The effects of curvature are accounted for by a simple beam tracing method. If a curved surface is illuminated by a beam with parallel sides, the reflected beam will diverge due to the curvature of the surface as shown in Figure 10.20. If the wavelength is assumed to be small compared to surface size, then simple geometric constructions can be used to calculate the attenuation due to curvature. For plane waves, this is given by:[3]

$$attenuation = \left| 1 + \frac{r^*}{R_c \cos(\psi)} \right| \tag{10.6}$$

where the composite radius r^* is defined in Equation 10.2, R_c is the radius of curvature of the panel and ψ is the angle of incidence and reflection. It is also possible to produce a formulation for spherical waves.[7] Figure 10.21 shows the scattered pressure versus
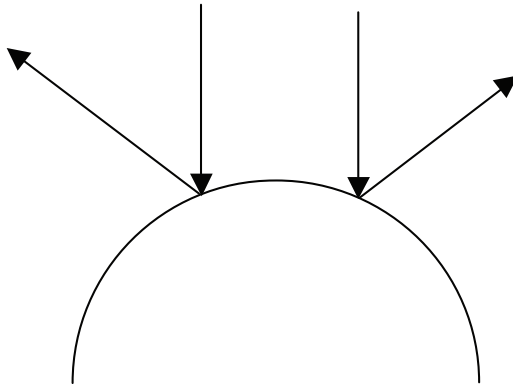
Figure 10.20 Effect of curvature on a sound beam.

frequency for the specular reflection direction for the two theories and the 3D BEM model. It is assumed that the BEM gives accurate results and so this indicates that the geometric model works to a certain degree – the magnitude is approximately right but the ripples are not predicted. Figure 10.22 shows a scattered polar response. The geometric theory of scattering is not successful for receivers where the geometric reflection point is not on the surface. For these receivers the effect of adding curvature should be to increase the scattered pressure, as energy is moved away from specular reflection angles to these receivers. The geometric formulation incorrectly applies an attenuation, whatever the angle of reflection.

The cut-off frequency for plane panels was a simple concept that readily allows some rough and ready design principles to be applied. Investigations have shown[8,9] that Equation 10.1 also works for curved surfaces, provided the receivers are close to the specular reflection direction, which was a necessary stipulation for plane surfaces also.
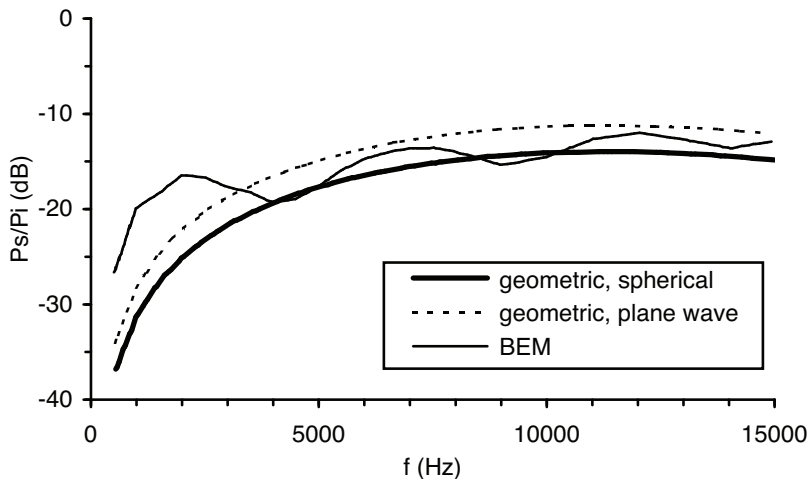
Figure 10.21 Prediction of scattered levels for a curved surface using three theories (after Cox[9]).
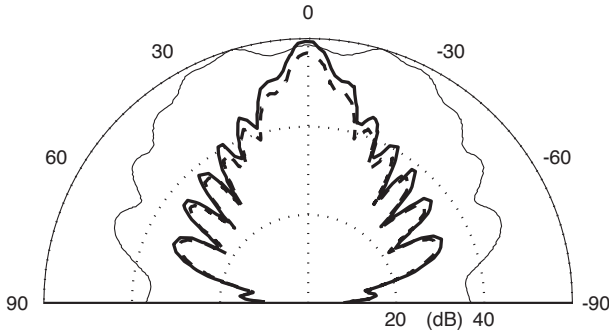
Figure 10.22 Prediction of scattered levels from a curved surface using three theories (data
from Cox[9]):
———— BEM;
▬▬▬ geometric, plane wave; and
– – – geometric, spherical wave.

10.4.2 *Performance of simple curved reflectors*

For normal incidence, reflectors based on part of an arc of a circle have good dispersion
performance. Figure 10.23 compares the predicted scattering from a semicylinder and
a flattened semicylinder (an ellipse) for normal and oblique incidence. For normal
incidence the semicylinder disperses the sound well, as it generates a virtual line
source. For oblique incidence, however, the performance is poorer for the flattened
semicylinder. The flattened semicylinder also has worse performance for normal
incidence. Incidentally, the trends are similar if a section of a circle is used instead
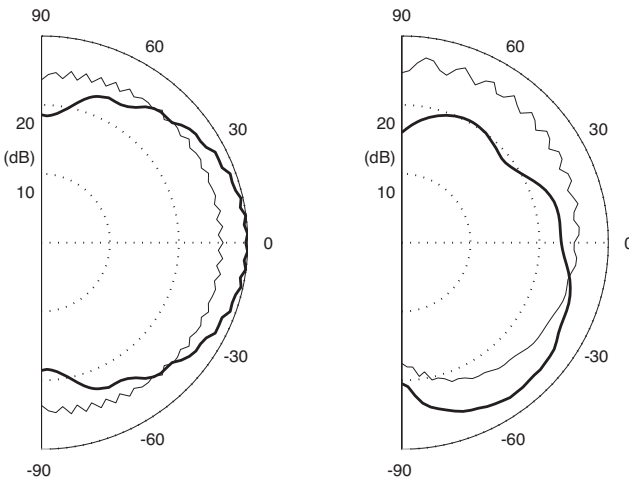
Figure 10.23 Scattered level for two surfaces for normal (left graph) and oblique (right
graph), 60° incidence:
———— semicylinder; and
▬▬▬ flattened semicylinder.

of a flattened circle – only a complete semicylinder at normal incidence produces the very good dispersion. Consequently, if a whole semicylinder cannot be used in an application, a better solution than flattening the semicylinder or taking part of a circle is needed. There are two possibilities: either use an array of semicylinders or use optimization to construct a more complicated curved shape. Arrays are considered below, and complicated curved shapes later in this chapter.

10.4.2.1 Arrays of semicylinders

Once cylinders are arranged in an array, the performance is dominated by a combination of the single cylinder response and the periodicity. If the simple analysis surrounding Equation 10.3 is considered, then the key to gaining good diffusion from a set of cylinders is mostly about how they are arranged. The scattered pressure distribution from one cylinder, $p_1(\beta)$ is constant if second order reflections are not considered. Consequently, the sum of the delta functions in Equation 10.3 dominates the scattered pressure distribution. Once again a modulation technique, where the cylinders are not arranged periodically, is needed to change the functional form of the last term in the Equation 10.3 to give more even scattering.

  The simplest method to follow is the modulation techniques described for Schroeder diffusers outlined in Chapter 9. For cylinders this means using two or more semicylinders, and arranging them randomly or pseudorandomly on the wall. This will reduce periodicity and so improve dispersion. Figure 10.24 shows this by comparing a periodic and a random array of semicylinders. At mid-frequencies, where there are some grating lobes, but not too many, the aperiodic arrangement helps to create extra lobes, thereby improving dispersion. In this case it is surprising how dominated the scattering is by lobing. A simple diffraction grating with one point source in the middle of each diffuser can produce reasonably accurate predictions of the scattering. At mid-frequencies, simple geometric base shapes very much mimic point sources.

  The overall envelope shows some reduction for reflection angles far from the specular reflection direction. This tailing off is presumed to occur due to second and higher
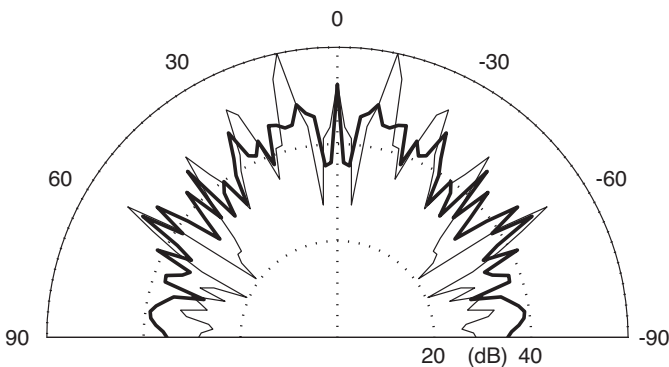
Figure 10.24 Scattered pressure distribution for a periodic and aperiodic arrangement of semicylinders. For the periodic set, $4\lambda \approx d$, where d is the diameter (chord) of the semicylinder:
———— periodic; and
━━━━ aperiodic.
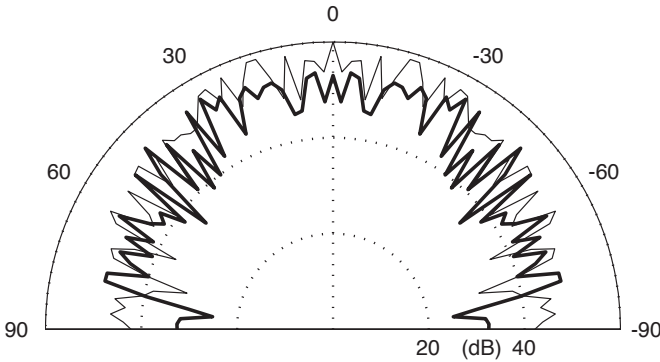
Figure 10.25 Scattered pressure distribution for a periodic and aperiodic (modulated) arrangement of semicylinders. For the periodic set, $15\lambda \approx d$, where d is the diameter (chord) of the semicylinder:
———— periodic; and
———— aperiodic.

order reflections from the array – neighbouring semicylinders get in the way of reflected sound. Similar results are seen for oblique incidence.

At high frequency, however, the modulation of the cylinders does not affect dispersion significantly for normal incidence. An example is shown in Figure 10.25. At high frequencies the grating lobes are so close together spatially that the local variation in minima and maxima is similar for periodic, modulated and random arrangements. Again, as in the mid-frequency range, there is a gradual tailing off at the edges of the overall envelopes of the polar responses. In the example shown in Figure 10.25 there is roughly a 15 dB drop from normal to grazing receivers. At oblique incidence (result not shown), the modulated arrangement is better at controlling the overall envelope, and a clear improvement on a periodic arrangement is achieved.
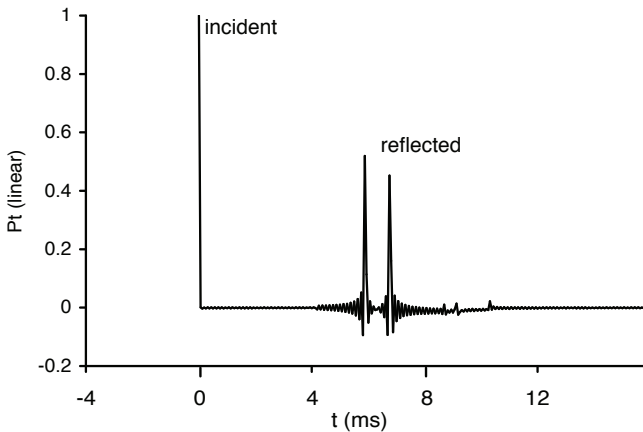
Figure 10.26 Scattered pressure from an array of four cylinders symmetrically arranged about the source (and hence only two unique reflection arrival times).
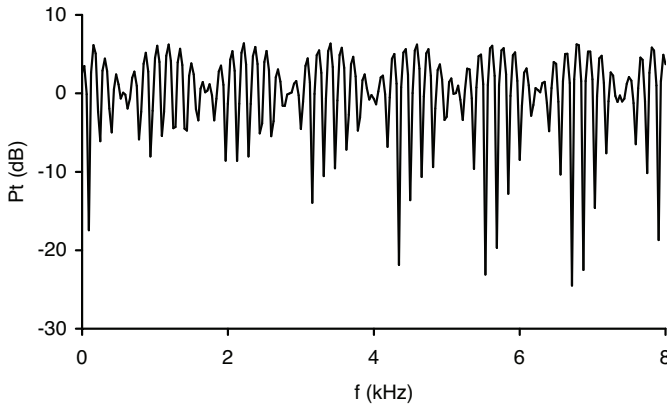
Figure 10.27 Frequency response for four periodic cylinders.

As previously discussed, dispersion is only one aspect of diffuser performance, although possibly the most important one. The total field response, incidence plus reflection, should also be considered. Figure 10.26 shows the total field for a periodic set of four cylinders. Only two arrivals are shown because the array was set up symmetrically and so there are only two unique arrival times. Figure 10.27 shows the frequency response for the total sound field. This can be compared to previous graphs in this chapter for plane and single semicylinder scattering. Using an array of cylinders has not destroyed the comb filtering, but it has somewhat reduced it. It might be expected that comb filtering aberrations such as coloration may well still be present, but may not be so noticeable. Figures 10.28 and 10.29 show the total field time and frequency responses for a complicated arrangement of many different-sized semicylinders. The use of a random arrangement of cylinder sizes and shapes has further broken up the regularity of the frequency response, making it much less likely that coloration will be heard.

   In conclusion, several key features will determine the performance of semicylinder
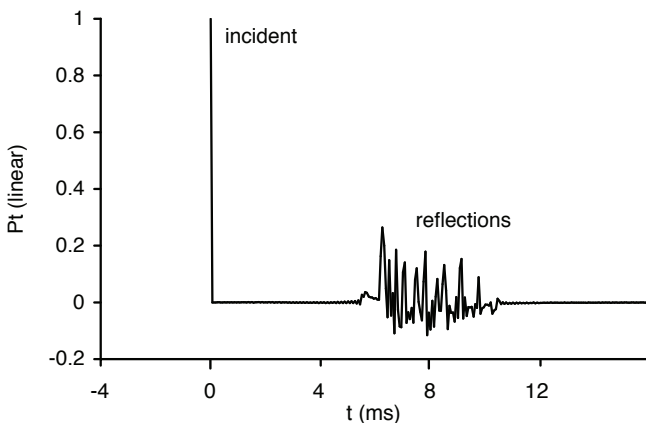
Figure 10.28 Total sound field for a complicated random array of many sized semicylinders.
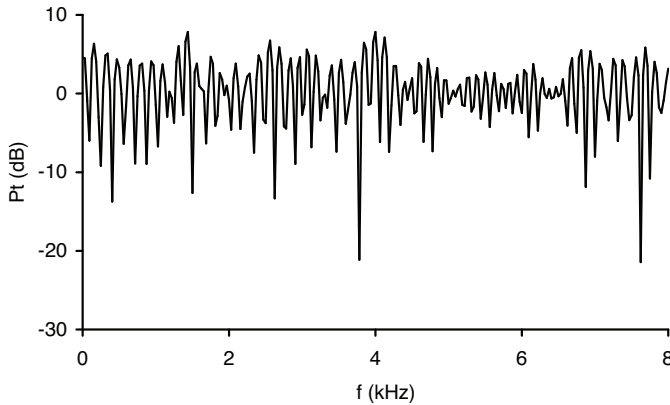
Figure 10.29 Frequency response of total sound field for a complicated random array of many sized semicylinders.

arrays. The low frequency limit of the diffuser will either be determined by the repeat distance or the diffuser depth. Multiple grating lobes need to be present for dispersion and hence repeat distance is important (see also Chapter 9). The issue of depth has not been discussed before for semicylinders, and unfortunately is as likely as not to be set by non-acoustic requirements. If the depth is the determining feature, then empirical results have shown that curvature produces significantly more scattering than a plane panel when the depth is greater than $\approx\lambda/10$. The mid-frequency performance is dominated by the arrangement of the semicylinders. The key to good performance is to avoid periodicity, or to ensure that the repeat distance is as large as possible. The high frequency performance, when the number of grating lobes is very large, seems difficult if not impossible to control.

10.5 Optimized curved surfaces

10.5.1 *Example application*

When designing a diffuser, the requirements of visual aesthetics and acoustics must be considered, and these are often in conflict. Schroeder diffusers may have well-defined acoustic performance, but they do that with a very specific visual appearance which it seems is either loved or loathed. Unless diffusers are visually acceptable to the architect they are unlikely to be used. Curved surfaces are common in modern architecture. Spurred on by the availability of new materials and computer aided design, architects are increasingly designing prestigious buildings where large flat surfaces appear to be outlawed in principle.

Curved diffusers are therefore appealing because they can complement modern architectural trends. They can have a form which blends with other structures in a building and they do not have to look like an obvious add-on. The Hummingbird Centre in Toronto is an interesting example[10] (shown in Figure 2.2). Diffusers were required on the side walls of the auditorium because a sound enhancement system was being installed which would generate echoes across the room, unless some surface

treatment was applied. The original design specification was for Schroeder diffusers, which were to be cloth wrapped to hide their visual appearance. After much discussion, a curved surface designed by optimization was accepted instead and because this fitted the visual appearance of the room there was no need to hide the diffusers. The curved diffusers blended with the room design while having good acoustic performance. Other examples of optimized curved surface were shown in Figures 2.24–2.27, 2.35 and 2.36.

10.5.2 Design process

Section 9.10 described how it is possible to get a computer to search for the best possible depth sequence for a Schroeder diffuser. It is also possible to get a computer to search for the best curved shape to generate dispersion.[11] For those unfamiliar with optimization, it may be necessary to read Section 9.10 before the description below because the background details of how optimization works are not repeated.

As with any diffuser optimization process, it is necessary to have a set of numbers that describe the surface shape. These shape parameters can then be changed by the optimizer to allow the computer to search through possible surface shapes. In the case of Schroeder diffusers this was straightforward; the shape parameters were the well depths. For a curved surface a different regime is needed. Any surface shape can be represented by a Fourier series and so the surface displacement, y, can be represented by:

$$y(x) = \sum_{n=1}^{N} a_n \cos(k_x x) + b_n \sin(k_x x) \tag{10.7}$$

where a_n and b_n are the shape parameters which are altered to change the surface shape. k_x is usually set so that the harmonic for $n = 1$ corresponds to half a wavelength across the panel in the x-direction. N is the number of harmonics used. This gives a single plane diffuser which has modulation in the y-direction only. It is also possible to use 2D Fourier transforms to form the shape in multiple dimensions – the only cost is computation time as the number of shape parameters to be optimized increases.

From Fourier theory, if an infinite series is used any diffuser shape can be produced. In reality it is necessary to truncate the series at some point as every extra element in the series gives a new dimension to the optimization process. Too many dimensions and the minimization becomes too slow. Furthermore, one advantage of curved diffusers over more complex surfaces is their simpler construction leading to potentially lower costs and lower absorption. An increase in the number of harmonics in the series increases the complexity of the diffuser shape which may cause excess absorption and increased cost. For these reasons, 4–6 harmonics are typically used. Once a surface shape is formed, it is necessary then to scale the shape to fit the maximum displacement in the y-direction required (i.e. fixing the maximum diffuser depth).

There are other mathematical representations of curved surfaces which can be used. For example, it is possible to define a number of variable points on the surface shape and use a cubic spline algorithm in one plane or a bicubic spline algorithm[12] in two planes to form a smooth curved surface between the variable points. It is possible to construct a harmonic series not based on sinusoidal basis functions. Frequency and amplitude modulation processes can also be used to generate many different

Fuzzy constraint point

(a) Surface passes through fuzzy constraint point, no penalty applied.

(b) Surface misses fuzzy constraint point, penalty applied proportional to d.

(c) Use of fuzzy constraints to ensure diffuser meets a wall at edges.

(d) Use of fuzzy constraints to ensure an S-shape.
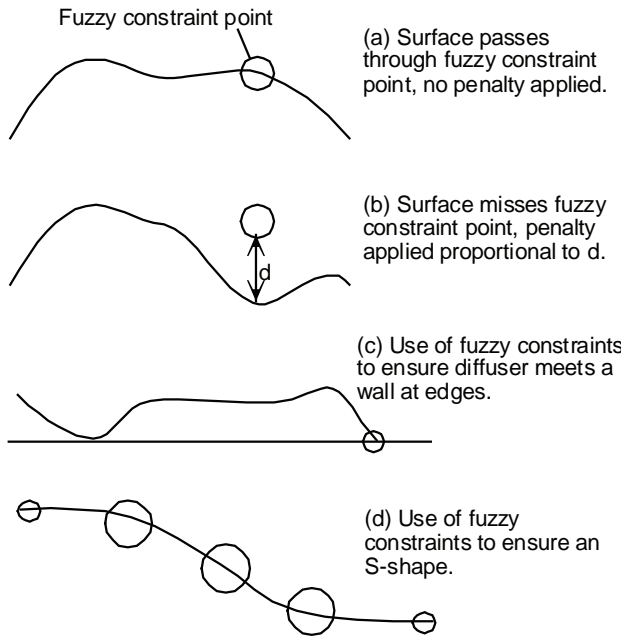
Figure 10.30   Use of fuzzy constraints to ensure optimized curved diffuser meets visual and physical constraints (after Cox and D'Antonio[13]).

shapes. Although there are many possibilities, the essential principle of needing shape parameters remains.

Problems sometimes arise when the best surface found by the computer does not meet the visual requirements of the architect. A curve is wanted, but the solutions produced are not quite what the designer originally envisaged. In addition, it is often necessary to ensure that the surface avoids other objects in the room, or has appropriate breaks to allow for lighting. In this case, non-acoustic constraints must be used in the optimization process to force the shape to meet visual and physical constraints. This can be done via a set of fuzzy coordinates through which the surface must pass. Figure 10.30 illustrates how such a system can be used to force a surface to pass through particular points. The error parameter in the optimization becomes a combination of the diffusion coefficient that measures the scattering quality and a penalty value that measures how close the surface is to the constraint points (this can be an additive or multiplicative penalty). This is often used to ensure that edges of diffusers meet walls as illustrated in Figure 10.30c. In addition, this technique can be used to ensure that:

- cusps are not formed between adjacent periods of periodic diffusers;
- the left and right edges of diffusers are at the same displacement so that periodic diffusers edges will meet without a discontinuity; and
- obstructions, such as pillars, are avoided.

While using such a constraint system is straightforward for physical problems, such as avoiding cusps, it is more problematic when trying to force the shape of the curve

Figure 10.31 Distortion in image processing (after Cox and D'Antonio[13]).

into the visual aesthetic demanded by the designer. Often during room design the interior designer has a definite idea about the general shape required for the diffuser, e.g. 'We would like an S-shaped diffuser'. Trying to come up with a suitable set of constraint points for this is possible, but involves some trial and error. Furthermore, the constraint point system lacks elegance and will slow down the optimization process by increasing the complexity of the error function surface to be searched. One solution is to use a spline construction, as then linear constraints on the shape parameters can be used.

A superior system is one where the surface is designed from shape variables in such a way that the only surfaces generated are ones that satisfy the visual constraints. One way to do this is distortion.[13] The architect supplies a base shape and distortion is used to change the acoustical performance of the shape while retaining the visual integrity. Such a process is familiar in image processing as a technique for adding effects to photographs. This is illustrated in Figure 10.31. In the distorted pictures, it is still possible to recognize the picture as being a person; the rough visual appearance is maintained, yet radically different pictures are obtained. The idea behind diffuser distortion is to alter the surface shape using image processing and other techniques in such a way that the general visual appearance is maintained, and yet a different acoustic performance is obtained. To achieve this, compression, modulation and warping techniques are used.

10.5.3 Performance for unbaffled single optimized diffusers

Initial work on curved diffusers examined whether they could perform better than arcs of a circle.[11] It was found that for all depths and widths tested the optimized diffusers were as good or better than arcs of circles. An interesting trend in the solutions from the optimization process was that when the maximum allowable depth and width of the surface were similar, so allowing a rough semicircular surface to be formed, this was the surface shape found by the optimization process. This near semicircle was similar to the arc of a circle and so for these geometries the optimization process could only produce diffusers which matched the performance of the circle arc. When the geometric constraints meant that a semicircle was not a possible solution then the
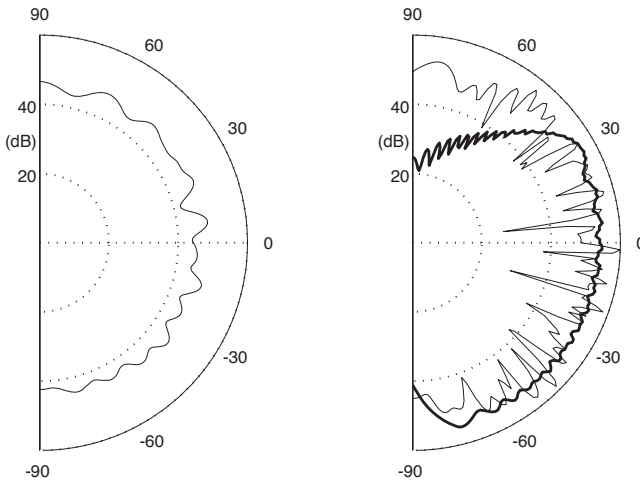
Figure 10.32 Scattered level from three surfaces at 2.8 kHz, 30° incident source. Left figure: standard curved diffuser (same as optimized diffuser) 1× 0.4 m. Right figure: ━━━ standard curved diffuser, dimensions 4 × 0.4 m; ── optimized diffuser 4 × 0.4 m (data from Cox[11]).

optimized surface found different, more complex shapes that were better at generating spatial dispersion than the standard curved surface.

The failure to improve on the simple arc does not show a fundamental weakness in the optimization process – it in fact illustrates how well it works! What has been shown is that, for the geometries tested, approximately semicircular diffusers have near optimal spatial dispersion and there is little room for improvement. (Remembering that spatial dispersion is not the only consideration for diffusers, time dispersion should also be considered.) This is illustrated in Figure 10.32 where the scattered pressures from two arcs and one optimized surface are shown. For the wide arc (right graph), the scattered pressure shows a noticeable fall off at large angles of incidence. The optimized diffuser provides more uniform scattering and does not suffer from such a fall off in pressure. For the narrower surface (left graph), the arc is nearly semicircular; the diffusion is fairly uniform, and it would be difficult for any surface to improve on the scattering produced in terms of spatial redistribution. The optimized diffuser shape is also a rough semicircle, indicating that this is almost certainly the best shape possible within the geometric constraints. Note that a single semicylinder is unlikely to give the necessary temporal dispersion and will not cover a large enough area.

Typical examples of a standard deviation diffusion parameter as a function of incident angle for an arc and optimized surfaces are shown in Figure 10.33. The figure is using an old diffusion evaluation technique and the lower the value of diffusion the greater the spatial dispersion. In this case the optimized diffuser has sacrificed a little performance for normal incidence sound, to improve the scattering for oblique sources. This shows the ability of the new surface to produce more uniform scattering for random incident sound.
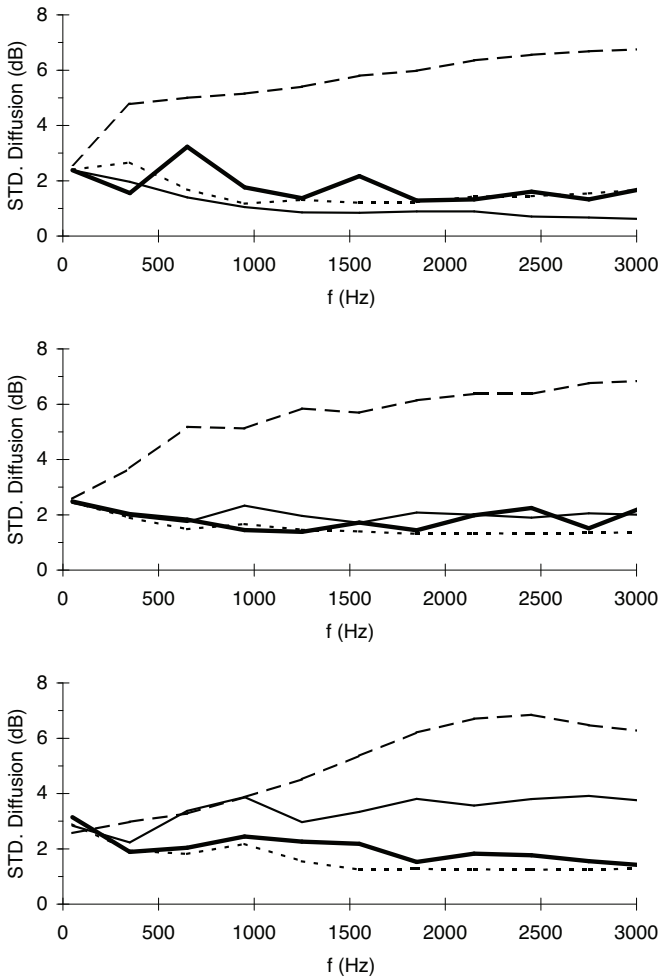
Figure 10.33   Diffusion from four surfaces; incidence sound angles different for each graph. Top: normal; middle: 30°; and bottom: 60° incidence sound. This uses an old standard deviation measure, where complete diffusion is when the standard deviation is zero.

– – – plane surface;
——— arc of a circle;
——— optimized fractal;
······· optimized curved surface (after Cox and D'Antonio[19]).

10.5.4 Periodicity and modulation

When placed in a periodic arrangement the quality of scattering at low to mid-frequencies is dominated as much by grating lobes generated by surface repetition as by the detailed surface shape. One solution to grating lobes (spatial aliasing) is to remove the periodicity completely by using a very large surface. Unfortunately, this is likely to be an expensive solution and consequently, a modulation scheme similar to that devised for Schroeder diffusers discussed in Chapter 9 can be used.
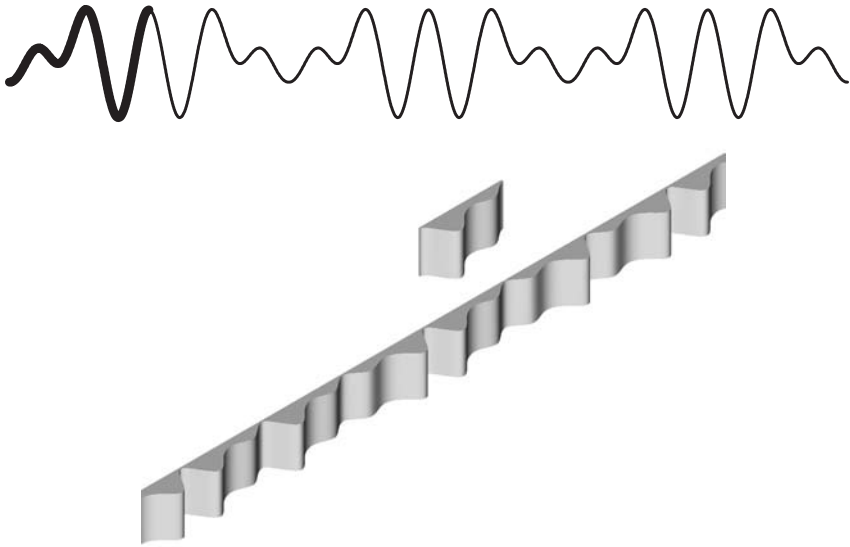
Figure 10.34   Top: a curved diffuser (not optimized for acoustics). The base shape is shown in bold. By changing the orientation between periods it is possible to increase the repeat length of the diffuser. Bottom: the same principle rendered in 3D showing one base shape and a modulated array.

Consider a single asymmetrical diffuser base shape shown at the top of Figure 10.34 in bold. If this base shape were arranged in a periodic fashion, grating lobes will arise. If, however, some of the periods are rotated, then the periodicity can be reduced. In the case shown in Figure 10.34 the repeat distance has been doubled by this modulation.[14] The figure also shows a 3D rendering of the idea. In general this will improve the diffusion. A key to this type of modulation is to form a shape which is sufficiently asymmetrical, so that flipping the shape produces completely different scattering. A further complication is ensuring that neighbouring diffusers tile together without discontinuity in surface displacement or gradient. By forming surfaces with zero end gradients and with the same surface displacement on both ends, it is possible to form a surface that will tile in any orientation. Then the architect can decide what pattern to form. More importantly, pseudorandom arrays enable diffusers of considerable extent to be created from small base shapes. If there is a discontinuity in gradient between panels then a cusp results. An inward facing cusp can be useful in generating additional scattering, but the appearance may not be desirable.

In its extreme, this modulation can result in a surface where the individual base shape is not clearly distinguishable.[15] The top of Figure 10.35 shows a single period of a 3D curved surface in various orientations and the bottom shows the same shape in a modulated array. The single period device has the same symmetrical shape on each edge, and the gradient around the perimeter is zero. This allows the surface to be tiled in any orientation. If the surface depth is z and is a function of the coordinates across the width x and length y of the diffuser, $z = F(x,y)$, then the requirements can be mathematically expressed as:
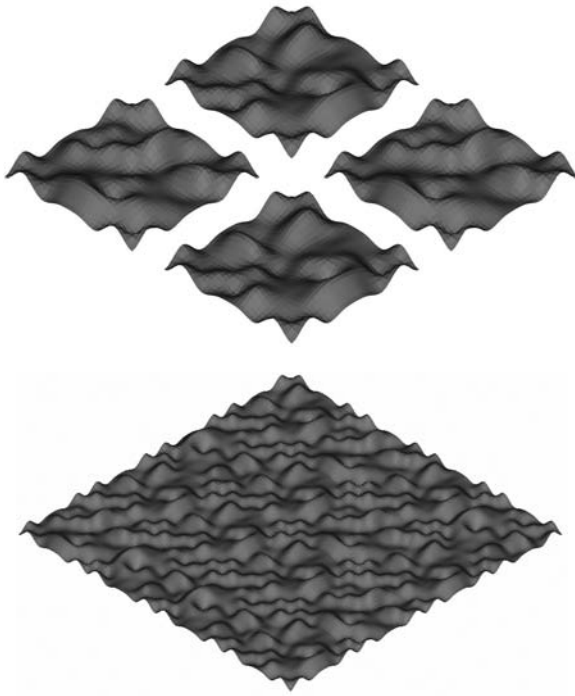
Figure 10.35 Top: an asymmetric single base shape used in modulation shown in different possible orientations. Bottom: a 4 × 4 modulated array of the base shape.

$$z(0, y) = z(L, y) \tag{10.8}$$

$$z(x,0) = z(x, L)$$

$$z(x,0) = z(L - x,0)$$

$$z(x,0) = z(0, x)$$

$$\frac{\partial z}{\partial x} = 0 \quad x = 0 \vee L$$

$$\frac{\partial z}{\partial y} = 0 \quad y = 0 \vee L$$

where L is the width (or length) of the diffuser.

When placed in a modulated array, the base shape disappears in a complex pattern of minima and maxima. This allows the use of one base shape and reduces manufacturing costs. Figure 10.36 shows an example application of modulated curved diffusers on the ceiling of a radio studio.

A periodic look is often favoured, however. It seems that a periodic object enables the eye to more easily decode the design. A completely random surface can be too difficult to interpret and hence not pleasing to the eye. This is, of course, a crass generalization – there are successful architectural designs where randomness is embraced – but it is

Figure 10.36 Modulated curved diffusers used in the ceiling of a radio production studio at KTSU, Texas Southern University, Houston, TX (Acoustician: HFP Acoustical Consultants). Insert shows close-up of ceiling.

more common for a periodic entity to be specified. Using this asymmetrical base shape gives designers control over the appearance. It can be made to look random or periodic, but the designers have to remember that short repeat distances will result in worse dispersion. Figure 10.37 shows the scattering from three surfaces showing how modulation can improve the scattering performance over a periodic array.
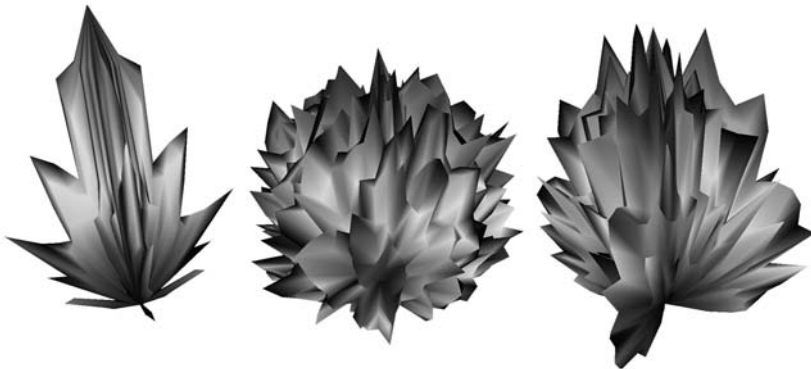
Figure 10.37 Three polar responses for scattering at 2 kHz. Left: plane surface; middle: optimized modulated array; right: periodic arcs.

10.5.5 Stage canopies

Overhead stage canopies are often designed with arrays of curved panels. The primary role of a stage canopy is usually to provide reflections back to the musicians or actors to allow them to hear themselves and others. Canopies may also be used to distribute some energy to the audience. There might be little delay between the direct sound and the overhead canopy reflection in the audience area, however, and care should be taken to avoid coloration due to comb filtering. If a completely flat large surface is used above the stage, plenty of energy will return to the musicians. Unfortunately, the energy will be too strong and likely to cause coloration. Consequently, a canopy often needs to be shaped to create temporal diffusion to reduce coloration. This is often done with curved surfaces. Figures 2.25–2.27 showed examples of curved canopies designed using optimization.

Canopies appear to fall into two rough categories which are determined by the amount of open area in the canopy. Sometimes canopies completely cover the stage (virtually no open area). This is most common where the canopy is being used to block sound entering a fly tower as was shown in Figure 2.32. Other canopies use elements sparsely, with plenty of open area between the canopy diffusers or reflectors, as is the case for the reflectors shown in Figure 2.27.

An optimization study[16] was carried out to investigate whether this design method could be used for stage shells with a reasonable amount of open area. Figure 2.25 showed a canopy designed using this principle. The canopy is such that there is a little open space between each of the reflectors to allow some energy to pass up to the void above. The canopy is about 7 m above the stage so that the reflections are delayed by an amount known to give a good chance of reflections aiding ensemble and support.[17] For the optimization study, five diffusers were arranged on the arc of a large circle from the front to the back of the stage. The diffusers were assumed to extend across the full width of the stage. The design criterion in the study was that for any source position
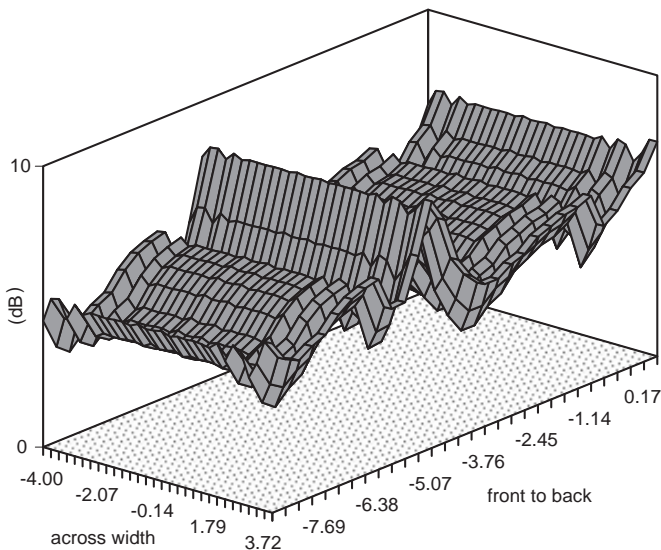
Figure 10.38 Scattering from a stage canopy with plane reflectors (after Cox and D'Antonio[16]).

on the stage, as even as possible energy distribution would be created to all positions on the stage. In other words, each musician has an equally good chance of hearing each other as far as the stage canopy reflections are concerned. This is a criterion that can be used in an optimization process described previously.

The optimized design was compared to several other reflector shapes, such as a plane surface and arcs of circles. The optimized surface outperformed the other diffuser shapes in producing the most even energy distribution across the stage area. Figure 10.38 shows the scattering coverage plot from the plane reflector canopy at 2 kHz for a source in the middle of the stage. The variation in pressures across the width is small because this was modelled as a large flat surface; any variation is due to spherical spreading and path length differences. There is a large reflection level directly below the source as much of the energy is being reflected straight back to the musician who is playing the instrument. Dips in the reflected pressures occur where there is no geometric reflection point on one of the reflectors due to the spaces in the canopy design. As discussed previously, shaping the reflectors can reduce the effects of pressure minima; this is often done by forming convex arcs.[5]

The effect of using a more complex optimized curved surface is shown in Figure 10.39. The effect of the surface diffusers is to reflect energy to receivers where specular reflections are missing. It also greatly reduces the strong specular energy being directed straight back to the musician. The reflected energy is more evenly distributed across the stage – all pressure levels along the front to back axis lie within 3 dB of each other.

The criterion of even energy across the stage needs to be used with caution, and is now considered not to be the best for all cases. Consider a canopy with a small open area, in other words a large surface with the same width and depth as the stage. A flat surface will give very good coverage on the stage, as noted before, but this does not make it a good stage canopy. Overhead reflections in this case will be strong, and the desire here is to reduce the coloration produced by these reflections. Consequently,
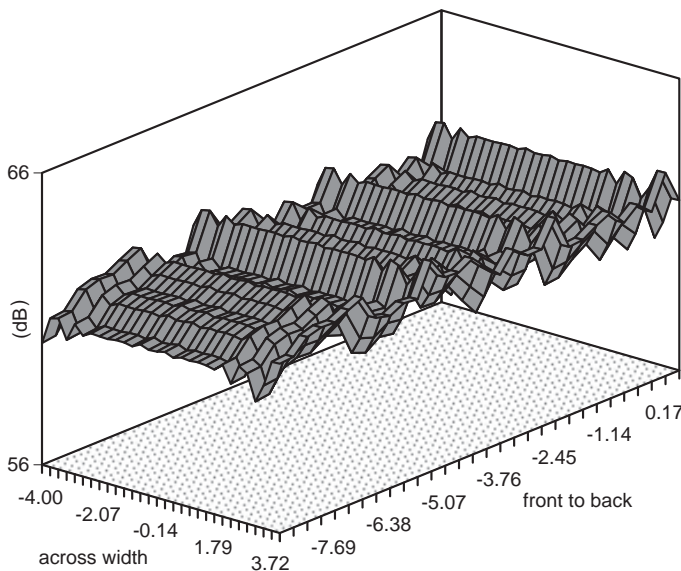
Figure 10.39 Scattering from a stage canopy with optimized curved diffusers (after Cox and D'Antonio[16]).
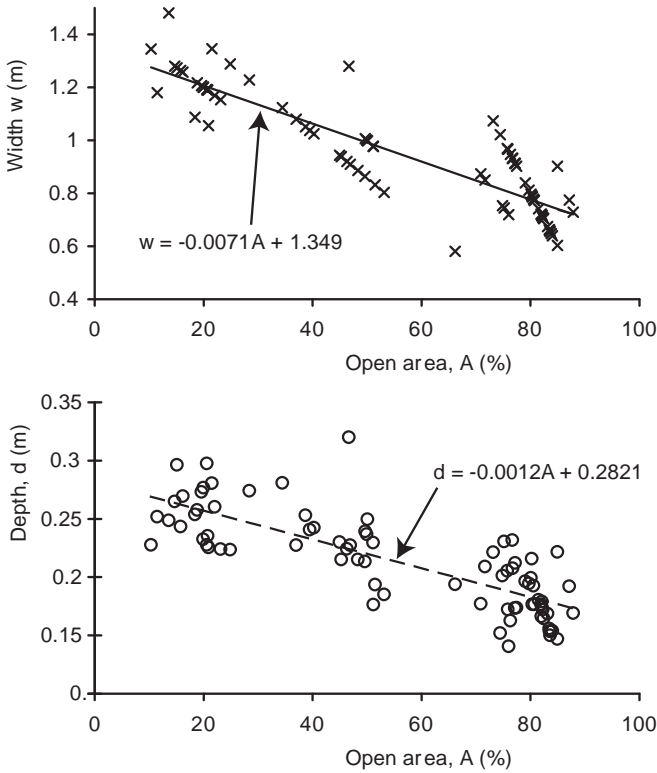
Figure 10.40 Changes in optimized reflector width and depth as a function of per cent open area, A. The best fit lines show the underlying relationship between optimum reflector size and canopy open area.

what is needed is a surface that produces temporal diffusion to minimize comb filtering. It is therefore usually better to design a stage canopy to promote maximum dispersion across a complete arc from –90 to +90°, in other words asking for maximum dispersion not just on the stage. If simple arcs are avoided, this maximizes the temporal dispersion from the overhead canopy and so minimizes coloration effects.

It is also possible to get the optimizer to look at the best locations, angles, number and sizes of canopy elements alongside examining the detailed surface shape of each element. While this can be carried out on a case-by-case basis, a study was also undertaken to explore what the underlying principles in canopy design might be and so develop some rules of thumb.[18] The optimizer was run many times with different target values for the reflection level on stage – this was done using the support measure[17] – resulting in many different canopy designs with different open areas.

Figure 10.40 shows how the width and depth of the best canopy designs varied with canopy open area. Figure 10.41 shows the variation in the number of canopy elements with open area. Fuller canopies with smaller open areas are shown towards the left of the figures. These canopies provide more reflections back onto the stage and have higher support. To the right of the figures the canopies provide lower level of reflections because the open area of the canopies is quite large. For the fuller canopies
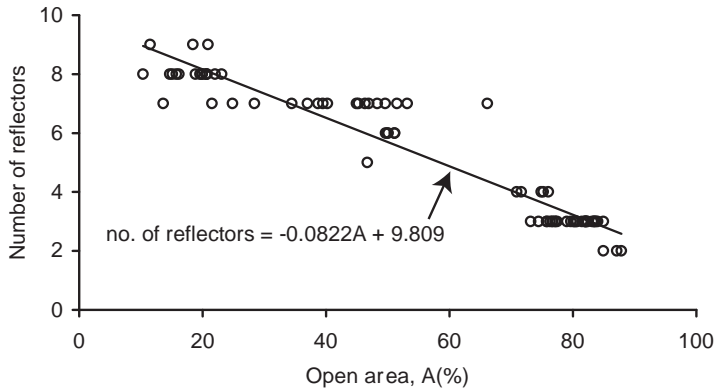
Figure 10.41 Variation in number of stage canopy reflectors with per cent open area, A. A least squares best fit straight line is also shown.

with small open area the best designs tend to have more canopy elements which are wider and deeper in comparison to more open canopies. Furthermore, fuller canopies have simpler, less wiggly shapes than canopies with larger open areas. Because fuller canopies have only a small open area there is less need for dispersion from the canopies to provide reflections to receivers who lack specular reflections.

It seems that relatively small panels are preferred. This supports the findings of Rindel[5] who studied the effect of density and panel size on array performance for flat elements. He concluded that panels needed to be relatively small so that energy is diffracted to receivers who do not receive a specular reflection from the canopy array. For this reason, high frequency performance was determined by panel size. The low frequency performance of the array was determined by the canopy density. The optimization study has also produced a new finding: that the desirable reflector width and depth is dependent on the open area of the canopy.

When a canopy is completely full and there are virtually no gaps between the panels, then the design issue is how to reduce coloration caused by the inevitable strong specular reflections. In this case, covering the surface with diffusing surfaces may be a good option. The situation is very similar to rear and side stage enclosure design, which was discussed in Section 2.8.

10.6 Fractals

Fractal mathematics is used to create natural objects in computer generated graphics, for example to make landscapes for animated films. Fractals are surfaces with a different visual aesthetic compared to common sound diffusers and so offer the possibility of expanding the pallet of surfaces available to designers.[19]

There is reason to believe that fractal surfaces may have good acoustic properties. Fractals are self-similar or self-affine; as a surface is magnified a similar looking surface is found. Consequently, the rough surfaces at different magnifications can be used to scatter different frequency ranges in an analogous way to the use of drivers of various sizes to radiate distinct frequency ranges from coaxial multi-way loudspeakers. This is

the principle of the Diffractal,[20] as discussed in Chapter 9 and shown in Figure 9.26, which imbeds small-scaled copies of an $N = 7$ QRD at the bottom of a larger $N = 7$ QRD. The small QRDs scatter mid-high frequencies and the large QRDs the bass frequencies. The construction is precisely self-similar; the exact shape is found upon magnification. This will not be true for surfaces considered here, where the surfaces are simply statistically self-similar or self-affine.

There are many established techniques for generating finite sample approximations to mathematically pure fractal shapes.[21,22] Single plane diffusers are described and are made from extruded 1D fractals. Construction methods for higher dimensioned surfaces are also available, but are ignored here for conciseness.

10.6.1 Fourier synthesis

Fractal surfaces can be constructed from spectral shaping of a Gaussian white noise source. Figure 10.42 is a schematic showing how the surfaces can be generated; such a scheme is more familiar in digital signal processing as a time signal filtering process. The Gaussian white noise is passed through a filter which is implemented using simple Fourier techniques. The shaping of the spectrum is done using a roll off with a defined number of dB per octave. The decrease in spectral content per octave is characterized by the gain of the filter at each spatial frequency. The filter gain $A(X)$ is given by:

$$A(X) = \frac{1}{X^{\beta/2}} \tag{10.9}$$

where X is the spatial frequency and β is the spectral density exponent which takes values between 1 and 3. This then ensures that the dimension lies between 1 and 2, as required for a 1D fractal shape. Figure 10.43 illustrates some typical surface shapes that are generated by such a scheme. The bottom line is the input Gaussian white noise. The
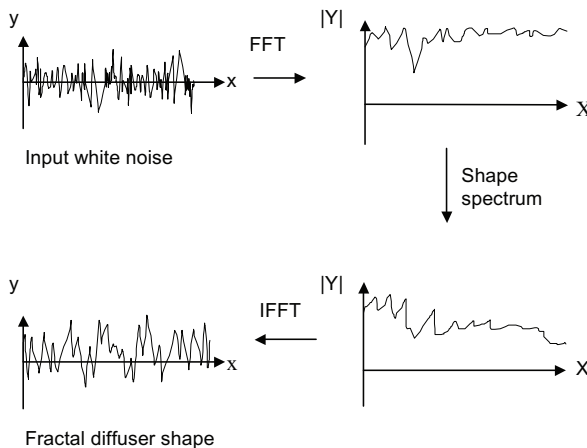
Figure 10.42 Schematic diagram showing Fourier synthesis construction technique (after Cox and D'Antonio[19]).
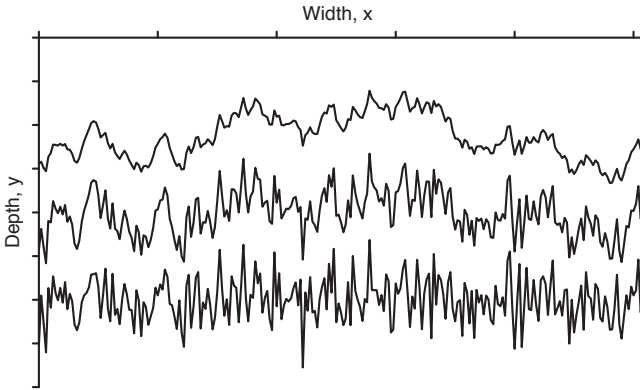
Figure 10.43   Different fractal surfaces generated by Fourier synthesis. Bottom line: input white
noise; middle line: pink noise; top line: brown noise (after Cox and D'Antonio[19]).

middle line was generated with a roll off of 3 dB/octave (β = 1) which gives 1/*f* noise, which in acoustics is termed pink noise. It is also a commonly occurring spectrum in other natural phenomena, for example in the pitch variations found in music. The top line is formed by a steeper roll off of 6 dB/octave (β = 2) and is characteristic of Brownian motion, random walk or brown noise.

   The shapes given in Figure 10.43 can be made into diffusers by extrusion, and will be termed fractional Brownian diffusers (FBD), as the functions represent fractional Brownian motion. By varying the spectral density exponent the spikiness of the surface shape can be altered. In the most general terms, to get the best low frequency scattering performance the spectral density exponent should be large, leading to a smooth shape. To get the best high frequency performance, however, a low spectral density exponent is needed as this makes a spiky shape. The story is, however, more complicated. It has been found that although the spectral density exponent does determine the scattering quality at low and high frequencies to a certain degree, the correct choice of the white noise sequence is most important. Unfortunately, it is not possible to optimize these surfaces, as there are too many governing shape parameters.

10.6.2 Step function addition

Brownian motion can also be simulated by adding a set of randomly displaced step functions. Although this is not always as mathematically pure as a Fourier synthesis technique, it facilitates a reduction in the number of parameters required to represent the surface shape.

   To get proper Brownian motion requires the addition of an infinite number of step functions. Each step function has a random amplitude and random step position along the width of the diffuser. The displacement of the diffuser from a flat surface *y* at a distance *x* along the diffuser is given by:

$$y(x) = \sum_{i=1}^{\infty} A_i f(x - x_i) \quad where \, f(\alpha) = \begin{cases} 0, \alpha < 0 \\ 1, \alpha \geq 0 \end{cases} \tag{10.10}$$
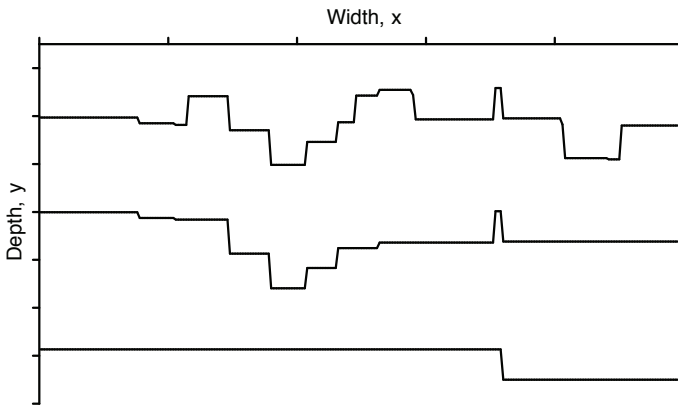
Figure 10.44 Fractal generation by step function addition. Bottom line: 1 step function; middle line: 10 step functions; top line: 20 step functions (after Cox and D'Antonio[19]).

where A_i are a set of Gaussian distributed random amplitudes and x_i a uniformly distributed random set of positions on the diffuser with $-a \leq x_i \leq a$, where $2a$ is the diffuser width. Figure 10.44 illustrates the random addition of step functions for a few terms.

To utilize this generation method efficiently the infinite sum in Equation 10.10 needs to be truncated. In acoustics, the difference in wavelength from the highest to the lowest frequency of interest is not so great that a sound diffuser requires self-similarity over a large range of magnifications. Instead of an infinite sum of terms, a finite number, N, has been used, with each successive term having a decaying amplitude.

$$y(x) = \sum_{i=1}^{N} B_i f(x - x_i) \text{ where } B_i = \frac{1}{i^\alpha}; 0 \leq \alpha \leq \infty \tag{10.11}$$

The decaying amplitude function produces a similar probability distribution of values as the original Gaussian random values A_i, except at the most extreme values of A_i. The other difference is that the amplitudes can now only be regularly spaced values, rather than being truly random. This reduces the number of independent parameters to $N + 1$, the set of displacements x_i and the amplitude decay rate α, and enables optimization to be used.

Using only a few step functions can lead to flat areas which might be prone to producing specular reflections at high frequencies, or sharp spikes which are undesirable. This can be seen in the 20 step function surface shown in Figure 10.44. Consequently, rather than step functions, $f(x)$ can be replaced with functions with more graceful transitions. For example, a hyperbolic tangent function can be used for this:

$$f(x) = \tanh(\gamma_i x) \tag{10.12}$$

The effect of using a hyperbolic tangent function is to round the top and the bottom of the step functions. The γ_i value changes the rate of transition from the top to the

bottom of the step and the amount of rounding. γ_i may either be a constant for all terms in Equation 10.11 or alternatively may be allowed to decay or increase:

$$\gamma_i = \frac{1}{i^\xi}; 0 \leq \xi \leq \infty \qquad (10.13)$$

The 'fractal' shape is now determined by $N + 2$ parameters. These are known as random addition diffusers (RADs).

When optimizing and testing these surfaces it was surprising to find that this generation technique can make semicylinders when the depth was roughly half the width. As discussed previously in connection with curved surface optimization, the semicylinder is very good at dispersing sound provided it is not in an array. This demonstrates that the optimization is working, but does raise the question as to whether the optimized shape can really be called a fractal!

When a more application realistic wide diffuser is optimized, the arc of a circle is no longer optimal, and better fractal diffusers are found. Figure 10.33 compared different diffusers using a standard deviation diffusion parameter (small is best). The fractal is better than the arc of a circle for random incidence sound. It seems that optimized fractal surfaces do produce reasonable diffusers; however, optimized curved surfaces often have better dispersion. Consequently, fractal construction techniques may produce different visual aesthetics to optimized curved surfaces, but not necessarily better diffusers.

10.7 Volumetric diffusers

Modern diffuser design has centred on the use of surface diffusers which are most often attached to the walls or ceiling of a room. But there is a different approach to achieving scattering in a room. The idea is to place the diffuser in the volume of the room rather than on surfaces. By placing scattering objects in the volume of the room the scattering elements have the possibility of influencing 4π space, whereas surface diffusers can only work on 2π space, and so volume diffusers have the potential to be more efficient. Surface diffusers often have limited bass response because of depth restrictions but it may be possible to overcome these by using volumetric designs. The problem with applying these structures is that they cannot be placed where they reduce sight lines or get in the way of the room's functionality. However, in some rooms it would be possible to find places for volumetric diffusers. Volumetric scatterers are commonly used in reverberation chambers, and there have been a few isolated examples of diffusing objects hung from the ceiling of auditoria. Overhead stage canopies could also be viewed as volumetric diffusers. But no one has tested the effectiveness or developed a design methodology, except in the case of reverberation chambers or stage canopies.

There is a recent body of literature[23] which has examined sonic crystals for the purpose of preventing sound transmission. Sonic crystals are regular arrangements of objects, say cylinders or spheres, which when placed in the path of sound waves result in frequencies which are not readily transmitted, known as band-gaps. Previous studies have concentrated on the propagation through periodic sonic crystals and how to maximize the band-gap effects, rather than studying the spatial distribution of the scattered sound field.
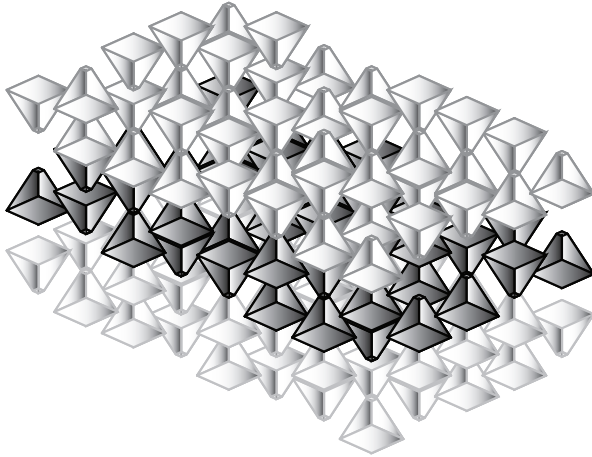
Figure 10.45 A volumetric diffuser.

Many of the key issues met with surface diffusers also arise with volumetric scatterers. Effects of periodicity, such as grating lobes which indicate uneven spatial distribution, or band-gaps which indicate an uneven frequency response, are undesirable. This means a random or pseudorandom arrangement of scattering elements in a multi-layered or 3D array will be needed, perhaps as seen in Figure 10.45. The elements that make up the volumetric diffuser, the cylinders and spheres, need to have a variety of sizes to scatter the different wavelengths of sound, so a fractal construction is most likely to be successful. The density of the elements within the array is important. With insufficient density too much sound will pass through the array unaltered; considering lines of sight through the structure can help understand the performance. It is unlikely that a single density throughout the whole structure will give the best performance. If outer layers are too dense, then too much sound will reflect from these and not reach the inner layers. A structure that gets progressively more dense towards the centre is likely to work best – a bit like impedance matching with absorbers.

10.8 Materials

Geometric reflectors and diffusers can be made from a variety of materials. Examples include wood in various species and finishes, light transmitting or thermoformed plastics, fibre reinforced gypsum, concrete, high density polystyrene and metal. The choice of material depends on factors such as visual appearance, weight and acoustic absorption. Nowadays, environmental effects are an additional consideration in choosing a suitable material. When using wood and plastics, fire resistance is an important factor, as are indoor air quality standards for low emitting products, such as formaldehyde, volatile organic compounds and other carcinogenic materials. In addition, recycled content, locally supplied materials and other characteristics are also important in sustainable or green design. The discussions in Section 5.2.3 about sustainable absorbers are pertinent here.

Geometric reflectors have potential to resonate and cause absorption. The resonant

frequency of a simply supported rectangular isotropic panel of width a and length b is given by:[24]

$$f_0 = \frac{\pi}{2}\sqrt{\frac{B}{m}}\left(\frac{i^2}{a^2} + \frac{n^2}{b^2}\right); \qquad i, n = 1, 2, 3, ...$$ (10.14)

where m is the surface density (kgm^{-2}) and B the bending stiffness given by:

$$B = \frac{Eh^3}{12\left(1 - v^2\right)}$$ (10.15)

where E is Young's modulus, h the panel thickness and v is Poisson's ratio. The fundamental resonance, $i = n = 1$, is of primary concern here, because this is usually the most easily excited and so has the greatest potential for absorption.

For large panels the coincidence phenomenon may also be important at higher frequencies. When the wavelength of the (bending) waves propagating in the reflector is the same as the wavelength of sound in air, then the panel is easily vibrated by the airborne sound, and absorption will result. This happens at the coincidence frequency, which is given by:

$$f_c = \frac{c^2}{2\pi}\sqrt{\frac{m}{B}}$$ (10.16)

where c is the speed of sound in air. If surfaces are orthotropic, for instance if a corrugated surface is used, then the coincidence effect will extend over a significantly wider bandwidth.

Some favour having stage enclosures with low frequency absorption, in which case the resonant frequencies in the above formulations need to be placed at appropriate bass frequencies and the panel should not be overly damped. Proponents of these 'diaphragmatic' enclosures, which are typically not sealed, argue that the surfaces surrounding an orchestra can be used to provide low frequency absorption to create more clarity on the stage. Furthermore, in a small hall, a sealed shell may overpower a small audience and typically these shells contain openings and/or diaphragmatic surfaces to dissipate energy. There are also occasions in small halls where the low frequency absorption from surfaces surrounding the audience can be used to control bass reverberance.

In a large hall, however, it is usual to preserve as much sound energy as possible. So surfaces around the stage and the audience should have low absorption. One way of achieving this is to make the surface heavy, placing the first resonance of Equation 10.14 at such a low frequency that resonant absorption is no longer important. However, the coincidence frequency of Equation 10.16 needs to be checked for large surfaces unless the bending waves are highly damped.

Heavy elements are often, however, undesirable, because they increase costs as the weight must be supported by the building somehow. This is especially true for suspended reflectors. An approach often used is to lighten the load by using a honeycomb core

with two lightweight faces. This laminated structure is very stiff and has low mass. However, Equation 10.14 shows that a high stiffness and low mass results in resonance at an elevated frequency. Furthermore, Equation 10.16 shows that this also lowers the frequency of coincidence. Consequently, increasing stiffness on its own risks increased absorption from both resonance and coincidence.

A better solution for lightweight surfaces is to heavily damp the resonance, which will prevent sound from significantly vibrating the material, and consequently minimizes absorption. Adding damping to increase reflectivity might seem counter intuitive. But by damping the resonances, the impedance mismatch between the air and the surface increases, leading to less absorption. Damping might be achieved by firmly bonding two materials together to form a constrained-layer damping system. For instance, rubber, cork-rubber or a viscoelastic material might be sandwiched between two layers of fibre reinforced gypsum or wood. Alternatively, some materials are inherently highly damped and using damping significantly reduces absorption due to panel resonances and the coincidence phenomenon.

10.9 Summary

This chapter has covered a wide range of different diffuser types. Starting with plane surfaces, it looked at the effects of edge diffraction. The performance of arcs, triangles, pyramids, fractals and curved surfaces was then considered. Current state–of-the-art is to use numerical optimization to allow the surface shape to meet both the acoustic and visual requirements. With good design there are many shapes that can make good diffusers, but only a few of these will ever be visually acceptable in a particular project. The next chapter looks at the use of absorption to promote diffuse reflections.

10.10 References

1 L. Cremer, "Early reflections in some modern concert halls", *J. Acoust. Soc. Am.*, **85**, 1213–25 (1989).
2 L. Cremer, "Fresnel's methods of calculating diffraction fields", *Acustica*, **72**(1), 1–6 (1990).
3 J. H. Rindel, "Attenuation of sound reflection from curved surfaces", *Proc. 25th Conference on Acoustics* (1985).
4 J. H. Rindel, "Attenuation of sound reflections due to diffraction", *Proc. Nordic Acoustical Meeting*, 257–60 (1986).
5 J. H. Rindel, "Design of new ceiling reflectors for improved ensemble in a concert hall", *Appl. Acoust.*, **34**, 7–17 (1991).
6 P. D'Antonio and J. Konnert, "The RFZ/RPG approach to control room monitoring", *Proc. Convention Audio Eng. Soc.*, preprint 2157 (I-6) (1984).
7 A. D. Pierce, *Acoustics: An Introduction to its Physical Principles and Applications*, McGraw-Hill (1981).
8 T. J. Cox and Y. W. Lam, "Evaluation of methods for predicting the scattering from simple rigid panels", *Appl. Acoust.*, **40**, 123–40 (1993).
9 T. J. Cox, "Objective and Subjective Evaluation of Reflection and Diffusing Surfaces in Auditoria", PhD thesis, University of Salford (1992).
10 J. P. O'Keefe, T. J. Cox, N. Muncy and S. Barbar, "Modern measurements, optimized diffusion, and electronic enhancement in a large fan-shaped auditorium", *J. Acoust. Soc. Am.*, **103**(5), 3032–3, also *Proc. 16th ICA* (1998).
11 T. J. Cox, "Designing curved diffusers for performance spaces", *J. Audio Eng. Soc.*, **44**(5), 354–64 (1996).
12 W. H. Press *et al.*, *Numerical Recipes, the Art of Scientific Computing*, Cambridge University Press, 289–92 (1989).

13 T. J. Cox and P. D'Antonio, "Holistic diffusers", *Proc. IoA(UK)*, **21**(6), 201–6 (1999).
14 P. D'Antonio and T. J. Cox, "Aperiodic tiling of diffusers using a single asymmetric base shape", *Proc. 18th ICA*, Mo2.B2.3 (2004).
15 P. D'Antonio and T. J. Cox, *Embodiments of Aperiodic Tiling of a Single Asymmetric Diffusive Base Shape*, US patent 6, 772, 859. (2004)
16 T. J. Cox and P. D'Antonio, "Designing stage canopies for improved acoustics", *Proc. IoA(UK)*, **19**(3), 153–60 (1997).
17 M. Barron, *Auditorium Acoustics and Architectural Design*, E&FN Spon, 55 (1993).
18 P. D'Antonio and T. J. Cox, "Canopy arrays: density, size, shape and position", *Proc. IoA(UK)*, **28**(2) (2006)
19 T. J. Cox and P. D'Antonio, "Fractal sound diffusers", *Proc. 103rd Convention Audio Eng. Soc.*, preprint 4578, Paper K-7, New York (1997).
20 P. D'Antonio and J. Konnert, "The QRD Diffractal: A new 1 or 2-dimensional fractal sound diffusor", *J. Audio Eng. Soc.*, **40**(3), 117–29 (1992).
21 H.-O. Peitgen and D. Saupe (eds), *The Science of Fractal Images*, Springer-Verlag (1988).
22 J. Feder, *Fractals*, Plenum Publishing Corporation (1988).
23 T. Miyashita, "Sonic crystals and sonic wave-guides", *Meas. Sci. Technol.*, **16**, R47–R63 (2005).
24 D. A. Bies and C. H. Hansen, *Engineering Noise Control*, 3rd edn, Spon press, 347 (2003).

11 Hybrid surfaces

A diffuser needs to break up the reflected wavefront. While this can be achieved by shaping a surface, it can also be done by changing the impedance of the surface. Indeed, Schroeder diffusers are often interpreted as being a surface with a spatially-varying impedance. In this chapter, variable impedance is achieved by patches of absorption and reflection. Unlike the Schroeder diffuser, these cannot be designed for minimum absorption. These surfaces are hybrids somewhere between pure absorbers and non-absorbing diffusers. Partial absorption is inherent in the design while any reflected sound is dispersed.

Using patches of absorption to generate dispersion is not particularly new. In studio spaces people have been arranging absorption in distributed patches rather than solid blocks for many years. In more recent times, however, a new breed of surface has been produced, where the absorbent patches are much smaller, and the arrangement of these patches is determined by a pseudorandom sequence to maximize the dispersion generated. This chapter will start by discussing some implementations of these surfaces to give a sense of how they can be constructed. Then a more detailed theoretical basis for their design will follow.

11.1 Planar hybrid surface

The Binary Amplitude Diffsorber, also known as a BAD™ panel,[1] is a flat hybrid surface having both absorbing and diffusing abilities. The panel simultaneously provides sound diffusion at high and mid-band frequencies, and crosses over to absorption below some cut-off frequency. Figure 11.1 shows a typical construction and an application in a music practice room. A porous absorber, such as mineral wool, is faced with a complex perforated mask and the panel might be fabric wrapped for appearance. The white patches on the mask are holes, and the black patches hard reflecting surfaces.

Figure 11.2 shows the random incidence absorption coefficient for a hybrid surface compared to the mineral wool alone; the effect of changing the backing depth is also shown. The additional vibrating mass within the holes of the mask causes the absorption curve to shift down in frequency generating additional low to mid-frequency absorption. At high frequency, the hard parts of the mask reflect sound and hide some parts of the mineral wool; this causes a reduction in the absorption coefficient. It is at these high frequencies, where the absorption is reduced, that the surface needs to disperse the reflected sound.

To accomplish mid- to high frequency dispersion a 31 × 33 2D array of absorptive and reflective areas is used. The reflective areas map to the 1 bit and the absorptive
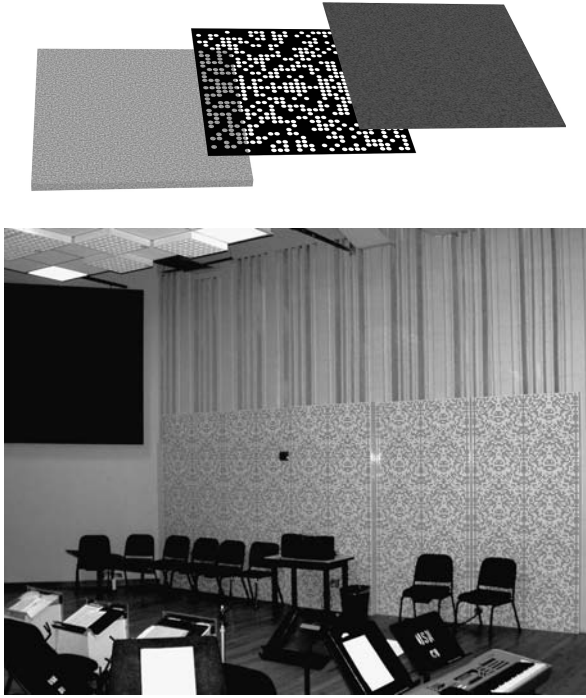
Figure 11.1 Top: construction of a hybrid surface: porous absorber (left), the mask (middle), and fabric covering (right). Bottom: an application on the lower part of the wall in the rehearsal room for the Commodores, the US Navy jazz ensemble. (Acoustician: Polysonics Corporation)
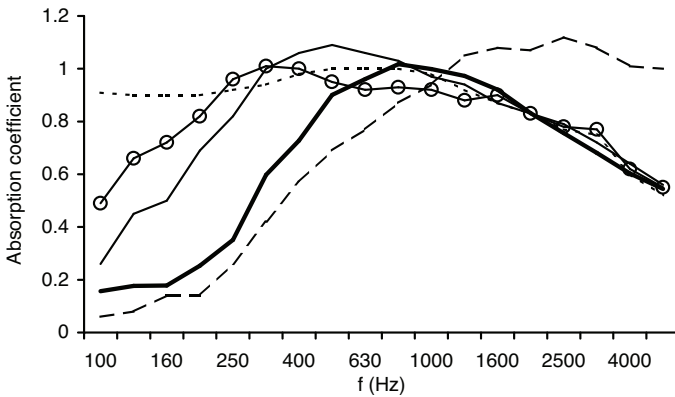
Figure 11.2 Random incidence absorption coefficient for a hybrid surface (BAD™ panel) compared to mineral wool. Four different backing depths for the panel are shown:
——— 2.5 cm BAD;
——— 5.1 cm BAD;
—⊖— 7.6 cm BAD;
------- 10.2 cm BAD; and
– – – 2.5 cm Fibreglass.
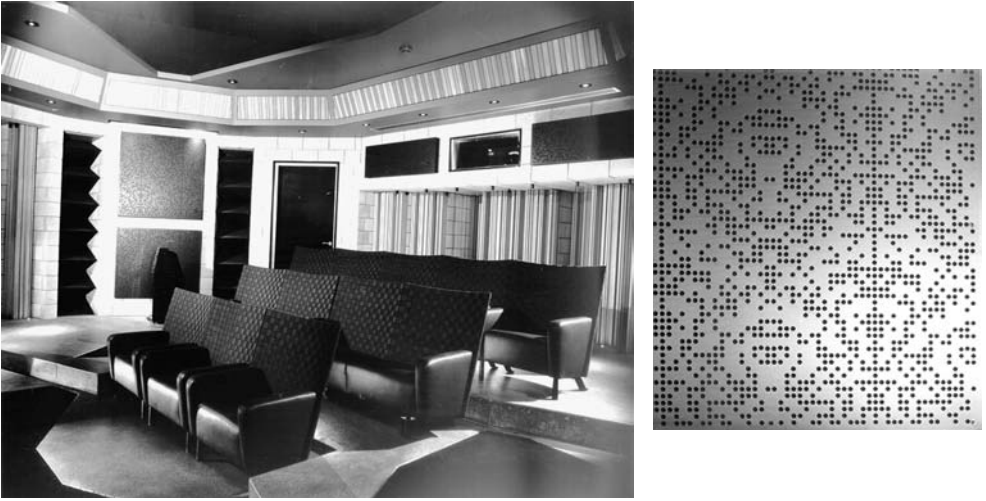
Figure 11.3 Example application of planar hybrid surface (BAD panel) in a home theatre (left). The BAD panels are on the back left wall, and are also shown magnified on the right. (Acoustician: Pilchner Schoustal International Inc.)

areas map to the 0 bit in a binary pseudorandom number sequence. The distribution of these binary elements is based on an optimal binary sequence with a flat power spectrum as this maximizes dispersion. For example, maximum length sequences (MLSs) can be used.

Hybrid surfaces extend the acoustical performance of traditional fabric wrapped absorbers and allow wide area coverage without excessive deadening at mid- to high frequencies. The treatment is used in facilities that need reflection control. The construction is simple and inexpensive. Furthermore, the acoustic function can be hidden, which can lessen the conflict between visual aesthetics and acoustic requirements. Alternatively, many architects are interested in seeing the mask due to its unique appearance and the fact that it offers an alternative to the traditional periodic perforated metal patterns. Figure 11.3 shows a home theatre installation in which a black anodized aluminium mask was used. The mask can be made from a variety of materials provided they are rigid and non-absorbing, such as wood and metal, and a non-woven matte can be used on the back surface to conceal the porous absorber.

11.2 Curved hybrid surfaces

Flat hybrid surfaces such as the BAD panel still generate a coherent specular reflection, albeit attenuated because it is partially absorbed. The hard parts of the mask still generate reflected waves that arrive in phase in the specular direction. One solution to this is to shape the surface, as then the specular reflection can be significantly reduced to achieve even more uniform diffuse reflections. Figure 11.4 illustrates such a construction with a simple curve as well as an application of the device. The absorption performance of curved hybrid surfaces will be similar to the planar surfaces, but as shall be shown later in this chapter, the dispersion will be greatly increased. This curved

Figure 11.4   A curved hybrid surface and its application in a control room at the Universal Music Mastering Studios in New York City (room design: Francis Manzella – FM Design Ltd, photo: George Roos).

construction has found favour in recording studios as it allows treatment away from the extremes of complete absorption, specular reflection or diffuse reflection. This enables the sweet spot, the place where the room acoustics are at their best, to be spatially expanded. Figure 11.5 shows an application of a curved hybrid surface[2] on the ceiling and walls of a post production studio.

As porous absorbents have a lower speed of sound than air, hybrid surfaces also have the ability to perturb the sound field more at lower frequencies when compared to hard diffusers of the same depth. In theory, hybrid surfaces can produce diffuse

Figure 11.5   A curved hybrid diffuser applied to the ceiling and side walls of SonyM1, New York. (Photo by Paul Ellis of The M Network Ltd, Acoustician: Harris, Grant Associates.)

reflections at lower frequencies, although at low frequency the effect of these surfaces can be dominated by absorption. Nevertheless, it appears that hybrid surfaces can make efficient use of a limited depth. As absorption is inevitable in these devices, they are not useful in spaces where absorption must be minimized, such as large auditoria for symphonic music.

Chapter 10 explained how optimization can be used to design rigid curved surfaces. This process can also be used to make hybrid curved surfaces. A binary sequence with good autocorrelation properties is chosen and then the computer is tasked to find the best shape.

11.3 Ternary and quadriphase surfaces

As noted above, a problem with planar hybrid surfaces is that energy can only be removed from the specular reflection by absorption. For instance, the specular reflection is only attenuated by about 6 dB for a surface with a 50 per cent absorptive area. To improve performance it is necessary to exploit interference and reflect waves out-of-phase with the specular reflection. This can be achieved by adding wells to the surface.[3] An example of this is shown in Figure 11.6A. The reflection coefficients of this surface are then made up of three values, which at the design frequency are –1, 0 and +1. As a result, optimal ternary sequences are required. By adding wells to hybrid surfaces a very useful improvement in performance is achieved for a modest depth penalty.[4] Performance is even better if two different well depths are used, in which case a quadriphase (4–level) sequence is used.

11.4 Simplest theory

First, a discussion of the design of hybrid surfaces using the simplest Fourier theory discussed in Chapter 8 will be given. As with Schroeder diffusers, much can be learned by considering the simplest equations but ultimately more exact theories will be necessary to match experimental results. For simplicity, consider a 2D world so that predictions in one plane only are considered. The pressure amplitude, $|p_s|$, reflected
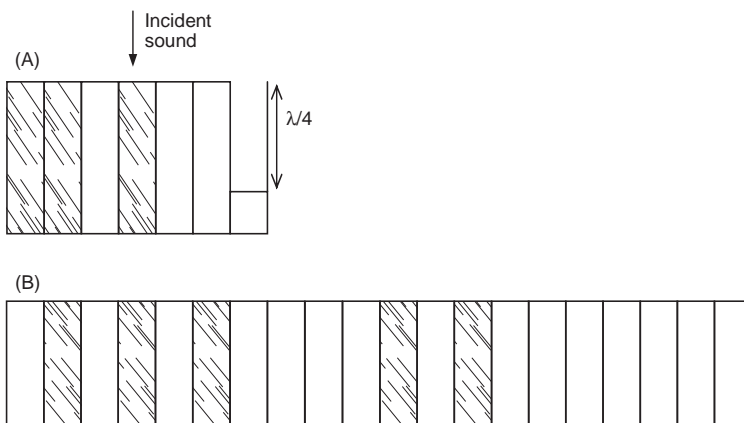
Figure 11.6   Two 1D hybrid surfaces where the shaded patches are reflective, and the clear patches absorptive. Constructed using a: (a) ternary sequence, and (b) binary sequence.

from a planar surface with a spatially-varying impedance is given by:

$$\left|p_s\left(\theta,\psi\right)\right| \approx \left|A\int_s R(x)e^{jkx[\sin(\theta)+\sin(\psi)]}dx\right| \tag{11.1}$$

where ψ and θ and the angles of incidence and reflection; $R(x)$ is the surface reflection coefficient at a distance x along the surface; k is the wavenumber; A is a constant, and s is the diffuser surface.

This is an approximate far field theory, which forms the basis of the hybrid surface design. This simple prediction theory and the subsequent design process are only applicable at mid- and high frequency. At low frequency the mutual interactions across the surface make the prediction model inaccurate, as shall be discussed later. Equation 11.1 is a Fourier transform in kx and transforms the reflection coefficients into $[\sin(\theta) + \sin(\psi)]$ space. To a first approximation, the absorptive parts of the hybrid surface will have a reflection coefficient of $R(x) = 0$, and the reflective parts have $R(x) = 1$. A pseudorandom number sequence with good autocorrelation properties is used to determine the spatial distribution of the hard and soft patches. For example, the number sequence might be {0, 1, 0, 1, 0, 1, 0, 0, 0, 0, 1, 0, 1, 0, 0, 0, 0, 0, 0, 0} and where there is a zero in the sequence a patch of absorption is used; where there is a one in the sequence the surface is reflective. Figure 11.6B illustrates a surface where the impedance variation is in one plane only, and the strips of absorption or reflection are extruded in one direction. Surfaces which scatter hemispherically, such as those shown in Figure 11.1, are formed from number sequence arrays; these are discussed in Section 11.8.1.

A number sequence with good autocorrelation properties will have a flat power spectrum with respect to kx. This means the pressure amplitude scattered is constant with respect to the transform variable $\sin(\theta) + \sin(\psi)$, which means good dispersion is generated in a polar response. If the surface is periodic, this will relate to grating lobes all having the same level except for the zeroth order lobe, in many ways similar to the theories behind Schroeder diffusers discussed in Chapter 9.

Consequently, the choice of number sequence is crucial to obtaining diffuse reflections. The initial development of this diffuser was carried out by Angus[5] who began by looking at MLSs. These sequences are a good starting point as they have desirable Fourier properties. There are many other bipolar sequences which have flat Fourier transforms, but MLSs are the best documented and known. The issue of sequences is discussed in more detail in the next section.

11.5 Number sequences

To gauge the quality of a number sequence for a hybrid surface, the autocorrelation function can be examined. This is because the autocorrelation function directly relates to the scattering performance of the surface, see Section 9.4.

11.5.1 One-dimensional maximum length sequences

The reflection coefficients for the hybrid surface are 0 (absorption) and 1 (reflection) and consequently, the number sequence used should have optimal autocorrelation
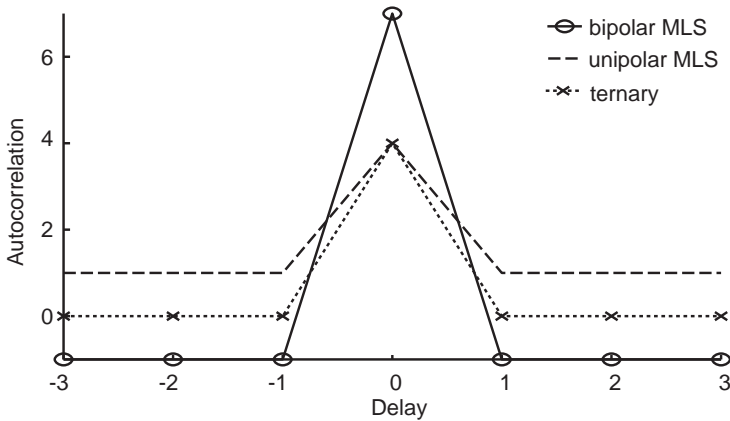
Figure 11.7   Autocorrelation function for a bipolar (+1s and –1s) and unipolar (+1s and 0s) MLS and a ternary sequence. The first is like a phase grating diffuser, the other two are like hybrid surfaces.

properties for 0s and 1s, which means a good unipolar sequence is needed. Most pseudorandom binary sequences, on the other hand, have autocorrelation properties designed with a bipolar sequence composed of 1s and –1s. The autocorrelation side lobe performance of a unipolar and bipolar sequence can be very different. Figure 11.7 demonstrates this for a MLS of length 7. When a sequence can be bipolar (positive and negative), the autocorrelation side lobes on either side of zero delay include cancelling effects, which enable a low side lobe energy to be created as desired. When the sequence is unipolar no cancellation can occur and the autocorrelation side lobe levels are higher. Consequently, it would be anticipated that the scattering performance would be worse for a unipolar sequence. The consequence of no cancellation is that the DC component in the power spectrum is large, as shown in Figure 11.8. This means that the energy in the specular reflection direction, when $\sin(\theta) + \sin(\psi) = 0$, will be attenuated less for a unipolar surface in comparison to a bipolar surface.
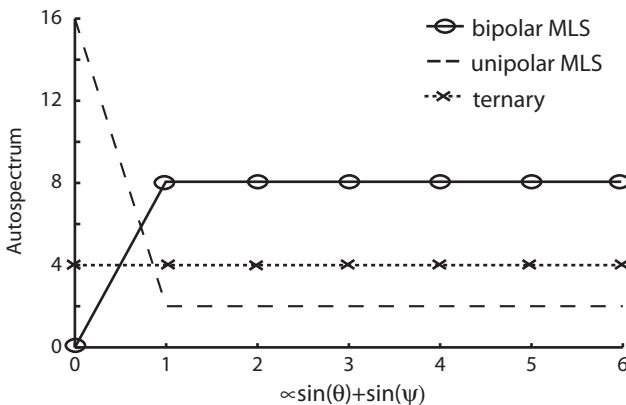
Figure 11.8   Comparison of power spectra for a bipolar MLS, a unipolar MLS and a ternary sequence.
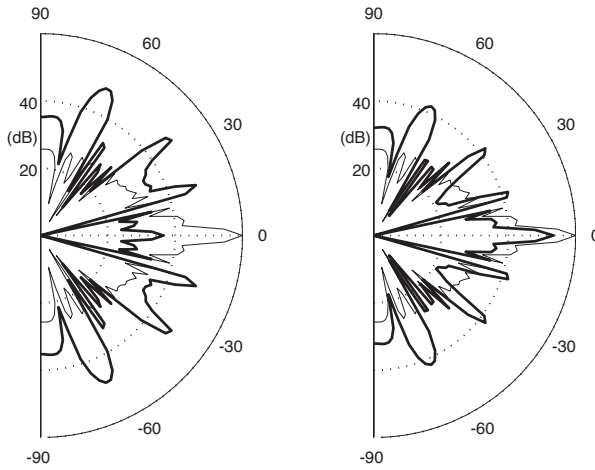
Figure 11.9   Scattering from diffusers constructed using bipolar and unipolar maximum
length sequences:
————— plane surface, shown in both figures; and
━━━━━ maximum length sequence, either bipolar (left figure) or unipolar (right
figure).

In a bipolar MLS the mean value of the reflection coefficients is close to zero, and consequently the DC value of its power spectrum is close to zero; see Figure 11.8. This means that suppression of the zeroth order lobe in the polar response, when $\sin(\theta) + \sin(\psi) = 0$ occurs; see Figure 11.9. The construction of diffusers based on bipolar MLSs was discussed in Section 9.4.1; these are a type of Schroeder diffuser.

With a unipolar MLS a hybrid diffuser is being constructed. The mean value of the reflection coefficients is no longer close to zero. Indeed the D.C. value is actually higher than the other spectral values, and consequently the zeroth order lobe is significantly greater than other lobes. Figure 11.8 illustrates this by comparing the power spectra of unipolar and bipolar MLSs. Figure 11.9 shows the polar response for a diffuser constructed from bipolar and unipolar MLSs. This is evidence that the planar hybrid surfaces will have a significant specular energy lobe, with the zeroth order lobe being about $10 \log_{10}(N)$ times larger than the other lobe energies, where N is the length of the MLS. The specular reflection lobe will be attenuated by about 6 dB compared to a plane hard surface (as expected for a surface which is 50 per cent absorptive by surface area). The scattering lobes are not even for the hybrid surface, but the scattering in the specular lobe is reduced.

When the open area of the panel is about 50 per cent then the MLS is a good choice. The performance of the MLS when composed of unipolar elements is worse than when it is bipolar as shown above, but the MLS will still be the best possible sequence achievable; there are no better unipolar sequences, although there are some which are just as good. Problems arise if the open area of the panel needs to be reduced, as common optimal binary number sequences usually have a similar number of 0s and 1s.

11.5.2 One-dimensional optical sequences

There are a set of sequences, called optical sequences,[6] which are unipolar and have a different number of 1s and 0s. Angus[7] suggested that these could be used to overcome some of the problems associated with MLS. For instance, they can be used to form a surface whose open area is not 50 per cent. Optical sequences were developed for use in fibre optical code division multiple access (CDMA) processes. CDMA systems enable multiple users to use a single digital transmission line efficiently. Fibre optic CDMA sequences, where the light intensity is either on or off cannot have cancellation, and hence unipolar sequences are needed. They use an optimal sequence defined as one where the maximum of the side lobes of the autocorrelation function has the smallest possible value.

The problem with optical sequences is that the typical construction methods available result in a very low number of 1s in a long sequence. For example, a typical length 20 sequence is {0, 1, 0, 1, 0, 1, 0, 0, 0, 0, 1, 0, 1, 0, 0, 0, 0, 0, 0, 0} which only contains five 1s and so would give a nominal open area of 25 per cent. This occurs because the sequences were devised for very low side lobe performance, which necessitates a low occupancy of 1s as this is the only way to achieve low side lobe energy in the autocorrelation function when no cancellation can occur. Unfortunately, for hybrid surface design this makes the sequences, especially the very long sequences, not that useful. The surface will either be very reflective (if the 1s are associated with absorption) or very absorptive (if the 1s are associated with reflection). Incidentally, the above sequence can also be written as {2, 4, 6, 11, 13}, where the index number gives the location of the 1s. For low occupancy cases, this is a much more compact representation of the sequences and so will be used below.

Optical sequences are usually generated in families. These are a set of sequences which not only have good autocorrelation properties, but also have low energies for the cross-correlation between family members. In an optical sequence, five parameters are used to specify their performance. ξ is the number of 1s in the sequence, N the length, M the family size (the number of sequences in the family), S_{xxm} the maximum side lobe value in the autocorrelation function, and S_{xym} the maximum value in the cross-correlation function between sequences in the same family. These parameters can be stated in an abbreviated form {ξ, N, M, S_{xxm}, S_{xym}}. For the length 20 sequence given above this would be expressed as {5, 20, M, 3, S_{xym}}.

There are some sequences with a reasonable occupancy, for example {3, 7, 1, 1, 1}, but the length of these sequences is too short to be of much use for hybrid surfaces. As with phase grating diffusers, a designer should always look to maximize the repeat length to minimize periodicity effects. This means that large N sequences are required, and then the number of 1s becomes too small using the normal optical sequence generation technique. Consequently, when N is large three construction techniques are suggested, as outlined below. In reality, a combination of techniques might be needed.

1. This technique involves starting with a sequence with too few 1s and increasing the number of 1s. Given a {ξ, N, M, S_{xxm}, S_{xym}} family of sequences, it is possible to increase the number of 1s, but at the penalty of increasing the maximum value of the autocorrelation and cross-correlation. This is best illustrated with an example:

A set of optical sequences {3, 25, 4, 1, 1} are: {1, 2, 7}, {1, 3, 10}, {1, 4, 12}, {1, 5, 14}. The sequences are taken in pairs and a bit-wise OR taken between the pairs to form new sequences. So if both sequences have a zero bit, then the new sequence has a zero bit; otherwise the new sequence has the bit set to one. In the above case there are six unique combinations, as sequences are not combined with themselves. The new sequences are: {1, 2, 3, 7, 10}, {1, 2, 4, 7, 12}, {1, 2, 5, 7, 13}, {1, 3, 4, 10, 12}, {1, 3, 5, 10, 13}, {1, 4, 5, 12, 13}. These form a new family of sequences with the property $\{\xi' = 5, N' = 25, M' = 6, S'_{xxm} = 2, S'_{xym} = 3\}$, where the prime is used to denote the new sequence. The number of 1s has increased from 3 to 5, but both the autocorrelation and cross-correlation properties have degraded. The maximum side lobe value in the autocorrelation has increased from 1 to 2.

The above process in general produces new sequences where the number of 1s is $\xi' \geq 2\xi - S_{xym}$, where ξ and S_{xym} are the values for the original sequences. If too many 1s are generated after the OR operations, some 1s are randomly chosen to be changed to 0s. This was not necessary in the above example. The autocorrelation and the cross-correlation of the new sequences will be $S'_{xxm} \leq 2S_{xxm} + 2S_{xym}$ and $S'_{xym} \leq \xi + 3S_{xym}$ respectively. In the construction example above, the new sequences are considerably better than the worst case given by these upper bounds. For diffuser design, repeated application of this process is likely to be needed.

2. A very similar approach to (1) would be to take a sequence with too many 1s and reduce their number. For example, it should be possible to start from a family of MLSs and via logical operations reduce the number of 1s to the desired value.

3. The last technique involves constructing a family of optical sequences and then concatenating these together. As the family will have mutual low correlation, they should work well in a concatenated longer sequence.

11.5.3 *One-dimensional ternary and quadriphase sequences*

Many of the standard construction methods for general ternary sequences are inappropriate because they do not generate the right balance of –1, 0 and +1 elements for hybrid surfaces. Many sequences have very few zero elements in them and consequently the surfaces would not be very absorbing. This arises because most applications of number theory want to maximize the efficiency of the sequence – efficiency in this context meaning the power carried by a signal based on the sequence. The sequence also needs to have a similar number of –1s and 1s, because this maximizes the attenuation of the specular reflection.

Correlation identity derived ternary sequences[6] can have an efficiency of ≈50 per cent, meaning that half the sequence are zeros, and will therefore have a nominal absorption coefficient of ≈0.5, provided the design parameters are chosen correctly. They are formed from two MLSs of order m and length $N = 2^m - 1$; the order of the sequences must obey $m \neq 0 \mod 4$.

First it is necessary to find a pair of MLSs with suitable cross-covariance properties. The process is to form an MLS and then sample this sequence at a different rate to form a complementary sequence. For example, if the sample rate is $\Delta n = 2$ then every second value from the original sequence is taken. The sample rate is chosen using either $\Delta n = 2^k + 1$ or $\Delta n = 2^{2k} - 2^k - 1$. A parameter e is defined as $e = \gcd(m, k)$ where gcd()

is the greatest common divisor. This must be chosen so that m/e is odd as this gives the correct distribution of cross-covariance values.

Under these conditions, the two MLSs have a cross-covariance $S_{ab}(\tau)$ which has three values. The total number of 1s and –1s in the sequence will be given by $\approx N(1 - 2^{-e})$. This is therefore the amount of reflecting surface on the diffuser, and so at high frequency it would be anticipated that the absorption coefficient of the surface, α, would be $\approx 1 - 2^{-e}$. If the aim is to achieve a surface with $\alpha \approx 0.5$, this means choosing $e = 1$, which means the order of the MLS, m, must be odd.

Consider an example of $N = 31 = 2^5 - 1$. e is required to be a divisor of m so that m/e is odd and this can be achieved with $k = 1$ as this makes $e = \gcd(k, m) = 1$. A possible sample rate is $\Delta n = 3$.

The first part of the MLS used is: {1, 0, 0, 0, 0, 1, 0, 0, 1, 0, 1, 1, 0, 0, 1, 1, 1, 1, 1, ...}. Taking every third value then gives a second MLS: {1, 0, 0, 0, 0, 1, 1, 0, 0, 1, 0, 0, 1, 1, 1, 1, 1, 0, 1, ...}. This then gives a cross-covariance (after the MLS sequences are made bipolar) where 7 occurs 10 times, –1 occurs 15 times and –9 occurs 6 times.

The ternary sequence, c_n, is formed from this cross-covariance – a rather surprising and remarkable construction method. The sequence is $2^{-(m+e)/2}(S_{ab}(\tau) + 1)$. This sequence has an ideal autocovariance with a peak value of 2^{m-e} and out-of-phase values that are zero. Applying this to the above pair of MLSs yields the ternary sequence: {0, 0, 1, 1, –1, 1, –1, 0, 0, 0, 1, 1, 0, 1, –1, –1, 0, 1, 0, ...}.

The autocovariance indicates the advantages that might be expected from ternary sequence diffusers in comparison to unipolar binary sequence diffusers. The auto-covariance functions for the ternary and unipolar binary sequences are shown in Figure 11.7. The unipolar binary sequence has constant out-of-phase values, but they are not zero. This leads to diffusers with a significant specular component in their polar pattern. Perfection can be achieved using a ternary sequence as the out-of-phase values are all zero.

The ternary sequence has a good reflection coefficient autospectrum because it is constant; an example is shown in Figure 11.8. This means that a surface based on a single ternary sequence produces more even scattering than one using an MLS. For a periodic structure where many repeats of the sequence are placed side by side, this will result in all the grating lobes having the same energy.

11.5.4 Optimized sequences

For short sequences it is possible to use a computer search to find the best sequence. For a small sequence length, say $N \leq 20$ for a binary sequence, it is possible to do an exhaustive search of every possible combination to find the best sequences. Every possible combination of bits with the correct number of 1s are tested by first constructing the autocorrelation function for each case, and then finding the sequence or sequences which have the smallest maximum value for the autocorrelation side lobes. As N increases, however, this rapidly becomes a very time consuming process to carry out. The number of unique combinations to search is given by:

$$^{N}c_r = \frac{N!}{\xi!(N - \xi!)} \tag{11.2}$$
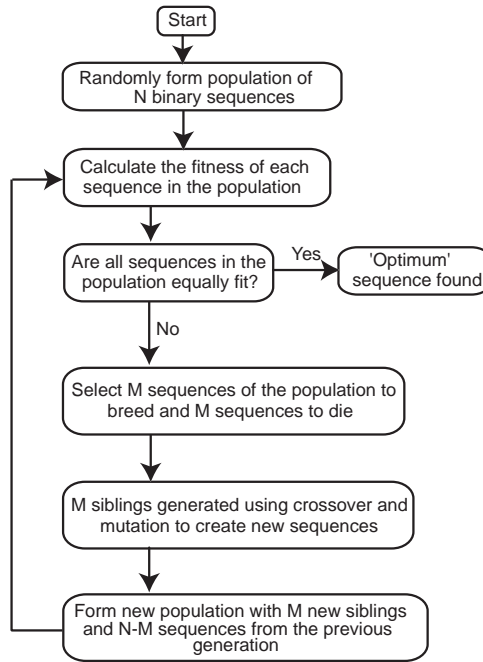
Figure 11.10 Optimization of numerical sequences using a genetic algorithm.

where ξ is the number of 1s in the sequence and ! indicates factorial. Consequently, for $N = 20$, $\xi = 10$ there are nearly 200,000 combinations, and this roughly doubles for every additional bit.

For say 20 $<N$ <48 a numerical optimization[8] can be used to search for the best sequence. In this case optimization algorithms are used to avoid the need to test every possible combination, but even so this is still going to be a slow process. As computing power increases, this will be applicable to larger sequence lengths. But even with increasing computing power, the length of sequence over which optimization can be carried out is not going to rapidly expand. For an $N = 48$ binary sequence with 24 1s and 24 0s there are about 10^{13} unique sequence combinations to search.

Unlike the numerical optimization of Schroeder well depths discussed in Chapter 9, this is a discrete function optimization. In other words, the values of the optimization parameters, which are the locations of the 1s in a binary sequence can only take discrete values. This means the best algorithm for tackling this problem is a genetic algorithm as it can explicitly represent the discrete sequences as genes.

A genetic algorithm is a technique for searching for optimum configurations in engineering problems. Figure 11.10 illustrates how a typical genetic algorithm works. It attempts to mimic the process of evolution that occurs in biology. A population of individuals is randomly formed. Each individual is determined by their genes, in this case the genes are simply the binary sequence values, indicating where hard and soft patches should be placed on the surface. Each individual has a fitness value that indicates how good they are. In this case, it is the largest energy in the autocorrelation side lobes. Over time, new populations are produced by breeding and the old populations die.
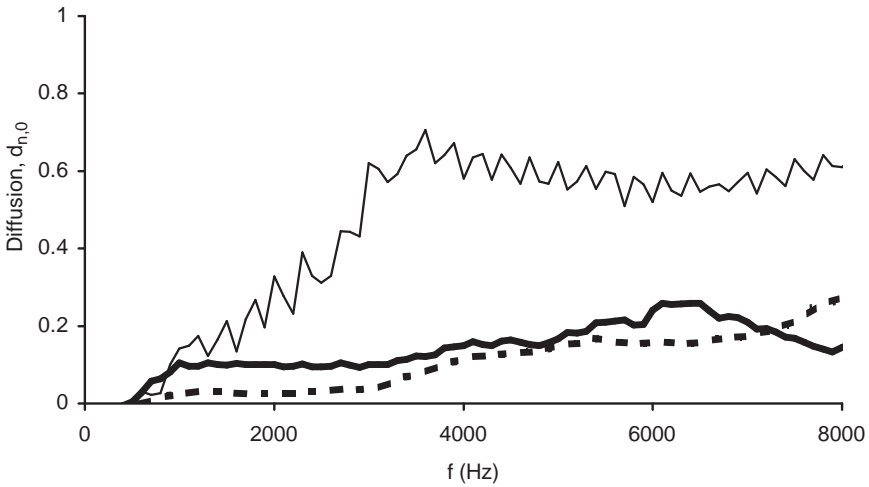
Figure 11.11 Normalized diffusion coefficient for three surfaces showing how an optimized
sequence can improve on a random sequence (normal incidence):
- - - hybrid surface formed using a typical random sequence;
——— hybrid surface formed using an optimized sequence; and
——— 25 cm fibreglass (original data from Cox and D'Antonio[8]).

Offspring are produced by pairs of parents breeding. An offspring has a gene sequence
that is a composite of the sequences from the parents. A common method for doing this
is multiple point cross over. For each bit in the sequence there is a 50 per cent chance
of the child's bit coming from parent A and a 50 per cent chance of the bit being from
parent B. Mutation is also used. This is a random procedure whereby there is a small
probability of any bit in the child sequence changing during breeding. Mutation allows
sequences outside the parent population to be made.

Selecting sequences to breed and die can be done randomly. As with conventional
evolution theory, the fittest are most likely to breed and pass on their genes, and the
least fit the most likely to die. By these principles, the fitness of successive populations
should improve. This process is continued until the population becomes sufficiently
fit, so that the sequence produced can be classified as optimum.

An additional advantage of using a numerical optimization is that it gives complete
control over the reflectivity of the diffuser. This can be specified as a desirable char-
acteristic; any individual not having the desired reflectivity will be scored as less fit.
Consequently, the trait of undesired reflectivity will die off.

Figure 11.11 shows the diffusion coefficient for a hybrid surface formed from an
optimized sequence, compared to a hybrid surface formed from a random sequence. An
improvement in performance is seen for most frequencies, although the improvement is
not great. The main problem with this design technique is that it is impossible to find
long optimal sequences, because the number of possible sequences to search becomes
too large. One solution to this problem is to generate a family of good sequences of
relatively low N with low mutual cross-correlation, and to concatenate them together
to get a longer sequence. This is possible because during the optimization both the
autocorrelation and cross-correlation properties can be considered at the same time.
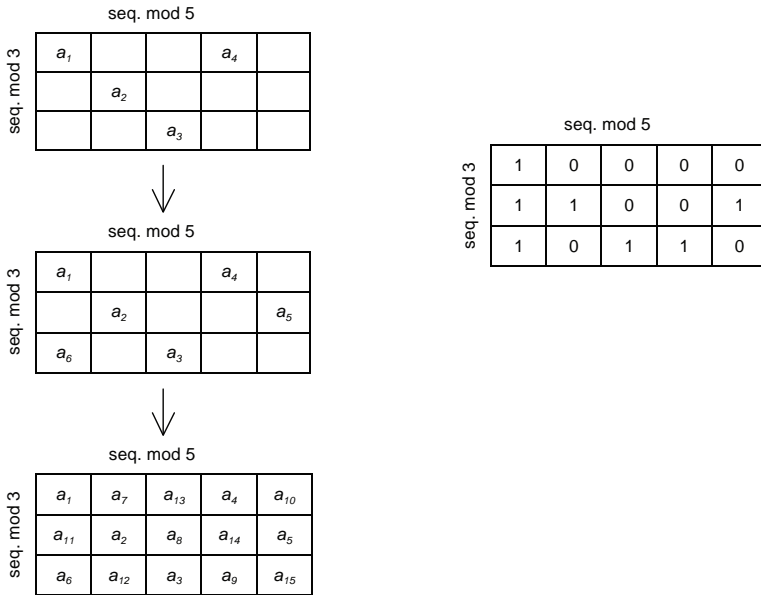
Figure 11.12 Left: some of the steps involved in folding a length 15 sequence, $a_1 \ldots a_{15}$ into a 2D array using the Chinese remainder theorem. The right table shows the wrapping of the MLS sequence {1, 1, 1, 0, 1, 1, 0, 0, 1, 0, 1, 0, 0, 0, 0}.

11.5.5 *Two-dimensional sequences*

A hemispherical scatterer such as that shown in Figure 11.1 requires a 2D sequence, and this can be achieved by three methods:[6,9] folding, modulation (Kronecker product in number theory) and periodic multiplication. Consider constructing a surface with dimensions (in terms of number of patches) of $N \times M$. Whether a sequence can be constructed depends on the values of N and M.

Schroeder[10] showed that a folding technique called the Chinese remainder theorem could be applied to phase grating diffusers based on polyphase sequences. D'Antonio[1] used the same technique for a binary hybrid diffuser. The Chinese remainder theorem folds a 1D sequence into a 2D array and yet preserves the good autocorrelation and Fourier properties. To use this method N and M must be co-prime. By co-prime it is meant that the only common factor for the two numbers is 1.

Consider a length 15 sequence which will be wrapped into a 3×5 array. The elements are sequentially labelled $a_1, a_2, a_3 \ldots a_{15}$. The 1D sequence is written down the diagonal of the array, and as it is periodic, every time the edge of the array is reached the position is folded back into the base period. The process is illustrated in Figure 11.12.

Figure 11.13 shows another way of viewing this process. The coordinates (column, row) of the elements $a_1 \ldots a_{15}$ are determined by modulo indexing. The subscript is

Index, n	0	1	2	3	4	5	6	7	8	9	10	11	12	13	14
Column coordinate = n modulo 5	0	1	2	3	4	0	1	2	3	4	0	1	2	3	4
Row coordinate = n modulo 3	0	1	2	0	1	2	0	1	2	0	1	2	0	1	2

Figure 11.13 The Chinese remainder theorem expressed as modulo indexing.
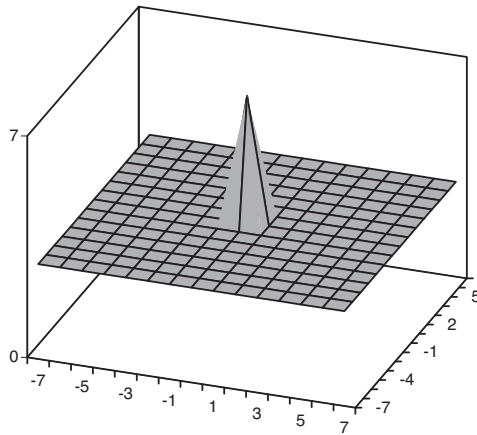
Figure 11.14 The autocorrelation function for a unipolar $N = 15$ MLS sequence folded using the Chinese remainder theorem.

called the index, n. The column for element a_n is determined by n modulo 5 and the row is determined by n modulo 3.

This folding technique still maintains the good autocorrelation properties of the sequence. For example, Figure 11.14 shows the autocorrelation for a unipolar maximum length sequence folded into a 3×5 array. The same autocorrelation properties are achieved in terms of the side lobe energy values. The Chinese remainder theorem can be applied before or after the Fourier transform, as illustrated in Figure 11.15. Consequently, the folding technique preserves the ideal Fourier properties.

Modulation is a process that allows diffusers to be arranged in a non-periodic fashion by modulating one or more base shapes with a binary sequence (see Section 9.5). Another way of viewing the outcome of this process is that it forms a single longer length sequence. A very similar process can be used to form arrays using ternary and binary sequences and arrays. Two sequences (or arrays) are modulated together to form a longer sequence (or array).

To illustrate this, consider making a ternary array by modulating a ternary sequence with a perfect aperiodic binary array. (Note that it is important to modulate the array by the sequence and not vice versa.) Consider a length 7 correlation identity derived
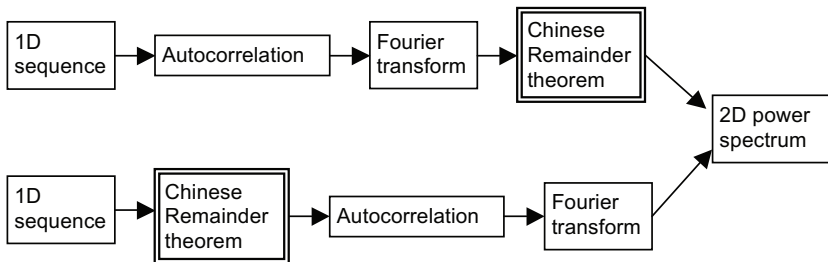
Figure 11.15 The Chinese remainder theorem can be applied before or after the Fourier transform, and consequently it preserves good autocorrelation properties when used to fold 1D sequences into 2D arrays.

ternary sequence $a = \{1, 1, 0, 1, 0, 0, -1\}$; this is used to modulate the perfect aperiodic binary array, b:

$$b = \begin{Bmatrix} -1 & -1 \\ -1 & 1 \end{Bmatrix}$$ to form a 2×14 length array, c, given by:

$$c = \begin{Bmatrix} -1 & -1 & -1 & -1 & 0 & 0 & -1 & -1 & 0 & 0 & 0 & 0 & 1 & 1 \\ -1 & 1 & -1 & 1 & 0 & 0 & -1 & 1 & 0 & 0 & 0 & 0 & 1 & -1 \end{Bmatrix}$$

This array has ideal periodic autocorrelation properties. As the binary array has no zeros, the modulated array has the same proportion of absorbent patches as the original ternary sequence; for long sequences, the proportion tends towards 50 per cent.

There is only one known perfect aperiodic binary sequence, the one shown above. Consequently, there are only six array sizes that can be constructed by this method with ≈ 50 per cent efficiency for $NM \leq 2^{16}$.

The final design process is to use periodic multiplication. Two arrays can be multiplied together to form a larger array. Consider array 1 to be $b_{p,q}$ of size $N_b \times M_b$ which has an efficiency of E_b, and array 2 to be $c_{p,q}$ of size $N_c \times M_c$ which has an efficiency of E_c. Then the new array is a product of the periodically arranged arrays, $b_{p,q} \cdot c_{p,q}$ of size $N_b N_c \times M_b M_c$ and the efficiency will be $E_b E_c$. A necessary condition is that N_b and N_c are co-prime, and so are M_b and M_c, otherwise the repeat distance for the final arrays will be the least common multiples of N_b and N_c in one direction and M_b and M_c in the other.

For example, consider a 7×3 ternary array derived by folding a sequence made using a Singer difference set:[7]

$$c = \begin{Bmatrix} 1 & 0 & 1 \\ 0 & 1 & 0 \\ -1 & 1 & -1 \\ -1 & 1 & -1 \\ 1 & 0 & 1 \\ -1 & 1 & -1 \\ 1 & 0 & 1 \end{Bmatrix}$$

This has an efficiency of 76 per cent. Consider also a perfect aperiodic ternary array d_2:

$$d_2 = \begin{Bmatrix} 1 & 1 \\ 0 & 0 \\ 1 & -1 \end{Bmatrix}$$

which has an efficiency of 67 per cent.

c and *d*$_2$ can multiplied together to from a 21 × 6 array with ideal autocorrelation properties and an efficiency of 0.76 × 0.67 × 100 per cent = 51 per cent.

It is also possible to use a combination of these design methods. Perfect array construction methods, ones that produce zero side lobe energy in the autocorrelation, tend to generate rectangular grids of holes. It is even possible to construct optimal binary sequences on a hexagonal array pattern as well.

In the design it is necessary to consider the balance between 0s and 1s for binary sequences and –1s, 0s and 1s for ternary sequences. The right balance needs to be struck to achieve the desired absorption characteristic. For ternary sequences, a rough balance between the number of –1s and 1s is needed so that the specular reflected energy is sufficiently attenuated.

Once the array is formed any periodic section can be chosen and many other manipulations can be carried out while still preserving the autocorrelation properties. Procedures that can be done on their own or in combination include:

- Using a cyclic shift to move the pattern around: $c_{p,q} = b_{p+u,q+v}$ where *u* and *v* are integers and the indexes *p* + *u* an *q* + *v* are taken modulo *N* and *M* respectively.

- Mirror image the array: $c_{p,q} = b_{\pm p, \pm q}$.

- Invert the sequence: $c_{p,q} = -b_{p,q}$.

- Rotation by 90°: $c_{p,q} = b_{q,p}$.

- Under sample the array: $c_{p,q} = b_{up,vq}$, provided both *u*, *N* and *v*, *M* are co-prime.

These will not change the acoustic performance, but may change the visual aesthetic. These processes can also help to make the array more asymmetric, which can be useful in modulation.

The main problem in forming these arrays is that there is only a limited set of array sizes. It has been shown,[11] however, that by relaxing the requirement for ideal auto-correlation enables more array sizes to be formed. For example, where there are a large number of elements in a sequence, it may be possible to truncate the sequence, losing 1 or 2 elements, and still gain good (but not ideal) autocorrelation properties. This type of truncation might then give the right sequence length for folding into an array with the desired size.

11.6 Absorption

Figure 11.2 showed the random incidence absorption coefficient for a planar binary surface with and without the perforated mask. This shows that the hybrid surface is behaving like the Helmholtz absorbers discussed in Chapter 6. It is possible to predict the absorption characteristics using the transfer function matrix method. Problems arise, however, because the hole spacing is not regular and many holes are too close together for the normal assumptions used when modelling sound propagation through a perforated sheet. Nevertheless, it seems possible to at least predict the trends of the absorption.

The amount of added mass in the holes determines the increase in absorption at
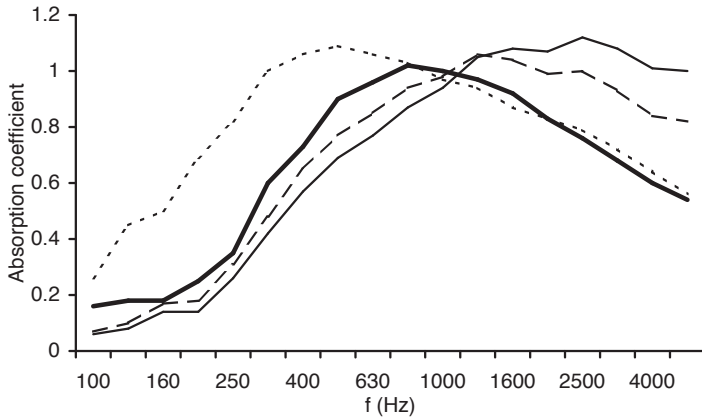
Figure 11.16 Random incidence absorption coefficients for various planar hybrid surfaces (BAD panels):
——— 25 mm fibreglass;
– – – BAD 16 mm hole, 25 mm fibre glass backing;
——— BAD 13 mm hole, 25 mm fibre glass backing; and
······· BAD 13 mm hole, 51 mm fibre glass backing.

bass frequencies. For the BAD panel, if additional bass absorption is required, it is possible to reduce the open area (this will not be true for all geometries), as shown in Figure 11.16. Alternatively, thicker mineral wool layers can be used, or the panel can be spaced from the wall to effectively increase the backing depth and so lower the resonant frequency. The effect of changing the backing depth is shown in Figure 11.2, giving the expected trends.

The drop-off in high frequency absorption can be explained by the open area of the panel. In a simplistic analysis, a surface with a 50 per cent open area would be expected to have an absorption coefficient of 0.5 at high frequency. Figure 11.16 shows the effect of reducing the open area on the absorption coefficient. BEM predictions show that the absorption coefficient response is similar for ternary diffusers, if a little less smooth with respect to frequency. It is assumed that this is due to reflections from wells providing out-of-phase reflections when compared to other parts of the surface, and therefore waves combine to put energy into the reactive field.

11.7 Accuracy of the Fourier theory

The Fourier theory used so far in this chapter is approximate. The absorption coefficient measurements give information about the likely accuracy of the design principles based on this simple theory. Some of the key assumptions behind the theory are:

1. The absorption coefficient of the soft patches is 1 and there is no phase change on reflection.
2. The Kirchhoff boundary conditions are true.

The absorption coefficient of the soft patches is not 1 at low frequency because there is insufficient depth of mineral wool to cause complete absorption. At mid- and

low frequencies mutual interactions across the panel render the Kirchhoff boundary conditions inaccurate. The Kirchhoff boundary conditions assume that the pressure on the hard patches is twice the incident pressure and on the soft patches is just the incident pressure. This is only true when the patch width is large compared to wavelength. It is only at high frequency, when the wavelength becomes smaller, that the Kirchhoff boundary conditions will be reasonable. Consequently, the discussions above are really only true for the highest frequencies of interest. To put this another way, for a 50 per cent open area sample predicted with the simple Fourier theory, the absorption should be 0.5. Figure 11.2 shows that this is not achieved, for instance at mid-frequency the absorption is around 1.

Despite these problems, it is still possible to learn something from the Fourier theory. For instance, the theory shows that as with all diffusers, periodicity is a problem as energy gets concentrated in the lobe directions. Consequently, the repeat distance of the diffuser should be made as large as possible. This can be done using a modulation scheme, as discussed for Schroeder diffusers in Chapter 9 and curved surfaces in Chapter 10, or by designing the diffuser based on a large number sequence.

Consider using a modulation scheme where two different hybrid surfaces are used. One of these is denoted A, the other B. A wall is filled by arranging the hybrid surfaces according to a pseudorandom sequence, for example if a length 5 Barker sequence is
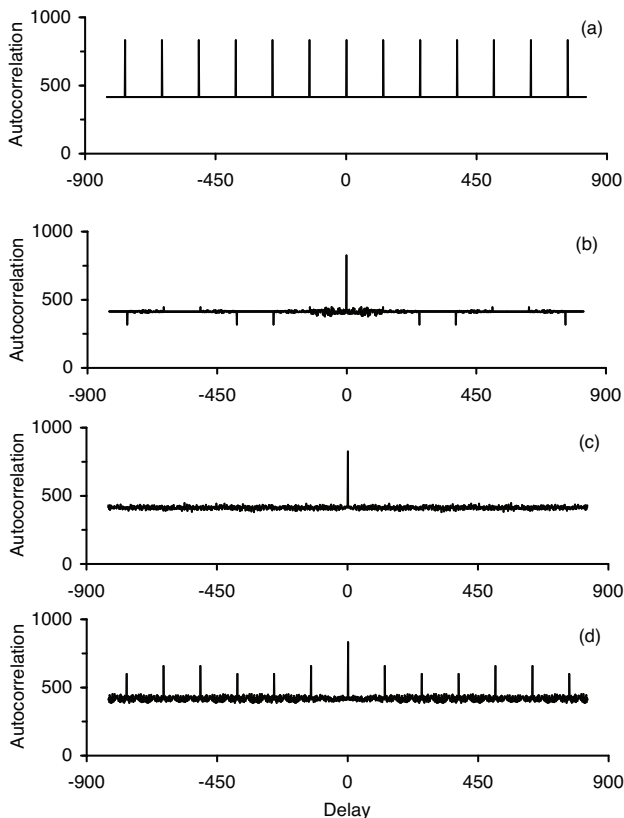
Figure 11.17 Autocorrelation properties for four sequences: (a) periodic; (b) modulated using inverse; (c) random length 1,651, and (d) one base shape modulation.

used, the arrangement of the surfaces would be: AAABA. This is a method for reducing periodicity effects.

Modulation schemes pose problems for devices based on unipolar sequences. The most successful modulation scheme for Schroeder diffusers was to modulate a surface with a phase inverted version of the surface. In a unipolar device, it is difficult to see how exact broadband phase inversion can be achieved. However, it is possible to go some way to achieving the inversion and therefore good performance. Consider a unipolar maximum length sequence a, an approximate inverse sequence can be found by adding 1 modulo 2, so the inverse sequence is given by $a + 1$ modulo 2. These two base shapes can then be arranged in a pseudorandom order to form a modulated array to reduce periodicity effects.

For example, consider the top three graphs in Figure 11.17. Graph (a) shows the autocorrelation properties for a periodic sequence of 13 $N = 127$ unipolar MLS sequences. As expected, there are periodicity lobes every 127 units. This is compared in graph (c) to a random sequence of length 1,651 (=13 × 127) showing no periodicity lobes. A modulated arrangement is shown in graph (b) using a hybrid surface and its inverse. The ordering of the two surfaces was determined by the length 13 pseudorandom sequence with the best unipolar aperiodic autocorrelation properties. The effects of periodicity have been greatly reduced. Figure 11.18 shows the effects of the modulation in terms of a scattered level polar distribution. The modulation has removed the periodicity effects for the non-zero order lobes. In that respect the modulation has been successful, but the dominant characteristic of the polar response is still the zero order specular lobe. The only way to deal with this is to introduce some possibility of phase cancellation, for example by curving the surface or using a ternary sequence.

A ternary sequence can be more readily modulated with its inverse. For instance, if the first ternary sequence was {1, 1, 0, 1, 0, 0, −1} then the complementary sequence used in modulation is the inverse of this {−1, −1, 0, −1, 0, 0, 1}. The modulated arrangement is highly effective, but only over certain frequency ranges. When multiples
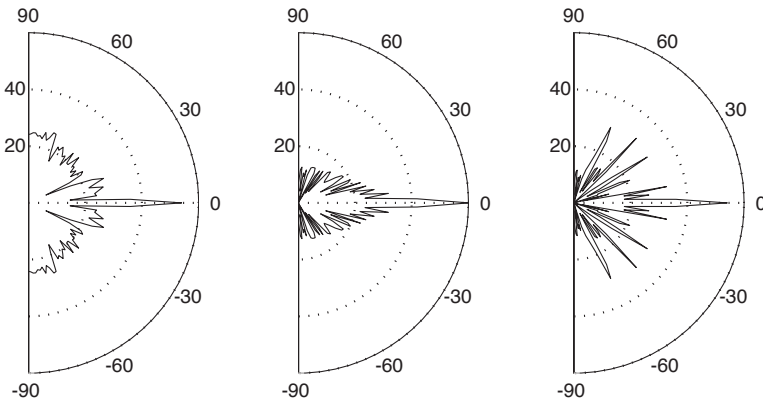
Figure 11.18 Scattering from three surfaces showing how modulation can improve the performance of hybrid surfaces:
(left) modulated MLS hybrid surface;
(middle) planar non-absorbing reflector; and
(right) periodic MLS hybrid surface.

of half wavelengths fit into the '–1' well, then the reflection coefficients of the ternary sequence and its inverse are identical, and undesirable periodicity lobes result.

Another technique for modulation would be to use two sequences from the same family with mutually good cross-correlation properties, although this does not work as well as the inverse process described above. It is also possible to modulate using number sequences of different lengths – a similar process was described for Schroeder diffusers in Chapter 9 where it was called orthogonal modulation.

As with Schroeder diffusers, it is possible to modulate a single asymmetrical base shape. The advantage of this technique is that it only needs one type of mask to be made. The mask shown in Figure 11.1 could be rotated by 90° and arranged with the original mask in a random arrangement. Brief tests on 1D sequences show this to be less successful than using two or more different base shapes. Graph (d) in Figure 11.17 shows the autocorrelation coefficient for a 1D asymmetric single base shape modulation. In this case the sequence order is just reversed to give the second base shape. While not as good as the modulation using two base shapes (graph b), one base shape modulation still gives a better result than the periodic arrangement.

11.8 Diffuse reflections

Measuring hybrid surfaces to get the scattering performance is awkward. The normal measurement techniques described in Chapter 3 have used scale models of diffusers to allow measurements far enough away from the surface. For hybrid surfaces, accurate scale models cannot be easily produced because the impedance properties of porous materials do not scale in the same way as the wavelength in air. It would be possible to empirically find a substitute material to use in the scale models which has the appropriate impedance properties, but this is a rather tedious process. Nevertheless, diffusion measurements have been carried out on full-scale samples, even though the receivers and source are rather too close. For example, Figure 11.19 shows the scattered polar response from a BAD panel and just the porous backing material for the 1.25 kHz one-third octave band. The energy in the specular zone is attenuated by 6 dB. This is
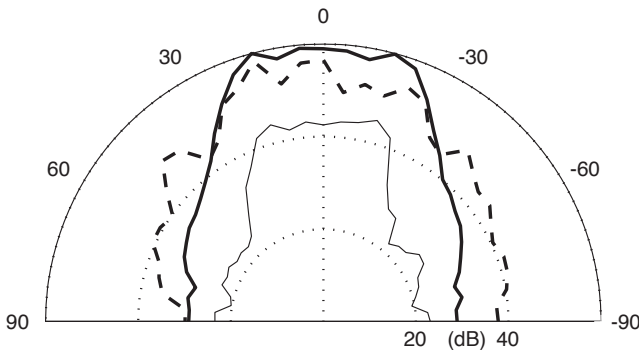
Figure 11.19 Measured scattering from a binary amplitude diffuser (BAD) compared to a hard surface and a piece of absorbent:
  – – – BAD;
  ——— non-absorbing flat reflector; and
  ——— 25 mm fibreglass (data from Angus and D'Antonio[7]).
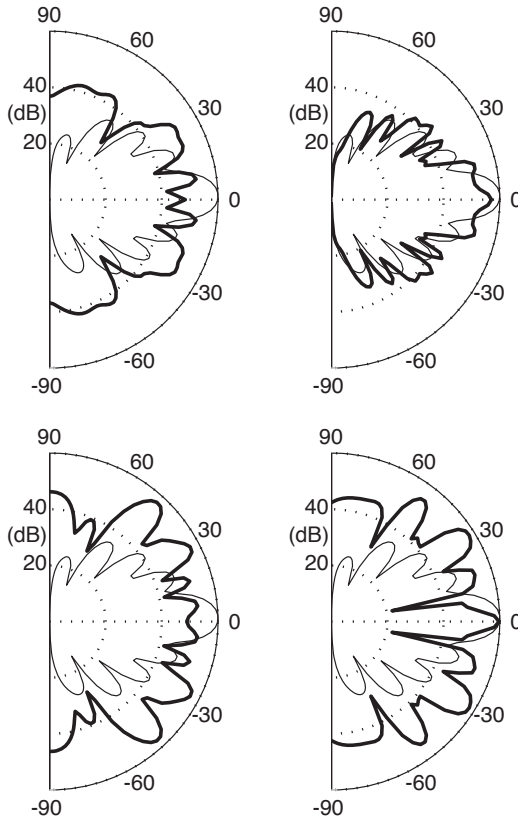
Figure 11.20 Scattering for five surfaces, in each case the thin line represents a planar non-
absorbing surface of the same size as the diffusers.
Top left: curved hybrid surface;   Top right: flat hybrid surface;
Bottom left: curved hard diffuser;   Bottom right: $N = 7$ QRD.

exactly as would be expected for a 50 per cent open area panel. Additional side lobe
energy is produced compared to the flat hard surface.

Consider an analysis now based on the simple Fourier model. Figure 11.20 shows
polar distributions for one example frequency. For this comparison, five surfaces were
predicted: a curved hybrid surface with a binary sequence of hard and soft patches;
a plane hybrid surface based on the length 31 MLS; a plane hard surface; an $N = 7$
QRD, and an optimized rigid curved surface. This last surface was 30 cm deep, which
is typical of the non-absorbing diffusers used in performance spaces; the hybrid curved
surface is much shallower, about 7 cm deep.

Moving from a flat hard surface to a plane hybrid device increases the dispersion,
as was also found in the measurements reported in Figure 11.19. However, curving
the hybrid surface produces more dramatic improvements. Interestingly, the quality of
dispersion for the curved hybrid surface is only a little worse than the rigid optimized
curved surface, which is four times as deep. This seems to indicate that a hybrid curved
surface is a good method for generating more diffuse reflections from a restricted
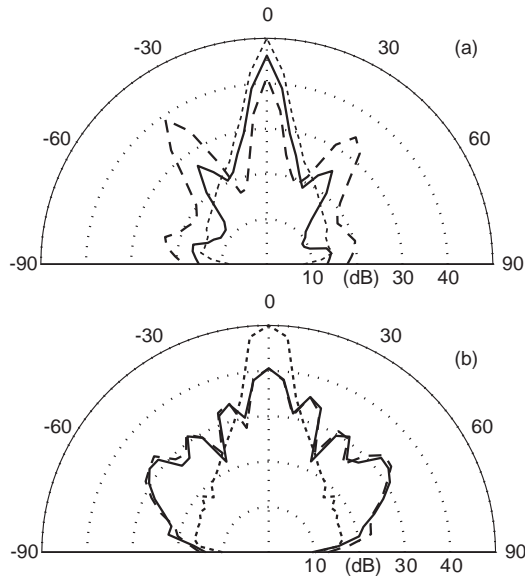
Figure 11.21 Scattering from three devices predicted using a BEM model. ———— planar binary hybrid; – – – ternary, and ······ plane surface, for the one-third octave whose centre frequency is: (a) the design frequency, and (b) twice the design frequency (after Cox and D'Antonio[4]).

depth, provided partial absorption is acceptable or wanted. It should be remembered that practical hybrid surfaces are often mainly absorptive up to about 2 kHz and consequently for these surfaces it is only at mid- to high frequencies that dispersion needs to be considered.

11.8.1 Boundary element modelling

It is known that the Kirchhoff boundary conditions are not accurate at low to mid-frequencies and so the Fourier model used in the previous section is unreliable. Using boundary element modelling (BEM) it is possible to calculate the scattering over a hemisphere including interactions across the surface, provided the absorbent patches remain locally reacting. BEMs have been shown to give accurate results for hybrid surfaces before, when compared with measurements.[12] They also give accurate results for Schroeder diffusers and consequently it would be anticipated that the BEM will be accurate for ternary diffusers as well.

First consider single plane predictions on a planar hybrid and a ternary device. Figure 11.21a shows the scattering for the one-third octave band centred on the design frequency; Figure 11.21b shows the scattering at an octave higher. At odd multiples of the design frequency (e.g. graph a) the well in the ternary diffuser provides waves which help cancel the specular reflection and so the device offers more even scattering and a reduced specular lobe in comparison to the planar hybrid surface. At even multiples of the design frequency, however (e.g. graph b), the scattering from the planar hybrid and ternary devices is similar. At these even multiples of the design frequency the waves
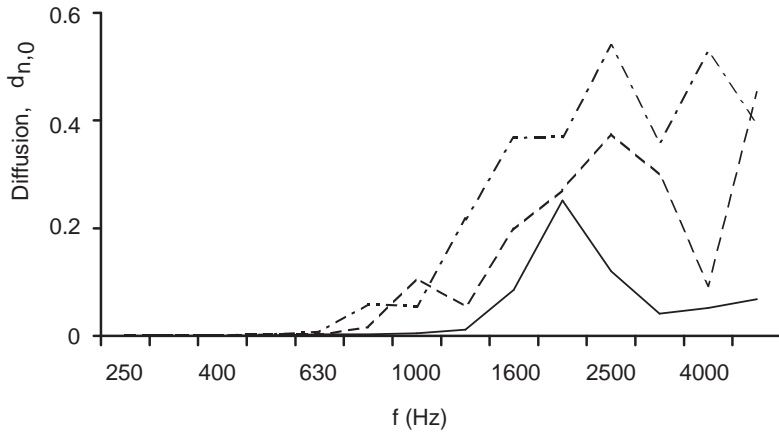
Figure 11.22 Predicted normalized diffusion coefficient for three hybrid surfaces: —— planar binary; – – – ternary; and ·–·–·· quadriphase.

propagating in the well of the ternary diffuser return in phase with reflections from the flat sections of the device, and so the wells are ineffective. To overcome these critical frequencies at even multiples of the design frequency, more well depths must be introduced. If two different well depths are used, for instance, a quadriphase diffuser results.[4]
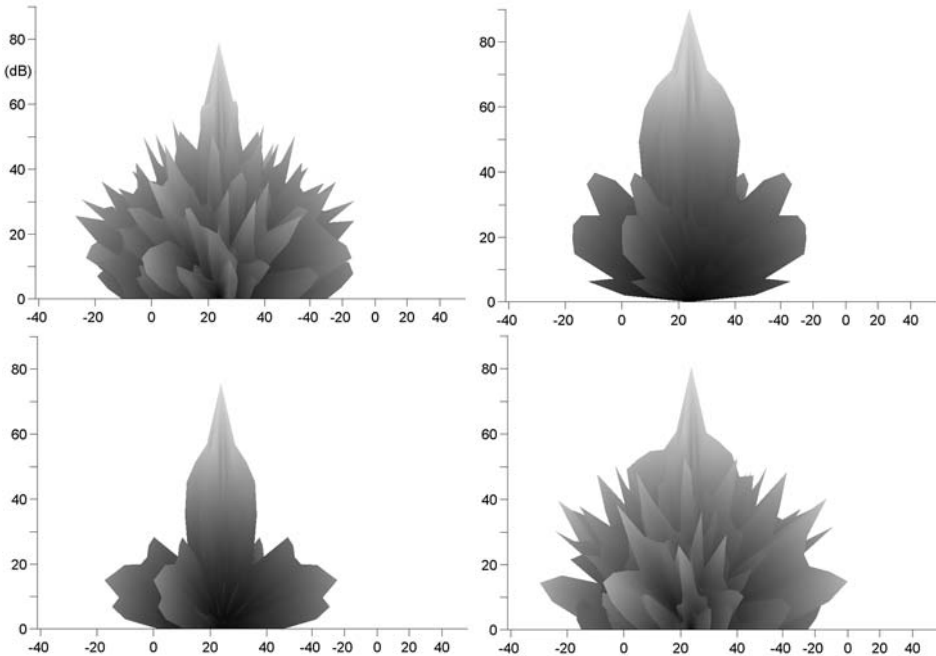
Figure 11.23 Scattering from arrays of three surfaces at 3 kHz. Top left: BAD panel; top right: plane surface; bottom left: a perforated mask with regular hole spacing; bottom right: a random perforated mask. 3D polar balloons viewed from side.
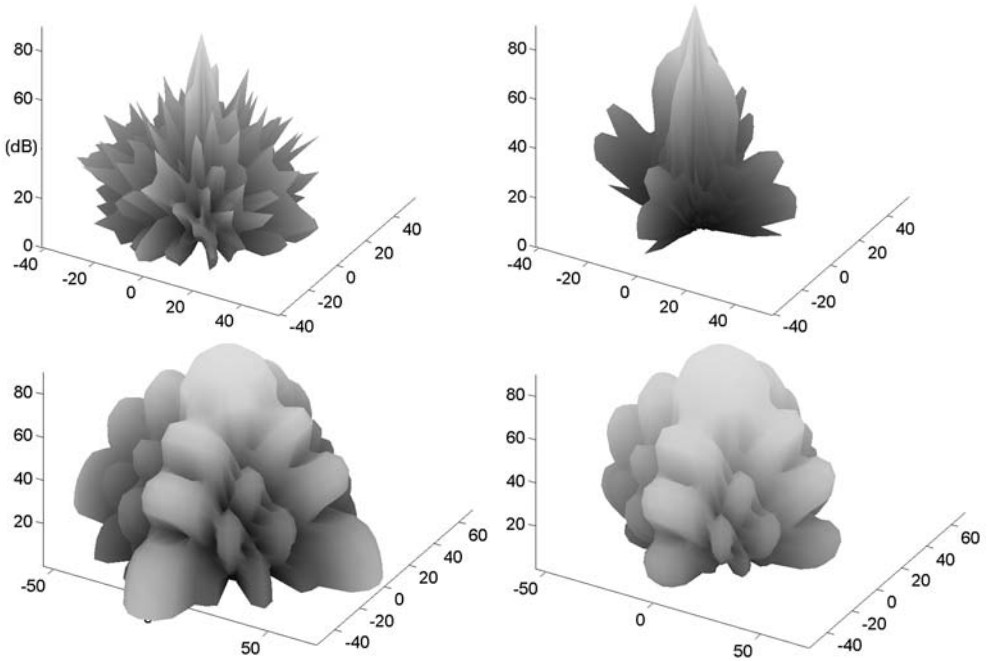
Figure 11.24 Hemispherical polar balloons. Top: 3 kHz; bottom: 400 Hz; left: BAD hybrid surface; right: plane hard surface.

Figure 11.22 shows the normalized diffusion coefficient for three hybrid surfaces. It shows how a ternary diffuser improves over the planar binary surface for most frequencies, except in the one-third octave band centred on 4 kHz where there is a critical frequency for the ternary device. It also shows how using an additional different well depth in a quadriphase diffuser overcomes the critical frequency.

So far the performance of the ternary devices has only been discussed at harmonics of the design frequency. Between these frequencies the phase of the reflection coefficient offered by the well of fixed depth is neither −1 or +1. The waves reflected from this well will be partly out-of-phase with the waves from the flat parts of the device. Consequently, the performance is still improved over the unipolar binary diffuser for these in-between frequencies.

Now consider predictions for hemispherical devices. Unfortunately, the BEM model rapidly becomes too slow and consequently a thin panel, periodic formulation must be used, as outlined in Chapter 8.

Figure 11.23 top left shows the scattering from a 4 × 4 array of the BAD panel at 3 kHz which is a MLS-based hybrid planar surface (shown in Figure 11.1). This is compared to a planar hard surface in the top right of the figure. The polar balloon is shown side on and it illustrates the drop in specular reflection energy as was found with the simpler theories. It also shows that a strong specular component still exists from the hybrid surface. The bottom left graph is for a perforated mask where the holes are regularly spaced. This shows that the side lobe performance is better for the BAD

panel, confirming the usefulness of a pseudorandom hole arrangement for getting more diffuse reflections. The bottom right graph is for a perforated mask where the hole locations are determined randomly. The performance is similar, but slightly worse than the BAD panel. This shows the superiority of using pseudorandom number sequences rather than a random hole arrangement.

Figure 11.24 compares the scattering from the BAD panel to a plane surface at two contrasting frequencies. At the low frequency (the bottom half of the figure) the mineral wool is not providing much absorption and so the BAD panel behaves similar to the planar hard surface, although a little additional dispersion is achieved. At the higher frequency (the top half of the figure) the difference between the surfaces is marked, as would be expected, with the hybrid surface generating dispersion.

11.9 Summary

Hybrid surfaces offer another solution to room designers who want both reverberation control and diffuse reflections in a single device. Flat hybrid surfaces have a considerable advantage in being cheap and in the treatment being hidden. By adding a few wells, ternary and quadriphase devices can be formed which significantly improve performance. Alternatively, the hybrid surface can be curved to break up the specular reflection.

11.10 References

1 P. D'Antonio, *Planar Binary Amplitude Diffusor*, US patent 5, 817, 992 (1998).
2 P. D'Antonio and T. J. Cox, *Acoustical Treatments with Diffusive and Absorptive Properties and Process of Design*, US patent 6, 112, 852 (2000).
3 P. D'Antonio and T. J. Cox, *Hybrid Amplitude-Phase Grating Diffusors*, US patent 7,428,948 B2 (2008).
4 T. J. Cox, J. A. S. Angus, P. D'Antonio, "Ternary and quadriphase sequence diffusers", *J. Acoust. Soc. Am.*, **119**(1), 310–9 (2006).
5 J. A. S. Angus, "Sound diffusers using reactive absorption grating", *Proc. 98th Convention Audio Eng. Soc.*, preprint 3953 (1995).
6 P. Fan and M. Darnell, *Sequence Design for Communication Applications*, John Wiley & Sons (1996).
7 J. A. S. Angus and P. D'Antonio, "Two dimensional binary amplitude diffusers", *Proc. Audio Eng. Soc.*, preprint 5061 (D-5) (1999).
8 T. J. Cox and P. D'Antonio, "Optimized planar and curved diffsorbors", *Proc. 107th Convention Audio Eng. Soc.*, preprint 5062 (1999).
9 M. F. M. Antweiler, L. Bomer and H. D. Luke, "Perfect ternary arrays", *IEEE Transactions on Information Theory*, **36**(3), 696–705 (1990).
10 M. R. Schroeder, *Chaos, Power, Laws: Minutes from an Infinite Paradise*, W. H. Freeman & Co. (1991).
11 H. D. Luke, H. D. Schotten and H. Hadinejad-Mahram, "Binary and quadriphase sequences with optimal autocorrelation properties: A survey", *IEEE Transactions on Information Theory*, **49**(12), 3271–82 (2003).
12 L. Xiao, T. J. Cox and M. R. Avis, "Active diffusers: some prototypes and 2D measurements", *J. Sound Vib.*, **285**(1–2), 321–39 (2005).

12 Absorbers and diffusers in rooms and geometric models

So far, this book has discussed how to design diffusers and absorbers, but mostly in isolation of where and how they are applied. This chapter starts by presenting some of the issues arising from the application of absorbers in rooms, especially the issue of translating absorption coefficients between the free field, reverberation chamber, and real room applications. It then proceeds to discuss how absorption and diffuse reflection properties are represented in geometric room acoustics models and how this affects prediction accuracy.

12.1 Converting absorption coefficients

12.1.1 From free field to random incidence

In Chapter 3, various methods for measuring absorption were outlined. These included free field and random incidence techniques. Unfortunately, it is not easy to translate between free field and random incidence values for a variety of reasons and these will be discussed in the following paragraphs. Being able to translate from the free field measurements to random incidence values is extremely useful because the free field experiments are done in a controlled environment which is ideal for validating prediction models. To make these measured coefficients useful to practitioners, however, they need converting into random incidence values.

The translation from a set of angle-dependent free field absorption coefficients to a random incidence value is normally carried out using Paris's formula:[1]

$$\alpha_s = \int_0^{\pi/2} \alpha(\psi)\sin(2\psi)d\psi \qquad (12.1)$$

where α_s is the random incidence absorption coefficient, and $\alpha(\psi)$ is the absorption coefficient in the free field, at an incident angle ψ.

This formula is derived by considering the sound incidence on a surface in a diffuse space, the $\sin(2\psi)$ term arising because of solid angle considerations. If the surface is locally reacting, then it is possible to just measure the normal incidence impedance, apply the formulations given in Equations 1.21 and 1.24 to get the angle dependent absorption coefficient and, from Equation 12.1, to get the random incidence value. For a locally reacting surface a single measurement at 55° will suffice, as this is the

same as the random incidence value. Many surfaces, however, are not locally reacting, as discussed in Chapter 5.

Makita and Hidaka[2] examined the problem of translating from free field to random incidence coefficients for homogeneous and isotropic porous materials. They measured different polyurethane foams in the impedance tube and the reverberation chamber and compared the random incidence absorption coefficients, derived from the impedance tube measurement using Paris's formulation, and the reverberation chamber measurements. Discrepancies arise because:

- The reverberation chamber is not completely diffuse, leading to the Paris' formula being inaccurate and some angles of incidence being emphasized over others.
- Diffraction at the edges of the sample creates excess absorption in the reverberation chamber measurements. The impedance discontinuity at the edges of the sample causes additional sound to bend into the sample as this has a lower speed of sound.
- The mounting conditions are different, which may affect how the frame of the absorbent vibrates.
- The assumption of local reaction, so that small sample experiments in the impedance tube can be translated to a large sample measurement in the reverberation chamber, may not be correct.

Makita and Hidaka carried out a series of reverberation chamber measurements on the foams with different sample sizes to get the absorption coefficient of an infinite array using extrapolation. Figure 12.1 shows the inferred absorption coefficient for an infinite sample, compared to the 12 m² sample, which is the recommended size in ISO 354.[3] These absorption coefficients are shown for one typical sample of the six different foams tested. The average difference in the absorption coefficient, between the finite and infinite samples for all six foams, is also shown. Figure 12.1 illustrates that great differences in the absorption can be obtained due to edge effects, even if the edges of the samples are covered with a reflective frame, as is normal practice and required by ISO 354.
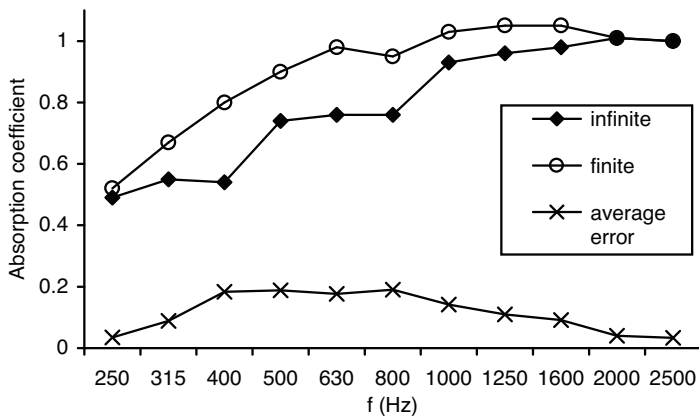
Figure 12.1   Comparison of measured random incidence absorption coefficients for finite and infinite samples for one material. Also shown is the average error between the finite and infinite sample absorption coefficients for six materials (data from Makita and Hidaka[2]).
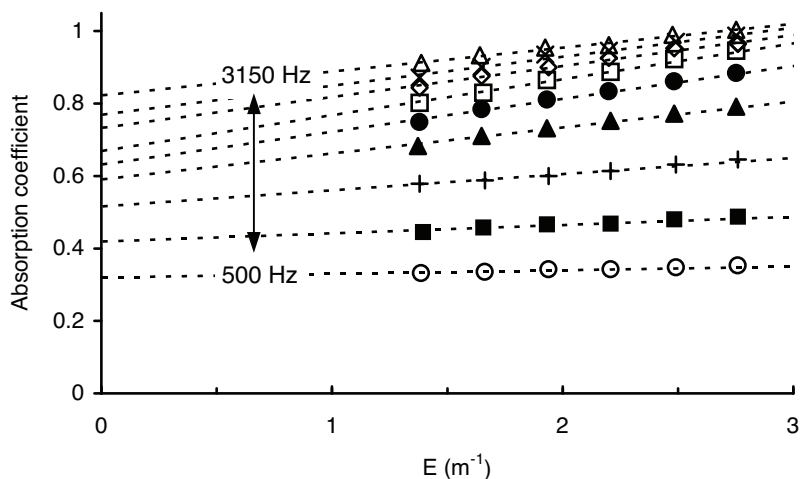
Figure 12.2 Random incidence absorption coefficient as a function of perimeter divided by sample area. Shown for different one-third octave bands.

○	500;
■	630;
+	800;
▲	1,000;
●	1,250;
□	1,600;
◇	2,000;
×	2,500; and
△	3,250 Hz (data from Bartel[4]).

Bartel[4] examined the extrapolation from finite to infinite area absorption. The paper also contains a useful and comprehensive literature review of previous work in this area. The simplest model for the absorption coefficient extrapolation assumes a linear relationship. This can be represented by:

$$\alpha_\infty = \alpha_s + mE \tag{12.2}$$

where α_∞ is the absorption coefficient for an infinite sized sample; α_s is the absorption coefficient for a finite sized sample, for example a 12 m² sample in a reverberation chamber measurement; m is a constant, and E is the ratio of the specimen perimeter to the specimen area.

The sensitivity of the absorption coefficient to the perimeter parameter, E, varies with material type and frequency. Figure 12.2 shows a plot of the absorption coefficient for different perimeter to area ratios, measured in the reverberation chamber, illustrating that the edge diffraction effects can be very significant. This is with the edges of the sample covered with a reflective strip. Figure 12.3 shows how the value of the constant m varies with frequency and material type. Bartel also investigated the effect of sample shape. Sample shape only affected the absorption coefficient by at most 3 per cent, so the size of the perimeter to area ratio is much more important than the shape of the sample's edge.
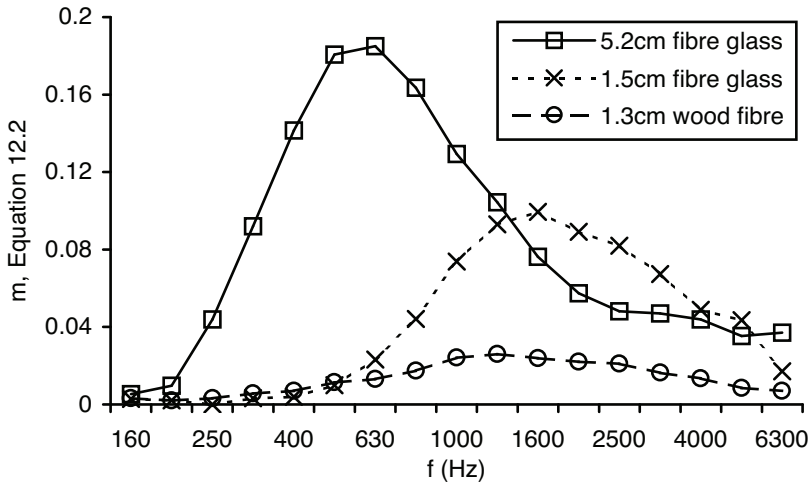
Figure 12.3   Variation of constant *m* in Equation 12.2, which measures the perimeter effect for random incidence absorption coefficient. Results for three different materials given as indicated (data from Bartel[4]).

To derive the constant *m* requires a series of measurements on different sample sizes in the reverberation chamber. Consequently, Equation 12.2 does not help derive random incidence absorption coefficients from impedance tube measurements because impedance tube experiments do not give values for *m*. Bartel[4] reports, however, a formulation attributed to Northwood[5] to allow the perimeter effect to be predicted, and so allow the translation from impedance tube to random incidence values. The normalized admittance *β* of the sample is measured in the impedance tube, and is given by:

$$\beta = \frac{\rho c}{z} = g - jb \tag{12.3}$$

where *z* is the surface impedance, *ρ* the density and *c* the speed of sound in air.

The average absorption coefficient for a finite rectangular sample is then given by:

$$\alpha = \frac{16g}{\pi} \int_0^{\pi/2} \int_0^{\pi/2} \frac{\sin^3(\phi)d\phi\, d\theta}{|\beta|^2(A^2 + B^2) + 2(gA + bB)\sin(\phi) + \sin^2\phi} \tag{12.4}$$

where:

$$A = \int_0^{ka\sin\phi} \cos(x\sin(\theta))J_0(x)dx - \frac{1}{ka\sin\phi} \int_0^{ka\sin\phi} x\cos(x\sin(\theta))J_0(x)dx \tag{12.5}$$

$$B = \int_0^{ka\sin\phi} \cos(x\sin(\theta))N_0(x)dx - \frac{1}{ka\sin\phi} \int_0^{ka\sin\phi} x\cos(x\sin(\theta))N_0(x)dx \tag{12.6}$$

where $a = 2/E$, and J_0 and N_0 are the Bessel functions of the first and second kind respectively. These formulations can also be used to gain random incidence predictions of absorbers based on the formulations derived in Chapters 5–7.

Makita *et al.*[6] presented a revised Paris's formula which accounts for inaccuracies in the cosine law formulation. The formulations derived are rather complex, but enable the effects of the boundary layer on the absorption to be accounted for. The boundary layer effect is not normally as big as the perimeter effect, but can still be significant.

12.1.2 *From the reverberation chamber to real rooms*

The problem of projecting from reverberation chamber measurements to whole room design has already been discussed in Section 3.4.1 in relation to audience seating. But seating is not the only surface to suffer from problems when making whole room predictions based on reverberation chamber measurements of absorption. Even when the inaccuracies in the absorption coefficient are numerically small, the inaccuracy in the resulting reverberation time in a space can be quite significant if large areas of the absorbent are used, as the inaccuracy in the total absorption will be large. The problems centre on two issues, edge diffraction and non-diffuseness.

1. *Edge diffraction*: The sample size tested in the reverberation chamber is usually smaller than that applied in the real space. Consequently, there is more edge diffraction in the reverberation chamber than in the real space. This can lead to significantly different absorption coefficients between the two spaces. The solution to the edge effect problem could be to determine the absorption of the edges, as was done for seating in Section 3.4.1. Alternatively, it is possible to test different sample sizes in the reverberation chamber, and from there extrapolate to the sample size used in the real room. The formulations given in the previous section for the influence of sample perimeter can also be used to extrapolate the absorption of large sample sizes from the smaller reverberation chamber samples.
2. *Non-diffuseness*: The acoustic conditions in the reverberation chamber and the real room may be very different. The reverberation chamber may be diffuse, while the real room is not diffuse. This could lead to the random incidence absorption coefficient measured in the reverberation chamber not matching the effective absorption coefficient in the real room. Actually, a more common scenario is that both the reverberation chamber and real room are non-diffuse, but they are non-diffuse in different ways.

The effect of the diffuseness of the space is difficult to account for. If the non-diffuseness is generated in a simple manner, for instance all the absorption on one surface of the room, then there are reverberation time formulae that can deal with these cases. (Gomperts carried out a comprehensive review of reverberation time formulations.[7]) A modern solution would be to use a geometric room acoustic model to properly model the sound distribution in both spaces rather than assume a diffuse field. This is an appealing solution, but as shall be discussed in the next section, the application of absorption coefficients in computer models is not necessarily straightforward. For instance, what should be done with absorption coefficients greater than 1, which commonly arise from reverberation chamber measurements? If a geometric model is used, it is best if both the reverberation chamber and the real room are modelled, rather

than making the assumption that the reverberation chamber is diffuse. This requires the modeller to have access to the reverberation times with and without the sample in the reverberation chamber, and these are not usually available.

12.2 Absorption in geometric room acoustic models

Geometric models are becoming a core tool for practitioners and researchers designing or investigating the propagation of sound within a space. To gain accurate predictions from these models it is necessary for the geometric models to correctly model absorption effects, but this is not always straightforward.

Geometric room acoustic models calculate the sound propagation within a space using ray tracing,[8] beam or cone tracing,[9] image source,[10,11] or hybrid approaches.[12] (Hybrid approaches are combinations of some of the other three methods.)[13] They are high frequency approximations to the true sound propagation and do not properly deal with the wave nature of sound.

For readers unfamiliar with geometric models it is necessary to describe how the sound might be modelled, but for brevity only one type of modelling will be described, and readers are directed to the literature for further reading. Here ray tracing will be considered, as this is the easiest to describe. In this method, the sound energy is modelled as rays that propagate around the room like rays of light. When the ray hits a surface in the room it is reflected from the surface and, if no scattering is considered, the angle of reflection equals the angle of incidence. There is a receiver in a room, usually a sphere, and every time a ray passes through this, the reflection contributes to the energy impulse response. This process is illustrated in Figure 12.4.

Every time a ray reflects from the surface the energy of the ray is decreased by a factor of $1 - \alpha$, where α is the absorption coefficient of the surface. One problem is that absorption coefficient tables published in the literature often contain values greater than 1. How should these be translated into use in the geometric model, where values greater than 1 are meaningless? Furthermore, many geometric models are now producing auralizations of the sound field within the space to allow designers to hear the effect of design changes. To get a natural rendition of the sound field a wide audio bandwidth is required, yet absorption coefficient data is normally only available for a restricted bandwidth of 100 Hz to 5 kHz.[14] These and other issues are discussed below.

Although a geometric room acoustic model has knowledge of the angle of incidence that a ray strikes a surface, it is usual for a random incidence absorption coefficient to
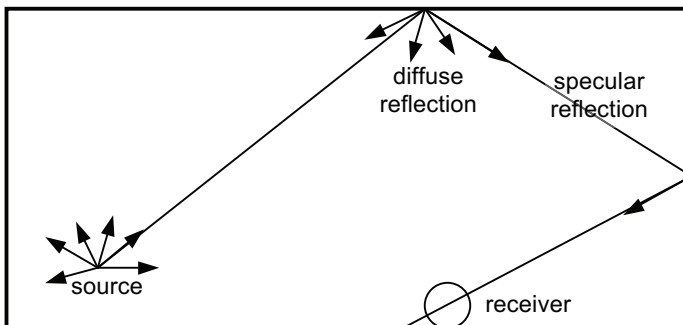
Figure 12.4   Picture of ray tracing in a room.

be applied to every reflection. If local reaction is assumed, and the normal incidence impedance of surfaces are known, it would be possible to predict the absorption coefficient as a function of incident angle and use these in computer models instead. Nijs *et al.*[15] examined this and found that for simple room geometries, in their case a reverberation chamber, angular dependent absorption coefficients made little difference to calculated levels and reverberation times. For a coupled room, however, Nijs *et al.* found that using an angular dependent absorption coefficient enhanced prediction accuracy. When using just random incidence absorption coefficients inaccuracies of 15–20 dB between the predicted and measured sound pressure levels in the coupled space were found; when using angular dependent absorption coefficients this error dropped to 4–7 dB. It would be interesting to know how parameters such as early lateral energy fraction,[16] which are highly dependent on correct modelling of early reflections, are affected by not using angular-dependent absorption, even in rooms with simple geometries.

One cause for the absorption coefficients to be greater than one in reverberation chamber measurements is that Sabine's formulation[17] becomes inaccurate when the absorption is high ($\alpha > 0.2$–0.4). According to Sabine's formula, a room constructed from completely absorbing walls still has a reverberation time greater than zero. A couple of authors have suggested that alternative reverberation time formulations should be used to calculate the absorption coefficients from the reverberation time measurements, as these absorption coefficients then give more accurate predictions in real spaces with geometric models. Nijs *et al.*[15] used the Eyring[18] equation to deal with some of the problems of excess absorption that occurs when using Sabine's formula. Dance and Shield[19] favoured the use of the Millington[20] reverberation time formulation. These formulations can be found in Chapter 1.

The problem with using alternative reverberation time formulations to get absorption coefficients from reverberation chamber measurements is that the geometric room acoustic modellers need access to the reverberation times measured in the reverberation chambers to re-derive the absorption coefficients. The data that is generally available in

$$\alpha_m = 0.071\alpha_s^3 - 0.416\alpha_s^2 + 0.99\alpha_s + 0.005$$
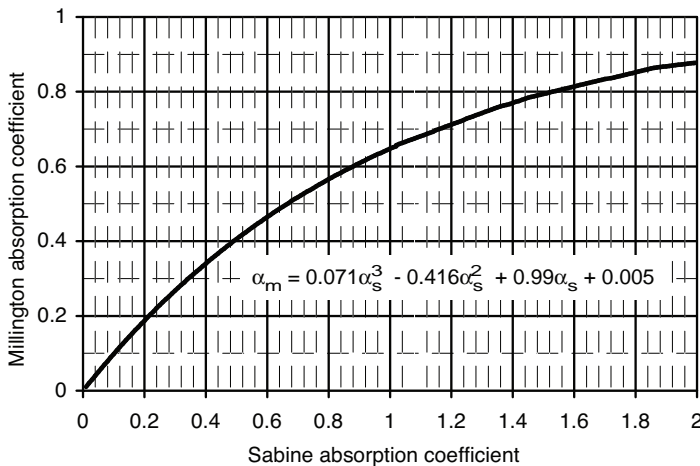
Figure 12.5   Chart and equation to translate from Sabine measurements of absorption coefficients, α_s, in reverberation chambers to Millington coefficients, α_m, to be used in real space predictions in geometric models (modified from Dance and Shield[19]).
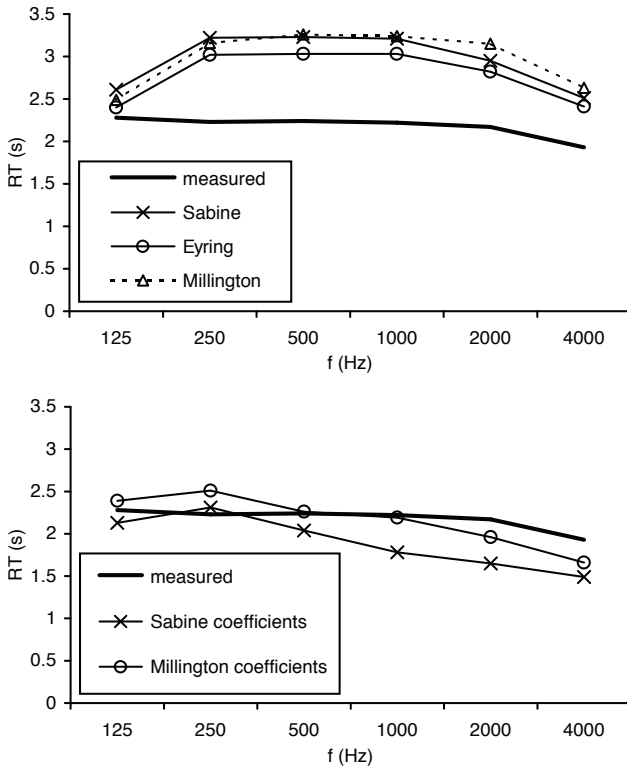
Figure 12.6 Predicted reverberation times compared to measurement for a concert hall. Top: predictions using various reverberation time formulations; bottom: predictions using a geometric model with different absorption coefficient formulations (data from Dance and Shield[19]).

literature is just the calculated absorption coefficients, using Sabine's formulation. Consequently, using other reverberation time formulations is awkward. Dance and Shield overcame this to a certain extent, however, by publishing a conversion chart to get from the Sabine absorption coefficients to the Millington values by carrying out some geometric room predictions which simulated typical reverberation chamber measurements. This chart is shown in Figure 12.5, along with an equation describing the relationship.

Figure 12.6 shows the reverberation times predicted for a concert hall from Dance and Shield. The top graph shows that classical reverberation time formulations are inaccurate in non-diffuse spaces, and using a geometric model can improve prediction accuracy – a finding also found by Antonio *et al.*[21] and many others. The bottom graph shows that using absorption coefficients derived using a Millington formulation in geometric models gives more accurate results. However, in some cases not shown here, the findings are less clear cut.

Using more exacting reverberation time equations may help predictions, but it does not prevent measured absorption coefficients often exceeding 1, due to edge effects and the non-diffuse nature of the reverberation chamber. Nijs *et al.*[15] recommend reducing

values measured in the reverberation chamber by 20 per cent as a good first guess for the input into a ray tracing program and hard limiting coefficients so they do not exceed 1. Summers[22] points out, however, that there is a great variation in measured absorption coefficients between different reverberation chambers, a point borne out by the results shown in Figure 3.6. Consequently, the 20 per cent rule suggested by Nijs *et al.* is unlikely to generalize.

The work could be extended to include the effects of edge diffraction, which previously in this chapter have been shown to cause significant estimation errors in the absorption coefficients. The work also needs to consider inter-laboratory variation in random incidence absorption coefficient measurement. An alternative solution to the problem of mapping from the reverberation chamber to the real room is empirical fitting. As a surface treatment is used over time, an understanding of how the absorption coefficient varies between the reverberation chamber and real rooms is developed. If the reverberation time was underestimated this time, next time the modeller might put in a smaller absorption coefficient. This is obviously not very satisfactory, but it is the reality of applying many scientific models to engineering problems. This is why experienced geometric modellers usually produce better predictions than novices. This also creates problems in verification of computer models. Too often the absorption coefficients for surfaces are found by fitting predictions to match measurements, and then the same measurements are used to show that the numerical method works!

So far, the issue of phase change on reflection has not been considered. The true reflection from a surface should include changes in magnitude and phase, and consequently the pressure reflection coefficient or impedance is needed. This is problematical for many reasons. Impedance data for surfaces are not readily available. Furthermore, many building surfaces have non-local reacting behaviour which creates problems in measuring and implementing the phenomena in geometric models. For many predictions it is probably unnecessary to go into this detail, which is fortunate, as it would pose some difficult problems to overcome. For small rooms, however, standing wave modes cause significant problems for geometric prediction models.[23]

In recent years there have been round robin trials of geometric room acoustic models, comparing the accuracy of the different techniques.[24] One of the key findings is that the accuracy of the prediction models is highly dependent on the quality of the input data, including the absorption coefficient of surfaces. So to summarize, defining absorption coefficients (and impedance) for geometric room acoustic models appears to be a tricky problem. Fortunately, experienced practitioners can usually produce estimations of absorption coefficients that are good enough, using previous knowledge. This is not an entirely satisfactory situation, as subjectivity should not be part of a prediction model.

12.3 Diffuse reflections in geometric room acoustic models

Early work on geometric models concentrated on the issue of modelling absorption. In recent years, much attention has been focussed on the modelling of scattering or dispersion from surfaces, often referred to as diffuse reflections. Geometric models inherently cannot precisely model sound as a wave. They approximate the sound to have a small wavelength, much shorter than any dimension within the room; this enables sound to be modelled as particles, rays, beams or as coming from image sources. Unfortunately, the wavelength of sound is relatively large at low to mid-frequencies

and, consequently, geometric models that do not attempt to predict the effects of surface and edge scattering are liable to produce inaccurate results. In real life, some incident sound will inevitably be scattered into angles other than the specular reflection direction upon reflection from most surfaces.

The problems of diffuse reflection modelling in geometric models are well established. For example, Hodgson[25] used a ray tracing model that took diffuse reflections into account by redistributing diffuse energy according to Lambert's law.[1] He concluded that in simple empty rooms the effects of diffuse surface reflections are negligible in small or proportionate rooms, while in large disproportionate rooms the effects can be considerable. To take another example, in the first round robin study of room acoustic models,[26] three prediction models were found to perform significantly better than others. These three prediction models produced results approximately within one subjective difference limen, while the less successful computer models produced predictions inaccurate by many difference limen. What differentiated the three best models from the others was the inclusion of a method to model surface scattering.

If the overall room shape and sizes and orientations of surfaces are such that they will cause reflections to be well mixed for purely geometrical reasons, a diffuse field may be created even if no rough or scattering surfaces are used. In this context, mixing means that the reflection paths involve all the surfaces of the room. For mixing room shapes the reverberation time can be well predicted even without diffuse reflection modelling, even if predictions of finer parameters such as clarity may suffer.[27] However, as it is difficult to know in advance if a room shape is mixing, it is best to always include diffuse reflection modelling in a geometric model, as otherwise inaccurate estimations of acoustic parameters may result.

The most obvious error created by a lack of diffuse reflection modelling is an overestimation of reverberation time.[28,25] This is especially true in enclosed spaces where absorption is concentrated on one surface, such as in concert halls, or when the room shape is highly disproportionate, such as in large factories. In some halls, the choice of scattering coefficients has a greater impact on the estimated reverberation times than the uncertainty in the absorption coefficients.[29] Torres and Kleiner[30] found that changes in the scattering coefficient in geometric models are audible in auralizations, and that the diffuse reflections should be modelled with frequency dependence. Gomes and Gerges[31] also found that using correct scattering coefficient values in a diffuse reflection model was important for gaining accurate predictions for an auditorium. A more recent round robin on geometric models[24] found that the biggest errors with geometric models were consistently at low frequencies, presumably because of their inability to model diffraction effects correctly because these are most prominent at low frequencies.

There are many different methods for incorporating diffuse reflections into a geometric room acoustic model. Dalenbäck *et al*.[29] gave a comprehensive survey of the techniques. Many of the techniques are similar or just variants. Consequently, only a few of the most important and commonly used techniques are outlined here, and readers are referred to Dalenbäck *et al*. for a more comprehensive review. While there are many possible diffuse reflection methods, it is not known which modelling technique, if any, is intrinsically more accurate. It is known that a diffuse reflection model is needed for accurate predictions, but it is not known if one model is better than any of the others. One key determining factor is, however, the computing time. Accurate diffuse reflection models are relatively simple for low orders of reflections, but often become increasingly computationally expensive as the reflection order increases.

12.3.1 Ray re-direction

This method is a ray scattering process as suggested by Kuttruff.[1] A wall is considered to reflect a proportion of all the incident sound energy diffusely. The proportion of diffusely reflected energy is given by the scattering coefficient *s*, and this is distributed according to Lambert's law. The remaining energy $(1 - s)$ is reflected in a specular manner. The direction of the diffuse reflection is determined by two random numbers. The angle of azimuth is chosen by a random number in the interval $\{-\pi, \pi\}$, and the elevation angle is given by the inverse cosine of the square root of a random number that is chosen from the interval $\{0, 1\}$.

Concentrating all the diffusely reflecting energy into one direction is not true in reality, but this method is reasonable for the reverberant sound field, as there are a large number of reflections to average out the response. For the early sound field, where there are fewer reflections, the method is not so good however. Instead of giving many weak reflections from diffusing surfaces spread over time, a receiver gets fewer stronger reflections. This can, to a certain effect, be solved by generating multiple rays from the diffuser in multiple directions, but this then becomes very computationally expensive as the number of rays rapidly increases.

12.3.2 Transition order using particle tracing

The reflection calculation method is separated by a user-defined transition order.[32] Reflections with orders lower than the transition order are purely specular. After the transition order, sound rays are treated as energy packets similar to a normal ray tracing method. At each subsequent wall reflection after the transition order, a secondary impulse source is created at the reflection point, which radiates into the room as an elemental area source. The energy is then re-grouped into a ray and traced forward in a direction given by a random process in which either a purely specular or a diffuse direction will be chosen depending on whether the value of a random number generated by the program is greater or smaller than the wall's scattering coefficient. If the reflection is diffuse, then its direction is determined by a second random process based on Lambert's diffusion law.

The choice of transition order is dependent on the hall shape rather than size.[33] In rectangular rooms, a transition order of 0 in low frequency bands and 1 to 3 in the high frequency bands is found to be appropriate. In fan-shaped halls, where correct modelling of the specular reflections is important to account for the influence of the hall geometry, a higher transition order is also required in the low frequency bands. Generally, the choice of transition order should be based on the importance of the specular components in the early reflections in defining the acoustic characters of the hall. An order of 1 or higher should be used only when the sound field is significantly affected by the specular components, such as at high frequencies or with strong reflecting surfaces. In real halls, where the sound field is expected to be more diffuse, lower transition orders should be used.

The main problem with this method of diffuse reflection modelling is that the concept of a transition order is not physically satisfactory, since diffuse reflections should occur even at the very first reflection, rather than suddenly being switched on at the transition order.

12.3.3 Diffuse energy decays with the reverberation time of the hall

Upon each reflection the scattering coefficient is used to define the fraction of energy diffusely scattered into non-specular angles, while the remaining energy is reflected into the specular reflection angle in the usual way. The diffuse energy is ambient energy spread throughout the room volume. This energy is assumed to decay exponentially, the decay constant being determined by Eyring's formulation. A visibility check is used to ensure that the right surfaces contribute to the received sound.[34]

The problem with this is that it assumes that the Eyring's formulation is correct, which is not necessarily true, especially if the space is non-diffuse. Some have used an iterative procedure to gradually improve the estimated reverberation time, but this slows computation as it requires multiple passes through the algorithm.

12.3.4 Radiosity and radiant exchange

The diffuse part of a reflection is stored in memory while the specular ray tracing is continued. Later, the stored diffuse energy is emitted and all subsequent surface reflections are assumed to be diffuse. These methods use a stochastic radiative exchange process to propagate sound between surfaces. This radiosity can be modelled by integral equations, but more commonly uses simple heat exchange formulations. The radiant exchange takes place at a time interval given by the mean free time between reflections.

12.3.5 Early sound field wave model

Another suggestion is to use wave based models, such as a time domain Fourier approach, to model the early sound field before resorting to a ray tracing with randomized ray redirection for the later sound field. This has the advantage of potentially being more accurate in modelling the early sound field, which is more important for perceived sound quality, while allowing ray tracing to take over where it is computationally more efficient and sufficiently accurate.

12.3.6 Edge scattering for small surfaces

Scattering coefficients are often used to account for the scattering caused by both the surface roughness and also the limited size of surfaces and edge diffraction. It is possible to deal with surface roughness and the effects of limited panel size separately.[35–37] This produces a more physically correct and robust model of scattering.

12.3.7 Distributing the diffuse energy

The models discussed above have many common features, one of which is that the diffusely reflected energy from a surface is modelled as radiating from the surface with a particular spatial distribution. In most current models, Lambert's law is used to determine this distribution. Another possibility is to disperse the sound reflected from a surface using a probability distribution based on the scattered pressure polar response measured or predicted in the free field. Problems would arise because the polar response would be from a surface of significant finite extent, whereas many geometric

models would require the correct dispersion from a point on the surface. This needs consideration in designing the model, and a method to reverse engineer the point reflectivity function from the finite-sized polar response is needed. This can be done using Farina's method for characterizing diffusers, which was discussed in Chapter 4. The situation is more complex with beam tracing as the beam may interact with part of a surface, and so the reflectivity function would neither be the point reflectivity function nor the finite-sized polar response. There is a further problem in dealing with situations where only part of the surface is illuminated, as might happen when objects cast shadows on surfaces, or with directional sources. Polar responses are usually measured or predicted using complete illumination by omnidirectional sources.

The most common dispersion law for computer models is Lambert's law, also referred to as the cosine law. It states that the intensity scattered from a surface follows a cosine distribution with respect to the incident and reflected sound angle to the wall. This is illustrated in Figure 12.7 for a normal incident source. Stated in terms of equations for a ray tracing case:[1]

$$I_r = \frac{I_0 \, dS \cos(\psi) \cos(\theta)}{\pi r^2} \tag{12.7}$$

where I_r is the reflected intensity at the surface; I_0 is the incident intensity at the surface; θ the angle of the receiver to the surface normal; ψ the angle of the source to the surface normal; dS the area of the surface being considered, and r the receiver radius.

This formulation is a simple statement of solid angle projections. For instance, the solid angle is zero for sources and receivers close to grazing. If the surface is partly absorbing, then the intensity should be attenuated by the corresponding intensity reflection coefficient, but to simplify discussions, the surface will be assumed non-absorbing in this discussion.
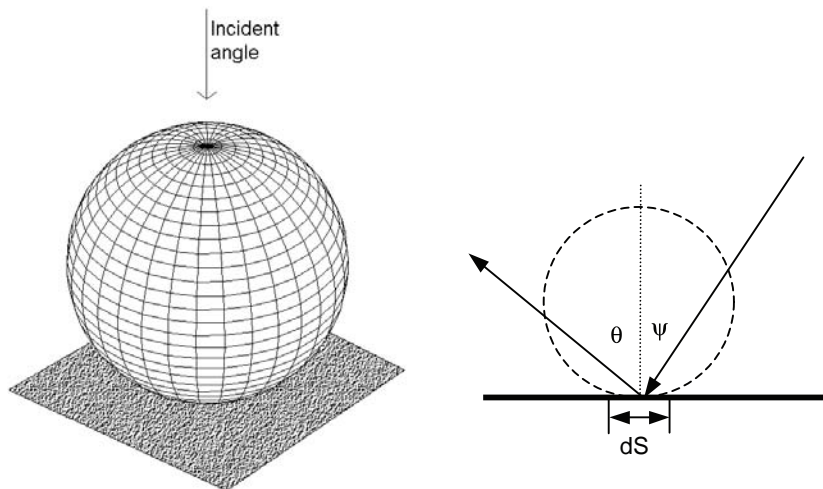
Figure 12.7 Two views of the Lambert distribution of intensity. Left: 3D view; right: cross-section.
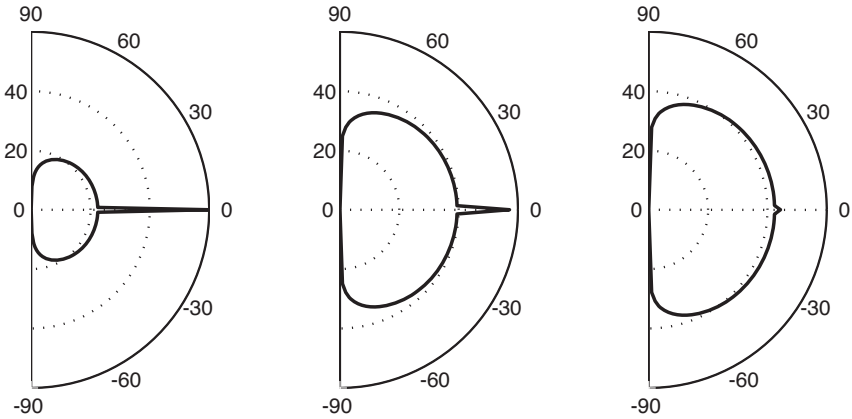
Figure 12.8   Typical far field energy distributions in a geometric model for different values of scattering coefficient *s* and a normal incident source. Left to right *s* = 0.01, 0.5, 0.99.

True rooms are not purely specular and nor are they purely diffuse following Lambert's law; they are somewhere in between. For the reverberant field, however, the evidence is that the sound field more closely matches a diffuse case than a specular one,[1] especially at mid- to high frequency.

Figure 12.8 shows the scattering distributions for a surface with 1, 50 and 99 per cent scattering, where the diffuse reflection is modelled using Lambert's law. Also included for comparison in Figure 12.9 are the polar distributions for a periodic diffuser, a single cylinder, a plane surface and a surface with small random roughness. Each surface was 2 m wide and the source and receivers are in the far field. The scattered distribution, using the Lambert model, does not match many of the real surfaces very well for many cases. The closest is the random rough surface, which approximately
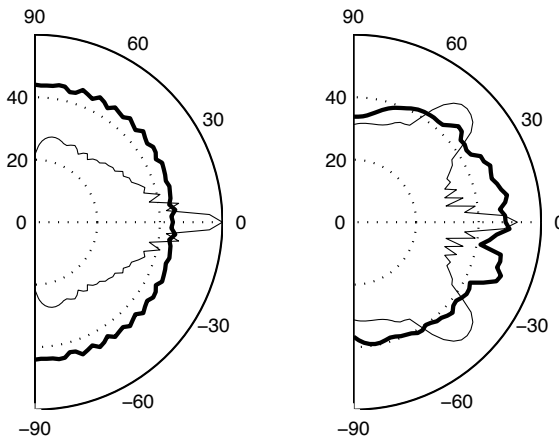
Figure 12.9   Some typical far field one-third octave polar response patterns for different surfaces.

Left figure	Right figure
——— plane surface;	━━━ random rough surface;
━━━ single semi-circle.	——— periodic diffuser.

matches the *s* = 0.99 case. Consequently, room acoustic models are not producing scattering distributions close to real diffuser scattering. However, this is probably not that important for the reverberant sound field, where there are a large number of reflections over which the errors in any one diffuse reflection tend to average out, or at least mask any inaccuracies. It is more of a problem, however, for the early sound field, when precise modelling of first order reflections is needed.

Lambert's law is a natural choice for room acoustic models because it is the asymptotic high frequency case, which is intrinsically the frequency range where the geometric models are most correct. Furthermore, it deals with scattering from a point, which fits with the philosophy of most models. Lambert's law deals with high frequency incoherent scattering, but in acoustics the wavelength is often comparable to surface roughness. Indeed, diffusers such as Schroeder diffusers would not function as designed if the scattering were incoherent. In rooms incoherence is not achieved, just a vast number of different reflections which give the impression of lacking coherence. It is true to say, however, that at high frequencies the scattering from surfaces will approximate Lambert's law. At the key frequencies for room design, and for first order reflections, some believe that it is better to approximate the scattering from specialist diffusers according to a uniform energy distribution rather than Lambert's law in geometric room acoustic models.

There is a further problem with Lambert's law with single plane diffusers. Single plane diffusers produce dispersion in one plane, and are very common in spaces; examples include pipe work, balcony fronts, 1D Schroeder diffusers and columns. Yet most current computer models disperse reflections according to Lambert's law, scattering the sound in all directions over a hemisphere. This has the potential to cause prediction errors, again particularly acute for the early sound field or some coupled spaces. It might be thought that this prediction inaccuracy is less important for the later sound field, and indeed the averaging effect of multiple numerous reflections probably makes the model less sensitive to incorrect modelling of the reflections. In recent years, however, attention has been drawn to the importance of late lateral energy in auditoria[38] and the role of spatial impression. Consequently, for a correct auralization of large music spaces, it may be important to correctly model the spatial distribution of late sound, and correct modelling of anisotropic scatterers is probably needed to achieve this.

12.3.8 Scattering coefficients

In Chapter 4 methods for measuring and analyzing the reflections from surfaces were given, including characterization, using a scattering coefficient. The scattering coefficient is intended to be used as an input to geometric room acoustic models. The success of the new scattering coefficient, however, appears to be mixed, with some suggesting that it works well within geometric room acoustic models, and others reporting problems.

Gomes and Gerges[31] found that errors greater than 20 per cent in the early decay time can occur if the scattering coefficients are incorrect, and that errors greater than 30 per cent can occur if the absorption coefficients are incorrect. In contrast, Nijs *et al.*[15] found that varying scattering coefficients had relatively small effects on predicted levels (3–4 dB) in a complex coupled set of rooms, although Summers[22] has questioned whether diffraction can be so insignificant in the coupled rooms they were considering.

In the past there has not been a defined way to gain scattering coefficients for surfaces, so researchers have adopted an empirical approach to investigations. They have examined what scattering coefficients are needed to gain accurate predictions in rooms by a trial-and-error process. The results from these investigations are presented below as they give some guidelines as to what scattering coefficients might be used. One problem with getting the correct scattering coefficient using this approach, however, is the interrelationship between the absorption and scattering coefficients used in the geometric model, and the predicted acoustic parameters. The reverberation time predicted in a space will depend on both the absorption and scattering coefficients. The effect is most marked for disproportionate spaces or ones where the absorption is unevenly distributed. It is therefore not correct to determine the scattering coefficient by simply adjusting the reverberation time prediction until it matches measurement, as there is usually considerable uncertainty as to what the absorption coefficient of surfaces should be, and this also affects reverberation time.

Prediction models use various approaches to model diffuse reflections and consequently it is likely that different prediction models will require different values of the scattering coefficient, even for modelling the same wall under the same room conditions. Lam[34] investigated the scattering coefficients required for three different diffuse modelling algorithms, using scale models with largely smooth walls. In simple proportionate rooms, where the room dimensions are comparable, the predictions were similar whatever the method used to model diffuse reflections and the scattering coefficient applied. In a highly disproportionate room, however, the scattering coefficient required to gain accurate results varied with the algorithm used to model the diffuse reflections. The required scattering coefficient varied between 0.25 and 1 for the three geometric models considered. It was also found that different scattering coefficients were required to give accurate predictions of different acoustic parameters within the same prediction model. Out of the three models tested, the models present in Sections 12.3.2 and 12.3.3 were most robust, and so were favoured by Lam.

Lam further investigated the effect of scattering coefficients in a concert hall. The trend with scattering coefficients is that going from a zero coefficient to a low value, say $s = 0.1$ or 0.2, can make a large difference to predicted acoustic parameters. Increases of the scattering coefficient from these low values create a much smaller effect.[34] Consequently, the sensitivity of volumetric acoustic parameters to scattering coefficients is non-linear. Figure 12.10 shows the early lateral energy fraction (ELEF) for different scattering coefficients in a real concert hall. Measurements are compared with various predictions. The difference limen for ELEF is about 0.075,[39] so differences bigger than this value are significant. ELEF is chosen because it is probably the parameter most affected by the diffuse reflection modelling algorithm, as it depends purely on the early sound field. This shows that the predictions are sensitive to getting the correct scattering coefficients.

There will be cases, however, where accurate predictions cannot be achieved whatever the values of the scattering coefficients. This will be particularly noticeable for acoustic parameters which are very sensitive to the early sound field, such as clarity and early lateral energy fraction.[16] The early sound field contains only a few reflections and consequently inaccuracies in the modelling of the sound field are most apparent. These cases show that the diffraction effects present in real life reflections are far more complicated than the simple scattering assumed in geometric models – as already indicated by Figures 12.8 and 12.9. It is only by summing over a large
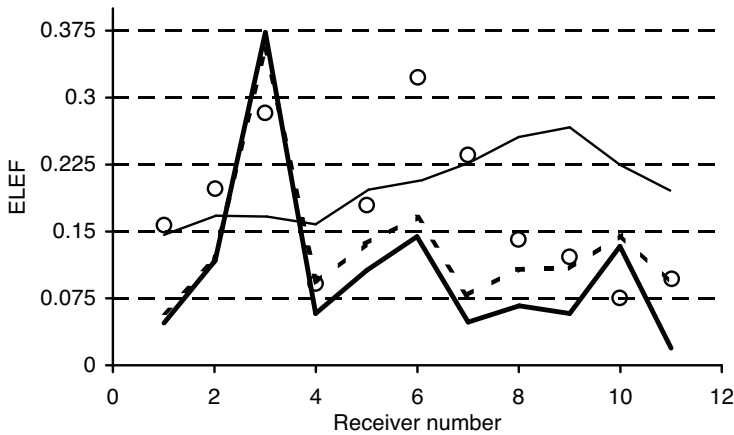
Figure 12.10 Variation of early lateral energy fraction (ELEF) with different scattering coefficients. The grid lines in the *y*-direction are spaced at the subjective difference limen.
    ○   measured;
    ——— *s* = 0;
    – – – *s* = 0.1 for walls, 0.7 for seats; and
    ——— *s* = 1 (after Lam[33]).

number of reflections that the simple scattering assumptions can be regarded as valid approximations. Fortunately, in many situations there are enough reflections that inaccuracies tend to average out, but in some cases, such as coupled rooms and under deep balconies, this will not be true. Certainly, a geometric room acoustic model should not be used to evaluate first order reflection paths, unless surfaces are simple, large and planar or generate diffuse hemispherical dispersion.

Lam recommends that a good starting point for scattering coefficients at mid-frequencies is to set the value to 0.1 for planar walls, as the value remains largely constant at around 0.1 in rooms of sizes ranging from 5,000 to 30,000 m³ and shapes ranging from rectangular to hexagonal.[33] Certainly, the scattering coefficient should never be set to zero because even with smooth walls edge diffraction is important. Nijs *et al.*[15] recommend lower scattering coefficients for plane walls of, at most, 0.02, although Summers[22] could not get accurate predictions using such a low value with a different geometric model. Zeng *et al.*[35] gives recommended mid frequency values of between 0.005 and 0.05 for smooth surfaces, and 0.05–0.2 for brickwork. Dalenbäck[40] recommends 0.1–0.2 as a minimum value on all surfaces, except very large planar surfaces where 0.08–0.1 is recommended.

Gomes and Gerges[31] found that in cases where early reflections are few, a higher scattering coefficient (as high as 1) can be used to improve the accuracy of the predicted early decay time. In the lower frequency bands, the correct scattering coefficient can change from 0.1 in smaller auditoria (volumes less than 10,000 m³) to over 0.4 in larger concert halls (volumes about 30,000 m³). A slight increase in correct scattering coefficient values was also observed in models with more complicated shapes.

Lam set the scattering coefficient to 0.7 for seating,[34] whereas Dalenbäck[40] recommends 0.4–0.7 for 125 Hz–4 kHz on audience areas and Zeng *et al.*[35] 0.6–0.7. For generally

rough surfaces, Dalenbäck suggests high values of 0.8 where the roughness is of the order of, or higher than, the wavelength, and gradually lower below. For example, if the roughness scale is 0.3 m, set 0.8 for 1–4 kHz, 0.6 at 500 Hz, 0.3 at 250 Hz and 0.15 at 125 Hz. He notes that there is generally greater risk associated with underestimating scattering coefficients than with overestimating them. Zeng *et al.*[35] recommend mid-frequency values of between 0.3 and 0.8 in large halls, where the geometric model has greatly simplified the geometry, and between 0.02 and 0.05 where the major details of the hall are explicitly modelled and the geometric prediction algorithm deals with finite-sized panel effects.

Scattering coefficients have also been used when modelling streets. Onaga and Rindel[41] estimated values for the sum of the absorption and scattering coefficients for building façades ranging from 0.1 to 0.25. Ismail and Oldham[42] found scattering coefficient values ranging from 0.09 to 0.13. Although these coefficients are relatively small the evidence is that, for late sound some way from the source, scattering is the dominant mechanism in street canyons. Kang[43] found that changing the scattering coefficient from 0 to 0.2 had a significant effect on the sound level and reverberation parameters within city squares, but increasing the scattering coefficient beyond 0.2 had much less effect.

As an additional approach to estimating scattering coefficients, Dalenbäck suggests testing for the sensitivity to diffusion settings. This is done by calculating acoustic parameters with an initial reasonable guess of scattering coefficients, and with diffuse modelling switched off. The modeller can then examine if the resulting acoustic parameters differ substantially. If the parameters vary greatly, then the scattering coefficients have to be more carefully estimated and it might be wise to include in the room design some options for final fine tuning of the reverberation time.

Appendix C gives a table of scattering coefficients for a variety of surfaces. These are correlation scattering coefficients, calculated using a method outlined in Chapter 4. These were calculated using a 2D BEM and so represent single plane surfaces, such as cylinders. The use of the table values within a geometric model will take a little interpretation. It has already been shown that the scattering coefficient required in geometric models varies between different diffuse reflection modelling algorithms. One deficiency in the table data is the raised values for random incidence scattering coefficients at low frequencies. This arises because the scattering from the edge and the rear of the test sample is different from a flat surface; an empirical fix might be required to gain lower values at low frequencies. Furthermore, the predictions are for the plane of maximum scattering, whereas most diffuse reflection algorithms will interpret these values as being for hemispherically scattering devices and distribute the scattered energy according to Lambert's law. So, although the predictions were produced using single plane scatterers, they will probably be better matched to hemispherical scatterers in many geometric models. The values in the table for semicylinders will probably better match the required values for hemispheres; the table values for 1D Schroeder diffusers will probably better match the required values for 2D Schroeder diffusers, and so on. When modelling a single plane device (cylinder, 1D Schroeder diffuser), it may be necessary to reduce the scattering coefficient table values if the geometric model distributes energy according to Lambert's law using a single scattering coefficient.

This section has summarized the current state of knowledge on using scattering coefficients in geometric models. There are many gaps in understanding and knowledge, and many problems still remain and need further research.

12.4 Summary

This chapter has presented some of the problems associated with going from isolated predictions or measurements of surface properties to whole room predictions. It has considered the problems associated with the use of absorption coefficients in simple statistical models, as well as the role of absorption and scattering coefficients in geometric room acoustic models. The next and final chapter will look at how active technology can provide absorption and diffuse reflections.

12.5 References

1 H. Kuttruff, *Room Acoustics*, 4th edn, Spon Press (2000).
2 Y. Makita and T. Hidaka, "Comparison between reverberant and random incident sound absorption coefficients of a homogeneous and isotropic sound absorbing porous material – experimental examination of the validity of the revised cos θ law", *Acustica*, **66**, 214–20 (1988).
3 BS EN ISO 354:2003, "Acoustics – measurement of sound absorption in a reverberation room".
4 T. W. Bartel, "Effect of absorber geometry on apparent absorption coefficients as measured in a reverberation chamber", *J. Acoust. Soc. Am.*, **69**(4), 1065–74 (1981).
5 T. D. Northwood, "Absorption of diffuse sound by a strip or rectangular patch of absorptive materials", *J. Acoust. Soc. Am.*, **35**, 1173–7 (1963).
6 Y. Makita, T. Hidaka, J. Kaku and J. Yoshimura, "Re-examination of the set of numerical values of the functions which the revised cos θ law and the revised Paris' formula comprise", *Acustica*, Research note, **74**, 159–63 (1991).
7 M. C. Gomperts, "Do the classical reverberation time formulas still have the right to existence?", *Acustica*, **16**, 255–68 (1965).
8 A. M. Ondet and J. L. Barbry, "Modeling of sound-propagation in fitted workshops using ray tracing", *J. Acoust. Soc. Am.*, **85**(2), 787–96 (1989).
9 I. A. Drumm and Y. W. Lam, "The adaptive beam-tracing algorithm", *J. Acoust. Soc. Am.*, **107**(3), 1405–12 (2000).
10 J. B. Allen and D. A. Berkley, "Image method for efficiently simulating small room acoustics", *J. Acoust. Soc. Am.*, **65**, 943–50 (1979).
11 H. Lee and B. Lee, "An efficient algorithm for the image model technique", *Appl. Acoust.*, **24**, 87–115 (1988).
12 M. Vorländer, "Simulation of the transient and steady-state sound propagation in rooms using a new combined ray-tracing/image-source algorithm", *J. Acoust. Soc. Am.*, **86**, 172–8 (1989).
13 U. Stephenson, "Comparison of the mirror image source method and the sound particle simulation method", *Appl. Acoust.*, **29**, 35–72 (1990).
14 M. Kleiner, B.-I. Dalenbäck and P. Svensson, "Auralization – an overview", *J. Audio Eng. Soc.*, **41**(11), 861–75 (1993).
15 L. Nijs, G. Jansens, G. Vermeir and M. van der Voorden, "Absorbing surfaces in ray-tracing programs for coupled spaces", *Appl. Acoust.*, **63**, 611–26 (2002).
16 ISO 3382:1997, "Acoustics – measurement of the reverberation time of rooms with reference to other acoustical parameters".
17 W. C. Sabine, *Collected Papers on Acoustics*, Cambridge (MA), Harvard University Press (1922).
18 C. F. Eyring, "Reverberation time in 'dead' rooms", *J. Acoust. Soc. Am.*, **1**, 217–26 (1930).
19 S. M. Dance and B. M. Shield, "Modelling of sound fields in enclosed spaces with absorbent room surfaces. Part I: performance spaces", *Appl. Acoust.*, **58**, 1–18 (1999).
20 G. Millington, "A modified formula for reverberation", *J. Acoust. Soc. Am.*, **4**, 69–81 (1932).
21 J. Antonio, L. Godinho and A. Tadeu, "Reverberation times obtained using a numerical model versus those given by simplified formulas and measurements", *Acta Acustica uw Acustica*, **88**, 252–61 (2002).

22 J. E. Summers, "Comments on 'Absorbing surfaces in ray-tracing programs for coupled spaces'", *Appl. Acoust.*, **64**, 825–31, (L) (2003).

23 I. Bork, "Report on the 3rd round robin on room acoustical computer simulation – part II: calculations", *Acta Acustica uw Acustica*, **91**(4), 753–63 (2005).

24 I. Bork, "A comparison of room simulation software – the 2nd round robin on room acoustical computer simulation", *Acustica*, **86**, 943–56 (2000).

25 M. Hodgson, "Evidence of diffuse surface reflections in rooms", *J. Acoust. Soc. Am.*, **89**, 765–71 (1991).

26 M. Vorländer, "International round robin on room acoustical computer simulations", *Proc. 15th ICA*, **II**, 689–92 (1995).

27 B.-I. Dalenbäck, "The importance of diffuse reflection in computerized room acoustic prediction and auralization", *Proc. IoA(UK)*, **17**, 24–34 (1995).

28 Y. W. Lam, "On the parameters controlling diffusion calculation in a hybrid computer model for room acoustics prediction", *Proc. IoA(UK)*, **16**(2), 537–44 (1994).

29 B. Dalenbäck, M. Kleiner and P. Svensson, "A macroscopic view of diffuse reflection", *J. Audio Eng. Soc.*, **42**, 793–807 (1994).

30 R. R. Torres and M. Kleiner, "Audibility of 'diffusion' in room acoustics auralization: an initial investigation", *Acustica uw Acta Acustica*, **86**, 919–27 (2000).

31 M. H. A. Gomes and S. N. Y Gerges, "On the accuracy of the assessment of room acoustics parameters using MLS technique and numerical simulation", *Acta Acustica uw Acustica*, **86**, 891–5 (2000).

32 G. Naylor, "Treatment of early and late reflections in a hybrid computer model for room acoustics", *Proc. 124th Acoust. Soc. Am. Meeting*, Paper 3aAA2, New Orleans (1992).

33 Y. W. Lam, "The dependence of diffusion parameters in a room acoustics prediction model on auditorium sizes and shapes", *J. Acoust. Soc. Am.*, **100**, 2193–203 (1996).

34 Y. W. Lam, "A comparison of three diffuse reflection modelling methods used in room acoustics computer models", *J. Acoust. Soc. Am.*, **100**(4), 2181–92 (1996).

35 X. Zeng, C. L. Christensen and J. H. Rindel, "Practical methods to define scattering coefficients in a room acoustics computer model", *Appl. Acoust.*, **67**, 771–86 (2006).

36 A. Farina, "A new method for measurement of the scattering coefficient and the diffusion coefficient of panels", *Acustica*, **86**, 928–42 (2000).

37 B.-I. Dalenbäck, *CATT Acoustic User's Manual V8* (2005).

38 J. S. Bradley, R. D. Reich and S. G. Norcross, "On the combined effects of early- and late-arriving sound on spatial impression in concert halls", *J. Acoust. Soc. Am.*, **108**(2), 651–61 (2000).

39 T. J. Cox, W. J. Davies and Y. W. Lam, "The sensitivity of listeners to early sound field changes in auditoria", *Acustica*, **79**(1), 27–41 (1993).

40 http://www.rpginc.com/research/reverb01.htm (accessed 11/4/2008).

41 H. Onaga and J. H. Rindel, "Acoustic characteristics of urban streets in relation to scattering caused by building facades", *Appl. Acoust.*, **68**, 310–25 (2007).

42 M. R. Ismail and D. J. Oldham, "A scale model investigation of sound reflection from building facades", *Appl. Acoust.* **66**(2), 123–47 (2005).

43 J. Kang, "Numerical modeling of the sound fields in urban squares", *J. Acoust. Soc. Am.*, **117**(6), 3695–706 (2005).

13 Active absorbers and diffusers

The absorbers and diffusers discussed in previous chapters have difficulty altering low frequency sound. Low frequencies have long wavelengths, which means the absorbers and diffusers have to be large to perturb or absorb the wavefronts. This can be overcome to a certain extent by the use of resonant structures, most often used in bass absorber design, but in recent years there has been growing interest in the use of active control technologies to absorb or diffuse low frequency sound.

Active control offers the possibility of bass absorption or diffuse reflections from relatively shallow surfaces, as well as the possibility of variable acoustics. An example application for active absorption is the control of modes in small rooms. The cost and difficulties of implementation are, however, considerable and this is the major reason why this technology has not been more widely applied.

Active absorption has much in common with active noise control, indeed in many ways it is the same concept just re-organized behind a slightly different philosophy. Olson and May carried out pioneering active control experiments and they suggested an active noise control method based on interference.[1] In their method, an electroacoustic feedback loop was used to drive the acoustic pressure to zero near an error microphone placed close to a secondary loudspeaker. This is illustrated in Figure 13.1. This was the first active absorber. More sophisticated active systems specifically alter the surface
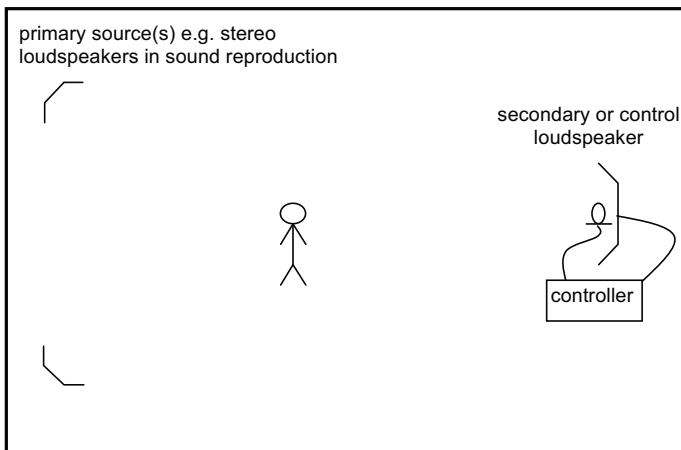
Figure 13.1   Schematic of active absorption in a small room. In this case, a microphone close to the secondary loudspeaker is used as an error signal for the controller to minimize.

impedance of the control loudspeaker towards a desired target value. They may be configured as feedforward or feedback devices and are often constructed around single channel, filtered-x least mean square (LMS) adaptive filter algorithms. Recent developments have moved away from the use of superposition or interference. Resistive material is used in front of the active surfaces to gain actual energy dissipation by, for example, using the active system to maximize the particle velocity through the material; this concept was also first suggested by Olsen and May.

13.1 Some principles of active control

In this section some basic principles of adaptive filtering and active control are outlined for readers unfamiliar with these concepts.

The particular form of a control system is dictated by the physics of the environment in which it operates and the control task to which it is set. However, broad classifications of control systems exist which are useful in differentiating between certain very different approaches to the control problem. These classifications distinguish feedforward from feedback control systems, which may or may not be adaptive to changes in their operating environment.

Consider the system in Figure 13.2. The signal s is corrupted by the addition of the noise signal n at the first summing node, generating the observable signal d. At the second summing node, a signal y is subtracted from d. The result of this subtraction is the error signal, e.

- If $y = n$, then the noise corruption on the signal s is removed, $e = s$; this is the ideal.
- If y is a reasonable approximation of n, then some of the noise contamination is removed, $e \approx s$; this is more realistic of what happens with active control systems.
- If y is largely uncorrelated with n, then the second summing node represents an additional source of noise, further corrupting the signal s in e; this is to be avoided.

The cancelling signal y is derived by filtering operations – through the filter block W which is an adaptive filter, i.e. a filter that can change its coefficients to achieve the required control – on the reference signal x. The optimal configuration of the adaptive cancelling filter, W, is the inverse of the filter relating n to x. Then, the noise added
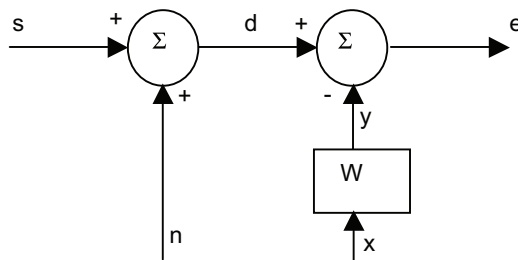
Figure 13.2   A basic active noise control system to remove noise n from signal s.

at the first summing node is perfectly cancelled at the second summing node. Such perfect performance is never achieved in practice for several reasons, most important among which are the imperfect implementation of the cancelling filter and the imperfect correlation between the noise n and the reference x.

Consider the problem of imperfect correlation. The attenuation of the noise component in d is a function of the coherence between the noise and reference signal. The attenuation increases as the coherence increases, and useful levels of noise attenuation can only be achieved with high coherence between the reference and the noise signal; this can pose problems in electroacoustic applications.

Ideally, an analytical solution for the necessary filter W would be derived; however, computing the coefficients of the filter W is usually a non-trivial problem. Fortunately, a computationally efficient iterative approach to the identification of the necessary filter coefficient exists; this is an adaptive filter running under the LMS algorithm.

The technique uses an iterative search process to find the filter W that minimizes the error e. The LMS algorithm discovered by Widrow and Hoff[2] has been found to be robustly stable in many practical applications. It is also a clear, simple and computationally efficient approach for identifying W. There are other techniques for solving minimization problems, but the LMS approach forms the basis of most adaptive noise cancelling systems.

The weights of the filter W are updated using the following equation. The coefficients of the adaptive filter at the $k + 1$ iteration are given by:

$$W_{k+1} = W_k + 2\alpha\, e_k x_k \tag{13.1}$$

where subscript k refers to iteration number; W_k is the vector of adaptive filter coefficients at iteration k; e_k is the error; α is the update rate; and x_k is input to the adaptive filter.

The performance of the LMS algorithm is illustrated below by an example which is also supplied in the MATLAB script *simple_lms.m*. A simulation of a discrete time implementation of Figure 13.1 was coded, in which:
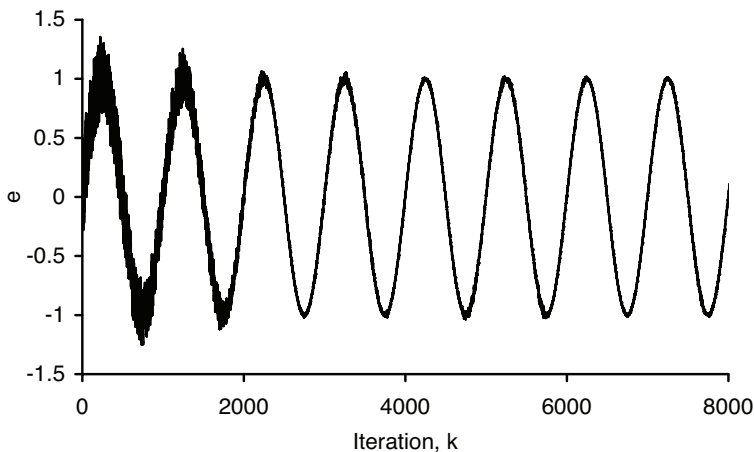
Figure 13.3 Removing noise from a sine wave using active control.
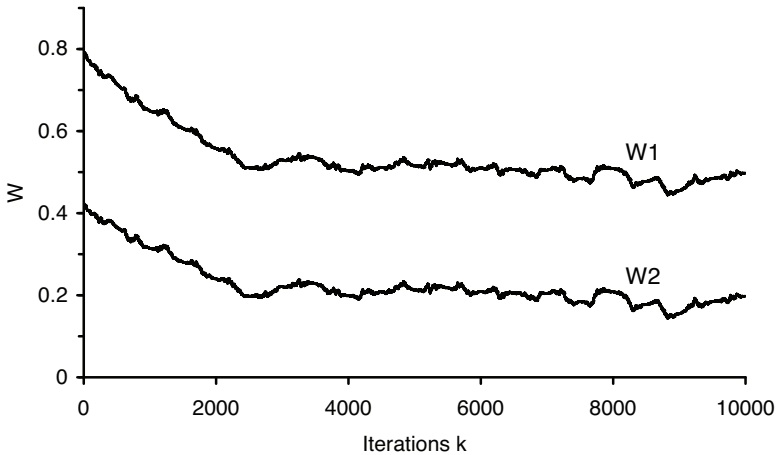
Figure 13.4 Filter coefficients for filter W during training.

$$n_k = 0.5x_k + 0.2x_{k-1} \tag{13.2}$$

A length 2 adaptive filter W was updated using the LMS algorithm (Equation 13.1) with s as a simple sinusoid and x a random process.

The error signal is shown in Figure 13.3. The initial noise is seen to be quickly cancelled leaving a sinusoidal wave, the signal s. The decay of the noise follows a roughly exponential form, which is due to the convergence behaviour of the LMS algorithm approximating the first-order convergence of a steepest descent algorithm.

The convergence of the two coefficients of the adaptive filter W is shown in Figure 13.4. The weights are seen to approach the optimal values implied by Equation 13.2. This is very similar to the system shown in Figure 13.2 except that the white noise signal is fed direct to x and then filtered to get the signal n.

Having studied some fundamentals of noise cancelling, it is now possible to consider the practicalities of active impedance systems.

13.2 An example active impedance system and a general overview

Figure 13.5 shows a possible feedforward controller for an active impedance system.[3-6] While there are other possible set-ups, this system allows some of the general principles to be explained. A signal generator is driving the primary source in the top left of the diagram. The role of the primary source is to generate acoustic waves for the controller to operate on. In the diagram shown this is constrained within a pipe (shown dotted), but it could be within other spaces. The sound from the primary source then propagates to the control surface (secondary loudspeaker) shown top right.

The control surface is instrumented to sense pressure and velocity. Consequently, the impedance at the surface of the controller is known. Using an LMS algorithm, it is possible to alter how the control loudspeaker moves to force the surface impedance to be some desired value.
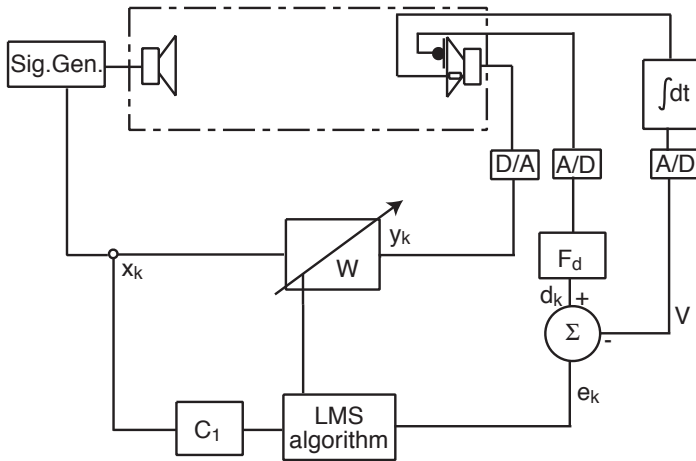
Figure 13.5 A feedforward active impedance control system.

The velocity v_k at the control surface is sensed by integrating the output from a miniature accelerometer mounted on the cone surface. An alternative technique would use two closely spaced microphones.[7,8] The pressure is measured using a surface microphone. This pressure is then passed through the filter F_d. F_d is the desired admittance, and consequently, the signal d_k is the desired velocity. The desired and actual velocity are subtracted to give an error signal, e_k. If this error was zero, then the surface admittance is as desired. If the error is non-zero, then the LMS algorithm is used to change the weights of the adaptive filter W, to reduce the error. Consequently, there is an adaptation time over which the error gradually converges to a small value, preferably zero. Setting the correct value for the update rate given in Equation 13.1 is crucial to achieving training – too large a value and the system never converges, too small a value and the convergence is very slow. There can be problems with instability during training.

The input to the adaptive filter is a signal x_k which must correlate with the primary source signal otherwise the control surface just adds additional noise. This signal can be derived from two places, forming either a feedback or feedforward system. In a feedforward case, the signal x_k is an electronic feed from the primary signal source. This is the case shown in Figure 13.5. The great advantage of feedforward is that it forms a stable system and no unstable feedback can occur. The disadvantage is that an electronic feed from the source signal is required, which means the active surface could be used with electroacoustic sound reproduction systems such as stereo systems, but not sound production systems such as acoustic musical instruments or speech.

In the feedback case, a microphone picks up the signal from the primary source, as illustrated in Figure 13.6. This can actually be the miniature microphone on the surface of the control loudspeaker. With this system, however, there is potential for instability, as a loop is formed which will become unstable if the gain of the loop exceeds 1. The solution to this problem is to insert a feedback compensation filter F_1 which is designed to cancel the feedback path. The feedback cancellation is awkward, however, and if not entirely successful the system will go unstable. Alternatively, highly directional
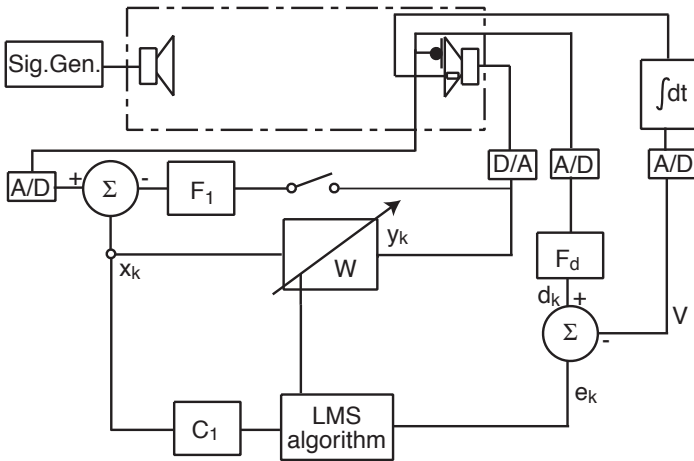
Figure 13.6 A feedback active impedance control system.

loudspeakers and microphones can be used to steer energy from the control source away from the microphone connected to the reference input, but performance is then frequency dependent.

The usual system is to train the coefficients of the adaptive filter, and once the error is sufficiently low, to fix the coefficients. In this example, adaptation is used purely as an efficient method for obtaining the filter coefficients W which may not be analytically derived.

In order that the impedance converges to the correct value, the measurements must provide a true and accurate measurement of the actual ratio of the pressure to the particle velocity. Any error in these measurements will result in convergence to a value other than that desired by the user. For instance, transduction will introduce non-flat frequency responses onto the signals. C_1 is called the plant model, and its role is to compensate for the frequency responses of the transducers and other components. The filter which models the plant is that referred to in the phrase 'filtered-x'.

The design of the plant model presents significant problems. It may be sufficient to measure the frequency response of the plant off-line with a noise or impulsive test signal, and fit this with a finite impulse response (FIR) filter providing a reasonable estimate of the actual plant response. The accuracy of the plant model appears to determine whether or not convergence of the filter will be achieved, and over what timescale adaptation may take place without the risk of instability.[9]

There is some tolerance to plant model errors, which is fortunate since sometimes the object of employing an adaptive active control system is to enable a controller to track changes in its environment during operation. Any such changes will introduce errors between the assumed and the current plant response. Where gross run-time alteration of the plant response is anticipated a run-time measurement of the plant which continually updates filter C_1 may be employed. This has been attempted using maximum length sequence (MLS) signals at very low levels presented simultaneously with program material.[10]

In fact, while people may refer to the active absorption systems as adaptive, this

is a rather misleading name in many cases. The system might be adaptive during the training of the system, but it is most often used with the adaptation turned off, as to do otherwise risks instability in operation. But without adaptation the system is vulnerable to changes in the physical acoustics such as temperature changes and room occupancy.

A theoretical analysis of the significance of transduction errors for active impedance control in a 1D waveguide is presented by Darlington *et al.*,[11] along with measured results derived from the intentional perturbation of pressure and velocity control signals. It is concluded that the transducers and associated signal-conditioning circuits should be calibrated to within 1 dB magnitude error and 5° phase error in order to achieve an absorption coefficient greater than 0.95. This analysis is helpful in that it identifies the significance of transduction errors, but a discussion of the measurement method itself and its relation to a theoretically modelled ratio of pressure and velocity at the surface of a loudspeaker cone is not attempted. This relationship is important in two ways.

Physical measurements of the impedance at the loudspeaker cone depend on two factors – the correct transduction of cone velocity and a suitable measurement of the pressure at the cone surface. Velocity measurement can be done via a two-microphone method or an accelerometer, but the position of the accelerometer is shown to be crucial. Nicholson reports[3] that at frequencies as low as 150 Hz significant differences appear in the magnitude and phase of the velocity between accelerometers mounted at different points on the cone, as the local mass load encourages the onset of non-pistonic motion. Accelerometer locations where the dust cap meets the cone are most suitable. Nicholson also investigated microphone locations immediately adjacent to the control source cone and found that a frame mounting 5 mm from the dust cap was best. It is important that the microphone does not pick up the effects of the cone vibration (the velocity) as otherwise the system becomes unstable.

Having given some sense of how an adaptive system might work in principle, the following sections detail the application of these types of controllers.

13.3 Active absorption in ducts

When the system described in Section 13.2 is constrained to 1D plane waves, the controller is very successful. This would be the case for low frequency control within ducts. Figure 13.7 shows the modes in a duct with the controller turned off (so the termination is the control loudspeaker, which is not being driven, the termination impedance being dictated by the mechanical characteristics of the loudspeaker). The plot shows the steady state response ($t = 0$) and the resulting decay when the primary source is turned off. Figure 13.8 shows the same situation but with the controller in operation. The ability of the controller to damp the modes and therefore make them decay faster is evident. In this case the target impedance for the active surface was the characteristic impedance of air for plane waves.

13.4 Active absorption in three dimensions

It is possible to train the active absorber in a duct to a characteristic impedance, turn the adaptation off, and then use the system within a room. Unfortunately, in this case only small reductions in pressure are obtained. The controller surface does achieve
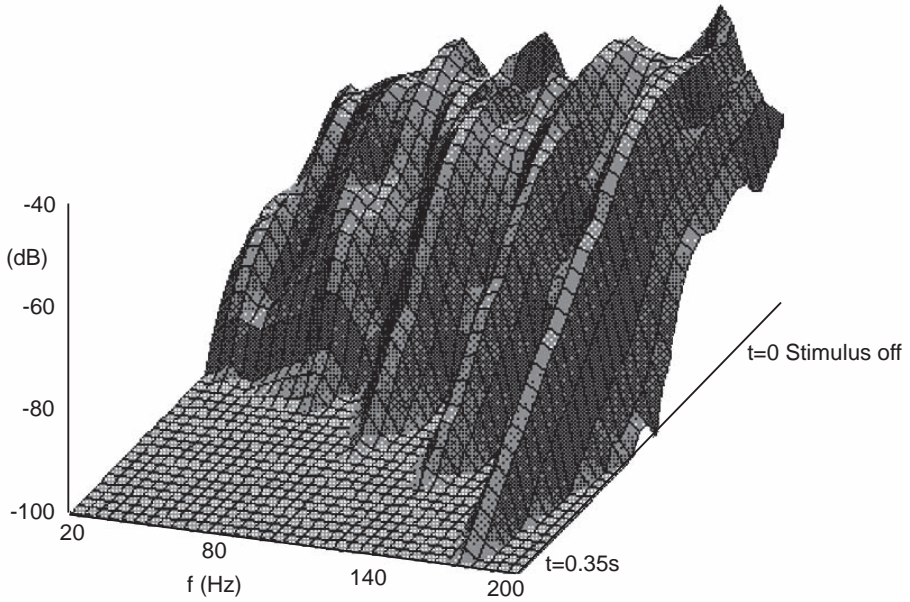
Figure 13.7   Waterfall plot of decay of modes in a 4 m duct, controller off (after Avis[5]).

high absorption coefficients, however. Furstoss *et al.*[12] report absorption coefficients of about 0.9, but only close to the loudspeaker cone. Consequently, while a high absorption coefficient is achieved, the total absorption added to the room is rather small and so there is little effect on most spaces.
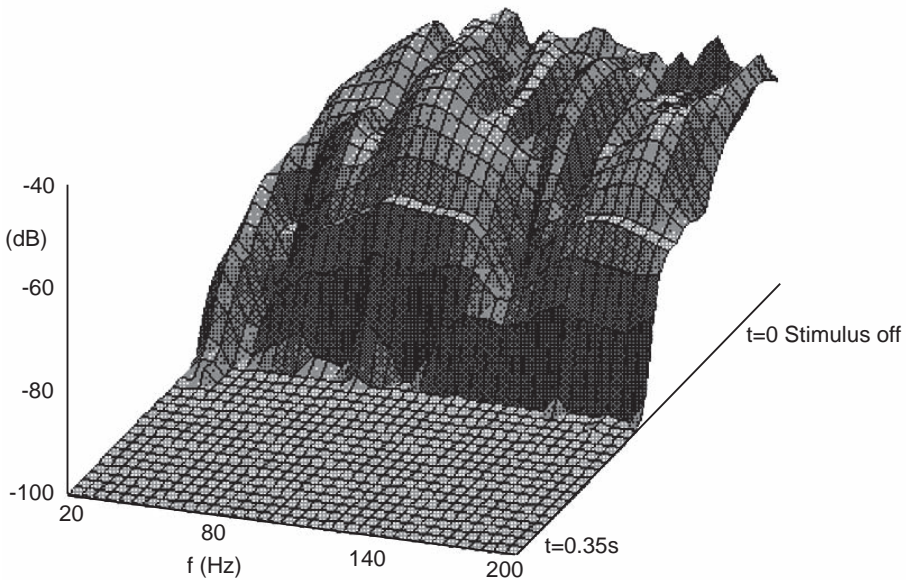
Figure 13.8   Waterfall plot of decay of modes in a 4 m duct, controller on (after Avis[5]).

In a 3D environment the relationship between the control source's surface impedance and the modal behaviour of the room is not simple. The sound field in the room is not plane, although it can be considered to result from the sum of a number of normal modes which individually are plane waves.[13] There exist three orthogonal coordinate axes for particle velocity rather than the single axis within the duct, and the velocity of the controlling driver may lie in the plane of one coordinate or perhaps none of the three. The meaning of a characteristic impedance is therefore no longer clear, and hence it follows that the solution for the duct is unlikely to result in optimal control in the room. Consequently, a different target function is required. For instance, it might be possible to train the system to minimize the pressure at one or more points in a room. This is then a traditional active control system, and more on these can be found in Nelson and Elliott.[14]

Alternatively, it is possible to consider the relationship between surface pressure and velocity in terms of the power radiated by the source. It can be shown that in certain circumstances the power radiated becomes negative, corresponding to absorption of energy by the source. When a pistonic sound source radiates acoustic power at low frequency, the power radiated is proportional to pv^*, where v is the velocity, p the total pressure and $*$ indicates a complex conjugate. If the velocity of the source can be controlled to minimize the power radiated, which is equivalent to maximizing the in-going intensity, the source is then absorbing acoustic power. This has, however, rather simplified the situation as the pressure across the cone is not constant, and the total pressure at the cone will contain direct and reflected components from the primary and secondary sources. The risk with maximizing the in-going intensity is that the controller will achieve this by maximizing the pressure, and so the sound pressure levels within the room will actually increase. For this reason, this control target is rather problematical.

Another problem with this system is that there is no energy dissipation. The active absorption is generated by superposition or interference. In effect, the active control system works by changing the radiation impedance of the primary sources rather than by absorbing energy from waves in the room. Consequently, what these active absorbers achieve is a reduction in radiated power.[15] To really achieve absorption requires a proper energy dissipation mechanism, and this can be achieved through hybrid designs, discussed in Section 13.5. In the following two sections, however, some experimental results from modal control using adaptive and non-adaptive techniques are presented.

13.4.1 Low frequency modal control – example results

Consider the system described in the previous section. This system will be used to try and deal with low frequency modes that are present in a room. Figures 13.9 and 13.10 compare the pressure distribution of the primary axial mode in a room with the controller on and off. In this example, the controller reduces the steady state pressure in the mode by about 6 dB. In this case, a single 8 inch loudspeaker is capable of almost halving the decay time of the first axial mode.

These systems work for single modes well isolated in frequency. As soon as modes become degenerate the active controller has problems. If many modes need to be controlled, many control loudspeakers need to be used. There is probably a need for one control loudspeaker per mode. Consequently, a full control system is going to be expensive to implement.
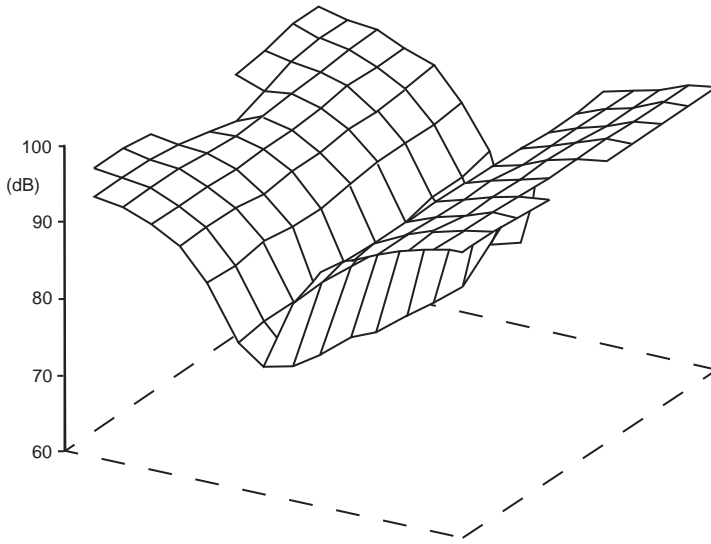
Figure 13.9 Distribution of pressures in a small room for the main axial mode (about 44 Hz); controller off (after Avis[5]).

13.4.2 Low frequency modal control – alternative control regime

Adaptive systems incur significant cost, both in terms of hardware and in terms of constraints on operation due to stability and convergence issues. This has motivated several authors to look for other non-adaptive control regimes for modal control.[16–19] Below is a short description of one of these. Avis[17] examined an analytical modal decomposition to derive a control filter which acts to reduce the modal quality factor by relocating system poles. The aim was to go further than conventional steady state
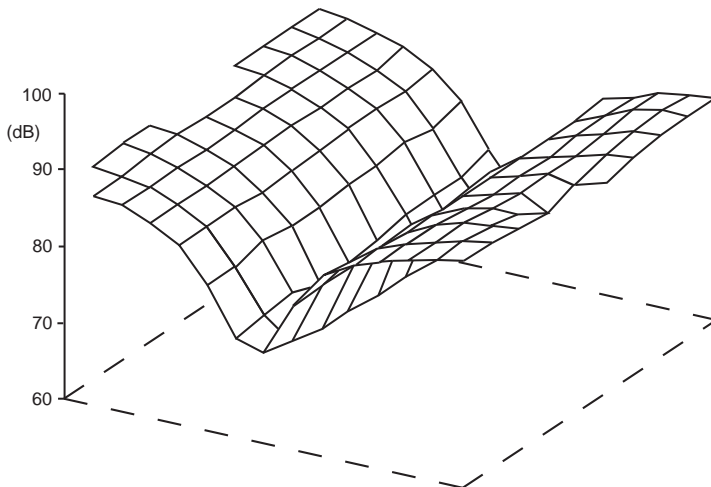
Figure 13.10 Distribution of pressures in a small room for the main axial mode (about 44 Hz); controller on (after Avis[5]).
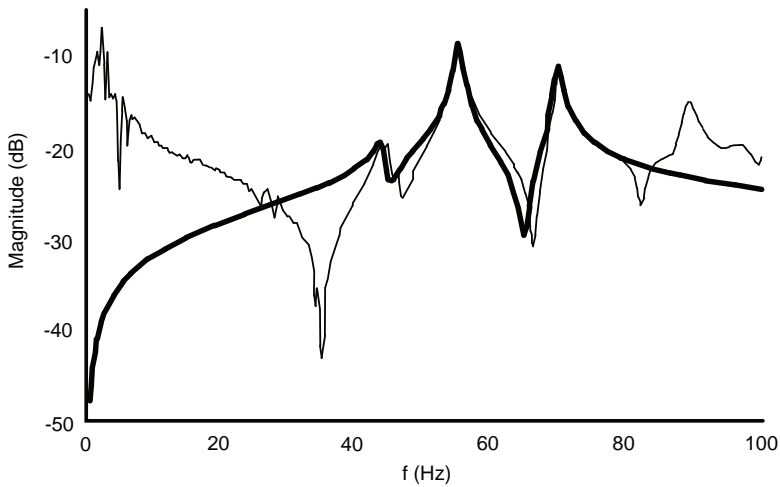
Figure 13.11 Example fitting of measured magnitude of ―――― modal response to ▬▬▬ biquad model (after Avis[17]).

equalization, since the detection of bass modes is more related to time than frequency domain artefacts.[20] Additionally, this has potential for controlled equalization across the whole sound field.

A sound field in a room can be expressed as a modal decomposition.[21] This implies that the sound field may be considered as the sum of a large number of second-order functions; these functions can be implemented as infinite impulse response (IIR) biquad filters. The coefficients of these filters are determined by fitting responses to measurements in the physical sound field. Figures 13.11 and 13.12 show an example of the fitting of magnitude and phase for two modes in a small room.
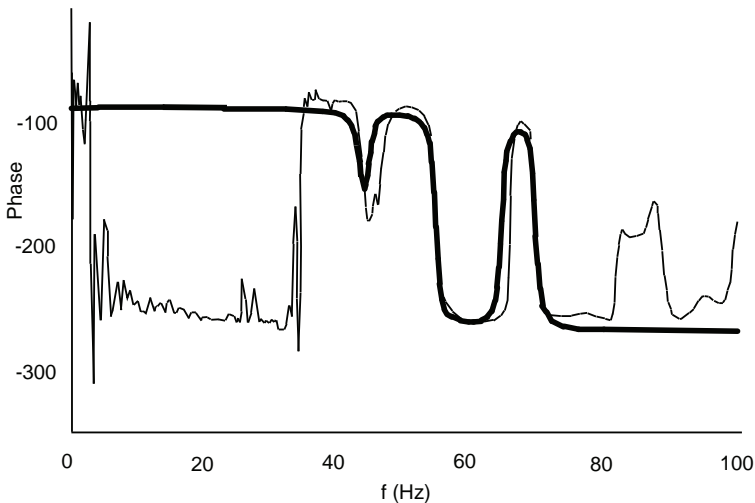
Figure 13.12 Example fitting of measured phase of ―――― modal response to ▬▬▬ biquad model (after Avis[17]).
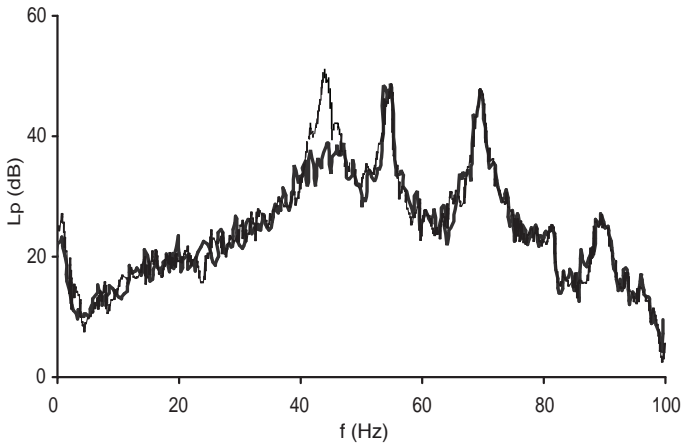
Figure 13.13 Effect of biquad controller designed for a single mode at 44 kHz (after Avis[17]).
——— controller off; and
——— controller on.

A secondary source is used to radiate pressures, which combine with the natural sound field of the room to generate modes with smaller Q factors, i.e. ones that decay faster. Figures 13.13 and 13.14 show a typical result. The controller is formulated such that the poles of the controlled sound field are relocated further away from the unit circle than the uncontrolled case. The controller works well at the measurement point used to fit the IIR filters, but operates less effectively at locations remote from that point.

This system can be used to control multiple modes simultaneously. Because the control technique mimics additional damping, the time, frequency and spatial aspects of the modal nature of the sound field are all addressed simultaneously and in sympathy.
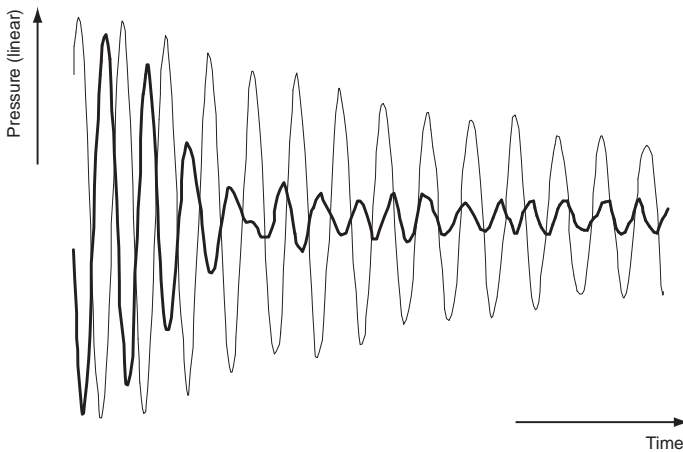
Figure 13.14 Effect of biquad controller designed for a single mode at 44 kHz (after Avis[17]).
——— controller off; and
——— controller on.

The effectiveness of control is again limited to situations where the modes are widely spaced and not degenerate. The sensitivity of this control regime to changes in room conditions is unknown. Presumably it would be necessary to regularly recalibrate the system for the damping to remain efficient.

13.5 Hybrid active–passive absorption

The above adaptive systems have not had explicit dissipation mechanisms included; they have worked by a process of interference or superposition. It makes sense to try to include some form of real resistance as better performance can be achieved. Consequently, this is a hybrid approach involving the combination of absorbent material with an active controller. Indeed, Olson and May[1] considered the possibility of using their secondary loudspeaker to absorb sound by placing it behind acoustically resistant cloth and to use the active controller to maximize the dissipation of energy in the cloth. A concise summary of the development of the hybrid approach is given by Smith *et al.*[22]

Furstoss *et al.*[12] picked up the hybrid concept in the 1990s and made it into a useable device. It is mostly their work which is reported below. A piece of resistive material is placed in front of the active element, and the absorber is made efficient by creating a virtual quarter wavelength resonator behind (as though the resistive material is a quarter of a wavelength from a rigid wall). A typical set-up is shown in Figure 13.15. In the example shown, the surface of the control loudspeaker is instrumented to measure velocity and pressure, and this is used as inputs to an active controller, which drives the control loudspeaker. The controller is tasked with setting the appropriate backing impedance condition. The active control system avoids the need for a large air gap as would be required for a passive resonant absorber at low frequency. Furthermore, it can produce broadband efficiency rather than the limited bandwidth achieved by the passive quarter wave resonant absorbers.

At low frequency the pressure drop across the resistive material can be given by the flow resistivity and particle velocity:

$$\frac{p_2 - p_1}{v} = \sigma d \tag{13.3}$$
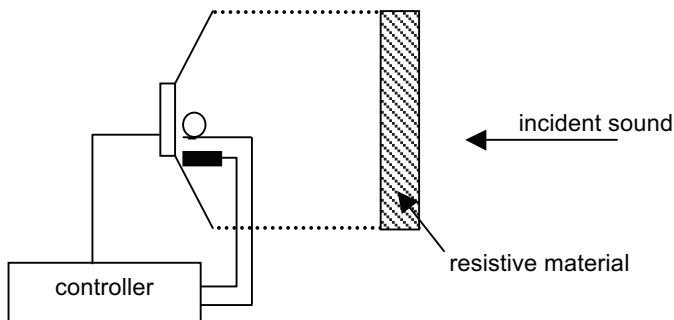
Figure 13.15 A hybrid active–passive absorber.

where p_2 and p_1 are the pressures at the front and the rear of the resistive material; v is the particle velocity; σ is the flow resistivity, and d the material thickness.

If the active element renders the backing pressure to be zero (as would be the case with a quarter wavelength tube), the impedance of the layer is:

$$z = \frac{p_2}{v} = \sigma\, d \tag{13.4}$$

This is the flow resistance of the resistive material, which should be set to the characteristic impedance to maximize absorption.

Therefore, an alternative set-up is to place a microphone at the rear of the porous material, and a controller is then tasked with minimizing the pressure at microphone. Figure 13.16 shows the results from such an arrangement. High absorption across a relatively wide frequency range is achieved. Absorption is not as high for oblique incident sound, averaging around 0.6–0.7 for an angle of incidence, $\psi = 60°$, because for that case the optimal backing pressure for maximum absorption is no longer zero (see below). When used in an array of active absorbers, good performance is achieved although transduction problems limit the useful frequency range to 1 octave around 280 Hz.

While the above regime works for low frequencies, this anechoic termination becomes less successful as the frequency increases. Furstoss *et al.*[12] showed that a better termination criterion is obtained by considering the optimal backing impedance more completely. Consider a porous layer between two fluids as shown in Figure 13.17. The impedance at the front face can be found using the transfer matrix approach described in Chapters 1 and 5. The impedance at the back face is:
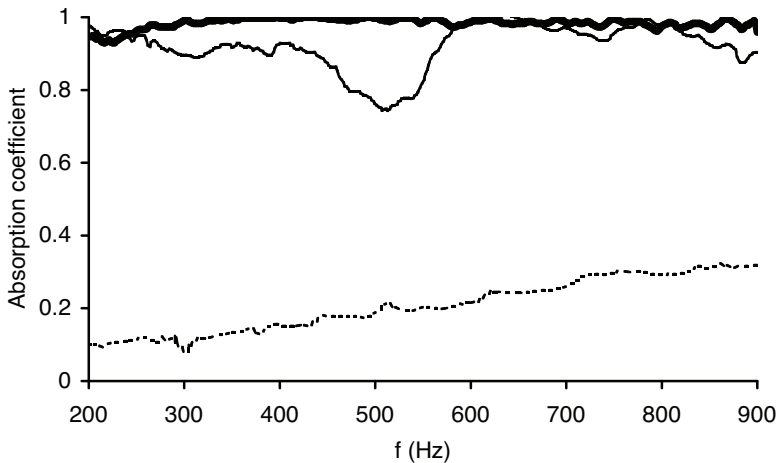
Figure 13.16 Absorption coefficient for a resistive material with and without an active controller backing minimizing the pressure at the rear of the material. The distance *r* refers to the distance of the microphone from the centre of the control loudspeaker: ------- material with rigid backing; —— hybrid absorber, *r* = 10 cm; and —— hybrid absorber, *r* = 0 cm (after Furstoss *et al.*[12]).
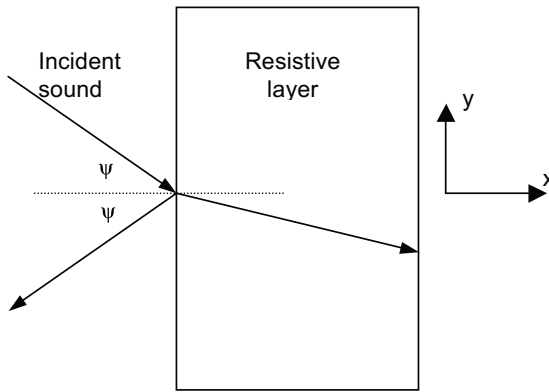
Figure 13.17 Geometry under consideration when determining optimal backing impedance for hybrid active–passive absorption.

$$z_b = \frac{z_c k}{k_x} \cdot \frac{-jz_f \cot(k_x d) + z_c k / k_x}{z_f - jz_c (k / k_x) \cot(k_x d)}$$

(13.5)

where z_f is the impedance on the front face and k_x is the component of the wavenumber in the porous layer in the x-direction (which can be found from Equation 5.7 and 5.8). The wavenumber k and characteristic impedance z_c in the porous medium can be found using the porous absorber models given in Chapter 5. By considering Equation 13.5, the optimal backing impedance for maximum absorption can be found for a particular angle of incidence by setting $z_f = p_0 c_0 / \cos(\psi)$.

Figure 13.18 shows the optimal backing impedance for a particular situation, where the porous material is offering a resistance close to $p_0 c_0$. At low frequency, the optimal backing impedance is zero similar to a zero pressure condition, as indicated before, but as the frequency increases, the optimal backing impedance also changes. It will also change with the porous material's resistance and the angle of incidence. Consequently, minimizing the backing pressure does not necessarily produce optimal absorption, although in the case shown it will be fairly effective below 1 kHz. This impedance matching approach requires pressure and velocity transducers on the active control surface.

Smith *et al.*[22] compared the impedance matching exemplified by Equation 13.5 and pressure release control conditions. They found that the impedance matching approach was superior, requiring less control effort and achieving higher absorption coefficients. Absorption coefficients ranged from 0.8 to 1 from 100 Hz to 1 kHz.

The active controller can also be placed behind a microperforated sheet to gain wideband absorption. The principles are similar to that outlined above for more conventional resistive material. Cobo and Cuesta[23] achieved an absorption coefficient of around 0.7 for a frequency range of 200 to 900 Hz from a full-scale system in an anechoic chamber measurement.

An alternative approach to hybrid absorption was developed by Guigou and Fuller.[24] They used a smart foam design which integrated a lightweight distributed piezoelectric
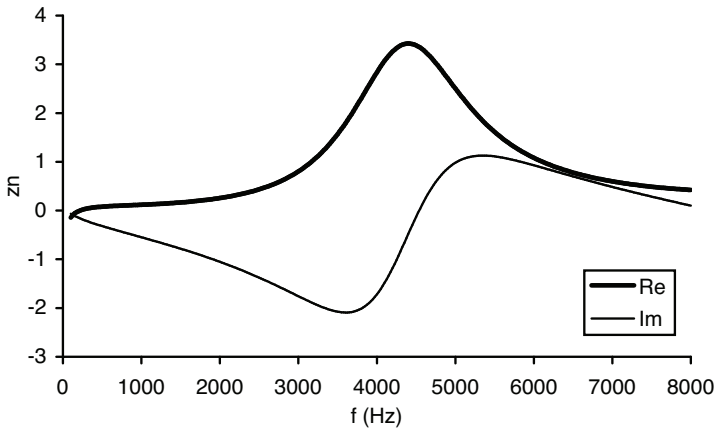
Figure 13.18 Optimal normalized backing impedance for a hybrid active–passive absorber.

PDVF actuator (the active component) between individual layers of sound absorbing foam (the passive component) such that the control can efficiently operate over a broad range of frequencies. The foam provides absorption passively at high frequencies, and the active element in collaboration with the foam provides absorption at low frequencies. In this case, the active surface is being used to reduce the radiated power from a vibrating surface.

13.6 Active diffusers

Active devices might offer significant advantages over passive devices. Most importantly, they allow diffusion over a wider bandwidth by extending the response of the diffusing surfaces to lower frequencies. This is useful because the space available for diffusers is usually limited. To achieve good diffusion, a passive diffuser must be significantly deep compared to the wavelength of sound, and at low frequencies building space costs generally limit the depth of treatments and so performance is compromised. By exploiting active technologies, it is possible to extend performance by 2–3 octaves.

Active diffusers also enable surfaces to be designed which are not physically realisable using passive technologies, for example surfaces where the well depth is frequency dependent. This enables active designs to perform better than passive diffusers. They do not suffer from the critical frequencies that affect many devices made from passive wells.

In the longer term, active diffusers may offer other advantages. Another limitation in diffuser design comes from the visual requirements of interior designers.[25] A good diffuser must be a unified part of the architectural design, rather than an obvious add-on. While it is possible to achieve rough surfaces that are pleasing to many, there is an appeal in having a flat surface that creates dispersion. Potentially, active surfaces could form surfaces that appear to be visually flat and uniform, acting like 'acoustic wallpaper' – but this has not yet been achieved. A final potential advantage is that active devices allow variability. Many rooms have to be multi-purpose, and active elements have the potential to enable the acoustics of a space to be easily changed. However, the variability can only be achieved electronically over the bandwidth that the active
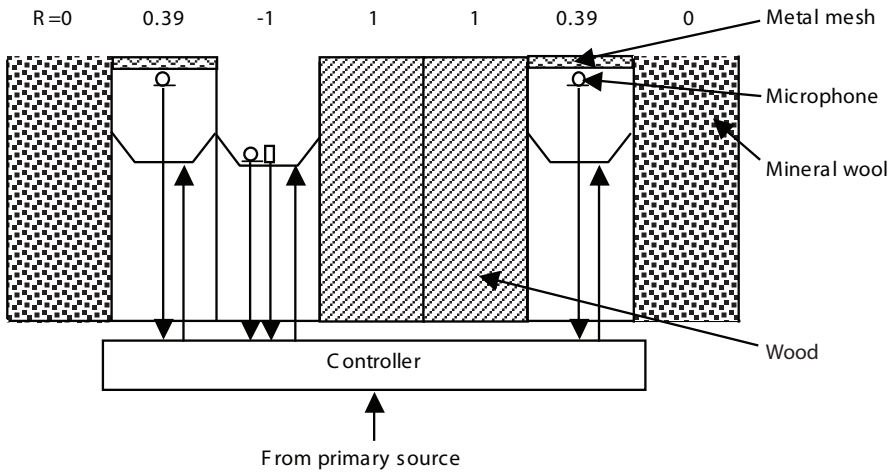
Figure 13.19 An active Bessel diffuser where *R* is the desired reflection coefficient (after Cox *et al.*[26]).

controller is working, which is about 3–4 octaves at low to mid-frequencies.

An example active diffuser is shown in Figure 13.19.[26] A Schroeder diffuser profile is used with active elements substituting for one or more of the wells. The diffuser uses the active elements to produce additional low frequency dispersion by controlling the well impedance, for instance simulating a virtual extension to the well.

A Schroeder-style device is appealing because the active element is constrained within a pipe, simplifying the modelling and measurement of the termination impedance. Only plane wave radiation and propagation need to be considered at the frequencies of interest. The disadvantage is that the surface is always going to look like a diffuser. The high frequency diffusion is provided by the passive elements in the diffuser, and the active elements deal with the low frequencies. There is a complementary relationship between the passive and active elements, as there was with hybrid active absorbers, which is again exploited.

13.6.1 Controllers

The structures and control regimes described for active absorbers can be adapted to make active diffusers. Two control regimes are shown in Figure 13.19. In the second well from the left, the simplest control structure is used. A microphone is placed behind a piece of thin material of known resistance, and the pressure at the microphone is forced to be zero across 3–4 octaves using either a feedback or feedforward configuration. This then means the well offers an impedance given by the resistance of the thin material alone. This type of structure has been exploited before to make a hybrid absorber with a characteristic impedance; here it is being used in a slightly different way to achieve a constant resistance less than characteristic. Wire mesh of known resistance is used to ensure the desired impedance. In the case of the second well from the left, the desire is for a reflection coefficient of 0.39, i.e. partial absorption but with no phase change on reflection.

The third well from the left shows the other type of control structure. The control loudspeaker is instrumented to measure pressure and velocity, and from this the surface impedance can be obtained and manipulated to a desired value using the techniques described previously for active absorption. In the case shown, the desire is for a broadband reflection coefficient of –1, which is equivalent to a well, which is a quarter of a wavelength long at every frequency, something that cannot be realized from a passive device.

The target surface impedance required for active diffusers is more complex than for active absorbers and more difficult to achieve. For instance, when trying to simulate a virtual extension to the well, there are singularities in the desired impedance function. This problem can be solved by including a small real part to the virtually simulated impedance or band, limiting the frequency range over which filter represents the desired impedance accurately. Furthermore, in comparison to active absorbers, active diffusers have a smaller region of stable control and are more sensitive to control impedance errors.[27] Target control impedances for a non-absorbing active diffuser must be achieved to a much higher level of accuracy than is the case for active absorption, because control impedance errors produce much larger changes in the performance of an active diffuser than an active absorber. This partly explains why active diffusers are so much more difficult to produce than active absorbers. It is also worth noting that processes developed to reduce the computational burden for active absorbers are not directly applicable to active diffusers, because it is not possible to trade off the final error achieved against the computation burden of the adaptation, as active diffusers are more sensitive to control impedance errors.

Despite these problems, a variety of diffusers can be made using these technologies, as detailed in the following sections.

13.6.2 Improving passive devices

One possibility is to use active wells to take the place of the longest wells in a quadratic residue diffuser.[28] The active wells are used to create virtual well extensions, and hence enable the construction of a shallower active diffuser which creates the same dispersion as a passive equivalent with longer wells.

Another possibility is to make a hybrid absorber–diffuser using a unipolar MLS. These diffusers cause dispersion by having some of the surface hard and reflective, and other parts absorbent. For the passive version of these devices, the low frequency bandwidth is limited by the depth of mineral wool that can be used. By using an active controller behind the mineral wool, and minimizing the pressure just behind the mineral wool, it is possible to extend the bandwidth of these hybrid diffusers by 2–3 octaves.[26] Furthermore, this is an active diffuser that can be operated in feedback mode.

13.6.3 Beyond passive devices

The performance of the unipolar MLS diffuser is limited because it only achieves reflection coefficients of 0 and 1. This means that, at best, all it can do is attenuate the specular reflection by absorption, it cannot use destructive interference to remove it. Consequently, a device with 50 per cent open area can only attenuate the specular reflection by 6 dB. By forming a device with reflection coefficients of –1 and 1, a bipolar MLS diffuser produces better scattering. While it is possible to form a passive
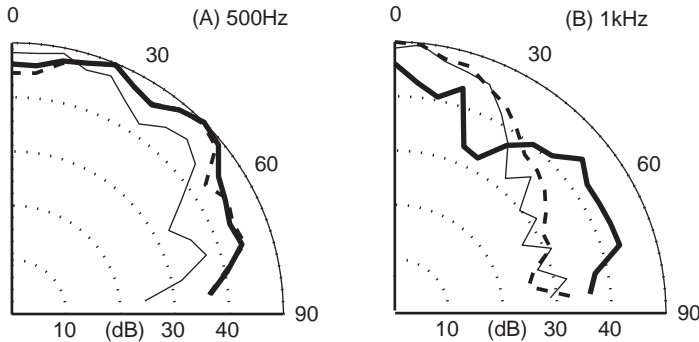
Figure 13.20 Measured scattering from three surfaces at two different frequencies.
——— plane surface;
━━━ active MLS diffuser; and
━ ━ ━ passive MLS diffuser (after Cox *et al.*[26]).

form of this diffuser, it can only operate at discrete frequencies, and the passive form also has a series of critical frequencies where it reflects like a planar surface. This is shown by the measurements in Figure 13.20. At 500 Hz the passive MLS diffuser produces scattering because the reflection coefficient is –1; at an octave higher, however, at 1 kHz, the passive surface behaves similar to the plane surface because all the reflection coefficients are 1.

An active bipolar MLS diffuser[26] can produce a reflection coefficient of –1 from about 100 Hz to 1.1 kHz, and overcome this problem, as shown in Figure 13.20. Good dispersion is achieved within this bandwidth, but the performance needs to be improved at higher frequencies. Due to intercell cancellation, energy is 'lost' into the reactive sound field, resulting in apparent absorption. For this reason there will be applications for which this type of diffuser would not be ideal, for example in large concert halls for classical music where the preservation of acoustic energy is a paramount concern. In other spaces, such as studios, the loss of energy would not be so important.

Bessel functions[29] are used with loudspeaker arrays to enable the radiation from the array to be more uniform. As the mathematics behind Schroeder diffusers has much in common with transducer arrays, Bessel array technologies can be adapted for diffusers. With passive Bessel diffusers it is only possible to construct a passive surface which works at a single frequency. Using active technologies, however, it is possible to gain a Bessel diffuser that operates over about 3–4 octaves.[26] The Bessel diffusers produce good dispersion, as illustrated by Figure 13.21, although with rather high absorption. Again, intercell cancellation is likely to be the cause of the problem.

A variety of problems with the Bessel diffusers need to be overcome. First the absorption needs reducing. Second, a modulation scheme which is more effective is needed. Unlike most sequences used for diffuser design and derived from number theory, the Bessel coefficients are not meant to be used in a periodic manner. And third, the scattering becomes poor at high frequency when the wavelength becomes small compared to the well width, and additionally the active controllers cease to generate the correct reflection coefficients at the well entrances. Some form of fractal construction might help overcome the well width problem, but methods for developing a fractal Bessel diffuser are not obvious.
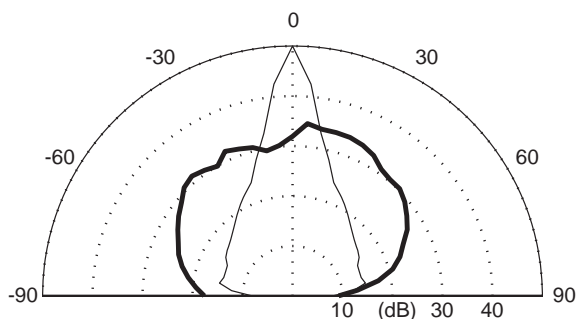
Figure 13.21 The predicted scattering from two surfaces for the 1 kHz one-third octave
bands:
——— plane surface; and
■■■ $N = 35$ Bessel diffuser (after Cox *et al.*[26]).

13.7 Summary

This chapter has discussed the use of active elements to achieve improved absorption
or greater dispersion. The main advantage of active control is that it overcomes the
requirement for large passive surfaces at low frequencies where sound wavelengths are
long. Unfortunately, the cost and practical difficulties associated with this technology
have meant that its use is not widespread. Some believe, however, that active systems
are the future of low frequency absorber and diffuser technology.

13.8 References

1 H. F. Olson and E. G. May, "Electronic sound absorber", *J. Acoust. Soc. Am.*, **25**, 1130–6
  (1953).
2 B. Widrow and S. D. Stearns, *Adaptive Signal Processing*, Prentice Hall, Englewood Cliffs
  (1985).
3 G. C. Nicholson and P. Darlington, "Active control of acoustic absorption, reflection and
  transmission", *Proc. IoA(UK)*, **15**(3), 403–9 (1993).
4 G. C. Nicholson, "The Active Control of Impedance", PhD thesis, University of Salford, UK
  (1995).
5 M. R. Avis, "The Active Control of Low Frequency Room Modes", PhD thesis, University
  of Salford, UK (2000).
6 G. C. Nicholson and P. Darlington, "Smart surfaces for building acoustics", *Proc. IoA(UK)*,
  13(8), 155–64 (1991).
7 F. Orduna-Bustamante and P. A. Nelson, "An adaptive controller for the active absorption
  of sound", *J. Acoust. Soc. Am.*, **91**, 2740–7 (1992).
8 J. Y. Chung and D. A. Blaser, "Transfer function method of measuring in-duct acoustic
  properties", *J. Acoust. Soc. Am.*, **68**, 907–21 (1980).
9 C. C. Boucher, S. J. Elliot, P. A. Nelson, *The Effects of Modelling Errors on the Performance
  and Stability of Active Noise Control Systems*, Recent Advances in Active Control of Sound
  and Vibration, Virginia State University, Technomic Publ. (291–301).
10 L. J. Ericksson and M. C. Allie, "Use of random noise for on-line transducer modeling in an
  adaptive active attenuation system", *J. Acoust. Soc. Am.*, **85**(2), 797–802 (1989).
11 P. Darlington, G. C. Nicholson and S. E. Mercy, "Input transduction errors in active acoustic
  absorbers", *Acta Acustica*, **3**, 345–9 (1995).
12 M. Furstoss, D. Thenail and M. A. Galland, "Surface impedance control for sound
  absorption: direct and hybrid passive/active strategies", *J. Sound Vib.*, **203**(2), 219–36
  (1997).

13 H. Kuttruff, *Room Acoustics*, 4th edn, Spon Press (2000).

14 P. A. Nelson and S. J. Elliott, *Active Control of Sound*, Academic Press (1993).

15 R. D. Ford, "Where does the power go?", *Proc. 11th ICA*, **8**, 277–80 (1983).

16 P. Herzog, A. Soto-Nicola and F. Guery, "Passive and active control of the low-frequency modes in a small room", *Proc. 98th Convention Audio Eng. Soc.*, preprint 3951(D1) (1995).

17 M. R. Avis, "Q-factor modification for low-frequency room modes", *Proc. Audio Eng. Soc., 21st Conference*, St Petersburg (2002).

18 J. Mourjopoulos, "Digital equalisation of room acoustics", *J.Audio Eng. Soc.*, **42**(11), 884–900 (1994).

19 Y. Haneda, S. Makino and Y. Kaneda, "Multiple-point equalisation of room transfer functions by using common acoustical poles", *IEEE Transactions on Speech and Audio Processing*, **5**(4), 325–33 (1997).

20 S. E. Olive, P. L. Schuck, J. G. Ryan, S. L. Sally and M. E. Bonneville, "The detection thresholds of resonances at low frequencies", *J. Audio Eng. Soc.*, **45**(3), 116–27 (1997).

21 P. M. Morse and K. U. Ingard, *Theoretical acoustics*, McGraw-Hill, 555–72 (1968).

22 J. P. Smith, B. D. Johnson and R. A. Burdisso, "A broadband passive–active sound absorption system", *J. Acoust. Soc. Am.*, **106**(5), 2646–52 (1999).

23 P. Cobo and M. Cuesta, "Hybrid passive-active absorption of a microperforated panel in free field conditions", *J. Acoust. Soc. Am.*, **121**(6), EL251–5 (2007).

24 C. Guigou and C. R. Fuller, "Adaptive feedforward and feedback methods for active/passive sound radiation control using smart foam", *J. Acoust. Soc. Am.*, **104**(1), 226–31 (1998).

25 T. J. Cox and P. D'Antonio, "Holistic diffusers", *Proc. IoA(UK)*, **21**(6), 201–6 (1999).

26 T. J. Cox, M. R. Avis and L. J. Xiao, "Maximum length sequence and Bessel diffusers using active technologies", *J. Sound Vibr.*, **289**, 807–29 (2006).

27 M. R. Avis, L. J. Xiao, T. J. Cox, "Stability and sensitivity analyses for diffusers with single and multiple active elements", *J. Audio Eng. Soc.*, **53**(11), 1047–60 (2005).

28 L. J. Xiao, T. J. Cox and M. R. Avis, "Active diffusers: Some prototypes and 2d measurements", *J. Sound Vib.*, **285**(1–2), 321–39 (2005).

29 R. M. Aarts and A. J. E. M. Janssen, "On analytic design of loudspeaker arrays with uniform radiation characteristics", *J. Acoust. Soc. Am.*, **107**(1), 287–92 (2000).

Appendix A

A.1 Table of absorption coefficients

Material	Frequency (Hz)					
	125	250	500	1000	2000	4000
Curtains or drapes						
Light velour 0.338 kg/m² hung straight in contact with wall[1]	0.04	0.05	0.11	0.18	0.30	0.35
Medium velour 0.475 kg/m², hung straight[1]	0.05	0.07	0.13	0.22	0.32	0.35
Medium velour 0.475 kg/m², draped to half area[1]	0.07	0.31	0.49	0.75	0.70	0.60
Heavy velour, 0.61 kg/m² hung straight[1]	0.05	0.12	0.35	0.48	0.38	0.36
Heavy velour, 0.61 kg/m² draped to half area[1]	0.14	0.35	0.55	0.77	0.70	0.60
Variation with draping						
Hung straight[2]	0.04	0.16	0.19	0.17	0.20	0.25
Draped to half area[2]	0.15	0.25	0.30	0.28	0.35	0.40
Draped to 40% of area[2]	0.19	0.31	0.35	0.34	0.44	0.50
Curtains in folds against wall[3]	0.05	0.15	0.35	0.40	0.50	0.50
Cotton curtains, 0.475 kg/m²						
Draped to 7/8 area[4,5]	0.03	0.12	0.15	0.27	0.37	0.42
Draped to 3/4 area[4,5]	0.04	0.23	0.40	0.57	0.53	0.40
Draped to 1/2 area[4,5]	0.07	0.37	0.49	0.81	0.65	0.54
Carpet						
Carpet heavy, on concrete[2]	0.02	0.06	0.14	0.37	0.60	0.65
Heavy carpet (same as line above) on foam rubber or 1.35 kg/m² hair felt[2]	0.08	0.24	0.57	0.69	0.71	0.73
Heavy carpet (same as 2 lines above) with latex backing on foam rubber or 1.35 kg/m² hair felt[2]	0.08	0.27	0.39	0.34	0.48	0.63
Haircord on felt[6]	0.10	0.15	0.25	0.30	0.30	0.30
Pile and thick felt[6]	0.07	0.25	0.50	0.50	0.60	0.65
No underlay (pad), woven wool loop, 1.2 kg/m² 2.4 mm pile height[2]	0.10	0.16	0.11	0.30	0.50	0.47
No underlay (pad), woven wool loop, 1.4 kg/m² 6.4 mm pile height[2]	0.15	0.17	0.12	0.32	0.52	0.57
No underlay (pad) woven wool loop, 2.3 kg/m² 9.5 mm pile height[2]	0.17	0.18	0.21	0.50	0.63	0.83
Loop pile tufted carpet, 1.4 kg/m², hair underlay 1.4 kg/m²[2]	0.03	0.25	0.55	0.70	0.62	0.84
Loop pile tufted carpet, 1.4 kg/m², hair underlay 3.0 kg/m²[2]	0.10	0.40	0.62	0.70	0.63	0.88
Loop pile tufted carpet, 1.4 kg/m², Hair and jute underlay 3 kg/m²[2]	0.20	0.50	0.68	0.72	0.65	0.90
Loop pile tufted carpet, 1.4 kg/m², no underlay[2]	0.04	0.08	0.17	0.33	0.59	0.75
Loop pile tufted carpet, 0.7 kg/m², 1.4 kg/m² hair underlay pad[2]	0.10	0.19	0.35	0.79	0.69	0.79
16 mm wool pile with underlay[1]	0.20	0.25	0.35	0.40	0.50	0.75
9.5 mm wool pile no underlay on concrete[1]	0.09	0.08	0.21	0.26	0.27	0.37
Cord carpet[3]	0.05	0.05	0.10	0.20	0.45	0.65
Thin (6 mm) carpet on underlay[7]	0.03	0.09	0.20	0.54	0.70	0.72

A.1 Table of absorption coefficients (*continued*)

Material	Frequency (Hz)					
	125	250	500	1000	2000	4000
6 mm pile carpet bonded to closed-cell foam underlay[7]	0.03	0.09	0.25	0.31	0.33	0.44
Thick (9 mm) carpet on underlay[2]	0.08	0.08	0.30	0.60	0.75	0.80
Needle felt 5 mm stuck to concrete[8,9]	0.01	0.02	0.05	0.15	0.30	0.40
Thin carpet cemented to concrete[11]	0.02	0.04	0.08	0.2	0.35	0.4
Other floors						
Wood block/lino/rubber flooring[6]	0.02	0.04	0.05	0.05	0.1	0.05
Parquet fixed with asphalt, on concrete[1]	0.04	0.04	0.07	0.06	0.06	0.07
Wood on solid floor[1]	0.04	0.04	0.03	0.03	0.03	0.02
Floors, wood[2]	0.15	0.11	0.10	0.07	0.06	0.07
Wood platform, large airspace below[1]	0.40	0.30	0.20	0.17	0.15	0.10
Floor boards on joist floor[6]	0.15	0.20	0.10	0.10	0.10	0.10
Floors, concrete or terrazzo[2,10]	0.01	0.01	0.015	0.02	0.02	0.02
Concrete floor[11]	0.01	0.02	0.02	0.02	0.02	0.02
Linoleum or vinyl stuck to concrete[12,9]	0.02	0.02	0.03	0.04	0.04	0.05
Linoleum, asphalt tile or cork tile on concrete[2,5,13]	0.02	0.03	0.03	0.03	0.03	0.02
Layer of rubber, cork, linoleum and underlay or vinyl and underlay, stuck to concrete[18,9]	0.02	0.02	0.04	0.05	0.05	0.10
Cork, lino or rubber tile on solid floor[1]	0.04	0.03	0.04	0.04	0.03	0.02
25 mm cork on solid backing	0.05	0.1	0.2	0.55	0.6	0.55
Slate[1]	0.01	0.01	0.01	0.02	0.02	0.02
Theatre seating, unoccupied						
Beranek's values[14]	0.19	0.37	0.56	0.67	0.61	0.59
Average of 9 modern seating designs, 0.9 m row spacing[15]	0.34	0.46	0.64	0.71	0.77	0.85
One seat type, 0.8 m row spacing[15]	0.29	0.39	0.61	0.74	0.83	0.88
Same seat as line above, 0.9 m row spacing[15]	0.25	0.35	0.58	0.70	0.78	0.84
Same seat as 2 lines above, 1 m row spacing[15]	0.23	0.34	0.52	0.65	0.73	0.75
Upholstered seating[6]	0.45	0.60	0.73	0.80	0.75	0.64
Upholstered seating, well upholstered[16]	0.44	0.60	0.77	0.89	0.82	0.70
Upholstered seating, leather covered[16]	0.40	0.50	0.58	0.61	0.58	0.50
Seating, occupied						
Occupied theatre seating average from refs 1 and 15	0.41	0.58	0.80	0.90	0.92	0.89
Audience on timber seats (1/m²)[2]	0.16	0.24	0.56	0.69	0.81	0.78
Audience on timber seats (2/m²)[2]	0.24	0.4	0.78	0.98	0.96	0.87
Orchestra with instruments (1.5 m²/person)[2]	0.27	0.53	0.67	0.93	0.87	0.8
Wooden pews (100% occupancy)[16]	0.57	0.61	0.75	0.86	0.91	0.86
Wooden chairs (100% occupancy)[16]	0.60	0.74	0.88	0.96	0.93	0.85
Wooden pews (75% occupancy)[16]	0.46	0.56	0.65	0.75	0.72	0.65
Miscellaneous						
Water surface in swimming pool[17]	0.01	0.01	0.01	0.01	0.02	0.02
Water surface in swimming pool[2]	0.008	0.008	0.013	0.015	0.02	0.025
Marble or glazed tile[2]	0.01	0.01	0.01	0.01	0.02	0.02
Solid wooden door[18,9]	0.14	0.10	0.06	0.08	0.10	0.10
Ventilation grille[8,9]	0.60	0.60	0.60	0.60	0.60	0.60
Egg boxes[19]	0.01	0.07	0.43	0.62	0.51	0.70

A.1 Table of absorption coefficients (*continued*)

Material	Frequency (Hz)					
	125	250	500	1000	2000	4000
Wood						
Plywood panelling, 1 cm thick[2,10]	0.28	0.22	0.17	0.09	0.1	0.11
22 mm chipboard, 50 mm cavity filled with mineral wool[18,9]	0.12	0.04	0.06	0.05	0.05	0.05
3-4 mm plywood sheets, >75 mm cavity with 25–50 mm mineral wool[8,9]	0.50	0.30	0.10	0.05	0.05	0.05
Plywood/hardwood, air space[6]	0.32	0.43	0.12	0.07	0.07	0.11
6 mm wood fibreboard on laths, cavity>100 mm deep[18,9]	0.30	0.20	0.20	0.10	0.05	0.05
Fibreboard, solid backing[6]	0.05	0.1	0.15	0.25	0.3	0.3
Fibreboard, 25 mm air space[6]	0.3	0.3	0.3	0.3	0.3	0.3
9.5–12.7 mm wood panelling, 5–10 cm air space behind[1]	0.30	0.25	0.20	0.17	0.15	0.10
Wood, 50 mm thick	0.01	0.05	0.05	0.04	0.04	0.04
Concrete						
Rough concrete[20]	0.02	0.03	0.03	0.03	0.04	0.07
Smooth unpainted concrete[18,9]	0.01	0.01	0.02	0.02	0.02	0.05
Smooth concrete, painted or glazed[18,9]	0.01	0.01	0.01	0.02	0.02	0.02
Concrete block, coarse[2]	0.36	0.44	0.31	0.29	0.39	0.25
Concrete block, painted[2,5,13]	0.10	0.05	0.06	0.07	0.09	0.08
Porous concrete blocks without surface finish, 400-800 kg/m³ [9]	0.05	0.05	0.05	0.08	0.14	0.20
Clinker concrete, no surface finish, 800 kg/m³ [8,9]	0.10	0.20	0.40	0.60	0.50	0.60
Bricks and blocks						
Brick, unglazed[2]	0.03	0.03	0.03	0.04	0.05	0.07
Brickwork, plain painted[6]	0.05	0.04	0.02	0.04	0.05	0.05
Smooth brickwork with flush pointing, painted[17]	0.01	0.01	0.02	0.02	0.02	0.02
Brick, unglazed, painted[2]	0.01	0.01	0.02	0.02	0.02	0.03
Smooth brickwork with flush pointing[18,9]	0.02	0.03	0.03	0.04	0.05	0.07
Smooth brickwork, 10 mm deep pointing, pit sand mortar[8,9]	0.08	0.09	0.12	0.16	0.22	0.24
Breeze block[6]	0.2	0.3	0.6	0.6	0.5	0.5
Plaster						
Lime cement plaster[18]	0.02	0.02	0.03	0.04	0.05	0.05
Glaze plaster[18,9]	0.01	0.01	0.01	0.02	0.02	0.02
Painted plaster surface[8,9]	0.02	0.02	0.02	0.02	0.02	0.02
Plaster with wallpaper on backing paper[18,9]	0.02	0.03	0.04	0.05	0.07	0.08
Plaster, gypsum, or lime, rough finish on lath[21,10]	0.02	0.03	0.04	0.05	0.04	0.03
Plaster, gypsum, or lime, smooth finish on lath[2]	0.14	0.1	0.06	0.04	0.04	0.03
Plaster, gypsum or lime, smooth finish on lath[21,10]	0.02	0.02	0.03	0.04	0.04	0.03
Plaster, on laths/studs, air space[6]	0.3	0.1	0.1	0.05	0.04	0.05
Plaster, gypsum, or lime, smooth finish on tile or brick[2]	0.013	0.015	0.02	0.03	0.04	0.05
Plaster, lime of gypsum on solid backing[6]	0.03	0.03	0.02	0.03	0.04	0.05
Acoustics plaster[6]	0.30	0.35	0.5	0.7	0.7	0.7

A.1 Table of absorption coefficients (*continued*)

Material	125	250	500	1000	2000	4000
	Frequency (Hz)					
Acoustics plaster, 40 mm thick[22]	0.31	0.55	0.84	0.78	0.71	0.54
Acoustics plaster, 68 mm thick[22]	0.47	0.74	0.76	0.65	0.62	0.49
Plasterboard						
Gypsum board, 1.27 cm nailed to studs with 4.1 m c-t-c[2]	0.29	0.1	0.05	0.04	0.07	0.09
Plasterboard on frame, 9.5 mm boards, 10 cm empty cavity[23,9]	0.11	0.13	0.05	0.03	0.02	0.03
Plasterboard on frame, 9.5 mm boards, 10 cm cavity filled with mineral wool[23,9]	0.28	0.14	0.09	0.06	0.05	0.05
Plasterboard on frame, 13 mm boards, 10 cm empty cavity[23,9]	0.08	0.11	0.05	0.03	0.02	0.03
Plasterboard on frame, 13 mm boards, 10 cm cavity filled with mineral wool[23,9]	0.30	0.12	0.08	0.06	0.06	0.05
2×13 mm plasterboard on steel frame, 5 cm mineral wool in cavity, surface painted[12,9]	0.15	0.10	0.06	0.04	0.04	0.05
Glazing						
Glass, ordinary window glass[2,10]	0.35	0.25	0.18	0.12	0.07	0.04
Single pane of glass, 3–4 mm[6]	0.2	0.15	0.1	0.07	0.05	0.05
Single pane of glass, >4 mm[6]	0.1	0.07	0.04	0.03	0.02	0.02
Single pane of glass, 3 mm[23,9]	0.08	0.04	0.03	0.03	0.02	0.02
Double glazing, 2–3 mm glass, 1 cm gap[8,9]	0.10	0.07	0.05	0.03	0.02	0.02
Double glazing, 2–3 mm glass, >3 cm gap[23,9]	0.15	0.05	0.03	0.03	0.02	0.02
Glass, large panes, heavy glass[2,5,13]	0.18	0.06	0.04	0.03	0.02	0.02
Wools and foam						
25 mm fibreglass, rigid backing[24]	0.08	0.25	0.45	0.75	0.75	0.65
2.54 cm fibreglass, 24 to 48 kg/m^3 [2]	0.08	0.25	0.65	0.85	0.8	0.75
2.5 cm fibreglass, 2.5 cm airspace[2]	0.15	0.55	0.8	0.9	0.85	0.8
5 cm fibreglass, rigid backing[24]	0.21	0.50	0.75	0.90	0.85	0.80
7.5 cm fibreglass, rigid backing[24]	0.35	0.65	0.80	0.90	0.85	0.80
10 cm fibreglass, rigid backing[24]	0.45	0.90	0.95	1.00	0.95	0.85
5 cm mineral wool (40 kg/m³), glued to wall, untreated surface[8,9]	0.15	0.70	0.60	0.60	0.85	0.90
5 cm mineral wool (40 kg/m³), glued to wall, surface sprayed with thin plastic solution[8,9]	0.15	0.70	0.60	0.60	0.75	0.75
5 cm mineral wool (70 kg/m³) 30 cm in front of wall[8,9]	0.70	0.45	0.65	0.60	0.75	0.65
5 cm wood-wool set in mortar[8,9]	0.08	0.17	0.35	0.45	0.65	0.65
5.1 cm fibreglass, panels with plastic sheet wrapping and perforated metal facing[2]	0.33	0.79	0.99	0.91	0.76	0.64
5.1 cm fibreglass, 24–48 kg/m^3 [2]	0.17	0.55	0.8	0.9	0.85	0.8
Acoustic tile, 1.27 cm thick[5]	0.07	0.21	0.66	0.75	0.62	0.49
Acoustic tile, 1.9 cm thick[5]	0.09	0.28	0.78	0.84	0.73	0.64
Polyurethane foam, 2.5 cm thick	0.16	0.25	0.45	0.84	0.97	0.87
Thermafleece, sheep wool absorbent 100 mm thick[25]	0.47	0.86	1.00	0.94	0.96	1.02

A.1 Table of absorption coefficients (*continued*)

	Frequency (Hz)					
Material	125	250	500	1000	2000	4000
Ballast						
Ballast or other crushed stone, 3.18 cm, 15.2 cm deep[2]	0.19	0.23	0.43	0.37	0.58	0.62
Ballast or other crushed stone, 3.18 cm, 30.5 cm deep[2]	0.27	0.58	0.48	0.54	0.73	0.63
Ballast or other crushed stone, 3.18 cm, 45.7 cm deep[2]	0.41	0.53	0.64	0.84	0.91	0.63
Ballast or other crushed stone, 0.64 cm 15.2 cm deep[2,10]	0.22	0.64	0.7	0.79	0.88	0.72
Microperforated absorber						
4 cm cavity[22]	0.08	0.27	0.70	0.35	0.11	0.04
40 cm cavity[22]	0.64	0.56	0.41	0.28	0.13	0.06
Diffusers						
Hybrid absorber-diffuser (BAD™ panel mounted on 2.5 cm fibreglass)[22]	0.17	0.40	0.86	1.00	0.84	0.61
2D N=7 QRD™, design freq. = 500 Hz[22]	0.14	0.12	0.14	0.20	0.09	0.12
2D N=7 QRD as line above, with cloth covering[22]	0.16	0.17	0.28	0.41	0.26	0.3
1D N=7 QRD, design freq. = 500 Hz[22]	0.11	0.1	0.07	0.08	0.06	0.06
1D N=7 QRD as line above, with cloth covering[22]	0.13	0.14	0.2	0.24	0.20	0.23

A.2 References

1 L. L. Beranek, *Acoustics*, McGraw-Hill (1954).
2 C. M. Harris (ed), *Handbook of Noise Control*, 2nd edn, McGraw-Hill (1991).
3 D. Templeton (ed), *Acoustics in the Built Environment*, 2nd edn, Architectural Press (1997).
4 V. S. Mankovsky, *Acoustics of Studios and Auditoria*, Focal Press (1971).
5 F. Alton Everest, *Master Handbook of Acoustics*, 4th edn, McGraw-Hill (2001).
6 A. Fry (ed), *Noise Control in Building Services*, Pergamon Press (1987).
7 P. H. Parkin, H.R. Humphreys and J. R. Cowell, *Acoustics, Noise and Buildings*, Faber and Faber (1979).
8 J. Kristensen, "Sound absorption coefficients – measurement, evaluation, application", Note #45, Statens Byggeforskningsinstitut, Hørsholm (in Danish) (1984).
9 C. Lynge, *ODEON Room Acoustics Program, User Manual*, DTU, Denmark (2001).
10 Physikalisch-Technische Bundesanstalt, http://www.ptb.de/en/index.html (accessed 2003).
11 L. L. Beranek and T. Hidaka, "Sound absorption in concert halls by seats, occupied and unoccupied, and by the hall's interior surfaces", *J. Acoust. Soc. Am.*, **104**(6), 3169–77 (1998).
12 J. Petersen, "Rumakustik", SBI-anvisning 137, Statens Byggeforskningsinstitut, Hørsholm (1983).
13 R. W. Young, "Sabine reverberation and sound power calculations", *J. Acoust. Soc. Am.*, **31**, 912–21 (1959).
14 L. L. Beranek, "Audience and chair absorption in large halls. II," *J. Acoust. Soc. Am.*, **45**, 13–19 (1969).
15 W. J. Davies, R. J. Orlowski and Y. W. Lam, "Measuring auditorium seat absorption", *J. Acoust. Soc. Am.*, **96**, 879–88 (1994).

16 D. A. Bies and C. H. Hansen, *Engineering Noise Control: Theory and Practice*, E&FN Spon, 2nd edn (1996).
17 V. O. Knudsen and C. M. Harris, *Acoustical Designing in Architecture*, John Wiley (1953).
18 H. W. Bobran, *Handbuch der Bauphysik*, Verlag Ulstein, Berlin (1973).
19 http://www.acousticsfirst.com/docs/egg.pdf (accessed 1/4/08).
20 ISO/TR 11690-3, "Acoustics – recommended practice for design of low-noise workplaces containing machinery. Part 3: Sound propagation and noise predictions in workrooms" (1997).
21 D. Davis and C. Davis, *Sound System Engineering*, Focal Press (1997).
22 RPG Diffusor Systems, Inc., www.rpginc.com (accessed 2003).
23 W. Fasold, and H. Winkler, *Bauphysikalische Entwurfslehre, Band 4: Bauakustik*, VEB Verlag f r Bauwesen, Berlin (1976).
24 L. E. Kinsler, A. R. Frey, A. B. Coppens and J. V. Sanders, *Fundamentals of Acoustics*, 4th edn, John Wiley & Sons (2000).
25 http://www.greenshop.co.uk/documents/Thermafleece/Thermafleece_acoustic.pdf (accessed 1/4/08).

Appendix B

MATLAB scripts

B.1 Chapter 5: script_5_1

```
%Absorption of a rigid backed porous absorber
%Using Delany and Bazley formulations
%Normal incidence absorption coefficients

close all
clear all

c = 340;              %speed of sound
rho = 1.21;           %density of air
Z0 = c*rho;           %characteristic impedance of air

sigma = 50000;            %flow resistivity
l = 0.0254;           %thickness

f = [100:50:10000]; %Frequency
nf = length(f);

%Delany and Bazley
X = rho*f/sigma;     %dimensionless quantity for Delany and Bazley
zc = rho*c*(1+0.0571*(X.^-0.754)-j*0.087*(X.^-0.732));
                     %characteristic impedance
k = (2*pi/c).*f.*(1+0.0978*(X.^-0.700)-j*0.189*(X.^-0.595));
                     %complex wave number

gamma = j*k;         %propagation constant
z = zc.*coth(gamma*l)        %surface impedance

figure
semilogx(f,real(z),'b',f,imag(z),'g');
title('Impedance of rigid backed porous absorber')
xlabel('Frequency(Hz)')
ylabel('Impedance')
legend('Real','Imaginary')

R = (z-Z0)./(z+Z0); %reflection factor

figure
semilogx(f,abs(R),'b',f,angle(R),'g');
title('Reflection factor of rigid backed porous absorber')
xlabel('Frequency(Hz)')
ylabel('Reflection factor')
legend('Magnitude','Phase')

anormal = 1-abs(R).^2;      %absorption coefficient
```

```
figure
semilogx(f,anormal);
title('Normal incidence abs. coeff. of rigid backed porous absorber')
xlabel('Frequency(Hz)')
ylabel('alpha')
```

B.2 *Chapter 5: script_5_2*

```
%Absorption of a rigid backed porous absorber
%Using Delany and Bazley formulations
%Normal incidence absorption coefficients

%Demonstrating effects of thickness

close all
clear all

c = 340;                %speed of sound
rho = 1.21;             %density of air
Z0 = c*rho;             %characteristic impedance of air

sigma = 20000;          %flow resisivity

f = [100:50:10000]; %Frequency
nf = length(f);

%Delany and Bazley
                        %dimensionless quantity for Delany and Bazley
X = rho*f/sigma;
                        %characteristic impedance
zc = rho*c*(1+0.0571*(X.^-0.754)-j*0.087*(X.^-0.732));
                        %complex wave number
k = (2*pi/c).*f.*(1+0.0978*(X.^-0.700)-j*0.189*(X.^-0.595));

figure(1)
hold on
for il = 1:4                         %thickness loop
    l = (il-0.5)*0.0254;            %thickness

    z = -j*zc.*cot(k*l)             %surface impedance
    R = (z-Z0)./(z+Z0);            %reflection factor
    anormal = 1-abs(R).^2;         %absorption coefficient
    str = dec2bin(il,3)
    semilogx(f,anormal,'color',[str2num(str(1)) str2num(str(2)) ...
    str2num(str(3))]);
    title('Abs. coeff., rigid backed porous absorber')
    xlabel('Frequency(Hz)')
    ylabel('alpha')
    strlegend(il,1:6) = char(num2str(l,4));
end
legend(strlegend)
axis([100,10000,0,1])
```

B.3 Chapter 5: script_5_3

```
%Absorption of a rigid backed porous absorber
%Using Delany and Bazley formulations
%Normal incidence absorption coefficients

close all
clear all

c = 340;     %speed of sound
rho = 1.21;  %density of air
z0 = c*rho;  %characteristic impedance of air

%Frequency
f = [100:50:10000];
nf = length(f);

%Consider absorbent layer alone

%Delany and Bazley
sigma = 20000;              %flow resisivity
X = rho*f/sigma;     %dimensionless quantity for Delany and Bazley
zc = rho*c*(1+0.0571*(X.^-0.754)-j*0.087*(X.^-0.732));
                     %characteristic impedance
k = (2*pi/c).*f.*(1+0.0978*(X.^-0.700)-j*0.189*(X.^-0.595));
                     %complex wave number
l = 0.0254;          %thickness
z = -j*zc.*cot(k*l) %surface impedance

figure(1)
semilogx(f,real(z),'b',f,imag(z),'g');
title('Effect of air gap')
xlabel('Frequency(Hz)')
ylabel('Impedance')
legend('Real','Imaginary')

R = (z-z0)./(z+z0); %reflection factor

anormal = 1-abs(R).^2;      %absorption coefficient

figure(2)
semilogx(f,anormal);
title('Effect of air gap')
xlabel('Frequency(Hz)')
ylabel('alpha')

%Consider absorbent with air layer behind
l = l/2;                    %Depth of air layer
kair = 2*pi*f/c;
zs1 = -j*z0*cot(kair*l);    %Impedance at top of air layer
zs2 = (-j*zs1.*zc.*coth(k*l)+zc.^2)./(zs1+zc.*coth(gamma*l));
                            %Impedance at surface of absorber

figure(1)
hold on
semilogx(f,real(zs2),'c',f,imag(zs2),'m');
title('Effect of air gap')
```

```
xlabel('Frequency(Hz)')
ylabel('Impedance')
legend('Real 25 mm','Imaginary 25 mm', ...
'Real 12.5 mm air gap','Imaginary 12.5 mm air gap')

R = (zs2-z0)./(zs2+z0);      %reflection factor
anormal = 1-abs(R).^2;                %absorption coefficient

figure(2)
hold on
semilogx(f,anormal,'r');
title('Effect of air gap')
xlabel('Frequency(Hz)')
ylabel('alpha')
legend('25 mm absorbent','12.5 mm absorbent and air gap')
```

B.4 Chapter 6: script_6_1.m

```
%Absorption of a perforated absorber
%Normal incidence

close all
clear all

c = 340;      %speed of sound
rho = 1.21;   %density of air
Z0 = c*rho;
viscosity = 15e-6;   %kinemetric viscosity of air

sigma = 20000;        %Flow resistivity of mineral wool
l1 = 0.025;           %backing thickness air
l2 = 0.025;           %backing thickness porous absorber

f = [100:50:2500];   %Frequency
nf = length(f);

kair = 2*pi*f/c;
w = 2*pi*f;

%Impedance at top of air layer
z1 = -j*Z0.*cot(kair*l1);

%calculate impedance of porous material (Delany and Bazley)
%dimensionless quantity for Delany and Bazley
X = rho*f/sigma;
%characteristic impedance
Zc = rho*c*(1+0.0571*(X.^-0.754)-j*0.087*(X.^-0.732));
                      %wavenumber
k = (2*pi/c).*f.*(1+0.0978*(X.^-0.700)-j*0.189*(X.^-0.595));

%Impedance at top of porous absorbent
z2 = (-j*z1.*Zc.*cot(k*l2)+Zc.^2 )./ (z1 -j*Zc.*cot(k*l2));

%Loop over different open areas
eta = [0.0625,0.125,0.25,0.50,1.00]
ne = length(eta);
for m = 1:ne
```

```
    a = 2.5e-3;                      %hole radius
    D = sqrt(pi/eta(m))*a;           %Hole spacing
    delta = 1.6*(1-1.47*eta(m)^0.5+0.47*eta(m)^3/2);
                                     %end correction
    t = 6.3e-3;                      %plate thickness
    rm = (rho/eta(m))*sqrt(8*viscosity*w)*(1+t/(2*a));
                                     %surface resistance

    z3 = (j/eta(m))*(2*delta*a+t)*w*rho+z2+rm;
                                     %impedance of resonant absorber
    R = (z3-rho*c)./(z3+rho*c);      %reflection factor
    alpha = 1-abs(R).^2;             %absorption coefficient

    figure(1)
    hold on
    str = dec2bin(m,3)
    plot(f,real(z3),'color', ...
[str2num(str(1)) str2num(str(2)) str2num(str(3))] ... ,'LineStyle','-');
    plot(f,imag(z3),'color', ...
[str2num(str(1)) str2num(str(2)) str2num(str(3))] ... ,'LineStyle',':');

    figure(2)
    hold on
    plot(f,alpha,'color', ...
[str2num(str(1)) str2num(str(2)) str2num(str(3))]);
end
```

B.5   *Chapter 6: script_6_2.m*

```
%Absorption of a slotted absorber
%Normal incidence

close all
clear all

c = 340;       %speed of sound
rho = 1.21;    %density of air

r0 = 32;       %air flow resistance of porous material =
               %flow resistivity*thickness

l = 0.1;                 %backing thickness

f = [100:10:1100];    %Frequency
nf = length(f);       %Number of frequency terms
k = 2*pi*f/c;         %wavenumber
w = 2*pi*f;           %Angular frequency

z1 = rho*c*coth(j*k*l);     %Impedance at top of air cavity

t = 15e-3;                  %Plate thickness
d = 0.01;                   %slot width
eta = (0.0465*4*d)/(pi*0.05^2);    %open area
delta = -(d/pi)*log(sin(pi*eta/2)); %end correction
%impedance of resonant absorber
z2 = (j/eta)*(2*delta+t)*w*rho+z1+r0/eta;
```

```
figure                          %Plot impedance
plot(f,real(z2),'b',f,imag(z2),'g');
title('Impedance')
xlabel('Frequency(Hz)')
ylabel('Impedance')
legend('Real','Imaginary')

R = (z2-rho*c)./(z2+rho*c);        %reflection factor
anormal = 1-abs(R).^2;             %absorption coefficient

figure                          %Plot absorption coefficient
plot(f,anormal);
title('Normal incidence absorption coefficient')
xlabel('Frequency(Hz)')
ylabel('alpha')
```

B.6 Chapter 6: script_6_3

```
%Microperforated
%Helmholtz absorber

close all
clear all

D = 2.5e-3;          %Hole separation
d = 0.2e-3;          %Hole diameter
a = d/2;             %Hole radius
t = 0.2e-3;          %Sheet thickness
l = 0.06;            %Cavity depth

f = linspace(50,8000,100);
nf = length(f);
w = 2*pi*f;
c = 340;
k = w/c;
rho = 1.21;
viscosity = 1.85e-5;
eta = pi*a^2/(D^2); %Open area

z1 = -j*rho*c*cot(k*l);     %Impedance, top of cavity;

%Impedance of covering sheet
kd = a*sqrt(rho*w/viscosity);
s = kd*sqrt(-j);
z2 = j*w*rho*t./(1 - 2*besselj(1,s)./(s.*besselj(0,s)));
z2 = z2/eta +j*w*0.85*2*rho*a/eta+sqrt(2)*kd*viscosity/(2*a*eta);
z = z1+z2;

R = (z-rho*c)./(z+rho*c);          %reflection factor
anormal = 1-abs(R).^2;             %absorption coefficient

hold on
plot(f,anormal,'g')
xlabel('f (Hz)')
ylabel('abs. coeff')
```

B.7 *Chapter 13: simple_lms.m*

```
%LMS demo

close all
clear all

N = 10000;                    %Number of time iterations
k = [1:N];                    %This is inefficient for storage, but allows
                              %graphs to be plotted

s = sin(2*pi*k*10/N)';        %Input signal
figure
plot(k,s)
title('Input signal s')
xlabel('Time k')
ylabel('(linear)')

x = (rand(N,1)-0.5)*2;        %Noise signal
figure
plot(k,x)
title('Noise signal x')
xlabel('Time k')
ylabel('(linear)')

W_1 = ([0.5,0.2]);   %This is W^-1 in Figure 13.2

W = rand(1,2);        %starting adaptive filter weights (assigned randomly)
alpha = 0.001;        %Update rate

e = zeros(N,1);
Wstore = zeros(N,2);
n(1,1) = 0;
for j = 2:N
   n(j,1) = W_1*x(j-1:j);       %This is convolution in matrix format
   %Note that W_1(2) is actually the first coefficient
   %and W_1(1) is actually the second coefficient
   d = s(j)+n(j);
   y = W*x(j-1:j);              %Output from adaptive filter
   e(j-1) = d - y;             %Error

   W = W + 2*alpha*e(j-1)*rot90(x(j-1:j),1);       %Update weights
   Wstore(j-1,:) = W;             %Store weights for future plotting
end

figure
plot(e)
title('Error')
xlabel('Time k')
ylabel('(linear)')

figure
plot(Wstore(:,1))
hold on
plot(Wstore(:,2),'r')
title('Adaptive filter coefficients')
xlabel('Time k')
ylabel('(linear)')
```

Appendix C

C.1 Normalized diffusion coefficient table

Surface	Angle of incidence (°)	Frequency (Hz)																	
		100	125	160	200	250	315	400	500	630	800	1000	1250	1600	2000	2500	3150	4000	5000
1. Effect of changing diffuser periodicity and width. Semicylinder(s) non-absorbing surfaces, radius 0.3 m, (1 cm flat section between each period)																			
1 period, 0.61 cm wide	0	0.02	0.00	0.00	0.00	0.65	0.96	0.92	0.96	0.97	0.90	0.93	0.95	0.94	0.95	0.97	0.98	0.98	0.98
	57	0.06	0.07	0.16	0.38	0.59	0.18	0.43	0.37	0.55	0.53	0.64	0.70	0.74	0.77	0.80	0.82	0.85	0.86
	random	0.06	0.07	0.11	0.28	0.56	0.50	0.56	0.66	0.80	0.76	0.77	0.80	0.82	0.82	0.84	0.85	0.86	0.87
2 periods, 1.22 m wide	0	0.16	0.18	0.15	0.06	0.02	0.17	0.60	0.62	0.71	0.43	0.50	0.72	0.65	0.77	0.77	0.73	0.77	0.80
	57	0.15	0.12	0.18	0.53	0.40	0.50	0.30	0.26	0.66	0.69	0.66	0.69	0.72	0.73	0.76	0.76	0.80	0.83
	random	0.23	0.16	0.09	0.26	0.32	0.38	0.38	0.33	0.64	0.55	0.62	0.69	0.71	0.73	0.74	0.74	0.78	0.79
4 cylinders, 2.44 m wide	0	0.02	0.00	0.01	0.05	0.03	0.04	0.13	0.58	0.32	0.16	0.24	0.38	0.31	0.48	0.44	0.41	0.43	0.54
	57	0.04	0.18	0.21	0.19	0.29	0.34	0.12	0.02	0.49	0.31	0.33	0.49	0.51	0.53	0.64	0.66	0.64	0.66
	random	0.00	0.05	0.03	0.07	0.09	0.18	0.19	0.19	0.38	0.29	0.34	0.45	0.47	0.49	0.54	0.59	0.61	0.62
6 periods, 3.66 m wide	0	0.00	0.02	0.02	0.01	0.02	0.02	0.05	0.21	0.22	0.10	0.19	0.21	0.26	0.39	0.32	0.38	0.49	0.72
	57	0.07	0.16	0.16	0.10	0.18	0.32	0.09	0.03	0.40	0.18	0.25	0.43	0.42	0.46	0.59	0.58	0.60	0.66
	random	0.00	0.00	0.00	0.00	0.07	0.14	0.14	0.12	0.28	0.19	0.26	0.36	0.40	0.42	0.48	0.55	0.60	0.65
12 periods, 7.32 m wide	0	0.00	0.00	0.01	0.01	0.01	0.01	0.01	0.04	0.14	0.08	0.17	0.48	0.35	0.63	0.57	0.72	0.66	0.81
	57	0.06	0.06	0.06	0.03	0.04	0.32	0.13	0.07	0.30	0.09	0.21	0.40	0.42	0.49	0.55	0.58	0.68	0.67
	random	0.00	0.00	0.00	0.00	0.03	0.10	0.10	0.09	0.20	0.12	0.22	0.38	0.42	0.46	0.56	0.64	0.66	0.70
2. Effect of surface depth, 6 semi-ellipses, non-absorbing, each width 0.6 m, total with 3.66 m (1 cm flat section between semi-ellipses)																			
1 cm deep	0	0.02	0.02	0.01	0.00	0.00	0.00	0.00	0.00	0.00	0.00	0.00	0.00	0.00	0.00	0.00	0.01	0.02	0.03
	57	0.01	0.03	0.02	0.00	0.00	0.00	0.00	0.00	0.00	0.00	0.00	0.00	0.00	0.00	0.00	0.01	0.02	0.03
	random	0.01	0.02	0.02	0.00	0.01	0.01	0.00	0.00	0.00	0.00	0.00	0.00	0.00	0.01	0.01	0.01	0.01	0.02

(*continued*)

C.1 Normalized diffusion coefficient table (continued)

Surface	Angle of incidence (°)	Frequency (Hz)																	
		100	125	160	200	250	315	400	500	630	800	1000	1250	1600	2000	2500	3150	4000	5000
2 cm deep	0	0.02	0.02	0.01	0.00	0.00	0.00	0.00	0.00	0.00	0.00	0.00	0.01	0.01	0.01	0.02	0.04	0.08	0.13
	57	0.01	0.03	0.02	0.00	0.00	0.00	0.00	0.00	0.00	0.00	0.00	0.00	0.01	0.01	0.01	0.03	0.08	0.10
	random	0.01	0.03	0.02	0.01	0.02	0.03	0.02	0.01	0.02	0.01	0.01	0.01	0.01	0.02	0.03	0.04	0.06	0.08
5 cm deep	0	0.01	0.01	0.01	0.00	0.00	0.00	0.00	0.01	0.03	0.03	0.04	0.07	0.10	0.14	0.24	0.24	0.34	0.36
	57	0.00	0.03	0.02	0.00	0.00	0.05	0.04	0.03	0.03	0.03	0.03	0.04	0.05	0.06	0.10	0.12	0.15	0.15
	random	0.01	0.03	0.03	0.02	0.05	0.06	0.04	0.03	0.04	0.04	0.03	0.05	0.08	0.12	0.14	0.15	0.20	0.25
10 cm deep	0	0.01	0.01	0.01	0.00	0.00	0.00	0.00	0.05	0.26	0.22	0.19	0.32	0.26	0.32	0.57	0.50	0.70	0.73
	57	0.00	0.03	0.02	0.00	0.02	0.22	0.15	0.12	0.14	0.14	0.16	0.17	0.19	0.24	0.31	0.40	0.41	0.40
	random	0.02	0.06	0.07	0.06	0.06	0.10	0.07	0.05	0.11	0.15	0.19	0.23	0.25	0.29	0.39	0.40	0.47	0.51
20 cm deep	0	0.00	0.01	0.01	0.00	0.01	0.01	0.02	0.28	0.41	0.18	0.02	0.16	0.28	0.27	0.57	0.58	0.58	0.54
	57	0.00	0.03	0.03	0.04	0.09	0.36	0.16	0.03	0.22	0.27	0.34	0.31	0.29	0.38	0.47	0.53	0.54	0.59
	random	0.00	0.00	0.00	0.01	0.06	0.11	0.11	0.11	0.20	0.25	0.23	0.31	0.32	0.37	0.45	0.50	0.56	0.61
30 cm deep (semi-cylinders)	0	0.00	0.02	0.02	0.01	0.02	0.02	0.05	0.21	0.22	0.10	0.19	0.21	0.26	0.39	0.32	0.38	0.49	0.72
	57	0.07	0.16	0.16	0.10	0.18	0.32	0.09	0.03	0.40	0.18	0.25	0.43	0.42	0.46	0.59	0.58	0.60	0.66
	random	0.00	0.00	0.00	0.00	0.07	0.14	0.14	0.12	0.28	0.19	0.26	0.36	0.40	0.42	0.48	0.55	0.60	0.65
3. Triangles, non-absorbing, 3.66 m wide, (0.01 cm flat section between each period)																			
15 periods, 60° angle	0	0.00	0.00	0.00	0.00	0.00	0.00	0.00	0.00	0.00	0.00	0.00	0.00	0.05	0.01	0.00	0.01	0.01	0.01
	57	0.07	0.09	0.07	0.05	0.09	0.06	0.06	0.11	0.07	0.05	0.05	0.04	0.23	0.17	0.15	0.23	0.24	0.23
	random	0.00	0.00	0.00	0.00	0.00	0.00	0.00	0.06	0.05	0.08	0.05	0.05	0.13	0.11	0.15	0.15	0.14	0.14
9 periods, 45° angle	0	0.00	0.00	0.00	0.00	0.00	0.00	0.00	0.00	0.01	0.03	0.03	0.00	0.02	0.02	0.01	0.01	0.01	0.01
	57	0.00	0.03	0.03	0.01	0.00	0.02	0.26	0.19	0.05	0.13	0.26	0.15	0.22	0.20	0.15	0.07	0.06	0.07
	random	0.00	0.00	0.00	0.00	0.00	0.00	0.12	0.11	0.07	0.13	0.16	0.14	0.18	0.20	0.16	0.13	0.15	0.10

(continued)

C.1 Normalized diffusion coefficient table (*continued*)

Surface	Angle of incidence (°)	Frequency (Hz)																	
		100	125	160	200	250	315	400	500	630	800	1000	1250	1600	2000	2500	3150	4000	5000
6 periods, 30° angle	0	0.00	0.00	0.00	0.00	0.00	0.00	0.00	0.07	0.39	0.21	0.22	0.35	0.40	0.33	0.36	0.33	0.22	0.17
	57	0.00	0.01	0.02	0.01	0.08	0.32	0.15	0.09	0.21	0.18	0.16	0.20	0.15	0.17	0.16	0.14	0.09	0.05
	random	0.00	0.00	0.00	0.00	0.04	0.09	0.08	0.09	0.17	0.18	0.19	0.22	0.24	0.24	0.23	0.20	0.16	0.12
3 periods, 18° angle	0	0.01	0.01	0.01	0.01	0.07	0.23	0.33	0.28	0.35	0.32	0.30	0.30	0.28	0.23	0.19	0.15	0.12	0.10
	57	0.02	0.15	0.34	0.29	0.19	0.19	0.16	0.18	0.16	0.16	0.16	0.17	0.19	0.17	0.13	0.10	0.09	0.02
	random	0.05	0.08	0.11	0.10	0.08	0.10	0.15	0.19	0.20	0.20	0.21	0.21	0.20	0.17	0.15	0.12	0.10	0.07
4. Semi-ellipses mounted on 3.63 m wide flat baffle, non-absorbing, each semi-ellipse 0.6 m wide, 0.2 m deep																			
1 semi-ellipse in middle of baffle	0	0.00	0.00	0.03	0.09	0.11	0.10	0.17	0.14	0.08	0.02	0.02	0.04	0.02	0.03	0.03	0.01	0.01	0.04
	57	0.11	0.27	0.23	0.29	0.31	0.29	0.26	0.26	0.22	0.16	0.11	0.08	0.06	0.09	0.15	0.15	0.07	0.06
	random	0.08	0.13	0.15	0.19	0.22	0.22	0.22	0.24	0.21	0.17	0.15	0.14	0.16	0.16	0.17	0.13	0.11	0.10
3 semi-ellipses with 0.6 m flat section between	0	0.01	0.02	0.01	0.02	0.12	0.50	0.33	0.28	0.30	0.10	0.12	0.16	0.17	0.10	0.08	0.16	0.17	0.25
	57	0.05	0.31	0.43	0.28	0.23	0.38	0.23	0.33	0.31	0.40	0.52	0.42	0.20	0.22	0.44	0.41	0.27	0.67
	random	0.05	0.13	0.14	0.14	0.17	0.27	0.24	0.31	0.31	0.29	0.25	0.33	0.33	0.32	0.34	0.37	0.34	0.35
5. Optimized curved surfaces, 3.6 m wide, modulated arrays																			
3 periods 30 cm deep	0	0.09	0.10	0.06	0.13	0.54	0.49	0.28	0.39	0.53	0.28	0.35	0.52	0.63	0.42	0.73	0.74	0.31	0.79
	57	0.21	0.51	0.50	0.33	0.20	0.23	0.12	0.16	0.31	0.60	0.59	0.52	0.59	0.58	0.56	0.57	0.55	0.47
	random	0.16	0.16	0.19	0.20	0.20	0.23	0.18	0.27	0.38	0.44	0.54	0.54	0.59	0.54	0.55	0.59	0.56	0.59
6 periods 20 cm deep	0	0.06	0.04	0.02	0.01	0.00	0.01	0.02	0.28	0.52	0.35	0.35	0.29	0.18	0.38	0.15	0.31	0.33	0.54
	57	0.08	0.06	0.05	0.00	0.08	0.38	0.21	0.11	0.31	0.44	0.53	0.60	0.51	0.64	0.57	0.54	0.52	0.58
	random	0.09	0.04	0.03	0.00	0.05	0.13	0.16	0.18	0.29	0.42	0.45	0.47	0.56	0.56	0.50	0.53	0.56	0.56

(*continued*)

Surface	Angle of incidence (°)	Frequency (Hz)																	
		100	125	160	200	250	315	400	500	630	800	1000	1250	1600	2000	2500	3150	4000	5000
6 periods 10 cm deep	0	0.04	0.02	0.01	0.02	0.01	0.01	0.03	0.04	0.05	0.05	0.05	0.41	0.56	0.30	0.64	0.29	0.63	0.63
	57	0.07	0.10	0.09	0.09	0.10	0.08	0.11	0.10	0.41	0.44	0.49	0.47	0.52	0.46	0.46	0.36	0.42	0.41
	random	0.07	0.10	0.11	0.10	0.10	0.11	0.13	0.10	0.20	0.27	0.33	0.44	0.47	0.44	0.47	0.46	0.48	0.51
6 periods 5 cm deep	0	0.06	0.03	0.02	0.01	0.00	0.00	0.00	0.01	0.00	0.00	0.01	0.10	0.16	0.29	0.45	0.56	0.51	0.64
	57	0.07	0.06	0.05	0.01	0.01	0.01	0.00	0.01	0.12	0.15	0.12	0.09	0.10	0.13	0.18	0.29	0.29	0.33
	random	0.07	0.05	0.04	0.02	0.04	0.04	0.03	0.05	0.10	0.12	0.09	0.10	0.13	0.21	0.30	0.36	0.39	0.45

6. Hybrid surfaces, 3.6 m wide, modulated arrays

Surface	Angle of incidence (°)	Frequency (Hz)																	
		100	125	160	200	250	315	400	500	630	800	1000	1250	1600	2000	2500	3150	4000	5000
3 periods, flat hybrid surface	0	0.07	0.02	0.02	0.01	0.00	0.00	0.00	0.00	0.00	0.00	0.00	0.00	0.01	0.01	0.01	0.01	0.01	0.02
	57	0.13	0.08	0.06	0.02	0.01	0.01	0.01	0.01	0.00	0.01	0.02	0.03	0.06	0.09	0.08	0.14	0.29	0.36
	random	0.15	0.11	0.09	0.06	0.04	0.04	0.02	0.01	0.01	0.01	0.01	0.03	0.07	0.10	0.11	0.13	0.13	0.16
3 periods, curved, 2.5 cm deep	0	0.06	0.02	0.02	0.00	0.00	0.00	0.00	0.01	0.01	0.01	0.01	0.03	0.04	0.05	0.06	0.15	0.22	0.28
	57	0.12	0.08	0.04	0.01	0.01	0.04	0.03	0.04	0.05	0.05	0.08	0.11	0.19	0.21	0.19	0.28	0.29	0.49
	random	0.15	0.10	0.08	0.05	0.04	0.07	0.05	0.05	0.07	0.06	0.06	0.10	0.15	0.16	0.19	0.24	0.28	0.32
3 periods, curved, 7.5 cm deep	0	0.05	0.01	0.02	0.01	0.00	0.00	0.01	0.03	0.05	0.08	0.24	0.39	0.52	0.52	0.24	0.32	0.67	0.56
	57	0.11	0.07	0.03	0.01	0.01	0.11	0.09	0.14	0.39	0.30	0.33	0.44	0.43	0.41	0.40	0.40	0.42	0.40
	random	0.15	0.10	0.06	0.04	0.04	0.10	0.09	0.11	0.21	0.20	0.24	0.36	0.42	0.40	0.33	0.40	0.49	0.47

7. Schroeder diffusers, 3.6 m wide

Surface	Angle of incidence (°)	Frequency (Hz)																	
		100	125	160	200	250	315	400	500	630	800	1000	1250	1600	2000	2500	3150	4000	5000
N=7 QRD, 6 periods, 0.2 m deep	0	0.07	0.01	0.02	0.00	0.01	0.01	0.01	0.07	0.16	0.21	0.12	0.10	0.07	0.23	0.39	0.04	0.19	0.27
	57	0.13	0.14	0.11	0.05	0.11	0.02	0.10	0.24	0.37	0.28	0.32	0.12	0.31	0.45	0.43	0.32	0.37	0.60
	random	0.07	0.04	0.00	0.00	0.00	0.00	0.04	0.22	0.25	0.22	0.23	0.09	0.23	0.35	0.36	0.23	0.25	0.42

(*continued*)

C.1 **Normalized diffusion coefficient table** (*continued*)

Surface	Angle of incidence (°)	Frequency (Hz)																	
		100	125	160	200	250	315	400	500	630	800	1000	1250	1600	2000	2500	3150	4000	5000
Optimized, modulated array, 6 periods, 8 wells/period, 0.17 m deep	0	0.07	0.02	0.01	0.00	0.06	0.07	0.07	0.30	0.58	0.40	0.41	0.49	0.59	0.38	0.33	0.38	0.30	0.33
	57	0.12	0.11	0.16	0.10	0.08	0.14	0.32	0.33	0.49	0.53	0.39	0.46	0.57	0.48	0.57	0.54	0.58	0.55
	random	0.08	0.05	0.06	0.00	0.00	0.07	0.18	0.27	0.43	0.47	0.37	0.41	0.51	0.43	0.43	0.48	0.42	0.46
N=7 PRD, 6 periods, 6 wells/period, 0.2 m deep	0	0.07	0.01	0.02	0.00	0.01	0.02	0.04	0.03	0.06	0.33	0.13	0.14	0.20	0.27	0.10	0.35	0.21	0.06
	57	0.15	0.15	0.12	0.08	0.07	0.24	0.31	0.25	0.21	0.26	0.15	0.20	0.34	0.34	0.19	0.27	0.32	0.19
	random	0.09	0.04	0.00	0.00	0.00	0.10	0.15	0.15	0.19	0.19	0.17	0.20	0.22	0.32	0.22	0.29	0.32	0.25
Diffractal, 1 period, 3 orders of size, N=7 (largest order only 6 wells), 0.5 m deep	0	0.06	0.25	0.10	0.27	0.30	0.36	0.56	0.31	0.39	0.40	0.42	0.52	0.56	0.49	0.49	0.40	0.47	0.54
	57	0.40	0.35	0.43	0.46	0.44	0.56	0.77	0.60	0.66	0.67	0.56	0.43	0.62	0.67	0.66	0.56	0.16	0.69
	random	0.19	0.20	0.29	0.35	0.36	0.44	0.61	0.45	0.51	0.51	0.49	0.40	0.54	0.53	0.50	0.47	0.35	0.53
Optimized, modulated array, 6 periods, 12 wells/period, 0.17 m deep	0	0.06	0.02	0.02	0.00	0.04	0.05	0.20	0.61	0.58	0.51	0.58	0.32	0.31	0.49	0.37	0.30	0.42	0.53
	57	0.09	0.10	0.12	0.07	0.24	0.53	0.44	0.74	0.54	0.43	0.66	0.52	0.60	0.52	0.48	0.41	0.48	0.72
	random	0.04	0.02	0.00	0.00	0.06	0.27	0.34	0.58	0.50	0.42	0.56	0.40	0.44	0.48	0.42	0.40	0.45	0.53

C.2 Correlation scattering coefficient table

	Angle of incidence (°)	Frequency (Hz)																	
		100	125	160	200	250	315	400	500	630	800	1000	1250	1600	2000	2500	3150	4000	5000
Plane surfaces, non-absorbing, any size	All/any	0.00	0.00	0.00	0.00	0.00	0.00	0.00	0.00	0.00	0.00	0.00	0.00	0.00	0.00	0.00	0.00	0.00	0.00
1. Effect of changing diffuser width and periodicity, semicylinder(s) non-absorbing surfaces, radius 0.3 m (1 cm flat section between each period)																			
1 period, 0.61 m wide	0	0.06	0.09	0.13	0.20	0.29	0.38	0.43	0.45	0.59	0.78	0.82	0.80	0.92	0.89	0.92	0.94	0.95	0.96
	56.9	0.27	0.24	0.23	0.26	0.32	0.45	0.69	0.79	0.80	0.92	0.88	0.91	0.90	0.90	0.91	0.92	0.94	0.96
	random	0.24	0.21	0.21	0.25	0.32	0.43	0.62	0.73	0.74	0.82	0.86	0.88	0.90	0.91	0.94	0.95	0.96	0.96
2 periods, 1.22 m wide	0	0.04	0.05	0.05	0.04	0.02	0.11	0.65	0.87	0.64	0.56	0.87	0.79	0.90	0.89	0.92	0.93	0.94	0.91
	56.9	0.13	0.12	0.18	0.40	0.43	0.71	0.85	0.93	0.80	0.71	0.81	0.87	0.90	0.89	0.93	0.92	0.94	0.96
	random	0.16	0.16	0.21	0.32	0.34	0.52	0.80	0.93	0.76	0.67	0.88	0.87	0.91	0.91	0.93	0.94	0.95	0.95
4 periods, 2.44 m wide	0	0.01	0.00	0.02	0.06	0.02	0.08	0.35	0.74	0.55	0.49	0.87	0.77	0.87	0.84	0.80	0.86	0.83	0.88
	56.9	0.14	0.19	0.24	0.34	0.36	0.82	0.87	0.96	0.76	0.52	0.77	0.86	0.90	0.88	0.92	0.92	0.95	0.98
	random	0.21	0.22	0.24	0.29	0.30	0.53	0.78	0.93	0.71	0.56	0.87	0.86	0.90	0.88	0.90	0.93	0.94	0.94
6 periods, 3.66 m wide	0	0.00	0.01	0.01	0.04	0.03	0.05	0.25	0.55	0.53	0.45	0.86	0.72	0.80	0.81	0.79	0.85	0.82	0.95
	56.9	0.15	0.20	0.23	0.26	0.24	0.84	0.89	0.97	0.74	0.48	0.75	0.85	0.89	0.87	0.94	0.95	0.97	0.98
	random	0.22	0.23	0.24	0.26	0.26	0.52	0.76	0.91	0.68	0.51	0.86	0.85	0.89	0.88	0.90	0.94	0.94	0.95
12 periods, 7.32 m wide	0	0.00	0.00	0.01	0.02	0.02	0.03	0.13	0.33	0.48	0.40	0.86	0.76	0.84	0.87	0.81	0.83	0.87	0.90
	56.9	0.16	0.15	0.10	0.08	0.12	0.81	0.89	0.97	0.71	0.40	0.74	0.88	0.93	0.90	0.91	0.94	0.93	0.94
	random	0.23	0.22	0.21	0.20	0.19	0.48	0.73	0.87	0.64	0.46	0.86	0.86	0.89	0.87	0.92	0.92	0.92	0.91
2. Effect of surface depth, 6 semi-ellipses, non-absorbing, each width 0.6 m, total with 3.66 m (1 cm flat section between semi-ellipses)																			
1 cm deep	0	0.00	0.00	0.00	0.00	0.00	0.00	0.00	0.00	0.01	0.01	0.01	0.02	0.02	0.04	0.04	0.10	0.14	0.37
	56.9	0.00	0.00	0.00	0.00	0.00	0.01	0.00	0.01	0.01	0.01	0.01	0.01	0.01	0.02	0.03	0.07	0.21	0.20
	random	0.00	0.00	0.00	0.00	0.00	0.02	0.01	0.01	0.02	0.01	0.02	0.02	0.03	0.04	0.06	0.10	0.13	0.20

(*continued*)

C.2 Correlation scattering coefficient table (*continued*)

Angle of incidence (°)	Frequency (Hz)																	
	100	125	160	200	250	315	400	500	630	800	1000	1250	1600	2000	2500	3150	4000	5000
2 cm deep																		
0	0.00	0.00	0.00	0.00	0.00	0.00	0.00	0.01	0.03	0.04	0.05	0.07	0.09	0.15	0.17	0.36	0.47	0.80
56.9	0.00	0.00	0.00	0.00	0.00	0.02	0.02	0.02	0.02	0.03	0.03	0.04	0.05	0.08	0.13	0.27	0.53	0.54
random	0.00	0.00	0.00	0.00	0.01	0.05	0.04	0.04	0.06	0.05	0.07	0.08	0.10	0.15	0.22	0.33	0.41	0.53
5 cm deep																		
0	0.00	0.00	0.00	0.00	0.00	0.00	0.01	0.06	0.20	0.23	0.33	0.40	0.51	0.67	0.77	0.86	0.84	0.92
56.9	0.00	0.00	0.00	0.00	0.01	0.12	0.11	0.11	0.15	0.16	0.19	0.24	0.29	0.39	0.54	0.85	0.93	0.94
random	0.00	0.00	0.01	0.01	0.06	0.16	0.16	0.18	0.22	0.25	0.31	0.38	0.47	0.59	0.71	0.80	0.82	0.85
10 cm deep																		
0	0.00	0.00	0.00	0.00	0.00	0.01	0.03	0.26	0.64	0.71	0.85	0.82	0.73	0.80	0.88	0.86	0.93	0.96
56.9	0.00	0.00	0.00	0.01	0.05	0.38	0.35	0.37	0.46	0.51	0.56	0.65	0.72	0.81	0.92	0.93	0.94	0.95
random	0.02	0.04	0.06	0.09	0.15	0.31	0.36	0.44	0.54	0.64	0.73	0.78	0.80	0.84	0.89	0.91	0.93	0.94
20 cm deep																		
0	0.00	0.00	0.00	0.01	0.01	0.03	0.12	0.66	0.91	0.61	0.26	0.78	0.86	0.76	0.91	0.88	0.87	0.86
56.9	0.03	0.04	0.06	0.09	0.19	0.75	0.76	0.88	0.87	0.81	0.70	0.72	0.85	0.92	0.91	0.96	0.97	0.98
random	0.14	0.16	0.18	0.20	0.25	0.47	0.64	0.87	0.90	0.76	0.62	0.80	0.90	0.87	0.92	0.93	0.94	0.95
30 cm deep (semi-cylinder)																		
0	0.00	0.01	0.01	0.04	0.03	0.05	0.25	0.55	0.53	0.45	0.86	0.72	0.80	0.81	0.79	0.85	0.82	0.95
56.9	0.15	0.20	0.23	0.26	0.24	0.84	0.89	0.97	0.74	0.48	0.75	0.85	0.89	0.87	0.94	0.95	0.97	0.98
random	0.22	0.23	0.24	0.26	0.26	0.52	0.76	0.91	0.68	0.51	0.86	0.85	0.89	0.88	0.90	0.94	0.94	0.95
3. Triangles, non-absorbing, 3.66 m wide (0.01 cm flat section between each period)																		
15 periods, 60°																		
0	0.01	0.01	0.00	0.00	0.00	0.01	0.02	0.03	0.04	0.06	0.05	0.06	0.37	0.12	0.06	0.12	0.13	0.17
56.9	0.49	0.60	0.68	0.71	0.58	0.19	0.18	0.33	0.25	0.45	0.23	0.27	0.68	0.65	0.95	0.92	0.93	0.98
random	0.34	0.35	0.35	0.34	0.32	0.28	0.24	0.30	0.27	0.32	0.24	0.34	0.50	0.53	0.67	0.69	0.72	0.75
9 periods, 45°																		
0	0.00	0.00	0.00	0.00	0.01	0.04	0.03	0.07	0.16	0.29	0.30	0.17	0.23	0.22	0.22	0.19	0.23	0.28
56.9	0.03	0.04	0.06	0.07	0.08	0.20	0.54	0.95	0.99	0.75	0.93	0.97	0.99	0.99	0.99	0.99	1.00	1.00
random	0.15	0.17	0.19	0.21	0.23	0.28	0.37	0.59	0.80	0.79	0.69	0.82	0.83	0.87	0.89	0.90	0.90	0.91

(*continued*)

C.2 Correlation scattering coefficient table (*continued*)

Frequency (Hz)

	Angle of incidence (°)	100	125	160	200	250	315	400	500	630	800	1000	1250	1600	2000	2500	3150	4000	5000
6 periods, 30° 3.66 m wide	0	0.00	0.00	0.00	0.00	0.01	0.02	0.06	0.36	0.96	0.98	0.81	0.99	0.89	0.97	0.97	0.99	1.00	0.99
	56.9	0.01	0.02	0.02	0.04	0.18	0.81	0.76	0.72	0.70	0.83	0.90	0.94	0.99	1.00	0.99	0.99	1.00	1.00
	random	0.11	0.13	0.14	0.17	0.26	0.47	0.61	0.72	0.81	0.90	0.93	0.95	0.95	0.97	0.97	0.98	0.98	0.98
3 periods, 18°	0	0.00	0.01	0.01	0.02	0.17	0.49	0.66	0.78	0.90	0.99	0.98	0.95	0.99	0.99	0.99	0.99	0.99	0.99
	56.9	0.01	0.10	0.37	0.42	0.37	0.39	0.43	0.51	0.59	0.71	0.82	0.94	0.98	0.94	0.94	0.98	0.97	0.98
	random	0.07	0.17	0.31	0.38	0.41	0.48	0.56	0.67	0.78	0.88	0.93	0.94	0.97	0.98	0.99	0.99	0.99	0.99
4. Semi-ellipses mounted on 3.63 m wide flat baffle, non-absorbing, each semi-ellipse 0.6 m wide, 0.2 m deep																			
1 semi-ellipse in middle of baffle	0	0.01	0.02	0.03	0.09	0.20	0.22	0.36	0.40	0.35	0.22	0.19	0.27	0.20	0.19	0.14	0.18	0.21	0.30
	56.9	0.09	0.17	0.24	0.29	0.37	0.39	0.43	0.48	0.52	0.47	0.44	0.43	0.37	0.48	0.67	0.74	0.77	0.60
	random	0.15	0.22	0.28	0.32	0.38	0.42	0.47	0.51	0.53	0.48	0.46	0.46	0.48	0.49	0.50	0.53	0.52	0.54
3 semi-ellipses with 0.6 m flat sections between	0	0.00	0.01	0.03	0.05	0.26	0.72	0.88	0.89	0.70	0.46	0.53	0.65	0.63	0.58	0.51	0.66	0.68	0.76
	56.9	0.03	0.17	0.52	0.62	0.56	0.66	0.78	0.80	0.90	0.95	0.94	0.72	0.54	0.72	0.90	0.80	0.91	0.91
	random	0.13	0.22	0.38	0.50	0.57	0.67	0.79	0.85	0.85	0.76	0.69	0.75	0.77	0.79	0.85	0.85	0.81	0.78
5. Optimized curved surfaces, 3.6 m wide, modulated arrays																			
3 periods, 30 cm deep	0	0.00	0.03	0.06	0.16	0.59	0.95	0.99	0.95	0.88	0.71	0.88	0.89	0.92	0.79	0.92	0.93	0.82	0.95
	56.9	0.05	0.31	0.74	0.76	0.70	0.68	0.85	0.88	0.92	0.95	0.94	0.89	0.94	0.96	0.95	0.99	0.97	0.99
	random	0.15	0.30	0.50	0.64	0.74	0.79	0.90	0.94	0.89	0.86	0.91	0.93	0.95	0.94	0.94	0.95	0.96	0.97
6 periods, 20 cm deep	0	0.00	0.00	0.00	0.01	0.02	0.04	0.14	0.61	0.81	0.94	0.80	0.78	0.68	0.84	0.60	0.84	0.78	0.86
	56.9	0.01	0.02	0.02	0.04	0.23	0.73	0.79	0.88	0.98	0.86	0.78	0.92	0.94	0.94	0.98	0.98	0.96	0.96
	random	0.09	0.11	0.14	0.16	0.27	0.48	0.68	0.85	0.94	0.89	0.80	0.86	0.90	0.93	0.89	0.94	0.95	0.94

(*continued*)

C.2 Correlation scattering coefficient table (*continued*)

	Angle of incidence (°)	100	125	160	200	250	315	400	500	630	800	1000	1250	1600	2000	2500	3150	4000	5000
												Frequency (Hz)							
6 periods, 10 cm deep	0	0.00	0.00	0.00	0.01	0.01	0.02	0.07	0.15	0.23	0.30	0.38	0.82	0.86	0.80	0.89	0.73	0.90	0.89
	56.9	0.00	0.01	0.01	0.03	0.11	0.15	0.20	0.24	0.67	0.71	0.77	0.81	0.82	0.89	0.96	0.97	1.00	0.99
	random	0.01	0.03	0.04	0.09	0.15	0.20	0.25	0.31	0.50	0.62	0.73	0.84	0.89	0.92	0.95	0.94	0.95	0.96
6 periods, 5 cm deep	0	0.00	0.00	0.00	0.00	0.00	0.00	0.01	0.02	0.03	0.04	0.13	0.49	0.62	0.80	0.90	0.93	0.90	0.91
	56.9	0.00	0.00	0.00	0.01	0.01	0.02	0.02	0.04	0.31	0.39	0.42	0.42	0.43	0.52	0.69	0.81	0.93	0.95
	random	0.00	0.01	0.01	0.02	0.05	0.06	0.06	0.12	0.29	0.36	0.43	0.50	0.58	0.70	0.82	0.88	0.91	0.92

6. Schroeder diffusers, 3.6 m wide

	Angle of incidence (°)	100	125	160	200	250	315	400	500	630	800	1000	1250	1600	2000	2500	3150	4000	5000
N=7 QRD, 6 periods, 0.2 m deep	0	0.00	0.01	0.02	0.05	0.08	0.07	0.04	0.35	0.51	0.67	0.57	0.52	0.44	0.73	0.85	0.39	0.71	0.86
	56.9	0.04	0.06	0.12	0.26	0.41	0.17	0.16	0.71	0.75	0.84	0.71	0.51	0.74	0.91	0.83	0.79	0.67	0.93
	random	0.12	0.15	0.19	0.27	0.36	0.30	0.25	0.69	0.78	0.72	0.69	0.51	0.66	0.86	0.82	0.69	0.70	0.88
Optimized, modulated array, 6 periods, 8 wells/period, 0.17 m deep	0	0.00	0.01	0.02	0.04	0.20	0.21	0.27	0.65	0.78	0.80	0.85	0.86	0.95	0.92	0.95	0.82	0.88	0.96
	56.9	0.03	0.07	0.11	0.22	0.40	0.43	0.55	0.58	0.76	0.90	0.74	0.89	0.95	0.96	0.94	0.96	0.96	0.97
	random	0.09	0.14	0.18	0.25	0.36	0.48	0.55	0.68	0.82	0.89	0.83	0.87	0.93	0.94	0.93	0.90	0.91	0.94
N=7 PRD, 6 periods, 6 wells/period, 0.2 m deep	0	0.00	0.01	0.02	0.05	0.04	0.14	0.19	0.14	0.32	0.81	0.65	0.69	0.88	0.88	0.97	0.98	0.97	0.42
	56.9	0.04	0.09	0.18	0.38	0.41	0.47	0.66	0.59	0.61	0.83	0.96	0.93	0.88	0.94	0.92	0.89	0.95	0.96
	random	0.11	0.15	0.20	0.29	0.34	0.47	0.52	0.52	0.62	0.88	0.85	0.82	0.88	0.92	0.92	0.90	0.93	0.75
Diffractal, 1 period, 3 orders of size, N=7, 0.5 m deep	0	0.16	0.45	0.28	0.39	0.70	0.85	0.87	0.83	0.73	0.79	0.89	0.86	0.96	0.96	0.89	0.84	0.91	0.90
	56.9	0.30	0.74	0.76	0.63	0.67	0.64	0.84	0.70	0.77	0.87	0.92	0.77	0.89	0.93	0.92	0.95	0.89	0.96
	random	0.33	0.56	0.66	0.61	0.72	0.80	0.88	0.80	0.78	0.85	0.91	0.80	0.91	0.92	0.91	0.91	0.90	0.91
Optimized, 6 periods modulated array, 12 wells/period, 0.17 m deep	0	0.00	0.01	0.01	0.03	0.14	0.20	0.50	0.78	0.82	0.84	0.92	0.81	0.89	0.87	0.84	0.92	0.92	0.94
	56.9	0.04	0.08	0.13	0.24	0.50	0.70	0.67	0.90	0.92	0.92	0.95	0.88	0.91	0.96	0.97	0.99	0.98	0.98
	random	0.14	0.17	0.21	0.27	0.40	0.61	0.69	0.90	0.90	0.91	0.92	0.87	0.87	0.90	0.91	0.93	0.94	0.94

Index